FACTORS INFLUENCING THE SUCCESSFUL PRODUCTION OF LARGE PLASMIDS FOR USE IN GENE THERAPY AND DNA VACCINATION

A THESIS SUMITTED FOR THE DEGREE OF ENGINEERING DOCTORATE

BY

THOMAS HENRY BURT

DEPARTMENT OF BIOCHEMICAL ENGINEERING
UNIVERSITY COLLEGE LONDON

SEPTEMBER 2006

ProQuest LLC
789 East Eisenhower Parkway
P.O. Box 1346
Ann Arbor, MI 48106-1346

TABLE OF CONTENTS

LIST OF FIGURES

LIST OF TABLES

LIST OF FIGURES (APPENDIX)

ACKNOWLEDGMENTS

This degree has represented the single hardest challenge in my life so far. Its completion is greatly down to the support and encouragement of many people whose help I would like to acknowledge.

Firstly, I would like to thank Claire, without whom I certainly would never have finished this project. Your help and support, not to mention the example you set when completing your own PhD, was inspirational. You are such an example to me and I just hope you realise how incredible you are. I promise never to forget the patience and kindness you showed to me through many tough years. **Thank you**.

I would also like to thank my family and friends who showed me so much kindness and put up with my 'Pretty horrible Disposition'. Mum & John, the support you gave me was well beyond any son's expectations and I apologise for the sleepless nights I may have caused you. To my brothers, James and Joseph, thank you for your help and empathy. You both are such remarkable people that my efforts were merely inspired by your own impressive achievements. To Dad & Laura, thank you for your helpful words of advice and encouragement. I would also like to thank my friends for putting up with me and keeping me sane through this time.

To Prof. Titchener-Hooker many thanks for the patience you showed in reading my work and the helpful, insightful corrections you suggested.

Crucially, I must acknowledge the generous help given to me by the staff at GSK, Beckenham. Their prudent advice and guidance was continually helpful and I was inspired to progress with the project by the passion they showed for their work. Specifically, I would like to thank Cora Henwood and Ronan O'Kennedy. There were times when nothing made sense and somehow you could always help. **Thank you**.

ABSTRACT

A thesis is presented which outlines investigations conducted to determine issues which may be faced should attempts be made to produce large plasmids (>3-10kb) for use in areas such as DNA vaccination and gene therapy.

Initial studies attempted to manufacture a series of large Bacterial Artificial Chromosomes (116kb – 242kb) and centered on the fermentation and downstream purification steps required to produce the plasmid material. It was determined that these constructs were not suitable models due to the low yields at which they were propagated. Additionally, many of the analytical protocols employed were found to be inadequate for monitoring the concentration and form of large plasmids.

In response to these issues large plasmids were constructed by the insertion of large fragments of *S.cerevisiae* DNA in to the relaxed, high-copy number vector; pGEM11. Plasmids ranging from 3kb to 50kb were created and used to probe the upstream and downstream steps of a plasmid production process. Efforts were also made to develop more suitable analytical methods.

The production of these plasmids was studied during pilot-scale fermentations at 37°C where it was discovered that the plasmids demonstrated a poor stability profile. In an attempt to improve plasmid stability, reduced temperature (25°C) fermentations were conducted which increased the stability and yields obtained from fermentations of these constructs.

Cell paste from the fermentations was subject to a purification process involving alkaline lysis and ultrafiltration steps. Described are balances of plasmid DNA, genomic DNA, RNA and contaminating protein. The topology changes displayed by the plasmids are also described. Finally, studies are outlined describing the binding behaviour of the large plasmids to chromatographic resins used for plasmid purification.

1 LITERATURE REVIEW

1.1 Chapter Aims

The aims of this section are as follows

1. Provide a brief summary to the field of gene therapy and the progression of the technology to date together with postulating about future developments in the field.
2. Describe some of the disease targets against which gene therapy treatments are being tested and the methods and means by which the treatments are delivered.
3. Describe the use of gene therapy in the field of vaccination and advantages offered by this mechanism of immunisation.
4. Outline the properties of plasmid DNA and briefly discuss the current processes used for its manufacture.
5. Highlight the importance of being able to reliably manufacture large plasmid DNA molecules.

1.2 Gene Therapy

Gene therapy is defined as the 'use of nucleic acid transfer, either RNA or DNA, to treat or prevent a disease'(Mountain, 2000). Generally, the nucleic acid is dsDNA encoding a therapeutic, destructive or marker protein but the above definition encompasses antisense therapy which uses ssDNA and RNA to prevent expression of a specific gene, by blocking mRNA expression or promoter activation. Gene therapy is regarded as potentially the fourth revolution in medicine, (the others being sanitation, antiseptics, antibiotics/vaccines) as it seeks to eliminate the cause of disease rather than just treat the symptoms.

The first gene therapy trial was initiated in 1990, on two girls with Severe Combined Immunodeficiency Disorder (SCID) resulting from the absence of the enzyme adenosine deaminase (ADA). In the protocol, T-lymphocytes were removed from each

patient and cDNA coding for the ADA gene introduced. After culturing, each patient received transfusions of their own genetically modified lymphocytes regularly for two years. Four years from the start, integrated vector and ADA expression (25% of normal levels) was still detectable in the girls' T-cells. SCID symptoms were alleviated. (Anderson, 1998; Crystal, 1995; Davis, 2002)

However, the initial excitement this technology generated was ill-founded as there are still only a handful of cases where gene therapy has proven efficacious. Even the trial described above was by no means conclusive, as it is uncertain whether the therapeutic advantage was provided by the replacement therapy, or the direct infusions of ADA the patients received. Reasons for this failure mainly lie with the fact that because gene therapy is so new and the number of diseases that could be treated by this broad-platform technology so diverse, a huge number of different strategies have been researched. Consequently, the past decade has been dedicated to developing the technology without any product successes. The most important development required for gene therapy is a clear demonstration of efficacy in clinical trials, which will lead to restoration of public and investor confidence. This development hopefully will be complemented by the completion of the Human Genome Project and the revolution in the field of genomics. It is becoming much more apparent that many diseases have a genetic component. Currently, pharmaceutical researchers have about 500 targets (genes) for intervention (Anderson, 1984; Edelstein *et al.*, 2004; Mhashilkar *et al.*, 2001). It is expected when mapping is completed this figure will be about 10,000, leaving a great scope for gene-based intervention.

Presently, fifteen years after the initial attempts, the first gene-therapy treatments are expected to gain market approval this year, and the predicted market for these kinds of product by 2010, exceeds $45billion (£27billion). However, with recent disappointments surrounding the safety of gene therapy (Fox, 1999) and the excitement generated by RNAi approaches, the acceptance of 'traditional' gene therapy remains as unsure as ever.

1.3 The Potential of Gene Therapy

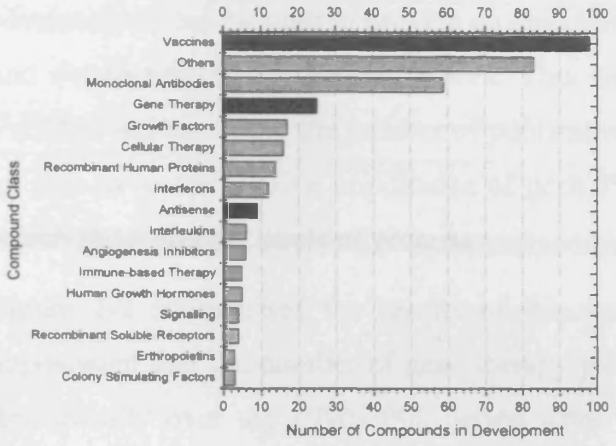

Figure 1-1 Figure displaying the number of biotech derived therapeutics currently in development. Highlighted in dark grey are classes for which plasmid DNA could be employed.

The figure above displays that at present gene/ antisense treatments only represent a small proportion of biotech-derived medicines in development. This is because the majority of drugs in development are still 1st generation biotech medicines, being recombinant human proteins and vaccines. Also, arriving after twenty years of development, are monoclonal antibodies. As with gene therapy, the therapeutic promise of monoclonal antibodies was hyped when first discovered in 1975. It has taken twenty years of development to overcome the problem of immune rejection but now the figures prove the technology is viable.

That there are gene therapy products in clinical trials is still an achievement after only fifteen-years. It is envisioned that the proportion will continue to increase as this technology supersedes and makes redundant existing treatments. For example, gene therapy could potentially replace many of the 1st generation of biotech compounds. Already this is being witnessed with gene therapy products in development for Heamophilia A, B and anaemia to replace the conventional recombinant protein treatments. As Professor W. French Anderson, director of the Gene Therapy Laboratories at the University of Southern California School of Medicine, and leader of the first gene therapy trial says "Thirty years from now, essentially every disease will have a gene-based therapy as a treatment option" (Anderson, 1984; Anderson, 1998).

1.3.1 Publication Analysis

Metaanalysis can be used to provide an objective opinion about the relative importance and development of a particular area. This can be achieved by searching terms in PubMed and recording the number of publications. This was performed to try and give an idea as to the relative importance of gene therapy compared to other technologies which show similar levels of promise.

Figure 1-2 summarises the results of this analysis. From Figure 1-2A, it can be appreciated that the number of gene therapy publications published per year increased dramatically over the 1990-2000 period when a high-level of spending, both public and private, was dedicated to the area. However, in 2000, the yearly increase of publications came to a halt and last year (2005) fewer publications were returned than the previous year. The reason for the slow-down is thought to be due to the death of a teenager which was directly attributed to a gene therapy protocol he was involved in (Fox, 1999).

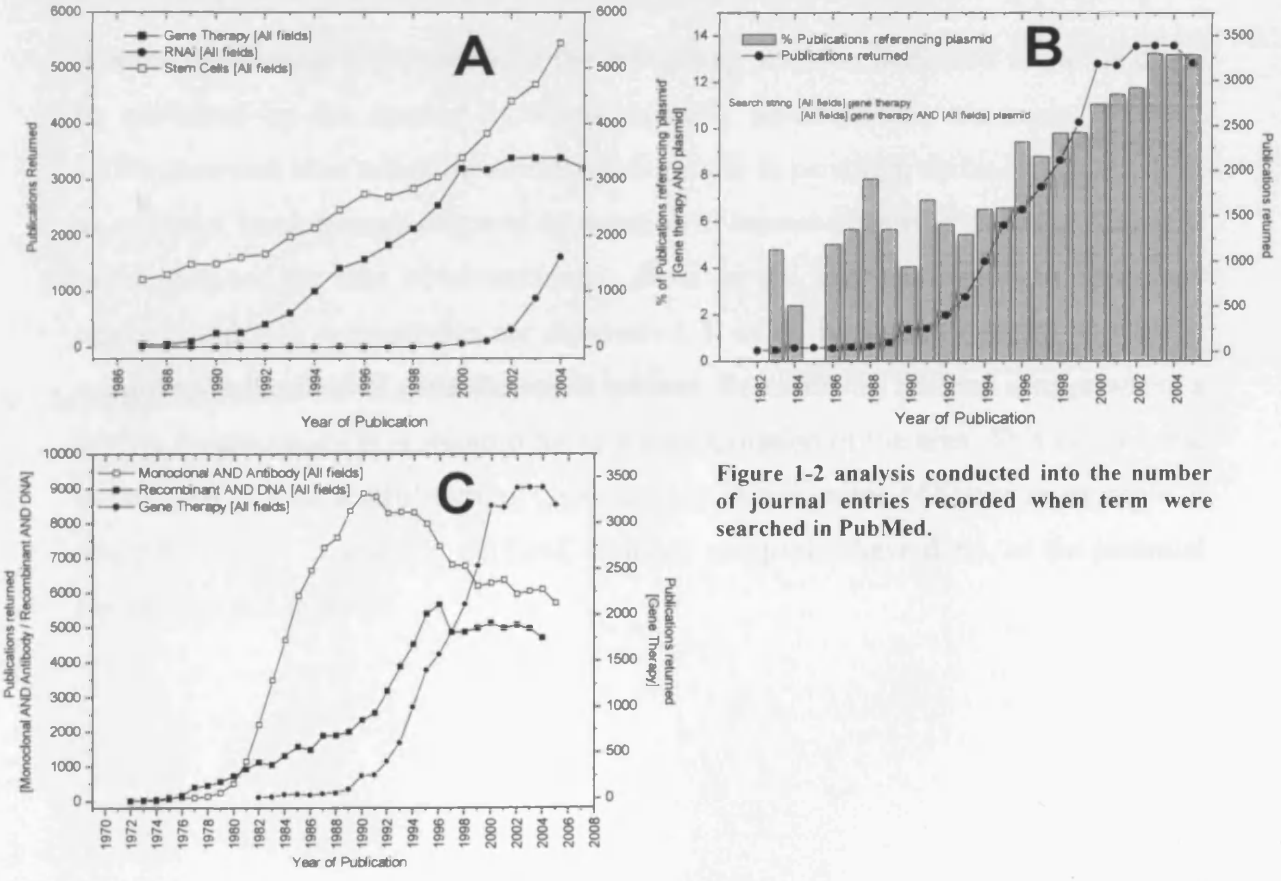

Figure 1-2 analysis conducted into the number of journal entries recorded when term were searched in PubMed.

As a result of the negative publicity generated by this event a number of gene therapy trials were halted. The research dollars went elsewhere and to an extent could explain the rapid increase in publications witnessed in the fields of stem cell therapy and RNAi. Where does this leave the field of gene therapy? On the face of it the numbers appear bleak but a similar situation has been seen previously with the more advanced fields of monoclonal antibodies and recombinant DNA technology.

Looking at Figure 1-2C demonstrates how both these fields displayed an exponential increase in publications followed by a subsequent decline. The comparision of the field of monoclonal antibodies to gene therapy is particularly apt. Monoclonal antibodies were hyped as the 'magic bullets' soon after their discovery, but the hype was unfounded as the delivery of commercial products was hampered for many years by problems of immune rejection. Figure C shows how the rise in publications reached a peak in 1990 from when on the number decreased year-on-year. It is important to remember that the first monoclonal antibody therapeutic (*Rituxan*®) did not receive approval until 1997. Therefore, if parallels are to be drawn to gene therapy, the decline in publications should not be seen as a wholly negative indication.

A more appropriate explanation for the decreasing attention dedicated to the field can be explained by the manner in which scientific advancements are made. (Popper, 1975) describes how scientific advancements occur in paradigm shifts, which manifest as an initial breakthrough followed by a period of intense activity. Following the initial rapid progress the rate of advancement slows as the initial impetus dissipates and newer competing technologies are discovered. It could be argued that this is what is occurring in the field of gene therapy at present. Research has reached a stage where a further breakthrough is required prior to a reinvigoration of the area. This could come in the form of a successful form of gene delivery. Again, using MAbs as an example, it could be foolish to abandon the field, as many companies have done, as the potential for success still remains.

1.3.2 Potential Targets for Gene Therapy

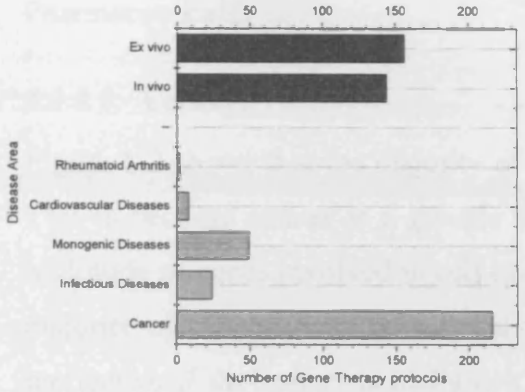

Figure 1-3 Number of genetherapy protocols by therapeutic application. From the grah the roughly equal number of *ex vivo* to *in vivo* procedures can be seen

Approximately 300 clinical protocols involving gene transfer have been conducted, involving some 3500 patients (Edelstein *et al.*, 2004). The majority have been small Phase I/ II trials mainly to assess safety before efficacy trials. Media speculation on these trials has been harsh, criticizing gene therapy for not living up to the hype the press created. It soon became apparent that gene therapies are technically more demanding than previously thought. However, progress has been made and shown below are some of the trials which have entered phase II and III trials.

Table 1-1 Table describing current gene therapy compounds in late-stage development

Name	Disease	Vector	Gene	Strategy	Company	Phase
Leuvectin	Prostate cancer/ renal cell carcinoma	Cationic lipid Tumour cells *in vivo*	*IL-2*	Immunogenicity Enhancement	Vical	II
E1A lipid complex	Breast/ head/ neck/ ovarian cancers	Cationic lipid Tumour cells *in vivo*	*AdE1A*	Apotosis induction	Targeted Genetics	II
ING N201	Head and neck cancer	Adenovirus Tumour cells *in vivo*	*P53*	Apoptosis induction	Introgen Therap.	III
ONYX-015	P53 deficient cancers	Adenovirus Tumour cells *in vivo*	*Ad death genes*	Killing by lytic virus	Onyx Pharm..	II
N/A	Ovarian cancer	Retrovirus. Fibroblasts *ex vivo*	*IL-12*	Immunogenicity enhancement	National Cancer Ins.	III
BioByPass	Limb ischaemia/ cardiac artery disease.	Naked DNA Muscle cells *in vivo*	*VEGF*	Angiogenesis stimulation	GenVec/ Valentis	II
AAV CFTR	Cystic fibrosis	AAV Airway cells *in vivo*	*CFTR*	Provision of functional protein	Targetted Genetics	II
TCR	HIV	Retrovirus T-cells *ex vivo*	*TCR*	Retargeting killer T-cells	N/a	II

At present only one gene therapy is licensed which is Vitravene®, an antisense treatment for cytomegalovirus retinitis in AIDS patients, produced by Isis Pharmaceuticals.

1.3.2.1 Cancer

Figure 1-3 shows that the majority of gene therapy trials are for treatment of cancers. This is because cancer is a genetic disease, caused by mutations in any one of the multitude of genes involved in cell cycle regulation. Main treatments at present for the majority of cancers involve surgical removal of the primary tumour, which is often ineffective if the cancer is malignant. Radio and chemotherapy do show success but which exhibit appalling side effects, meaning treatment is essentially a race to kill the tumour before the treatment kills the patient.

Gene therapy offers a rational treatment that could complement existing methods and make treatable presently untreatable cancers. New approaches are desperately needed. The five-year survival rates of patients diagnosed with any one of a number of different cancers remain static. Existing gene therapy strategies include:-

(i) Gene Directed Enzyme Prodrug Therapy (GDEPT).

(ii) Immunogenicity enhancement e.g. by vaccination.

(iii) Oncolytic viral therapy.

(iv) Transfer of therapeutic genes-tumour suppressor/ apoptosis inducing.

(v) Antisense e.g ISIS 2503/ 3521/ 5132.

1.3.2.2 HIV/ AIDS and related conditions

Referring to (Figure 1-3) it can be seen that there are approximately 25 gene therapy protocols being developed for infectious diseases, of which the vast majority are targeting HIV. Development has been spurred in this area because of the lack of effective antivirals, the main one being AZT, but resistance to present drugs is spreading. Antisense prevails for HIV treatment aimed at blocking the expression of several key genes namely *gag*, *pol* and *env*.

1.3.2.3 Blood, Cardiovascular and Heart disorders

Figure 1-3 also highlights the importance this technology has in the development of treatments for blood, heart and cardiovascular disorders. Gene therapy treatments for Haemophilia A and B are in phase I trials. Within the past year, clinical benefit has been demonstrated by the administration of naked DNA encoding the angiogenic protein VEGF. Injections into the skeletal muscles of patients with critical limb ischaemia, resulting from inadequate blood supply has resulted in dramatic long-term benefit in a large proportion of patients. The treatment is now completing phase II trials and is showing success in the alleviation of coronary artery blockage, a major symptom of heart disease. In addition to HIV, cancer and cardiovascular disorders infectious diseases, skin disorders and transplant rejection are also being targetted.

1.3.2.4 Monogenic Disorders

Perhaps one of the most media attentive areas has been the potential of gene therapy to alleviate genetic disorders that afflict people from birth and at present are incurable. Appendix 1 details two treatments, which are in clinical trials for the treatment of cystic fibrosis, using gene replacement to provide patients with the transmembrane regulator they lack. It is expected that this area will be one of intense research, because of the lack of cures or effective treatments Table 1-2 shows a selection of monogenic disorders which could benefit. As the technology is developed, it may be possible to treat more complex genetic disorders.

Table 1-2 Table listing a number of monogenic disorders which may benefit from gene therapy

Gene Product	Disease	Frequency	Current Therapy	Prognosis
Adenosine deaminase	SCID Loss of T and B cells	1:1,000,000	Bone marrow transplant	Without therapy fatal by 2yrs. With therapy limited improvement
LDL receptor	Familial hypercholesterolemia Elevated cholesterol leading to heart disease	1:500	Diet, drugs, Liver transplant	Some improvement
Glucocerebrosidase	Gaucher disease Accumulation of glucocerebroside causing liver, spleen, bone damage	1:2,500	Removal of spleen, antibiotics,bone marrow transplant	Some improvement
Blood clotting factor VIII	Haemophilia A Defective blood clotting, chronic internal bleeding	1:10,000 (males)	Transfusions of recombinant factor VIII	Extended life expectancy requiring continual treatment
Phenylalanine hydroxylase	Phenylketonuria Can cause retardation	1:10,000	Control of dietary phenylalanine	Good if treatment started early

α_1-Antitrypsin	Emphysema Damage to lungs Cirrhosis of liver	1:3,500	Replacement therapy. Reduce environmental risks	Progression is slowed but not stopped.
Cystic fibrosis transmembrane regulator	Cystic fibrosis Blocked airways Intestinal blockage Damaged pancreas	1:2,500 (Caucasians)	Antibiotics, physical clearing of lungs, diet control	Fatal by late twenties
Orthinine trans-carbamylase		1:40,000	Restricted protein diet, Drugs, liver transplant	Symptoms diminished
Dystrophin	Duchenne muscular dystrophy Progressive muscular wasting	1:7,500 (males)	Only supportive treatments:-wheelchair, breathing aids	Fatal by early twenties
β-Globin	Sickle-cell anemia Damage to spleen, heart, kidneys, liver and brain	1:500	Blood transfusions, drugs, analgesics, bone marrow	Symptoms diminished but treatments suboptimal

1.4 Vaccines

1.4.1 Traditional Vaccination

Vaccination protects a recipient from pathogenic agents by establishing an immunological resistance to infection. Present day vaccines consist of either inactivated, attenuated or components of the infectious agent. Notwithstanding the considerable success vaccines have had in combating diseases such as poliomyelitis, smallpox and diptheria etc, there are a number of limitations to the current mode of vaccination

(i) Not all infectious agents can be cultured meaning no vaccines have been developed for many diseases.

(ii) Production of human/ animal vaccines by animal cell culture is expensive but often necessary to produce correct form of vaccine.

(iii) Batches of vaccine may not be killed/ attenuated (or may revert) sufficiently leading to the recipient contracting the disease, they pose severe safety problems

(iv) Extensive safety precautions are necessary to protect production personnel.

(v) Not all diseases (e.g AIDS, malaria and tuberculosis) are preventable through the use of present day vaccines

(vi) Most current vaccines have a shelf-life and require refrigeration which limits their usage in third world countries.

1.4.2 Novel Vaccine classes

The advent of recombinant DNA technology has provided a means of creating new generations of vaccines that overcome the above drawbacks:-

1.4.2.1 Recombinant viruses

(i) Removal of virulence genes enables the pathogen to be used as a live vaccine as it is impossible for a whole gene to be reacquired spontaneously.

(ii) Live non-pathogenic virus (e.g vaccinia virus) could have antigenic genes inserted into its genome. Vaccinia virus is harmless and inserted antigen gene would be expressed using viral machinery in the cytoplasm.

(iii) Virus like particles.

1.4.2.2 Subunit vaccines

Genes for immunologically active proteins of a dangerous pathogen are cloned into a host such as E.coli. These subunit vaccines can be produced safely, purified and administered. It is a safe option and allows vaccines to be made against pathogens, which cannot be maintained in culture. Although the preparation is ensured to be safe and defined, isolated, subunit proteins may not have the same conformation and thus not the same antigenicity. Also, the host used to make the subunit may not correctly post-translationally modify and glycosylate.

1.4.2.3 Passive Immunisation

Using monoclonal antibody technology it is possible to create a specific, murine mAbs against a pathogen. Using humanization the monoclonal antibody can be administered to patients, providing them with antibodies to a pathogen they have yet to encounter, therefore immunising them.

1.4.2.4 Anti-idiotypic Antibodies

Antibodies raised against the variable domains of antibodies generated against an original antigen can be used to mimic the original antigen and can be used as a 'surrogate antigen' to generate an immune response targeting the original antigen.

1.4.2.5 Peptide Vaccines

These new classes of vaccines do have benefits over traditional vaccines, but are still not ideal. Recombinant vaccines are expensive to develop and produce, are unstable and can only be produced for pathogens able to be cultured. Subunit, passive and idiotypic vaccines suffer the same problems of instability and do not elicit as strong an immune response or memory as traditional vaccines. Fortunatelty there are another class of vaccines on the horizon which show considerable promise; DNA vaccines.

1.4.3 DNA Vaccines

DNA vaccines represent an exiting area of gene therapy. They employ plasmid DNA, encoding proteins of pathogens or tumours, directly transfected in to animals to elicit an immune response. They consist of a bacterial plasmid with a strong, viral promoter (CMV/ SV40), the gene of interest and a polyadenylation/ transcription termination sequence. They must have a bacterial origin of replication (ori) but a eukaryotic ori is omitted so the plasmid does not persist in the vaccinee's cells. They are delivered to cells, usually muscle cells, by microinjection or using compressed gas to fire DNA coated gold particles.

1.4.4 Advantages of DNA vaccines

(i) One major reason that DNA vaccines are considered so important is the way by which they are able to stimulate the immune system. The immune system is composed of two arms. The humoral arm consists of B-lymphocytes, which detect antigens on the surface of pathogens and produce antibodies, molecules that bind the antigen and alert other immune cells to destroy the pathogen. The cellular arm is carried out primarily by cytotoxic T-lymphocytes (CTL). These cells have the ability to detect antigens expressed on the surface of cells infected by a pathogen and destroy any infected cells. Once an antigen has been encountered by the immune system, some B-lymphocytes differentiate into 'memory' cells, which rapidly divide if the antigen is detected again, making the second response quicker and more effective.

Vaccination is far more efficient if both arms of the immune system are alerted. For this to occur the proteins of the pathogen must be expressed in the cells of the patient. When this occurs these foreign proteins are then automatically presented on the surface

of the cells where they are recognized by CTL, initiating the cellular arm and the humoral arm of the immune system. Heat killed, subunit, idiotypic, peptide and passive vaccines cannot induce cellular arm and are thus less effective vaccines. Attenuated and recombinant vaccines are able to but they have other disadvantages.

(ii) A second major advantage is the simplicity of this form of vaccination. The only steps required are construction of the plasmid and its purification. There are more issues involved in the scale-up and manufacture of these pharmaceuticals but less so than involved with subunit vaccines. Development of subunit vaccines requires the plasmid to be constructed, expression must be assured to be correct and at high-titres in a suitable host (usually animal cell culture, which is expensive) followed by purification through a multitude of different steps. With DNA vaccines, the antigen is expressed in vivo guaranteeing correct processing for viral proteins and more often than not for bacterial and parasitic antigens. This helps generate antibodies of optimal specificity.

(iii) Traditional vaccines (excluding attenuated types) only stimulate the humoral response, producing antibodies that bind proteins on the surface of the pathogen. To escape antibody detection, pathogens (especially viruses) mutate their surface proteins often to escape recognition. Functional proteins that require a specific sequence function are conserved and protected from attack by these surface proteins (Rossman's Canyon hypothesis). DNA vaccines can be produced encoding these conserved proteins so when they are exposed to function the immune system can rapidly respond.

(iv) Certain motifs of bacterial DNA, notably Cytidine-Phosphate-Guanosine (CpG) are known to be immunostimulatory. Studies have revealed these motifs, (present twenty times more commonly in bacterial DNA than eukaryotic DNA) activate T-helper-1 and T-helper-2 cells (Th1/ Th2). These cells produce cytokines such as γ-interferon and interleukin 4,5,12 and 13. Such T-cell and cytokine activation appears to augment antibody and CTL responses to the antigen encoded by the plasmid. Essentially, the construct has in-built adjuvants.

(v) Pre-clinical efficacy/ immune response has been clearly demonstrated for a wide range of disease models, including viral, bacterial, parasitic diseases together

with allergies and tumours. Table 1-3gives examples of disease models against which DNA vaccination has shown positive responses.

(vi) Many DNA vaccines protocols followed thus far have demonstrated positive, long-lasting responses from even small doses. Figure 1-4 demonstrates the survival of mice immunized with 200μg of plasmid DNA encoding NP from influenza against

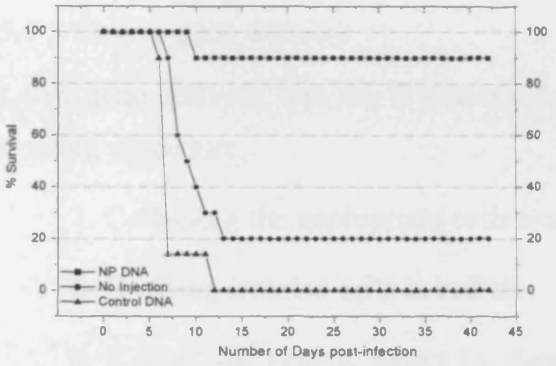

Figure 1-4 Demonstrates the survival of mice immunized with 200μg of plasmid DNA encoding NP from influenza against control DNA (plasmid without the coding region) or not injected. Groups of 10 mice were injected three times at three-week intervals and then challenged intranasally with LD_{90} of influenza A/HK/68 (H3N2) three weeks after the third injection.

control DNA (plasmid without the coding region) or not injected. Groups of 10 mice were injected three times at three week intervals and then challenged intranasally with LD_{90} of influenza A/HK/68 (H3N2) three weeks after the third injection.

Table 1-3 Table detailing the disease models against which DNA vaccination has proved effective

Disorder	Vaccine Type
Viral	Influenza Nucleoprotein / Haemagglutinin, HIV envelope protein / Bovine herpes virus glycoprotein / Rabies virus glycoprotein / Hep B surface antigen / HSV glycoproteins B and D / Papillomavirus L1 / Hep C virus nucleocapsid / Hep B core protein / HIV gp120 and gp160 /HIV Nef protein
Bacterial	*B.thuringensis* delta-toxin / *Mycobacterium tuberculosis* antigen 85 and hsp65 / *Mycobacterium pulmonis* / Tetanus toxin C / *Salmonella* OmpC protein,
Parasitic	*Schistosoma japonicum / Leishmania major / Plasmodium yoelli / Plasmodium falciparum*
Tumour	Human carcinoembryonic antigen / Polymorphic epithelial mucin (MUC-1) Idiotypic antibody of a B-cell lymphoma / Human IgV region / MHC class 1 molecules

(vii) DNA vaccines could facilitate the combination of diverse immunogens into a single preparation to facilitate the immunisation of several disorders. Indeed for viruses that undergo antigenic variation, such as HIV and influenza it may be necessary to include DNA constructs encoding surface proteins from several distinct stains to provide protection against strains which may be circulating.

1.5 Gene Delivery

At the heart of any gene therapy procedure is the delivery of a corrective gene, together with the appropriate regulatory machinery into the cells of the designated tissue and the subsequent expression of the gene. Two methods have been developed to that end

1.5.1 *Ex vivo* gene delivery

Ex vivo gene delivery was the first method to be developed and usually involves the following procedure;

1. Collecting the appropriate cells from affected individual.
2. Growing isolated cells in culture.
3. Correct the genetic defect by transferring appropriate gene into the isolated cells.
4. Select and culture the corrected cells.
5. Either infuse or transplant the corrected cell back into the patient.

The advantages of this technique are that it uses the patient's own cells, ensuring no adverse immunological response occurs after infusion of the corrected cells. Additionally, this technique of gene delivery has a high transfer efficiency ensuring multiple copies of the corrective genes are delivered to the cells. Furthermore, only transfected cells are selected for and delivered back to the patient. These transfected cells tend to have numerous copies of the gene stably inserted into the genome of the cell, meaning the construct persists in the cells for reasonably long periods of time (~18 months). However, it is by no means a cure as ultimately the expression of the gene is transient and the procedure will need to be repeated.

Unfortunately, this technique is only applicable to a small number of cell types; endothelial, haematopoeitic and skin. A preferred method of *ex vivo* delivery would use totipotent stem cells. These cells have the ability to develop into any differentiated tissue once exposed to the correct growth factors. Unfortunately, at present it is very hard to isolate stem cells from a patient, being present in only very small numbers in bone marrow, blood and adipose tissue and the ethical debate surrounding the use of

embryonic stem cells, remains sadly unresolved. Furthermore, this method is very time consuming taking months to generate sufficient number of cells, and highly labour intensive.

1.5.2 *In vivo* gene delivery

In vivo gene transfer would be the preferred technique of introducing a corrective gene into the required cells, once the many technical hurdles have been overcome. It requires the direct introduction of the gene construct in to the patient. This form of delivery would mean gene therapy would become as simple as administering a traditional pharmaceutical, thus allowing the huge number of people in need of some possible form of gene therapy to benefit.

If gene therapy is to become a viable treatment option able to compete with traditional, small-molecule pharmaceuticals, *in vivo* transfer is the only way it will succeed. There simply are not the medical or economic resources to treat the huge number of people who could benefit from gene therapy by the *ex vivo* transfer procedure. Unfortunately, the hurdles in terms of producing a suitable *in vivo* vector, which can be targetted to the correct cells, enter those cells in sufficient numbers and in many cases stably integrate in to the host chromosome and be expressed for long periods of time, are huge. At present *in vivo* methods produce low transfection efficiency and non-stable integration. In many cases, namely tumour therapy and vaccination, transient expression is favourable but high rates of targetted transfer are still required.

1.6 Gene Therapy Vectors

In order to deliver the corrective gene to the correct cells and to ensure its expression, the gene is inserted in to a vector. An ideal vector should be efficient in delivering the gene, target the correct cells, protect the gene from degradation, allow for control of expression aswell as being non-toxic or immunogenic. There exist two broad categories of vector; viral and non-viral vectors.

1.6.1 Viral Vectors

Viruses have evolved specifically for hijacking cellular machinery of the cell to express the nucleic acid it carries. Consequently, they became an obvious choice as a

vector, by removing the virulence/replication genes and replacing them with the gene for transfer. The most commonly used viral vectors are; Adenovirus, Retrovirus and Adeno-assocoiated virus. Viral vectors have a high transfection efficiency, meaning the majority of viral particles deliver the gene into the cells. Because of the nature of viruses, these vectors can be targetted very specifically to certain cells. Additionally, some virus are lysogenic meaning they insert into the genome of the cell allowing prolonged expression of the construct. Transient expression is also possible with other viral species.

Disadvantages with the viral method centre around the highly immunogenic nature of the viral particle. Continual administration of the viral vector leads to a strengthening immune response by the patient, meaning greater and greater doses need to be given, which in one case has proved fatal. Because the virus exists as a self-assembling, precise, geometric particle the cavity where the genetic material is encased, limits the size of the insert allowed to usually less than 8kb. A further drawback, which applies not just to the viral delivery method, but any method which leads to integration of the construct into the host genome, is the possible deactivation of important genes, namely those which control cell proliferation. The chances of insertional deactivation are slight, due to the small amount of coding DNA within the genome and are considered to be a necessary evil. However, one trial in France has already had to be ceased since the patient contracted leukemia, due to the insertion of a lysogenic virus.

Other problems encountered include the potential risk of recombination between vector and viral DNA resulting in the generation of wild-type, infectious particles. This vector class also have to be produced by contained, animal cell culture leading to high cost of manufacture.

Retroviral vectors (MMLV/ HIV):- the advantage of this vector class are their ability to efficiently and stably integrate nucleic acids into the host chromosome. The integrated DNA is expressed throughout the life of the cell and passed on to daughter cells. Retroviral vectors require mitosis for integration so subsequently can only be used to infect rapidly dividing cells.

Adenoviral vectors are used due to their ability to carry large inserts ~10kb. They are also able to infect non-dividing cells. Their chromosome remains episomal, leading to

transient expression, useful in tumour therapy. However, this vector class is highly immunogenic and was the one used in the trial which resulted in the death of one volunteer.

Adeno-associated vectors have recently been used as vectors. They are a small, ssDNA virus carrying an insert of ~5kb. It is their absence of pathogenicity which makes this vector class so attractive. They also have the ability to integrate into a specific site on chromosome 19. Injection of this virus into brain and muscle tissue has produced stable and long-term expression.

1.6.2 Non-viral vectors

Increasingly, the emphasis for gene delivery method is shifting from viral to non-viral means. In non-viral delivery, genes are carried on plasmids, produced most commonly in *E.coli*. The advantages of using non-viral delivery systems are that it eliminates the concerns relating to the transfer of unwanted viral sequences, together with reduced immunogenicity. The reduced immunogenicity allows greater potential for serial *in vivo* administrations than viral vectors (Davis, 2002).

Additionally, this method allows for larger expression cassettes to be used. At present trials have used constructs of less than 10kb, but this is expected to increase. Larger constructs allow for multiple expression cassettes, meaning several corrective genes can be expressed together or the inclusion of cell signaling molecules, cytokines allowing greater control over cellular processes. Thus, treatment of multigene and metabolic disorders becomes a possibility. There is even talk about the possible transfer of artificial chromosomes.

The main disadvantages of this method are the relatively low levels of delivery. It is estimated that for every 1000 plasmid molecules only one reaches the cell and is expressed. Another drawback is the very transient nature of expression demonstrated by these vectors. Although generally regarded as being safer than the viral alternative, there still remain some safety concerns with this delivery method. DNA itself is immunogenic (specifically unmethylated CpG sequences) this can be advantageous if the purpose of transfer is for vaccination. However, a severe immune response could possibly cause patients to develop systemic autoimmune disease, triggered by activation of auto-reactive B-cells.

1.6.3 Naked DNA

Administration of naked DNA gives a surprising level of gene transfer following local injection into skin/muscle. Reports have described transgene expression lasting several months for intramuscular injection, but only a few days for intradermal. The mechanism of DNA uptake into muscle/skin cells is unclear, but the fact that this delivery method does lead to the priming of both the humoral and cellular arms of the immune system has led to enormous interest in this method for DNA vaccination. Success has been demonstrated by this method for stimulating immune responses against the protein product of a gene from *Plasmodium falciparum* (the malaria parasite). The other important application is the injection of naked DNA encoding VEGF into the muscles of patients with critical limb ischaemia, now in Phase II trials.

The advantage of this method is that naked DNA can be manufactured and administered simply. However, gene delivery efficiency is still poor, very brief expression is seen and the method is only an option for a few tissues as targeting is not an option. As detailed earlier naked DNA is a powerful adjuvant, an advantage when used to administer a one-off vaccine but becoming a serious problem if the therapy requires multiple injections as it could lead to the development of autoimmune diseases.

1.6.4 Needle-free injection

Two 'biolistic' devices have been developed as an alternative to the injection of naked DNA. The 'gene gun' uses high-pressure helium to deliver DNA coated gold particles directly into the cytoplasm of cells, and can be used for both *in vivo* and *ex vivo* transfer procedures. The 'Intraject' device uses liquid under high pressure to force the DNA into interstitial spaces. Both methods report higher immune responses than naked DNA injection, but again suffer from the same drawbacks, namely that they can only be applied to a few tissue types (Yoshida *et al.*, 2000; Zagon *et al.*, 2005)

1.6.5 Condensed DNA particles

This method uses cationic polymers to condense DNA by electrostatic interaction into small particles. The hope is to protect the DNA from degradation and enhance its uptake by endocytosis. The most important polymers continue to be polylysine and

polyethyleneimine (PEI). There are a number of examples, which suggest that these formulations give reasonably efficient transfection *ex vivo* but very few reports to suggest any improvement over naked DNA transfer for *in vivo* protocols. Indeed, the polymers seem to cause aggregation of the particles in physiological conditions, resulting in entities too large to effectively penetrate tissue. The main advantage of this approach are that it offers a way of improving specificity by the attachment of ligands or antibody to the condensing polymer.

1.6.6 Cationic Lipids

Cationic lipids bind DNA tightly by electrostatic interaction. Like cationic polymers, lipids offer some protection to the DNA aswell as neutralizing the anionic charge of the DNA so condensing its structure. Cationic lipid-DNA complexes have been extensively tested for delivery of the cystic fibrosis transmembrane receptor gene. Unfortunately, the level and duration of expression was too low for clinical benefit. As with cationic polymers the main drawbacks with this method are the low transfection efficiency, poor targeting and formulation instability. Two therapeutic strategies involving cationic lipids for the treatment of cancer have reached Phase II trials. However, the investigation of the efficacy of cationic lipids has led to the development of cationic liposomes, which are the most widely used non-viral vector.

1.7 Plasmid DNA Properties

The plasmid DNA used in non-viral gene delivery applications is required to possess certain qualities in terms of size, gene sequences and conformation. Plasmids, the workhorse of the biotechnology revolution, are naturally occurring entities of bacterial origin. These DNA units are found as extra chromosomal DNA within bacterial species such as *E.coli* (Caldwell, 1997; Felgner, 1997; Middaugh *et al.*, 1997). Plasmids are usually isolated as covalently closed circular DNA in a negative supercoiled form (i.e. the DNA is interwound, containing fewer helical turns, compared to relaxed forms, resulting in torsional tension in the plasmid loop). The conformation of the plasmid is important and for gene delivery purposes it is preferable to keep the plasmid DNA in its native conformation of negative super coiled (SC) conformation. This conformation is known to produce the highest transfection

efficiency as it dissociates from and complexes with the greatest ease aiding uptake of the DNA to the cell nucleus (Adami *et al.*, 1998; Even-Chen and Barenholz, 1999). Conversion of the SC DNA to a circular conformation has only a minor effect but conversion to a linear state reduces the efficiency of gene expression by 90% (Adami *et al.*, 1998). The natural sequence of these plasmids does not however contain all the genes required for effective gene delivery and further manipulation is required to produce a sequence suitable for effective gene delivery.

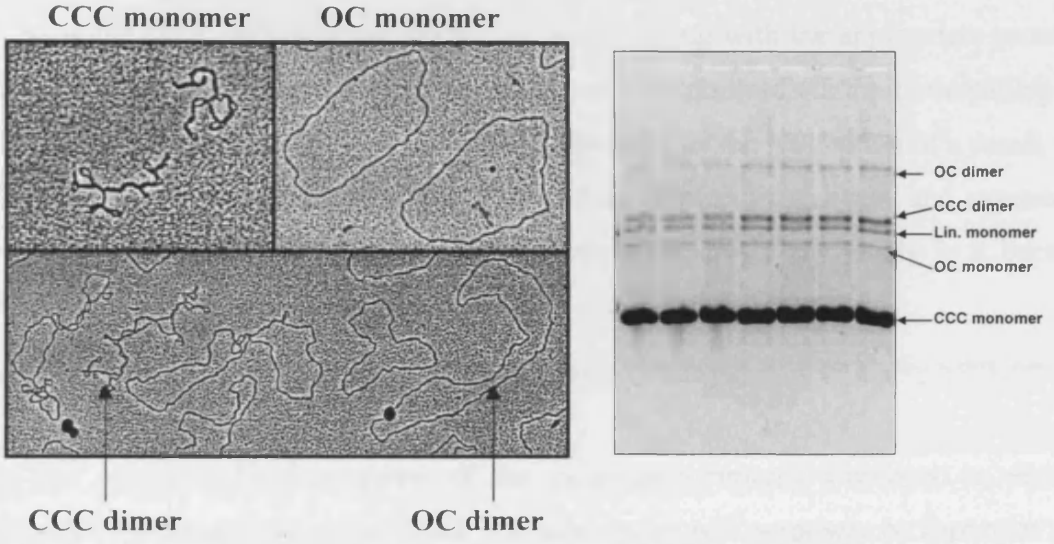

Figure 1-5 Electronmicrograph displying the different forms that plasmid DNA molecules can exist and how they are represented by electrophoresis

There is a limit to the size of the construct that can be packaged into the delivery system and easily inserted into the target cells. DNA macromolecules are relatively large, for example, DNA of seven kilo bases (kb) has a theoretical hydrodynamic diameter of 300nm and the upper limit for packaging is at present 30kb (Tsai *et al.*, 1998). The sequences contained in the plasmid are therefore important and only essential genetic information can be included. Essential information includes the therapeutic gene, which must be identified and cloned into the appropriate expression vector, the signal sequences for gene expression such as promoters and enhancers and in some cases genes that aid integration into the genome of the diseased cell (Mhashilkar *et al.*, 2001).

Ideally the vector should also contain an on/off switch to provide a level of control, however, currently available switches need further development (Prud'homme *et al.*,

2000). To limit the possibility for chromosomal integration during the delivery of genes to a patient the homology of the pDNA sequences to known sequences in the human genome should be examined and described and strong homology avoided if possible (Zoon, 1996). To tailor plasmids to contain the essential gene sequence for production of the desired protein a recombinant DNA technology process is employed (Caldwell, 1997). The tailoring process begins with cleaving the plasmid and therapeutic genes at precise locations, using restriction enzymes, in order to produce compatible DNA ends and the therapeutic genes, along with the appropriate promoter and enhancer sequences, can then be ligated into the plasmid via their compatible end (Stribley *et al.*, 2002). The result of this manipulation is the production of a small, well designed, custom-built expression vector, aiding therapeutic delivery and expression, which can then be produced in significant quantities relatively easily in a bacterial fermentation.

1.8 Plasmid DNA manufacture

In this section a brief overview of the methods commonly employed to produce plasmids for therapy will be outlined. The description will purposely be kept brief as to avoid repeating subject matter encountered later.

1.8.1 Fermentation

Escherichia coli is by far the most common choice as the host for the production of plasmid DNA. The organism is well characterised and there exists a multitude of strains with various characteristics which may be desirable. The choice of fermentation strategy is designed to achieve high cell densities under conditions which allow for high plasmid specific yields. Although plasmid copy number is primarily a function of the control mechnisms coded on the molecule it can be strongly influenced by growth conditions, including growth rate. Further discussion concerning the impact of manipulating the upstream conditions in order to maximise plasmid yield is discussed in 3.1. Such manipulation can take the form of media adaptation and the use of fed-batch operation.

1.8.2 Downstream processing

Following the fermentation step a sequence of unit operations must be set up with the combined task of purifying the plasmid, commonly achieved by the removal of impurities away from the product, as well as concentrating the plasmid product. Due to the variety of unit operations on offer many different process flow sheets have been described. Generally, the downstream operations can be divided in to four distinct phases: Cell harvest, Cell Lysis, Clarification and concentration and Purification. More detail concerning these operations can be found in Chapter 7

1.9 The requirement for large plasmids

There are many processes described in the literature capable of producing plasmid DNA (Table 7-1), but the overwhelmingly majority describe the production of plasmids up to 10kb in size. Plasmids of this size range can comfortably accommodate all the necessary coding sequences for the own plasmid's replication, whilst in the bacterial host, with sufficient capacity remaining to accomodate the necessary sequence information for the protein of interest. As such, what are the drivers for the larger plasmid manufacture? It is envisioned that there are several reasons why larger plasmids could be required, all of which are linked to the increase in coding capacity available.

Increased coding capacity promises to allow for the expression of multiple proteins of interest, enable more sophisticated control of gene expression and also allow for the delivery of whole gene sequences, inclusive of introns and other regulatory factors.

In the shorter term more coding capacity is envisioned to be critical to the further development of DNA vaccines. At present, it is believed that to become a truly functional technology the immune response generated by such vaccines needs to be strengthened. One proposed stategy is to include sequences coding for immunomodulatory proteins, such as cytokines and interleukins, to be expressed in conjunction with the antigen and so boost the resulting immune reaction. In addition, it is hoped that constructs could be produced which express multiple antigens simultaneously. This would be useful for strengthening the response against one target/pathogen or would allow the immunisation against multiple targets/pathogens

using one construct. Obviously, both of these strategies would require either an increase in coding capacity or could be achieved through the administration of multiple invidual constructs. However, the manufacturing, formulation and logistical issues associated with such the administration of multiple constructs would be complicated.

Furthermore, current targets for gene replacement technology are mainly directed against monogenic disorders. It is hypothesised that future targets may be more complicated involving the correction of entire biochemical pathways and, as such, multigenic in nature. Larger coding capacity would be essential to achieve correction of such disorders.

1.10 Conclusions

A brief background to the field of gene therapy has been outlined. Details have been given about current progress and the potential future developments of this technology, and specifically DNA vaccination. Limited detail was given surrounding to the properties of plasmid DNA and the current methods on manufacture as these subjects will be dealt with in more detail in later sections. Finally, reasons were outlined as to the requirement of being able to manufacture large plasmids.

2 MATERIALS AND METHODS

2.1 Cultures

2.1.1 *Escherichia coli* bacterial strain genotypes

E.coli K-12 strains used as plasmids hosts were:

DH1 [F⁻ *rec*A1 *end*A1 *gyr*A96(Nal^r) *thi*-1 *hsd*R17 *sup*E44 *rel*A1].

DH10β [F⁻ *mcr*A Δ(*mrr-hsd*RMS-*mcr*BC) Φ80*lac*ZΔM15 Δ*lac*X74 *deo*R *rec*A1 *end*A1 *ara* Δ139 Δ(*ara,leu*)7697 *gal*U *gal*Kλ⁻ *rps*L *nup*G].

DH5α [F'/ *end*A1 *hsd*R17 (r_K^- m_K^+) *sup*E44 *thi*-1 *rec*A1 *gyr*A (Nal^r) *rel*A1 Δ(*lac*ZYA-*arg*F) U169 (Φ80d*lac* Δ(*lac*Z)M15] (Woodcock *et al.*, 1989; Blattner *et al.*, 1997).

2.1.2 Preparation of cell stocks

E.coli strains were maintained in 20% glycerol and stored at -70°C. Glycerol stocks were prepared by plating out cells from a master cell bank on to selective agar plates using a sterile inoculation loop. Plates were incubated at either 37°C or 25°C depending on the fermentation regime. Single colonies were picked off and used to inoculate 5mL of media in a sterile universal.

Bacteria were grown at either 37°C or 25°C on LB media in rotary shaker at 230rpm (New Brunswick Scientific). Plasmid harbouring strains were maintained by supplementing the liquid/solid media with selective antibiotics as appropriate, depending on plasmid phenotype; ampicillin sodium salt (100μgmL^{-1} to 1000μgmL^{-1}) for ampicillin resistance (pSVβ and pGEM® series), kanamycin sulphate (50μgmL^{-1}) for kanamycin resistance and chloramphenicol powder (25μgmL^{-1}) for chloramphenicol resistance (Oxford series). All selective agents were provided by Sigma-Aldrich, Dorset, UK and were added to the media after it had been sterilised and cooled so as to prevent degradation.

The seed culture was used to inoculate 50mL of sterile media, containing the appropriate antibiotic in a 1L baffled shake-flask, to 0.1OD. Shake-flasks were incubated until the optical density fell between 2.5-3.0 (early log phase). The flasks were removed from the incubator and 12.5mL of sterile 100%(v/v) glycerol was added. The cell suspension was

then aliquoted in 1.8mL volumes into 2mL Nunc cryovials and stored at -70°C. These formed the working cell bank.

2.1.3 Growth of bacterial strains.

In order to produce plasmid for cloning and gel studies, cultures were grown in 1L baffled shake-flasks. A cryovial from the working cell bank was removed from cold storage, defrosted and used inoculate 50mL of sterile, selective nutrient-broth in the shake-flask. Because the working cell bank was banked at an OD of ~2.5, inoculating 50mL of media with a 1.8mL cryovial of cell suspension led to a starting OD of 0.1. Shake-flasks were incubated overnight and the cell paste harvested by centrifugation.

To produce larger amounts of cell paste for the downstream operations bacteria were grown in a 5L (4L working volume) Applikon bioreactor. The sterile media in the fermenter was inoculated from Shake-flasks prepared as above to a starting OD of 0.1.

2.2 Plasmid Constructs

2.2.1 Oxford Series of large plasmids

The Oxford series of plasmids were provided by the The Wellcome Trust Centre for Human Genetics. Their construction and use is described by (Wade-Martins *et al.*, 1999; White *et al.*, 2003). Three constructs were provided: p5176 (116kb), p5206 (172kb) and p5204 (242kb). All the constructs were Bacterial Artificial Chromosome (BAC) based plasmids, constructed by the insertion of human genomic DNA segments into p5170 (12kb). The vector p5170 is based on the *NotI-XhoI* fragment of the BAC vector pBAC108L. This vector carries *parA, parB, parC, repE* and *oriS* which are F factor regulatory genes controlling BAC replication and copy number. These genes encourage stable propagation of the constructs and maintain copy number at ~2 copies/cell. The vector also carries Cm^r providing resistance to chloramphenicol.

The p5170 vector was developed as an episomal shuttle vector and as such was designed to be constructed and produced in bacterial cells for subsequent transfection into mammalian cells so as to investigate the effect of the inserted sequences on mammalian cell physiology. This trait means the vector also carries several genes enabling it to express sequences in mammalian cells. These include green-fluorescent protein (*GFP*) open-reading frame under the control of cytomegalovirus promoter (P_{CMV}) for visualisation

studies. The hygromycin-B phosphotransferase (*HPH*) gene under the control of the Rous sarcoma virus promoter (P_{SRV}) is included in order to allow selection in mammalian cells and the Epstein-Barr virus *FR* region is present to provide nuclear retention of the construct in cells expressing EBNA-1 (Figure 2-1).

2.2.2 Control plasmid pSVβ (6.9kb)

The plasmid pSVβ was used as a control in many experiments. It is a high-copy number pUC-based plasmid which confers ampicillin resistance and expresses β-galactosidase under the control of SV40 promoter (Figure 2-1).

2.2.3 pGEM® constructed plasmid models

(Tao and Zhang, 1998) describe the propagation of large DNA fragments using conventional vectors, specifically pGEM11. This vector was employed to create a series of larger constructs under the control of a high-copy number replicon using the method outlined in their report.

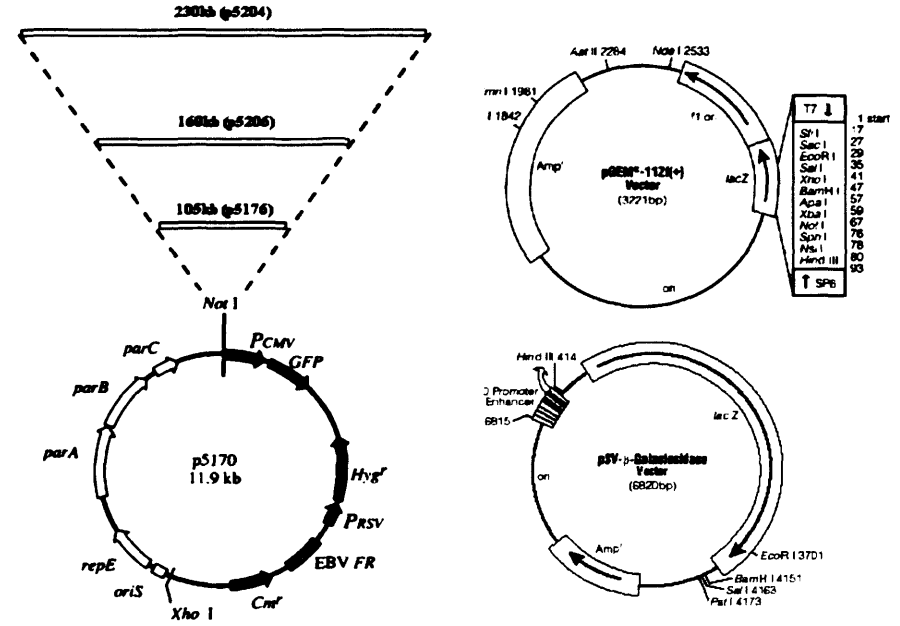

Figure 2-1 Maps of the plasmid vectors employed throughout this study. P5170 is the BAC vector in to which had been cloned several large fragments of human genomic DNA form the Oxford series of 116kb, 172kb and 242kb in size. Note the presence of active partition elements (*par A,B,C*) to ensure stable propagation. These combined with *Ori S* form the F-replicon. Also shown is the pSVβ construct which was a small, high-copy number plasmid often employed as a positive control plasmid. The pGEM11 vector is also detailed. Into this vector was cloned a series of large fragments of *S.cerevisiae* DNA to create large plasmid models using a method based on that of Tao and Zhang, (1998).

2.3 Bacterial Growth Media

2.3.1 Growth Media

Unless otherwise stated, chemicals and media components were supplied by BDH Laboratory Suppliers, Dorset, UK. Deionised water was drawn from a Milli-Q system (Millipore, Billerica, Massachusetts, USA) and used for media preparation. Media sterilisation was performed by autoclaving except additions which were heat labile. Autoclaving was peformed in either a PAC Autoclave set on Media cycle (121°C / 30mins/ 15psi) or for smaller items a benchtop autoclave was used.

2.3.1.1 Nutrient agar

Plate media was Luria-Bertani (LB) medium agar. LB agar consisted of per litre, mycological peptone (10g; Oxoid, Hampshire, UK), Yeast Extract (5g; Oxoid), NaCl (10g) and Agar Technical (15g; Oxoid, Hampshire, UK). The pH was adjusted to 7.5 with 4M NaOH prior to sterilisation by autoclaving.

2.3.1.2 SOC Media

This complex media was used in the revival of cells following electroporation. It consisted of per litre; Tryptone (20g; Oxoid), Yeast extract (5.0g; Oxoid), NaCl (10mL of 1M soln) and KCl (2.5mL of 1M soln). These components were mixed and the pH brought to 7.0 with 4M NaOH before adjusting the volume to 960mL and autoclaving. Following sterilisation additions of separately sterilised components were added. These were $MgCl_2.6H_2O$ (10mL of 1M soln), $MgSO_4.7H_2O$ (10mL of 1M soln) and D-Glucose (20mL of 1M soln). (Sambrook *et al.*, 1989)

2.3.1.3 SuperBroth media

SuperBroth media is a complex media. It consisted of, per litre; Yeast Extract (20g; Oxoid, Hampshire, UK), NaCl (5.0g) and Tryptone (32.0g; Oxoid, Hampshire, UK). The pH was adjusted to 7.5 with 4M NaOH prior to sterilisation.

2.3.1.4 SDCAS media

SDCAS media is semi-defined. Its preparation is slightly more involved than that of SuperBroth. The basal media was prepared as outlined in Table 2-1 and autoclaved to sterilise. The additions outlined in the same table were all sterilised separately either by autoclaving or filter sterilising and recombined aseptically once sterile in order to avoid

browning. Table 2-2outlines the constituents of the stock solutions used to prepare SDCAS media, together with the method of their sterilisation and storage.(O'Kennedy *et al.*, 2000)

Table 2-1Table detailing the constituents of SDCAS media

SDCAS MEDIA (PH 6.3)	COMPONENT	AMOUNT PER LITRE
Base Media	$(NH_4)_2SO_4$	4.0g
	KH_2PO_4	13.3g
	Citric acid	1.7g
	Trace element soln. (TES)	1mL
	4M NaOH to pH6.3	~10mL
	dH_2O	To 920mL
Additions	Iron (III) citrate stock	1mL
	Thiamine stock	1mL
	$MgSO_4.7H_2O$	2mL
	Glucose stock	25mL
	Casamino acids stock	50mL
Selective agent	Chloroamphenicol stock	0.74mL

Table 2-2 Table detailing the constituents of the stock solutions used to make SDCAS media

SOLUTION	COMPONENTS	G PER 100ML STOCK	STERILISATION	STORAGE
Trace Element Solution (TES)	$Na_2EDTA.2H_2O$	0.84	A/C	RT
	$CoCl_2.2H_2O$	0.25		
	$MnSO_4.4H_2O$	1.5		
	$CuSO_4.2H_2O$	0.15		
	H_3BO_3	0.3		
	$NaMoO_4.2H_2O$	0.25		
	ZnCl	1.3		
	Iron (III) citrate	10	A/C	RT
	$MgSO_4.7H_2O$	60	A/C	RT
	D-Glucose	40	A/C	RT
	Casamino acids	20	A/C	RT
	Thiamine	0.45	F/S	-20°C
	Chloramphenicol	3.4	N/A	-20°C

2.3.1.5 Seed Media

Used for shake-flask studies and inoculum preparation. A complex media prepared from yeast extract and tryptone, supplemented with glycerol as an additional carbon source. The media was sterilised prior to use. The precise contents remain proprietary.

2.3.1.6 Fermentation media

Used for 4L fermentations. A complex media prepared by dissolution of yeast extract, tryptone and mineral ion supplements in deionised water. Glycerol was added as an additional carbon source. Polypropylene glycol (PPG) was added on a fixed volumetric basis to control foaming. The media was sterilised *in situ* prior to use. The exact contents remain proprietary.

2.3.2 Antibiotic solutions

Both ampicillin and kanamycin were produced at stock concentrations of $50mgmL^{-1}$ by dissolving in sterile-filtered, cell-culture tested water. The stocks solutions were filter sterilised through 0.22μm filters (Acrodisc, Gelman Sciences, Ann Arbor, USA) before being aliquoted in 1mL fractions into sterile Sarstedt tubes and stored at -20°C. Chloramphenicol was prepared as a $34mgmL^{-1}$ solution in HPLC grade ethanol. With no need to filter sterilise the stock was aliquoted as above and also stored at -20°C. (Sambrook *et al.*, 1989)

2.4 Buffers and other solutions

2.4.1.1 TE buffer

10mM Tris-HCl (pH 8.0); 1mM Na_2EDTA (Sambrook *et al.*, 1989)

2.4.1.2 Phosphate buffered saline buffer (PBS)

A 10x stock of PBS was prepared by dissolving NaCl (80.0g), KCl (2.0g), Na_2HPO_4 (14.4g) and KH_2PO_4 (2.4g) in 800mL of dH2O. The pH was adjusted to 7.4 through dropwise addition of 1M HCl. The solution was then made up to 1L and autoclaved. A 10x dilution using dH2O was made when required and the solution re-sterilised (Sambrook *et al.*, 1989).

2.4.1.3 Qiagen® buffers for small-scale plasmid DNA preparation

All buffers for small scale preparations of plasmid were provided by Qiagen, Crawley, Sussex, UK. The buffer contents listed below are taken from (Qiagen, 2005).

P1 (Resuspension buffer)	50mM Tris-HCl (pH8.0); 10mM Na_2EDTA; 100μgmL^{-1} RNase A. Stored at 4°C.
P2 (Lysis buffer)	200mM NaOH; 1% (w/v) SDS. Stored at RT
P3 (Neutralisation buffer)	3.0M Potassium acetate (pH 5.5). Stored at 4°C
N3 (Neutralisation buf.-spin)	Proprietary composition similar to P3 but also containing guanidine hydrochloride. Stored at RT.
QBT (Equilibration buffer)	750mM NaCl; 50mM MOPS, pH 7.0; 15%(v/v) IPA; 0.15%(v/v) Triton® X-100.
QC (Wash buffer)	1M NaCl; 50mM MOPS; pH 7.0; 15%(v/v) IPA
QF (Elution buffer)	1.25M NaCl; 50mM Tris.Cl; pH 8.5; 15%(v/v) IPA.
EB (Elution buffer-spin)	10mM Tris-HCl; pH8.5
QS (Adjustment buffer)	1.5M NaCl; 100mM KH_2PO_4; pH 7.5
EX (Reaction buffer)	50mM Tris-HCl; 10mM $MgCl_2$; pH8.5

2.4.1.4 3M Sodium acetate

Sodium acetate (24.6g) was dissolved in 80mL of dH_2O. The solution was made up to 100mL and sterilised by filter sterilising through a 0.22μm filter (Acrodisc, Gelman Sciences, Ann Arbor, USA). It was stored at 4°C (Ausubel, 1987).

2.4.1.5 0.5x Tris-Borate-EDTA (TBE) buffer for electrophoresis

A 10x stock of TBE (0.45M Tris-Borate; 0.1M EDTA) was produced by dissolving Trizma base (54.0g) and Orthoboric acid (27.5g) in 0.8L of dH_2O. 20mL of 0.5M Na_2EDTA (pH8.0) was added to the solution which was then made up to a final volume of 1L. The buffer was autoclaved and subsequently diluted 1:20 with distilled water prior to use.(Sambrook *et al.*, 1989)

2.4.1.6 SYBR Gold Staining buffer

30µL of 10,000x concentrate of SYBR Gold (Molecular Probes, Leiden, NL) was added to 300mL of 0.5xTBE. (Molecular Probes Inc, 2003)

2.4.1.7 Loading buffer

0.25% (v/v) bromophenol blue; 0.25% (v/v) xylene cyanol; 30% (v/v) glycerol; 0.1M Na2EDTA

2.4.1.8 LMP Agarose

Low-melting point agarose was prepared by dissolving 0.8g of LMP agarose (Sigma, Dorset, UK) in 0.5xTBE. The solution was autoclaved to dissolve.

2.4.1.9 TBE/ Ethidium bromide staining buffer

$10mgmL^{-1}$ EtBr (Sigma, Dorset, UK) was added to 0.5xTBE to a final concentration of $0.2\mu gmL^{-1}$.

2.4.1.10 HPLC buffers

(i) Buffer A (20mM Tris; pH7.5).

9.69g of Trizma base (Sigma, Dorset, UK) was dissolved in 1.5L of dH_2O in a 2L volumetric flask. The pH was adjusted to 7.5 through dropwise addition of 1M HCl before being made up to 2L. The solution was filtered through a Millipore Type HA 0.45µm filter (Millipore, Billerica, Mass. USA) to degas.

(ii) Buffer B (20mM Tris+1M KCl; pH7.5)

9.69g of Trizma base (Sigma, Dorset, UK) and 149.0g of KCl was dissolved in 1.5L of dH_2O in a 2L volumetric flask. The pH was adjusted to 7.5 through dropwise addition of 1M HCl before being made up to 2L. The solution was filtered through a Millipore Type HA 0.45µm filter (Millipore, Billerica, Mass. USA) to degas.

(iii) Cleaning solution (20% (v/v) Methanol)

To 500mL of dH_2O 200mL of HPLC grade methanol was added. The solution was allowed to cool before being made up to 1L.

2.4.1.11 PicoGreen Working Solution

100µL of PicoGreen stock solution (Molecular Probes, Leiden, Netherlands) was diluted 1:200 in 19.9mL of TE buffer in an opaque universal immediately prior to use(Molecular Probes Product Information, 2003).

2.4.1.12 Bicinchoninic acid (BCA) assay reagents

All reagents were supplied by Pierce Scientific BCA Protein Assay kit (Perbio Science, Northumberland, UK) and as such the exact contents were proprietary (Pierce Scientific, 2006).

Reagent A: Contained Sodium carbonate; Sodium bicarbonate; bicinchoninic acid; Sodium tartrate in 0.1M Sodium hydroxide.

Reagent B: Contained 4% cupric sulphate (CuSO4)

Working reagent: 50:1 dilution of Reagent A to B.

2.4.1.13 Quant-IT™ Working Solution.

100µL of Quant-IT™ RNA reagent (Molecular Probes, Leiden, Netherlands) was diluted 1:200 in 19.9mL of Quant-IT RNA buffer in an opaque universal immediately prior to use (Molecular Probes Inc, 2006).

2.4.1.14 Restriction Enzyme buffers

All restriction enzymes were purchased from Promega, Madison, USA and the buffers supplied were used. Bovine serum albumin (BSA) was added to restriction digests from a stock solution provided ($10mgmL^{-1}$) to form a $100\mu gmL^{-1}$ solution in the reaction mixture.

2.4.1.15 100mM ATP solution

Adenosine 5'-triphosphate disodium salt (2.75g; Sigma, Dorset, UK) was dissolved in 40mL of dH_2O. The pH was adjusted to 7.5 using 4M NaOH and the volume corrected to 50mL. The solution was sterilised through a 0.22µm filter before being aliquoted in 300µL volumes and stored at -20°C (Qiagen, 2005).

2.4.1.16 β-Agarase buffer

10mM Bis Tris-HCl; 1mM EDTA; pH 6.5 (Promega, Madison, USA)

2.4.1.17 Phenol/Chloroform

Phenol:Chloroform:Isoamyl alcohol (25:24:1), saturated with 10mM Tris-HCl (pH 8.0); 1mM Na_2EDTA (Sigma, Dorset, UK). The phenolic phase was pH 6.7±0.2

2.4.1.18 1x T4 DNA ligase buffer

50mM Tris-HCl (pH 7.5); 10mM $MgCl_2$; 10mM dithiothreitol; 1mM ATP; 25μgmL^{-1} BSA(Promega, Madison, USA).

2.4.1.19 MagNA Pure LC DNA Isolation Kit 1

Contents of the buffers provided for use in the kit remain proprietary (Roche Diagnostics, Indianapolis, USA). The MSDS provides indications to some of their contents but not as to their proportions (Roche Diagnostics, 2004).

Lysis/ Binding buffer	20% Triton® X-100; 25%Guanidinium isothiocyanate
Proteinase K solution	2% Proteinase K; 50% Glycerol
Magnetic Glass Particle soln	1-Methyl-2-pyrrolide
Wash Buffer 1	38% Ethanol; Guanidine hydrochloride
Wash Buffer 2	Not known
Elution Buffer	10mM Tris-HCl (pH8.0)

2.4.1.20 TaqMan 2xUniversal MasterMix Buffer (Applied Biosystems, CA, USA)

Exact contents remain proprietary but the mix is known to contain AmpliTaqGold® DNA polymerase (a heat activated enzyme designed to reduce background signal), ROX™ passive reference dye, dNTP's at 200μM each in 100mM Tris-HCl, 100mM KCl (pH8.3). The remaining buffer components including Mg^{2+} concentration are optimised for high-performance. with total $MgCl_2$ being 1.5mM; 0.7mM of which remains unbound.

2.4.1.21 Primer-Probe Mix

Supplied as 500nM primer and 250nM probe solution in 25mM Tris-HCl; 0.1mM Na_2EDTA; 0.15%(v/v) Tween-20; 0.15% (v/v) NP-40 (pH8.3).

2.4.1.22 Resuspension Buffer

25mM Tris+10mM EDTA+55mM Dextrose. Stored and used at room temperature.

2.4.1.23 0.96% (w/v) Sodium hydroxide (Lysis buffer 1)

2.4.1.24 6% (w/v) Sodium dodecylsulphate solution (Lysis buffer 2)

2.4.1.25 Neutralisation buffer (3M Potassium acetate)

3M Potasium acetate pH to 5.5 using glacial aceitic acid. Stored and used at 4°C.

2.4.1.26 RNA precipitation solution (5M Calcium chloride)

5M Calcium chloride stored and use at room temperature.

2.4.1.27 Diafiltration buffer 1 (10mM Tris)

10mM Tris buffer (pH 7.1) stored and used at room temperature.

2.4.1.28 Diafiltration buffer 2 (10mM Tris+0.54M NaCl)

10mM Tris + 0.54M NaCl (pH 7.1) stored and used at room temperature.

2.5 Analytical methods

2.5.1 Optical density measurement

Optical density was used as the primary measure of bacterial cell growth in liquid culture. All recordings were taken using the same spectrophotometer; Shimadzu UV-1700 (Shimadzu Corp, Duisburg, Germany) set to 600nm. Measurements were taken by diluting culture broths, using blank media being used for cultivation, until the reading fell within the linear range of the assay 0.1-0.6OD units.

2.5.2 Wet Cell Weight (WCW) determination

Wet cell weight measurements were taken in duplicate per sample point. All mass measurements were carried out using a Sartorius MasterPro five-point balance (Sartorius AG, Surrey, UK). 1mL of culture broth was pipetted into a pre-weighed sarstedt tube and centrifuged for 5 minutes at 13,000rpm in a benchtop centrifuge. The supernatant was carefully decanted off and any remnants of media removed using a cotton swab. The tube was then reweighed and the cell weight calculated from the difference.

2.5.3 Dry Cell Weight (DCW) determination

Dry cell weight measurements were taken in duplicate per sample point. All mass measurements were carried out using a Sartorius MasterPro five-point balance (Sartorius AG, Surrey, UK). 5mL of culture broth was pipetted into pre-weighed, glass universal bottles. These were placed in a vacuum oven at 80°C and left for ~24hours before being reweighed and the cell weight calculated from the difference.

2.5.4 Replica plating assay for determination of plasmid retention

Broth samples for analysis needed to produce between 50-200 colonies per 100mm diameter plate to produce a significant result. Each sample for analysis was processed in triplicate by loading each of the dilutions on to three plates. The optical density of the broth was determined and the level of dilution required chosen from Table 2-3 which lists the dilutions used (figures decided upon assuming 1OD unit~2.5×10^8 cellsmL^{-1} (Figure 6-1). The broth was diluted using sterile PBS buffer by serial $\log_{10}$ dilution in sterile universal bottles by adding 1mL of culture broth to 9mL of PBS. 100µL of the correct dilution was then pipetted on to the centre of a non-selective TSA 100mm plate.

The plates were then incubated at whatever temperature the culture was being cultivated at (25°C, 30°C or 37°C) for 18-24hrs in a benchtop incubator. The dilution plates with the most applicable number of colonies were chosen as the master plates.

Table 2-3 Table outlining the two dilutions which were plated out on to separate 100mm TSA plates. The table demonstrates the increase in dilution required with OD progression, calculated by assuming $1OD_{600}$ unit ~ $2.5x10^8 cells mL^{-1}$. Dilutions were performed by log_{10} dilution in sterile PBS buffer.

OD_{600}	Cells per 100µL	Dilutions required
0 – 0.04	$0 - 1x10^6$	10^{-3} and 10^{-4}
0.04 – 0.4	$1x10^6 - 1x10^7$	10^{-4} and 10^{-5}
0.4 – 1.0	$1x10^7 - 2.5x10^7$	10^{-5} and 10^{-6}
1.0 – 4.0	$2.5x10^7 - 1x10^8$	10^{-5} and 10^{-6}
4.0 – 10.0	$1x10^8 - 2.5x10^8$	10^{-6} and 10^{-7}
10.0 – 50.0	$2.5x10^8 - 1.25x10^9$	10^{-6} and 10^{-7}

The master plates were marked on the base as a reference point. In a hood, the replica-plating block was disinfected by spraying with 70% (v/v) ethanol. A sterile, velveteen square was then placed on the block and locked in place by a locking ring. Aligning the mark on the master plate with the mark on the plating block, the master plate was inverted and the colonies transferred to the cloth by applying gentle pressure to the back of the plate. A marked, non-selective TSA plate was then placed on the plating block and gently pressured to ensure colonies are transferred. A selective TSA plate was then placed on the block and the process repeated. The plates were incubated at the cultivation temperature for 18-24 hours to allow colony formation after which the colonies were counted using a colony counter. The colonies on the three selective and three non-selective plates for each sample point were counted and totalled. The proportion of plasmid bearing cells was calculated using the binomial equation shown in Equation 2-1.

$$\text{Proportion of plasmid bearing cells} = \sqrt{\frac{\left(\frac{\text{Colonies on selective}}{\text{Colonies on non-selective}}\right) \times \left(1 - \left(\frac{\text{Colonies on selective}}{\text{Colonies on non-selective}}\right)\right)}{\text{Colonies on non-selective}}}$$

Equation 2-1 Binomial equation which was used to calculate the proportion of plasmid bearing cells from data gathered by replica plating. It was used to improve the accuracy of the result, since the equation used the sum of the colonies from all the triplicate plates. This produces a more precise result than calculating the proportion of plasmid bearing cells from each of the triplicate plates and then averaging the results.(O'Kennedy and Patching, 1999)

2.5.5 Sample preparation for plasmid quantification by HPLC and gel analysis

Bacterial pellets of 5OD units, equivalent to approximately $2.5x10^9$ cells were resuspended to homogeneity in 250µL of buffer P1(2.4.1.3) by pipetting. 250µL of buffer P2 was then added and the solution gently mixed by inverting 4-6 times. The lysis reaction was left to proceed for no longer than 5 minutes before 250µL of 4°C buffer P3 was added and the solution mixed as before. The tubes were then left on ice for 30minutes to complete the precipitation reaction. The lysate was cleared by centrifugation in a benchtop centrifuge (Eppendorf, Cambridge, UK) at 13,000rpm for 10minutes. The clarified lysate was decanted off into fresh Sarstedt tubes.

To the 0.75mL of lysate, 0.53mL (0.7vols) of isopropyl alcohol (IPA) was added together with 0.1 volumes (75µL) of 3M sodium acetate. The tubes were gently mixed by inversion. The plasmid DNA was recovered by centrifugation at 13,000rpm for 25mins. The liquor was decanted off and the pellet washed with 1mL of 70%(v/v) ethanol before being centrifuged again for 10 minutes at 13,000rpm. The ethanol fraction was discarded and the tubes air-dried. The plasmid DNA pellet was then resuspended in 100µL of TE buffer. (Sambrook *et al.*, 1989)

2.5.6 Preparation of samples for plasmid quantification by PicoGreen assay

Bacterial pellet samples were prepared in an identical fashion to above (2.5.4) except that the procedure was halted once the clarified lysate was decanted into fresh sarstedt tubes. The PicoGreen assay was conducted directly on clarified lysates or spin-prep eluents where specified. (Noites *et al.*, 1999)

2.5.7 Preparation of samples by Qiagen spin-prep

Bacterial pellets of 5OD units, equivalent to approximately $2.5x10^9$ cells, were resuspended in 250µL of buffer P1(2.4.1.3) by pipetting. 250µL of buffer P2 was then added and the solution gently mixed by inverting 4-6 times. The lysis reaction was left to proceed for no longer than 5 minutes before 350µL of buffer N3 (2.4.1.3) was added to neutralise and the solution mixed as before. The lysate was cleared by centrifugation in a benchtop centrifuge (13,000rpm 10minutes) and the clarified lysate instantly applied to the anion-exchange resin of a QIAprep spin-column (Qiagen, Crawley, UK), which was centrifuged for 1 minute. The flow-through was discarded and 0.75mL of the wash buffer PE was applied to the column before being centrifuged for 1 minute. The column was then

re-centrifuged to remove any residual enthanolic wash buffer. Finally, the plasmid DNA was eluted from the column into a fresh eppendorf tube by applying 50μL of EB buffer directly to the surface of the resin. The columns were left to incubate for 5 minutes to encourage maximum recovery before eluting the plasmid solution by centrifugation. (Qiagen, 2005; Pederson, 1996)

2.5.8 Preparation of plasmid material by Qiagen kits

When larger quantities of plasmid were required for standard curve preparation, for use as markers or in binding studies, commercially available Qiagen kits were utilised (Qiagen, Crawley, UK). Three different methodologies were used depending on the quantity and purity of the desired plasmid. Each of the methodologies were as outlined in Qiagen technical literature (Qiagen, 2005) and all were based upon the use of Qiagen Tip-500 columns capable of binding a maximum 500μg of pDNA product.

2.5.8.1 Qiagen Maxi-preps (Refer to Figure 2-2)

2.0g of frozen cell paste was resuspended to homogeneity in 10mL of buffer P1 (2.4.1.3) in a Sorvall centrifuge pot by vortexing, forming a cell suspension of ~150gL^{-1}. The cells were lysed through the addition of 10mL of buffer P2 and the solution mixed by inverting the bottle 4-6 times. The lysis reaction was allowed to proceed for 5 minutes before neutralising through the addition of 10mL of 4°C buffer P3. The centrifuge pot was then incubated on ice for 30minutes to maximise precipitation, before clarifying the solution by centrifugation in a Sorvall centrifuge (SLA-1500 rotor) at 12,000rpm for 30minutes. The lysate was further clarified by filtration through a double-layer of Kimwipe® tissue into a clean, sterile Nalgene flask.

A Tip-500 column was equilibrated by applying 10mL of the buffer QBT, which passed through the resin by gravity flow, before the clarified lysate was introduced to the column. Once the clarified lysate had passed through the column, 2x30mL volumes of the wash buffer QC were applied. The plasmid DNA was eluted from the column using 15mL of buffer QF heated to ~60°C.

The eluant was collected in a clean SS-34 centrifuge tube, to which was added 10.5mL (0.7vols) of IPA and 1.5mL (0.1vols) of 3M sodium acetate to precipitate the pDNA. This step was followed by centrifugation using a Sorvall SS-34 rotor at 12,000rpm for 30mins. The IPA liquor was decanted off, being careful not to disturb the pellet and 10mL of 70%

(v/v) ethanol was added before re-centrifuging the tube for 15minutes at 12,000rpm. The ethanol liquor was decanted off and the tube allowed to air-dry before the plasmid DNA was resuspended in 0.5mL of TE buffer.

2.5.8.2 Qiagen Very Low-copy number preps (Refer to Figure 2-2)

This protocol was identical to the Maxi-prep method (2.5.8.1) except that it used more starting material and required an additional IPA precipitation step. It was employed because many of the plasmids studied existed at very low copy numbers making them hard to isolate using a traditional maxi-prep approach. Consequently, this protocol used 4.0g of starting material resuspended in 20mL of buffer P1 so forming a cell suspension of identical concentration as above. The lysis and neutralisation buffers were added in the same ratio as before (1:1:1) equating to 20mL each. Consequently, 60mL of clarified lysate was produced as opposed to 30mL.

The second difference with this protocol is that the clarified lysate was not applied directly to the Tip-500 column as was the case with the maxi-preps. Instead, the lysate was precipitated in order to concentrate through the direct addition of 42mL (0.7vols) of IPA and 6mL (0.1vols) of 3M sodium acetate. The DNA was recovered by centrifugation in a Sorvall centrifuge (SLA-1500 rotor) at 12,000rpm for 30minutes. The waste liquor was discarded and the pellet resuspended in 1mL of TE buffer to which was added 12mL of equilibration buffer QBT. This plasmid containing solution was then applied to the equilibrated Tip-500 column and the remainder of the protocol matched that of the Maxi-prep method.

2.5.8.3 Qiagen Large construct preps (Refer to Figure 2-2)

This protocol mirrored that of the Very Low-copy number prep (2.5.8.2) except for two key differences. Because many of the plasmids being studied were low-copy number they were very difficult to obtain in sufficient quantities. That issue was addressed by the Low-copy number prep by doubling the starting quantities used. However, because of the low-copy number and low yields the ratio of plasmid DNA to contaminating genomic DNA at the end of the purification regime was often unacceptably low, especially when preparing the plasmids to form a standard curve for PicoGreen or HPLC. This is because the level of contaminating gDNA would give a false overestimation of plasmid yield when measured spectrophotometrically at 260nm. In attempt to remedy the problem this prep was used when preparing large plasmids for use as standards. The key difference of this prep was

that it employed an exonuclease to degrade the genomic DNA so as to increase the ratio of plasmid DNA to genomic DNA achieved.

The beginning of the protocol was identical to the Very low-copy number prep in that 4.0g of cell paste was resuspended, lysed and neutralised using 20mL of the various buffers. Again the clarified lysate was precipitated in the same fashion as before but after centrifugation the pellet was washed with 70% (v/v) ethanol and recentrifuged using a Sorvall centrifuge (SLA-1500 rotor) at 12,000rpm for 15minutes. Once the ethanol liquor had been discarded and the tube air-dried, the pellet was dissolved in 9.5mL of buffer EX. To this was added 300µL of 100mM ATP solution (2.4.1.15) together with 200µL of ATP-Dependent exonuclease (supplied in kit) and the tube incubated in a water bath for 60 minutes at 37°C. Following incubation, 10mL of buffer QS was added to the mixture, which was then applied to an equilibrated Tip-500 column. The remainder of the protocol was as outlined in the Maxi-prep method (2.5.8.1).

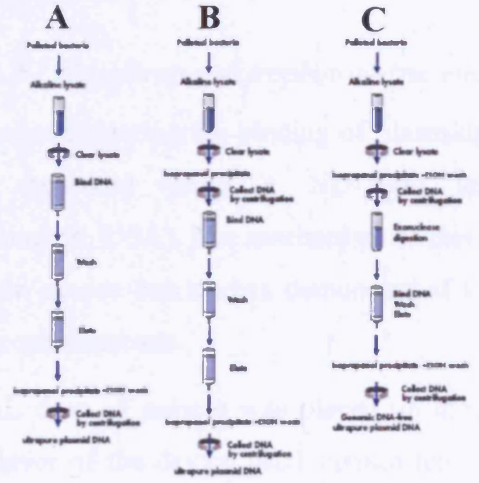

Figure 2-2 Schematic outlining the three different methods of Qiagen column chromatography employed throughout this project. All methods employed Tip-500 packed bed columns containing Qiagen's proprietary anion exchange resin. There are subtle differences in the operation of the protocols. A; Standard maxi-prep B; Low-copy number protocol C; Large construct kit protocol.

2.5.9 Concentration of plasmid DNA by UV absorbance

This method quantified plasmid preparations through their absorbance at 260nm. The extinction coefficient (ε) of dsDNA at this wavelength is $20gL^{-1}cm^{-1}$. According to Beer's law, absorbance is the product of the path length, concentration and the extinction coefficient. Using a path length of 1cm means absorbance is equal to optical density, which itself is the product of the concentration and the extinction coefficient. This means that an optical density of 1.0 equates to a DNA concentration of $0.05gL^{-1}$ or $50\mu g\ mL^{-1}$(Ausubel, 1987). This method of quantification formed the bench mark against which all the other methods of plasmid quantification (HPLC/ PicoGreen) were calibrated. Due

to the nature of the assay, absorbance could only be used on pure, concentrated solutions of plasmid DNA and so was mostly employed to quantify material for calibrating the other methods of plasmid quantification, which could be performed on less pure and more dilute plasmid solutions. Two different spectrophotometers were used during the course of the investigations.

2.5.9.1 Standard spectrophotometric measurement

Absorbance was measured by diluting the plasmid solution so that the A_{260} reading fell into the linear range of 0.2-0.8, using the buffer in which the plasmid was contained. Most commonly this was TE buffer except when measuring spin-prep eluents when buffer EB was used. A Uvikon XL double-beam scanning spectrophotometer (North Star Scientific, Bedford, UK), blanked against the correct buffer, was used to measure the absorbance of the plasmid solution in a 100µL quartz cuvette. The purity of samples was checked by the ratio of absorbance at 260nm to 280nm, a ratio below 1.8 being indicative of protein contamination.

2.5.9.2 NanoDrop spectrophotometric measurement

When investigating the binding of plasmids to chromatographic matrices, A_{260} absorption was measured using a ND-1000 spectrophotometer (NanoDrop Technologies, Wilmington, USA). The mechanism of this spectrophotometer differed considerably to the Uvikon device but studies demonstrated a high level of comparability between the two spectrophotometers.

A 2µL drop of sample was placed on the sample pedestal and the automated, magnetic cantilever of the device used surface tension to pull the drop into a column of liquid of known path length. The sample pedestal was the end of an optical fibre down which the light from a xenon flash lamp was directed. The device consisted of a 2048-element linear silicon CCD array detector, enabling the absorption measurement of a continuous spectrum. The machine was blanked against the sample buffer but dilution was not required as the spectrophotometer was capable of quantifying DNA solutions up to 3700µgmL^{-1}. The attached software produced a continuous spectrum trace but quantified the solution by using the absorbance reading as found at 260nm and the dsDNA extinction coefficient of 20gL^{-}cm^{-1}. The device also reported the A_{260}/A_{280} and A_{260}/A_{230} ratios as measures of plasmid purity (NanoDrop Tech.Lit, 2005).

2.5.10 PicoGreen quantification of plasmid

PicoGreen (Molecular Probes, Leiden, NL) was used in the quantification of plasmid DNA solutions including both clarified lysates and spin-prep eluents. PicoGreen has been demonstrated to be a sensitive dye that can be used to detect dsDNA in the presence of ssDNA, RNA and other compounds which commonly contaminate nucleic acid preparations. The dye becomes intensely fluorescent upon binding dsDNA due to its high quantum yield (~0.5) and large, molar extinction coefficient (~70,000$cm^{-1}M^{-1}$) (Singer *et al.*, 1997). The lower detection limit of the assay has been determined to be 25$pgmL^{-1}$ and the linear range found to extend over four-orders of magnitude; 25$pgmL^{-1}$ to 1μgmL^{-1}. However, investigations did reveal that the linearity of the assay was sensitive to salt contamination. Also, the signal emitted from linear dsDNA was greater than that of an equivalent concentration of CCC plasmid DNA, due to the capability of linear dsDNA to bind more flurophore molecules per mole.

2.5.10.1 Sample preparation and measurement

All assays were performed in BD-Falcon™ 96-well polystyrene plates (clear/ flat-bottomed/ 370µL volume) and based on the method of (Noites *et al.*, 1999). The fluorescence of the unknowns was calculated by calibrating against a standard curve of solutions of known plasmid DNA concentration, determined by A_{260} (Refer to 2.5.9.1). Duplicate samples for analysis were prepared as described in 2.5.4 for clarified lysates and 2.5.7 for spin-prep eluents. In both cases the final dilution of the samples (unless stated otherwise) and PicoGreen stock was 1:400.

In sterile sarstedt tubes, 20µL of each sample was diluted with 180µL of TE buffer, representing a 1:10 dilution. Triplicate 5µL volumes of the diluted sample were loaded into separate wells of a 96-well plate. To each well was added 95µL of TE buffer. A standard curve was constructed by preparing a 2μgmL^{-1} stock of the plasmid being quantified. The material for the standards was prepared by Qiagen kit (2.5.8.1) except in the case of linear DNA which used λ DNA (Sigma, Dorset, UK). This stock was diluted by serial dilution, using TE buffer to create three other standard solutions of concentration; 0.2μgmL^{-1}; 50$ngmL^{-1}$; 5$ngmL^{-1}$. The standard curve was then prepared as outlined in Table 2-4.

Immediately before use, 100µL of PicoGreen stock (200x concentrate in DMSO) was added to 19.9mL of TE buffer in an opaque universal and inverted to mix, representing a

1:200 dilution. Using a multiwell Gilson® 200µL pipette, 100µL of the diluted PicoGreen reagent was added to each well. The plate was wrapped in aluminium foil and incubated in the dark for 5 minutes prior to reading.

Table 2-4 Table outlining the volumes of the standard curves added to a 96-well plate to form the standard curves for the PicoGreen assay. Rows A-D represent the concentrated standard curve and E-H formed the dilute standard curve. Typical R^2 values were 0.99. Wells A4-A12 were blank and recorded background fluorescence. The mean value of the background was subtracted from each sample and standard value before calculation of the concentration.

Well	Total DNA (ng)	DNA Conc. μgmL^{-1}	Vol(µL) of $2\mu gmL^{-1}$	Vol (µL) of $0.2\mu gm^{-1}$	Vol (µL) of $50ngm^{-1}$	Vol(µL) of $5ngml^{-1}$	Vol of Te (µL)	Vol (µL) of PicoGreen
A1-3	40	8	20	0	0	0	80	100
B1-3	20	4	10		0	0	90	100
C1-3	2	0.4	0	10	0	0	90	100
D1-3	0.2	0.04	0	1	0	0	99	100
E1-3	5	1	0	0	100	0	0	100
F1-3	0.5	0.1	0	0	10	0	90	100
G1-3	0.05	0.01	0	0	0	10	90	100
H1-3	0.005	0.001	0	0	0	1	99	100
A4-12	0	0	0	0	0	0	100	100

The plate was read using a Gemini EM Microplate Spectrofluorometer (Molecular Devices, Wokingham, UK). Readings were taken using Excitation filter EX 480/20 (470-490nm) and Emission filter EM 520/10 (505-515nm). Gain was set to 80 and each well was automatically read six times and the average value taken. The data was analysed using SoftMax Pro® software. The software plotted the standard curve using a Quadratic fit, subtracted the background, calculated the DNA concentration and corrected for dilution and so returned the value of DNA concentration in the starting sample.

Table 2-5 Table depicting the concentrations of components in the samples tested by the PicoGreen assay and their tolerable limits as reported by (Singer *et al.*, 1997). * refers to average levels of contaminants determined in the clarified lysate from the DSP operations and assumed to be at similar levels for the analytical preparations used here.

Feed Stream	Component	Concentration In Undiluted Stream	Acceptable Limit	Concentration Post 400x Dilution (mM)
Clarified lysate	Potassium acetate	1000mM	30mM	2.5mM
	SDS	11.5mM	3.5mM	0.03mM
	Protein*	0.1%	2%	<0.1%
	ssDNA*	33.6µgmL-1	0.13µgmL-1	0.08µgmL-1
	RNA*	112µgmL-1	0.13µgmL-1	0.28µgmL-1
Spin-prep eluant	Tris	10mM	No reported effect	Blanked against TE
	EDTA	1mM		

2.5.11 Concentration of plasmid by HPLC

Plasmid concentration was determined by anion-exchange high performance liquid chromatography (IE-HPLC) using a Dionex DNAPac PA-100 column (4mm x 250mm) (Dionex, Camberley, UK). The DNAPac PA-100 packing material is composed of 100-nm, quaternary-ammonium functionalized MicroBeads™ bound to a 13µm diameter, solvent-compatible, nonporous substrate. The HPLC system was a Waters Alliance 2690/5 Separations module coupled to a 996 Photodiode Array Detector recording absorbance at 260nm (Waters, Elstree, UK). Injection of a sample was followed by a linear gradient of 20mM Tris + 0.7M KCl (pH 7.5) to 20mM Tris + 0.9M KCl (pH 7.5) over a 9.5minute period (Refer to 2.4.1.10). The column was then requilibrated with Buffer A for 4.5minutes. The exact programmed flow gradient is detailed in Table 2-6. Buffer flowrate was maintained constant at around 1.0mLmin^{-1} producing a pressure drop during normal operation of ~1500psi. Samples for analysis were maintained at 4°C ± 0.5C in the refrigerated carousel whilst the column was operated at 40°C. (Stowers *et al.*, 1988; Strege and Lagu, 1991; Eon-Duval and Burke, 2004)

Table 2-6 Table detailing the programmed flow for a HPLC run

TIME (MINS)	FLOWRATE (MLmin^{-1})	% BUFFER A	% BUFFER B
0 to 5	1.0	30.0	70.0
5.0	1.0	18.0	82.0
5.5	1.0	10.0	90.0
9.5	1.0	10.0	90.0
10.	1.0	30.0	70.0
14.0	1.0	30.0	70.0
14.99	1.0	30.0	70.0
15.0	0.0	30.0	70.0

HPLC trace data was logged by the attached PC and Empower 2 Chromatography Data Software (Waters, Elstree, UK) was used for its manipulation and interpretation. The software was instructed to integrate peaks between the time points 4.59mins and 8.118mins, the time region in which plasmid DNA was found to elute.

Plasmid streams quantified using HPLC included fermentation time-point samples together with samples recovered during the various steps of the downstream process. These samples were run in an identical fashion on the same column but their method of preparation, volume loaded and calibration curve differed, the reasons for these differences are outlined in (4.5.2).

2.5.11.1 Calibration of HPLC

During the course of investigations it was necessary to calibrate the HPLC column on numerous occasions. It was observed that plasmid quantification by HPLC was, to a much lesser extent than the PicoGreen assay, affected by the form and purity of the plasmid sample being analysed. As such, it was necessary to use three standard curves during the course of process. For more on the development on this assay refer to (4.5.2). The standard curve used depended on the stage of the process from which the sample was generated. Each standard curve set was comprised of a calibration curve for each construct under investigation.

(a) Standard Curve Set for Specific Yield progression during fermentation (Upstream)

This standard curve was generated through the loading of 10μL volumes of plasmid standard in TE buffer. The plasmid standard was produced using Qiagen Large construct kit*. The plasmid stock was quantified by absorbance at 260nm (2.5.8.1) and serially diluted to create standard solutions of concentration; 0/ 1/ 2.5/ 5/ 7.5/ 12.5/ 25/ 50/ 75/ 100/ 150/ 200/ 250μgmL^{-1}. The standard solutions were run on HPLC in triplicate in increasing concentration order, with buffer blank runs between each sample to prevent carryover. The resulting areas were used to construct the calibration curve shown in Figure 9-26

(b) Standard Curve for Pre-Ultrafiltration samples (Downstream)

This standard curve was created using Qiagen Large construct kit* as above but instead serially diluted in parental clarified lysate. The parental clarified lysate would remove the small but observable distortion produced by the presence of genomic DNA fragments in the lysate. The parental clarified lysate was prepared by conducting a 50g prep (2.8) on parental cell paste. The plasmid stock was quantified by absorbance using the NanoDrop spectrophotometer and serially diluted using clarified lysate to the following concentrations; 0/ 0.1/ 0.25/ 0.5/ 0.75/ 1.25/ 2.5/ 5/ 7.5/ 10/ 15/ 20 and 25μgmL^{-1}. Triplicate 100μL samples of the standard solutions were run in ascending concentration order separated by buffer blanks. The resulting areas were used to construct the calibration curve shown in Figure 9-27

* The Qiagen Large construct kit was employed on all plasmid constructs since it was necessary to use it for the BAC p5176, so for reasons of consistency the kit was used to prepare all plasmid stock solutions. It was preferential because for BAC preparations contaminating chromosomal DNA could represent ~30-50% of recovered DNA, as assayed by A_{260}. Looking at the standard curves for some constructs it was not possible to recover sufficient plasmid to prepare standards above 50μgmL^{-1}.

(c) Standard Curve for Post-Ultrafiltration samples (Downstream)

This standard curve was generated from each of the plasmids recovered from the Ultrafiltration rig. Recovered plasmid solutions were concentrated by IPA precipitation and ethanol wash and resuspended in 20mM Tris/0.54M NaCl (the buffer used to recover plasmid from the UF rig). The plasmid stocks were quantified using the NanoDrop spectrophotometer and serially diluted to create the standard solutions. Triplicate 100µL samples of the stock solution were run in ascending concentration order separated by buffer blanks. The resulting areas were used to construct the calibration curve shown in Figure 9-27.

2.5.11.2 Determining specific yield progression during fermentation by HPLC

To measure specific yield progression during fermentation, hourly cell pellet samples were obtained as outlined in 2.7.5 and prepared as in 2.5.4. Duplicate 5OD samples from each time point were prepared and 50µL of the final plasmid containing solution was added to polypropylene HPLC vials. 10µL of this solution was run on the HPLC column for analysis. The area values reported from the HPLC were converted to plasmid concentrations using the calibration curves shown in Figure 9-26. The values of concentration of the purified plasmid samples were used to determine the plasmid specific yield, volumetric yield and copy number as shown in Figure 9-26 using the equations detailed in Equation 2-2 and Equation 2-3

$$\text{Plasmid Mass (µµg)} = 0.1 \; x \; Plasmid\ Concentration(\mu g ml^{-1})$$

$$\text{Pellet Mass (g)} = \left(\frac{5}{Optical\ Density}\right) x \left(\frac{Wet\ Cell\ Weight}{1000}\right)$$

$$\text{Specific Yield (µµg}^{-1}) = \left(\frac{Plasmid\ Mass(\mu g)}{Pellet\ Mass(g)}\right)$$

$$\text{Volumetric Yield (mgL}^{-1}) = Specific\ Yield(\mu g g^{-1}) \; x \; WCW$$

Equation 2-2 Equations used to calculate the specific and volumetric yield from the value of plasmid concentration obtained from inputting the HPLC peaks areas into the respective calibration curves.

$$Plasmid\ Copy\ Number = \frac{Copies\ of\ Plasmid}{Number\ of\ Cells}$$

$$5\ Optical\ Density\ Units = 2.5x10^{9}\ cells$$

$$Copies(moles)\ of\ Plasmid = \frac{Plasmid\ Mass}{RMM}$$

$$1bp = 660Da$$

$$1Da = 1.66x10^{-24}$$

$$Plasmid\ RMM\ (gmol^{-1}) = (Plasmid\ Size(bp)\ x\ 660)\ x\ 1.66x10^{-24}$$

$$Moles\ of\ Plasmid = \left(\frac{Plasmid\ mass(\mu g)}{RMM}\right)/1x10^{6}$$

$$Plasmid\ Copy\ Number = \frac{Moles\ of\ Plasmid}{2.5x10^{9}}$$

Equation 2-3 Equations used to calculate the plasmid copy number progression during the fermentations from the plasmid concentration information.

2.5.11.3 Monitoring plasmid mass through downstream operations

Plasmid DNA progression was monitored through the downstream operations using the same HPLC assay. Samples were obtained from the streams outlined in Table 7-4. The peak areas produced were converted to plasmid concentrations using the calibration curves shown in Figure 9-27. Once the plasmid concentration had been determined a mass balance for plasmid could be constructed across the process using the volumes of the various streams. From each downstream run, duplicate samples were analysed for each stream.

2.5.12 Desalting samples for assays using PD-10 columns

During the downstream procedure, RNA removal was achieved through precipitation by the addition of 5M $CaCl_2$. This resulted in the final clarified lysate having a salt concentration of 1M, a salt level which was found to interfere with all the assays for plasmid, protein, RNA and gDNA quantification. To overcome this, Post-$CaCl_2$ and Permeate samples were desalted using PD-10 desalting columns (Amersham Biosciences, Buckinghamshire, UK). PD-10 columns are pre-packed, disposable columns containing Sephadex™ G-25 Medium for group separation of high (M_r > 5000) from low molecular weight substances (M_r < 1000) by desalting and buffer exchange.

A column was equilibrated by applying 25mL of TE buffer. To the equilibrated column, 2.5mL of either Post-$CaCl_2$ or Permeate sample was added and allowed to run-through by gravity feed. The large molecular weight compounds were then eluted by the addition of 3.5mL of TE buffer. The literature supplied with the columns claims that 95% recovery of large molecular weight species is achieved, with only 4% of the salt remaining. Because the compounds are loaded in 2.5mL and eluted in 3.5mL of volume, there is a dilution of 1.4 fold which was accounted for when mass balancing. The final salt concentration of the eluted material was ~28.5mmols a level in the acceptable range of all the assays.

2.5.13 BCA Protein assay

To quantify protein levels through the downstream process the BCA assay was performed on all the streams. Assay materials were all contained within the Pierce Scientific BCA Protein Assay kit (Perbio Science, Northumberland, UK). The BCA assay, as opposed to the Lowry method, is a detergent compatible formulation based on bicinchoninic acid (BCA) for the colourimetric detection and quantification of total protein. The method combines the reduction of Cu^{2+} to Cu^{+} by protein, which occurs in an alkali environment (the biuret assay), with the selective and sensitive colourimetric detection of Cu^{+} using a proprietary reagent containing BCA (Smith *et al.*, 1985). The reaction produces a purple colouration being the result of a Cu^{+} cation chelating with two molecules of BCA. This complex exhibits strong absorbance at 562nm which is linear over a working range of 20 to 20,000μgmL^{-1}. The absorbance of the unknown samples was determined by calculation from a calibration curve prepared from supplied Bovine Serum Albumin (BSA).

Samples from the downstream operations were removed from -70°C cold storage and defrosted. A fresh vial of BSA solution (2mgmL-1) was opened and diluted by serial log_2 dilution in sterile sarstedt tubes using sterile PBS, in order to form a standard curve; 2/ 1/ 0.5/ 0.25/ 0.125/ 0.0625/ 0.03125/ 0$mgmL^{-1}$. To a 96-well plate[1] (Fisher Scientific, Loughborough, UK) triplicate 25µL volumes of each of the standards was pipetted. In a sterile Falcon tube, 50mL of the supplied Regent A was mixed with 1mL of Reagent B to form the working solution (2.4.1.12). Each of the unknowns was diluted to form three different dilutions all within the acceptable linear range of 20-20,000μgmL^{-1}. Three dilutions were used to improve assay accuracy and the specific dilutions chosen depended on the level of contaminating compounds present in the different streams. Table 2-7 details

[1] Corning® 96 Well Clear/ Flat Bottom/ Polystyrene/ TC-Treated Microplate/ Individually Wrapped/ Sterile/ with Lid

the dilutions chosen for each feed stream and the reasons why whilst Figure 2-2 shows the plate template used. (Pierce Scientific, 2006; Brown *et al.*, 1989)

Table 2-7 Table depicting the concentrations of components reported to effect the BCA assay. The concentrations were determined by calculating the dilutions of the components that occurs when the lysis buffers were combined, knowing their original concentrations. Concentrations of components in desalted samples were calculated by assuming 4% of original component remained from the original solution and accounting for 1.4x dilution achieved by desalting. The dilutions chosen had to decrease the level of the contaminating component to below the acceptable limit whilst maintaining the protein concentration within the linear range of 20-20,000µg/mL. All dilutions used 1xPBS (0.1M Phosphate; 0.15M NaCl levels which are perfectly compatible with the assay). Figures in bold highlight contaminant levels in the feedstream which were above the acceptable limit. The dilutions employed removed this contaminant levels to below the limit.

Feed Stream	Component	Concentration In Undiluted Feed (mM)	Acceptable Limit (mM) In Final Assay Solution	Dilutions Employed*
PRE-LYSIS	Tris EDTA	10 1	100 4	1x 2x 5x
PRE-$CACL_2$	Tris EDTA Dextrose Sodium hydroxide Potassium acetate SDS	6.5 2.6 14.3 100 730 17	100 4 4 40 160 68	2x 5x 10x
PD-10 POST-$CACL_2$ (samples desalted by PD-10 column)	Tris EDTA Dextrose Sodium hydroxide Potassium acetate SDS Calcium chloride	6.5 2.6 0.41 2.9 20.9 0.49 28.5	100 4 4 40 160 68 4	1x 2x 5x
PD-10 PERMEATE (samples desalted by PD-10 column)	Equivalent to Post-$CaCl_2$	See above	See above	1x 2x 5x
DIAFILTRATE 1 (represents a 1:20 dilution of Post-$CaCl_2$)	Tris EDTA Dextrose Sodium hydroxide Potassium acetate SDS Calcium chloride	10 0.1 0.7 5 36.5 0.85 50	100 4 4 40 160 68 4	5x 8x 10x
DIAFILTRATE 2	Tris Sodium chloride	10 540	250 1000	1x 2x 5x
RECOVERED FRACTIONS	Tris Sodium chloride	10 540	250 1000	1x 2x 5x

All unknowns were diluted with PBS and 25µL of each of the dilutions was added in triplicate to the 96-well plate. To each well was added 200µL of the working reagent and

* Dilutions employed must be multiplied by factor eight to reach the final dilution factor since 25µl of diluted unknown was added to 200µl of working reagent.

the plate was covered with an adhesive plate cover and incubated at 37°C for 30mins. The plate was removed from the incubator and left to stand for 5 minutes to cool to room temperature. The plate was read at 562nm using a SpectraMax 190 Microplate reader (Molecular Devices, Wokingham, UK) using the attached SoftMax Pro software. The software was instructed as to the layout and dilutions of the samples on the plate and so automatically plotted the standard curve using Quadratic fit, calculated the mean value of the triplicate wells and corrected for the dilutions and so returned the value of the protein in the original solution. The software also calculated the %CV and standard deviation enabling quantification of assay precision and accuracy.

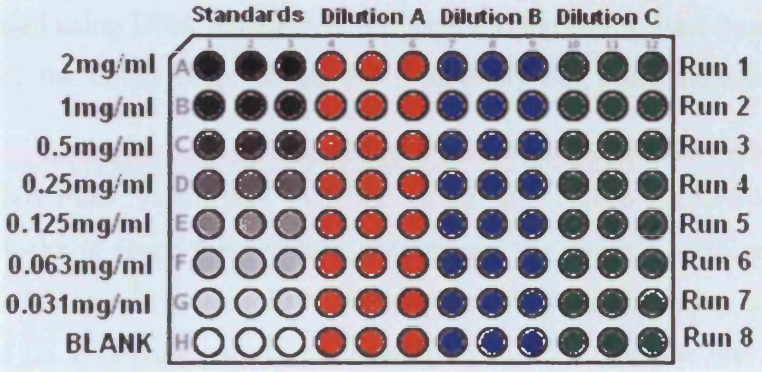

Figure 2-3 Schematic displaying the plate template used to assay the same one process stage sample (e.g.pre-$CaCl_2$) from 8 runs for total protein concentration, using the BCA assay. Each process stage sample (pre-lysis, pre-$CaCl_2$, post-$CaCl_2$, permeate, diafiltrate 1, diafiltrate 2, retentate, wash 1, wash 2) from each of the 24 runs was diluted to form three differing dilutions, each of which was assayed in triplicate. The average of each triplicate was returned as a separate concentration value and the average of each of these values, from each dilution set, was taken as the final value.

In order to track the removal of contaminating *E.coli* genomic DNA through the downstream process, it was necessary to purify the total genomic DNA from samples taken at stages during the process, allowing for their quantification by quantitative PCR. This was achieved using a MagNA Pure LC system (Roche Diagnostics, East Sussex, UK). More detail into the background of the assay is provided in 4.7 .

The MagNA pure system is robotically automated and capable of isolating the total DNA from 32 samples simultaneously (equating to 16 duplicate samples). The system was used in conjunction with Roche's proprietary extraction technology, which binds the DNA to glass-magnetic particles, from which contaminants (proteins/ RNA/ salts etc) could be washed and then from which the nucleic acids could be eluted. The operation followed pre-programmed actions throughout to isolate the DNA, then loaded the purified DNA on

to a PCR plate with all the necessary components (primer/probes/dNTPs/polymerase) ready to insert into a ABI PRISM 7700 PCR cycler (Applied Biosystems, CA, USA) as 30µL reaction volumes. The minimal manual involvement and the physical enclosure of all the samples for preparation, massively reduced the potential of any contamination of the samples for analysis by free DNA, together with increasing the assay reproducibility. (Roche Diagnostics, 2006; Roche Diagnostics, 2004)

Samples analysed by qPCR were taken from Pre-lysis, Pre-$CaCl_2$, Retentate, Wash 1 and Wash 2 streams. Analysis of these samples would allow the construction of a partial mass balance for gDNA across the plasmid recovery process. Although not a full mass balance the information provided would be useful in describing the main steps where gDNA is removed and give values as to the final levels of contamination. The MagNA pure system was operated using DNA Isolation Kit 1 (Roche Diagnostics, East Sussex, UK). The exact contents of the buffer preparations are proprietary but some indications are outlined in 2.4.1.19.

The MagNA Pure system was switched on an hour before use to allow the cooling and heating blocks to reach temperature. Before use the internal surfaces were wiped down with RNA/DNAzap®(Ambion Ltd., Huntingdon, UK) and following use the UV lamp was left turned on to degrade any contaminating DNA. The machine was instructed that total DNA was to be extracted from the samples using the Total DNA Kit 1(Roche Diagnostics, 2004) and that the purified DNA should be eluted in 100µL volumes of the elution buffer. Because 100µL volume of sample was purified and eluted in 100µL of elution buffer, meant no dilution occurred. The program used for extraction was DNA I Blood_Cells Fast.blk. This program uses the minimum lysis time. Since all the DNA in the samples was free in solution no lysis was really required but the lysis operation also places the samples in the correct buffer for binding to the MGPs.

For each extraction, 15 samples were processed in duplicate, meaning samples (Pre-lysis/ pre-$CaCl_2$/ retentate/ wash 1 and wash 2) from three 50g preps could be processed simultaneously. Samples were removed from cold storage and defrosted. In a DNA-free hood, duplicate 100µL volumes of sample were pipetted into separate wells of a 32-well sample cartridge, which was then covered with an adhesive plastic cover and placed in the cooling block of the MagNA pure machine ready for processing (1). The identity of the samples in each of the wells was entered into the PC. From Figure 2-5 it is possible to see the arrangement of samples as they were when loaded into the MagNA pure in a 32-well

sample cartridge. Following processing the eluted samples were arranged in the same pattern, in a 32-well sample cartridge placed in cooling block (9), as they were when loaded. From here 3µL volumes were pipetted into separate wells of a PCR, also shown.

The master mix buffer and primer/probe mix (2.4.1.20) were combined in a DNA-free facility to prevent any background contamination. 1450µL of 2x Master Mix buffer (Applied Biosystems, CA, USA) was mixed with 1160µL of Primer/Probe mix in a sterile bijou and vortexed. This solution was aliquoted in 1300µL volumes into two sterile sarstedt tubes and placed in the cooling block of the MagNA pure system.

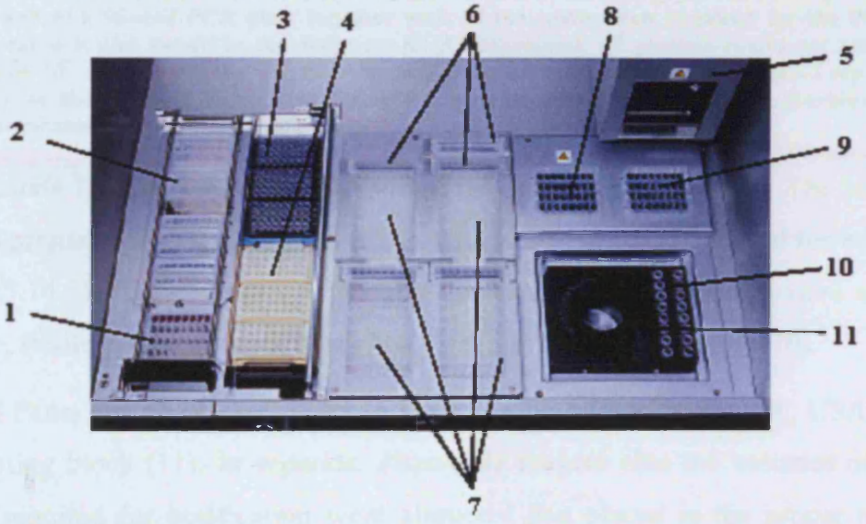

Figure 2-4 Picture (overleaf) displaying the setup and arrangement of the MagNA Pure LC system. All is enclosed in a DNA-free hood to reduce contamination. Duplicate 100µl volumes of 15 raw process samples and 1 duplicate sample of sterile water are loaded in a 32-well sample cartridge and placed in the cooling block (1). All buffers for purification and the magnetic-glass beads are placed in separate buffer cartridges and correctly positioned in their racks (2). The robotic arm (5) uses disposable pipette tips of two sizes; blue > 200µl (3) and yellow <200µl (4) for the processing. Tips are rested between different functions in tip-rests (6). Washing steps occur in the four 64-well processing cartridges (7). Heating is used to promote elution of DNA from the magnetic-glass particles in a sample cartridge contained in a heating block (8). Once eluted the DNA is transferred to a cooling block (9). The purified DNA is now ready to be loaded on to the PCR plate positioned in a cooling block (11). Duplicate 3µl volumes of each of the DNA samples in the 32-well elution cartridge, in cooling block (9) are transferred to known positions on the PCR plate (11). The sarstedt tubes containing six known concentrations of *E.coli* gDNA (10^6-10^1 copies/3µl), which form the standard curve, are positioned in the cooling block (10). Triplicate 3µl volumes of each of these are then pipetted into precise wells on the PCR plate (11). As a control, triplicate 3µl volumes of sterile water from a sarstedt tube in cooling block (10) are also added to the plate. Finally, the MagNA pure aliquots 27µl volumes of the pre-combined master mix buffer/primer+probe mixture (located in 2 sarstedt tubes positioned in cooling block (10)) into each well of the PCR plate. The process is now complete and the plate placed into the cycler.

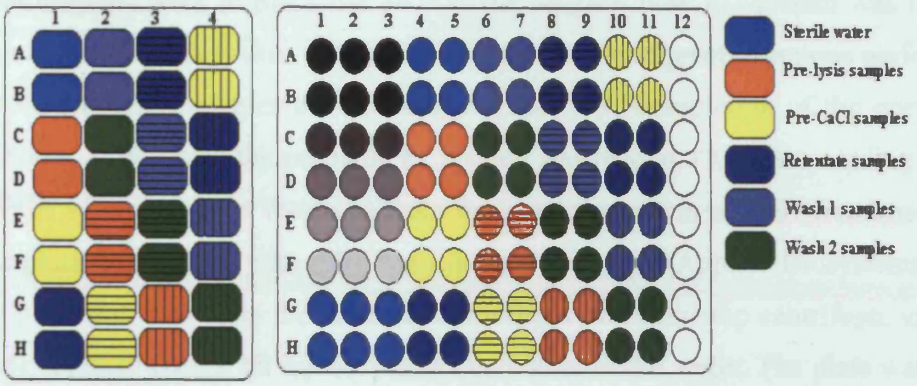

Figure 2-5 Schematic displaying the arrangement of samples on the MagNA Pure plates. Samples from three 50g runs were processed simultaneously. The colours represent the different sample types and the horizontal/vertical lines represent the three different runs. 100µl volumes of duplicate raw samples from each run were loaded into the sample cartridge. These were processed by the MagNA pure system and eluted in 100µl volume so no dilution occurred. Duplicate 3µl volumes of each of the processed samples was loaded into a separate well of a 96-well PCR plate together with all the components required for the PCR reaction. The standard curve is also shown in the diagram; A1-A3 represents 10^6 genome copies per well down to F1-F3 representing 10^1 copies per well. Sterile water was included as a control. Well G&H1-3 represent the value 0 copies/well on the standard curve, whilst A&B4-5 were actually processed by the machine and included to record ant contamination during processing

In a separate facility the *E.coli* gDNA standard curve was aliquoted. The standard curve was pre-prepared so that the same batch of standard material was used for every PCR run (er to 2.5.14.1). 15µL volumes of each of the standard curve samples were aliquoted into separate, sterile 1.5mL sarstedt tubes and placed in the cooling block (10).

An ABI PRISM optical 96-well reaction plate (Applied Biosystems, CA, USA) was placed into cooling block (11). In separate, disposable reagent tubs the volumes of each of the buffers required for purification were aliquoted and placed in the proper rack (2). The details of these buffers are outlined in Table 2-8.

Table 2-8 Table detailing the volumes of the various buffers used by the MagNA Pure LC system during processing and their functions. The buffers are described in the order in which they are used and the volume of each which was aliquoted into individual disposable reagent tubs.

BUFFER	VOLUME (ML)	FUNCTION
Lysis/ Binding Buffer	12	Lyses cells/ denatures proteins and promotes binding of DNA
Proteinase K	Lyophilised powder; dissolved by vortexing in 4mL of Elution buffer	Digests proteins
Magnetic Glass Particle Suspension	Provided in bottle as 5mL. Vortexed to resuspend	Solid Phase Matrix for binding DNA
Wash Buffer 1	40	Removes unbound substances; proteins (nucleases)/ membranes/ inhibitors (heparin)
Wash Buffer 2	40	Removes chaotropic salts and some proteins
Elution Buffer	20	Elution of DNA/ resuspending Proteinase K and tip washing

Once all the reagents were in place the door to the MagNA pure LC system was locked and through the attached software, the run was initiated. The sequential actions performed by the system to purify samples are detailed in Table 2-9. Completion of the operation took three hours, after which the prepared PCR plate was held at 4°C in the cooling block (10). The PCR plate was then removed from the machine and in a DNA-free hood, the wells of the plate were sealed with ABI PRISM optical strip caps (Applied Biosystems, CA, USA). The plate was then spun for 1minute at 1000rpm in a benchtop centrifuge, using a 96-well plate rotor, to ensure all liquid was at the bottom of the wells. The plate was now loaded into the PCR cycler (2.5.15)

Table 2-9 Table outlining the sequence of actions carried out by the MagNA Pure LC system. This sequence of events occurs after the machine has been initiated. More details of the exact program the MagNA pure system follows are outlined in the program supplied with the software; DNA I Blood_Cells Fast.blk

STEP	ACTIONS PERFORMED BY THE MAGNA PURE LC INSTRUMENT
(0)	Dispensation of all necessary reagents into the processing cartridges (7)
(0)	Dispensation of the Elution Buffer into the heated Elution Cartridge (8) to equilibrate
1	Mixing of 300µL of Lysis/Binding buffer with the samples (1)
2	Addition of 100µL of Proteinase K to each sample, mixing and incubation (1)
3	Addition of 150µL of MGP suspension/ mixing/ incubation and separation (1)
4	Transfer of MGPs to 850µL of Wash buffer 1, mixing and separation (7)
5	Transfer of MGPs to 450µL of Wash buffer 2, mixing and separation (7)
6	Transfer of MGPs to 450µL of Wash buffer 2, mixing and separation (7)
7	Transfer of MGPs into heated Elution Buffer (Heating block)(8) mixing, incubation, elution of DNA in 100µL
8	Transfer of 100µL eluate to the Storage cartridge (Cooling Block) (9)
9	Transfer of duplicate 3µL volumes of each processed sample to an individual well on the PCR plate (11)
10	Transfer of triplicate 3µL volumes of each standard curve sample to a individual wells on PCR plate (11)
11	Addition of 27µL of Primer/ Probe mix to each well on the PCR plate. Cooled. (11)

2.5.14.1 Preparing E.coli Genomic DNA standard curve

Due to the nature of the software used by the PCR cycler (Applied Biosystems, CA, USA) the standard curve for the measurement of contaminating genomic *E.coli* DNA used copies/well as the unit. The standard curve employed, consisted of six-points; $1x10^6$ genome copies/well down to $1x10^1$ genome copies/well, created by $\log_{10}$ dilution of the starting material in water (Figure 4-31). Conversion of the copies/well into a mass based concentration figure used the equations shown in Equation 2-5. From the calculation it can be seen that the highest standard point used of $1x10^6$ copies/ well required an *E.coli* genomic DNA stock of $1.7\mu gmL^{-1}$.

$$\begin{aligned}
Size\ of\ E.coli\ genome &= 4.64x10^{6}\ bp \\
1bp &= 660Da \\
1Da &= 1.6605x10^{-24}\ g^{\otimes} \\
\therefore dsDNA &= 1.096x10^{-21}\ gbp^{-1} \\
Mass\ of\ E.coli\ genome &= 4.64x10^{6}\ x\ 1.096x10^{-21} \\
&= 5.087x10^{-15}\ g\ copy^{-1} \\
1st\ standard\ curve\ pt &= 1x10^{6}\ copies/well \\
&\because 3\mu l\ of\ standard/sample\ injected\ per\ PCR\ well \\
&\therefore standard = 0.33x10^{6}\ copies/\mu l \\
&= 0.33x10^{6}\ x\ 5.087x10^{-15} \\
&= 1.696x10^{-9}\ g\mu l^{-1} \\
&= 1.696\mu gml^{-1}
\end{aligned}$$

Equation 2-4 Calculation demonstrating the conversion of the values of genome copies to a mass based concentration value. PCR reactions commonly use copies as their basal unit and conversion to more applicable units uses commonly trusted values for *E.coli* genome size and base pair mass. (Blattner *et al.*, 1997) [⊗] Value obtained from National Physical Laboratory.

To prepare gDNA stocks, cultures of *E.coli* DH1 [F⁻ *rec*A1 *end*A1 *gyr*A96(Nal^{r}) *thi*-1 *hsd*R17 *sup*E44 *rel*A1] were grown on 50mL of seed media (2.3.1.5) contained in a 1L baffled Shake-flasks according to 2.1.3. The Shake-flasks were incubated overnight at 37°C and 230rpm in a shaking incubator (New Brunswick Scientific, NJ, USA).

1mL volumes of the cell suspension were transferred to sterile sarstedt tubes and centrifuged for 5 minutes at 13,000rpm. The supernatant was decanted and the pellet resuspended in 1mL of TE buffer by pipetting. The suspension was again centrifuged as before to pellet. The wash buffer was discarded and the pellet resuspended in 0.5mL of TE buffer.

To the suspensions were added 30µL of 10% SDS and 3µL of 20mgmL^{-1} Proteinase K. The tubes were mixed and incubated in a 37°C water bath for 1 hour. To the tubes was added 1 volume of 25°C phenol:chloroform (2.4.1.17) and the tubes gently agitated until an emulsion formed. The tubes were then centrifuged at 13,000rpm for 15 minutes in a benchtop centrifuge. The aqueous, top-layer was gently removed using a wide-bore Gilson to a fresh sarstedt tube and the process repeated two more times, until no interfacial layer could be seen. To the aqueous fraction, 1 volume of chloroform was added to remove any

phenolic traces and the tube re-centrifuged. Once more, the aqueous layer was removed to a clean tube and to it added 0.1 volumes of 3M sodium acetate and 2 volumes of -20°C 100% ethanol. The tube was mixed and left at -70°C for 1 hour. The tubes were then spun down at 13,000rpm for 15minutes. The supernatant was discarded and the pellets washed in 1mL of -20°C 70% ethanol. The tubes were then re-centrifuged as before and the supernatant discarded and the pellet left to air-dry for 10 minutes before being resuspended in 200µL of sterile water (Sigma, Dorset, UK) (Ausubel, 1987).

The stock solution was pipetted to shear the gDNA into smaller fragments before being quantified using the NanoDrop spectrophotometer. This stock solution was then diluted down with water to a concentration of $1.7\mu gmL^{-1}$ to form the first calibration. The remaining standards were created by $\log_{10}$ dilution of the top standard in water. The standards were then frozen at -70°C. To demonstrate the consistency of the new standard curve, samples were run in the PCR cycler against an existing standard curve and the C_t values produced compared 4.7.4

2.5.15 Quantitative Polymerase Chain Reaction (qPCR)

The technology described here is an automated kinetic PCR, which allows for real time quantification of target nucleic acids. More in depth information into the mechanism of the qPCR reaction can be found in 4.7. In brief, the approach involved the binding of a forward and reverse primer to the DNA sequence of interest as with traditional PCR (Saiki *et al.*, 1985a). Additionally included was a probe sequence specific to a region within the boundaries of the sequence set by the primers. Attached to the 5'end of the probe sequence was reporter dye (in this case FAM™) and to the 3'end a quencher dye (TAMRA™). The approach utilised the 5' exonuclease activity of *Taq* DNA polymerase to digest the probe region and so release the reporter dye away from the quencher dye so increasing its fluorescence. Accumulation of PCR products could then be monitored in real time by scanning the increase in fluorescence in the PCR wells using a PCR cycler coupled with a fluorescent plate reader; ABI PRISM 7700. (Fykse *et al.*, 2003; Heid *et al.*, 1996; Weissensteiner and Lanchbury, 1996)

The system was used quantitatively by using standards of known DNA concentration and recording the number of PCR cycles required to raise the fluorescence reading above a threshold value. The number of PCR cycles required to cross the threshold value is directly proportional to the starting concentration of DNA. The threshold cycle values (Ct) of the

standards were used to construct a calibration curve against which the unknowns could be plotted.(Holland *et al.*, 1991; Gelfand *et al.*, 1993) From Table 2-10 it can be seen that the total mass of *E.coli* gDNA in each of the standard wells starts from $5x10^{-9}$g/well down to $50x10^{-15}$g/well. Such a broad standard curve allowed the assaying of all the samples from the downstream process on an identical standard curve.

The PCR plate as prepared by the MagNA Pure LC instrument was inserted in the carousel of an ABI PRISM 7700 PCR cycler (Applied Biosystems, CA, USA). The reaction volume of each of the wells totalled 30µL. Table 2-10 details the breakdown of the final components in the PCR wells and Table 2-11 details the components of the Master Mix buffer and their individual functions.

Both primer and probe sequences were directed at a region of the single copy *E.coli* DNA polymerase gene. The primer sequences were about 20bp in length and probe sequence was a 27bp sequence covalently coupled to the two dyes; FAM™ and TAMRA™. Further details about the primer and probe sequences are recorded in Table2-12.

Table 2-10 Table describing the concentrations of the various components used in the PCR before they were diluted by the MagNA Pure during plate preparation and the final concentrations they existed in the PCR wells.

COMPONENT	INITIAL CONCENTRATION	COMPOUND DILUTION[2]	FINAL CONCENTRATION
Master Mix Buffer	2x	2	1x
Primers (Fwd and Rev)	500nM each	2.5	200nM
Probe	250nM	2.5	100nM
Genomic DNA Standards	$1.7\mu gmL^{-1}$ to $17pgmL^{-1}$	10	5ng to 50fg per well (10^6 to 10^1 copies/well)

[2] Compound dilutions calculated from reagent mixing. Since 1450µl of 2xMaster Mix added to 1160µl of primer+probe mix. Represents a 1.8x dilution for the master mix and a 2.25x dilution for primer probe mix. Both are then further diluted by the addition of 27µl of the mix to 3µl of sample/standard representing a 1.11x dilution. Samples and standards are diluted by a factor 10.

Table 2-11 Table detailing the components of the master mix buffer and their importance to the functioning of the quantitative polymerase chain reaction.

COMPONENT	FUNCTION
AmpliTaq Gold DNA Polymerase	Possesses 5'-3' nuclease activity but lacks 3'-5' exonuclease activity. It is a thermostable enzyme allowing hot start PCR, which reduced background signals normally created by amplification of non-target sequences before thermal cycling had begun.
AmpErase® uracil-N-glycosylase	Due to the enormous amplification possible, false positives can be created caused by amplicon carryover. This enzyme removes incorporated uracil bases reducing contamination
Deoxynucleosidetriphosphates (dNTPs)	dTTP/dGTP/dCTP/dATP/ dUTP at 200µM
Passive Reference Dye (ROXTM)	Does not interfere with reporter dye. Present to normalise fluorescence signals to correct for buffer or volume deviations.
Mg^{2+}	1.5mM; optimised for highest specific yield of target PVR product.

Table 2-12 (overleaf) Describes key features of the primers (forward and reverse) and the probe used to bind complementary regions of the *E.coli* DNA polymerase gene. The shortest amplicons are the most effective and 20bp-45bp is optimum. The GC content of the amplicons should be in the 40-80% range to avoid formation of internal structures. The melting temperature of the primers should be between 58 ° C to 60 ° C and the probes >68 ° C. The 5'end of the probe should not end in G. The probe strand sequence chosen should be the one with the hihest number of C residues and for all amplicons less than 2 G or C bases should comprise the last 5 bases of the 3'end. Information calculated by Primer Express software v1.5a (Dieffenbach C W *et al.*, 1995)

CRITERION	FWD PRIMER	REV PRIMER	PROBE
Length (bp)	20	19	27
GC content (%)	60	47	48
Melting Temp (°C) (50mM salt)	61.47	61.65	71.47
Molecular weight (fwd) Da	6118	5751	8188
Molecular weigh (rev) Da	6118	5863	8370
G on 5' end	N/A	N/A	NO
Strand with more C than G	N/A	N/A	YES
Less than 2 G or C bases in last 5 bases of 3' end	NO	YES	YES

The thermal cycler conditions were Stage 1: 50C for 2:00mins, Stage 2: 95°C for 10:00mins, Stage 3: 95°C for 0.15secs and then 60°C for 1:00mins, repeated 40 times. The software of the ABI PRISM was instructed as to the identity of the wells on the plate, since the plate outline was always as shown in Figure 2-5 a template was used. The threshold value was set at $0.04\Delta R_n$ and the baseline to be taken as the average fluorescence of all wells between cycles 3-13. The software then plotted the standard curve of starting DNA quantity against threshold cycle as shown in Figure 4-31, against which it calculated the

starting quantities of all the unknowns. The software took the average figure of the quadruplicate samples and returned the data as genome copies/well as shown in (Figure 9-28). To convert the copies per well value into μgmL^{-1} of the initial sample material the data was pasted into Excel and the following formula applied.

$$DNA\ mass\ \left(\mu gml^{-1}\right) = \left(\frac{(Copies\ /\ well)\ x\ 1000}{3}\right) x\ \left(5.087x10^{-9}\right) x\ Correction\ Factor$$

Equation 2-5 Relationship used to convert the values of DNA mass presented by the software in terms of copies per well into the more standard mass-based figures.

2.5.16 Quant-IT RNA assay

The progression of RNA removal was tracked through the downstream process using the Quant-IT™ RNA assay kit (Molecular Probes, Leiden, Netherlands). More background into the nature and development of the assay is given in 4.8. This assay was very similar to the PicoGreen assay in its design and operation. The RNA specific dye becomes intensely fluorescent upon binding RNA. The assay has been demonstrated to be highly selective toward RNA over dsDNA (Molecular Probes Inc, 2006) and the fluorescence signal produced is linear with RNA over a range of 5ng to 100ng per well (0.5-10μgmL^{-1} starting material).

All assays were performed in BD-Falcon™ 96-well polystyrene plates (clear/flat-bottomed/ 370µL total vol.) and based upon the method as described by the enclosed literature (Molecular Probes Inc, 2006). The fluorescence was calculated by calibrating against a standard curve of solutions of known RNA concentration. The *E.coli* rRNA standards were provided in the kit. Samples from each stage of the DSP were removed from -70°C cold storage and defrosted. Each sample was diluted to form three different dilutions. Dilutions were chosen to ensure the signal produced fell within the range of the standard curve and also to remove the possibility of any contaminating substances interfering with the signal (Table 2-13). Triplicate 10µL volumes of each of the three dilutions made from each process sample were loaded into separate wells of the 96-well plate as shown in Figure 2-6. Triplicate 10µL volumes of the 8 provided standards (0, 0.5, 1, 2, 4, 6, 8 and 10μgmL^{-1}) were also included on the plate.

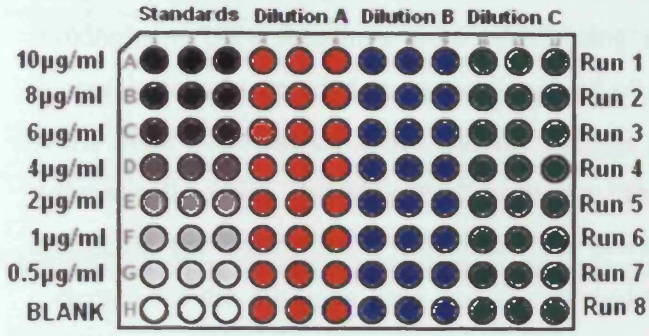

Figure 2-6 Schematic displaying the plate template used to assay the same one process stage sample (e.g.pre-$CaCl_2$) from 8 runs for RNA concentration, using the Quant-IT RNA assay. Each process stage sample (pre-lysis, pre-$CaCl_2$, post-$CaCl_2$, permeate, diafiltrate 1, diafiltrate 2, retentate, wash 1, wash 2) from each of the 24 runs was diluted to form three differing dilutions, each of which was assayed in triplicate. The average of each triplicates was returned as a concentration value and the average of each of these values, from each dilution set, was taken as the final value.

Immediately prior to use, the Quant-IT ™ working solution was prepared as outlined in 2.4.1.13. Using a multiwell Gilson® pipette 200µL of the working solution was added to each well of the plate. The plate was then wrapped in aluminium foil and incubated in the dark for 5 minutes.

Table 2-13 RNA concentration of diluted sample must fall between 1 and 10µgmL^{-1}. Table shows the components and their concentrations in the different streams which underwent analysis. The table also shows the dilution used to dilute away any interfering effects these components mat have had.

FEED STREAM	COMPONENT	CONCENTRATION IN UNDILUTED FEED (mM)	ACCEPTABLE LIMIT (mM) IN 10µL SAMPLE	DILUTIONS EMPLOYED
PRE-LYSIS	Tris EDTA	10 1	N.S N.S	4x 10x 20x
PRE-$CACL_2$	Potassium acetate SDS	730 17	200 6.9	100x 200x 400x
PD-10 POST-$CACL_2$ (samples desalted by PD-10 column)	Potassium acetate SDS Calcium chloride	20.9 0.49 28.5	200 6.9 40	5x 10x 20x
PD-10 PERMEATE (samples desalted by PD-10 column)	Equivalent to Post-$CaCl_2$	See above	See above	5x 10x 20x
DIAFILTRATE 1 (represents a 1:20 dilution of Post-$CaCl_2$)	Potassium acetate SDS Calcium chloride	36.5 0.85 50	200 6.9 40	4x 5x 10x
DIAFILTRATE 2	Sodium chloride	540	200	4x 5x 10x
RECOVERED FRACTIONS	Sodium chloride	540	200	4x 5x 8x

The plate was read using a Gemini EM Microplate SpectroFlurometer (Molecular Devices, Wokingham, UK). Readings were taken using a Excitation wavelength of 644nm and fluorescence was recorded at a wavelength of 673nm with a cut-off of 665nm. Each well of the plate was read six times and the average taken. The data analysis was processed automatically using SoftMax Pro® software. The software plotted the standard curve, subtracted the background, calculated the RNA concentration of the unknowns and corrected for the dilutions used and so returned the value for RNA concentration of the nascent sample. The software also gave the standard deviations and %CV values of the recordings made.

2.5.17 Conventional Agarose gel electrophoresis

In some applications, typically cloning procedures, it was necessary to run plasmid samples by conventional agarose gel electrophoresis, even though this technique was not suitable for visualising and sizing large constructs. Depending on the separation required the agarose concentration used varied between 0.6-1.0% (w/v). For cloning purposes 1xTAE buffer was used, otherwise 1xTBE was standard. Between 0.6g and 1.0g of agarose (Sigma, Dorset, UK) was added to the selected buffer in a conical flask and dissolved by boiling. After cooling to around 60°C, agarose was poured into casting trays and the wells formed using combs containing the appropriate number of teeth. Once set, the casting blocks were removed and the gel placed in the electrophoresis chamber. The gel was then submerged in the appropriate buffer and the electrodes connected. Samples for analysis were prepared as described in 2.5.5. 0.6-0.8µg of plasmid was loaded into each well in loading buffer. Electrophoresis conditions varied depending on the level of separation required but fell between 100V running for 2 hours down to 15V running overnight. (Sambrook *et al.*, 1989; Ausubel, 1987)

2.5.18 Pulsed Field Electrophoresis (PFGE)

This technique is capable of separating megabase sized DNA molecules and as such had a slightly more complex methodology. More detail on the nature of this assay can be found in 4.6.2. PFGE was carried out in a CHEF-DR II system (Bio-Rad Laboratories, Herts, UK). Gels were cast as 1.0% (w/v) solutions of Pulsed-Field certified agarose (Bio-Rad Laboratories, Herts, UK) by dissolving 3.5g of agarose in 350mL of 0.5xTBE. The agarose was dissolved by boiling and allowed to cool prior to pouring the solution into the

supplied gel frame. Once the gel had solidified, 0.8-1.0μg samples of plasmid for analysis (2.5.5) were loaded onto the gel in 0.8% (w/v) low-melting point (LMP) agarose. Size standards used were Mid-Range I and II PFG markers (New England Biolabs, Herts, UK).

A fresh 2L volume of pre-chilled 0.5xTBE was added to the electrophoresis chamber and the loaded gel submerged in the chamber. The buffer was circulated at speed 70 on the supplied pump and the temperature of the buffer maintained at 14°C by the chiller. Running conditions varied depending on the operation but typically were; Run time: 22hrs, Initial switch time of 50s, Final switch time of 90s, Fixed angle of 120° using a $6Vcm^{-1}$ gradient. After running the gel was removed to stain. (Barton *et al.*, 1995; Carle *et al.*, 1986; Clark *et al.*, 1988; Fangman, 1978; Hightower *et al.*, 1987; Levene and Zimm, 1987; Olson, 1989; Wang and Lai, 1995)

2.5.19 Field Inversion Gel Electrophoresis

This technique is a derivative of PFGE with the only exception being the angle of field inversion. In PFGE, separation of larger DNA species is possible because the electric field can switch at 120° intervals, with FIGE the angle of inversion is fixed at 180°. More detail into the background of this assay is provided in 4.6.2.2. A FIGE Mapper Electrophoresis System (Bio-Rad Laboratories, Herts, UK) was used. The agarose gel was prepared in an identical fashion as described in 2.5.18. Also as above, 0.8-1.0μg of plasmid samples were loaded into the gel in 0.8%(w/v) LMP agarose. Size standards employed included; 2.5kb ladder, 5kb ladder, 8-48kb ladder and Lambda DNA standard (Bio-Rad Laboratories, Herts, UK).

2L of fresh, chilled 0.5xTBE buffer was added to the electrophoresis chamber and circulated at ~$750mLmin^{-1}$ (~70 on supplied pump). Electrophoresis was carried out in a 4°C cold-room to improve resolution of the separated bands. Running conditions again varied but typically were; Run time 40hrs, Forward Voltage 180V, Reverse Voltage 120V, Switch time 0.1-3.5secs increasingly linearly over run time. After running the gel was removed to stain. (Carle *et al.*, 1986)

2.5.20 Staining with SYBR Gold

All gels were stained with SYBR-Gold (Molecular Probes, Leiden, Netherlands). There are a number of advantages in the use of SYBR-Gold over traditional Ethidium bromide for gel staining (4.2.3). Unlike EtBr it does not bind plasmid isoforms differently. (Even-Chen and Barenholz, 2000). Also, it is considerably more sensitive having a much lower limit of detection. This is because it exhibits a 10,000 fold increase in fluorescence upon binding nucleic acids, rather than a corresponding 30-fold increase witnessed with EtBr.(Tuma *et al.*, 1999; Le Pecq and Paoletti, 1966)

The gel was placed in a foil covered Tupperware box to which was added 300mL of 0.5xTBE and 30µL of SYBR-Gold Reagent (1:10,000 dilution). The gel was left to stain for ~24hours on a platform shaker in a 4°C cold-room. Following staining the gel was destained in an equivalent volume of distilled water for 1 hour, to improve contrast.

2.5.21 Quantitative Gel analysis

Gels were scanned using a GelDoc-It Imaging system (Ultraviolet Products, Cambridge, UK). Excitation at 480nm and emission of 530nm were used with an exposure time of 10-30s, depending on detection level. Band quantification was performed using LabWorks 3.0 software.

2.6 Cloning and cell line development methods

2.6.1 Enzymatic manipulation

Restriction digests and other DNA modifications were carried out using the conditions recommended and buffers supplied by the enzyme manufacturers; Promega, Madison, USA, New England Biolabs, Herts, UK. Typical plasmid digests were performed using 1μg of DNA, using 10units of restriction enzyme, in a total volume of 20μL with 2μL of 10x buffer, as supplied with each enzyme. Reaction mixtures were incubated at 37°C for 2 hours in a waterbath. Dephosphorylation of linearised vectors was achieved by the addition of 0.1 Units of Shrimp Alkaline Phosphatase (New England Biolabs, Herts, UK) per pmol of DNA and incubation at 37°C for 30 minutes.(Sambrook *et al.*, 1989; Ausubel, 1987)

2.6.2 Insert preparation

Large DNA fragments for insertion into pGEM11 were prepared in three ways, either by partial digestion of *Saccharomyces cerevisiae* DNA (Promega, Madison, USA) by *HindIII* or complete digestion by *NotI*or by digestion of the BAC p5176 by *NotI* to release the 112kb fragment. (Tao and Zhang, 1998; Hong-Bin Zhang *et al.*, 1995). More information on the precise procedure is outlined in 5.3.2. Duplicate samples of the digested fragments were then run on a 0.8%(w/v) Low-melting point agarose gel using conditions outlined in 2.5.19. Following electrophoresis, the marker lane (MidRange PFG marker 1, New England Biolabs, Herts, UK) was cut from the gel and stained using SYBR Gold. The marker lane was then visualised under an UV transilluminator and the migration distances of the various size fragments recorded.

The areas of the gel lanes containing the digested DNA fragments of interest were excised using a scalpel, placed in separate eppendorf tubes and dialysed overnight at 4°C in 1xTE+30mM NaCl. The gel slices excised ranged from 30-85kb in 5kb increments for the *NotI* digestions, 15-65kb in 5kb increments for the *HindIII* digestions and 112kb for the p5176 digestions. The dialysis buffer was removed and replaced with 2 x gel volume (~100μL) of 1xβ-agarase buffer and left on ice for 30 minutes. This step was repeated twice more. Each of the gel slices was then melted by heating to 65°C in a heating block and then transferred to a 42°C waterbath to equilibrate before 3 units of β-agarase (New England Biolabs, Herts, UK) was added to each eppendorf. The slices were left at 42°C for

2 hours for the LMP agarose to be completely digested. On removal from the waterbath the tubes were incubated on ice for 15 minutes to coagulate any carbohydrate fragments remaining and spun at 13,000rpm for 2 minutes in a benchtop centrifuge.

The solutions of large DNA fragments were then quantified by running 20μL of each on a conventional 0.6% gel at $6Vcm^{-1}$ for 2 hours. The gel was stained in SYBR Gold overnight and destained for 1 hour in 0.5xTBE. The gel was scanned and the software calculated the mass of DNA in each of the wells by comparing the image intensity to bands contained in three standard lanes. From the mass calculations the concentrations could be determined.

2.6.3 Ligations

Ligations were prepared using a 5:1 molar ratio of vector DNA to insert DNA. The ligations were all based upon 50ng of insert DNA. More detail on the ligation preparations is shown in 5.3.4. Ligation controls were also prepared using linearised, phosphorlylated (-ve control) and dephosphorylated (+ve control). The prepared ligation mixtures were then heated to 56°C for 10 minutes to encourage ligation. The reaction mixtures were cooled to room temperature when 0.1 volumes of 10x ligation buffer and 2Units of T4 Ligase (New England Biolabs, Herts, UK) were added to each. The ligation mixtures were then incubated at 4°C overnight. The lowered ligation temperature having been shown to aid ligation of large fragments (Promega, 2005).

2.6.4 Electroporation

Ligation products were electroporated into ElectroMAX DH5α-E cells (Invitrogen, Paisley, UK) to increase the chance of successful transformation and capture of any large plasmids created. Cells were removed from -70°C storage and defrosted on ice. 1μL of ligation mixture was added to an ice-cold, sterile sarstedt tube and mixed with 20μL of cells using a cold Gilson pipette tip and left on ice for 1 minute. The mixture was then pipetted into a chilled 0.1cm electroporation cuvette (Bio-Rad Laboratories, Herts, UK) making sure both electrode plates were contacted. Electroporation was achieved using a MicroPulser™ (Bio-Rad Laboratories, Herts, UK). Electroporation conditions adopted were as described by (Sheng *et al.*, 1995) and were $13kVcm^{-1}$(1.3kV across 0.1cm) using a 10μF capacitor, which decayed with an exponential waveform time constant of 5ms.(Bio-Rad Labs., 2003)

Immediately following pulsing, 0.9mL of pre-warmed SOC media was added to the cuvette. The contents were then transferred to a sterile sarstedt tube and incubated at 37°C for 2 hours and 230rpm in a shaking incubator (New Brunswick Scientific).

2.6.5 Recombinant selection and sizing

The SOC broth containing the transformants was serially diluted by $\log_{10}$ dilution in sterile PBS buffer. 100µL of neat broth and on separate plates, 100µL of 1:10 diluted broth was plated out on to selective, 100µgmL^{-1} ampicillin plates. On each 100mm diameter TSA plate, had been spread 40µL of 50mgmL^{-1} 5-bromo-4-chloro-3-indoyl-β-galactopyranoside (X-Gal) and 4µL of 200µgmL^{-1} isopropyl-B-D-thiogalactopyranoside (IPTG) to allow blue/white colony screening. When recording transformation efficiency, 100µL volumes of 1:10^5 and 1:10^6 diluted broth samples were plated onto non-selective TSA plates. All plates were incubated at 30°C in a benchtop incubator for over 24 hours, after which time the recombinants were counted and efficiencies of transformation were calculated using the equations described in Equation 2-6.

$$Transformant\ Ratio = \left(\frac{(CFU\ on\ selective\ plate)\ x\ dil.factor}{(CFU\ on\ non-selective\ plate)\ x\ dil.factor} \right) x100\%$$

$$T.efficiency\ (CFU\ /\ \mu g) = \left(\frac{CFU\ on\ selective\ plate}{Mass(pg)\ of\ pDNA\ used} \right) x \left(\frac{1x10^6\ pg}{\mu g} \right) x \left(\frac{vol.\ of\ transformants(\mu l)}{vol.\ plated} \right) x\ dil.factor$$

Equation 2-6 Different equations used to determine the transformation efficiency of electroporation procedures

White colonies from the selective plates were picked off using a sterile inoculum loop and streaked on to separate, selective TSA plates. These were incubated for over 24 hours at 30°C. From these plates colonies were picked and used to inoculate 5mL of sterile, seed media containing 100µgmL^{-1} ampicillin in universal bottles. These were incubated at 30°C and 230rpm in a shaking incubator for 16 hours. Duplicate 1mL samples of each of the cultures were spun down in a benchtop centrifuge and the plasmid extracted as described in 2.5.5. The plasmid samples were then run by FIGE to size the constructs.

2.6.6 Preparing electrocompetent cells

All large constructs created were transformed by electroporation into GSK's host cell line *E.coli* DH1. Electrocompetent cells were produced by inoculating 100mL of seed medium, in a 1L baffled Shake-flask, with 1 vial of DH1 working cell bank stock. The flask was incubated at 37°C for ~4hrs and harvested when the optical density reached 1.5. The resulting broth was recovered into a 250mL sterile Falcon tube and incubated on ice for 1 hour. The cells were then spun down at 4°C in a Sorvall Legend RT Tabletop centrifuge at 20,000g for 20 minutes. The supernatant was poured off and as much of the media remnants removed using a tissue swab. The cells were then washed by resuspending in 100mL of ice-cold 10%(v/v) glycerol. The cells were then re-centrifuged. The washing process was repeated twice more. Finally, the cells were resuspended in 500µL of 10%(v/v) glycerol and aliquoted into an ice-cold cryovial and stored at -70°C. Throughout the entire process the cells were constantly maintained at a temperature as close to freezing as possible by incubation on ice. (Sheng *et al.*, 1995; Siguret *et al.*, 1994). The cells were then electroporated together with the large constructs isolated from the previous step.

2.6.7 Cell Banking

Cells having undergone electroporation and so contained a known large plasmid were isolated on selective TSA plates (100µgmL^{-1} ampicillin). These colonies were then used to create a working cell bank. Single colonies were picked off and used to inoculate 5mL of media in a sterile universal. Cells were incubated at 30°C, 230rpm overnight and used as a seed culture to inoculate 50mL of sterile selective media in a 1L baffled Shake-flask to 0.1OD. Shake-flasks were incubated until the optical density fell between 2.5-3.0 (early log-phase). The flasks were removed from the incubator and 12.5mL of sterile 100% (v/v) glycerol was added to each. The cell suspension was then aliquoted in 1.8mL volumes into 2mL Nunc cryovials and stored at -70°C.

2.6.8 Plasmid stability assay

Following duplicate 4L fermentations of the selected large constructs, from which no plasmid could be isolated, stability studies were conducted on the large plasmid bearing strains. These consisted of cultivating the plasmid-bearing cells in 50mL of selective medium in 1L baffled shake-flasks over a 60 hour period, which required four passages of the cells to fresh, selective media. The conditions employed during the stability trials

(temperature, selective agent, concentration of selective agent and host cell line) varied in attempt to improve plasmid retention but the general methodology remained fixed. Refer to 5.6.1.

Two working cell vials of cells bearing each construct were removed from -70°C storage and defrosted. These were used to inoculate duplicate 50mL volumes of sterile, selective media to a starting OD ~0.1. The flasks were incubated at 230rpm and either 37°C, 30°C or 25°C in a shaking incubator. In a hood, samples of culture broth were removed at regular intervals over an eight hour period. The samples were used to determine optical density progression to measure growth rate and were also used to determine plasmid retention using the replica plate assay as outlined in 2.5.5. At the end of the eight-hour period, sufficient inoculum was drawn from each Shake-flask to inoculate a corresponding flask containing fresh, sterile, selective media to 0.05OD. (the lower initial starting OD was used due to a longer incubation period). The passaged flasks were incubated in an identical fashion overnight, after which the process was repeated for a total of four passages.

2.7 Upstream processing methods

2.7.1 Shake-flask fermentations

Shake-flask fermentations were conducted to produce sufficient plasmid material for purification by Qiagen kits, to investigate plasmid stability and as scale-down mimics of larger scale fermentations or to prepare inoculum for such fermentations. Two methods of Shake-flask fermentation were conducted throughout this project.

Early work utilised 2L total volume baffled shake-flasks in which 500mL of sterile media was cultured. Later 1L total volume shake-flasks were employed in which 50mL of sterile culture media was added. The smaller volume Shake-flasks enabled a larger number of runs to be conducted. Shake-flask cultures were all inoculated to 0.1OD by inoculating from a seed culture in a glass universal bottle, in the case of the larger shake-flasks or directly from the working cell bank for the smaller volume flasks.

2.7.2 Inoculum preparation

The inoculum with which to seed the vessels was prepared by shake-flask fermentations. 50mL of fresh, sterile seed media supplemented with the appropriate antibiotic was inoculated to 0.05OD from a 1mL cryovial. The shake-flasks were then incubated at either 37°C or 25°C for 10-12hours or 20-24 hours depending on the regime in a shaking incubator at 230rpm. If multiple fermentations were being conducted the inoculum would be pooled to ensure for each vessel the inoculum was uniform.

2.7.3 Fermentation

Batch fermentations were performed in 5L total volume, jacketed, autoclavable, glass bioreactors (Applikon, Worcs., UK) containing 4L of sterile media. The shake-flask inoculum was pooled, the optical density determined and the volume of inoculum required to produce a starting OD of 0.1 was asepetically transferred into each vessel. Dissolved oxygen tension (DOT) was monitored using an Ingold polarographic probe (Mettler-Toledo Ltd., Leics., UK) (Buhler and Ingold, 1976). DOT was maintained at 30% saturation initially by cascade control of impeller speed from 600rpm to 1000rpm and adjustment of sparging rate from 0.5vvm to 1vvm. When action on the DOT control loop had been >90% for a period of 10 minutes the control algorithm switched the sparger from

compressed air to enriched air (40% O_2). Again the DOT was maintained at 30% by cascade control of the impeller speed and adjustment of sparging rate from 1vvm to 2vvm. Fermentations were deemed complete when the DOT spiked and the progression of OD had stopped.

pH was maintained at 7.00±0.1 through the automatic additions of 1M NaOH and 1M H_2SO_4 under proportional control. Temperature was maintained at either 37°C or 25°C, depending on the cultivation regime, by proportional and integral control of water temperature flowing through the vessel jacket. Antifoam addition was controlled by the timed addition of 10%(v/v) polypropylene glycol at 5secs/hour. Both optical density (2.5.1) and wet cell weight (2.5.2) were used to monitor culture growth and samples were also taken to determine plasmid retention (2.5.4). Exit gas analysis of O_2 and CO_2 levels was carried out by mass spectrometry (VG Gas Analysis Systems Ltd., Cheshire, UK).

Culture broth was centrifuged immediately following the end of the fermentation by aliquoting 4L of broth into centrifuge pots and centrifuging at 20,000g for 20 minutes at 4°C. (Heraeus centrifuge). The supernatant was discarded and the cell paste collected and frozen at -70°C.

2.7.4 Calculation of specific growth rate (μ)

A standard method of calculating specific growth rate was used. From the growth curve the period of exponential growth was identified covering at least four data-points. A plot of the natural log of these points was constructed and linear regression performed. The result was only accepted if the R^2 value returned exceeded 0.96.

2.7.5 Samples for specific plasmid yield progression

Using the correlation that 5OD units at 600nm is equal to $2.5x10^9$ cells (Figure 6-1A), the volume of culture required to produce samples was calculated[3]. For each fermentation, per time point (~hourly), 5OD equivalent volumes of broth were aliquoted into 10 separate sartstedt tubes and centrifuged at 13,000rpm for 5 minutes. The supernatant was decanted

[3] Using a constant mass unit (5OD) rather than a constant volume unit when sampling meant that when the samples were analysed, the cell mass being lysed would be constant (~120gL^{-1}) irrespective of culture cell density when the sample was taken. This meant the lysis conditions would remain the same for each sample, which is critical when trying to accurately determine plasmid specific yield progression and would not be the case if samples were taken on a fixed volume basis. The mass of the sample pellet was easily calculated by recording the volume of the sample taken and also recording the WCW of the culture at the time of sampling.

off and any media remnants removed using a cotton bud. Cell pellets were then frozen at -20°C for retrospective analysis.

2.7.6 Oxygen Uptake Rate (OUR) determination

OUR and Carbon dioxide evolution rate were calculated by mass balancing the proportion of both compounds entering and leaving the fermentation vessel. A macro was used for the calculation, using the values for oxygen and carbon dioxide entering the vessel (obtained by directing a proportion of the entry gas to the mass spectrometer) and subtracting the masses of both the compounds detected in the exit gas. The mass spectrometer (VG Gas Analysis Systems Ltd., Cheshire, UK) returned the values of each of the components as % of total, therefore the basic equation for OUR and CER calculation used by the macro was as described in Equation 2-7.

$$Oxygen\ Uptake\ Rate\ (mmolsL^{-1}hr^{-1}) = \left(\frac{(Gas\ Flowrate\ x\ 60)}{22.4\ x\ Fermentation\ Vol} \right) x \left(100 - \left(O_{2\,IN} - O_{2\,OUT}\right)\right)$$

Equation 2-7 Basic equation used by OUR macro to calculate oxygen uptake rate. The equation uses gas flow rate as Lmin^{-1} and assumes 1mole of gas occupies 22.4L at standard temperature and pressure.

2.7.7 Online parameter logging

Fermentation conditions and variables were constantly logged using BioXpert software (Applikon, Worcs., UK). Progression of pH, temperature, DOT, impeller speed and the % action on each of these control loops was used in combination with OUR/CER progression and the discrete variables recorded (WCW/OD/Specific Yield) in the multivariate analysis of each of the fermentations.

2.8 Downstream purification methods

2.8.1 Cell Resuspension

50g of cell paste was removed from the freezer, broken into pieces and resuspended in 250mL of resuspension buffer in a glass vessel equipped with an overhead magnetic stirrer. The solution was left mixing for 1 hour to allow complete resuspension of the cell paste, after which the solution was incubated on ice for 10 minutes to chill. The wet cell weight of the solution was then determined using the assay described in 2.5.2

2.8.2 Cell Lysis

Cell lysis was achieved in a 1.5L total volume, round-bottomed, glass vessel equipped with a 4-blade, 45° pitched blade impeller. The dimensions of the vessel are recorded in Figure 7-6. At all times during the lysis and neutralisation operations the vessel was surrounded by ice. 395mL of cold 0.96%(w/v) NaOH was added to the lysis vessel along with 78mL of 6%(w/v) sodium dodecylsulphate (SDS) solution to form the lysis buffer. The impeller was switched to 100rpm and after a short time a white precipitate could be seen as the temperature of the SDS dropped. After the precipitate had formed the cell suspension was removed from the ice and poured into the lysis vessel, which continued to be agitated at 100rpm. Immediately upon addition of the cells the sudden increase in viscosity could be seen, typical of the cell lysis operation.

The vessel was left agitating for 30 minutes to allow for complete lysis[4] at which time 236mL of ice-cold 3M Potassium acetate was added to the vessel to neutralise the solution. The neutralisation reaction was allowed to proceed for a further 30 minutes to reach completion. At the end of the neutralisation reaction a 10mL sample was taken representing the Pre-$CaCl_2$ sample point. The sample was aliquoted in 1mL volumes into sterile sarstedt tubes which were centrifuged for 5 minutes at 13,000rpm to clarify. The clarified lysates were poured into fresh tubes, labelled and frozen at -70°C for retrospective analysis. The total volume of the lysate in the vessel at this point was 959mL and the component concentrations were as shown in Table 2-14 .

[4] Although lysis would be complete much quicker in a vessel of the size used, a 30-minute mixing time was used to mimic the likely mixing time that would be normal for a production (500L) operation. Refer to section for the calculation.

Table 2-14 Table detailing the concentrations of the various constituents used in the lysis procedure. Also showb are the concentrations following combination. In bold are recorded the concentrations after the addition of the 5M $CaCl_2$.

COMPONENT	VOLUME ADDED (mL)	CONC. (mM)	DILUTION FACTOR	RESULTANT CONC. (mM)
Tris	250	25	3.84 (4.82)	6.5 (5.19)
EDTA	"	10	3.84 (4.82)	2.6 (2.07)
Dextrose	"	55	3.84 (4.82)	14.32 (11.41)
Sodium hydroxide	395	240	2.43 (3.05)	98.8 (78.7)
SDS	78	210	12.29 (15.45)	17.1 (13.6)
Potassium acetate	236	3000	4.06 (5.11)	738.9 (587.1)
Calcium chloride	246	5000	4.9	1020

2.8.3 RNA removal

The ice-surrounding the vessel was removed and 246mL of room temperature 5M $CaCl_2$ was added to the unclarified lysate in the reaction vessel. Agitation of the vessel was continued for a further 5 minutes, to ensure adequate mixing of the components, after which the impeller was turned off and the mixture incubated at room temperature for 10 minutes.

2.8.4 Clarification

The unclarified lysate was distributed equally into six centrifuge pots and centrifuged in a Sorval-1500 rotor for 30 minutes at 12,000rpm/ 4°C to clarify. The supernatant was poured off into a clean, sterile 2L Duran bottle through a double-layer of Kimwipe tissue (Merck KGaA, Darmstadt, Germany) to remove any large particulates. Further clarification was achieved by pumping the clarified lysate through a 5µm PTFE depth filter in series with a 0.45µm/0.22µm PTFE depth filter (Sartorius, Surrey, UK) using a Watson-Marlow peristaltic pump set to 80mLmin^{-1}. This step ensured the removal of micron and sub-micron size particulates which would block the UF membrane. The filters were primed before use by passing through 1L of TE buffer. A clean 2L Duran was used to collect the clarified lysate which had a volume of 1205mL. The concentrations of the various components of the clarified lysate are shown emboldened in Table 2-14.

2.8.5 Ultrafiltration operation

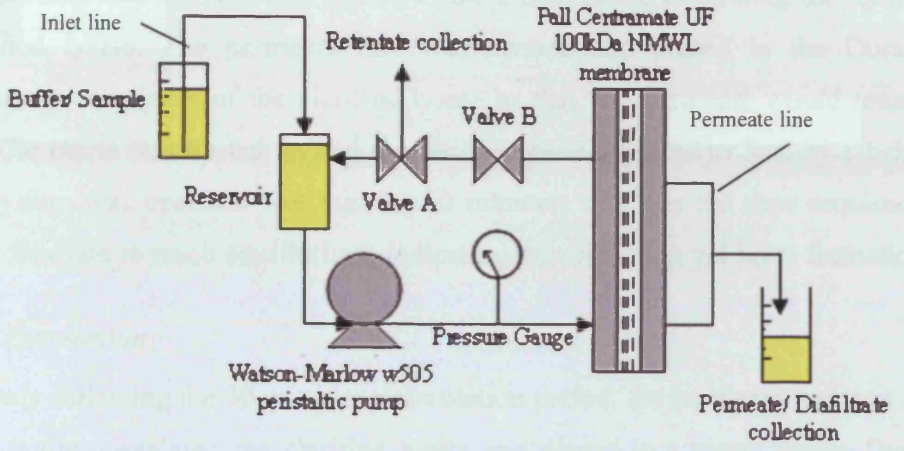

Figure 2-7 Schematic showing the setup of the ultrafiltration rig. The clarified lysate was added to the reservoir and sealed such that capillary action could be used to draw more fluid into the system from the inlet line. The fluid was pumped around the system in an anti-clockwise direction with the plasmid remaining in the retentate side of the membrane. Permeate and diafiltrate was collected for analysis. The TMP was regulated by the back-pressure valve (B) and the retentate collected from valve (A).

The setup of the Ultrafiltration system is outlined in Figure 2-7. The system used a 0.1sqft, 100kDa NMCO, Omega open-channel[5], Pall Filtron Centramate membrane (Pall Corporation, Portsmouth, UK). Liquid was passed around the system through 7.5mm ID tubing, the lengths of which were kept to minimum to reduce liquid hold-up volume. A Watson-Marlow 505 peristaltic pump was used for operation, set to either 500mLmin^{-1} or 250mLmin^{-1}.

2.8.5.1 Ultrafiltration preparation

After each use the membrane was cleaned by circulating with 500mL of 0.5M NaOH for 5 minutes. This was drained and replaced with a fresh volume which was circulated for 30minutes. This was drained off and the membrane stored in 500mL of 0.1M NaOH. Before use the alkali had to be drained and the system equilibrated. The system was equilibrated by passing 2L of Milli-Q water through the membrane followed by circulation of 1L of 10mM Tris (pH 8.0) for 30 minutes. This was drained and the membrane ready for use.

[5] Open channel meant there were no spacers between the outer wall of the membrane and the membrane itself. This resulted in less turbulent flow being created and so less shear at the membrane surface.

2.8.5.2 Recirculation

Approximately, 400mL of clarified lysate was loaded into the reservoir, the lid sealed and the tube leading into the reservoir placed in the Duran bottle containing the remainder of the clarified lysate. The permeate line was opened and placed in the Duran bottle containing the remainder of the clarified lysate so that any permeate would return to the system. The pump was turned on and the back pressure adjusted to 5psi by closing valve B. The system was operated like this for 30 minutes, this was the time required for the permeate flux rate to reach equilibrium, indicating the maximum gel layer formation.

2.8.5.3 Permeation

Immediately following the 30 minutes recirculation period, the permeate line was removed from the bottle containing the clarified lysate and placed in a clean, sterile Duran. The clarified lysate was allowed to concentrate from 1200mL to 100mL, representing a 12-fold concentration step.

2.8.5.4 Diafiltration

Once the clarified lysate had been concentrated to 100mL the inlet line was transferred to a bottle containing 3L of sterile-filtered 10mM Tris (pH7.5) DF1 buffer. The diafiltration was allowed to continue until all the volume had passed through the membrane. The filtrate was collected for analysis. Immeadiately, following the use of all DF1 buffer the inlet line was transferred to 2L of 10mM Tris+50mMNaCl. This was allowed to penetrate the membrane and the filtrate collected for analysis.

2.8.5.5 Retentate collection

Following both diafiltration steps there remained 100mL of clear fluid in the UF system. In order to recover the plasmid from the gel layer, the TMP was removed and the Retentate recirculated at the set crossflow velocity for 20minutes. The pump was then stopped and the fluid collected from the system. To fully recover the plasmid from the membrane two more sequential wash steps were employed, both using ~80mL of DF2 buffer which was circulated for 20 minute periods. The washes were drained from the system and the volume determined by weight

2.8.6 Determining Mass-Volume coefficients of anion-exchange resins

To separate, pre-weighed (5d.p) glass McCartney bottles were added 7mL, 5mL, 2.5mL and 1mL volumes of each anion-exchange resin under study (TMAE Fractogel and DEAE Fractogel). For each volume triplicates were prepared. These were left in a vacuum oven (80°C) for 24 hours. The bottles were reweighed and the mass of the residue calculated. Taking the average of the triplicate measurements and of each volume repeat, the mass-volume coefficient of the resins was calculated.

2.8.7 Binding Studies

The TMAE and DEAE Fractogel (Merck, USA) resins to be used were mixed well to resuspend. Multiple 20μL volumes of each were pipetted in to separate, autoclaved eppendorf tubes. To each was added 2mL of sterile 10mM Tris+0.54M NaCl (Diafiltration buffer 2). This was done to equilibrate the resin into the buffer used for loading in the normal course of the process. The tubes were then left overnight at 4°C to allow the resin to settle.

To perform the binding studies the equilibration buffer was drained away. To the sedimented resin was added 1mL of a 50μgmL^{-1} solution of the plasmid under study. The plasmids were purified by Qiagen Large Construct kit (2.5.8.3) which employs an exonuclease to digest any genomic DNA. Immediately following addition a 2μL volume of the solution was extracted and the plasmid concentration measured using the NanoDrop spectrophotometer (2.5.9.2). The tubes were then attached to an inversion mixer to agitate and promote effective mixing. At regular intervals the tubes were assayed for the presence of free, unbound plasmid by removing 2μL volumes and assaying by NanoDrop. The binding was monitored for 90 minutes. In total about 15 measurements were recorded over this period, equating to 30μL. This represented 3% of the total volume of the mixture under study. Following the 90 minute period the tubes were left to agitate at room temperature for a total of 24 hours. At this point the agitation was halted and the final measurements of free, unbound plasmid recorded. It was maintained that equilibrium would have been reached by this point and as such this measurement formed the value for maximum specific binding capacity.

3 INITIAL STUDIES: RESULTS AND DISCUSSION

3.1 Chapter Aims

This chapter concentrates on the initial studies conducted on the series of large, BAC based, Oxford plasmids (Wade-Martins *et al.*, 1999). At the outset of this EngD no data existed as for the potential for these constructs to be produced or purified and previously their production had been purely laboratory scale, utilising caesium chloride gradient purification. A number of preliminary experiments were designed to assess the feasibility of manufacturing these plasmids at a larger scale.

The main questions to be answered by these studies were;

1. Whether the host-cells were able to grow sufficiently when bearing constructs of this size and whether the plasmid size had any deleterious effect on the growth rate of the culture. If the growth rate was severely impinged by the propagation of such large macromolecules, their large-scale manufacture may not be feasible due to the excessively long time scales predicted for the fermentations.

2. Investigations would be done to determine the plasmid yields, which could be expected from fermentations of these constructs. It was known in advance that these plasmids existed at a very low copy number (1-2 copies/ cell) (Frame and Bishop, 1971). However, due to the much greater linear DNA length it remained to be seen whether a similar mass of plasmid DNA existed for purification, as compared to that of a smaller, high-copy number plasmids, by balance of the sheer plasmid size. Experiments would also be done to determine whether it was possible to increase the productivity of the strains producing these plasmids by altering the medium used for their cultivation.

3. By completing pilot-scale (4L) batch fermentations of these large constructs, sufficient cell material could be produced to conduct purification trials upon these plasmids. Additionally, it would be possible to monitor the growth and productivity of cells bearing these constructs in a system which would closer mimic their manufacture, should attempts ever be made.

4. Using the cell material produced from pilot-scale fermentations, downstream purification trials could be conducted to investigate if it was possible to purify these large

constructs and in what amounts, together with identifying the steps in the downstream process, which were the most problematic.

5. In the process of monitoring plasmid yields though the fermentation and downstream operations it would be possible to determine whether the current analytical techniques, used for plasmid quantification and visualisation, were applicable and whether developments or new assay techniques were required.

The following sections detail the attempts made to answer these unknowns.

3.2 Investigating the effect of plasmid size on culture growth rates

3.2.1 Introduction

It has been recognised for some time that strong, constitutive promoters severely limit the growth of bacterial cells by forcing the cell to generate large amounts of the desired protein (Glick, 1995; Dong *et al.*, 1995). Essentially a significant amount of the host cell's resources, either in the form of energy such as ATP or raw materials such as nucleotides and amino acids, are diverted to maintain or express foreign DNA. This metabolic burden can cause a variety of changes to the physiology and functioning of the host cell. One of the most commonly observed changes is a decrease in the rate of cell growth but a reduction in final cell yield has also been reported (Summers, 1991). Attempts have been made to quantify the level of metabolic burden placed upon cultures expressing recombinant proteins by measuring the level of the starvation signal molecule ppGpp (Andersson *et al.*, 1996; Cserjan-Puschmann *et al.*, 1999).

With burdened cells having a slower growth rate, in the absence of selective pressure, this can lead to complete plasmid loss from the culture, as the plasmid-free cells soon come to dominate the population. Due to the industry focus being mainly upon recombinant protein production, several strategies have been developed to try and overcome the problem of excessive expression leading to an unsustainable metabolic burden. One of the most common is to employ an inducible promoter to ensure protein expression occurs only at high cell densities, thereby reducing the metabolic burden on the dividing cells leading to a higher proportion of cells maintaining the plasmid up until they are induced. (Grabherr and Bayer, 2002) reported that expression vectors should be carefully designed to ensure a balance exists between expression rate of the plasmid-encoded protein and the plasmid copy number (and hence the resultant metabolic burden placed upon the cell). The desired

result is the maximisation of protein yield, with the minimal burden placed upon the cells, so that fast growth rates and high cell densities can be achieved.

The obvious difference with the strategies employed for processes aimed at producing recombinant proteins and those for the manufacture of plasmid DNA, are that for the latter no expression of the plasmid DNA is strictly required. The reason for this being that excluding the necessary control machinery the plasmid genes remained unexpressed in the bacterial cell since it is the genes themselves that are the product, as such metabolic burden should be less of a problem. It has become clear that the metabolic burden associated with the propagation of a plasmid is small compared to the effect of expression of recombinant protein (Bentley W.E., 1990; Jones and Keasling, 1998). (Andersson *et al.*, 1996) demonstrated that inducing expression of a plasmid-bearing culture led to 23% drop in the biomass produced as compared to the plasmid-free culture of the host. The result for the non-induced plasmid-bearing culture was a reduction in final biomass, which fell between the other two. Indeed several studies have identified the fact that when propagating non-coding sequences in bacteria the extra metabolic burden is the result of the cells expressing the selective agent employed to maintain the plasmid and not the plasmid itself (Rozkov *et al.*, 2004; Lee and Edlin, 1985). Attempts have been made to remove the selective resistance gene from plasmid constructs and maintain plasmid presence by novel section techniques such as repressor-titration (Cranenburgh *et al.*, 2001; Williams *et al.*, 1998b).

It appears to be the case that it is protein expression which leads to the higher metabolic burden rather that the propagation of the plasmid itself. The extent to which this idea can be applied when the cells are being asked to propagate large plasmids such as in this study is, however, unknown. (Stouthamer A.H., 1973) calculated that to synthesize 1g of plasmid-free cells requires 34.7mmoles of ATP. Of that total, 20.5mmoles is required for protein synthesis and only 1.1mmoles is needed for DNA synthesis. These figures mask the fact that the constituent mass breakdown of a log-phase *E.coli* cell (Bailey and Ollis, 1986) includes 15% protein and 1% DNA. Proportionally, this means that the energy required for the synthesis a unit mass of protein is highly comparable to the identical mass of DNA. This analysis is relevant, since the figure of 1% DNA represents 4.7Mbp of DNA (i.e 1 bacterial genome) (Blattner *et al.*, 1997). Hypothetically, the propagation of a plasmid may cause a significant metabolic burden when the plasmid exists at levels where the amount of extrachromosomal plasmid DNA is equal to, or at least approaching, the

amount of DNA in the genome. With large plasmids, it becomes feasible that this limit could be reached, such that the host cell's resources for synthesising genomic DNA may become strained by the burden of having to maintain and replicate the plasmid DNA. The only unknown is by how much the task of replicating such quantities of DNA would effect the cell's normal functioning and the resultant metabolic burden and whether the demands are at all comparable to the high metabolic burden caused by the constituitive expression of proteins.

Certainly there are some reports that plasmid size does result in additional metabolic burden. In one study, the behaviour of four different pUC8-based plasmids was compared, with each plasmid carrying different amounts of unexpressed *Drosophilia melanogaster* chromosomal DNA (2.7-8.7kb). Although the growth rates in rich medium of *E.coli* cells transformed with one of these four plasmids were identical, as plasmid size increased, maximum cell density decreased, and with the largest plasmid, cell death was accelerated once the stationary phase of cell growth was reached (Cheah *et al.*, 1987). Similarly, report that inserting non-coding sequences from *Metarhizium anisopiliae* of sizes 3-9kb into pBluescript caused a reduction in growth rate by increasing the length of the lag phase period of growth (Smith and Bidochka, 1998).

The other factor observed during these preliminary studies was whether the use of semi-defined media (SDCAS) provided any benefit over complex SuperBroth media. *E.coli* is a non-fastidious microorganism and as such is capable of growing both on rich, complex media as well as in salt-based, chemically defined media, provided a source of organic carbon is provided. Though the type and concentration of the components used, growth medium composition directly dictates the amount of biomass produced, and therefore directly dictates the plasmid volumetric yield (mg plasmid/L). In addition, the medium composition directly affects the host-cell physiology and metabolism and therefore influences plasmid copy number or specific yield (μgmL^{-1}) (Prather *et al.*, 2003). Once again a balance must be met. A high specific yield is critical so that for the downstream processing stages the plasmid exists in high amounts relative to other cellular components, which exist as contaminants in the purification process. However, the high specific yield should not impact too negatively on the final biomass yields or the maximum specific growth rate, by applying excess metabolic burden, as this reduces the overall efficiency of the fermentation process.

The advantages of using either defined media over complex media remains disputable. (Shoham and Demain, 1990; O'Kennedy and Patching, 1997; Kim *et al.*, 1987) report that defined media can support higher plasmid copy numbers than complex media by reducing segregation-rate associated plasmid instability and the maximum specific growth rate. It is generally accepted that plasmid copy-number varies inversely with growth rate in batch culture. Indeed, this has been mathematically established by (Vasuki, 1989) in the form of an unstructured model based upon Michaelis-Menton type kinetics to derive the relationship outlined in Equation 3-1.

$$p_S = \frac{(V_P{}^0)(V_H{}^0)}{\mu + K_H} - K_P$$

Equation 3-1 Relationship derived from a model for plasmid replication (p→2p) using Michaelis-Menton kinetics, demonstrating an inverse relationship between plasmid copy number and specific growth rate. P_S is the intracellular plasmid copy number or concentration. μ is the specific growth rate. K_H is the host-cell saturation constant and as such is effectively a measure of the dependence of the plasmid on the host cell machinery for replication. K_P is the plasmid saturation constant and represents the level of all the host components involved in plasmid replication exist at $0.5V_p{}^0$. $V_0{}^P$ represents the maximal rate of plasmid synthesis, whilst $V_H{}^0$ represents the maximal rate of host-cell activities required for plasmid synthesis such as RNA synthesis.

A proposed basis for this response is a negative control system, which suggests that the activities of the RNAI and RNAII promoters, and the efficiency with which RNAI inhibits plasmid replication, are controlled by the growth rate. Reducing the culture growth rate from $1.7h^{-1}$ to $0.4h^{-1}$ led to an increase in copy number from 15-23 plasmids per genome (Lin-Chao and Bremer, 1986). Similarly, the use of a stoichiometrically designed, defined medium produced plasmid yields of $60\pm5.0mgL^{-1}$ as compared to $4.0\pm0.4mgL^{-1}$ for LB medium by reducing the growth rate from $0.61h^{-1}$ with complex LB to $0.33h^{-1}$ with the defined media (Wang *et al.*, 2001). For complex media, opposite results have been seen (O'Kennedy *et al.*, 2000). They describe how semi-defined SDCAS media was capable of producing lower growth rates, higher cell densities and improved plasmid stability than LB media. However, these studies made use of LB media for comparison, which is quite a simple, complex media formulation (O'Kennedy and Patching, 1997; Wang *et al.*, 2001). Increasing complex medium strength by employing richer formulations, such as SuperBroth, supports higher volumetric yields without compromising specific yields, and this solely attributable to increased biomass levels at harvest.

3.2.2 Characterising the growth rates of the Oxford series in Shake-flasks

The main difference between previous studies and this study is down to the nature of the plasmids employed. All studies referenced thus far made use of ColE1 based, reasonably small, high-copy number plasmids whose replication was relaxed. In this study the plasmids are derived from the pBAC108L vector and so the replication is stringently controlled at 1-2copies per cell by the F-factor (Frame and Bishop, 1971). However, the plasmid sizes are considerably larger than previously encountered at 116kb, 172kb and 242kb. It was unknown when embarking on these studies whether the low-copy, large size would place a similar level of burden upon the cells as high-copy, small plasmids. Additionally, due to the nature of stringent replication control demonstrated by these plasmids, the use of semi-defined media may have little impact on yields since the RNA promoter control system is not in effect and so reducing the growth rate may only serve to reduce the efficiency of the fermentation.

Figure 3-1A and B display the results of shake-flask experiments conducted on the large plasmid series. Each large construct; p5176 (116kb), p5206 (172kb) and p5204 (242kb) was grown in triplicate in 2L shake-flasks containing 500mL of either complex (SuperBroth) media or semi-defined (SDCAS) media. Referring to Figure 3-1A and B, it can be appreciated that the cultures grown on SuperBroth displayed shorter lag-phases than the same cultures grown on SDCAS media. The lag-phase was deemed complete when the optical density of the culture had increased from its 0.1 starting figure to over 0.5OD. The lag phase for the complex media had a three hour duration, whilst the figure for the semi-defined media was four hours. A possible explanation for this difference could be catabolic repression. The main carbon source in SDCAS media is glucose, which *E.coli* will metabolise preferentially over any other carbon source. Because of this fact it is unlikely that any glucose remained in the starter culture used to inoculate the SDCAS shake-flasks, since they had been growing for over 12 hours. This would have meant that when the culture was passaged into fresh media containing glucose, the cells would have responded by synthesising the required enzymes to metabolise the glucose, as this would take preference over any other carbon source, a course of action which would have

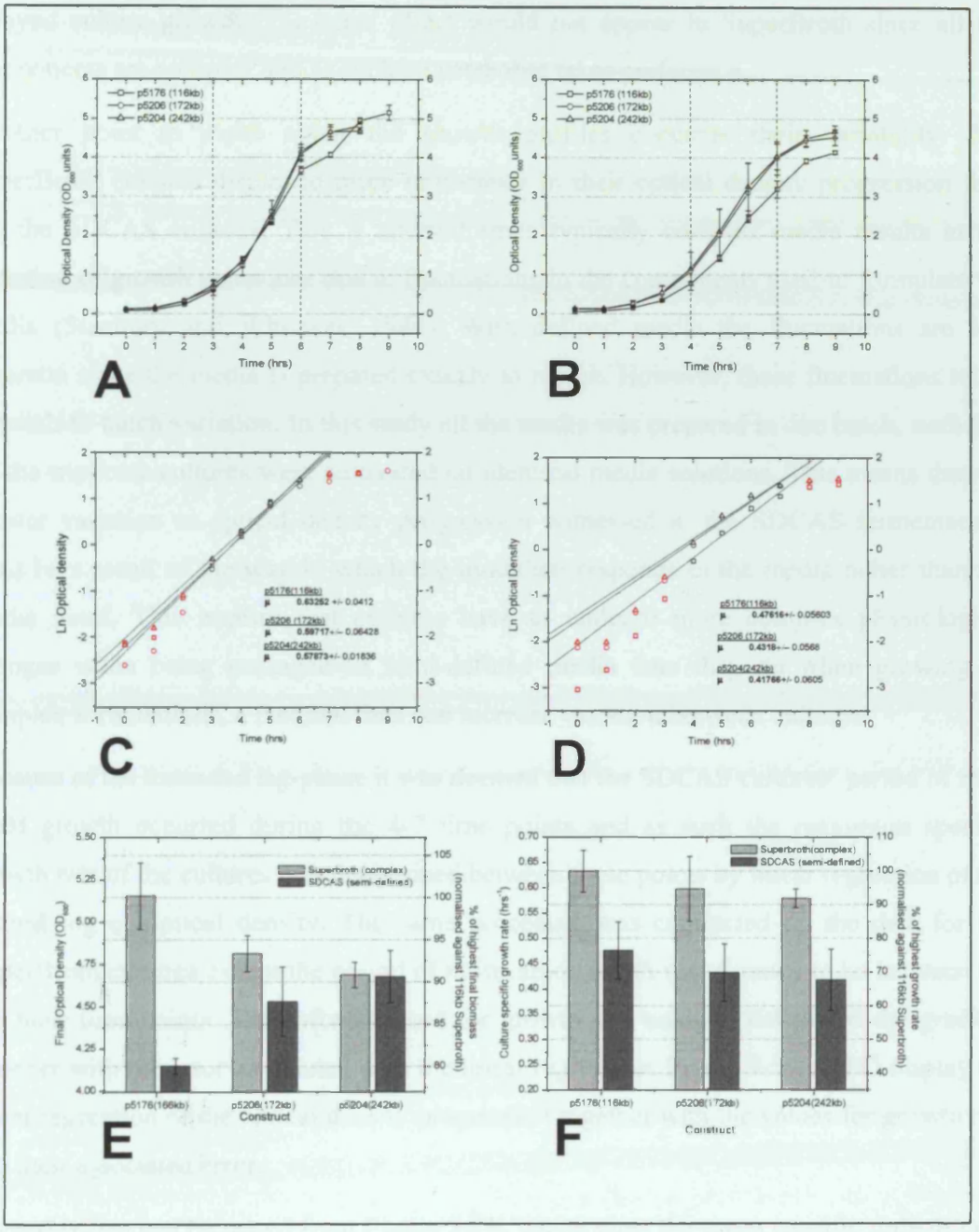

Figure 3-1 Results of Shake-flask studies designed to determine whether the size of the large Oxford series of constructs had any effect on the growth characteristics of the plasmid bearing cells. Plasmids were propagated in *E.coli* DH10β and grown on 500mL of either complex SuperBroth media or semi-defined SDCAS media in 2L baffled shake-flasks supplemented with 25μgmL^{-1} chloramphenicol. Each construct on each media variety was studied in triplicate by inoculating each flask to 0.1OD starting density though the use of a starting culture grown on the appropriate media. Flasks were incubated at 37°C and 230rpm in a shaking incubator. Hourly samples of broth were extracted and diluted to within the linear range (0.1-0.6) using the appropriate blank media and analysed using a Novaspec spectrophotometer set to 600nm, blanked against media. Specific growth rates were determined by linear regression of natural log of optical density though the time period, which displayed maximum growth.

[A; growth profiles of the constructs on SuperBroth / B; Growth profiles of the constructs on SDCAS media. / C; Growth rates on SuperBroth. / D; Growth rates on SDCAS. / E; Final biomass levels at harvest. / F; Maximum specific growth rates]

delayed culture growth. The same effect would not appear in SuperBroth since all the components are complex and as such no catabolite takes preference.

Another point to make about the growth profiles concerns their variability. The SuperBroth cultures displayed more uniformity in their optical density progression than did the SDCAS cultures. This is unusual since typically complex media results in the variation of growth behaviour due to fluctuations in the components used to formulate the media (Stanbury and Whitaker, 1984). With defined media the fluctuations are less common since the media is prepared exactly to recipe. However, these fluctuations relate to batch-to-batch variation. In this study all the media was prepared in one batch, such that all the triplicate cultures were cultivated on identical media solutions. This means that the greater variation in optical density progression witnessed in the SDCAS fermentations must be a result of the way in which the inoculum responds to the media rather than the media itself. This implies that cultures have to undergo more complex physiological changes when being passaged in semi-defined media than they do when growing on complex formulations, a fact that than can increase variation between cultures.

Because of the extended lag-phase it was deemed that the SDCAS cultures' period of most rapid growth occurred during the 4-7 time points and as such the maximum specific growth rate of the cultures was determined between these points by linear regression of the natural log of optical density. The same procedure was conducted on the data for the SuperBroth cultures except the period of most rapid growth was deemed to be between the 3-6 hour time points. The software used for growth rate analysis calculated the gradient together with the error associated with the linear regression. Figure 3-1C and D display the linear regression of the optical density progression together with the values for growth rate and their associated error.

Several points can be raised from Figure 3-1F, which plots the mean specific growth rates of the triplicate cultures. The most apparent observation is the effect that semi-defined media had on growth rate, as it can clearly be seen that the use of this media resulted in a ~25-30% decrease in the growth rate for each construct. Highlighting one example is the drop from $0.63h^{-1}$ to $0.48h^{-1}$ displayed by p5176 culture. This is very similar to other reports (O'Kennedy *et al.*, 2000). In their report they described a decreasing growth rate of $0.63h^{-1}$ to $0.42h^{-1}$ when growing *E.coli* DH5α [pSVβ] on LB and SDCAS media respectively.

Alongside the decrease in growth rate due to the media change, plasmid size also has a suppressing effect on growth rate. From Figure 3-1F it can be seen that growth rate on SuperBroth drops from $0.63h^{-1}$ for 116kb to $0.59h^{-1}$ for 172kb plasmid and $0.57h^{-1}$ for 242kb. Overall this accounts for a 10% drop in growth rate upon doubling the plasmid size from 116kb to 242kb. Similarly with the SDCAS cultures, growth rate drops from $0.48h^{-1}$ for 116kb to $0.42h^{-1}$ for 242kb plasmid, representing a 12.5% drop. Since the plasmid backbone of the constructs is identical, such that the expression rate of the chloramphenicol resistance gene is the same, the decreasing growth rate has to be due to the increase in non-coding DNA the cells are required to maintain and replicate.

Figure 3-1E throws up some disparities as it plots the final biomass yield attained (determined from optical density) of cultures carrying the different constructs on the different media types. Increasing plasmid size reduces the final biomass attained by fermentations (Cheah *et al.*, 1987). The same effect is seen here with optical density dropping from a 5.15 OD units for the 116kb plasmid down to 4.69OD units for the largest 242kb plasmid, when cultivated on SuperBroth media. This represents a 10% decrease in final biomass yields. This effect is understandable, once again by assuming the effect of metabolic burden placed upon the cells by increasing plasmid size.

$$r_S = r_{S(X)} + r_{S(P)}$$

$$-r_S = \frac{1}{Y_{X/S}} r_X + \frac{1}{Y_{P/S}} r_P$$

Equation 3-2 Equations describing the relationships between substrate utlisation and product formation. R_S is rate of substrate utilisation; $r_{S(x)}$ describes the rate of substrate utilisation for biomass production; $r_{S(P)}$ is rate of substrate utilisation for product formation. R_X is rate of biomass accumulation; r_P is rate of product formation; $Y_{X/S}$ and $Y_{P/S}$ are the yield coefficients for biomass and product synthesis

The relationships between substrate utilisation and product formation are outlined in Equation 3-2 (Luedeking *et al.*, 1957). Since plasmid is the product, as plasmid size increased the product yield coefficient ($Y_{P/S}$) would decrease since more substrate is required to make one mass unit of product. This would increase the rate of substrate utilisation for product formation and since the amount of substrate would be fixed would mean less would be available for biomass synthesis.

A potential disparity is seen in the results for the SDCAS fermentations, whereby biomass accumulation appears to increase with plasmid size. The only possible way for this to occur would be for the product yield coefficient ($Y_{P/S}$) to increase with increasing plasmid

size, such that product formation consumes less substrate material as size increases. However, this suggestion does not have a rational explanation as to why this would be the case, so the only possible explanation is that the result for the biomass accumulation on SDCAS media is an anomaly. Despite this it could be claimed that the SDCAS media does reduce the maximum cell mass attainable, since all the biomass levels produced are lower than when SuperBroth media was used. A possible explanation for this is that cells growing on semi-defined media have a lower biomass yield coefficient ($Y_{X/S}$), such that per unit mass of substrate consumed less biomass is produced. The remainder of substrate utilised could have been taken up with a higher amount of endogenous respiration which occurs due to the increased number of metabolic actions the cells must perform on the substrate to produce useful cell metabolites.

So far it has been demonstrated that the Oxford series of large plasmids do exert an increasing metabolic load with increasing size on the cells employed to replicate them and also that using SDCAS media reduced the growth rate and final cell density reached. However, the magnitude of this load compared to that from a plasmid-free culture has not been established nor whether the metabolic load is as great as in a culture propagating a relaxed, high-copy number plasmid, the type of which is normally used for plasmid production.

3.2.3 Comparative control studies using parental and high-copy number strains

Further shake-flask trials were performed which characterised the variation in growth of one of the large plasmids; DH10β p5176 (116kb) against a negative control in the form of wild-type, parental DH10β and a positive control in the form of a small, high-copy number construct; DH10β pSVβ (6.9kb). As before, all constructs were grown in triplicate in 500mL of SuperBroth media in 2L Shake-flasks at 230rpm and 37°C in a shaking incubator. Again, growth was monitored by recording optical density progression at hourly intervals.

Figure 3-2 displays the results from these shake-flask experiments. Figure 3-2A plots the mean growth profiles of the triplicate cultures of each construct. Again it can be seen that the short lag-phase which occurs with complex media, but also how the parental culture soon overtakes the other two cultures and does so for the remainder of the fermentation. Indeed, it appears that p5176 and pSVβ display remarkably similar growth profiles.

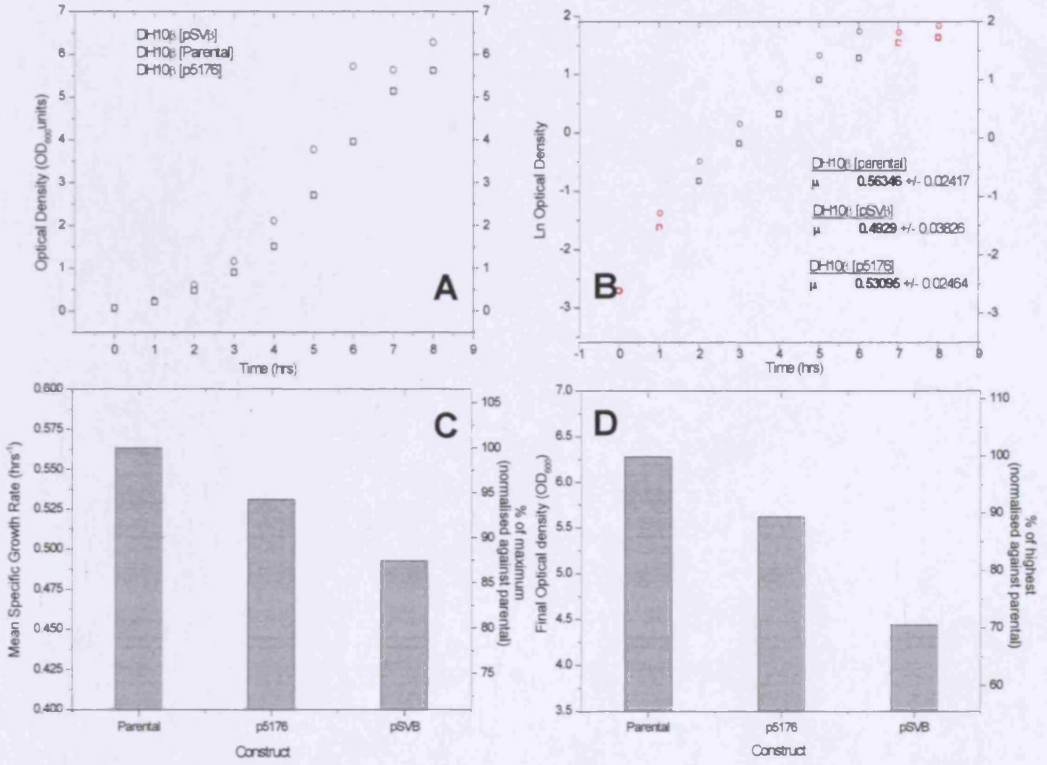

Figure 3-2 Results from shake-flask trials designed to determine the extent of metabolic load on the propagation of the large 116kb plasmid exerted upon the host-cells as compared to a parental plasmid –free culture and a culture bearing the small, high-copy number plasmid pSVβ. All cultures were *E.coli* DH10β grown in triplicate on 500mL of SuperBroth media, supplemented with either 25μgmL^{-1} chloroamphenicol or 100μgmL^{-1} ampicillin where appropriate, in 2L baffled shake-flasks. Each flask as inoculated to 0.1 starting OD from an inoculum culture. Flasks were incubated at 37°C and 230rpm in a shaking incubator. Hourly samples of broth were extracted and diluted to within the linear range (0.1-0.6) using blank SuperBroth media and analysed using a Novaspec spectrophotometer set to 600nm and blanked against the media. Maximum specific growth rates were determine by linear regression of the natural log of optical density though the time period which displayed maximum growth. [A; growth profile on SuperBroth/ B; growth rate determination/ C; Maximum specific growth rates/ D; final optical densities

One difference between the two constructs becomes apparent once the stationary phase is reached. In the pSVβ cultures the stationary phase is very abrupt and as such the cell concentration soon goes into decline.

It was decided that the maximum specific growth rate should be calculated over the 2-6 time points during which maximum growth was occurring. Figure 3-2B shows the linear regression used to determine the growth rates. The first thing to notice from the growth rates is the difference they display to the previous shake-flask cultures, as outlined in Figure 3-1. The growth rate recorded previously for DH10β [p5176] on SuperBroth, using the same growth conditions and flask geometry, was 0.63h^{-1} whereas in this series for the same culture the figure was 0.53h^{-1}. This represents a 15% drop-off, the only explanation

of which can be down to growth conditions and media preparation. As described earlier, complex media can vary significantly between batches, as can the inoculum used. All this goes to signify how critical it is to employ controls and to maintain the conditions and media components as consistently as possible. However, although it becomes hard to compare the two shake-flask studies directly, it is still possible to draw conclusions from the independent studies.

From the previous studies it can be appreciated that increasing plasmid size does increase the metabolic load upon the cells, an effect noticeable by the reduction in both growth rate and biomass yields. Comparing the culture growth rates outlined in Figure 3-2C shows that the effect of the metabolic burden of both p5176 and pSVβ compared to the wild-type. It can be seen that the propagation of the large 116kb plasmid does reduce the mean maximum growth rate slightly from $0.56h^{-1}$ -$0.53h^{-1}$. However, the error associated with this decrease is large and as such the significance of this result is questionable. Despite this, it can be said that the growth rate of the BAC-bearing culture falls in between that of the parental and of the high copy number plasmid.

The propagation of the small, high-copy number plasmid pSVβ does reduce growth rate significantly, in this study by roughly 15%. This amount is half of that described by others when comparing the growth rates of DH5α parental and DH5α [pSVβ], where they describe a 30% reduction in growth rate (O'Kennedy *et al.*, 2000). However, this earlier result is due to the more rapid growth of DH5α parental cell-line in their study. Indeed, this is a reason the large constructs are propagated in the DH10β strain, since the slower growth characteristics of this cell line are meant to promote plasmid retention. In line with the reduction in growth rates witnessed, there also occurs a significant reduction in biomass levels attained by the cultures. As shown in Figure 3-2 there was a roughly 10% reduction in biomass yield when propagating the 116kb plasmid but a 30% reduction with pSVβ cultures. The large difference in the biomass yields attained from the pSVβ cultures was described by the rapid decline in optical density that these cultures displayed upon reaching stationary phase.

3.2.4 Conclusions

It has been found that the propagation of the Oxford series of large plasmids is not too problematic. They do contribute a metabolic burden on the growing cells but not to the extent that small, high-copy number plasmids do. Growth rates are suppressed and reduce further with increasing plasmid size, but by small margins. The biomass levels reached by the end of the fermentations, were found to be reduced but again by a small degree. It has also been determined that the use of semi-defined SDCAS media lowers the growth rate and final biomass levels of the cultures. It has been described elsewhere that reducing growth rate can be beneficial to increasing plasmid specific yield, a fact that remains to be determined with these plasmids. Lowered biomass levels would certainly reduce plasmid volumetric yield (O'Kennedy *et al.*, 2000; Wang *et al.*, 2001). The propagation of these plasmids is no different to any other plasmid and indeed there propagation does not place much additional burden on the host cell.

It is thought appropriate to highlight an error with the experimental setup, which was not appreciated until later. In the past experiment references were made to how negative controls, in the form of plasmid-free, wild-type *E.coli* were used to allow comparison to cultures bearing large plasmids. From these studies conclusions were drawn about the effects propagation of these large plasmids had on the cell growth and biomass yields. However, it was realised that the studies were not strictly equivalent due to the fact that plasmid-free fermentations were conducted in the absence of chloroamphenicol, whilst the plasmid-bearing cultures were supplemented with this antibiotic up to 25μgmL^{-1}. It is not known the effect of inclusion of this antibiotic may have had on the results. Perhaps it may have been more scientifically correct to perform the shake-flask studies of the cultures bearing the plasmids in the absence of the antibiotic. The problem with this strategy would have been the potential for plasmid loss from the culture and the resultant inaccuracies such an event would cause. As a result of this oversight it, it should be considered that the inclusion of the antibiotic may have an impact on the reduced growth witnessed for the larger plasmids (as compared to the plasmid-free wild-type) especially when it is appreciated that the mode of action of the antibiotic involves the disruption of protein synthesis.

3.3 Progression of p5176 (116kb) yield during 2L Shake-flask fermentations

3.3.1 Introduction

It has been established that the propagation of the series of large plasmids does not pose a significant challenge and that indeed they demonstrate faster growth rates and higher biomass yields than cell lines propagating small, high-copy number plasmids. What needs to be determined is whether the mass of plasmid DNA carried by the cells bearing these plasmids is sufficient to enable purification.

As described previously a high specific plasmid yield is very desirable, since it immediately increases the efficiency of the fermentation stage, whilst also facilitating downstream processing by decreasing the ratio between contaminants and plasmid product in the initial starting material (Prather *et al.*, 2003). As such many strategies have been employed to increase the plasmid specific yield. Briefly, these fall into two groupings; genetic and process strategies.

3.3.2 Genetic-led Strategies

The genetic strategies employed centre on the choice of replicon chosen for the plasmid. pMB1 replicons, as used in pBR322 based plasmids, are traditionally chosen since they have successfully been modified to replicate at high copy numbers of ~50 per cell (Bolivar *et al.*, 1977). pBR322 was modified to exclude the Rop/Rom protein that controls its replication and as such copy number increased three fold to ~150cpc (Balbas *et al.*, 1986). Further modification by a single G→A point created the pUC series of vectors which demonstrated a further increase in copy number to ~500-700 copies per cell. The point mutation lies within the region coding for the RNAII sequence and impacts upon the binding of the RNAI:RNAII complex in a temperature sensitive manner. The effect of the mutation is suppressed at 30°C but becomes elevated at 42°C, a technique employed to produce yields of 10.3μgmg^{-1}DCW (Lahijani *et al.*, 1996). Additional to a high-copy replicon, vectors engineered for production have also included short *cer* sequences, which occur naturally in *E.coli* ColE1. This sequence enhances the resolution of concatomeric DNA and the distribution of plasmids among daughter cells. Inclusion of this sequence assists plasmid maintenance and stability and therefore maintains a high specific yield. It should be noted that despite the choice of replicons, the size and sequence of the DNA being propagated in the plasmid also has an effect on the growth rate and copy number of

the plasmid (Summers, 1991). For instance some cloned, non-coding sequences are found to be toxic to the host cells.

3.3.3 Process-led strategies

Process driven strategies of improving specific yield focus on the fermentation media employed together with the mode of cultivation.

3.3.3.1 Media effects

As described earlier in this section, both specific and volumetric yield are affected by the media used for cultivation. In general, rich complex-media leads to faster growth rates and higher biomass and therefore volumetric yields. Plasmid specific yields attained propagating high-copy plasmids on complex LB media, have been shown to display remarkable similarity, all reaching yields of 4-6μgmg^{-1} DCW (Prather *et al.*, 2003).

Utilising defined media can slow the growth rate which leads to higher specific yields (O'Kennedy and Patching, 1997; Wang *et al.*, 2001; Kim *et al.*, 1987). Additionally, defined media can reduce the growth rate differential that exists between plasmid-free and plasmid-bearing cells thereby reducing plasmid instability and so positively influencing specific yield. Defined media can also be improved by rational design of required metabolites. In one study, stoichiometric analysis of fermentation media led to the identification of six amino acids found to be key to the successful propagation of plasmid DNA. Supplementing a basal salt-glucose media with these amino acids led to a 50% increase in specific yield, as compared to LB media. Further enhancement of the defined media though the inclusion of ribonucleosides (adenosine, guanosine, cytidine, thymidine) led to an additional 250% increase in specific yield, up to 17.1μgmg^{-1}DCW (Wang *et al.*, 2001). Similarly, the carbon to nitrogen ratio of the fermentation media has been found to have a strong influence on plasmid specific yield (O'Kennedy *et al.*, 2000). Traditional media formulations typically possess a C:N ratio of 12:1, lowering the ratio to 2.78:1 led to a 600% increase in specific yield to 12μgmg^{-1}DCW.

3.3.3.2 Mode of cultivation

Both batch and fed-batch cultivation strategies have been used for the manufacture of plasmid DNA (Riesenberg *et al.*, 1991; Knorre *et al.*, 1991; Lee, 1996). Batch fermentations used for pDNA production are associated with technological and economic drawbacks. For batch fermentations, complex or semi-defined media are most commonly

used and result in a pDNA yield that ranges between 3.5 and 68 mgL^{-1} (Huber and et al., 2005a). With batch culture, oxygen transfer capacity becomes limiting sooner and as such the culture anaerobically respires producing toxic by-products such as acetic acid, which limits growth and ultimately leads to cell death. Typically, biomass yields at the end of batch fermentations are between 5-15gL^{-1} DCW. Conversely, fed-batch culture supplies nutrients over an extended period of time and so controls the nutrient availability to a level compatible with the oxygen transfer capacity of the bioreactor. This management enables the attainment of high cell densities in the range of 50-100gL^{-1}DCW. Batch cultivation can be improved by reducing oxygen limitation though the use of enriched air, enabling higher biomass yields up to 25gL^{-1}DCW (as shown in this report) but still failing to reach the levels achievable using fed-batch strategies.

Perhaps more important is that fed-batch techniques allow control over cell growth rate, which just like reducing growth rate by changing medium composition, leads to higher plasmid copy numbers. A feeding strategy designed to maintain slow growth at around 0.15h^{-1} for the majority of the fermentation, resulted in a final biomass yield of 50g L^{-1}DCW and a specific yield of 4.1μgmg^{-1}DCW (Schmidt *et al.*, 1997). Fed-batch feeding strategies are becoming increasingly sophisticated. A process using an automated, feed-back control nutrient-feeding strategy, based on dissolved oxygen tension (DOT) and pH has been described (Chen *et al.*, 1997). The process was automated though a computer-aided data processing system to regulate the cell growth rate by controlling interactively both the nutrient feed rate and agitation speed based on DOT. The control increased the total yield of the plasmid DNA by approximately 10-fold as compared to a manual fed-batch culture but to only 1.7μgmg^{-1}DCW. With such feed-back algorithms, plasmid yields between 100 and 230 mgL^{-1} have been obtained, mostly due to increasing biomass yields (Prather *et al.*, 2003). However, the application of feed-back algorithms is accompanied with a number of disadvantages. One is that the feeding rate depends on current measurable process parameters such as the DOT. Fluctuations in the process for whatever reason may influence the control parameter and therefore impact on the feeding rate and consequently on growth and plasmid yield. Another disadvantage of feed-back control is that the specific growth rate cannot be exactly predefined or controlled.

Precise control of the specific growth rate can be achieved by another fundamental feeding mode based on the supply of feed medium using an exponential function. Exponential feeding of glucose to control growth at 0.05h^{-1} resulted in an 800% increase in plasmid

specific yield to 7.6μgmg^{-1}DCW (O'Kennedy *et al.*, 2003). This technique is effective as it controls growth at a low-rate, a fact known to increase yield of pUC based plasmids. Also, by culturing cells in a carbon-limited environment, the cellular machinery responds by down-regulating other metabolic pathways, thus inadvertently providing more nutrients for plasmid replication. One possible drawback with fed-batch strategies have centered on concerns over the resultant plasmid quality. Reports have shown how fed-batch process result in low plasmid quality, (Schleef, 2001) however, this conflicts with others who maintain that percentage supercoiling decreases over the course of a batch fermentation, but remains fairly constant at 50-70% during fed-batch operations (O'Kennedy *et al.*, 2003).

3.3.4 Conclusions

The importance of obtaining a high plasmid specific yield is critical to the efficiency of the fermentation but also to the success and ease of the downstream processing stages. Many strategies have been tested and refined. However, it is clear that the best routes to a high specific yield are to employ relaxed plasmid replicons, which generate high-copy numbers. Ideally, they should not express any protein including for selection as this adds additional metabolic burden. Traditional batch techniques are increasingly being replaced by fed-batch strategies, most employing exponential feed, as this can positively affect plasmid specific and volumetric yields. Also, although at present complex media is common, the use of fully defined media offers greater advantages in terms of reproducibility and higher specific yields. These advantages are coupled with better approval ratings by the regulatory authorities and so easier and quicker process validation.

Once again the problem with comparing the findings of current literature concern differences in the plasmids being studied here. It is already understood that the large constructs are present at very low copy numbers of 1-2 per cell. This figure is so precise because it is known that the replication of these plasmids is stringently maintained at this level by host-cell control. This difference makes redundant any of the techniques used to influence plasmid specific yield since copy number regulation is outside the control of the environmental factors of growth rate and medium design. What was hoped for was that by virtue of the large plasmid size, sufficient plasmid mass would be present to make purification applicable. However, simple arithmetic shows that for these constructs the total cellular plasmid mass of two copies of a 116kb plasmid would be far less than that for a 6kb plasmid maintained at 500 copies per cell. The picture becomes bleaker when it is

appreciated that even high copy number plasmids form only 1-3% by mass of the total material to be purified (Shamlou, 2003). Having understood the potential drawbacks the results of the yield studies were not too surprising.

3.3.5 Results of investigations into the yield progression of the Oxford series

Figure 3-3 displays the results of triplicate shake-flask studies where progression of p5176 (116kb) yield was measured though the course of the fermentations. The shake-flask fermentations were carried out in an identical manner to be before by inoculating 500mL of either SDCAS or SuperBroth media, supplemented with 25μgmL^{-1} chloramphenicol, to a starting optical density of 0.1. The shake-flasks were incubated at 37°C and 230rpm in a shaking incubator. Wet cell weight and optical density progression were measured though out the fermentations. Duplicate 1mL samples of broth were taken hourly from each of the shake-flasks, centrifuged, the liquor discarded and the pellets frozen at -20°C. The pellets from both culture sets were processed by Qiagen spin-prep. The plasmid containing streams from the spin-preps were then quantified by PicoGreen, calibrating against a linear, lambda DNA standard curve. These studies were part of a larger investigation performed to identify suitable methods of quantifying BAC DNA containing streams. In this section are reported the results which were found to be the most accurate. Details of the remaining investigations determined to validate the different quantitative methods can be found in Analytical development: results and discussion.

Cultures grown on SDCAS media demonstrated longer lag-phases as the cells adapted to the fresh media. Additionally, as previous studies highlighted, Table 3-1 shows that cultivation on SuperBroth produced a faster growth rate, with SDCAS media showing a 20% relative reduction, comparable to the result described earlier. In line with a reduction in growth rate, SDCAS cultures also demonstrate a reduction in final biomass yields obtained, averaging 9.2gL^{-1} as opposed to 11.3gL^{-1} demonstrated by SuperBroth. Again in line with earlier results.

Considering the plasmid yields produced by these fermentations shows a high degree of comparability between the two media types and fairly constant yields. Considering Table 3-1 highlights how plasmid yields in both fermentations remained quite constant at ~50$\mu ggWCW^{-1}$ equating to 1-2 copies per cell. This result fits well with the yields predicted according to the copy number of these constructs. It will be outlined in Chapter 4 about how the validity of these yield results was confirmed

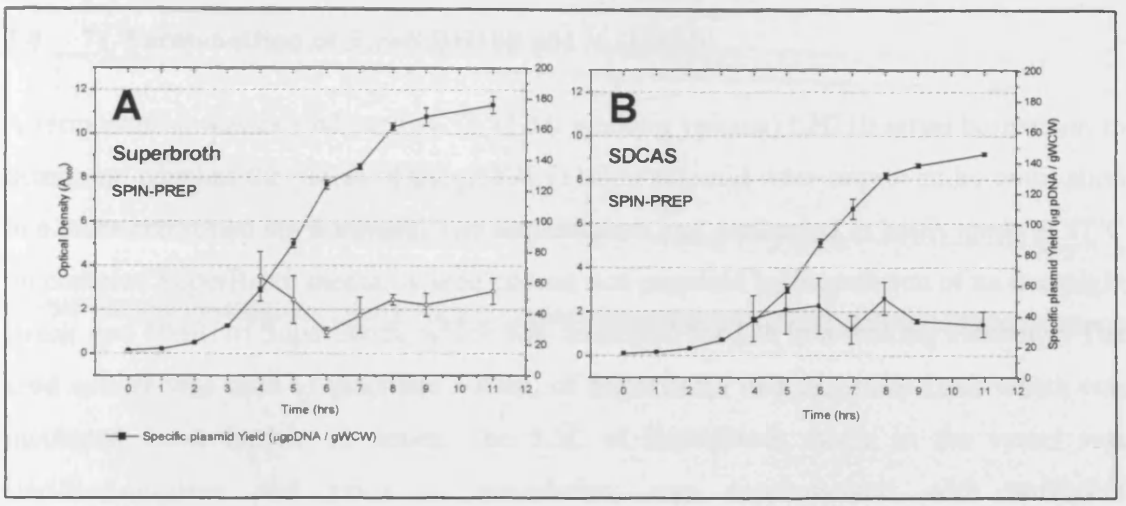

Figure 3-3 Chart depicting the progression of wet cell weight (gL-1) and specific plasmid yield (µg pDNA/ gWCW) though triplicate shake-flask fermentations of DH10β [p5176 (116kb)] on two media types; complex SuperBroth and semi-defined SDCAS media.

2L shake-flasks (500mL media) were inoculated with 50 OD units and incubated in a shaking incubator (230rpm) at 37 ° C. Hourly 1mL samples of broth were taken, centrifuged and the plasmid extracted from the cell pellets using Qiagen spin-prep® extraction. The plasmid containing streams were then quantified by PicoGreen against a λDNA standard curve.
[A; SuperBroth media – Qiagen spin-prep / B; SDCAS media – Qiagen spin-prep]

Table 3-1 Summarising the yield data produced by p5176 cultures grown on both SDCAS and SuperBroth media by Qiagen spin-prep. The plasmid containing streams were quantified by PicoGreen calibrating against a linear λDNA standard curve.

Sample		Spin-Prep Eluent		
Measure / Media	μ_{max} (h^{-1})	Final Specific Yield (µg/ gWCW)	Final Volumetric Yield (mgL^{-1})	Final Copy No. (Copies/cell)
SDCAS	0.56	34.8 ±8.2	0.32 ±0.08	1.14 ± 0.27
SuperBroth	0.69	54.8 ±8.46	0.62 ± 0.1	1.80 ± 0.28

3.4 7L Fermentation of *E.coli* DH10β p5176 (116kb)

A fermentation was carried out in a 7L (5.5L working volume) LH210 series bioreactor, to determine whether the yields of the p5176 (116kb) plasmid were improved by cultivation in a more controlled environment. The fermentation was performed in batch mode at 37°C on complex SuperBroth media. A seed culture was prepared by inoculation of an overnight streak into 10mL of SuperBroth, which was incubated for 12h in a shaking incubator. The seed culture was used to inoculate 500mL of SuperBroth in a 2L shake-flask which was incubated for a further 12 hours. The 5.5L of SuperBroth media in the vessel was sterilised-in-place and prior to inoculation was supplemented with sufficient chloramphenicol to produce a 25μgmL^{-1} concentration in the media. The broth was then inoculated to a starting optical density of 0.5 and aeration maintained at 5.5Lmin^{-1} (1vvm). During the fermentation optical density, wet cell weight and plasmid retention were monitored using the techniques outlined in 2.5.1, 2.5.2 and 2.5.4.

3.4.1 Fermentation Growth analysis .

Figure 3-4 and Table 3-2 details the information obtained from the fermentation. From the growth profile it can be seen how quickly the culture adapted in larger scale culture, since the lag-phase is almost non-existent. This is confirmed by the OUR profile which shows a rapid drop-off from saturation to the 30% control level within one hour. Maximum oxygen uptake rate of 34.5mmolsL^{-1}h-^{1} was reached at 6.33h coinciding with the point of highest biomass concentration. Between this point and harvest, biomass concentration dropped slightly. The fermentation was harvested at the DOT spike, occurring at 7.92h, an identifying signal that the culture was limited and as such was respiring anaerobically. However, it is believed that the culture was not O2 limited as the maximum impeller speed used was 692rpm, with 1000rpm being the maximum capable using the algorithm. The culture most likely became substrate limited. Biomass levels at harvest are improved on shake-flask studies by roughly 25-30% indicating improved oxygen supply. The harvest cell concentration of 15gL^{-1} (~4gL^{-1}DCW) matches well with similar studies reported in the literature,(Wang *et al.*, 2001; Lahijani *et al.*, 1996; Horn *et al.*, 1995) who all report harvest yields of 4-5gL^{-1} DCW, when cultivating plasmid-bearing *E.coli* in batch on complex media

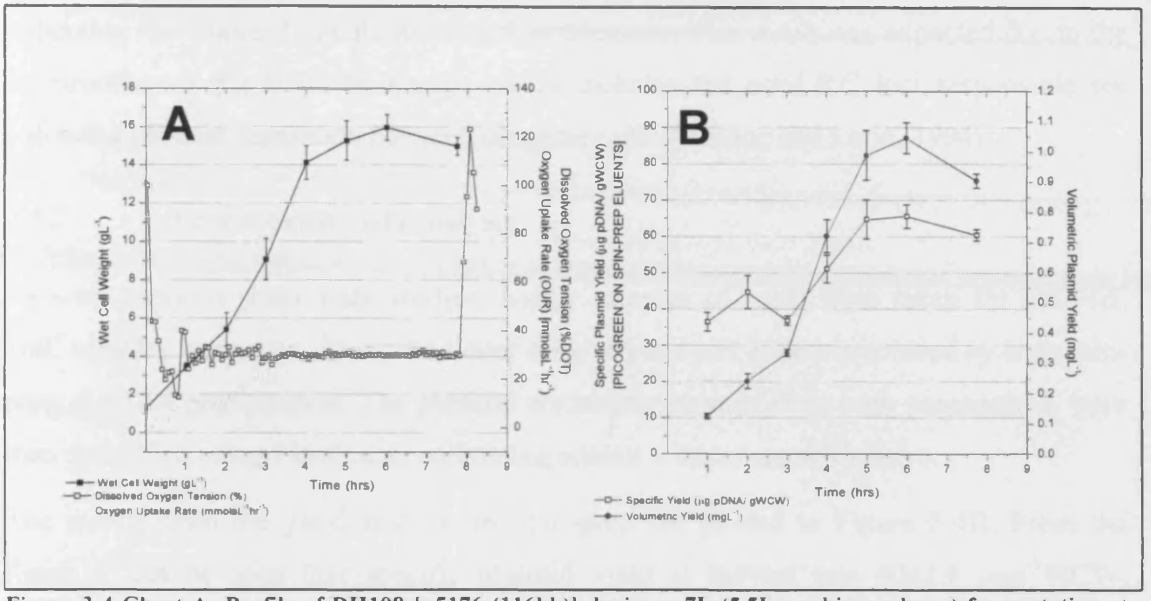

Figure 3-4 Chart A: Profile of DH10β [p5176 (116kb)] during a 7L (5.5L working volume) fermentation at 37°C on SuperBroth supplemented with 25µgmL^{-1} chloramphenicol. The vessel was inoculated to 0.5OD a from shake-flask culture of the same media. Oxygen saturation was maintained at 30% by cascade control of impeller speed. The impeller speed response time was set 10-fold faster than the Ingold polarographic probe response time in order to maintain stable control. Optical density and wet cell weight were followed throughout the fermentation. Multiple 1mL samples of broth were extracted hourly, spun down to remove broth and frozen for retrospective analysis of plasmid specific yield. At harvest the broth was aliquoted into 0.5L centrifuge pots and centrifuged. The cell paste was frozen at -80°C for later analysis.

Chart B: Graph charting the progression of plasmid yield during a 5.5L working volume, batch fermentation of DH10β p5176 (116kb) on complex, SuperBroth media. Hourly, triplicate 1mL broth samples were centrifuged, the supernatant discarded and the pellets stored at -20°C for retrospective analysis. The cell pellets were processed using Qiagen spin-preps and the plasmid in the eluents quantified by PicoGreen against a λ DNA standard curve. The specific yield was calculated by dividing the total mass of plasmid DNA in the sample by the mass of cell paste processed in 1mL sample, calculated from the wet cell weight at the time of sampling. Volumetric plasmid yield was calculated by multiplying the specific yield by the wet cell weight at the appropriate time point.

Table 3-2 Table highlighting the key measurable values from a 5.5L working volume fermentation of DH10β p5176 conducted in batch mode on SuperBroth media. Growth rate was calculated by linear regression of the natural log of wet cell weight progression between the 1-4 time points. OUR was calculated using the exit gas data recorded by the mass spectrometer. Total oxygen demand was calculated by integration of OUR curve and accounting for total volume of 5.5L.

Measure / Strain	Final OD (A600)	Final WCW (gL^{-1})	Max. OUR ($mmolsL^{-1}h^{-1}$)	Total O_2 Demand (mmols)	µ (h^{-1})	Plasmid retention at harvest (%)
DH10β [p5176 (116kb)]	7.4	14.9	34.5	352.1	0.475	100

The plasmid stability profile was 100% at each assay point during the fermentation, indicating that plasmid retention was not problematic. This result was expected due to the construction of the BAC backbone, which includes the *parA,B,C* loci responsible for enforcing plasmid separation between daughter cells (Monaco and Larin, 1994).

3.4.2 Fermentation yield analysis

As with previous shake-flask studies, hourly samples of broth were taken for analysis. 1mL samples were spun-down, the liquor removed and cell pellets processed by both spin-prep and IPA precipitation. The plasmid containing streams from both preparations were then quantified using PicoGreen, calibrating against a linear standard curve.

The results from the yield analysis by spin-prep are plotted in Figure 3-4B. From the figure it can be seen that specific plasmid yield at harvest was 60±1.6 μgg^{-1}WCW, resulting in a final volumetric yield of 0.9±0.02 mgL^{-1}. The specific yield value is within 10% of that achieved in the shake-flask studies outlined in Table 3-1. The average specific yield over the course of the entire fermentation was 51.4±12.5 μgg^{-1}WCW, a figure very much in line with that shown in.

The specific yield does display a rise (~70%) during the log-phase of growth, specifically between the 3-5h time-points. As postulated earlier, this coincides with the period of maximum cell growth when any cell will likely have greater than 1 genome equivalent of DNA.

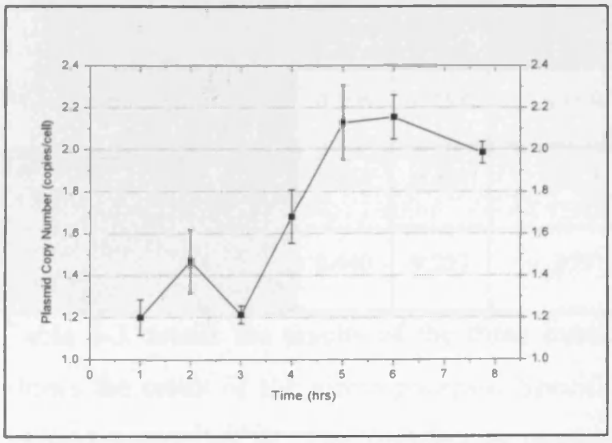

Figure 3-5 Graph outlining the progression of plasmid copy number during a 5.5L batch fermentation of DH10β p5176 on complex SuperBroth media. Copy number was calculated from the specific plasmid yield figures obtained by PicoGreen on spin-prep purified hourly samples.

The same logic can be applied to these plasmid molecules, whose replication is controlled in-line with genome replication. It is highly likely that the individual cell would posses a greater number of plasmid molecules during periods of rapid cell growth. Copy number analysis confirms this suspicion. Figure 3-5 plots the copy number progression calculated

from the yield data. The rise during the log period of growth is from an average of ~1.2copies to over 2.0 copies per cell. During periods of slow growth the copy number hovers between 1.2-1.4. In this respect these plasmid molecules are produced in a growth associated manner, meaning the optimum harvest point is at the end of the log-phase. Continuing fermentation could result in 50% lower yields as the plasmid copy number would return to its low growth copy number, which seems to be occurring 6-8 hours from the onset of cultivation.

3.4.3 Qiagen Column chromatography studies

Further studies into the plasmid yield from the 5.5L fermentation of p5176 were conducted by 'larger-scale' Qiagen-prep analysis on the harvested cell paste. Three methods of extraction were employed, all utilising the Qiagen anion-exchange columns but using three distinct protocols. The eluents from all three preps were quantified by absorbance at 260nm. The A_{260}/A_{280} ratio was used to determine the relative purity of the samples and approximately 1μg of each of the purified samples was run by conventional electrophoresis to enable comparison of the purity and relative form of the various plasmid samples. The gel was also useful for comparing the plasmid streams obtained from the samples taken during the fermentation and extracted by both spin-prep and IPA precipitation.

Table 3-3 Table detailing the total masses of plasmid obtained from three protocols based around the Qiagen Maxi-prep methodology and the resultant specific yields.

Measurement Extraction protocol	A_{260}	A_{280}	Conc. (μgmL^{-1})	Total mass (μg)	Specific Yield (μgg^{-1})	A_{260}/A_{280}
Maxi-prep (2.0g)	0.306	0.188	153.0	76.5	38.3	1.63
Low-copy number prep (4.0g)	0.603	0.467	301.5	150.8	37.7	1.29
Large construct prep (4.0g)	0.440	0.227	110	55.0	13.8	1.94

Table 3-3 details the results of the three extraction methods employed and Figure 3-6. shows the result of the electrophoresis. Specific plasmid yield varies considerably from 13.8-38.3 μgg^{-1}WCW. The simplest extraction technique was the Qiagen® Maxi-prep where 2.0g of cell paste was lysed and the clarified lysate purified using a Tip-500 column.

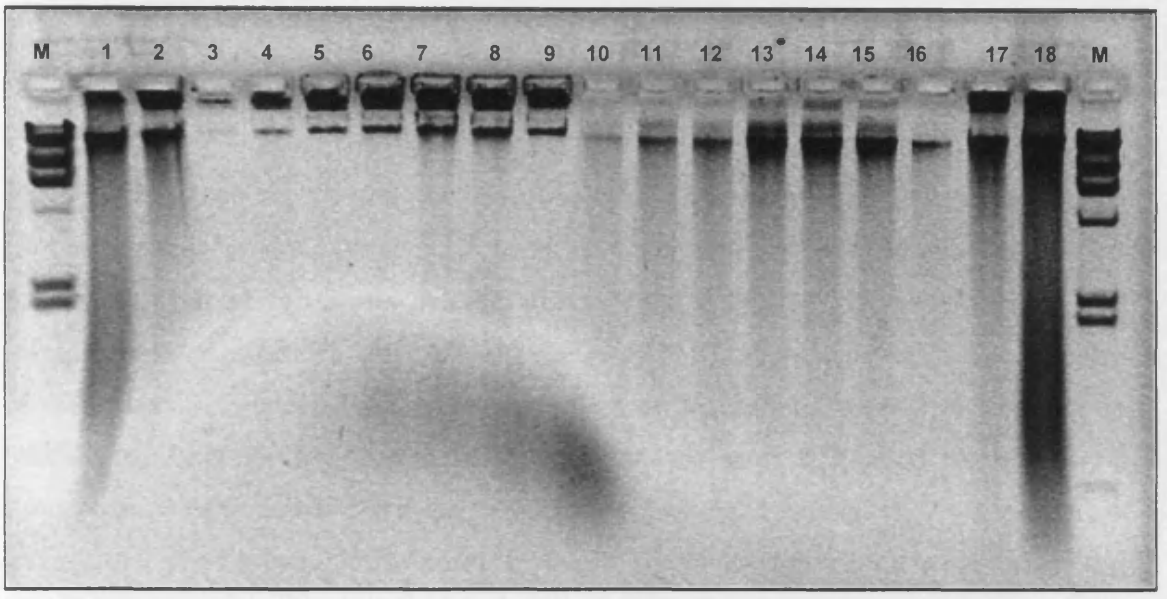

Figure 3-6 Conventional gel electrophoresis of samples prepared from hourly cell collections from the 5.5L fermentation of DH10β [p5176 (116kb)]. Approximately 1μg samples of plasmid were loaded into each well of a 0.8% agarose gel and run for 4 hours at 6Vcm^{-1} in 0.5xTBE. The gel was then stained in a 1:10,000 dilution of EtBr before being photographed using a UV transilluminator.

M **..... λ*HindIII* digest**
1**..... Qiagen Maxi-Prep**
2**..... Qiagen Large Construct prep**
3**..... IPA precipitated lysate (Time-point 3)**
4**..... IPA precipitated lysate (Time-point 4)**
5**..... IPA precipitated lysate (Time-point 5)**
6**..... IPA precipitated lysate (Time-point 6)**
7**..... IPA precipitated lysate (Time-point 7)**
8**..... IPA precipitated lysate (Time-point 8)**
9**..... IPA precipitated lysate (Time-point 9)**
10**..... Qiagen spin-prep (Time-point 3)**
11**..... Qiagen spin-prep (Time-point 4)**
12**..... Qiagen spin-prep (Time-point 5)**
13**..... Qiagen spin-prep (Time-point 6)**
14**..... Qiagen spin-prep (Time-point 7)**
15**..... Qiagen spin-prep (Time-point 8)**
16**..... Qiagen spin-prep (Time-point 9)**
17**..... Qiagen Large Construct prep**
18**..... Qiagen Low copy number Maxi-prep**
M**..... λ*HindIII* digest**

The yield produced was ~35% below that obtained by PicoGreen on spin-prep purified samples. Also, the low A_{260}/A_{280} ratio points to contamination by protein, meaning the specific yield could be even lower. Analysis by electrophoresis indicates that the sample was heavily contaminated by genomic DNA. Genomic DNA contamination can be identified by a continuous smear of DNA extending down the lane in which the sample was loaded. By comparing the spin-prep purified samples with the maxi-prep eluents suggests that the spin-prep matrices are far more efficient at removing genomic DNA. However, this cannot be definitively stated since the concentrations of cell material in all the Qiagen large-scale preps at 200gL^{-1}WCW was 3-fold greater than that of the samples taken during the fermentation (60gL^{-1}WCW), resulting in a higher amount of contaminating gDNA in the starting material. Despite this unequivalence, the gel shows roughly equal masses of plasmid loaded and there is no doubt that the eluent from the gravity fed, maxi-prep column has a far higher ratio of genomic to plasmid DNA. This

ratio analysis is important as it suggests that the maxi-prep is either less capable of purifying the large construct or not as efficient at removing genomic DNA as the spin-preps.

The low-copy number Qiagen protocol was used to improve the yield of the large construct. Its operation differed little from the maxi-prep protocol, except it employed double the mass of cell paste, in twice the volume of buffer, with an additional IPA precipitation step to concentrate the feed material prior to column loading. The philosophy of the protocol is simple. By doubling the mass of the starting material the amount of plasmid available for purification is doubled, but the same applies to the masses of contaminants. From Table 3-3 it can be seen that double the amount of DNA is purified and as such gives a very similar specific yield to the maxi-prep. However, as before the specific yield could be misleading as the A_{260}/A_{280} ratio is even poorer indicating the greater mass of starting protein is not removed as effectively. Also, from the gel profile, shown in lane 18, it becomes clear that the prep merely succeeds in purifying a higher amount of genomic DNA than the maxi-prep, such that the plasmid to genomic DNA ratio is worse than when using the maxi-prep.

This highlights how critical the harvest specific yield is to the plasmid purification process. If the plasmid specific yield is low, simply increasing the mass of cell paste processed will do nothing to solve the problem as it only serves to increase concomitantly the mass of contaminants. The key factor is the initial starting ratio of plasmid DNA to genomic DNA. Although other contaminants like protein and RNA are present, their removal is less of an issue than that of genomic DNA, the physicochemical similarities of which being so close to that of the plasmid product that separation becomes difficult.

Looking at lanes 2 and 17 it can be seen that the gDNA contamination problem is improved by the use of the Qiagen Large construct kit. The operation of this kit was similar to the low-construct prep except that it employed an exonuclease digestion step to enzymatically clear gDNA contamination. The yield results from this prep were very low at 13.8$\mu g g^{-1}$WCW. From PicoGreen quantification on spin-prep eluents it is known that the specific yield at harvest was ~60$\mu g g^{-1}$WCW, which means that the Tip-500 columns used in these protocols are capable of recovering only ~25% of the plasmid that is present in the sample. Therefore, large plasmids do elute better from spin-preps, where 70-80% recovery has been established (Figure 4-10), than from gravity-fed Qiagen columns. What is believed to occur in the maxi-prep column is that the small, contaminating genomic

DNA fragments are not cleared as efficiently by the wash steps but are eluted at a higher rate than the plasmid during the elution step, even more so since the elution buffer was heated in these investigations. However, the large plasmid size means their elution or even their binding is problematic. Later studies using PD-10 desalting columns and Qiagen columns (6.5.3)showed that the large constructs were eluted poorly from the columns and it is possible that a similar effect occurred here.

3.4.4 Topology of Fermentation samples

The gel also displays interesting differences in plasmid topology resulting from processing. Although the samples were only run by conventional gel electrophoresis it is understood and corroborated by later studies (4.6.1) that the linear/ open-circular forms of the large plasmid are incapable of penetrating into the gel and remain trapped in the wells. However, it is believed that the smaller diameter SCC form of the plasmid and indeed smaller fragments created by shear degradation of the plasmid are capable of running into the gel. Comparing the spin-prep processed samples to the IPA precipitated samples highlights how damaging the spin-prep methodology is to the plasmid topology. From the gel it can be seen that in the IPA samples the supercoiled plasmids runs slightly behind a similar species found in the lanes of the spin-prep purified samples. It is believed that for IPA this band represents supercoiled BAC DNA. For the spin-prep purified samples this is believed to be sheared plasmid DNA, because it runs slightly ahead. The sheared fragments are believed to be large, and as such are not well resolved by conventional gel electrophoresis, but there is also evidence of smaller sheared fragments since a slight smear continues down the lanes of the spin-prep purified samples. It is thought that since the spin-preps force the plasmid through the column matrix explains the higher levels of recovery but also the damage caused to the plasmid topology.

3.4.5 Conclusions

The 5.5L fermentation study confirmed that large-scale cultivation of cells bearing large constructs remains unproblematic. Specific growth rate is adequate and the final biomass yield is within the range reported by authors adopting similar media and cultivation conditions. There was nothing observed that would suggest that the plasmids cause oxygen limitation in the growing cells, indeed substrate limitation was believed to be the limiting factor. Further evidence was provided as to the very low specific yields at which these plasmids exist. Additionally, it was determined that cultivation of these plasmids in a more

controlled environment does little to improve the specific yield. Important conclusions can also be drawn about approaches to downstream processing and how the specific yield is the root problem for effective genomic DNA clearance. Simply increasing the mass of cells for processing does not alleviate the problem. Direct visual evidence was also provided for the damaging effects of spin-prep processing on plasmid topology.

3.5 Electroporation of the large series of plasmids into *E.coli* DH1.

3.5.1 Introduction

The series of large plasmids was transformed into GSK's host strain, *E.coli* DH1, by electroporation using the methodology outlined in (2.6.4). This was performed to enable studies of the large plasmid series to begin, using the process for manufacturing plasmid DNA employed by GSK. Following cell banking, shake-flask studies were performed on the plasmids in the new host to determine any influence on growth the host change may have had. The studies compared the large plasmid series in DH1 to the same plasmids propagated in DH10β. The cells were cultivated on GSK's complex media recipe, which was compared to historical shake-flask studies performed using SuperBroth.

Shake-flask studies were performed by inoculating 50mL of sterile seed media, containing 25μgmL^{-1} chloramphenicol, in 1L baffled shake-flasks. Inoculation of each flask was achieved by the addition of one vial of defrosted cell stock (1.8mL), which was banked at ~2.5OD and so gave a starting OD of 0.1 when added to 50mL. The flasks were all incubated at 37°C, 230rpm in a shaking incubator. Samples were taken hourly to determine optical density.

3.5.2 Effect of host-strain on fermentation growth profiles

Figure 3-7 and Table 3-4 detail the results of the shake-flask studies. From Figure 3-7A the optical density progression of the shake-flasks is shown. It is immediately apparent that the host-cell line does effect the growth of the cultures. The *E.coli* DH1 strain demonstrated a much shorter lag phase than the DH10β cultures, which remained 1-1.5h behind the DH1 cultures. The reason for this is postulated to be due to the complex media having been specifically optimised for propagation of DH1 cells. One of the key factors in medium development is to reduce the period of lag-phase of growth (Stanbury and Whitaker, 1984). Media optimisation would have been achieved using either Plackett-Burman or factorial design studies to determine the optimum concentrations of the media components that produced the best growth and yield characteristics. Since these optimisation studies would have been performed using the DH1 strain, the media would be specifically adapted for its cultivation.

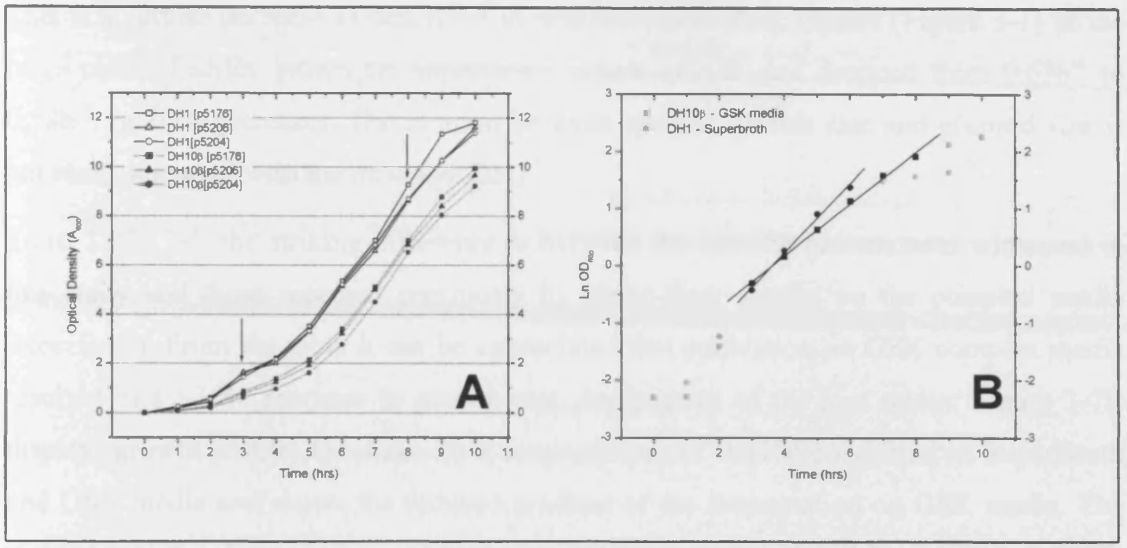

Figure 3-7Chart A displays the progression of optical density of cultures of *E.coli* DH1 and DH10β propagating each of the plasmids from the Oxford series. The fermentations were carried out in 1L shake-flasks, using 50mL of GSK proprietary media supplemented with 25μgmL^{-1} chloramphenicol, from a starting OD of 0.1. The flasks were incubated at 37 ° C / 230rpm in a shaking incubator with hourly samples removed from each, diluted appropriately and optical density determined at 600nm using a Shimadzu spectrophotometer. The arrows mark the period of logarithmic growth over which linear regression was performed. Chart B plots the natural log of the mean optical density for the fermentations of the large plasmid series in DH10β in this study and compares the maximum specific growth rate to the same strains grown on SuperBroth in (Figure 3-1)

Table 3-4 Table compiling the growth and final optical densities reached during shake-flask fermentations of the large plasmid series in the original host strain, DH10β and in the GSK host strain, DH1. The data obtained in this study was compared and normalised to the figures obtained in the first shake-flask studies with the cultures grown on SuperBroth.

Strain/media	DH10β - SuperBroth			DH10β - GSK media			DH1 - GSK media		
Construct	p5176	p5206	p5204	P5176	p5206	p5204	p5176	p5206	p5204
μ (h^{-1})	0.63	0.60	0.58	0.45	0.41	0.40	0.44	0.43	0.44
%	100	100	100	70.2	72.3	75.8	70.7	69.1	68.7
Final OD	5.15	4.81	4.69	9.94	9.66	9.22	11.8	11.6	11.38
%	100	100	100	193	200.8	196.6	229.1	241.1	242.6

However, when both DH1 and DH10β cultures enter logarithmic growth the difference in specific growth rate is quite minimal, even from the optical density progression it can be seen that the profiles run roughly parallel. Table 3-4 details the specific growth rate for each fermentation. The GSK media provided an average specific growth rate in all the cultures is 0.43±0.02 h^{-1}. There is a decrease in growth rate with increasing plasmid size from 0.45h^{-1} to 0.40h^{-1} in the DH10β cultures, representing an 11% decrease.

This is a similar decrease as described in previous shake-flask studies (Figure 3-1) of the large plasmid series grown on SuperBroth, where growth rate dropped from $0.63h^{-1}$ to $0.58h^{-1}$, (a 10% decrease). The relation between specific growth rate and plasmid size is not really apparent with the new host DH1.

From Table 3-4, the striking difference is between the specific growth rates witnessed in this study and those reported previously by shake-flask studies on the complex media SuperBroth. From the table it can be appreciated that cultivation on GSK complex media resulted in a ~30% decrease in growth rate, irrespective of the host strain. Figure 3-7B displays growth profiles for shake-flask fermentations of DH10β conducted on SuperBroth and GSK media and shows the reduced gradient of the fermentation on GSK media. The geometry of the shake-flasks used in the two different studies did differ, but it is unlikely that such a significant decrease in growth rate can be solely due to flask geometry and as such the media employed must be affecting the change.

3.5.3 Effect of host-strain on biomass yields

The second striking difference is the improvement in harvest biomass yields as a result of cultivation on GSK media. The final biomass yields for the large plasmid series propagated in DH10β are double that for the same strains cultivated on SuperBroth. In both DH1 and DH10β cultivations the final biomass yields decrease slightly with increasing plasmid size. This effect was reported earlier where the final biomass yield dropped about 10% when plasmid size increased from 116kb to 242kb. In this study the biomass reduction attestable to increasing plasmid size is between 5-7%. The DH1 strains consistently produced the highest biomass yields at harvest, more than 2.3-fold higher than the same strains cultivated on SuperBroth and ~20% higher than DH10β cultures grown on the same GSK media. This increase over DH10β is believed to be attributable again to either the media optimisation having been specific to DH1 or the fact that this strain is a *relA* mutant. Such mutants are unable to produce ribosome-dependent ppGpp synthetases. These are activated during amino-acid starvation and produce the signalling molecule ppGpp, which induces the stringent response in bacteria. The stringent response causes the down-regulation, of among other things, protein synthesis, cell division and genome replication. This response in DH10β could explain the decreased biomass produced as the cells effectively enter hibernation as they become starved whilst the DH1 strain carries on dividing (Baracchini and Bremer, 1988; Hecker *et al.*, 1983).

3.5.4 Conclusions

From the growth profile of the large plasmid series propagated in DH10β on SuperBroth, shown in Figure (Figure 3-1), the extent of the difference in growth profiles can be seen. Cultivation on GSK media extends the logarithmic growth period by approximately three hours. It is believed that the reduced growth rate and extended log-phase is a characteristic of the media, which is enhanced by media optimisation. As explained earlier a reduced growth rate is preferable when culturing cells containing relaxed plasmids, as evidence suggests this increases specific plasmid yield (Lin-Chao and Bremer, 1986; Byung Gee Kim, 2006).

The GSK media differed from SuperBroth in several ways. Firstly, GSK media employed glycerol as a carbon source. The use of this more complex carbohydrate has been shown to reduce the maximum specific growth rate and also allow the attainment of higher biomass yields (Thatcher , 1997). Also, glycerol can be used at much higher concentrations than glucose without suffering the inhibitions of growth caused by acetate accumulation. Secondly, the GSK media was richer in the concentration of yeast extract together with the inclusion of additional minerals providing extra sources of potassium, phosphorus and an inorganic nitrogen source. This richer medium formulation supplemented with more minerals necessary for bacterial growth and metabolism are believed to be the reason for the GSK media consistently producing higher biomass yields.

These studies demonstrate that the DH1 host-strain is capable of increasing biomass yields, possibly due to an improved genotype. Additionally, the use of GSK's richer media formulation reduces specific growth rate, extends logarithmic growth phase and so doubles the final biomass yield. If this media were to be used for production of a relaxed plasmid species, a simultaneous increase in specific and volumetric yields could be expected. Consequently, further pilot-scale fermentations were conducted to determine whether this improved media and host-cell combination could generate any improvements in the specific yields of the Oxford series of plasmids despite previous studies having confirmed the vector architecture makes this outcome unlikely.

3.6 Triplicate 4L working vol. fermentations of *E.coli* DH1 p5176 (116kb)

3.6.1 Introduction

Pilot scale fermentations were run to investigate the growth and yield characteristics of the large plasmids propagated in the DH1 cell line further.

Triplicate fermentations of the large plasmid [p5176] were conducted along with triplicate fermentations of DH1[pSVβ] and DH1[parental]. The pSVβ and parental fermentations were conducted to form positive and negative controls respectively. Fermentations were carried out at 37°C in 7L total volume, water-jacketed fermenters using 4L of sterile media supplemented with the appropriate antibiotic where required. DOT was maintained at 30% saturation by cascade control of impeller speed. Aeration was achieved by sparging at 1vvm until the DOT fell below 30% and the impeller speed was at the maximal 1000rpm, when the airflow was switched to enriched air, initially at 1vvm and later 2vvm. The fermentations were deemed complete when DOT spiked. Optical density and wet cell weight progression were monitored throughout the runs. Multiple broth samples, equal to 5OD unit volumes, were taken at each time-point, centrifuged, the liquor discarded and the pellets stored at -80°C for retrospective analysis of plasmid specific yield progression.

3.6.2 Results

Figure 3-8 and Table 3-5 detail the mean results of the triplicate fermentations. The specific growth rates (μ) calculated by linear regression of the OD and WCW progression were very comparable, differing only by an average 5%. Both sets of specific growth rates display a decrease in growth rate for plasmid bearing cells, as compared to the parental strain. This decrease in growth rate has been reported previously (3.2) and the decline comparable to before, with the high-copy number strain displaying a ~10% decrease and the large plasmid; p5176 displaying a ~5-10% decrease.

The impact of the improved media recipe and aeration regime, achieved by sparging enriched air, can be seen in the large increase in final biomass yields as compared to previous fermentations. Comparing the data for DH1[p5176] in Table 3-5 with the data for the same strain, cultivated on SuperBroth without enriched air aeration (Table 3-2) it can be seen that the harvest OD in these fermentations displayed a 7-fold increase and the WCW increased 6-fold.

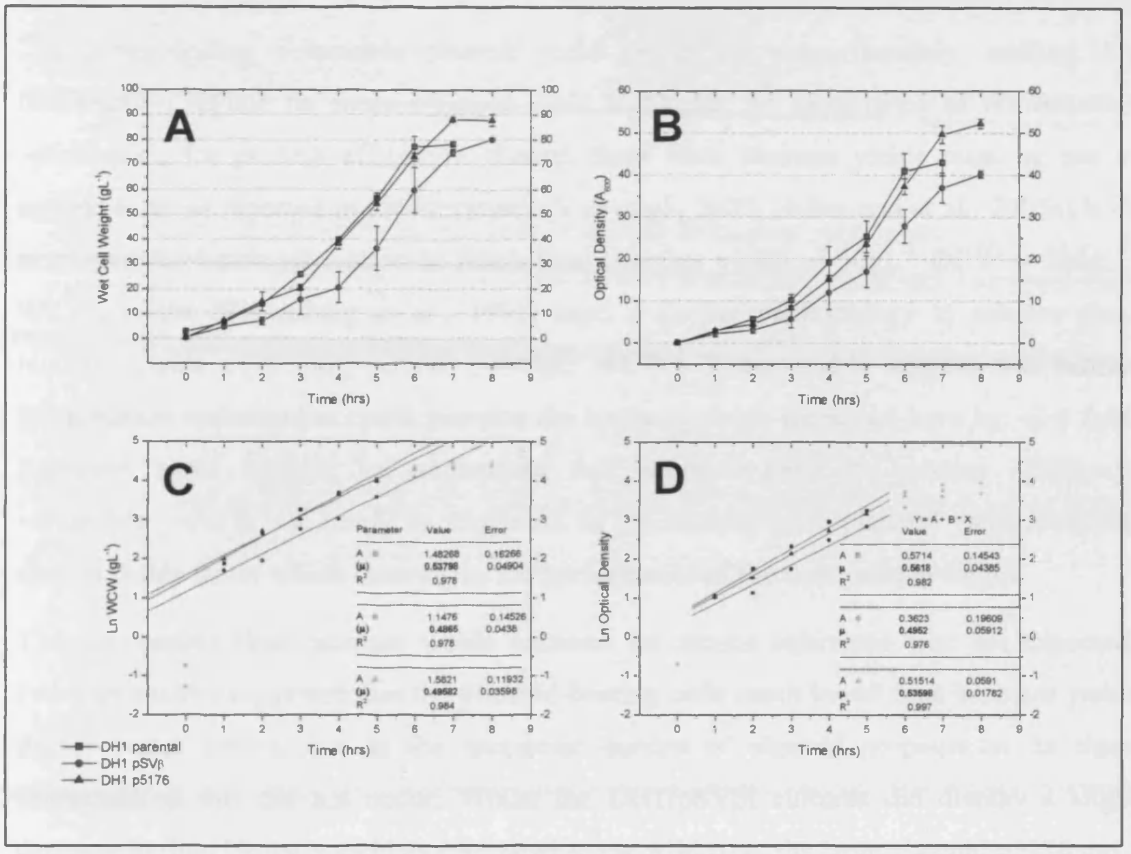

Figure 3-8 Chart outlining the mean progression of optical density and wet cell weight of triplicate 4L working volume fermentations of *E.coli* DH1 parental, pSVβ (6.9kb) and p5176 (116kb). Wet cell weights from each vessel at each time-point were determined by spinning down duplicate 1mL broth samples in pre-weighed Sarstedt tubes. The supernatant was decanted off and any liquid traces removed using a cotton bud, these tubes were then re-weighed on a five-point balance. Optical density measurements were taken by diluting samples of the broth with blank media to a level consistent with the region of linearity (0.1-0.6OD) and measuring absorbance in a Shimadzu spectrophotometer at 600nm. 5OD unit equivalent volumes of broth from each vessel were aliquoted into sterile Sarstedt tubes at hourly intervals. These were prepared in a similar fashion to the WCW samples except were frozen at -80°C for retrospective determination of plasmid yield.
[A; Wet cell weight progression / B; Optical density (A600 progression / C; μmax determination for WCW / D; μmax determination from OD]

Table 3-5 Table outlining the mean maximum growth rates of the cultures grown at 4L scale, as measured by two methods, together with the average final biomass yields. The table shows the percentage difference between the results normalised against that recorded for the parental fermentations

Parameter / Strain	DH1 PARENTAL	DH1 [p5176]	DH1 [pSVβ]
μ OD (h^{-1})	0.5618 ± 0.0439	0.5360 ± 0.0178	0.4952 ± 0.059
%	100	95.4	88.14
μ WCW (h^{-1})	0.5380 ± 0.049	0.4958 ± 0.036	0.4865 ± 0.044
%	100	92.2	90.4
Final OD	42.9 ± 3.0	52.2 ± 1.11	40.2 ± 0.85
%	100	121.7	93.7
Final WCW (gL^{-1})	78.1 ± 0.99	87.9 ± 2.4	80.15 ± 0.59
%	100	112.5	102.6

The corresponding volumetric plasmid yield would rise proportionately, making this fermentation regime far more efficient. This highlights the importance of fermentation optimisation for process efficiency, though these final biomass yields must be put in context to those reported in the literature. (Voß *et al.*, 2003; Huber and et al., 2005a) both employed fed-batch cultivation to reach final biomass yields of $50gL^{-1}$ DCW (~$200gL^{-1}$ WCW) whilst (Riesenberg *et al.*, 1991) used a similar methodology to achieve final biomass yields of $110gL^{-1}$ DCW (~440gL WCW). These yields suggest that further fermentation optimisation could increase the biomass yields witnessed here by ~2-4 fold. However, again it must be emphasised that whilst essential to process efficiency, volumetric yield is not nearly as important as the final specific plasmid yield obtained, since it is this factor which determines the performance of the downstream stages.

The comparable final biomass yields between the strains cultivated was not expected. Previous studies suggested that the plasmid-bearing cells reach lower final biomass yields than parental strains, due to the metabolic burden of plasmid propagation. In these fermentations this did not occur. Whilst the DH1[pSVβ] cultures did display a slight decrease in final biomass yield as compared to the wild type, the large plasmid p5176 gave a relative increase in final biomass yield. A possible explanation for this lies in the media formulation. The triplicate fermentations of each strain were performed simultaneously, 16L of cultivation media was prepared in bulk, so that the same cultures were grown on batch-identical media. Differences could have occurred during the media preparation between the different sets of triplicate fermentations and this may account for growth disparities. A possible improvement would have been to perform triplicate fermentations simultaneously but with each fermentation running a different strain. This would not have removed any differences caused by variation in the inoculum used, but an understanding of this effect would have been useful.

3.7 Progression of plasmid yield during 4L fermentations

3.7.1 Introduction

It was hoped by conducting these fermentation trials of the large construct in the new host; DH1 and on media specifically adapted for its cultivation that an increase in plasmid yield may be recorded. So, together with monitoring the fermentation growth, broth samples were taken during the runs and used to determine plasmid yield through the course of the process.

The samples taken for yield analysis were processed by a variety of methods since at this stage in the project a suitable method of accurately recording the yield of these constructs had yet to have been found and validated. More details into the background of the investigations concerned with determining the suitability of the various analytical techniques can be found in the Analytical development chapter. The method that will be reported here was the method found to describe the situation most accurately for this particular investigation. However, the samples obtained during these fermentations were used to validate the different analytical techniques so the yield curves presented here will be encountered again in later sections (4.3 and 4.4).

3.7.2 Results

The yield profiles from the 4L fermentations are described by Figure 3-9. Graph A plots the specific yield profile for the small, high-copy number plasmid pSVβ (6.9kb) whilst B describes the same for the large construct p5176 (116kb). The plots were generated from data obtained from A_{260} analysis of Qiagen spin-prep purified cell pellets. The method of quantification is a very common one for determining yield progression of small, high-copy number plasmids, since the spin-prep can be relied upon to remove the majority of contaminants, whilst absorbance on pure DNA samples can be regarded as a highly accurate, and indeed is the method employed to calibrate other methods of plasmid quantification.

Considering the smaller plasmid pSVβ first. It can be seen that plasmid specific yield begins at ~175μg $gWCW^{-1}$ and rises to ~320μg$gWCW^{-1}$ by the end of the fermentations. The results for the three vessels show a high degree of comparibility.

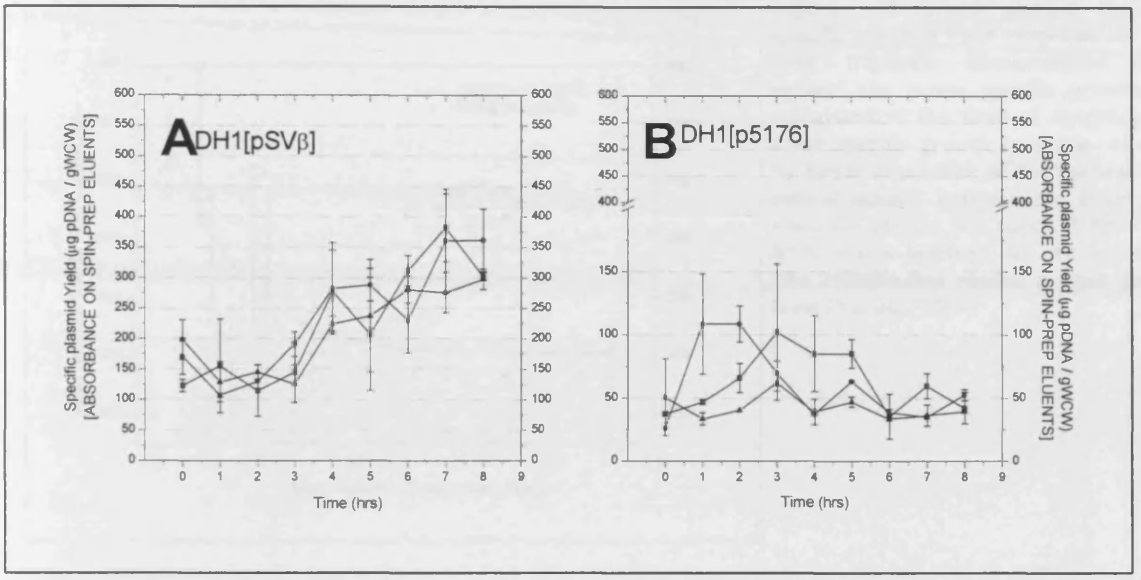

Figure 3-9Chart describing the progression of specific plasmid yield (µg pDNA/ gWCW) throughout triplicate 4L 37°C of *E.coli* DH1 pSVβ (6.9kb) and p5176 (116kb). Duplicate 5OD-unit equivalent volumes of broth were taken at each time point for each fermentation and centrifuged. The resultant cell pellets were then processed using using Qiagen spin-preps. The plasmid recovered from the spin-preps was then quantified by absorbance. The specific yield could be then calculated from the mass of plasmid recovered and the size of the pellet from which the plasmid was extracted

The increase in plasmid yield with the progression of the fermentation was postulated to be due to relative decreases of the specific growth rate with time. As outlined in earlier sections plasmid copy number and hence specific yield vary inversely with growth rate. In order to test this, the mean specific yield of the pSVβ was plotted against the culture growth rate recorded at the time of sampling. This was performed by linear regression between the natural log of the OD at the time prior and after the sample was taken. It is appreciated that the use of only three data points will lead to inaccuracies in the returned value but the aim was only the illusatration of connection between plasmid yield and growth rate for relaxed plasmid. The result of the analysis is detailed in Figure 3-10. From the graph it can be seen that the relationship described by (Vasuki, 1989) is in action for these fermentations. The importance of such a relationship is that it means that a degree of control can be exerted over the specific yield of the fermentation by manipulation of the environmental parameters which influence growth rate.

Turning attention to the yield profile of the larger p5176 construct (116kb) shows that no predictable increase was witnessed during the fermentations. Again as was witnessed during the fermentation of this construct reported in 3.4 the increase in

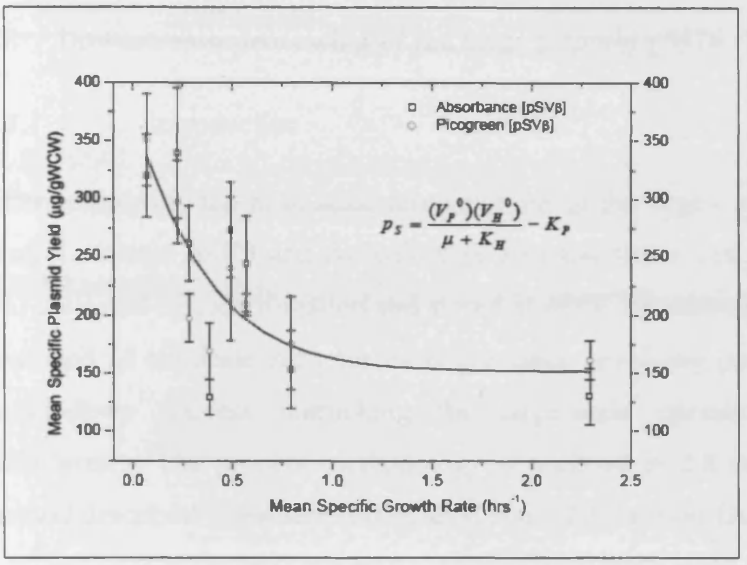

Figure 3-10 Graph plotting the mean specific plasmid yield recorded for pSVβ from triplicate fermentations plotted against the mean specific growth rate calculated at the time of sampling. The mean specific growth rate was calculated by linear regression of the natural log of optical density between the hour points when the sample was taken. A line of best fit is drawn between the average values. The relationship shown is that adapted from (Vasuki, 1989)

yield is reported during the exponential phase of growth. This was outlined before as being due to the replication of this construct being growth-linked since its replication is coupled to that of the host genome. As such unlike the relaxed plasmid pSVβ the specific yield of this construct cannot be increased by growth rate manipulation. Not much more can be said about the yield curve presented for the p5176 fermentations as later studies will call into question the accuracy of the data presented. One final point should be made about the specific yield at harvest. A figure of ~50µggWCW^{-1} is reported, very much in-line with previous estimates.

3.7.3 Conclusions

The yields of the fermentations demonstrate an increase of pSVβ yield upto ~300µggWCW^{-1}. It was demonstrated that the production of this plasmid is related to the culture specific growth rate. Profiles of the yield progression of the p5176 plasmid were also recorded and a harvest yield of ~50µggWCW^{-1} reported.

One of the aims of this series of fermentation was the creation of cell paste with which to conduct downstream purification trials on. This will be the subject of the next section.

3.8 Downstream processing of the large plasmid p5176 (116kb)

3.8.1 Introduction

After completing the pilot-scale fermentations of the large construct p5176, the high-copy control plasmid pSVβ and the wild-type parental strain, cell paste from the fermentation was collected by centrifugation and stored at -80°C for retrospective analysis. The analysis consisted of triplicate runs for each construct, involving purifying the plasmid using a scaled-down process mimicking the large-scale operation employed for plasmid manufacture. The process methodology is outlined in 2.8 and 7.3 and is based upon a method described elsewhere (Eon-Duval *et al.*, 2003a; Eon-Duval *et al.*, 2003b).

3.8.2 Brief Methodology

Briefly 50g of frozen cell paste was resuspended in a Tris-based buffer to a concentration of $200gL^{-1}$. To resuspend fully, the cells were agitated by a magnetically-driven overhead impeller. During resuspension, the lysis buffer, consisting of sodium hydroxide and SDS, was prepared in the lysis tank. The lysis tank was a round bottomed CSTR, surrounded by ice and equipped with a 4-blade, 45° up-pumping pitched-blade impeller agitated at 100rpm. The resuspended cells were added to the lysis buffer and the lysis operation was allowed to proceed for 30 minutes before the solution was neutralised using 4°C potassium acetate (A and B). The process was designed such that RNA removal was achieved by precipitation using a divalent cation as the precipitation agent. Calcium chloride was the agent used, by addition of 250mL of 5M solution to the neutralised lysate, which was then incubated for 10 minutes with agitation and 10 minutes without. The precipitated lysis mixture was clarified by centrifugation, a step replacing the traditional 200μm sieve filter used for clarification on the large scale for purposes of ease of operation. The clarified lysate was depth filtered to remove sub-micron particulates prior to loading on to the UF membrane (Figure 3-12C). The UF step achieved concentration and purification by trapping the plasmid on the membrane surface and allowing the lysis solution, containing salts, proteins and small molecular weight RNA and genomic DNA through (Figure 3-11)

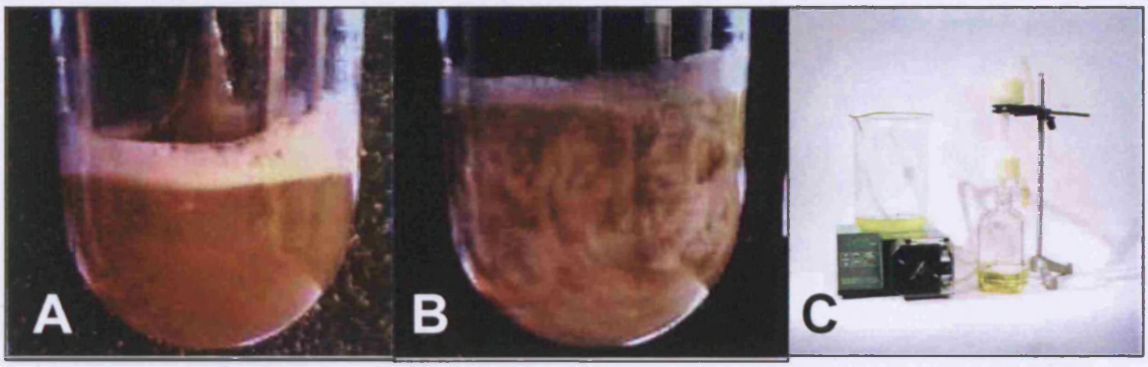

Figure 3-12 Images displaying some of the key steps in the downstream process. A; Lysis operation; the addition of the cell suspension to the NaOH/SDS lysis buffer was accompanied by a dramatic increase in viscosity and the occurrence of the Weissenberg effect indicative of laminar/ transition phase mixing B; Neutralisation operation; the neutralisation of the lysis mixture was achieved though the addition of Potassium acetate, leading to precipitation of the majority of cellular contaminants. C; Microfiltration (5µm followed by 0.45µm/0.2µm depth filters), clarified lysate was filtered to remove sub-micron sized particulates prior to loading the ultrafiltration rig.

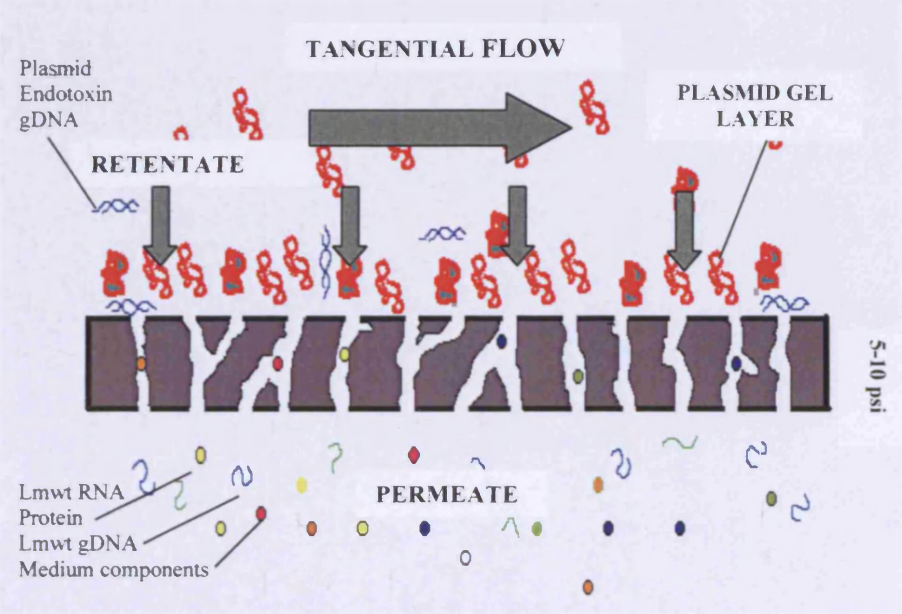

Figure 3-11 Schematic displaying the operation of the ultrafiltration membrane. Fluid flow is adjacent to the membrane surface (500mLmin^{-1}) and pressure is applied across the membrane (5-10psi). The result is an equilibrium between the rate of build-up of plasmid on the membrane surface with the TMP forcing membrane accumulation and the fluid-flow removing membrane accumulation. This equilibrium enables the formation of a plasmid gel-layer thick enough to act as a secondary membrane layer and prevents plasmid loss though the membrane but allowing penetration of small M.Wt solutes including proteins, salts. Ultimately, the plasmid is concentrated and purified.

Further purification was achieved by two diafiltration steps employing 3L of a Tris-based buffer for washing and 2L of a Tris-based salt buffer for buffer exchange. Finally, the plasmid solution was recovered from the membrane by three consecutive wash steps

3.8.3 Plasmid DNA primary purification

On the laboratory scale plasmid purification can be accomplished by either column purification of the clarified lysate using supplied kits such as Qiagen or though intensive methods such as caesium chloride centrifugation. However, these techniques do not lend themselves to scale-up due to the relatively dilute concentration of the starting material, the use of large amounts of organic solvents or unachievable equipment specifications i.e. ultracentrifugation (Feliciello and Chinali, 1993). There are some similarities in the processes used at bench scale and the processes employed on the larger scale, the most notable being the lysis operation.

As with vector design, the most common bacterial cell lysis operations, including homogenisation, freeze-thaw and detergent lysis, have been optimised for recombinant protein extraction. By far the most common lysis method encountered for plasmid purification is alkaline lysis (Birnboim and Doly, 1979). This procedure uses sodium hydroxide and sodium dodecylsulphate to disrupt the cell membrane and cause the release of intracellular components. Subsequent neutralisation with potassium/sodium acetate leads to the precipitation of protein and genomic DNA. Plasmid DNA, due to its enclosed conformation, is able to re-circularise into its native form, whilst the large genomic DNA cannot diffuse and reform properly such that it is precipitated. In addition, a large amount of dissolved protein is precipitated and at high pH's RNA degradation occurs. Both effects being beneficial to the downstream processing steps.

A disadvantage of this lysis method is the large increase in viscosity encountered, in the 35-200mPas range, which makes mixing difficult (Levy *et al.*, 1999a; Ciccolini *et al.*, 1999). This can lead to areas of extreme pH within the lysis vessel leading to irreversible plasmid denaturation and the creation of multimeric and open-circular forms. The high pH and agitation-induced shear has also been shown to lead to plasmid degradation and fragmentation of genomic DNA into smaller sizes which are harder to purify in later stages due to their physicochemical similarities to the plasmid product (Chamsart *et al.*, 2001).

Several studies have been performed to optimise the lysis step in terms of plasmid yield and gDNA contamination by alteration of the agitation rate, exposure time to high pH, sodium hydroxide concentration and impeller type (Meacle *et al.*, 2004; Clemson and Kelly, 2003). Table 3-6 summarises some of the key findings of the optimisation studies.

Table 3-6 Table summarising the findings of several authors and the resulting conclusions which can be drawn about optimising the shear rates and mixing times used in the lysis operation.

Shear rate	Plasmid	gDNA	Comments
Low ($<600s^{-1}$)	• Lower plasmid release as lysis operation is inefficient. (Clemson and Kelly, 2003)	• gDNA fragments larger (300-1000kb) (Meacle *et al.*, 2004)	• Poor macro and micromixing resulting in poorer cell lysis as a result lysis operation may be extended. • Possibly the plasmid associates with floc during neutralisation
Moderate ($600\text{-}10^4s^{-1}$)	• More plasmid released more quickly (Clemson and Kelly, 2003) • No shear of plasmid molecule (Levy *et al.*, 1999b)	• Higher shear does not appear to increase gDNA contamination (Meacle *et al.*, 2004; Chamsart *et al.*, 2001) • Decreased size of gDNA fragments (Meacle *et al.*, 2004) 50-200kb	• Better micromixing means lysis operation is more rapid and effective. Less time required for lysis operation. • gDNA fragments released are slightly smaller due to shear
High ($>10^4s^{-1}$)	• Shear of plasmid molecule (Levy *et al.*, 1999b)	• Slight increase in gDNA contamination (Meacle *et al.*, 2004) • Fragments smaller size (10-100kb)	• High shear rates physically damage plasmid molecule and reduce size of gDNA fragments which hinders DSP. • Only at this rate are there reports of increase in gDNA in lysate
LYSIS MIXING TIME -scale dependent			
SHORT	• If lysis time too short complete lysis does not occur and poor plasmid yields obtained (Clemson and Kelly, 2003)		
LONG	• Longer lysis periods increase plasmid yields by ensuring complete lysis (Ciccolini *et al.*, 1999) • More gDNA present in lysate but by virtue of more complete lysis (Ciccolini *et al.*, 1999) • Too long lysis periods lead to decrease in plasmid supercoiling. (Meacle *et al.*, 2004; Clemson and Kelly, 2003; Sayers *et al.*, 1996) • Suggested that longer lysis times required for larger plasmids (Clemson and Kelly, 2003)		

To achieve maximum yield and purity of plasmid from the lysis operation several points must be considered when deciding on mixing conditions and the lysis time-scales.

(a) That high final NaOH concentrations (>0.1M) are required in order to convert all gDNA to single-stranded form so that maximum precipitation occurs in the neutralisation stage.

(b) Exposure of plasmids to NaOH concentrations >0.15M (pH12.9) leads to irreversible plasmid denaturation.

(c) Extended lysis periods lead to a rapid decrease in plasmid supercoiling.

(d) Sufficient time is required to complete lysis otherwise yields will be low.

(e) Moderate to high shear rates are required to encourage good macro and micromixing and thus ensuring complete lysis and plasmid release and to discourage areas of high pH/molarity in the vessel.

(f) Shear rates in the order of $10^5 s^{-1}$ can cause plasmid damage and increase the level of contaminating gDNA.

Whether these conditions were optimal during the lysis regime employed in this protocol is subject to later analysis in the Downstream processing chapter (7.7).

3.8.4 Plasmid DNA purification

Tangential flow ultrafiltration is one potential method for intermediate purification of plasmid-containing lysates. This step enables simultaneous concentration, purification and buffer exchange. The use of this technique has been demonstrated to remove >99% of RNA and >95% of protein from clarified lysate (Kahn *et al.*, 2000). The mechanism of action involves trapping the plasmid molecules, the diameters of which exceed the 160nm pore size of the $0.1m^2$ ($1ft^2$) membrane used in this study (Millipore, USA), on the surface of the membrane whilst allowing the passage of smaller sized contaminants (Figure 3-11). The retention of the plasmid on the surface allows washing of the plasmid to facilitate the removal of maximum amounts of contaminants and also buffer exchange to place the plasmid in the correct buffer for later chromatographic steps. The build-up of plasmid on the surface of the membrane forms a boundary or gel layer which inhibits permeate flux. This gel layer is kept at an acceptable thickness by employing a crossflow of fluid. The gel layer is functional, since plasmid molecules are potentially able to cross the membrane depending on their size distribution, this is rendered much harder by the creation of the gel layer. The disadvantage of maintaining a crossflow is, as with any fluid in motion that the shear forces created may be of a magnitude sufficient to damage the plasmid molecule, a problem which could become more apparent when processing larger plasmids. So far tangential flow ultrafiltration has been demonstrated to be an acceptable method of intermediate purification and concentration of plasmids up to 10kb.

Use of UF is the subject of a patent claim (Butler *et al.*, 2000) which covers this technique up to a plasmid size of 50kb, though only data for a maximum plasmid size of 10kb is reported (Kahn *et al.*, 2000).

3.8.5 Results of preliminary investigations into purification of the Oxford series

The overall aim of this study was to investigate the possibility of purifying the large construct p5176 (116kb) using the established plasmid purification protocol. The results of the study are outlined in Figure 3-13.

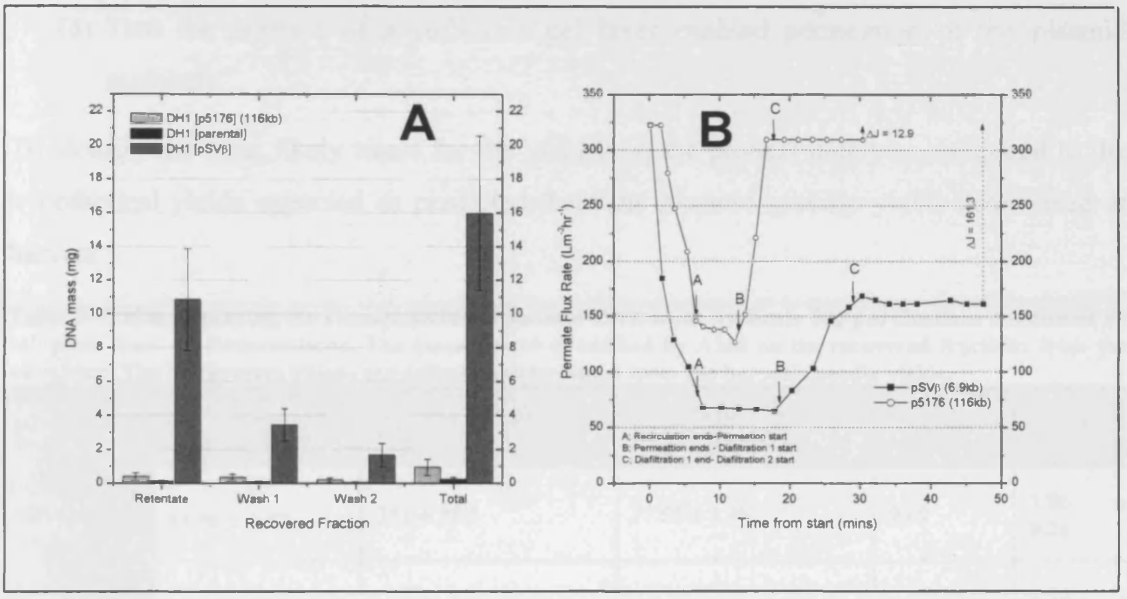

Figure 3-13 Graph displaying the results of preliminary investigations into the possible purification of the large construct p5176 using the small, high copy number plasmid pSVβ and DH1 parental as positive and negative controls. Figure A shows the plasmid masses recovered from the ultrafilter by the three consecutive wash steps which follow the permeation and diafiltration steps. Figure B tracks the changes in permeate flux as the ultrafiltration step progressed.

Figure 3-13 shows that large differences exist in the recovered masses of pSVβ and p5176. The recovered yields of p5176 mirror that of gDNA from the parental controls indicating that little plasmid was actually recovered. Comparison of the flux profiles between two of the runs highlights the problems with ultrafiltration of the large construct; p5176. Permeate flux drops much more rapidly and to a greater extent for the pSVβ runs than for the p5176 runs, indicating greater membrane loading. During the first diafiltration period the flux of the p5176 run increases sharply suggesting that the majority of the material on the membrane, thoughout the permeation stage, may be washed though the membrane; it was evidently not plasmid.

Several factors may account for the low yields of p5176;

(a) That the large construct was sheared by fluid forces in the UF rig, degrading it sufficiently such that the fragments permeated the membrane

(b) That there exists only trace amounts of plasmid to begin with because of degradation in the lysis step.

(c) That there exists only trace amounts in the lysate by virtue of the low copy number of the plasmid.

(d) That the absence of a sufficient gel layer enabled permeation of the plasmid molecule.

To identify the most likely cause for the yield loss, the process data was compared to the hypothetical yields expected as predicted from the plasmid specific yields determined at harvest

Table 3-7Table displaying the average yields of plasmid DNA from triplicate 50g purifications conducted on cell paste from 4L fermentations. The masses were quantified by A260 on the recovered fractions from the ultrafilter. The % recovery values are estimates determined from the harvest specific yields.

	Total DNA recovery (mg)	Harvest specific yield ($\mu g g^{-1}$WCW)	Maximum plasmid recovery (mg)	% Recovery	A_{260}/A_{280}
DH1 [pSVβ]	15.96 ± 4.57	351 ± 39.5	17.55 ± 1.98	90.9	1.86 ± 0.26
DH1 [p5176]	0.94 ± 0.06	44.7 ± 6.8	2.2 ± 0.34	42.7	1.78 ± 0.31
DH1 [parental]	0.246 ± 0.97	1,410[6] 10,000[2] 12,140[3]	70.5 500 607*[3]	0.35 0.05 0.04	1.74 ± 0.25

From Table 3-7 it can be seen that the from the harvest yields the total mass of p5176 present at the start of the DSP process is 2.2mg, meaning that if the contamination by gDNA is ignored around 40% of the plasmid was recovered. The same result for pSVβ suggests that 90% of the plasmid is recovered.

[6] Assumes that *E.coli* genome is 4.7Mbp and is present at 1copy per cell at harvest. [2] Assumes DNA present at 1%(w/w) WCW (Bailey and Ollis, 1986). [3] Value placed upon specific gDNA yield by sonication and qPCR in later Chapters.

3.8.6 Conclusions

It was not possible to determine which factors led to the low plasmid yields as there remain too many unknowns. The low yields meant further analysis was difficult as insufficient plasmid could be concentrated to analyse by electrophoresis. The only conclusion which could be confidently stated is that the low p5176 recoveries are a direct result of either the low starting yields or the large size of the construct. Shear forces are certainly likely to impact on the recoveries, due to the large diameter of the plasmid molecule, ~1μm (7.7.3.1). This large size also means that the plasmid molecules are unlikely to have penetrated the 0.16μm pores of the membrane, at least not in their native form. An additional fact is that this process was designed to operate at a loading value of 500-700mg of plasmid per m^2 of membrane and the loading values used here were far below that level. Smaller sized membranes ($0.01m^2$) were used to increase the plasmid load but this led to rapid fouling and ultimately complete blockage of the membrane. The problem faced in resolving these questions is that the low yield and large size are inextricably linked making resolution of the problem difficult.

As the process stands it was unable to effectively purify the large construct p5176 (116kb) a fact attributable to either the large plasmid size or low initial yields. An interesting analysis of the results concerns the contamination by genomic DNA. The total recovery of genomic DNA from the process was low at ~250μg, representing a clearance of gDNA in excess of 99.5%. This level of clearance compares well to that reported elsewhere for similar purification strategies (Kahn *et al.*, 2000). Although the level of gDNA is acceptable the ratio of plasmid DNA to gDNA at the end of the process are not. The regulatory authorities have been demanding for some time that the level of genomic DNA contamination in plasmid vaccine preparations should not exceed 0.05μg gDNA /μg plasmid (5% w/w) (WHO, 1997) and indeed industry standards are beginning to accept an even lower level of <0.01μg gDNA/μg plasmid (<1% w/w) (Zoon, 1996). In the studies reported here the level of genomic DNA contamination represents 1.5% (w/w) of the total plasmid DNA when considering pSVβ but 26% (w/w) when considering p5176. Even if the p5176 demonstrated 100% recovery the genomic DNA would still account for 11% (w/w). These figures are difficult to improve upon further downstream in the chomatography and polishing stages and as such the only effective method of ensuring the ratio is maintained <1% is to achieve high plasmid yields from the fermentation.

3.9 Initial Studies Conclusions

To conclude this chapter involves confirming whether the questions posed at the start have been satisfactorily answered. The first query posed was whether cultures harbouring these large plasmids were able to grow sufficiently well when bearing constructs of this size. Both shake-flask investigations and pilot-scale fermentations have confirmed that the growth rates of these cultures are not severely impinged by the propagation of these constructs. Decreases in maximum growth rate and final biomass yields were reported, as compared to parental strains, but were to a lesser degree than cultures bearing small, high-copy number plasmids and as such would not cause problems in their larger scale manufacture.

In regards to the yields of these plasmids the view is less optimistic. It seems by virtue of the low-copy number at which these plasmids are maintained (1-2 copies/cell) the yields, as determined during various studies, were very low (~0.2μgmg^{-1}DCW). This yield figure compares poorly to small, high-copy number plasmids reported in the literature as commonly being 4-6μgmg^{-1}DCW, resulting in 25-fold less material for purification. If compared to the yields of more optimised productions systems, the large plasmid yields are almost 100-fold lower. It was also established that due to the vector architecture of these plasmids, strategies often employed to improve specific yield by reducing specific growth rate, could not be used with these plasmids as different control mechanisms are in action. Boosting volumetric plasmid yield was achieved by improving aeration during fermentation but this yield measure is of less critical importance.

The low specific yield also impacted negatively on the downstream processing of these molecules. Lab-scale purifications involving gravity-fed, anion-exchange resins were judged to be poor at purifying these constructs. It was found that the expected yields from such protocols were not obtained. Variations in the operations of these lab-scale protocols by doubling the starting cell mass, achieved little except to increase the level of contaminants. The use of a lab-scale purification technique employing an exonuclease to digest the contaminating gDNA succeeded in its aim but the resulting yields suggested that only ~25% of the expected plasmid was recovered by these columns, implying that the binding or elution of these plasmid to the resins was problematic. Purification of these plasmids on a larger scale employing ultrafiltration was also found to be far from optimal. The % recoveries of the large construct was found to be ~40% compared to ~90% with a

small, high-copy number plasmid. The low % recoveries were accompanied by low mass yields. At this stage it was impossible to determine whether the low recoveries produced by the DSP runs was symptomatic of the large size of the constructs or the fact that purification was being attempted on lysate containing little plasmid. A recurring problem though out the purification of these large plasmids was the co-purification of contaminants. It was found that with both lab-scale and pilot-scale purification runs, the ratio of plasmid to contaminants was high, not due in fact to poor processing techniques but attributable to the low initial yields. The low-level of starting material also made determination of the most troublesome DSP stages hard, due to the difficulty faced in quantifying changes in low amounts.

Accurate and precise quantification of the large plasmids was also found to be fraught with problems, mostly due to the high ratio of contaminants to plasmid in the purified streams used for analysis. Spin-prep purification results were found to be heavily influenced by the residual levels of co-purified protein, levels of which have little impact when the recovered plasmid yields are high. PicoGreen analysis on both clarified lysates and spin-prep purified samples was also troublesome. When PicoGreen was conducted on clarified lysates, the resulting yields were misleading by virtue of contaminating gDNA, which due to its relatively high concentration and linear topology gave stronger signals than the supercoiled plasmid. When conducting PicoGreen on spin-prep purified eluents the problem lay with the standard curve employed. It was determined that the process of spin-prepping destroyed any topology possessed by the plasmid molecules reducing them entirely to linear form. As such, PicoGreen calibration against a standard composed of the plasmid under analysis, as is traditional with the protocol, led to misleading over-estimations of plasmid yield. An alternative method was devised, involving calibration of spin-prep purified samples against a linear λDNA standard curve. This method by-passed the problem of residual protein contamination in the eluents and the linear standard represented the plasmid DNA in the correct form it demonstrated after processing. However, since this assay relies on exacting a physical change upon the plasmid under investigation it becomes more likely for errors to creep in and as such the assay would never be acceptable from a validation perspective. As a result of these conclusions new methods of large plasmid quantification are required. It was possible to visualise the plasmids using PFGE but separation of the plasmid topologies proved difficult. Further optimisation of the assay for plasmid visualisation is required.

3.10 Discussion

The findings of these initial studies makes determining the problems faced when manufacturing large plasmids difficult. The reason being that the problems faced thus far are intrinsically linked to the low plasmid yields and not to the size of the plasmids per se. Indeed, the most pressing problems encountered during fermentation, downstream and analytical protocols remains their low yield a fact which makes determining the other challenges impossible. If the other problems faced when manufacturing large plasmids are to be determined, the impact of the large size has to be decoupled from the impact of the low plasmid yield

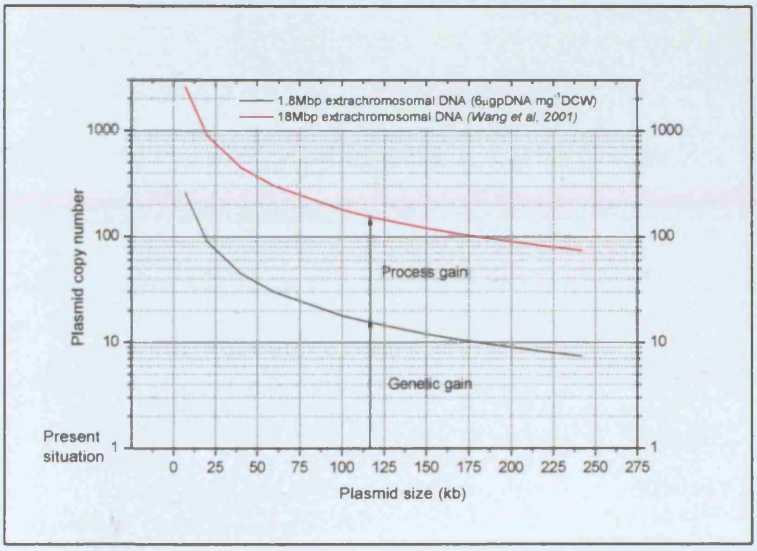

Figure 3-14 Schematic displaying the expected plasmid copy number of various sized plasmids when cells are producing 1800kb of extrachomosomal DNA and when the medium and processing conditions have been optimised for production of 18Mb of extrachomosomal DNA

This conclusion contradicts the accepted belief that large plasmids have to be present in low yields. The plasmids employed in this study are at low yields due to the nature of their origin of replication and not due to their large size. Ultimately, they remain tools for molecular biology and genome mapping and as such were not intended for production. Conceptually, if the cell is regarded as a manufacturing unit, it is being persuaded to under perform when synthesising these constructs. Literature evidence confirms that when bacterial cells record yields of 4-6µgmg^{-1}DCW, as they commonly do when maintaining high-copy number replicons, each cell is in effect synthesising ~1.8Mbp of extrachomosomal DNA. When the medium and process conditions are optimised this value has been found to rise to a maximum recorded level of 18Mbp per cell (Adapted from (Wang *et al.*, 2001)). Using these figures the expected copy numbers of plasmids of various sizes can be estimated as shown in Figure 3-14. From the graph it can be reasoned

that the yields of large plasmids could be much improved though the use of a more suitable origin of replication.

Another major consideration is the size of the plasmid molecules under investigation, the smallest of which being 116kb. At present manufacture of plasmids has been focused on constructs 3-10kb. To attempt to monitor plasmid processing with constructs ranging from 116kb to 242kb represents quite a dramatic leap in size. A more reasoned approach would make use of more incrementally increasing plasmid sizes. It was for these reasons that the decision was taken to attempt to clone a series of large plasmids making use of a high-copy number replicon.

4 ANALYTICAL DEVELOPMENT: RESULTS AND DISCUSSION

4.1 Chapter Aims

The main aims of this chapter are to describe the analytical techniques which were developed and used for quantifying the concentrations and analysing the topology of large plasmids. Also, the techniques used to determine the masses of other constituents encountered during plasmid processing, will be outlined. Additionally in this section, information will be given on why the techniques required development, as well as details about their operation and accuracy.

The main issues which will be answered by this chapter are;

1. Whether the techniques commonly employed for plasmid quantification are applicable to larger constructs. By virtue of the large size of the plasmids being studied and the low-copy numbers they exist at (as determined by previous studies), exact quantification may result in difficulties when using techniques developed for small, high-copy number plasmids. Several methods for plasmid quantification including absorbance, PicoGreen and HPLC were studied.
2. Together with plasmid quantification, useful information about the process and the plasmid product are provided by gel electrophoresis analysis. This chapter will describe the efforts which went into developing suitable techniques for visualisation of large plasmids.
3. The most important contaminant to consider when manufacturing plasmid DNA is contaminating bacterial genomic DNA (gDNA). The reason for its importance is due to the physicochemical similarities of gDNA to the plasmid product, which makes removal of this contaminant critical to ensuring a production process is feasible. Due to the similarities, presence of this contaminant can also lead to significant errors in the accuracy of analytical techniques used for quantifying plasmid. Consequently, this chapter will describe the development of techniques aimed at accurately quantifying genomic DNA.

4. In order to assess the removal of protein and RNA by the process, suitable methods of determining their concentration, in all streams of the process, were required. The development of assays to achieve this will be outlined.

5. Finally, the development of the sonication assay will be described. This technique was employed to determine the initial masses of the contaminants such that their emoval could be balanced over the lysis step.

4.2 Techniques Used for Plasmid Quantification

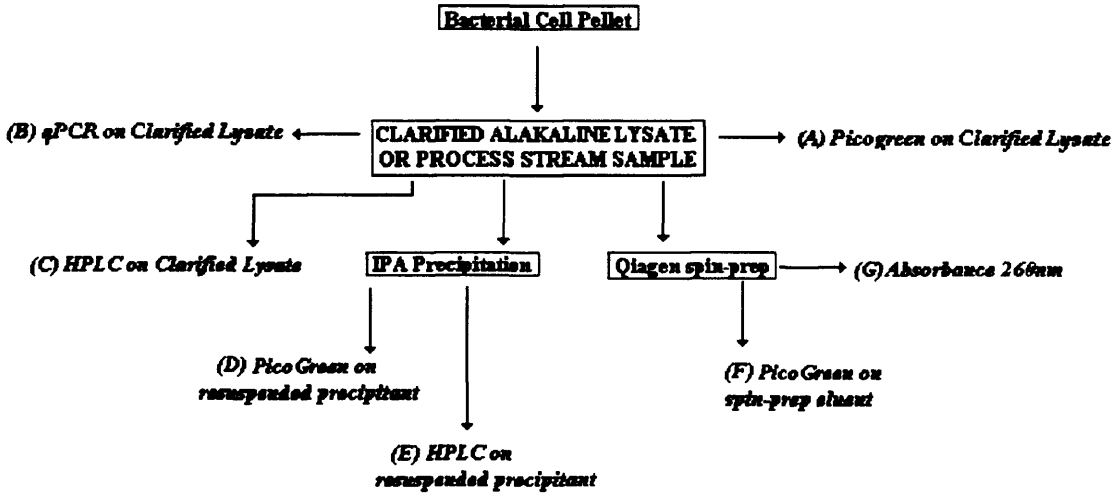

Figure 4-1 Schematic describing the analytical techniques which can be employed to quantify plasmid in either clarified lysates obtained from either bacterial cell pellets or from process streams of the downstream process. The analytical techniques are italicised.

4.2.1 Introduction

The plasmid quantification techniques employed during this project were developed concurrently as the project progressed. At the outset, it was unknown whether the commonly applied techniques for plasmid quantification could be employed with these large, low-copy plasmids. Consequently, many of the studies employed during the early stages of the project were as much about investigating the analytical techniques, as they were about investigating the production issues associated with the manufacture of large plasmids.

In this project, plasmid concentration was a measured variable in two situations; Fermentation and Downstream Processing. During the fermentations, plasmid progression was monitored to record the efficiency of the fermentation and to determine the relative

productivity of the large plasmid constructs. During downstream processing, measurement of plasmid concentration in the different process streams was essential for mass balancing, in order to determine the feasibility of processing large constructs using the adopted process. These two scenarios describe the situations where plasmid concentration was measured as a process variable, but alongside these investigations there were other instances where plasmid quantity needed to be determined, for instance when cloning or preparing standard curves. On these occasions plasmid was not being recorded as a variable, however, it was important to be confident that the analytical technique being employed was accurate and precise. Figure 4-1 outlines the different techniques that can be employed to determine plasmid concentration. All methods shown in the diagram, except qPCR, were scrutinised as to their accuracy and precision in determining the correct plasmid yield, and as such will be described in this chapter. From the schematic it can be appreciated that the analytical technique employed depended on what processing method was used to purify samples for analysis. Since plasmids are intracellular products, all techniques required a lysis step to release the molecules enabling their analysis (excluding process samples in which plasmid, after the lysis step, existed free in solution). Conceptually, the most accurate techniques promised to be those where processing was kept to a minimum (i.e. A, B and C) as the introduction of further processing steps (D, E, F and G) could be expected to lead to greater losses and make the sample less representative.

Table 4-1 describes the numerous methods available for quantifying plasmid DNA in solution. The analytical techniques can be categorised as one of three methods: ultraviolet absorbance, fluorescent dyes or quantitative PCR. Historically, quantification of DNA was often achieved by measurement of deoxyribose or phosphate groups following hydrolysis, but these techniques have largely been superseded due to their high error and labour-intensive nature, and so are not considered here.

Table 4-1 Table outlining the various methods available for the determination of DNA concentration. The three major techniques detection by are Absorbance, Fluorescent dyes, and qPCR. The other two, involve hydrolysis reactions which are laborious and less accurate.

ANALYTICAL TECHNIQUE	USES	REFERENCE
Absorbance 260nm	Direct measurement/ HPLC	(Sambrook *et al.*, 1989)
Fluorescent dye	Hoechst 33258/ PicoGreen/ AGE	(Singer *et al.*, 1997)
Quantitative PCR	Most specific and accurate technique	(Lee *et al.*,)
Quantification of deoxyribose	Superseded due to high errors introduced by hydrolysis and the labour intensive nature of the assays.	
Quantification of phosphate		

4.2.2 UV absorbance

Ultraviolet absorbance quantification of plasmid solutions is the most simple and widely applied method, and is the technique used by direct absorbance as well as HPLC (which uses an in-line UV spectrophotometer). Indeed, the use of this technique forms the basis for all the other techniques, since they all rely on standard curves calibrated from absorbance readings. The rationale for the method is that the presence of conjugated heterocycles (the purine and pyrimidine bases) in DNA gives rise to strong electronic transitions upon absorption of light at 260nm in wavelength, the near-UV region (Middaugh *et al.*, 1998). Consequently, DNA absorbs maximally around 260nm. However, the absorbance method is incapable of distinguishing dsDNA plasmid from ssDNA and RNA, which due to their highly comparable chemical make-up, also absorb strongly in this region. And, although proteins absorb maximally near 280nm, they do display absorbance at 260nm. This means that for a plasmid sample to be accurately quantified it must be very pure and free of contaminating RNA and protein.

Spin-prep processed samples are assumed to have had the majority of protein contaminants removed by processing, whilst HPLC purifies the plasmid DNA away from protein, prior to quantification by absorbance. In all techniques used, the resuspension buffer was supplemented with RNase. This highly efficient enzyme is able to quickly degrade all of the RNA in a lysed sample, such that none can be detected by gel electrophoresis. As such, RNA contamination of analytical samples rarely occurs.

An estimate of sample purity can be achieved from absorbance readings by calculating the ratio between the absorbance value of the sample at 260nm and 280nm. If the ratio is

found to be lower than 1.8 then the sample is contaminated by protein and as such the 260nm reading used to calculate plasmid concentration would be erroneous. The impact of contaminating protein on the absorbance result is displayed in Figure 4-2.

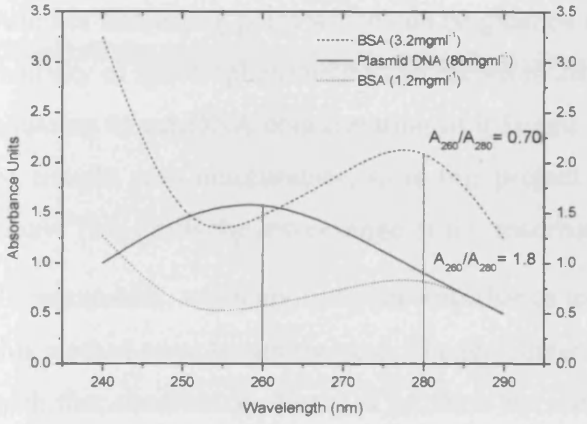

Figure 4-2 Schematic adapted from (Davidson, 1972) displaying the absorbance profiles of solutions of plasmid DNA and comparing to those of the protein BSA. From the schematic it can be appreciated that for an accurate estimate of plasmid concentration the plasmid concentration must be more than 60-fold higher than the contaminating protein.

The figure demonstrates the absorbance profile a plasmid DNA solution, which produces a maximum absorbance reading of 1.6,* which when multiplied by 50 (since the extinction coefficient of dsDNA is $20gL^{-1}cm^{-1}$, and the path length used here is 1cm then 1AU = $50\mu gmL^{-1}$DNA) the concentration is found to be $80mgmL^{-1}$. The traces of two BSA solutions are also shown. Although the peak of these solutions is at 277nm, the 280nm reading is taken as the maximal due to the sensitivity of the majority of spectrometers not being greater than ±5nm. The problem arises due to the lower extinction coefficient of proteins. The value for this parameter varies depending on the specific protein, but using BSA as an example highlights the problem. The extinction coefficient of BSA is $0.66gL^{-1}cm^{-1}$ (See figure and (Pierce Scientific, 2006)) meaning that 1AU = $1,500\mu gmL^{-1}$. From Figure 4-2, this means that the higher protein peak is produced by a BSA solution of $3.2mgmL^{-1}$ (AU 2.1*1.5). Recording the A_{260}/ A_{280} ratio, between the absorbance peak produced by plasmid DNA (260nm) and the absorbance peak produced by protein (280nm), produces a value of 0.7. This indicates that an $80mgmL^{-1}$ solution containing $3.2mgmL^{-1}$ of protein would be out of spec, and as such the value produced for the concentration of plasmid would be erroneous, since the impact of protein absorbing at 260nm would corrupt the true result. Therefore, to have confidence in the reading produced by absorbance, a plasmid solution of $80mgmL^{-1}$ could contain no more than

* In this study the range of linearity of absorbance was taken to be 0.2-0.8 where % Coefficient of variation (%CV) between assays is <2%. Dilution was used to achieve this. Absorbance readings >1.0 are accompanied by increases in %CV to around 2-5%. (Qiagen, 2005).

1.2mgmL^{-1} protein, as shown by the figure, as at this point the impact of the protein on absorbance is deemed to be minimal. Ultimately, due to the differences in the extinction coefficient of protein and DNA, to correctly record the concentration of a plasmid solution it must exist in a ratio > 60:1 plasmid mass to protein mass.

Another interesting point which can be gleaned from this analysis are the assay limits. The majority of spectrophotometers can record to 2d.p resulting in the lowest value being 0.01, equating to a dsDNA concentration of 0.5μgmL^{-1}. However, using such low values would be fraught with inaccuracies, so in this project 0.05 was taken as the lower range of the assay. This limits the lower range of the absorbance assay to 2.5μgmL^{-1}.

To summarise, when applying the absorbance technique consideration of the drawbacks of this method must be appreciated. The technique can only be applied on very pure solutions such that absorbance effects of proteins are minimised and it must be acknowledged that this technique is incapable of distinguishing small traces of ssDNA remaining from the bacterial genome and that the lower limit of application of this assay is ~2.5μgmL^{-1}.

4.2.3 Fluorescent Dye Quantification

Quantification of plasmids using fluorescent dyes offers two important advantages over absorbance.

(a) Their use can extend the lower limit of detection below the 0.5-2.5μgmL^{-1} limit reached by absorbance.

(b) They can be selective for plasmid molecules and so reduce the over- estimation of plasmid concentration caused by the contributory effects on absorbance readings produced by the contaminants; RNA, protein, ssDNA.

The mechanism of action of all fluorescent dyes is comparable, but their individual uses and application can differ. The most common dyes used for DNA quantification in solution are Ethidium bromide, Hoechst 33258 and PicoGreen, whilst for gel visualisation Ethidium bromide and SYBR-Gold are used. The structures of fluorophore molecules used for plasmid quantification are all similar in that they are all heterocyclic compounds. As such, the molecules possess the dispersed electron clouds necessary to display fluorescent behaviour. The core structure of the monomeric cyanine dyes, of which PicoGreen, SYBR-Gold and YO-YO are included, is shown in Figure 4-3C.

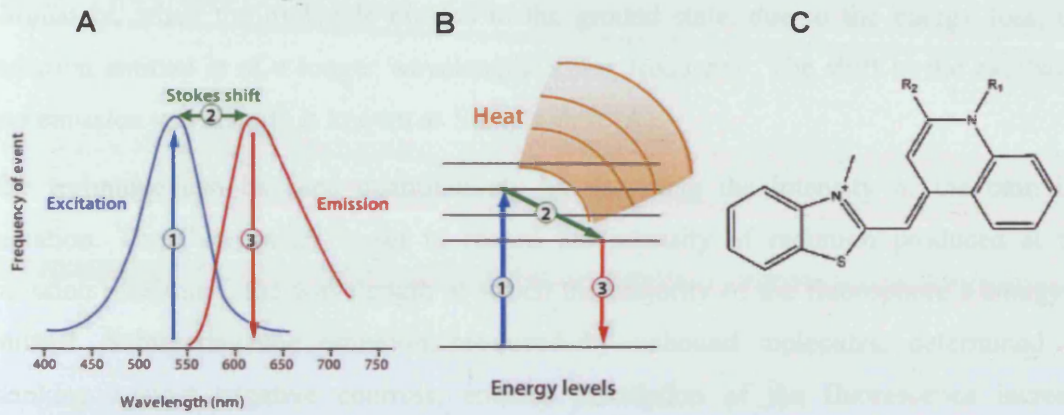

Figure 4-3 Schematic displaying the process of fluorescence. The flurophore molecule, such as monomeric cyanine dye base (C), is excited by radiation of wavelength which most excites the electrons in the dispersed electron cloud of the molecule (its excitation maximum). The excitation wavelength is set by the filter used on the fluorometer. The absorption of energy raises the molecule from its ground state to its excited state (1). Whilst in the excited state, (an unstable state which is extremely short ~10^{-9}-10^{-15}s) collisions with solvent molecules leads to dissipation of some of the energy as heat. Following such energy loss, the molecule is in its semi-excited state (2) and returns to its ground state by emission of the excess energy as light (3). Due to the energy lost during the excited to semi-excited transition, the wavelength of the light emitted is of lower frequency than it absorbed. The molecule is now free to repeat the process

Improvements to the binding behaviour of these molecules, depending on desired function, can be achieved by alteration of the two R groups. PicoGreen and SYBR-Gold have almost homologous R groups, accounting for the similarities between the two fluorophores (Zipper, 2004). In both cases the R_1 is a phenyl group, but PicoGreen carries an additional positive charge on its R_2 group. The planar, hydrophobic structure and positive charge at the appropriate position, facilitates binding of these molecules to DNA. It is known that PicoGreen and SYBR-Gold display biphasic binding, such that they intercalate into the DNA superstructure, as well as binding the minor groove of DNA molecule. Contrastingly, Hoechst 33258 does not intercalate and only displays minor groove binding. The mechanism of action of these molecules, as with any fluorophore, is that binding to the target compound increases the molecule's fluorescence, as compared to unbound molecules, due to minor structural or electrochemical changes induced by binding.

Figure 4-3 A and B displays the progression of a fluorescent transition. Upon irradiation of the fluorophore molecule, photons of the correct wavelength excite the electrons of the distributed electron cloud, resulting in them occupying a higher energy state (B). During the period of this excited state, a proportion of energy is dissipated as heat through collision with solvent molecules.

Ultimately, when the molecule returns to the ground state, due to the energy loss, the radiation emitted is of a longer wavelength/ lower frequency. The shift in the excitation and emission wavelength is known as Stoke's shift (A).

The technique can be used quantitatively by recording the intensity of the emission radiation. The fluorometer is set to record the intensity of radiation produced at the emission maximum, the wavelength at which the majority of the fluorophore's energy is emitted. Subtracting the emission produced by unbound molecules, determined by blanking against negative controls, enables calculation of the fluorescence increase attributable to binding. By plotting the fluorescence produced by standards of known concentration, this increase in fluorescence due to binding can be linearly correlated to DNA mass. The nature of the fluorescence transition dictates certain criteria required by the fluorophore molecule for it to be functional for assay purposes.

A main criterion for efficacy is a large increase in fluorescence upon binding. Ethidium bromide has long been used for quantification of DNA in solution, as well as gel visualisation. A drawback with this molecule is that the unbound form displays a high degree of intrinsic fluorescence, such that the increase upon binding is relatively low (~20-fold). This makes the background fluorescence of the molecule hard to eliminate, reducing the sensitivity of the assay. Hoechst 33258 is an improvement as it displays a ~95-fold increase in fluorescence upon binding. However, the new generation of monomeric cyanine dyes are reported to display a ~2000-fold enhancement of fluorescence upon binding, and as such the background intrinsic fluorescence is less of a problem (Singer *et al.*, 1997). See Figure 4-4.

A second criterion is the specificity of the fluorophore molecule. The use of dyes in this project requires the fluorophore to report the concentration of dsDNA plasmid molecules. Reporting the presence of contaminating ssDNA, RNA and protein leads to inaccuracy. Again, ethidium bromide is not optimal as it displays strong specificity for all nucleic acids including ssDNA and RNA. Hoechst 33258 does display specificity for dsDNA, but requires high salt conditions to detect dsDNA in the presence of RNA and low salt conditions to enable dsDNA detection in the presence of ssDNA, meaning two assay conditions must be run to achieve adequate selectivity.

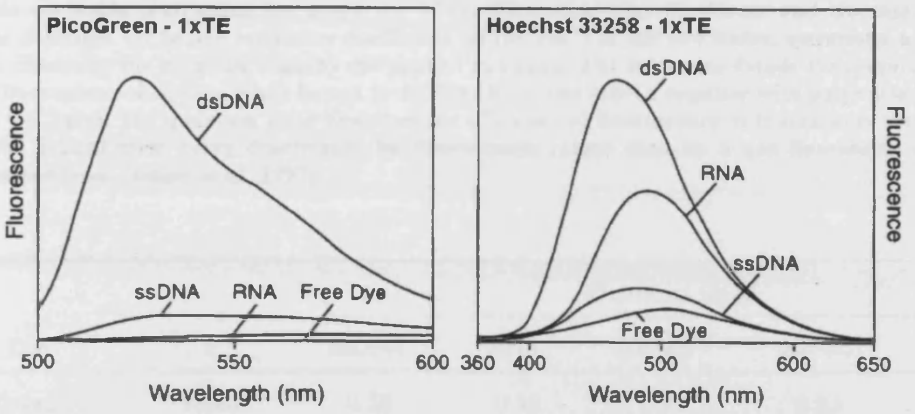

Figure 4-4 Fluorescence spectra of PicoGreen and Hoechst 33258 dyes when free dye or bound to dsDNA, ssDNA and RNA. The PicoGreen trace shows minimal background fluorescence due to the contaminants. The Hoescht profile shows the large contributory effect of RNA in a low-salt buffer. Should any RNA be remaining in the sample then the result would be affected by its presence. From (Singer *et al.*, 1997)

Figure 4-4 shows the emission spectra of assays employing both PicoGreen and the competing dye Hoechst 33258, when unbound and when bound to contaminating ssDNA, RNA and dsDNA. From the figure it can be appreciated the increase in fluorescence displayed by PicoGreen upon binding dsDNA, as compared to the presence of free dye. What is also apparent from the figure is the specificity the molecule displays for dsDNA over contaminating RNA and ssDNA.

The fluorescence quantum yield of the fluorophore is the ratio of photons absorbed to photons emitted through fluorescence (ranging from 0.1-1.0). Therefore, the quantum yield gives the probability of the excited state being deactivated by fluorescence rather than by another, non-fluorescent mechanism. From Table 4-2 it can be seen that the quantum yield results for PicoGreen, upon binding various types of polynucleotide, are relatively comparable. However, the values for RNA and ssDNA are lower than the same for dsDNA. This means that the specificity of PicoGreen is partly down to the reduction in fluorescence displayed when the molecule binds either ssDNA or RNA, since the quantum yields of these complexes are lower, such that less of the energy of the excited state is released by fluorescence.

However, the main reason for PicoGreen's specificity for dsDNA over ssDNA and RNA is due to the red-shift phenomenon. At the concentrations suggested for its use, PicoGreen molecules bind ssDNA/RNA at high *dye molecule: base pair* ratios. The overall effect of this is that the emission maximum of the complex is shifted to longer wavelengths, such that the effect is not recorded at the wavelength used to record the emission of dsDNA.

Table 4-2 Table contrasting the properties of the fluorescent dyes PicoGreen and Hoechst 33258. The table describes the molar extinction coefficient (ε) ($M^{-1}cm^{-1}$) of the two stains, essentially a measure of how efficiently the molecule absorbs the applied radiation. The table also details the quantum yields of the fluorophore molecules when bound to dsDNA/ RNA and ssDNA together with polynucleotides of AT and GC bases. The quantum yield describes the efficiency of fluorescence as it measures the probability of the excited state being deactivated by fluorescence rather than by a non-fluorescent mechanism. Obtained from (Singer *et al.*, 1997)

		Quantum yield				
Dye	ε	dsDNA	RNA	dA·dT	dG·dC	ssDNA
PicoGreen	70,000	0.53	0.42	0.53	0.53	0.34
Hoechst 33258	40,000	0.59	0.03	0.52	0.05	0.40

A final criterion for the fluorophore molecule concerns the limit of its range. With low quantities of material available to bind, the efficiency at which the fluorophore absorbs radiation *combined* with the intensity of the fluorescence produced by the molecule upon binding, must be maximal. Absorption and emission efficiencies are quantified by the molar extinction coefficient (ε) for absorption and the quantum yield for fluorescence. The fluorescence intensity per dye molecule is proportional to the product of both these value. As can be seen from Table 4-2 the extinction coefficient of PicoGreen is high at $70,000M^{-1}cm^{-1}$, compared to $\sim 5500M^{-1}cm^{-1}$ for EtBr. Also, the quantum yield of PicoGreen when bound to dsDNA is higher at 0.53, compared to <0.3 for EtBr. As a result PicoGreen can quantify solutions of dsDNA down to $25pgmL^{-1}$, representing a 10^4 fold lower limit than achievable by absorbance, and ~20 fold that achievable by EtBr.

The advantages of PicoGreen and SYBR-Gold, as outlined above, mean they have been applied to plasmid quantification for several years. (Singh *et al.*, 2005; Thwaites *et al.*, 2002; Molecular Probes Product Information, 2003; Rengarajan *et al.*, 2002; Kay *et al.*, 2003). SYBR-Gold is used for plasmid quantification by densitometric gel scanning, as the use of this fluorophore improves contrast and a lower detection limit of plasmid DNA as compared to EtBr. However, determination of plasmid concentration by gel scanning is not a particularly robust assay, due to inter-assay fluctuations and the inaccuracy associated with calibration from a marker (Friehs, 2004). As such, DNA binding dyes are more commonly used for quantifying plasmid in solution, through the use of a fluorometer. A drawback of this is that due to the error associated with the more complex nature of the fluorescence assay, PicoGreen quantification has been found to be less accurate than absorbance, when analysing pure solutions of dsDNA (Rengarajan *et al.*

(2002a)) compared the accuracy of quantification of solutions of dsDNA by PCR, PicoGreen and Absorbance against a reference standard. The absorbance method was found to be the DNA quantification method most concordant with the reference sample among the three methods evaluated (Rengarajan *et al.*, 2002). However, the advantage of PicoGreen is its capacity to determine dsDNA concentration in the presence of contaminants, in which case the use of this assay has clearly demonstrated its credentials (Noites *et al.*, 1999).

Despite the advantages of PicoGreen its use has two drawbacks, the extent of which will be explained in the results section. PicoGreen has been demonstrated to display impressive sensitivity toward dsDNA. Obviously though, it is incapable of differentiating genomic dsDNA from plasmid dsDNA, as for all intent and purposes they are identical molecules. This is not a pressing problem when the sample being quantified has a high plasmid to genomic dsDNA ratio, since the contributory effect of genomic dsDNA will be minimal. The problem arises when the plasmid DNA mass approaches the mass of contaminating genomic dsDNA. Secondly, the fluorescence reading has been reported to vary according to the topology of the DNA (Singer *et al.*, 1997). The authors describe how linear dsDNA produced a higher fluorescence reading than the same mass of supercoiled DNA, which they attribute to the high rate of intercalation of the PicoGreen molecule into linear DNA. Ultimately, this means that the topology of the sample used for calibration must be highly representative of the topology of the plasmids under analysis.

4.2.4 Plasmid quantification by qPCR

Plasmid quantification by quantitative PCR is more an enabling technology than an analytical technique per se. It facilitates extremely accurate and specific quantification of plasmid molecules (or indeed any RNA/DNA), but the actual detection method employs fluorescent dyes as described above. The use of qPCR is largely replacing historical methods of quantifying specific gene sequences based around radio-labelling of nucleic acids and quantifying their hybridisation. Such methods present safety problems in handling radioactively labelled probes, and the procedure is laborious and time-consuming. Additionally, the radioactive probe used for hybridization can also cause inaccuracy due to its short life span (Pushnova et al., 2000). One of the main advantages of qPCR is the assay's specificity. The technique is capable of quantifying dsDNA specific to the plasmid under investigation, even in the presence of other forms of dsDNA, ssDNA, protein and RNA.

It achieves this through the use of sequence specific primers, which bind only to the plasmid molecule and so initiate only its replication.

End-point qPCR was the traditional mode of operation of this assay. In essence, the PCR reaction would be used to amplify the sequence of interest, be it part of a plasmid or genomic fragment, alongside control fragments of known concentration. At the end of the reaction the amplified DNA and controls would be analysed by agarose gel electrophoresis, followed by densitometric scanning of the bands. The problem with this method included poor sensitivity and precision combined with long running times. The technique at best was semi-quantitative and hardly an improvement on Southern blot. The insensitivity of gel scanning was combined with the fact that when using end-point PCR reaction, identical masses of DNA at the start could differ significantly by the finish, due to chaotic and unpredictable events (rector-Myska *et al.*, 2001; Mallet, 2000). Figure 4-5 attempts to display how random events during a PCR reaction can lead to differences in the final DNA mass despite the starting mass being identical. It can be appreciated that during the exponential part of the PCR reaction replicate samples are in concordance. However, due to random events this synchronicity deviates during the linear phase of the reaction.

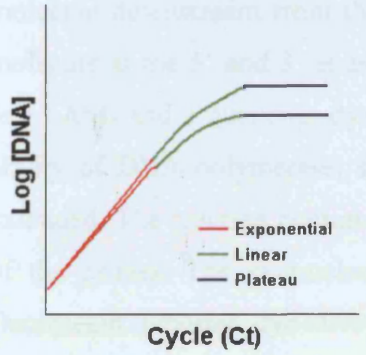

Figure 4-5 Schematic demonstrating the progression of two PCR reactions on two replicate samples. The same starting yield means that progression of the reaction is highly comparable during the exponential phase. However, slight differences and random events cause the deviation of the two reactions such that by the end-point large deviations can be created. Real-time PCR exploits the concordance between individual PCR reactions demonstrated in the exponential phase.

Development of real-time PCR massively improved the sensitivity and accuracy of qPCR. There are two methods of real-time PCR but they both rely on the same principle to improve accuracy. Real-time PCR tracks the difference in DNA mass produced during PCR, but only during the exponential phase of the reaction, where no significant deviation between replicate samples will have occurred. The technique exploits the fact that there will be a quantitative relationship between the amount of starting target sample and the amount of PCR product at any given cycle number. To do this requires *in situ* and continuous monitoring of the PCR products during the reaction.

This is achieved in one of two ways, but both rely on the use of fluorescent dyes. The constant monitoring of the DNA mass allows determination of the number of reaction cycles required to raise the starting mass of DNA above a threshold value. By calibrating against a standard curve, the cycle number at which the threshold value is crossed, can be linearly related to the mass of starting DNA material (Wang *et al.*, 2005). The two methods of real-time PCR are described below.

The SYBR-Green method traces the progression of the PCR reaction through the fluorescence of this fluorophore, an analogue of PicoGreen. As new PCR products are formed, fluorophore molecules intercalate into the newly formed DNA whereupon the fluorescence enables real-time detection of the DNA mass increase. The only drawback of this method is that the molecule will detect all dsDNA formed, including any unexpected PCR products. Although the probability of a defined probe binding to an unintentional sequence is low, it can occur. For example, a probe sequence 20bp length will occur every 160kb (20^4). The situation can be worse if the probe contains repetitive sequence (Lee *et al.*, Providenti *et al.*).

An improvement on the SYBR-Green method is the fluorescent primer-probe method. This technique employs a sequence-specific probe which binds to a sequence on the DNA molecule downstream from the sequence where the primer binds. Attached to the probe molecule at the 5' and 3' ends respectively are two molecules; a fluorescent reporter dye (e.g.FAM) and a quencher dye (e.g. TAMRA). The reaction relies on the 5' exonuclease ability of DNA polymerase, such that when the PCR reaction is initiated the primer is extended. The reaction continues until the probe sequence is reached, slightly downstream of the primer. The exonuclease action of DNA polymerase causes the release of the fluorescent reporter dye away from the quencher dye. The quencher dye works by stabilising the excited state of the fluorescent molecule such that it does not fluoresce. Upon release of the reporter dye, the molecule is able to fluoresce enabling real-time monitoring of the PCR reaction. Due to the proximity of the primer and probe sequence the probability of both binding to a sequence, except the one of interest, is highly unlikely. Ultimately, this technique is more precise than the SYBR-Green method as rogue PCR products will not be reported.

It is evident that qPCR is the most sensitive and accurate method of monitoring DNA concentration, be it plasmid or genomic DNA (Gibson *et al.*, 1996; Heid *et al.*, 1996). At the time of writing there existed no published data for the use of the primer-probe method

for quantifying plasmid DNA. The use of the SYBR-Green technique for plasmid quantification has been reported and its precision determined to be high at %CV of 2.8-3.9% (Lee *et al.*,). The use of the primer-probe method has displayed its sensitivity in being able to enable detection down to the single-copy number level (Lockey *et al.*, 1998). The application of this technique to allow precise determination of the contamination of plasmid preparations by gDNA has also been reported by (Vilalta *et al.*, 2002; Smith, III *et al.*, 1999). On the basis of the reported accuracy and precision it is believed that qPCR will be adopted further. At present it is the method of choice for quantifying gDNA contamination in plasmid preparations and is believed it will become more widely adopted for plasmid quantification.

4.2.5 Conclusions

The different methods of plasmid quantification have been outlined. Essentially, all the analytical technique make use of either absorbance or fluorescence for plasmid detection. However, how these two techniques are deployed depends on the method used to prepare the sample for analysis. As outlined in Figure 4-1, a number of methods were tried and analysed as to their efficacy. The philosophy behind this is that no evidence existed that the large plasmids used in this project could be reliably monitored using conventional techniques. The following results sections highlight the problems identified with commonly used plasmid quantification techniques and the improvement of such techniques required to allow quantification of large constructs.

4.3 PicoGreen quantification of IPA precipitated lysates and spin-prep eluents

4.3.1 Outline

The first analytical methods used for quantification of large constructs were performed on the Oxford series of plasmids grown in shake-flasks. Hourly samples of broth were analysed for the presence of plasmid by PicoGreen on samples purified by both Qiagen spin-prep and IPA precipitated clarified lysate. The streams were calibrated against a standard curve prepared from linear λDNA. Referring to Figure 4-1 this represents streams D and F.

Figure 4-6 displays the results of triplicate shake-flask studies where progression of p5176 (116kb) yield was measured through the course of the fermentations. The shake-flask fermentations were carried out by inoculating 500mL of either SDCAS or SuperBroth media, supplemented with 25μgmL^{-1} chloramphenicol, to a starting optical density of 0.1. The shake-flasks were incubated at 37°C and 230rpm in a shaking incubator. Wet cell weight and optical density progression were measured throughout the fermentations. Duplicate 1mL samples of broth were taken hourly from each of the shake-flasks, centrifuged, the liquor discarded and the pellets frozen at -20°C. The pellets from both culture sets were processed by two means; Qiagen spin-prep and IPA precipitation of clarified lysate. The plasmid containing streams were then quantified by PicoGreen calibrating against a linear, lambda DNA standard curve.

4.3.2 Comparing specific yield curves

The differences between the yield curves are quite apparent, the most apparent being between the different processing techniques employed. Yield progression shows a much higher variation when analyzing IPA precipitated clarified lysate. For example, the standard error on the harvest point of SuperBroth media, using IPA precipitation, is 34%. Comparing that error to the same result obtained by spin-prep extraction is 15%. It is clear then that PicoGreen quantification on spin-prep clarified lysates is a much less error prone technique.

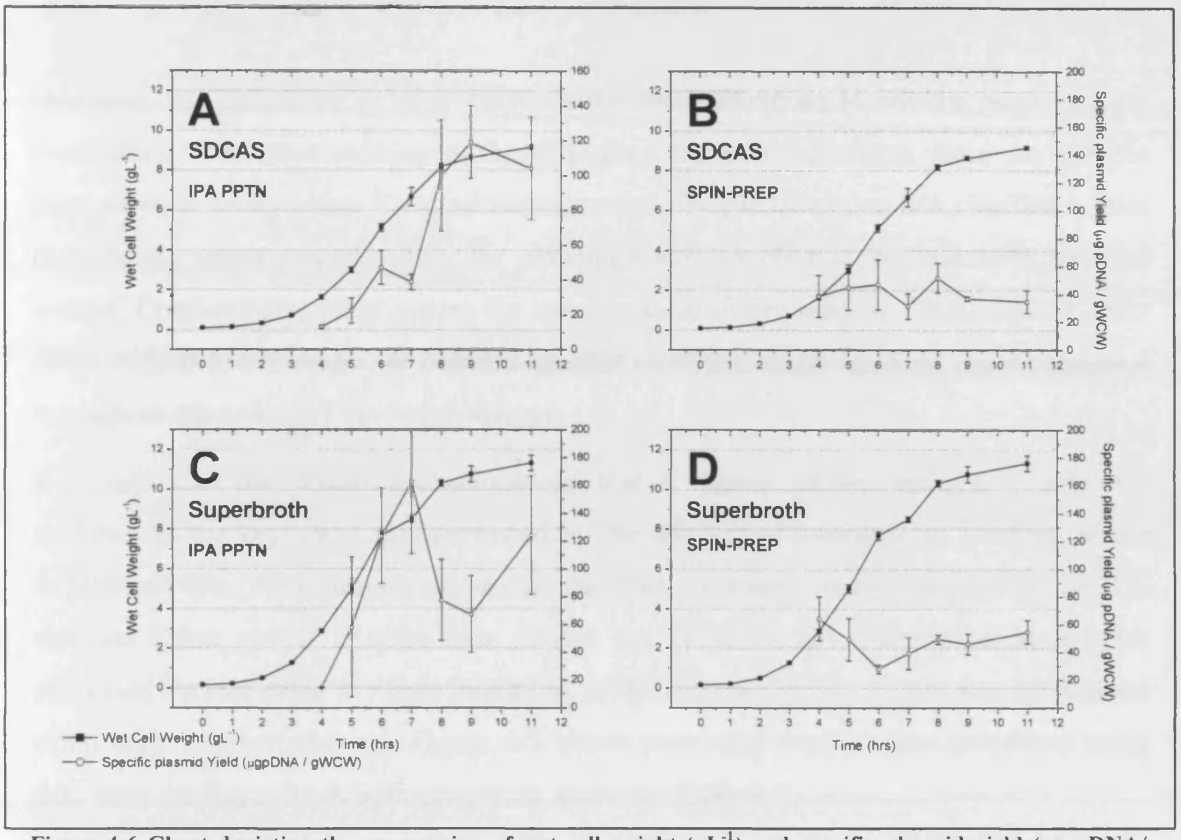

Figure 4-6 Chart depicting the progression of wet cell weight (gL^{-1}) and specific plasmid yield (µg pDNA/ gWCW) through triplicate shake-flask fermentations of DH10β [p5176 (116kb)] on two media types; complex SuperBroth and semi-defined SDCAS media.

2L shake-flasks (500mL media) were inoculated with 50 OD units and incubated in a shaking incubator (230rpm) at 37 ° C. Hourly 1mL samples of broth were taken, centrifuged and the plasmid extracted from the cell pellets using both Qiagen spin-prep® extraction and IPA precipitation of clarified lysate. The plasmid containing streams from both procedures were then quantified by PicoGreen against a λDNA standard curve.

[A; SDCAS media – IPA precipitation of lysate / B; SDCAS media – Qiagen spin-prep / C; SuperBroth media – IPA precipitation of lysate / D; SuperBroth media – Qiagen spin-prep]

Table 4-3 Summarising the yield data produced by p5176 cultures grown on both SDCAS and SuperBroth media by two extraction methods IPA precipitation of clarified lysate and Qiagen spin-prep. The plasmid containing streams from both extraction methods were quantified by PicoGreen calibrating against a linear λDNA standard curve.

Sample		IPA precipitated Clarified Lysate			Spin-Prep Eluent		
Measure / Media	µ (hrs^{-1})	Final Specific Yield (µg/ gWCW)	Final Volumetric Yield (mgL^{-1})	Final Copy No. (Copies/cell)	Final Specific Yield (µg/ gWCW)	Final Volumetric Yield (mgL^{-1})	Final Copy No. (Copies/cell)
SDCAS	0.56	104 ±29.4	0.96 ±0.27	3.42 ± 0.97	34.8 ±8.2	0.32 ±0.08	1.14 ± 0.27
SuperBroth	0.69	124.4 ±42.5	1.41 ±0.48	4.08 ± 1.4	54.8 ±8.46	0.62 ± 0.1	1.80 ± 0.28

However, the difference in error between the two techniques is not the most striking observation. The most striking is the difference the two techniques place on specific plasmid yield at any point. Yield curves determined by PicoGreen on IPA clarified lysates demonstrate much greater values for plasmid yield, which also increase with wet cell weight. Conflictingly, yield curves for specific yield determined by PicoGreen on spin-preps suggest lower values for plasmid specific yield, but which are must more consistent throughout the course of the fermentations.

It is not until the results are scrutinised that a clearer picture emerges. Table 4-3 summarises the key yield data produced by the triplicate fermentations. Looking at the SuperBroth data, for example, shows that the final volumetric yield predicted by the IPA clarified lysate results is more than double the value identified for identical samples processed by spin-prep. A rough indication of the accuracy of the results was determined using copy number analysis. Figure 4-7 shows how copy number was calculated using data from the SuperBroth/Spin-prep trials shown in Table 4-3.

$$\text{Final volumetric yield} = 0.62\text{mgL}^{-1}$$

$$\text{Final optical density} = 5.42\text{OD units}$$

$$1\text{OD unit} = 5\text{x}10^{8}\ \text{cells/ml}$$

$$1\text{ml of sample processed} = 0.62\mu\text{g}$$

$$= 0.114\mu\text{g / OD unit}$$

$$\text{Plasmid RMM}(\text{gmol}^{-1}) = \left[(\text{plasmid size x } 660)\text{x } 1.66\text{x}10^{-24}\right]$$

$$= \left[(116\text{x}10^{3}\text{ x } 660)\text{x } 1.66\text{x}10^{-24}\right]$$

$$= 1.2709\text{x}10^{-16}\ gmol^{-1}$$

$$\text{Moles of plasmid} = \left(\frac{\text{Plasmid mass}\ (\mu\text{g})}{\text{RMM}}\right)/1\text{x}10^{6}$$

$$= \left(\frac{0.114}{1.2709\text{x}10^{-16}}\right)/1\text{x}10^{6}$$

$$= 8.97\text{x}10^{8}\ mols$$

$$\text{Plasmid Copy Number} = \frac{\text{Moles of plasmid}}{\text{Number of cells}}$$

$$= \frac{8.97\text{x}10^{8}}{5\text{x}10^{8}}$$

$$= 1.79\ \text{copies/cell}$$

Figure 4-7 Calculation used to estimate the copy number of p5176 at harvest using the yield data provided by PicoGreen analysis on Qiagen spin-prep eluents from SuperBroth Shake-flask fermentations.

The other results from the copy number analysis are shown in Table 4-3. From them, it appears that the values placed on copy number by spin-prep extraction are the most trustworthy. The reason being that the figures calculated for the mean copy number at harvest for samples extracted by IPA precipitation; 3.42 and 4.08, are much higher than could be physically achieved. More likely are the numbers calculated for copy number by samples extracted by spin-prep; 1.14 and 1.8, as these place the result within the 1-2copies per cell range, known to be the copy number of plasmids possessing the F-factor replicon (Frame and Bishop, 1971; Burke *et al.*, 1987; Monaco and Larin, 1994; Sinnett *et al.*, 1998). Although not conclusive proof of the accuracy of certain techniques, copy number analysis can provide a good estimate of whether the result is likely or not. Further evidence supporting the inaccuracy of the IPA technique, and relative accuracy of the spin-prep technique, was provided by control studies.

4.3.3 Control studies using DH10β

The assumption that the spin-prep processing technique produces the most likely result of plasmid specific yield was backed up by control studies. Figure 4-8 details the results of yield traces, produced using an identical methodology and extraction regime as before, but on triplicate cultures of DH10β parental strain grown on SuperBroth. From Figure 4-8A, it can be appreciated that the specific yield of genomic DNA over the course of the fermentations, shows a remarkably similar trace to that presented by the yield curves for the IPA precipitated clarified lysates of samples extracted from the 116kb fermentations. It would seem that the results presented as plasmid specific yields in Figure 4-6A and C are heavily contaminated by residual genomic DNA, meaning that the traces are not at all indicative of the actual plasmid yields. The contamination also goes someway to explain the variation in IPA results as being due to fluctuations in the mass of genomic DNA removed by the individual lysis operations conducted on the samples. It is not known what form the contamination takes, it is either ssDNA or dsDNA. What can be said is that PicoGreen is unable to differentiate between the plasmid p5176 and this contaminant. Contamination is somewhat expected, due to the crude nature of the IPA processing technique. Although alkaline lysis will result in the removal of large amounts of genomic DNA, some small fragments obviously remain in the clarified lysate and are co-precipitated together with the plasmid in the IPA precipitation step.

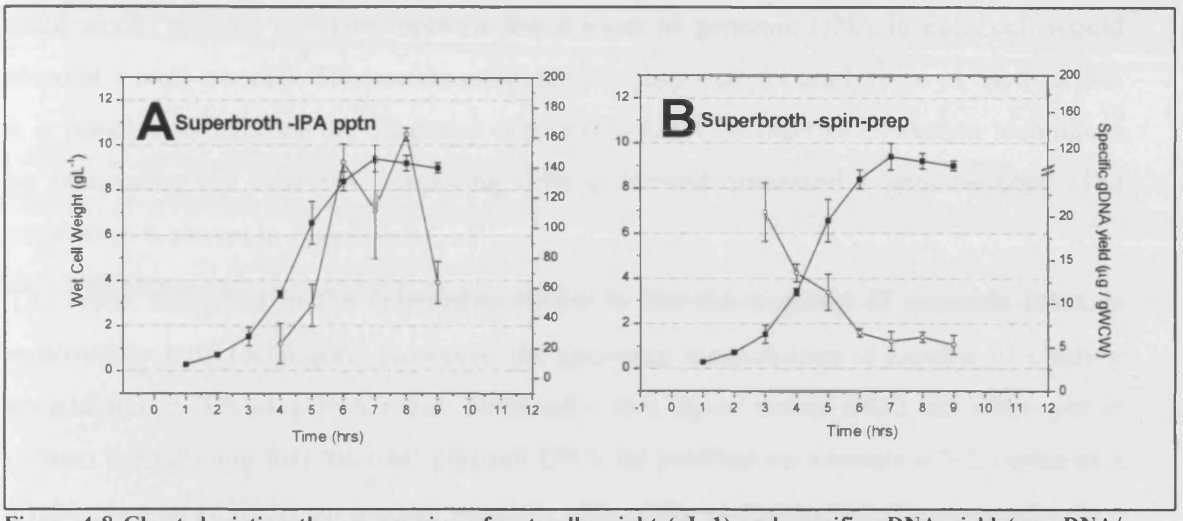

Figure 4-8 Chart depicting the progression of wet cell weight (gL-1) and specific gDNA yield (µg gDNA/ gWCW) through triplicate shake-flask fermentations of DH10β [parental] on complex SuperBroth.
2L shake-flasks (500mL media) were inoculated with 50 OD units and incubated in a shaking incubator (230rpm) at 37 ° C. Hourly 1mL samples of broth were taken, centrifuged and the DNA extracted from the cell pellets using both Qiagen spin-prep extraction and IPA precipitation of clarified lysate. The DNA containing streams from both procedures were then quantified by PicoGreen against a λDNA standard curve in order to provide a measure of the background reading produced by the co-purification of gDNA.
[A; SuperBroth – IPA precipitation / B; SuperBroth – Qiagen spin-prep]

Figure 4-8B displays the results of background genomic DNA as measured by PicoGreen on spin-preps eluents of DH10β parental fermentation samples. The background level of genomic DNA contamination is far reduced compared to IPA precipitation. Indeed at harvest the spin-prep samples recorded an average of ~5µgg^{-1} WCW as opposed to the same figure for the IPA clarified lysates being ~60µgg^{-1}WCW genomic DNA. This is confirmed by the manufacturer's literature (Qiagen, 2005) which claims the protocol is able to promote the elution of small dsDNA fragments over plasmid DNA by the salt content and pH of the wash buffers employed during the washing stages of the column (Qiagen, 2005).

4.3.4 Calculating the clearance of genomic DNA by the two extraction regimes

The profiles of the progression of genomic DNA during the fermentations are quite illuminating. The genomic DNA yield trace shown in Figure 4-8B describes a reduction in genomic DNA specific yield as the course of the fermentation progresses. This should be the case, since a typical cell during early log phase of growth will be doubling at a maximum rate, and so will most probably have greater than 1 genome copy of DNA, meaning specific yield would be at a maximum. As growth slows, in late log phase and early stationary phase, less of the cell population will be doubling and so DNA specific yield begins to decrease. Eventually, at stationary phase, growth stops and the specific

yield would become constant, because the amount of genomic DNA in each cell would stand at 1 copy per cell. This means using similar copy number analysis to as used earlier, it is possible to estimate the clearance of genomic DNA by the two extraction techniques by calculating the clearance supposing cells at harvest possessed 1 genome copy. The estimation is shown in Figure 4-9.

The result described in the calculation below is that the majority of genomic DNA is removed by both techniques. However, the spin-prep methodology is capable of clearing an additional ~4% of gDNA mass. Nominally, this figure seems small but when put in context by outlining that the total plasmid DNA for purification consists of ~2 copies of a 116kb plasmid (232kb), an amount equal to ~5% of the genome mass. Consequently, in a typical IPA processed sample it can be expected that there was a 1:1 ratio of plasmid mass to contaminating genomic DNA mass, meaning the results obtained for pDNA yield are approximately double the actual amount.

$$
\begin{aligned}
\text{Volumetric gDNA yield } (\mu g L^{-1}) \text{ at harvest} &= 48.1 \text{ [spin - prep]} \\
&= 575.1 \text{ [IPA pptn]} \\
\text{OD at harvest} &= 5.2 \\
&= 2.6\text{x}10^{9} \text{ cells} \\
\text{1 genome copy mass (g)} &= 4.669\text{Mbp} \\
&= \left[\left(4.7\text{x}10^{6} \text{ x } 660\right) x\ 1.66\text{x}10^{-24}\right] \\
&= 5.15\text{x}10^{-15} \text{ g / copy} \\
\text{Mass of genomic DNA in 1ml at harvest}(\mu g) &= (2.6\text{x}10^{9}) \text{ x } (5.15\text{x}10^{-15}) \\
&= 13.4\ \mu g \\
\text{Mass of gDNA recovered from 1ml by spin - prep } (\mu g) &= 0.048\ \mu g \\
\text{Mass of gDNA recovered from 1ml by IPA pptn } (\mu g) &= 0.575\ \mu g \\
\textbf{\% removal by spin - prep} &= \left(\frac{13.4 - 0.048}{13.4}\right) x100 \\
&= \mathbf{99.64\%} \\
\textbf{\% removal by IPA pptn} &= \left(\frac{13.4 - 0.575}{13.4}\right) x100 \\
&= \mathbf{95.7\%}
\end{aligned}
$$

Figure 4-9 Calculation to determine the mass of genomic DNA cleared by IPA precipitation and spin-prep assuming each cell has 1 genome equivalent at harvest.

4.3.5 Validation of the PicoGreen assay for use on spin-prep eluents

One conclusion for the yield analysis is that the results for plasmid yield progression are more precisely described by the spin-prep results. However, although precise, it is not known definitively how accurate the results are. Copy-number analysis suggests that the figures are accurate but two unknowns remain. For the figures to be accurate, it has been assumed all the plasmid is recovered by spin-prep processing. Secondly, there is a disparity over the calibration standard employed. Typically, when using PicoGreen the unknown fluorescence is calibrated against a signal of known concentration. The calibration curve is made up from the DNA species being quantified, such that when measuring the concentration of p5176 plasmid in samples, the standard curve should be composed of known concentrations of the same plasmid. In this study, the calibration standard was composed of known concentration of lambda DNA, differing from plasmid DNA in that it is linear and so displays no supercoiling. This fact could result in the yield data plotted in Figure 4-6B and D being inaccurate.

4.3.5.1 Plasmid recovery over a spin-prep column

The effect of the first unknown; the efficiency by which large plasmids could be purified by spin-preps, was quantified by recording the percentage recovery of various plasmid solutions across the column step of a Qiagen spin-prep. Figure 4-10 displays the results of the recovery trials. The irregularity with this study was that spin-preps are designed to recover plasmid from clarified lysate and not TE buffer. However, this effect was decided to be minimal and the results back this up. The graph displays the percentage recovery of the small plasmid pSVβ against the same for the large construct, p5176. Although recovery for both plasmids is quite poor at low concentrations, (deemed mainly to be due to assay error) the recoveries of the two constructs display a similar profile of between 75-90%. The pSVβ solutions demonstrate only a slightly higher level of recovery. In conclusion, using spin-prep purification recovers the majority of large plasmid DNA present in the samples, and hence the results presented in Figure 4-6 B and D can be taken as being an accurate reflection of the process output.

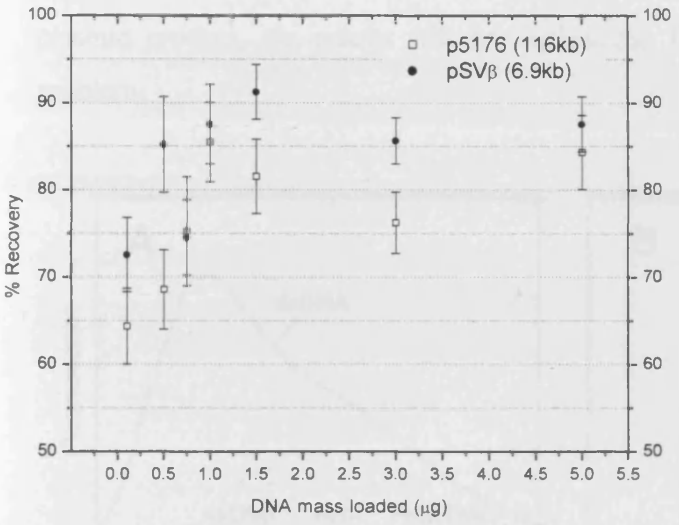

Figure 4-10 Figure displaying the recovery of two plasmid varieties over triplicate spin-prep column purification. 1mL volumes of known plasmid concentration (quantified by NanoDrop) in TE buffer were loaded on to the matrix of a spin-prep column and incubated at room temperature for five mins. The columns were then washed with the requisite buffers as described by the spin-prep protocol. The eluted plasmid was then quantified by NanoDrop absorbance and the percentage recovery calculated.

4.3.5.2 Standard curve for PicoGreen analysis of spin-prep eluents

The second unknown about the accuracy of PicoGreen analysis on spin-prep purified samples, concerns the disparity between the standard curve material and the samples being analysed. In this study the samples were calibrated against a linear DNA standard curve. As explained earlier, it had been reported that the fluorescence signal produced by PicoGreen is dependent upon the topology of the DNA. At the stage of conducting these investigations, it was believed that the plasmids in the p5176 samples were supercoiled and as such would not be well represented by a linear DNA standard curve. It was perceived that further studies were needed to confirm the accuracy of PicoGreen on spin-prep purified samples, by calibration against a standard curve composed of p5176 plasmid.

4.3.6 Conclusions

It has to be concluded that PicoGreen quantification of IPA clarified lysates is not an accurate method of determining the concentration of large plasmid in the sample. The reason determined for this is that the signal produced by the plasmid is heavily corrupted by the presence of contaminating DNA of either single-stranded of double-stranded form. This technique can and does form the basis for reliable quantification when the concentration of the plasmid in the sample is high, as with high-copy number plasmids, but due to the similar quantities of plasmid to contaminant gDNA in the samples of large plasmids, the results cannot be trusted. It is not an issue with the PicoGreen either, as the

fluorophore does demonstrate a high specificity for dsDNA over contaminants. The issue remains that since the level of contaminants is at a comparable concentration to the plasmid product, the results will be misleading. Figure 4-11 attempts to highlight the problem.

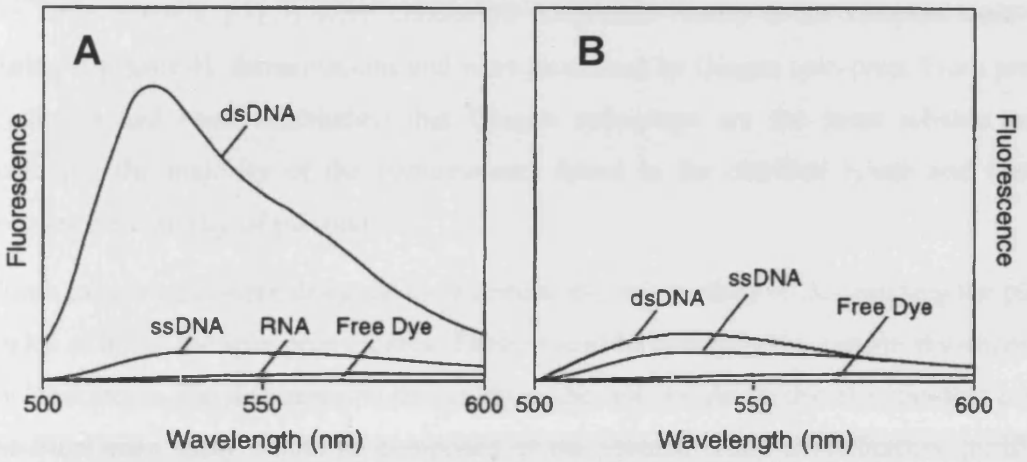

Figure 4-11 Figure attempting to illustrate how contamination issues can corrupt the signal produced when assaying large, low-copy number plasmids. Figure A demonstrates a hypothetical fluorescence trace when assaying a high-copy number plasmid. The result of the combined fluorescence result can be trusted since the effect of the contaminants on the overall result is small. However, when the ratio of contaminants to plasmid is high as in B, the contributory effect of the contaminants cannot be ignored since it forms a large part of the overall signal.

PicoGreen analysis of spin-prep purified samples did show a higher degree of precision. It was determined that the spin-prep process removed a higher quantity of contaminating genomic DNA (99.64%), sufficient to believe that only small traces of contaminants remain. However, issues still surround the accuracy of this technique. Studies revealed that the majority of plasmid is purified when using spin-prep processing. The problem lay in the standard used for PicoGreen analysis and more specifically the topology it displayed.

4.4 Comparing Plasmid Quantification by Absorbance and PicoGreen

4.4.1 Outline

This section compares two methods of quantifying plasmid samples extracted as time-points during 4L fermentations. Fermentations of the small, high-copy plasmid pSVβ and the large plasmid p5176 were conducted. Duplicate hourly broth samples were taken during triplicate 4L fermentations and were processed by Qiagen spin-prep. From previous studies it had been established that Qiagen spin-preps are the most reliable way of removing the majority of the contaminants found in the clarified lysate and that they recover the majority of plasmid.

These experiments were designed to determine the best method of determining the plasmid yields of the of the spin-prep eluents. These would be quantified by simple absorbance and by PicoGreen. The difference in this study to the last, would be that the standard used for the PicoGreen assay would be composed of the plasmid under investigation, purified by Qiagen maxi-prep. As such, the topology of the plasmid standard should be identical to that of the native plasmid. Referring to Figure 4-1 this study will compare quantification of streams G and F.

4.4.2 Methodology

Samples taken during the 4L fermentations were processed by Qiagen spin-prep. Duplicate samples from each fermentation at each time-point were processed. The eluted plasmid containing streams were quantified by two means; Absorbance (A_{260}) and PicoGreen. Absorbance measurements were recorded using the method explained in (2.5.9) and the PicoGreen method followed that described in (2.5.10). There was one key difference with this set of studies. Up until this point, PicoGreen measurements on spin-prep eluents, had been made by calibrating against a linear λDNA standard curve. It was understood at the time that this could lead to discrepancies in the returned values, due to differences in the topology of plasmid and linear DNA. Consequently, in these studies, the plasmid containing streams were calibrated against known concentrations of the same plasmid purified by maxi-prep (i.e. p5176 standards for p5176 samples). The gentler processing regime of maxi-preps ensured that the plasmid standards existed in a form closely matching their native topology. Samples purified from the parental fermentations

continued to be calibrated against λDNA. Figure 4-12 and Table 4-4 detail the results of the yield investigations.

Table 4-4 Table detailing the key measurables taken from investigations into the plasmid yields of triplicate fermentations of DH1[pSVβ] and DH1[p5176]. The yield results were obtained by PicoGreen and absorbance (A_{260}) readings recorded from duplicate samples through the course of the fermentations and processed by Qiagen spin-preps.

Strain Quantification method	Mean % CV	Coefficient of correlation	Final mean specific yield ($\mu g g^{-1}WCW$)	% Average deviation from mean	Final mean volumetric yield (mgL^{-1})	Final copy number
DH1 [pSVβ] Absorbance	16.14	0.883	320±35.7	31.6	25.65±2.86	168±18.8
DH1 [pSVβ] PicoGreen	12.06		351±39.5	24.3	28.1±3.17	185±20.9
DH1 [p5176] Absorbance	17.72	0.572	44.7±6.8	23.6	3.93±0.6	1.2±0.18
DH1 [p5176] PicoGreen	16.06		205.3±49.8	24.2	18.05±4.38	5.4±1.3

4.4.3 Comparing the results of PicoGreen and Absorbance for pSVβ

The results from the pSVβ fermentations in Figure 4-12A and B, demonstrate a high degree of comparability between the yield profiles from both methods of quantification. The mean %CV records the average % coefficient of variation between each duplicate sample, from each time-point, from each of the three fermentations. The values produced suggest that the PicoGreen method, with a lower value of 12% is the more precise of the two assaying methods. This contradicts (Haque *et al.*, 2003) who maintained that due to the higher complexity of the PicoGreen assay, the %CV was higher than for absorbance.

Figure 4-12F correlates the mean values for specific yield determined by each method for each time point. For the pSVβ results, the coefficient of correlation is high at 0.883, suggesting good correlation between the results produced by absorbance and those of PicoGreen. The results of linear regression through the axis, reveals that quantification by absorbance places the value for specific yield roughly 6% higher than PicoGreen. Because absorbance has been demonstrated to be the more error-prone technique, it is assumed that PicoGreen quantification is also more accurate.

It is believed that PicoGreen would be more likely to record a more accurate value, since the absorbance readings would be affected by contaminating protein in the recovered

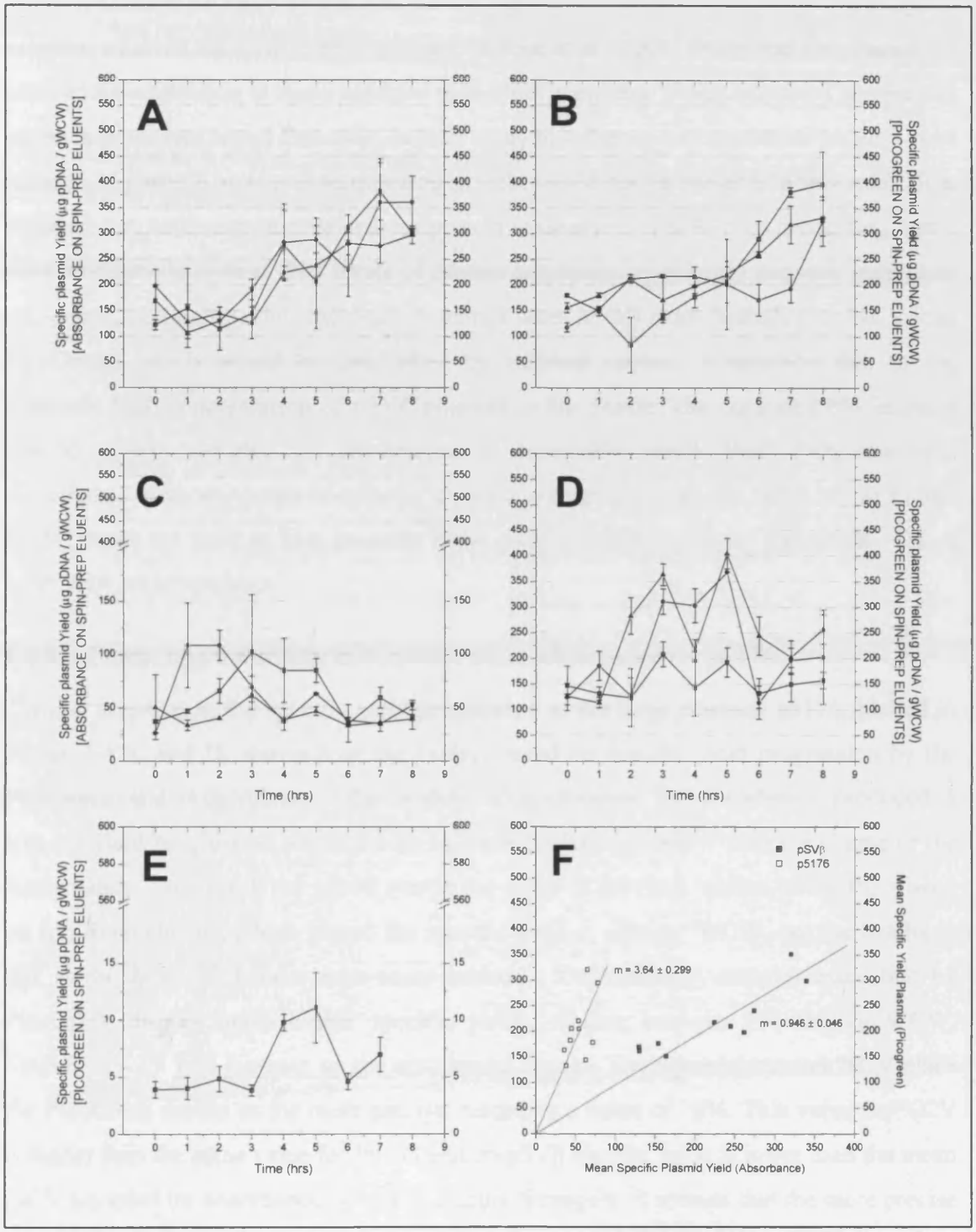

Figure 4-12 : Chart describing the progression of specific plasmid yield (µg pDNA/ gWCW) throughout triplicate 4L 37°C fermentations of *E.coli* DH1 parental, [pSVβ (6.9kb)] and [p5176 (116kb)]. Duplicate 5OD-unit equivalent volumes of broth were taken at each time point and centrifuged. The resultant cell pellets from each of the fermentations were then processed using Qiagen spin-preps. The plasmid recovered from the spin-preps was then quantified by both absorbance and PicoGreen. For PicoGreen the appropriate standard was employed, either; maxi-prep purified pSVβ (6.9kb)/ p5176 (116kb) respectively or λDNA for parental extracts. [A; pSVβ (6.9kb)-Absorbance / B; pSVβ (6.9kb)-PicoGreen / C; p5176 (116kb)-Absorbance / D; p5176 (116kb)- PicoGreen /E; Parental-PicoGreen (Background) / F; Correlating PicoGreen and absorbance methods for the two plasmid constructs].

samples, whereas the PicoGreen would not. (Haque *et al.*, 2003) report that absorbance for plasmid quantification is more accurate than PicoGreen, due to the increased complexity of the fluorescence assay. However, in their study absorbance was conducted on ultra-pure samples of plasmid and so contaminating protein would not be present. In this study, it is believed that while the vast majority of protein is removed by spin-prep processing, some trace amounts do remain. The levels of protein remaining would vary between individual spin-preps, explaining why absorbance readings taken in this study had a higher %CV than PicoGreen, which would be unaffected by residual protein. Ultimately, due to the relatively high concentration of pSVβ plasmid in the eluents, the estimated 6% increase due to protein reported by absorbance, is acceptably small. Both PicoGreen and Absorbance methods would be affected by trace amounts of genomic DNA but as Figure 4-12E shows the level of host genomic DNA contamination at harvest represents ~1% of total DNA under analysis.

4.4.4 Comparing the results of PicoGreen and Absorbance for p5176

Turning attention to the specific yield progression of the large plasmid; p5176, plotted in Figure 4-12C and D, shows how the values placed on specific yield progression by the PicoGreen and Absorbance differ widely. Quantification by absorbance produced a specific yield progression which varied between 50-100$\mu g g^{-1}$WCW over the course of the fermentation. This result for p5176 was in the range of previous studies, using PicoGreen on spin-prep eluents, which placed the specific yield at ~50$\mu g g^{-1}$WCW, but the results in this study show a lot more intra-assay variation. Contrastingly, samples quantified by PicoGreen display much higher specific yields, ranging between 150-350$\mu g g^{-1}$WCW, roughly a 3-3.5 fold increase on the absorbance figures. The figures for mean %CV place the PicoGreen results as the more precise, recording a value of 16%. This value for %CV is higher than the same value for PicoGreen on pSVβ eluents, but it is lower than the mean %CV recorded for absorbance on p5176 eluents. Strangely, it seemed that the more precise technique was recording values for plasmid yield three times higher than had been previously encountered.

The striking difference between the values estimated for specific yield by the two methods is shown in Figure 4-12F, which plots the values produced for each time point by the two methods against each other. The correlation between the two sets is low at 0.572 making linear regression uneasy. However, the value produced suggests that indeed PicoGreen quantification produced a value for specific yield on average 3.6 fold higher than

absorbance. Copy number analysis was performed to give an estimate about which technique was producing a value closest to that assumed to be the case, i.e. 1-2 copies per cell. Shown in Table 4-4 are the values for harvest copy number estimated by the two techniques. The analysis suggests that the absorbance method is the more accurate since it places copy number in the 1-2 copy range, whereas PicoGreen places the figure much higher at 5-6 copies per cell.

The situation was clarified when the standard curves used for PicoGreen were analysed, as plotted in Figure 4-13A. From the graph, the difference in the fluorescence produced per unit mass of DNA can be seen to vary depending on the DNA used. Comparing the linear λDNA standard curve to the other two curves demonstrates that linear DNA produces a 6.5-fold stronger fluorescence signal than pSVβ and a 2.6-fold stronger signal than p5176. (Singer *et al.*, 1997) reported similar differences when studying the fluorescence of supercoiled and linear DNA species and reasoned it was due to conformational differences in the DNA. Essentially, the increased supercoiling of DNA makes it increasingly difficult for the PicoGreen fluorophore to intercalate into the DNA. The results above suggest that linear DNA is capable of binding over 6-fold more molecules of PicoGreen per kilobase of DNA than the same length of supercoiled pSVβ DNA. Interestingly, p5176 DNA is able to

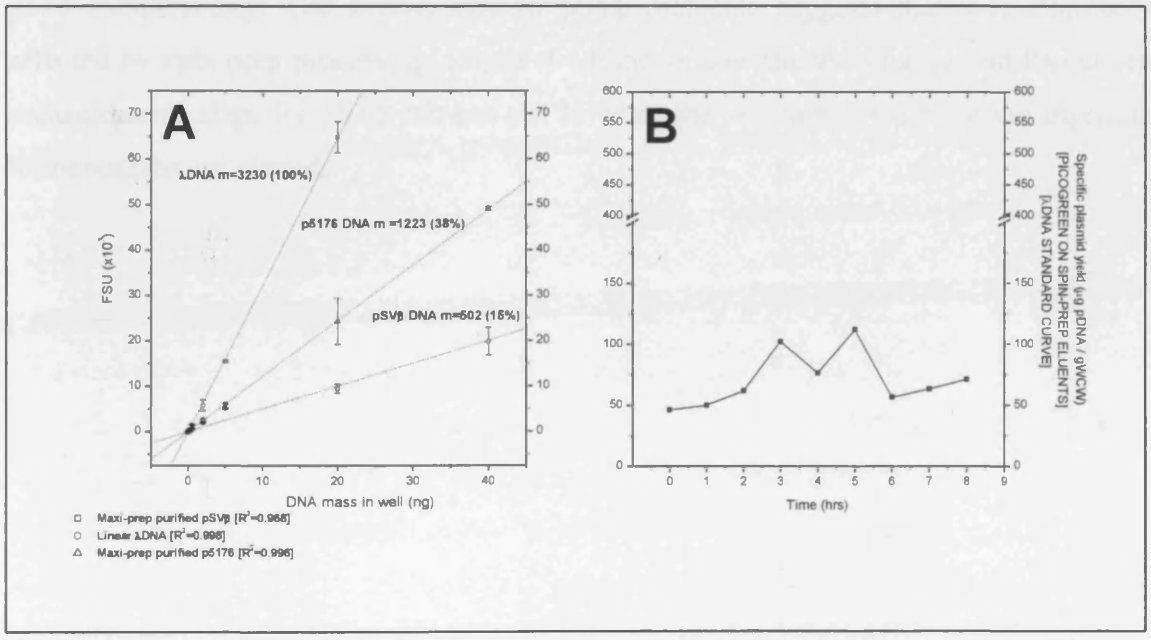

Figure 4-13 Chart A shows the calibration curves used in PicoGreen quantification. Fluorescence was recorded for each DNA species in triplicate at concentrations of [0.005/0.05/0.2/0.5/2/5/20/40 ng per well]. The gradients produced by linear regression are shown on the graph. Chart B records the values produced for mean specific plasmid yield for the p5176 fermentations when the linear λDNA standard curve was used for calibration.

bind 2.5 fold more DNA than the same mass of pSVβ, suggesting p5176 samples displayed less supercoiling than pSVβ, a fact supported by the increased plasmid size causing an increased probability of plasmid shear during standard preparation.

This analysis suggests that for accurate estimation of plasmid yield using the PicoGreen assay, requires that the standard employed must be highly representative, in terms of topology, of the samples under analysis. By such logic, it was reasoned that the standard curve used in this study was representative for the pSVβ cultures and so reliable specific yields, which correlated well with the absorbance readings, were produced. However, the same could not be said for the p5176 fermentations, where it was believed the standard curve did not closely mimic the samples being analysed.

This belief was evidenced by earlier studies, as shown in (Figure 3-6), where the differences between the relative topologies displayed by the IPA/maxi-prep and the spin-prep purified samples were striking. The effect of the shear induced by spin-prepping and the resultant over-estimation by PicoGreen was only appreciated at this stage. Consequently, it was realised that purifying p5176 samples by spin-prep and then assuming that their topology matched that of its native state was wrong. This error only seemed to apply to the large constructs, since the PicoGreen values for the pSVβ did show good comparability. The smaller size of pSVβ molecule suggests that it is minimally affected by spin-prep processing. Figure 4-14 shows how the absorbance and PicoGreen measurements align for pSVβ but not p5176 when the volumetric yields of the triplicate fermentations are plotted.

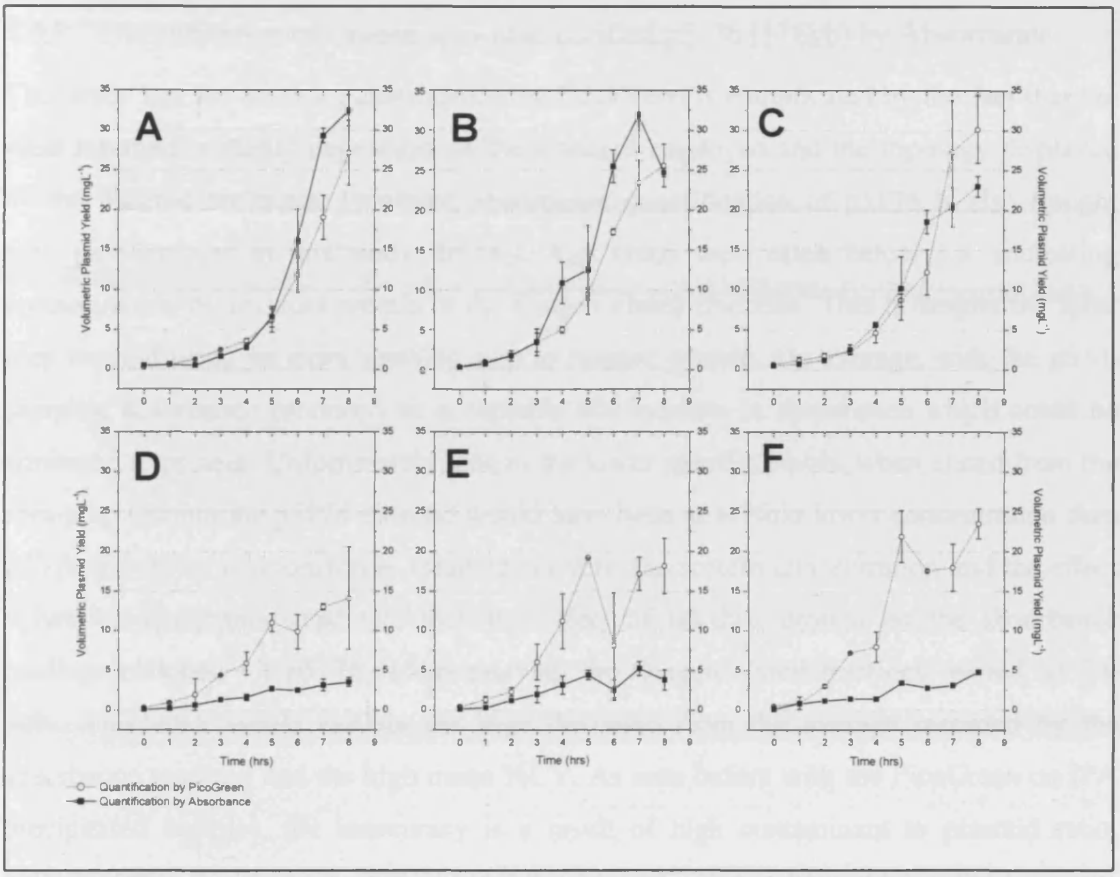

Figure 4-14 Figure contrasting the differing estimations of volumetric yield produced by quantifying plasmid by PicoGreen and Absorbance (A260). Figures A/B/C compare the values for volumetric yields produced during 4L fermentations of DH1 pSVβ (6.9kb) determined by both PicoGreen (using maxi-prep purified pSVβ for the standard) and Absorbance on Qiagen spin-prep eluents. Figures D/E/F contrast the volumetric yields determined by absorbance and PicoGreen (using maxi-prep purified p5176 (116kb) for the standard) for the 4L fermentations of DH1 p5176 (116kb). In all cases plasmid quantification (either by absorbance or PicoGreen) was conducted on Qiagen spin-prep purified material generated from (5 OD unit volume equivalent) cell pellets collected during 4L fermentations

As an estimate, the fluorescence values produced by the spin-prep eluents of the p5176 plasmid were calibrated against the standard curve for λDNA, and the results plotted in Figure 4-13B. This analysis is not entirely accurate, since for PicoGreen to be accurate a standard curve is included on each assay plate as the level of fluorescence will vary between plates. However, despite the associated error, the yield profile produced suggests that the λDNA curve does form a more representative standard, since the yield profile more closely resembles the values estimated by absorbance. This realisation, that using a λDNA standard curve with spin-prep purified p5176, produced a more accurate estimation of yield validated previous studies which employed the same standard for quantification.

4.4.5 Quantification of Qiagen spin-prep purified p5176 (116kb) by Absorbance

This study has shown that quantification by PicoGreen is complicated by the fact that the yield returned is highly dependent on the standard employed and the topology displayed by the plasmid molecule. However, absorbance quantification of p5176 is also fraught with problems, as in this study the A_{260}/A_{280} ratios were often below 1.8, indicating contamination by residual protein in the Qiagen eluted fractions. This is despite the spin-prep method using an extra washing step to remove protein. On average, with the pSVβ samples, absorbance produced an acceptable 6% increase in absorbance which could be attributed to protein. Unfortunately, due to the lower specific yields, when eluted from the spin-prep column the p5176 plasmid would have been at 6-7fold lower concentration than pSVβ. If a linear relationship is assumed between the protein concentration and the effect it has on absorbance readings, then the effect of residual protein on the absorbance readings obtained for p5176, when assaying the Qiagen eluted fractions, would be 30-40%. This error would explain the high deviation from the average recorded by the absorbance readings and the high mean %CV. As seen before with the PicoGreen on IPA precipitated samples, the inaccuracy is a result of high contaminant to plasmid ratio. Unfortunately, background residual contamination will always be present in the spin-prep purified samples, making the situation difficult to improve upon.

4.4.6 PicoGreen quantification on clarified lysates

As described previously, absorbance on spin-prep purified samples has been shown to be an accurate and precise method of quantifying high-copy number, small plasmids. However, its employment for use with large, low-copy number plasmids was found to be hampered by the corrupting influence of trace amounts of residual protein. Additionally, using PicoGreen quantification on spin-prep eluents has been shown to be highly dependent on the topology of the plasmid used for calibration. It was found that the topology of the small plasmid pSVβ, in the spin-prep eluent, did not differ widely from the maxi-prep standard, the same could not be said for the large plasmid.

In response to these issues, samples taken from both the pSVβ and p5176 fermentations were lysed in the normal fashion and attempts made to determine the plasmid concentration directly in the clarified lysate. This technique, it was hoped, would describe the plasmid in a more native state. Referring to Figure 4-1 this corresponds to stream A.

The plasmid samples were calibrated against a standard curve composed of maxi-prep purified plasmid. The results are outlined in Figure 4-15.

From the graph it can be appreciated that the results for pSVβ, as determined by spin-prep on clarified lysate and directly on clarified lysate, correlate well. Linear regression through the origin reveals that PicoGreen directly on clarified lysate produced ~60% higher reading than on spin-prep eluents. The reason for this increase will be down to two reasons. Firstly, there will have existed higher levels of bacterial genomic DNA in the clarified lysate, the presence of this linear dsDNA contamination would be expected to produce an increased fluorescence signal, the effect of which would have been exacerbated by the calibration against a pure, supercoiled standard. Secondly, as shown in, spin-prepping does result in 10-15% loss of plasmid. This plasmid would still be present in the clarified lysate, partly explaining the increased specific yield. As a result of this analysis, it has to be assumed that PicoGreen on clarified lysate places an upper limit on pSVβ yield with PicoGreen on spin-prep eluents placing a lower limit on the yield.

Turning attention to the progression of specific yield of the culture bearing the large construct p5176 as shown in Figure 4-15B. The results of PicoGreen quantification on the clarified lysate of hourly cell pellets taken from the p5176 fermentations revealed a great

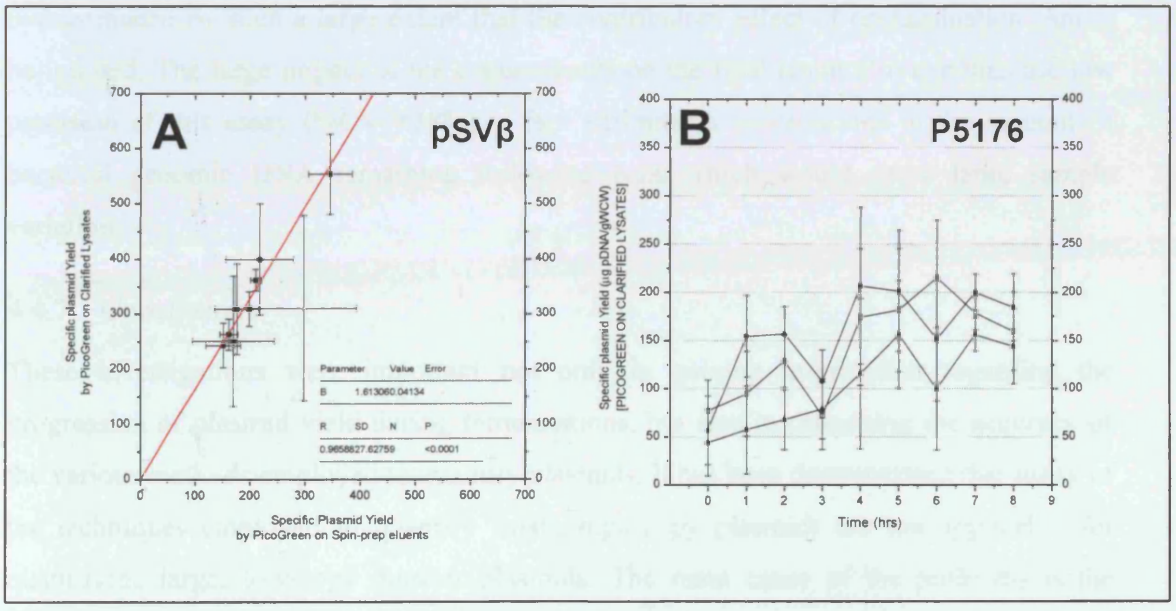

Figure 4-15 Graph A correlates the mean specific yield calculated by PicoGreen on spin-prep purified pSVβ against the values produced from the same time-point in the fermentation determined by PicoGreen on clarified lysates. A point has been masked to improve the correlation. Graph B shows the calculated specific yields of the p5176 fermentations as determined by PicoGreen on clarified lysates.

deal of variation, with the average %CV recorded at 38%. Such lack of precision of the results is mirrored by the assay's poor accuracy. The results from the fermentation recorded by absorbance (Figure 4-12C) are taken as the most accurate in explaining the progression of p5176 yield during the fermentations. The absorbance values, although probably adversely affected by residual protein, place the plasmid yield at 50-100μgg^{-1}WCW. Using PicoGreen quantification on clarified lysates it can be seen that the values ranged from 100-250μgg^{-1}WCW. As such, it is believed that these results do not accurately describe the yield progression.

Referring back to the results of PicoGreen on IPA precipitated clarified lysates shown in Figure 4-6 suggests that similar contamination effects are being witnessed by performing PicoGreen on clarified lysates. As reported with quantification of IPA lysates the results were heavily contaminated by residual bacterial genomic DNA. The situation is made worse in this scenario since in this study the lysates were calibrated against a standard curve composed of supercoiled p5176. The net result of this is that the residual linear DNA will bind more fluorophore molecules giving a higher estimate of plasmid DNA. Whilst the residual DNA effect impacts on all quantification of plasmids by this method, partly explaining the increase witnessed for the pSVβ fermentations, the effect becomes more noticeable when the plasmid yield is low, as with p5176. The results are overestimated by such a large extent that the contributory effect of contamination cannot be ignored. The large impact of the contaminants on the final result also explains the low precision of this assay (%CV =38%), a fact attributable to variations in the amount of bacterial genomic DNA remaining following lysis which would show large sample variation.

4.4.7 Conclusions

These investigations were important not only in gaining information regarding the progression of plasmid yield during fermentations, but also in discerning the accuracy of the various methods employed to quantify plasmids. It has been demonstrated that many of the techniques employed to quantify small, high-copy plasmids are not applicable for quantifying large, low-copy number plasmids. The main cause of the problems is the contaminant to plasmid ratio. High-copy plasmids exist at high enough concentration in the streams used for analysis that the impact of background signals produced by contaminants has little impact on the accuracy of the results. However, with the drop in

plasmid concentration witnessed when using low-copy number plasmids, the impact of the contaminants on the overall value becomes too large to be ignored.

Table 4-5 highlights the problems associated with the application of various quantification methods for determination of plasmid concentration when low-copy plasmids are being assayed. The asterisked methods can and have been applied for the accurate quantification of small, high-copy number plasmids.

Table 4-5 Table displaying the extraction and quantification combinations used so far and their relative suitability for monitoring yield progression of the large plasmid series. Asterisks denominate methods which would be suitable for small, high-copy number plasmids.

QUANTIFICATION METHOD / EXTRACTION METHOD	ABSORBANCE [A_{260}]	PICOGREEN [USING LINEAR λDNA STANDARD]	PICOGREEN [USING MAXI-PREP PLASMID STANDARD]
IPA precipitated clarified lysate OR directly on Clarified Lysate	**Not Possible**; sample heavily contaminated by protein and gDNA	**Inaccurate and imprecise**; BAC remains supercoiled meaning plasmid yield would be underestimated. However, reading masked by residual gDNA contamination	**Inaccurate and imprecise**; overestimation of plasmid yield due to background gDNA fluorescence. *
Qiagen spin-prep	**Roughly accurate**; most plasmid eluted but due to the low elution concentration, small traces of protein can lead to large errors in absorbance readings.*	**Accurate and precise;** spin-prep removes the most contaminants and majority of plasmid eluted. Shear forces remove all supercoiling meaning standard and sample share the same topology.	**Inaccurate;** large difference between plasmid and standard topology means plasmid yield is over-estimated.*

From the table it can be appreciated that absorbance on either clarified lysate or IPA precipitated lysates is not a feasible technique, in any case, due to the solvent and high contaminant levels. PicoGreen quantification can be employed to quantify all of the aforementioned streams when high-copy number plasmids are being quantified, since the overall level of the contaminants is not sufficient to corrupt the final reading. However, this is not the case with low-copy number plasmids.

Again, spin-prep purification of plasmids followed by absorbance quantification, is a perfectly acceptable technique for quantification of high-copy number plasmids. In this study it was established that the trace levels of protein would lead to an acceptable 6% overestimation of plasmid yield. However, due to the lower plasmid concentration in the spin-prep eluents of low-copy plasmids, the residual levels of protein were found to produce A_{260}/A_{280} ratios below the acceptable margin of 1.8. As a result, the use of this

technique for quantifying low-copy plasmids was accompanied by a high error level and the certain possibility that the residual protein increased the final estimate placed upon plasmid yield.

An interesting effect was reported for the quantification of spin-prep eluents using PicoGreen. From standard curve data, it was shown that the topology of the DNA affected the fluorescence signal produced, and as such it was deemed that the topology of the standard had to mimic the sample under investigation very closely, in order to be confident about the accuracy of the result. For small plasmids, the action of spin-prepping did not have a detrimental effect on the plasmid topology, meaning that spin-prep purified samples could be accurately calibrated against a standard curve composed of maxi-prep material. However, it was deemed that the action of spin-prepping on the large plasmid; p5176, did cause the loss of supercoiling such that calibrating the samples against the supercoiled maxi-prep standard led to an overestimation of plasmid yield. It was determined that the spin-prep samples could be accurately quantified by calibrating the samples against a standard curve composed of linear λDNA. This method overcame the problem with residual protein in the eluents and also accurately mimicked the DNA topology of the plasmid in the eluent.

The final technique of accurately quantifying large plasmids by spin-prepping to remove the majority of contaminants, followed by PicoGreen detection and calibration against a linear standard curve could be employed. The drawback with this technique is that the spin-prepping technique involves exacting a physical change upon the plasmid molecule and assumes that the spin-prep does this reliably and completely. To make this assumption makes it likely for errors to be overlooked and from an industrial perspective, such an assay would be unlikely to be validated. A second consideration concerns one of the main aims of this project, which is the creation of descriptive plasmid balance over the process. This will involve quantifying the plasmid through fermentation and all streams of the purification process. During this it is expected that the topology of the plasmid, and the contaminant profile of the solution it is in, will vary a great deal. As such, it is important that an analytical technique be found that is not affected by alterations in plasmid topology, contaminant concentration or the buffer environment. With this in mind it was decided to investigate the use of HPLC for plasmid quantification.

4.5 Plasmid quantification by HPLC

4.5.1 Introduction

Separation of biological molecules by High Performance Liquid Chromatography (HPLC) is long established. Commonly used for analytical studies on biological compounds, it enables effective separation of different molecular species in a sample by one chromatographic step, so allowing their analysis and quantification. The high degree of separation and high purity that can be achieved is produced due to the high theoretical plate number of HPLC columns which, depending on column length, is in the order of 10^5. This high plate number is created by virtue of the small particle size used for the stationary phase (which is commonly between 3-50μm) combined with the large aspect ratio of HPLC columns. As with traditional column chromatography, HPLC can be operated in different modes i.e. hydrophobic interaction, gel filtration and ion-exchange, by employing specific column matrices which enable its use for separating a wide variety of compounds. The small particle size is the cause of the large pressure drops encountered during HPLC operation, which again depend on column length, but are often over 1000psi.

The use of HPLC for plasmid analysis has been reported in the literature. The advantages of using this analytical technique for quantifying plasmid in clarified lysate is that it many cases it can allow separation of plasmid DNA from contaminating protein, RNA and linear DNA such that only the plasmid is quantified. Indeed, the technique has even been reported to enable separation of the different topoisomers of plasmid DNA, allowing the obtainment of detailed information on the plasmid quantity and quality (Kapp and Langowski, 1992). It is this ability to separate the plasmids away from the contaminants that led to the adoption of this technique for use in this project, as previous investigations had been hampered by misleading quantification due to the high ratio of contaminants to plasmid in the streams used for analysis. Four modes of operation have been reported for plasmid separation, as well as mixed mode.

4.5.1.1 Hydrophobic Interaction HPLC

Hydrophobic Interaction HPLC (HIC-HPLC) has been applied successfully for quantifying total plasmid in clarified lysates. The technique takes advantage of the more hydrophobic character of nucleic acid impurities (RNA, denatured genomic DNA, oligonucleotides and denatured plasmid forms) when compared with double-stranded

plasmid DNA. The advantage of this technique is that no prior removal of RNA is required. Diogo *et al.*(2003) employed HIC, using Sepharose CL-6B gel derivatized with 1,4-butanediol diglycidyl ether, to achieve base-line separation of plasmid DNA. The precision of the technique was reported to be 2%, and it was found capable of accurately quantifying pDNA in heavily contaminated samples, where plasmid was <5% w/w and at concentration levels down to $1\mu gmL^{-1}$ (Diogo *et al.*, 2003). The technique is also reported to be capable of separating of open-circular and supercoiled plasmid forms (Diogo *et al.*, 1999; Iuliano *et al.*, 2002; Onishi *et al.*, 1993). However, this degree of selectivity can only be achieved with longer running times of about 40 minutes.

4.5.1.2 Size Exclusion HPLC

Size-exclusion HPLC has also been demonstrated to separate plasmid molecules from clarified lysate. It is capable of separating large M_r molecules (plasmid isoforms/ gDNA) away from smaller M_r species (oligonucleotides/ RNA/ Proteins). The plasmid containing peak is Gaussian in form, with the leading edge containing the OC/multimers/ large gDNA, whilst the smaller size CCC form is found in the trailing edge. Traditional matrices were not effective since the small pore sizes did not allow the penetration of the large plasmid molecules. Introduction of rigid and highly porous composite polyacrylamide/dextran stationary phases has alleviated the problem. Despite the drawback, plasmid isolation has been reported using TSK-Gel G6000PW which separated plasmid from clarified lysate by size exclusion alone. However, there are no reports of this method being able to resolve the different topoisomers. The majority of methods using size exclusion HPLC do so in mixed mode.

4.5.1.3 Reverse Phase HPLC

The use of this HPLC method has been reported to separate different plasmid topoisomers. The retention of nucleic acids on the column is attributed to hydrophobic interactions between the aromatic hydrophobic bases and the hydrophobic ligands of the matrix. Bound molecules are eluted in order of increasing hydrophobicity, a property which is defined by characteristics such as base composition, chain length and secondary structure. Consequently, nucleic acids of increasing size will be retained longer, also AT-rich sequences leads to an increase in interaction strength, suggesting that separation can be sequence dependent. (Kapp and Langowski, 1992; Weiner *et al.*, 1988)

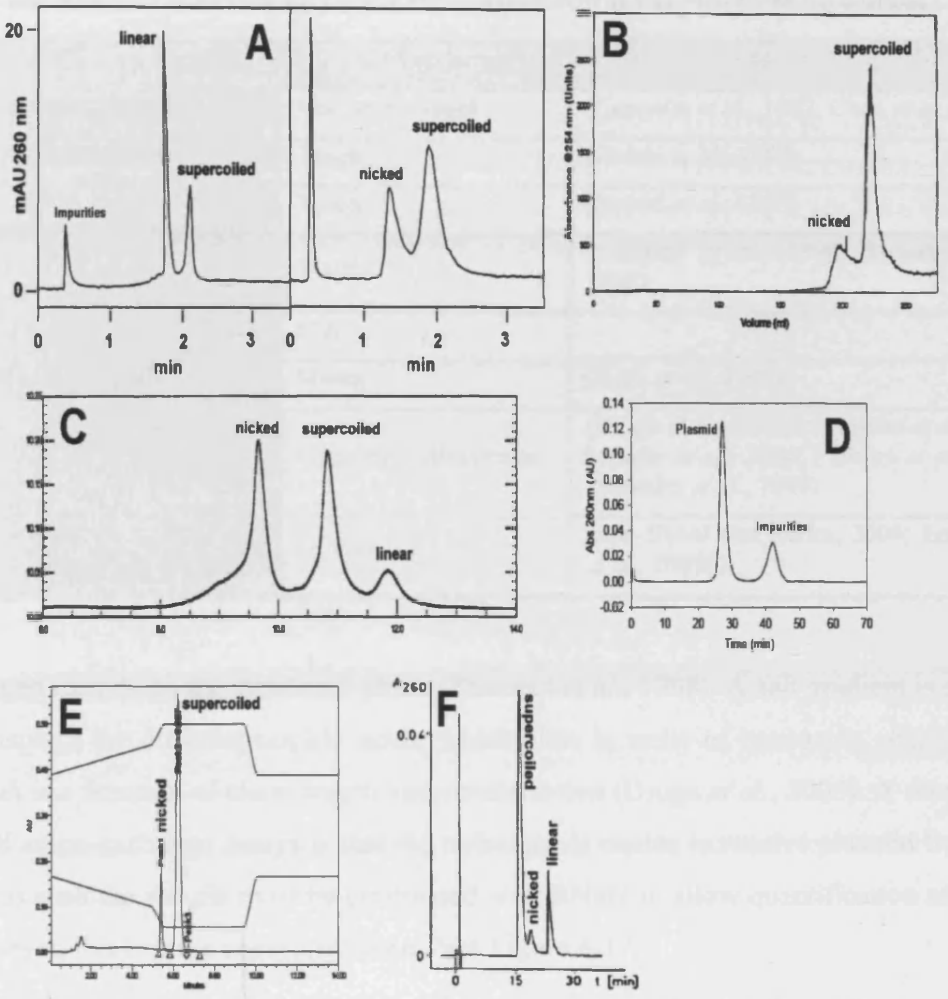

Figure 4-16 Figure displaying reported HPLC traces of plasmid samples separated by different forms of HPLC. A shows the profile generated by anion exchange HPLC using DEAE-PS-DVB matrix. Reasonable separation of plasmid isoforms is witnessed (Huber, 1998). B shoes the trace following Reverse Phase HPLC using copolymer beads with attached Hexyl residues (Kapp and Langowski, 1992). C shows the results of HIC-HPLC using TSKgel Butyl-NPR column and effective baseline line separation is achieved (Iuliano *et al.*, 2002). D shows the results of size-exclusion HPLC using TSKgel G6000PW, showing the separation of plasmid from smaller size contaminants. E shows the profile of 3kb plasmid run in this project on anion-exchange column DNA-Pac PA-100, which allowed separation of topoisomers of small plasmids. F displays the trace of another anion exchange matrix; Nucleogen 4000 with effective separation of a small plasmid pBR322 (4.3kb) produced.

4.5.1.4 Anion Exchange HPLC

Anion exchange HPLC is the most common form of HPLC used for plasmid quantification, and is the type employed in this project. It relies on the interaction between the negatively charged phosphate groups in the DNA backbone and positively

Table 4-6 Table outlining a selection of ion-exchange HPLC columns used for plasmid separation. Details are given into the nature of the stationary phase, the manufacturers and any associated publications.

Stationary Phase	Manufacturer	References
Nucleogen-DMA-4000	Macherey-Nagel	(Coppella *et al.*, 1987; Chen *et al.*, 1997)
DEAE-NPR	Tosoh	(Onishi *et al.*, 1993)
DEAE-5PW	Tosoh	(Onishi *et al.*, 1993)
DEAE-Gen-Pak	Waters	(Lahijani *et al.*, 1996; Stowers *et al.*, 1988)
DEAE-PS-DVB	N/A	
DMAE-LiChrospher	Merck	(Horn *et al.*, 1995)
Poros HQ, QE, PI	PerSeptive Biosystems	(Diogo *et al.*, 2001b; Prazeres *et al.*, 1998; Meacle *et al.*, 2004; Ferreira *et al.*, 1999; Monteiro *et al.*, 1999)
DNAPac PA-100	Dionex	(Eon-Duval and Burke, 2004; Eon-Duval *et al.*, 2003b)

charged ligands on the stationary phase (Prazeres *et al.*, 1998). A salt gradient is employed to displace the different nucleic acids, which elute in order of increasing charge density, which is a function of chain length and conformation (Diogo *et al.*, 2005). A disadvantage of all anion-exchange assays is that the technique is unable to resolve plasmid from RNA, and as such the sample must be pre-treated with RNase to allow quantification of plasmid. However, this is not a significant issue. See Figure 4-17.

The use of anion-exchange HPLC for plasmid quantification has been described in numerous publications, as outlined in Table 4-6. Total pDNA analysis and quantification, for use as a process analytical tool has been described using Poros HQ, Poros PI and DMAE-LiChrospher (Table 4-6). None of these methods were capable of resolving the different plasmid forms, but were used for accurate assessment of the purity and pDNA quantification in process solutions.

However, the separation of different plasmid isoforms by AE-HPLC has been reported.

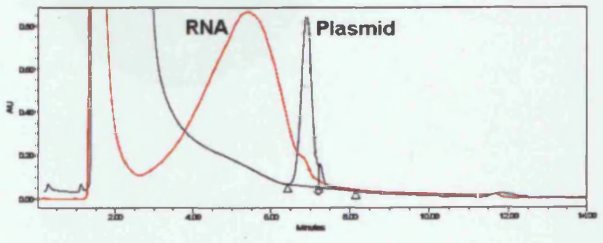

Figure 4-17 Impact of RNA in the HPLC sample when run on Dionex DNAPac100 column. While a degree of separation is achieved the contaminating presence of RNA makes accurate quantification of plasmid difficult. Consequently, samples treated with RNAse.

(Colpan, 1999) used macroporous Nucleogen-DMA-4000 to separate gDNA and RNA

from pDNA, and achieve separation of isoforms (Figure 4-16F). Similarly, (Onishi *et al.*, 1993) achieved the same objective using DEAE-NPR and DEAE-5PW columns. Both these reports could be referred to as mixed-mode HPLC as the columns separated using both AE and SE principles. Consequently, the run times of these columns were ~30mins.

A much more rapid method, allowing the resolution of pDNA isoforms was obtained using a non-porous, micropellicular DEAE anion-exchanger, based upon highly crosslinked PS-DVB particles. The favourable mass transfer properties of this type of support allowed the resolution of different pDNA isoforms within 3 minutes (Liu *et al.*, 2004). It is this type of matrix that is employed in this project, as found in DNAPac PA-100 columns (Dionex). The Nucleopac PA-100 stationary phase of the column consists of 100nm quaternary-ammonium functionalised Microbeads, bound to a 13μm non-porous core. The solid core allows steeper gradients to be applied allowing more rapid elution, and the microbeads ensure good mass-transfer. Furthermore, the material is more stable and pressure resistant, and due to its configuration, the area available for binding is not much lower than totally porous substrates.

The micropellicular nature of the substrate used in the HPLC column, along with its high aspect ratio (250mm x 4mm) allows for excellent separation and resolution of plasmid samples. Consequently, as shown in Figure 4-16E the column is capable of resolving the nicked and supercoiled plasmid forms.

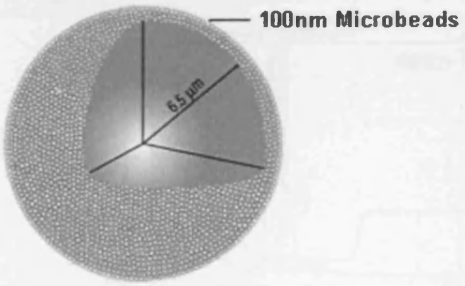

Figure 4-18 Figure displaying the physical make-up of the beads which form the stationary phase of the DNA Pac PA-100 column. The functional groups of crosslinked quaternary ammonium form 100nm microbeads, attached to a 13μm solid core of fused silica. The design enables good mass transfer and pressure resistance.

4.5.2 Use of Anion-Exchange HPLC

The use of HPLC in this project was pervasive, as it was the main analytical tool for plasmid quantification in both upstream and downstream studies. Test runs carried out established the feasibility of using this technique for quantifying plasmids up to 116kb. From the HPLC traces produced for the smallest plasmid analysed (3.2kb), it was estimated that the HPLC column possessed ~10^3 theoretical plates. A figure not as great as reached by some preparative columns, but still outperforming other HPLC systems, as evidenced by the shape of the peaks as compared to competing methods shown in Figure 4-16. It was noted however, that the degree of resolution was better for small plasmids, and as such plasmid isoforms could be resolved. Unfortunately, it was found that resolution decreased with increasing plasmid size, such that it was not possible to resolve the topologies of the larger plasmids. This was not a major problem as other techniques were developed for analysing plasmid topology. The main use for HPLC was for a technique that could reliably and accurately determine plasmid yield. The precision of the HPLC assay was determined by running replicate samples and was determined to be ~4%CV.

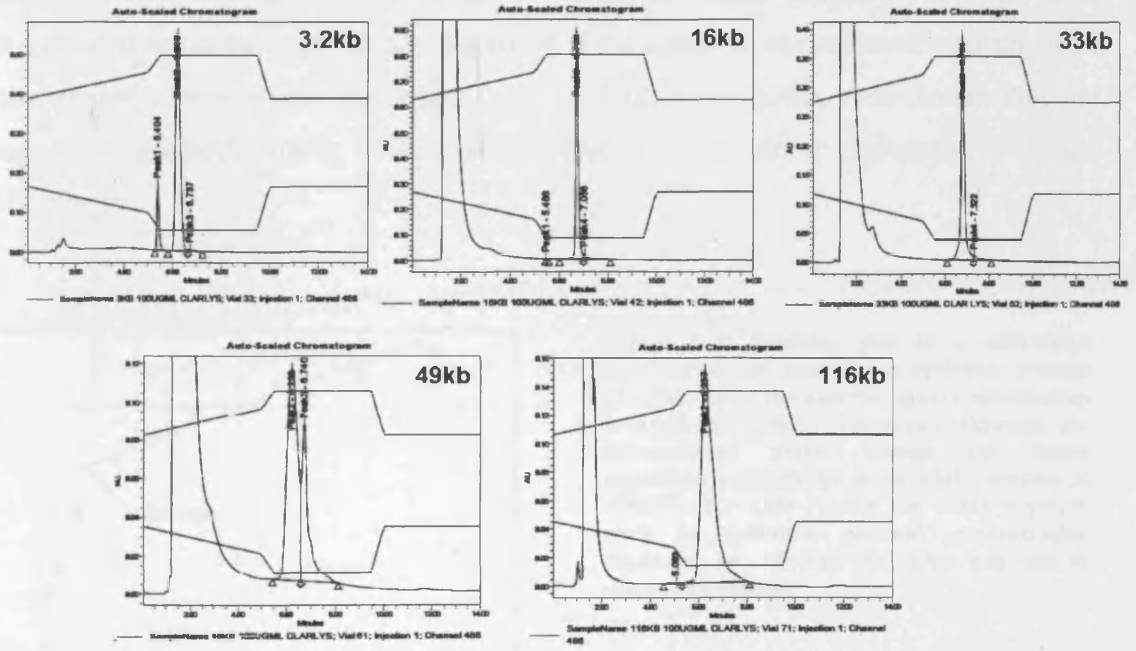

Figure 4-19 Figure displaying the decrease in resolution achieved with increasing plasmid size. Traces of equal concentrations of the various plasmids shows that as size increased the ability to resolve isoforms could not be achieved. Also, as plasmid size increased the width of the peaks increased indicating the greater number of plasmid conformations that were in existence.

Details about the operation of the HPLC system can be found in (2.5.11). In all cases the operation remained the same in terms of flow rate, buffers used and the method of detection. Detection was achieved by absorbance at 260nm and the traces recorded by the software. Integration of the peaks from the HPLC traces was also automated by the software. The algorithm controlling the integration was instructed to ignore peaks before 4.5mins and after 8.2mins, as all the plasmids investigated were found to elute between these time points. The peak areas were calibrated against standard curves prepared for each plasmid.

All the standard curves used, were plots of the concentration of the plasmid solution loaded (determined by A_{260} of ultra-pure samples) against the resultant HPLC peak area. The application of the standard curve depended on the HPLC area value returned. If the peak area of the unknown was found to be ≥400,000 then a different standard curve would be employed to when the peak area was ≤400,000. The reason for this was to improve accuracy of the standard curve and is explained by recording a semi-log plot of a typical standard curve (Figure 4-20). Because the standard curve describes an area term, the increase in area obeys a square relationship. Consequently, for more dilute plasmid solutions, the standard curve was found to be more representative if the linear fit was performed over the points describing the dilute solutions. Similarly, for the more concentrated solutions accuracy was improved if the linear fit was achieved over the more concentrated solutions. For this reason each standard curve shown, even though they are seen to be perfectly linear, will be accompanied by two linear regression plots and relationships.

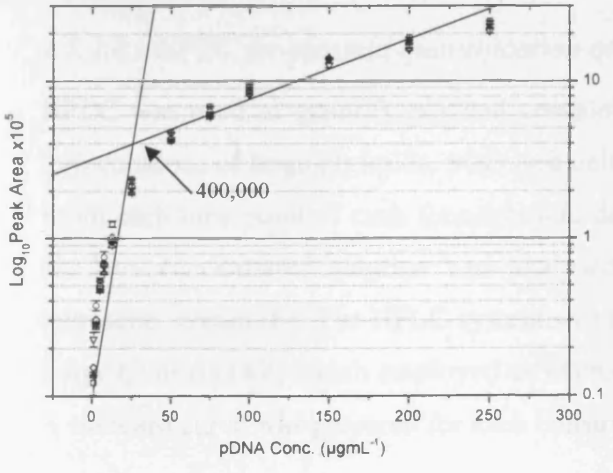

Figure 4-20 Semi-log plot of a calibration curves used for quantifying upstream process samples. From the plot the square relationship is apparent. Linear regression through the concentrated points crosses the linear regression through the more dilute samples at 400,000. For that reason the exact equation used to calculate plasmid concentration depended on whether the value was less or more than 400,000.

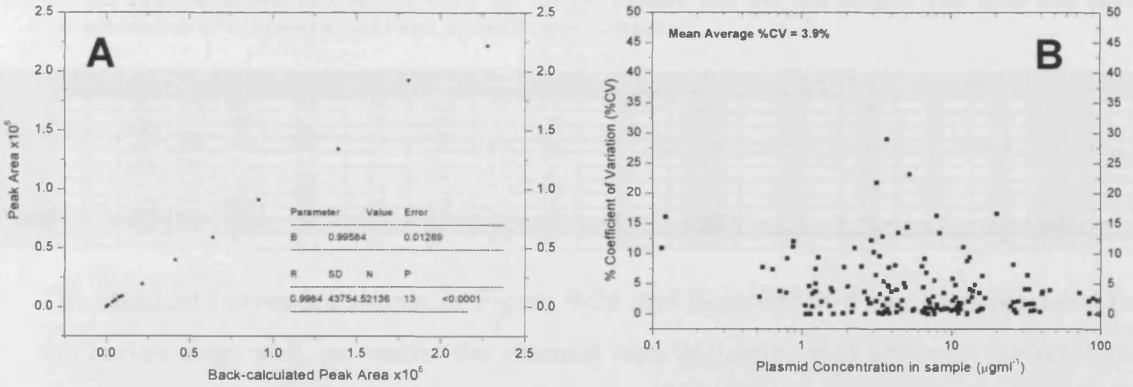

Figure 4-21 Figure A displays a check made to confirm the accuracy of the HPLC system. The figure correlates the areas produced from running solutions of known plasmid concentration against the values predicted for the area terms from the current standard curve. Performing this check regularly allowed detection of any drift in the calibration. Figure B plots figures the results of investigations into precision of the HPLC system. The %CV produced by running replicate samples on the HPLC equipment is plotted against the resultant concentration of the plasmid sample.

The accuracy of the HPLC assay was regularly checked by running plasmid standards of known concentration. The results were then correlated against the expected peak area, as determined from the current standard curve. Figure 4-21A shows the result of such an investigation, using a 16kb plasmid. From the figure it can be appreciated that the accuracy of the HPLC assay was never in doubt. Figure 4-21B also plots the results of investigations into the assay's precision.

Despite the similarities in the operation of the HPLC assay for its use in upstream and downstream studies, there remained some subtle differences between the two, in terms of the standard curves employed and the volumes injected. These differences shall be outlined in the following sections.

4.5.2.1 HPLC for plasmid quantification of Fermentation Samples

HPLC was used to quantify plasmid containing streams from samples taken during the fermentations of large plasmids. 5OD unit cell pellets were prepared as outlined in (2.5.5). From each time point of each fermentation, duplicate samples were prepared and 10μL of the IPA concentrated solution was analysed by HPLC (Referring to Figure 4-1, this represents stream (E). The HPLC system was calibrated using material prepared by Qiagen Large Construct kit, which employed an exonuclease to digest any residual genomic DNA. A standard curve was prepared for each construct under investigation.

Table 4-7 Table outlining the calculations performed to determine plasmid specific yield from the HPLC peak areas. Peak areas were calibrated from the standard curves enabling the plasmid mass produced from a 5OD cell pellet sample to be found. The specific yield was calculated from this value and the mass of the cell pellet analysed determined from the optical density and wet cell weight. The table also shows the calculation of volumetric yield and plasmid copy number.

pQEM 19kb V2 Time point	Elapsed Time (hrs)	HPLC Area A	HPLC Area B	Mean Area	Plasmid [conc. (ug/ml)]	Plasmid Mass (ug)	Std Dev	WCW [g/L]	WCW [SD Dev]	Optical Density (A600)	WCW Pellet Mass (g)	Plasmid Specific Yield (ug/gWCW)	Spec Std [St Dev]	Volumetric Yield [mg/L]	Vol Yield [St dev]	Moles of Plasmid	Plasmid Copy No. [copies/cell]	Copy No [St Dev]
0	0	618827	537920	578373.5	69.58	6.96	0.6178	40.7	0.141	12.6	0.0158984	437.54	36.857	0.14	0.012	3.98823E+11	317.46	28.19
2	9	234731	241837	238289	28.14	2.81	0.0609	14.55	0.601	2.885	0.0252166	111.59	2.417	1.82	0.035	1.60625E+11	128.42	2.78
3	10	201941	218921	210931	24.81	2.48	0.1548	17.4	0.849	4.6	0.0189130	131.18	8.187	2.28	0.142	1.41531E+11	113.22	7.07
4	11.5	206172	190872	198522	23.05	2.31	0.1882	25.55	0.318	7.4	0.0172635	133.56	9.828	3.41	0.246	1.31152E+11	105.22	7.69
5	12.5	239007	258380	248654.5	29.40	2.94	0.1662	26.45	0.177	8.12	0.0175185	167.85	9.485	4.76	0.270	1.6774E+11	134.16	7.58
6	13.5	247886	260999	254232	30.08	3.01	0.1097	37.25	0.601	13.12	0.0141959	211.92	7.725	7.86	0.286	1.71618E+11	137.29	5.00
7	15	240875	249219	245047	28.96	2.90	0.0719	51.15	0.530	18.1	0.0141298	204.99	5.086	10.49	0.260	1.65234E+11	132.19	3.28
8	16	241862	257447	249654.5	29.53	2.95	0.1342	65.6	0.071	22.7	0.0144493	204.34	9.289	13.40	0.809	1.68436E+11	134.75	6.13
9	17	237902	241584	239743	28.32	2.83	0.0321	83.4	1.344	31.1	0.0134084	211.18	2.391	17.61	0.199	1.61639E+11	129.23	1.46
10	18	273429	276461	274455	32.55	3.25	0.0177	95.1	2.051	38.7	0.0122868	264.89	1.438	25.19	0.137	1.85888E+11	148.53	0.81
11	18.5	293636	264448	279042	33.11	3.31	0.2514	92.45	0.601	39.5	0.0117025	282.89	21.480	26.15	1.986	1.88853E+11	151.06	11.47

The standard curves are shown in Figure 9-26 and from which it can be appreciated that the curves align well, no matter the plasmid size, indicating that although the resolution decreased as plasmid size increased, the area under the curve remained for an equal plasmid mass. This indicated that the recovery of the plasmid from the column was comparable no matter the size of the plasmid loaded.

Following the analysis of the cell pellet sample by HPLC, the trace was analysed the peak area recorded and converted to a concentration using the standard curve (Figure 9-26). Once the plasmid concentration of the plasmid stream was known, the total plasmid mass could easily be determined. The specific yield of the fermentation at the particular time point could then be calculated. Details of the calculation process for one vessel is shown in Table 4-7, the other vessel records can be found in Figure 9-29. The volume of the broth samples taken during the fermentation were all 5OD unit volume equivalent. The reason to assay on the constant mass basis was that as the wet cell weight of the fermentation increased, sampling on a constant volume basis would lead to increased masses of the cell pellets. This would cause inaccuracies in the analysis when the cell pellets were lysed. For instance, sampling on a constant volume basis would lead to inefficient cell lysis of samples taken toward the end of the fermentation. Since the wet cell weight and optical density of the fermentations were known at the point of sampling the pellet mass could be calculated and the specific yield was the plasmid mass determined by HPLC divided by the mass of the cell pellet.

The precision of IPA precipitation of clarified lysate and subsequent plasmid quantification by HPLC was determined to be 7%CV. As such, this assay was deemed more precise than both absorbance and PicoGreen on spin-prep eluents which recorded %CV values between 12-16%.

As outlined earlier the accuracy of the HPLC system for quantifying plasmids was never in doubt. However, the checks described earlier were performed on ultra-pure plasmid standards. In this scenario, IPA precipitated samples were being run on the system. As such, the assumption was being made that the peaks recorded only contained plasmid. It was known that HPLC has the ability to separate pDNA away from protein and low mol.weight gDNA, and that the RNA was removed by RNase. However, it was discovered that the system did co-elute some large gDNA fragments, which remained in the IPA precipitated sample along with the plasmid. There was little that could be done to improve this, as there would always be some degree of contamination. It was reasoned that a size exclusion column could be placed in-line with the anion-exchange column to remove the effect. However, it was believed that since the impact of the contamination was small, the potential plasmid loss which could be incurred by including an additional column would negate the point of its inclusion.

It was important to quantify the level of this residual contamination. As such, when the upstream studies were conducted, negative controls were also carried out in the form of DH1 parental fermentations. Samples were taken during the fermentations and processed in the same fashion as the plasmid bearing samples. These were run on HPLC to provide information on the background signal. The resulting contaminant profile is not a measure of the amount of gDNA in the sample, since the vast majority would be removed by IPA

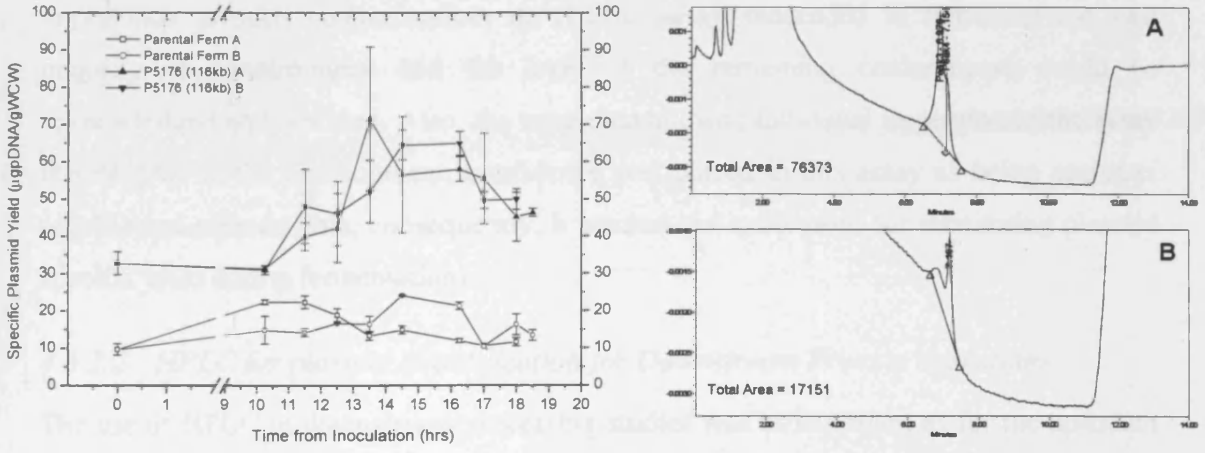

Figure 4-22 Graph showing the yield profiles of the large plasmid p5176 (116kb) through duplicate fermentations as determined by HPLC on IPA precipitated clarified lysates. The graph also charts the progression of the contaminants detected by HPLC by loading IPA precipitated samples obtained during fermentations of wild-type parental fermentations. The HPLC traces compare that produced from loading 10µL of IPA precipitated sample from a p5176 time-point (A) and the same time-point from a parental time-point.

precipitation, as later studies demonstrate (6.5.4). Additionally, it was not considered accurate to subtract the reported gDNA contaminant profile from the plasmid yield profiles, since this would make the assumption that the contamination in all the samples is equivalent. Consequently, the contaminant profile is reported alongside the plasmid yield data. For this reason, when looking at the yield curves for the plasmid fermentations, it is important to note that a proportion of the signal is due to contamination (Figure 6-5).

However, the overall level of contamination detected by this assay should be put in context. Overall, the level was small and it did not have nearly the same impact on the plasmid yields, as was witnessed when attempting to quantify similar samples with PicoGreen. Figure 4-22 compares the yield profiles of the plasmid whose quantification was most affected by the residual contamination: p5176 (116kb). This construct was the most affected, since it was found to exist at the lowest concentrations. On average, the co-elution of residual gDNA accounted for ~20% of the returned value. Contrast this situation with the PicoGreen studies on IPA precipitated clarified lysates and the improvement delivered by the HPLC assay becomes clear. With PicoGreen analysis the residual, linear gDNA bound proportionally more fluorophore molecules than the plasmid molecule and so the estimated plasmid yield was often over twice the expected.

The development of the HPLC assay produced a method of plasmid quantification more accurate and precise than any previously used. Other assays were affected far worse by the trace level of contaminants remaining in the streams used for analysis. Whilst not impervious to such contamination, the HPLC assay succeeded in removing the vast majority of contaminants and the level of the remaining contaminants could be acknowledged and reported. Also, the trace data allowed for visual inspection of the assay results. Due to the development, confidence was placed in this assay as being accurate, reliable and reproducible, consequently, it became the assay used for monitoring plasmid specific yield during fermentations.

4.5.2.2 HPLC for plasmid quantification for Downstream Process operations

The use of HPLC in downstream processing studies was as important as for the upstream investigations. The technique was used to determine plasmid concentration at several stages during the downstream process, and on streams leaving the process, in order to devise a full plasmid balance. As outlined previously, the operation of the HPLC remained constant no matter whether analysing upstream or downstream samples. However, the

samples injected, the volumes injected and the calibration curves used did differ when analysing downstream samples as from when running upstream samples. There were several reasons for this.

Firstly, it was noted from the results of the upstream samples that the sample concentrations never exceeded 20μgmL^{-1}, even for the most concentrated samples. As a result of the narrow concentration range encountered, calibration of values on a standard curve ranging from 0-250μgmL^{-1} reduced the sensitivity of the assay. Also, for the downstream process assay, it was hoped to perform HPLC directly on samples so removing the need for IPA precipitation. Without the IPA precipitation step, the samples for analysis would be ~7.5x more dilute, since the IPA step achieved that level of concentration. With these considerations in mind, the HPLC standard curves prepared for downstream process samples were prepared over a narrower range of 0-25μgmL^{-1}. Since no IPA concentration step would be performed, to ensure sufficient plasmid material was injected to generate large enough peak areas to allow accurate quantification, 10-fold more volume would be loaded. Consequently, all DSP analyses involved loading 100μL volumes of sample. The net effect of loading higher volumes of more dilute streams, was that the peak areas produced were comparable to those produced by the upstream analysis.

The second difference in the HPLC assay for DSP samples also involved the standard curve and the impact of gDNA contamination. As described previously, the small effect of gDNA could not be eliminated from the analysis of the upstream samples and as a result its presence was reported alongside the results for plasmid yield. With DSP analysis the potential existed to 'calibrate out' the impact of the small amount of contamination. In the process runs, identical masses of cell paste were lysed and as such the concentration of the contaminants in the clarified lysate would be comparable. To 'calibrate out' the gDNA contamination, the DSP standard curve material was prepared by serial dilution of known concentrations of the individual plasmids, using clarified lysate prepared from parental wild-type cell paste. By performing the dilutions with the blank lysate, the peak areas returned for the standard curve would be the concentration of the plasmid, plus the small contamination. In this way when lysate samples were run, the peak area of the contaminants would be effectively 'blanked out'. These standard curves were used to quantify plasmid in the clarified lysate before the UF step.

The final difference with the HPLC assay, as it was used for the mass balancing of plasmid through the downstream process, was a correction to an issue which had not been envisaged. Having performed several of the DSP runs, it was noted that the plasmid concentration value, as determined by HPLC on the material recovered from the ultrafilter, was less than the value placed upon the same solution by direct absorbance. It was also noted that this issue did not occur with the smaller plasmids, indicating that the problem was a result of plasmid size. Repeated calibration of the HPLC did not resolve the issue. The reason was only determined when the HPLC profiles were compared.

Figure 4-23 compares the HPLC profiles of Qiagen purified 49kb plasmid against the same plasmid recovered after ultrafiltration. The plasmids are both at ~100μgmL^{-1}. The difference between the two profiles is the bulge seen on the post-UF profile (Figure 4-23B) between the column run-through peak and the plasmid peak. This 'peak' was present on all traces of the large plasmid samples following ultrafiltration, and as such was reasoned to be small dsDNA fragments generated by shear during UF operation. These smaller sized DNA fragments were later sized by electrophoresis at being between 10-25kb. Due to their smaller size and linear conformation, their charge density would be lower than an intact plasmid molecule, so explaining their elution before the plasmid. The ill-defined nature of the peak made it impossible to integrate accurately, complicating the quantification of the plasmid in the UF streams.

However, for correct mass balancing of pDNA, it was essential that the sheared plasmid be accurately quantified. Although no longer plasmid molecules, the sheared fragments represented a proportion of the plasmid stream and as such was required to be quantified.

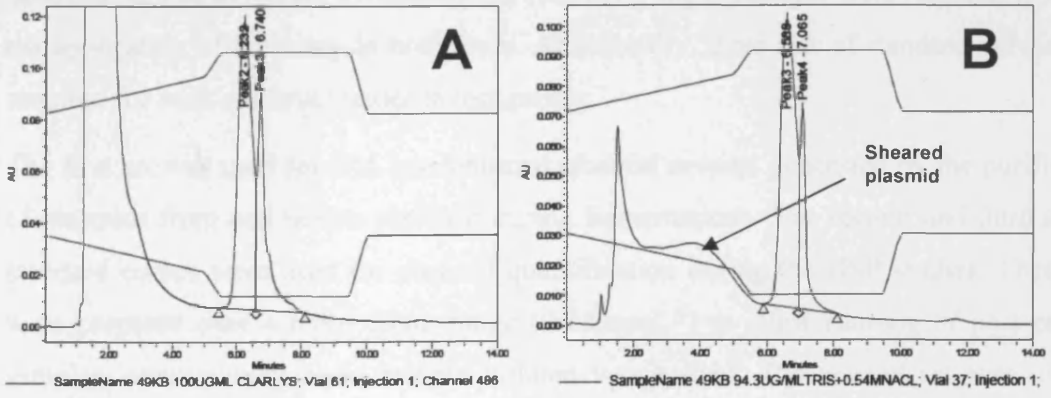

Figure 4-23 Figure comparing the HPLC profiles of similar concentrations of a large 49kb plasmid. Figure A shows the HPLC trace of a plasmid in clarified lysate. Figure B shows the same plasmid following ultrafiltration.

The solution required the preparation of post-UF standard curves for each construct, which took account of the sheared portion of plasmid in the samples.

The standard curves for the post-UF samples were prepared from plasmid recovered from the UF step and suspended in Tris + 0.54M NaCl buffer. The stock plasmid was serially diluted to the desired concentrations, and to improve accuracy the precise concentration of all the standards was determined using the NanoDrop spectrophotometer. From Figure 9-27 it can be appreciated how the peak area produced from the same quantity of plasmid material differed between the curves of intact plasmid and sheared plasmid. The curves can be used as an indication of the susceptibility of the constructs to shear. Looking at Figure 9-27 it can be seen how the standard curves for the 3kb and 16kb plasmids align well. It is the increase in size to 33kb, 49kb and 116kb where the differences manifest themselves with increasing magnitude. This observation confirms that shear damage is size dependent.

4.5.3 Conclusions

Following the problems identified with the application of PicoGreen and direct Absorbance to the quantification of large, low-copy plasmids, it was decided to investigate the use of HPLC. It was found that anion exchange offered an effective means of quantifying the concentration of large plasmids in solution. Plasmids up to 116kb in size were found to be separated and eluted from the chosen column, however, the broadening of the peaks produced was observed with increasing plasmid size. Furthermore, the accuracy and precision of the technique was found to be very favourable.

The HPLC assay was applied to the quantification of plasmid streams encountered in both upstream and downstream investigations. However, slight changes were required to enable the application of the assay in both areas. Additionally, three sets of standard curves were required for each construct under investigation.

The first set was used for IPA concentrated plasmid streams generated by the purification of plasmids from cell pellets obtained during fermentations. The second and third sets of standard curves were used for plasmid quantification during the DSP studies. These sets were prepared over a more dilute range (0-25μgmL^{-1}) to allow running of neat process samples, consequently more sample volume was loaded. The second set was used to quantify plasmids in the clarified lysate following lysis and as such the standards were prepared using blank parental lysate to 'calibrate out' the impact of small traces of gDNA

contamination. The third set was prepared upon discovering that shear effects on the larger plasmids was generating linear dsDNA fragments, which were not being integrated by the HPLC and leading to errors in the plasmid balancing. To correct the third standard curve was prepared from plasmid material recovered from the UF, suspended in the buffer used in the recovery steps from the membrane.

4.6 Gel Electrophoresis

Direct visualisation of plasmids by electrophoresis is a useful method of investigating the relative purity of a plasmid sample, giving information on contamination by gDNA and more importantly the ratios of supercoiled to other plasmid topologies. It use is mandatory for the analysis of plasmid batches for bulk release (Zoon, 1996), although its use may become superseded by more quantitative techniques of assessing plasmid topology, such as capillary electrophoresis.

The principle behind electrophoresis centres around the force exerted on a charged particle in an electric field; the Lorentz force. The force induced is dependent on both the electric properties of the body under study and the magnitude of the electric field. The migration of the body by the force is countered by the resultant frictional force, such that the migration of the charged body in a constant, homogeneous electric field is steady. There are relationships which can predict and describe the movement of bodies in electric fields i.e Smoluchowski equation, but due to the number of potential variables, precise prediction is complicated. However, some fundamental parameters affecting migration rate have been identified:

Particle properties: Charge density/ Size
Solution properties: Ionic strength/ Electrical permivitty/ pH/ Temperature
Matrix properties: Gel conc./ Gel type; Crosslinking and Electroendosmosis (EEO)
Electric field properties: Magnitude/ Field arrangement

4.6.1 Conventional Gel Electrophoresis

Conventional gel electrophoresis is the most common form of electrophoresis encountered for plasmid DNA analysis. The technique employs a constant, homogeneous electric field and separates different plasmid molecules and topologies on the basis of their charge density and size. The application of conventional electrophoresis in this project was hampered by the fact that the distance migrated by the DNA molecules becomes independent of their size at around 20kb, such that molecules exceeding that size all co-migrate.

However, conventional gel electrophoresis was attempted on the Oxford series of plasmids, the results of which are displayed in Figure 4-24. To improve the separation several parameters were altered by trial and error. Firstly, the running time was extended

to ~15hrs, with smaller plasmids separation can be achieved using run times of 1-4hrs. Secondly, the gel concentration was lowered to 0.8%, any lower and the gels tended to melt due to the long running times. To abate the temperature increases encountered during the extended running times, the gel-case was surrounded by ice.

From the images it can be appreciated that whilst the plasmid molecules can be visualised, the level of information provided by such analysis is poor. The gels resolve the supercoiled plasmid form but there is no evidence of the other plasmid forms. It is believed that due to the outstretched size of the open-circular/ linear forms they remain trapped in the wells. Increasing the running time did little to improve the resolution, as shown in Figure A. The band running ahead of the supercoiled form in the wells containing the large plasmids is contaminating linear, gDNA remaining in the preparations, the size range of which is between 15-30kb. By comparison when running a smaller plasmid by traditional electrophoresis, all the topologies which were present can be elucidated, as shown by pSVβ; Lane 1/ Fig. B

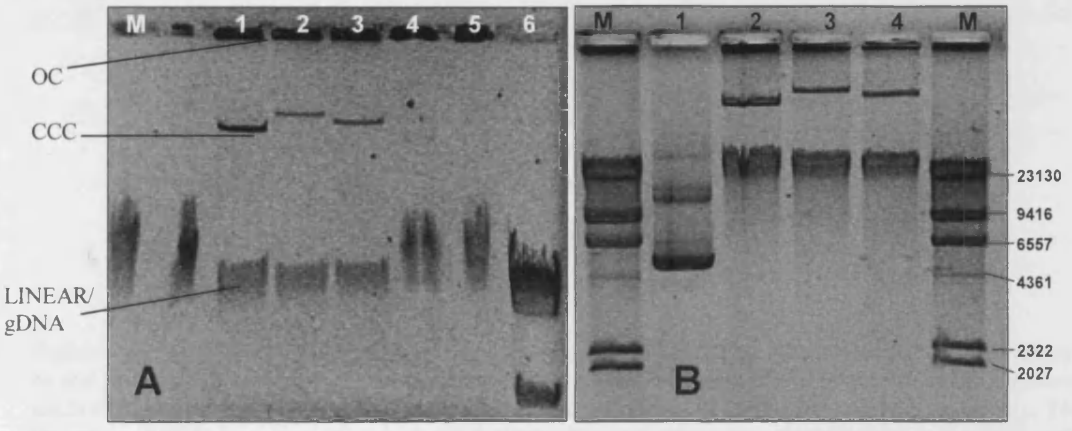

Figure 4-24 Two conventional gel electrophoresis gels displaying the running characteristics of the large constructs. Figure A shows a 0.8% gel run in 2xTBE for 15 hours at a current strength of ~80mA generated from a fixed field strength of 1.5Vcm^{-1}. To prevent the overheating of the system due to the extended running period the gel case was surrounded by ice. Figure B shows the result of an identical operation except the plasmids were run at higher field strength of 4.2Vcm^{-1} for a period of 6 hours.

M ; Mid-range PFGE marker
1; p5176 (116kb)
2; p5204 (242kb)
3; p5206 (172kb)
4; 86kb plug
5; λ DNA HindIII digest
6; λ DNA ladder

M; λDNA HindIII digest
1; pSVβ (6.9kb)
2; p5176 (116kb)
3; p5204 (242kb)
4; p5206 (172kb)
M; λDNA HindIII digest

It was realised that useful information regarding the topology of large plasmids was not going to be achieved by conventional electrophoresis.

4.6.2 Pulsed-Field Electrophoresis

Pulsed field electrophoresis was developed to allow resolution of large DNA molecules which could not be separated by normal electrophoresis. The technique was developed by (Schwartz and Cantor, 1984) and originally intended for whole genome mapping, electrophoretic karyotyping and for discerning strain homogeneity. The crucial difference between PFGE and conventional electrophoresis is that during operation, the polarity of the electrodes is switched at defined and variable intervals, causing the re-orientation of the electric field and so the molecules in the field. The rate of switching can alter during the run period and is essential to effective resolution. There are several different arrangements of PFGE, but the ones considered in this project are Field Inversion Gel electrophoresis (FIGE) and Contour clamped Homogeneous Electric field (CHEF).

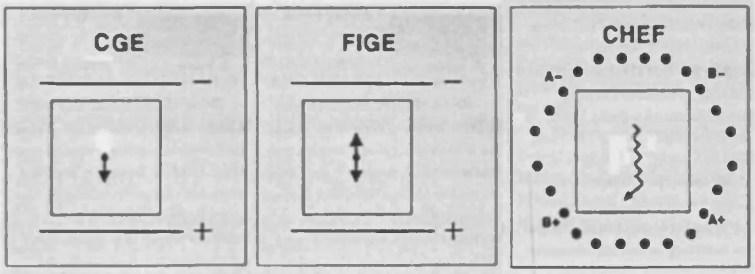

Figure 4-25 Figure displaying the orientation of electric fields of three types of electrophoresis employed in this project. Conventional gel electrophoresis (CGE) employs a constant, unidirectional homogeneous electric field and the DNA molecules are separated by virtue of their size and charge density. Field inversion (FIGE) is a type of pulsed field electrophoresis where the electric field is inverted casing periodic 180° reorientation. Contour clamped homogeneous electric field (CHEF) is a more complicated form of pulsed field electrophoresis whereby the DNA is reorientated at oblique angle of 120° causing the molecules to follow a zig-zag pattern through the gel.

Currently, there are three models that attempt to describe the behaviour of DNA during PFGE ; the biased reptation model, the chain model, and the bag model (Chu, 1990), but these focus on linear DNA molecules. Although the exact theory of pulsed field electrophoresis is still a matter of debate, qualitative statements can be made about the movement of DNA during PFGE. As outlined earlier, during conventional electrophoresis, DNA above 20kb migrates with the same mobility regardless of size producing a single large diffuse band (Figure 4-24). However, if the DNA is forced to change direction

during electrophoresis, different sized fragments within this diffuse band begin to separate from each other. With each reorientation of the electric field relative to the gel, smaller sized DNA molecules are capable of switching direction more easily and begin moving in the new direction more quickly than the larger DNA molecules. Thus, the larger DNA lags behind, providing a mechanism for separation from the smaller DNA. The rate of re-orientation combined with the extended running times and longer running distances (the reorientation means the path followed by the molecules is far longer) account for the technique's ability to resolve DNA molecules of megabase size. Of note, is that fact that the constant field re-orientation can also lead to changes in the order in which the plasmid topologies are resolved, again because the separation is dependent on the rate at which the molecules are able to change direction.

Although PFGE was developed in the 1980s, its use has mainly been for linear DNA and genome analysis, but there are reports of the technique's use for plasmid analysis. (Levene and Zimm, 1987) reported the differences in migration rates seen for supercoiled, linear and open-circular plasmid forms for plasmids extending from 3-56kb. (Wang and Lai, 1995) compared CHEF, FIGE and conventional agarose gel electrophoresis. They report how SCC forms of large constructs can be separated by CGE, stating that the mobility of SCC forms is independent of size. However, the report also describes the difficulties experienced in resolving OC forms of large plasmids, maintaining that the OC configuration results in the molecules being trapped in the wells.(Barton *et al.*, 1995) report a method for detecting and sizing BACs which are traditionally hard to isolate from bacterial preparations. Despite the several reported methods, the specifics of their individual operation did not translate well to the situation of this project. For that reason, the development of the PFGE assay was very much a trial and error affair.

4.6.2.1 CHEF Pulsed Field Electrophoresis

The CHEF system was the first of the Pulsed Field variety that was used to determine the topology of constructs studied in this project. Exact details of the system, its configuration and operation are outlined in 2.5.18. It was the most sophisticated of the systems employed, and is reportedly capable of resolving chromosome-sized DNA molecules (Bio-Rad Labs., 2000).

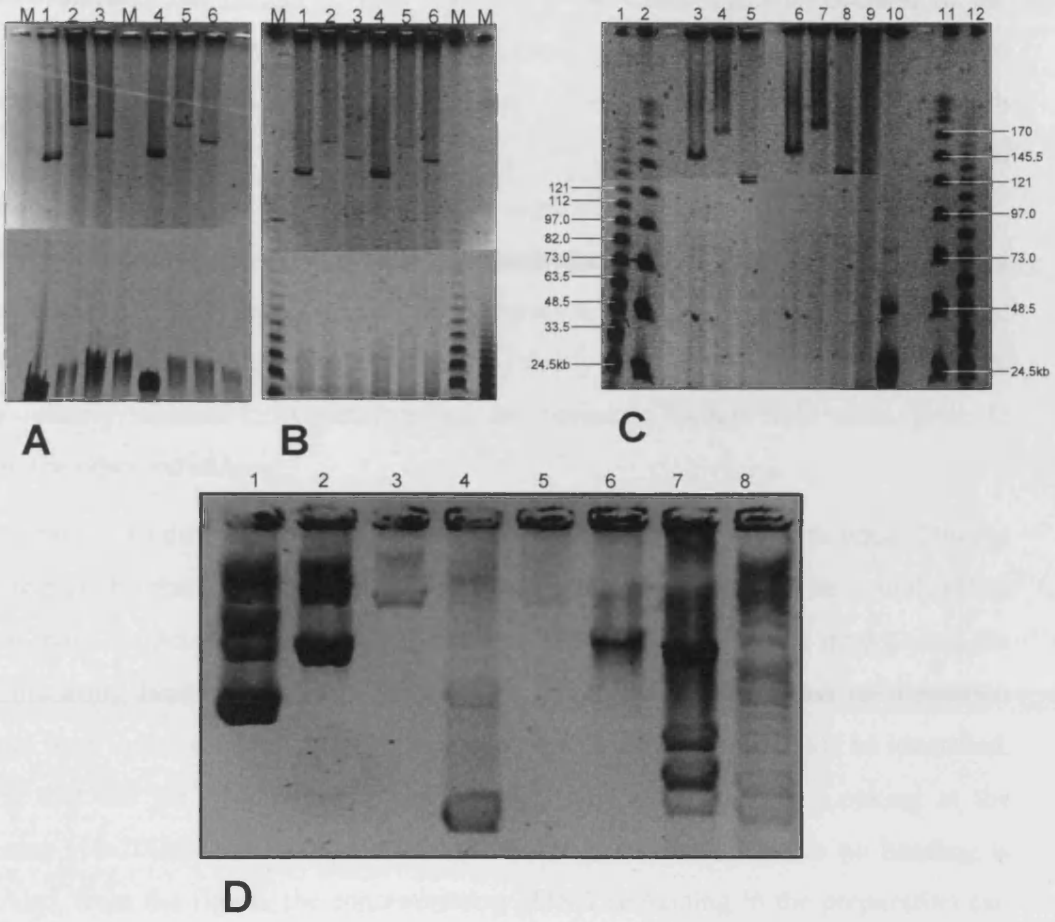

Figure 4-26 Results of Pulsed-Field Gel Electrophoresis on the large plasmids as the conditions for use were determined. The pictures are segmented because the large size of the gel meant that to fully photograph usng the gel imager, several pictures had to be taken and reassembled.

A: [0.5xTBE/ 16hrs/ 125mA/ 6.0Vcm^{-1}/ 14°C/1% agarose/ Initial switch time 0.1s/ Final switch time 0.1s (Ratio 1:1)

1/4 : p5176 (116kb) Lane order applies to B also.
2/5 : p5204 (242kb)
3/6 : p5206 (172kb)

B: [0.5xTBE/ 16hrs/ 125mA/ 6.0Vcm^{-1}/ 14°C/ 1% agarose/ Initial s.t 5s/ Final s.t 120s] (1:24)

C: [0.5xTBE/20hrs/ 125mA/ 6.0Vcm^{-1}/ 14°C/ 0.8% agarose/ Initial st 1.4s/ Final st 21.6s] (1:15)

Lane 1/ 12: Mid-Range marker I 5/ 8: Maxi-prep p5176 (116kb)
2/ 11: Mid-Range marker II 9: Maxi-prep pMT103 (29kb)
3/ 6: Maxi-prep p5206 (172kb) 10: Maxi-prep pQR150 (20kb)
4/ 7: Maxi-prep p5204 (242kb)

D: [0.5xTBE/ 16hrs/ 125mA/ 6.0Vcm^{-1}/ 14°C/ 1% Agarose/ Initial s.t 100s/ Final s.t1000s] (1:10)

1: pQR186 (13kb)
2: pQR150 (20kb)
4: pSVβ (6.9kb)
3/5: pMT103 (29kb)
6: λ DNA
7: λDNA HindIII digest
8: Supercoiled ladder.

Figure 4-26 displays the results of four runs using the CHEF system. Because of the number of combinations feasible, in the development of this is assay it was decided to keep a number of possible variables constant and concentrate on optimising the switch times. (Levene and Zimm, 1987; Wang and Lai, 1995) both report the large impact the choice of suitable switch times have on effective separation of plasmid moieties by PFGE. Whilst gel concentration, run-time and field strength also have an impact on the degree of separation achieved, their value affects the separation in a reasonably predictable and linear fashion. Consequently, it was important to firstly to ensure the plasmid topologies could be reliably separated, by determining the optimum switch time ratio, prior to optimising the other variables.

The first attempt (A) displays the results using the variables listed but with equal forward and reverse switch times, the duration of which were very short (0.1s). The overall effect of this was that the operation of the PFGE was effectively in conventional mode, since the rapidly fluctuating field would have little impact on the separation as no re-orientation would have been induced. From the figure, it can be seen that plasmid could be identified, suggesting that the gel concentration and running time were suitable. Looking at the marker lanes (10-200kb) it can be seen that they are not resolved, since no banding is evident. Also, from the figure, the contaminating gDNA remaining in the preparation can be seen as it forms a smear towards the base of the plasmid containing lanes. The aim was to optimise the switch times such that the marker bands are effectively resolved.

Repeating the above run using identical parameters but with a switch time ratio of 1:24 achieved a degree of separation of the marker lanes (Figure 4-26B). However, the separation was not optimal and still only one plasmid topology, most likely supercoiled, was seen on the gel. The gel in Figure 4-26C shows an improvement on the previous trials, as the marker lanes are quite effectively separated. However, once more, the plasmids only display one topology. Looking at Lane 10 in Figure C shows the results of the pQR150 (20kb) the profile seems to suggest the presence of another topology. Indeed as shown in Figure D the topologies of a selection of smaller plasmids could be resolved. It was disappointing that despite the separation of the marker lanes, which indicated workable parameters, the plasmid topologies were not resolved. It was surmised that the OC form of the large BACs were being trapped in the wells of the gel as reported by (Wang and Lai, 1995).

4.6.2.2 Field Inversion Gel Electrophoresis

FIGE is a simpler form of Pulsed field electrophoresis. As the name suggests the field is inverted around 180°, causing the DNA molecules to constantly switch their direction of movement back and forth. The technique was found to be more applicable for the plasmids under study, as although the system doesn't enable separation over the size range achievable with the CHEF system, it is extremely useful for separating smaller DNA of the order 4-1000kb (Carle *et al.*, 1986).

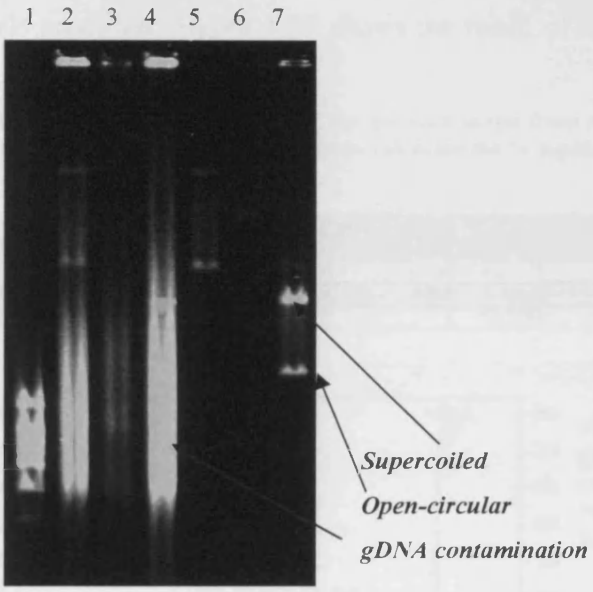

Figure 4-27 Figure showing the separation of the Oxford series of BAC by FIGE.

Lane 1:marker
Lane 2: 172kb maxi-prep Lane 5: 172kb Large construct kit
Lane 3: 242kb maxi-prep Lane 6: 242kb Large construct kit
Lane 4: 116kb maxi-prep Lane 7: 116kb Large construct kit
[1xTBE/ 0.8%/ 30hrs/ Forward voltage 180V/ Reverse Voltage 120V/ Initial st 0.3/Final st 5.5/ Linear ramp]

Figure 4-27 displays the results of a preliminary run using the FIGE system. Each of the Oxford series of plasmids was analysed. Two different methods were employed for their purification; conventional Qiagen maxi-prep and Qiagen Large construct kit. As described in 2.5.8.3 the large construct kit employs an exonuclease to digest any linear DNA. From the figure the importance of this step can be seen in the level of contamination removed. The normal maxi-prep samples display a large degree of contamination which is almost all removed by treatment with the exonuclease.

However, the important factor was that both plasmid topologies could be resolved. It was determined that the supercoiled plasmid topology runs behind the open-circular form. The reason for this is due to the smaller diameter/ size of the supercoiled form enables it to switch direction more easily than the open-circular form, as a result it is able to travel further in the reverse direction. The system was checked as to the linearity in which it resolved linear markers and as shown in Figure 4-27, the distance migrated was found to be proportional to the size of the fragments above 10kb. Below 10kb the linearity ended.

Further development of the FIGE assay led to incremental improvements in the quality of the gels produced. Figure 4-29 shows the result of a sizing FIGE using the final adopted

Table 4-8 Table showing the results of the gel-scan taken from the gel image captured in Figure 4-29. The relative amounts of each species were used to calculate the % topologies.

Sizing Gel	3.2kb		16kb		33kb		49kb		116kb	
Lane	(amount)	% Topology	(amount)	% Topology	(amount)	% Topology	(amount)	% Topology	(amount)	% Topology
SUPERCOILED	46.974	100	64.954	90.66	48.002	84.51	41.813	83.62	14.432	46.40
OPEN-CIRCULAR	0	0	6.6926	9.34	8.7969	15.49	8.1884	16.38	16.672	53.60
Sum	46.974		71.647		56.799		50.001		31.104	

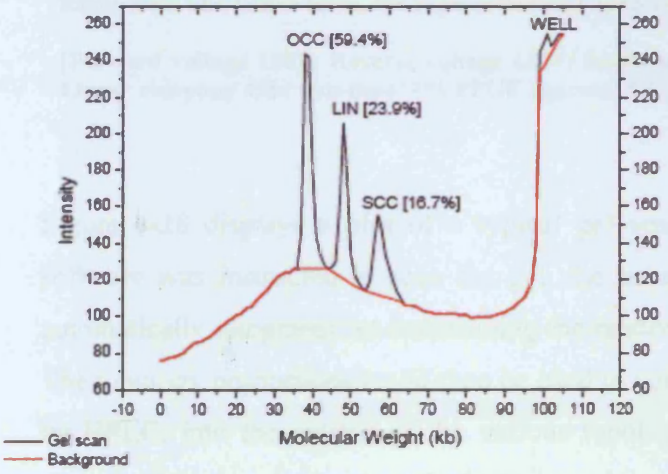

Figure 4-28 Figure displaying the results of a gel-scan of a lane on which the pGEM49kb construct had been analysed. The scan also records the fluorescence produced as background.

conditions. The small improvements were to use 1% PFGE agarose and run at 4°C for longer running periods. Previously, using shorter run-times, 0.8% gels at room temperature had resulted in good separation but more diffuse bands. Also, the gels were stained for >24hrs at 4°C using SYBR-Gold and destained for ~4hrs to improve contrast. These conditions led to effective separation of the various topologies and discrete bands which could be accurately quantified by gel scanning. The results of the gel scan of the gel shown in Figure 4-29 can be seen in Table 4-8.

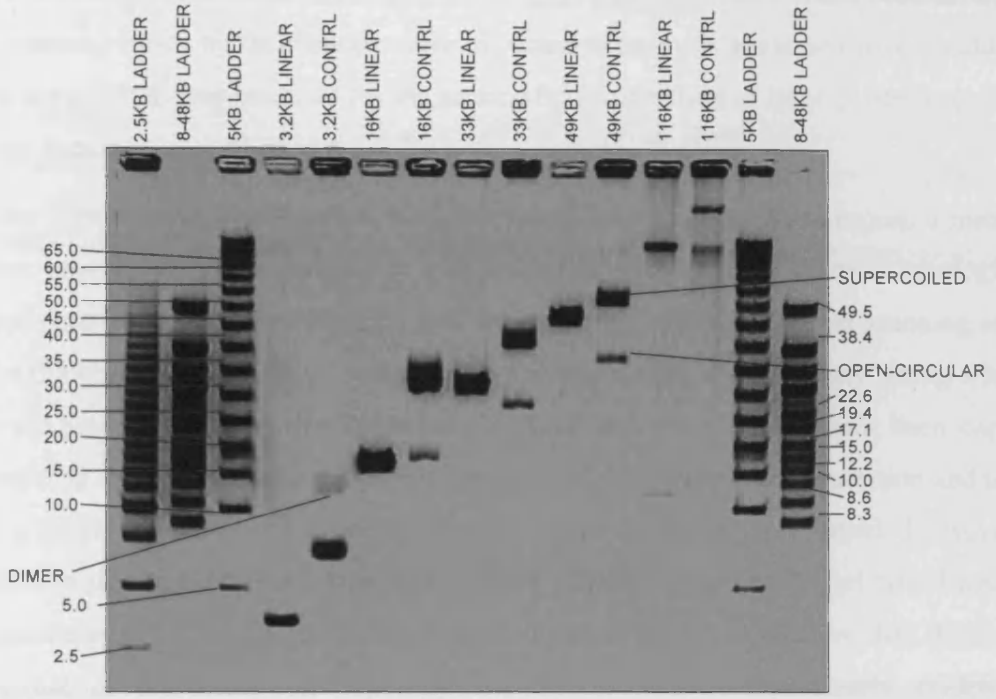

Figure 4-29 FIGE of the plasmid series employed in this project. The plasmids are run in the linear form and native form, the supercoiled and open-circular forms clearly visible.

[Forward voltage 180V/ Reverse voltage 120V/ Initial switch time 0.4s/ Final switch time 3.5s/ Linear ramping/ 40hr run-time/ 1% PFGE agarose/ 4°C]

Figure 4-28 displays a plot of a typical gel scan produce by the UVP software. The software was instructed to scan the gel, the bands were fitted manually and the peaks automatically integrated, so determining the relative proportions of the various topologies. The topology proportions could then be used to convert the plasmid masses, as determined by HPLC, into the masses of the various topologies. It would be feasible to determine masses of the topologies directly from the gel, by loading samples of known mass on the gel and calibrating from the signal produced. However, there are several inaccuracies involved in such a method, especially gel to gel variation, so it was decided to use the FIGE to determine the proportions of the topologies, and then calculate the masses of the various topologies from the HPLC data.

4.6.3 Conclusions

An effective assay for plasmid topology was fundamental for the analysis of the plasmid containing streams from both the fermentation and the downstream stages, since topology

is a critical process variable and one which grows in importance when considering larger constructs, which by their nature were expected to be more shear sensitive. Additionally, the use of FIGE was essential for the successful construction of large plasmids using high-copy vectors as described in 5.3.2.2.

After considerable development, with too many individual results to report, a method has been established which resulted in effective separation of large plasmid topologies. The bands produced were discrete and could be accurately quantified by gel scanning software. The drawback with the assay was the long run-times with a single assay taking a few days to produce results. It would have been optimal had the HPLC system been capable of resolving the different plasmid forms, since measuring plasmid concentration and topology in a single assay would have been more convenient and more rapid. However, it is believed that the information provided about plasmid topology by gel based assay is as accurate as HPLC and certainly provides a higher degree of qualitative data. For instance, the use of this assay for topology analysis in later studies clearly evidenced the vulnerability to shear the large constructs demonstrate during DSP stages, it is unlikely that HPLC would have been able to as neatly describe the situation.

4.7 Determining Genomic DNA contamination by quantitative PCR

4.7.1 Introduction

Accurate and precise determination of the level of bacterial genomic DNA contamination is important in any plasmid manufacturing process. However, its description became even more critical in this project as many of the plasmids under study were present in low quantities. As a result of the lower plasmid masses, the ratio of genomic DNA to plasmid DNA was often high. The persistence of relatively high levels of gDNA has been responsible for many of the issues surrounding the development of accurate analytical techniques for plasmid quantification, since it became more important to distinguish the contributory signal produced due to the gDNA contamination from the signal produced by the plasmid DNA. Looking at Figure 4-27, showing the level of gDNA contamination detected by gel analysis, and it can be appreciated the importance of not mis-representing plasmid yield by assuming that gDNA is plasmid. Because of this pressure, a HPLC assay was utilised which went a long way to removing the contributory effect of gDNA from the overall signal, allowing accurate plasmid quantification.

Thus far the methods used to quantify plasmid and plasmid topology through the process have been outlined. Knowing the impact that gDNA contamination had wrought in the development of suitable analytical techniques, it was expected that its persistence in the downstream processing steps was likely to be as important to describe. Consequently, a specific method of quantifying the level of gDNA in samples obtained during DSP was required. Fortunately, qPCR offered the potential of precise detection and measurement specifically of genomic DNA.

4.7.2 Purification and preparation of samples for analysis by qPCR

The genomic DNA from samples obtained throughout the downstream process needed to be purified prior to analysis by quantitative PCR. This was achieved using the automated MagNA pure system, the operation of which is outlined in (2.5.14). The robotic system was able to purify the total DNA from 32 samples simultaneously, equating to 16 duplicate samples. This meant that 5 duplicate samples from 3 different DSP runs could be analysed simultaneously. The samples were taken from the Pre-lysis, Pre-$CaCl_2$, Retentate, Wash 1 and Wash 2 stages of the process. As a result, the gDNA assay could not produce a full mass balance, but could demonstrate clearance of gDNA through the process.

The MagNA pure system employed Roche's proprietary extraction technology, which binds the DNA to glass particles, from which contaminants can be washed prior to eluting the DNA. The advantage of the technique was its ease of operation, combined with its reproducibility, and the fact that purification was performed in a DNA-free hood, so reducing the potential for contamination. The same could not be said had the samples been purified by conventional spin-prep.

Following purification, the system loaded the purified DNA into the wells of a PCR plate in a programmed order, with all the necessary reagents required for the PCR reaction. 100µL of each of the duplicate DSP samples was loaded into the sample cartridge and the machine purified the DNA and eluted it in 100µL of buffer, meaning no dilution occurred. 3µL volumes of the eluted material was then loaded into a well of the PCR plate with the necessary primers, probes and materials for the PCR reaction, with the volume in each well totalling 30µL. After loading, the plate could be removed from the machine and placed in the PCR cycler for analysis. Since duplicate samples from each step in the process were run, and duplicate volumes of each purified sample were loaded on to the reaction plate, the net result was four values for gDNA concentration for each sample point (Figure 4-33). The mean of the four values was taken as the concentration. It should be noted that because the mean of the four samples was taken, the coefficient of variation recorded is a measure of the combined differences encountered during both the *processing* of the duplicate samples and the *measurement* of the four samples.

Calculating the precise amount of DNA present in the initial DSP sample from the data produced by the PCR, the proportion of DNA purified by the MagNA pure system was required. Recording the concentration of DNA in the PCR well as being the concentration of DNA in the initial sample would be false, as it would make the incorrect assumption that all DNA from the sample was purified and eluted. As a result, the MagNA pure system was calibrated in order to account for the DNA that is lost during the purification process. Fortunately, the MagNA pure instrument employed in this project had been calibrated prior to its use for this assay. The calibration of the machine took account of the different buffer make-up of the samples being purified, as this was a major factor in influencing the binding of the DNA to the glass particles. Additionally, samples of varying concentration were run and the average taken. The calibration was represented by a correction factor (Table 4-9) which when multiplied by the result obtained from the PCR

reaction would describe the DNA concentration in the original sample 2.5.15/ Equation 2-5. The requirement for calibration was not really a drawback to the procedure, since the same action would have to be conducted had the purification been carried out by conventional spin-prep. Furthermore, the reproducibility of the MagNA pure system improved the confidence that the correction factor would be consistently applicable.

Table 4-9 Table describing the different streams of the process which were purified by MagNA Pure and then quantified by qPCR. The MagNA pure was capable of purifying small amounts of DNA but could not be relied upon to extract all the gDNA fragments from a sample. The reason had a great deal to do with the ionic environment of the buffer affecting binding of the gDNA to the glass particles. From the table it can be appreciated that in low-salt buffer (TE) the equipment was capable of extracting ~15% of the gDNA. However, as the salt content of the buffer was increased the recoveries decreased. No analysis was performed on samples from the Post-$CaCl_2$ stage of the process but its inclusion in the calibration table was to demonstrate the inverse relationship of increasing the ionic strength of the buffer on the recoveries.

Sample stream	Buffer Constituents	Correction Factor (% Recovery of DNA)
PRE-LYSIS	10mM Tris/ 1mM EDTA	7.05 (14.2%)
PRE-$CACL_2$	6.5mM Tris/ 2.6mM EDTA/ 14.3mM Dextrose/ 100mM NaOH/ 730mM Potassium acetate/ 17mM SDS	8.93 (11.2%)
RETENTATE/ WASH 1/ WASH 2	10mM Tris/ 540mM NaCl	13.61 (7.3%)
POST-$CACL_2$ **[No samples from this stream were run but the MagNA pure system had been calibrated for them to be analysed]**	Roughly equal to Pre-$CaCl_2$ but with 1000mM $CaCl_2$	43.47 (2.3%)

4.7.3 Background of the qPCR assay

The different modes of PCR are outlined in 4.2.4 and the operation of the PCR is described in (2.5.15). In this project, kinetic qPCR, employing primer-probe system was the type used for real-time quantification of gDNA at various points of the process. The technique followed a similar method to that described by (Smith, III *et al.*, 1999). The samples removed from the process were purified using the automated MagNA pure system described in (2.5.14). The MagNA pure system purified the DNA from the samples and prepared the qPCR plate containing all the necessary reagents, primers, probes and standards

Table 4-10 Table detailing the components of the master mix buffer and their importance to the functioning of the quantitative polymerase chain reaction.

Component	Function
AmpliTaq Gold DNA Polymerase	Possesses 5'-3' nuclease activity but lacks 3'-5' exonuclease activity. It is a thermostable enzyme allowing hot start PCR, which reduced background signals normally created by amplification of non-target sequences before thermal cycling had begun.
AmpErase® uracil-N-glycosylase	Due to the enormous amplification possible, false positives can be created caused by amplicon carryover. This enzyme removes incorporated uracil bases reducing contamination
Deoxynucleosidetriphosphates (dNTPs)	dTTP/dGTP/dCTP/dATP/ dUTP at 200µM
Passive Reference Dye (ROX™)	Does not interfere with reporter dye. Present to normalise fluorescence signals to correct for buffer or volume deviations.
Mg^{2+}	1.5mM; optimised for highest specific yield of target PVR product.

PCR wells. The mechanism of the qPCR reaction involved the binding of a forward and reverse primer to the DNA sequence of interest as with traditional PCR (Saiki *et al.*, 1985b). However, additionally included in the reaction mixture was a probe-sequence, specific to a region within the boundaries of the sequence set by the primers. Attached to the 5'end of this probe sequence was reporter dye (in this case FAM™) and to the 3'end a quencher dye (TAMRA™). Whilst the reporter dye was in proximity to the quencher dye, the molecule did not fluoresce. The approach utilised the 5' exonuclease activity of *Taq* DNA polymerase to digest the probe region, releasing the reporter dye away from the quencher dye, so enabling it to fluoresce. Accumulation of PCR products could then be monitored in real time by scanning the increase in fluorescence in the PCR wells using a PCR cycler coupled with a fluorescent plate reader; ABI PRISM 7700. (Fykse *et al.*, 2003; Heid *et al.*, 1996; Weissensteiner and Lanchbury, 1996). Figure 4-30 describes the progression of a primer-probe PCR reaction.

Both primer and probe sequences were directed at a region of the single genome copy *E.coli* DNA polymerase gene. The primer sequences were about 20bp in length and probe sequence was a 27bp sequence covalently coupled to the two fluorescent dyes; FAM™ and TAMRA™. Further details about the primer and probe sequences are recorded in Table 2-12.

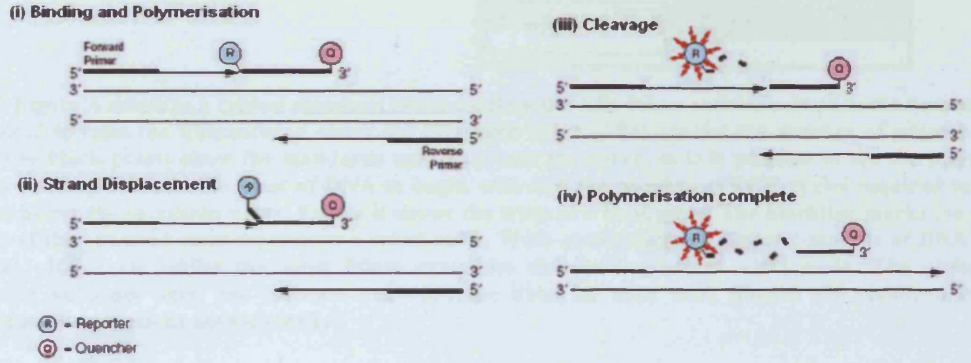

Figure 4-30 Figure describing the progression of the PCR reaction. (i) the forward and reverse primers bind to their complementary regions on *DNA pol* and the probe binds to the site between the two. The polymerisation reaction begins. (ii) the *Taq* DNA polymerase extends the 5' strand of DNA until the probe region is reached. (iii) the exonuclease activity of *Taq* polymerase causes the release of the fluorophore away from the quencher molecule, the fluorophore can now fluoresce. (iv) polymerisation complete.

Table 4-10 Describes key features of the primers (forward and reverse) and the probe used to bind complementary regions of the *E.coli* DNA polymerase gene. The shortest amplicons are the most effective and 20bp-45bp is optimum. The GC content of the amplicons should be in the 40-80% range to avoid formation of internal structures. The melting temperature of the primers should be between 58°C to 60°C and the probes >68°C. The 5'end of the probe should not end in G. The probe strand sequence chosen should be the one with the highest number of C residues and for all amplicons less than 2 G or C bases should comprise the last 5 bases of the 3'end. Information calculated by Primer Express software v1.5a (Dieffenbach C W et al., 1995)

CRITERION	Fwd Primer	Rev primer	Probe
Length (bp)	20	19	27
GC content (%)	60	47	48
Melting Temp (°C) (50mM salt)	61.47	61.65	71.47
Molecular weight (fwd) Da	6118	5751	8188
Molecular weigh (rev) Da	6118	5863	8370
G on 5' end	N/A	N/A	NO
Strand with more C than G	N/A	N/A	YES
Less than 2 G or C bases in last 5 bases of 3' end	NO	YES	YES

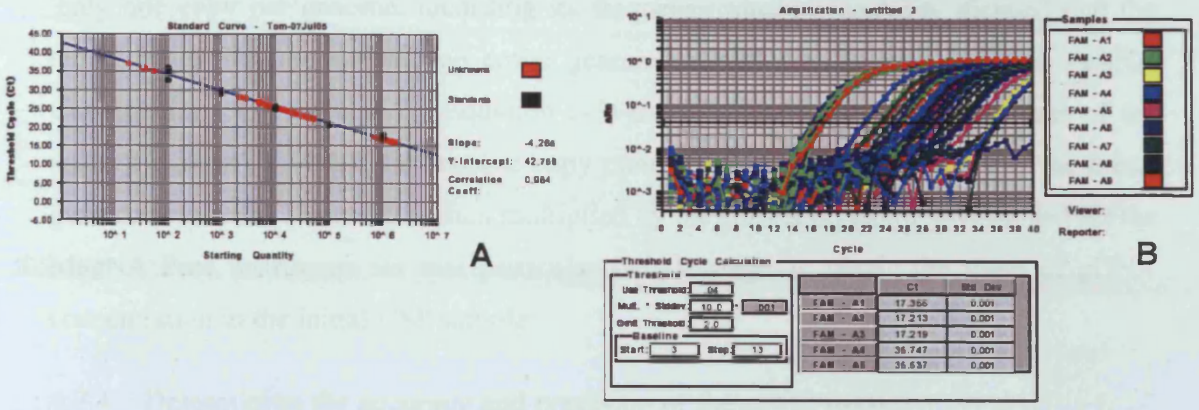

Figure 4-31 Figure A displays a typical standard curve used by the ABI Prism software. It plots the number of PCR cycles required to raise the fluorescence above the threshold value (0.04) against the number of genome copies in each well. The black points show the standards used to create the curve, so it is possible to see the inverse linear relationship existing between the mass of DNA to begin with and the number of PCR cycles required to raise the fluorescence above the threshold value. Figure B shows the trace of a PCR plate. The blackline marks the threshold value. Each of the coloured lines represents a set of wells. Wells containing the highest amounts of DNA cross the threshold at ~16th cycle whilst the most dilute cross the threshold value at ~30th cycle. The picture is for demonstration purposes only, the software recorded the data for each well, plotted the standard curve and calculated the concentrations automatically.

The system was used quantitatively by using standards of known DNA concentration and recording the number of PCR cycles required to raise the fluorescence reading above a threshold value. The number of PCR cycles required to cross the threshold value is directly proportional to the starting concentration of DNA. The threshold cycle values (Ct) of the standards were used to construct a calibration curve against which the unknowns could be plotted.(Holland *et al.*, 1991; Gelfand *et al.*, 1993). A standard curve was included on each PCR plate and was prepared from the same batch of standard genomic DNA stored at -80°C. The standard curve extends from 10^2copies/well to 10^6copies/well as shown in Figure 4-31A. Such a broad standard curve allowed the assaying of all the samples from the downstream process on an identical standard curve.

The ABI Prism software recorded the progression of the PCR reaction, constantly monitoring the fluorescence increases in each well, and the cycle number at which the threshold value was exceeded. Following completion of the reaction, the software plotted the standard curve and automatically calculated the gDNA concentration in each well, averaging the four values representing identical sample points and returning the mean value and error. The results of each qPCR plate were given by the software in PDF form as shown in Figure 9-28. The values for gDNA concentration were given in copies per well. Since the target sequence of the primers/probe was present at

only one copy per genome, recording its frequency meant probability dictated that the remaining gDNA (comprising an entire genome) would also be present in the sample. Consequently, the calculation (Equation 2-5) used to determine the gDNA mass of the nascent sample converted the genome copy number to mass, since the mass of the *E.coli* genome is known. The result is then multiplied by the correction factor, determined for the MagNA Pure instrument for that particular sample stage, to obtain the value of gDNA concentration in the initial DSP sample.

4.7.4 Determining the accuracy and precision of the qPCR assay

Compared to other methods of DNA quantification, such as PicoGreen and absorbance, the qPCR assay employed during this project was fairly complex. However, the far greater sensitivity and specificity of the assay was sufficient justification for the additional complexity. As the results will demonstrate, the assay was capable of accurately and specifically quantifying gDNA concentrations over 3000-fold more dilute than the lower limit of the absorbance assay. Automation of sample purification simplified the operation tremendously and enabled far more replicates to be processed and so improving the accuracy obtained. However, the accuracy and precision of the assay needed to be quantified to be sure of the assay's usefulness, as increased complexity can often lead to reductions in accuracy.

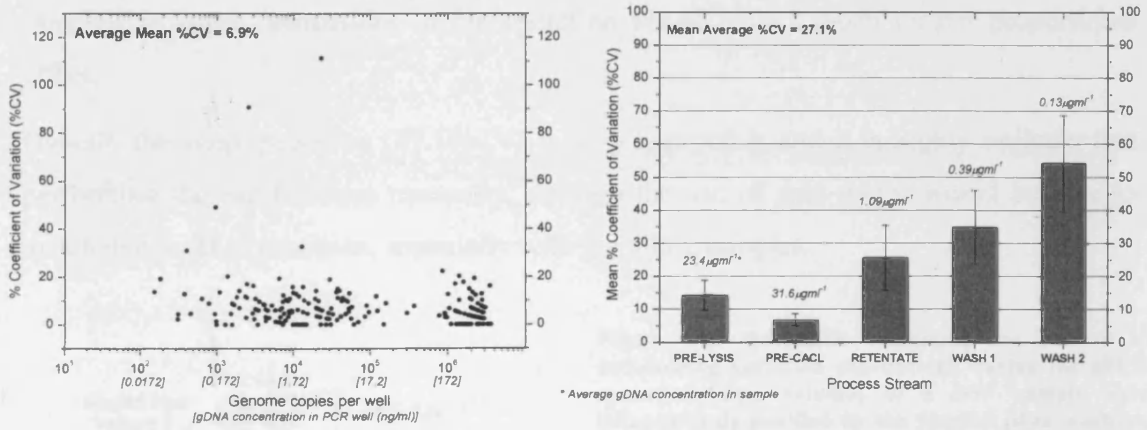

Figure 4-32 Graph A plots the coefficient of variation recorded for every pair of PCR wells against the mean concentration determined for the wells, and as such records the intra-assay variation introduced by the PCR reaction. Note that the average %CV is 6.9%. Plot B records the total variation between the two independently purified samples as a function of the stream under analysis. It also displays the average concentration of the streams analysed. Note that the average total variation (%CV) of the entire qPCR operation is 27.1%

Figure 4-32 shows the results of studies completed to quantify the assay's precision. The precision was recorded by % Coefficient of variation in two ways. Figure 4-32A records the intra-assay variation whilst Figure 4-32B records the total assay variation as a function of the process stream assayed. It can be stated that the total assay variation is the sum of the variation introduced by the variation encountered during the PCR reaction and the variation introduced by the sample's purification.

Looking first at the intra-assay variation shown in Figure 4-32A. It demonstrates that the variation introduced by the measurement of the PCR plate is very consistent never mind the concentration of the sample under analysis. There are a few anomalies but the average variation introduced to the total variation by the PCR reaction is 6.9%CV. This compares well to the precision of PCR reactions in the literature, where precision levels of 2.8-3.9% have been demonstrated (Lee *et al.*,). Regarding Figure 4-32B shows that the total variation of the qPCR operation is on average 27.1%, which is much higher than the 6.9% due to the intra-assay variation. Consequently, it can be confidently stated that the decrease in precision is due to the purification of the samples by the MagNA pure machine. What is interesting to note is that the total variation is dependent on the stream under analysis, and as such the concentration of the gDNA in the stream. It appears that the MagNA pure machine is capable of very consistent purification of relatively concentrated samples, but that this consistency is reduced with more dilute samples. However, it is to be expected that the precision would drop when purifying more dilute samples, as small fluctuations in the operation would have a much greater proportional effect.

Overall, the assay precision (27.1%CV) is very acceptable and it is highly unlikely that performing the purifications manually, through the use of spin-preps, would be able to match that level of precision, especially with the dilute samples.

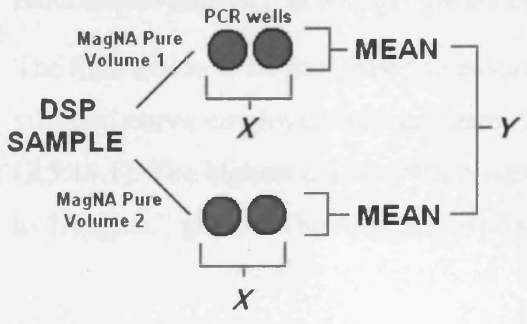

Figure 4-33 Schematic explaining the method of determining variation encountered during the qPCR operation. Two volumes of a DSP sample were independently purified by the MagNA pure machine. Two volumes of each of these samples were loaded on to the PCR plate, giving a total number of 4 wells per sample. X records the intra-assay variation and as such is a measure of the variation introduced by the PCR reaction. Y records the variation between the independently purified samples and as such is the total variation encountered during the assay

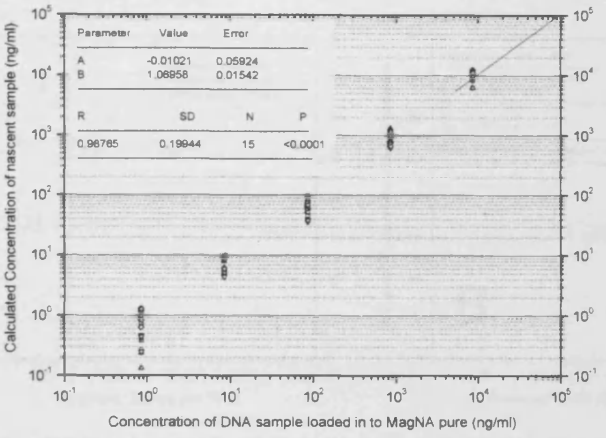

Figure 4-34 Figure shows the results of the experiment run to determine the accuracy of the qPCR assay. Triplicate samples of known concentrations of gDNA standard material (10μgmL^{-1} to 0.001μgmL^{-1}) prepared by serial dilution in TE buffer, were purified by the MagNA pure system and loaded on to the PCR plate as would occur in a normal operation. The results from the PCR plate were then back-calculated using the correction factor and correlated against the values of their known concentration. The concentration of the top standard was determined by NanoDrop spectrophotometer.

Studies to record the accuracy of the qPCR assay are displayed in Figure 4-34. Duplicate volumes of standard gDNA material of known concentrations dissolved in TE buffer were processed by the MagNA pure equipment and loaded on to a PCR plate, as would be the case for normal operation. The results from the qPCR plate were then used to calculate the DNA concentration of the original solutions using the equation (Equation 2-5). The quadruplicate results were then correlated against their known values as shown in the graph. From the figure the coefficient of correlation was found to be high at 0.987. The gradient of the linear regression was determined to be 1.07, indicating that the qPCR had the tendency to overestimate gDNA yield by ~7%. This deviation is acceptable and probably attributable to a combination of error in the calibration of the MagNA pure, and the possible detection of contaminating sequences in the preparations. From the figure the increase in variation is seen toward the lower concentrations which are predicted by the reduction in precision at low gDNA concentrations.

The final action to be performed to ensure the accuracy of the qPCR was to ensure that the standard curve employed was accurate. The standard curve was prepared as described in (2.5.14.1). The highest concentration standard was 10^6 genome copies per well, equivalent to 1.7μgmL^{-1} gDNA. This was prepared and the concentration validated by the NanoDrop

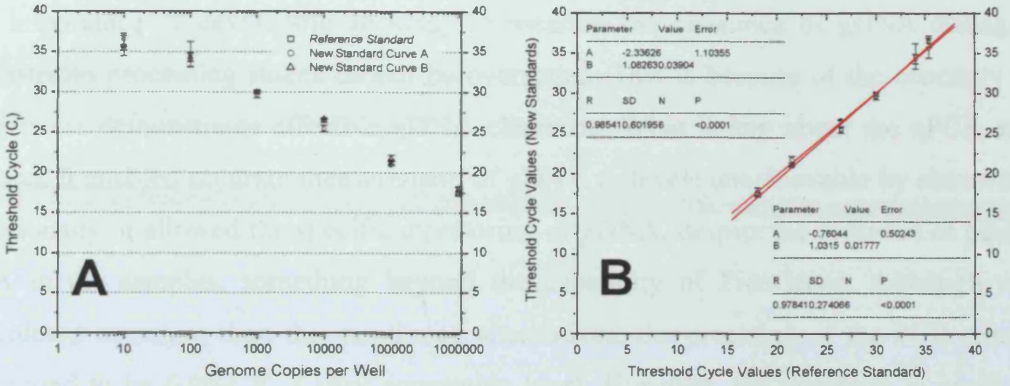

Figure 4-35 Graphs plotting the results of the standard curve validation experiments. Figure A plots the threshold values of each standard curve point at each gDNA concentration. The threshold value is the cycle number at which the fluorescence in the PCR well exceeds the pre-defined boundary of 0.04, a value in the middle of the exponential part of the PCR reaction. From the figure it can be appreciated that the different standard curves are in alignment and that the inverse relationship between threshold cycle number and DNA concentration is in effect. The anomalous result for 10 copies/well is ignored to improve fit.

Figure B correlates the threshold values produced for the prepared standard curve points against those of the reference standard. The coefficient of correlation for each standard curve is high and the average deviation from the reference standard is ~5%.

spectrophotometer. The remaining points on the standard curve were prepared by serial $\log_{10}$ dilution, and were beyond the capacity of the spectrophotometer to validate. Consequently, the validity of the standard curve was checked against the reference-standard gDNA standard material. Triplicate volumes of each standard curve point were loaded on to a PCR plate, with all the necessary reagents. Similarly, equal volumes of the reference standard material were loaded on and the plate analysed by the ABI Prism PCR cycler. From Figure 4-35A it can be appreciated that the freshly prepared standard curve aligned well with the reference standard. Each PCR reaction which was run in this project carried a standard curve on the plate ranging from $10^1 - 10^6$ copies/ well. However, as can be appreciated from Figure 4-35A the points for 10^1 copies were ignored in order to improve fit. It seems that the limit of sensitivity for the qPCR reaction is around 10copies per well, equating to a gDNA concentration of ~1.72pgmL^{-1}.

Correlating the threshold values produced for the new standard material against the reference standard, as shown in Figure 4-35B demonstrated good correlation (~0.98) and suggested that the new standard curve values lay on average ~5% within the figure for the reference standard. The acceptable degree of variation from the reference standard was 10%, meaning that the freshly prepared standard was acceptable.

4.7.5 Conclusions

The importance of developing an assay to measure the clearance of gDNA during the downstream processing stages cannot be overstated. This is because of the necessity that the process demonstrates effective gDNA clearance. What is key about the qPCR assay was that it enabled accurate measurement of gDNA to levels unachievable by absorbance. Additionally, it allowed the specific monitoring of gDNA, despite the presence of plasmid DNA in the samples, something beyond the capability of PicoGreen. Although more convoluted in nature than the mentioned alternatives, the precision of the PCR reaction was found to be 6.9%CV, a very acceptable level. However, the necessity to purify the gDNA prior to quantification meant that the overall assay precision dropped to 27%CV. However, the necessity to purify the sample would be required whatever the analytical method employed, and the automation of the assay meant that reproducibility would be better than manual purification, aswell as allowing more replicates to be processed.

The accuracy of the assay was also something important to demonstrate. Overall, the assay was found to overestimate the gDNA present by ~7%. This was surmised to be due to residual contamination, although that remains conjecture. The entire operation was performed in a DNA-free hood ensuring contamination was minimised. However, due to the impressive sensitivity of the PCR reaction (found to be sensitive to ~1.72pgmL^{-1}) extremely slight contamination would contribute. In short the assay's impressive capabilities made it such an important assay to use and demonstrated why it is becoming the recognised industry standard method of quantifying gDNA in process streams. Furthermore, the capabilities of this assay make it an ideal candidate for plasmid quantification, and it is believed that it will be employed for such in an increasing way.

4.8 RNA quantification by Quant-IT assay

4.8.1 RNA assay background

One of the desired achievements of this project was the construction of a mass balance for plasmid and contaminants over the main steps of the downstream process. A great amount of process information can be gleaned from a descriptive mass balance and although the plasmid is the product, and therefore the most important species to track, a fundamental concern in process development is tracking the progression of the contaminants, of which RNA is a major one. Indeed, in the order of contaminant mass following the lysis procedure, RNA represents the second most prevalent contaminant, second only to dissolved protein (Ciccolini *et al.*, 2002). To construct such an RNA balance would require an accurate and precise assay for quantifying RNA from process streams, which had to be robust enough to do so in samples which contain other nucleotides, proteins and salts.

During the preparation of samples for plasmid analysis, RNA is typically removed through the inclusion of RNase in the resuspension buffer. This highly efficient enzyme is capable of clearing all of the RNA contamination in a short period. However, from a process validation perspective the use of bovine material in plasmid production processes is disallowed. Consequently, the main RNA removal step employed in this process was the addition of 5M Calcium chloride to the bulk lysate, immediately following completion of the neutralisation step. The addition of this divalent salt, forming a final 1M solution, causes the precipitation of the vast majority of the RNA in the lysate. It was important to describe the level of this removal achieved over this step, together with characterising the removal of RNA by the other steps known to facilitate RNA clearance, namely UF.

Unfortunately, there is not an abundance of suitable analytical techniques capable of quantifying RNA. From an historical perspective, the number and sophistication of techniques for assaying and quantifying DNA far exceed those available for RNA measurement, by virtue of DNA's greater importance in a larger number of fields. Table 4-11 details a number of available techniques used for RNA quantification and their associated drawbacks.

Table 4-11 Table describing competing methods for quantification of RNA in process streams and their associated drawbacks.

Technique	Analytical method	Drawbacks
Gel detection	Run sample on gel, stain and scan.	- Can and is used to prove RNA removal but not particularly quantitative - Time-consuming - High inter-assay variability
Hydrolysis and dephosphorylation of RNA in sample (Gehrke and Kuo, 1989)	Guanosine residues in hydrolysate quantified by Reverse-phase HPLC.	- Hydrolysis reaction takes >24hrs. - Each HPLC run takes ~30 mins, reducing the number of samples which can be screened. - Contamination by residual guanosine residues on glassware etc.
Direct HPLC (Eon-Duval *et al.*, 2003a)	Sample analysed by HPLC using an Anion exchange and Size exclusion column in series.	- Cannot give a definitive measure of RNA, but a ratio of plasmid: RNA - Each sample takes ~30 mins, reducing the number of samples which can be screened.
MagNA Pure Total RNA isolation (Roche Diagnostics, 2006)	Total RNA from samples purified by glass beads and DNA digested enzymatically. Detection by absorbance at 260nm	- Additional processing decreases accuracy - Detection by absorbance requires samples to be >6μgmL^{-1} for accurate quantification - Time consuming
Qiagen RNA purification kits	Qiagen kits used to purify RNA in sample. Detection by absorbance at 260nm	- Cannot purify total RNA, species <200bp lost - Additional processing decreases accuracy - Detection by absorbance requires samples to be >6μgmL^{-1} for accurate quantification - Time consuming -Cannot guarantee full clearance of DNA.
RT-qPCR (Roche Diagnostics, 2006)	RNA purified by one of the above two methods. RNA detection by RT-qPCR	- Cannot measure total RNA only quantity of RNA species targeted by the primers. Therefore must know the proportion the target RNA represents of total RNA. This value is variable and hard to determine.

Fortunately, Molecular Probes had just produced the Quant-IT RNA assay kit, which promised to make the construction of an RNA balance a possibility. It also promised to be a lot simpler and less complex assay than those detailed in Table 4-11. Due to the relative novelty of the assay no reported results of the use of this assay, except the manufacturer's guidelines, were available (Molecular Probes Inc, 2006). More detail about the assay methodology can be found in 2.5.16. In brief, the assay follows a similar format to the PicoGreen assay, in that it employs an RNA specific fluorophore and is conducted in a 96-well plate format. The advantages of this technique become obvious in that no purification of samples is required and that due to the high-throughput nature many samples and sample replicates can be read, improving ease and precision.

Although many problems were encountered with the PicoGreen assay, it was envisaged that these problems would not be a hindrance to this assay. The PicoGreen assay is a rapid and accurate method of plasmid quantification, the problems with the assay found in this

project were the direct result of the plasmids under investigation and not the assay itself. As outlined earlier, the relatively high abundance of gDNA corrupted the results for the plasmid quantification, which was confounded by the wide-range in signal variation produced by linear and supercoiled DNA. For the Quant-IT RNA assay, the manufacturer's outline claimed the fluorophore to be highly specific for RNA, even in the presence of DNA. Additionally, the handbook goes on to state that the fluorophore is specific for all types of RNA (mRNA/ tRNA/ rRNA) no matter the molecules' conformation (Molecular Probes Inc, 2006).

As with the PicoGreen assay, the sample for analysis is diluted to lie within the assay range (0-10μgRNA mL^{-1}) and 10μL loaded on to a 96-well plate. The fluorophore concentrate is then mixed, in a 1:200 ratio, with the proprietary dilution buffer, 200μL of which is then added to each well of the plate. Included on each plate was an RNA 8-point RNA standard curve using material provided by the manufacturer, which ranged from 0-10μgmL^{-1}. After a 5 minute incubation period the plate can be read using a fluorescent plate-reader.

4.8.2 Determining the accuracy of the Quant-IT RNA assay

Since the assay involved no purification of RNA in the streams used for analysis, the potential for contaminants in the samples to corrupt the result was a real possibility. To determine whether this was the case, standard curve material was used to create solutions of known RNA concentration using mimics of the solutions found in the downstream process. These solutions were then read and the results correlated against the solutions of the RNA in TE buffer. Table 4-12 displays the results of the correlation experiments. It can be seen that RNA solutions in the DF1 and DF2 buffers demonstrated good comparability to the standard curve indicating the contents of those streams would not affect the results. However, the correlations for the Pre-$CaCl_2$ and Post-$CaCl_2$ streams did not show good comparability, indicating that components of those streams had the potential to heavily influence the assay results.

Table 4-12 Table detailing the results of experiments into the effect of buffer components on the Quant-IT assay. Known concentrations of RNA were prepared using solutions found at various stages of the downstream process. The Pre-$CaCl_2$ and Post-$CaCl_2$ solutions were prepared from a blank lysis run using *E.coli* parental cell paste. The Diafiltrate 1 buffer was prepared by a 1:20 dilution of the Post-$CaCl_2$ buffer, mimicking the dilution achieved in the process. The prepared standards were run in triplicate against a reference standard consisting of RNA of known concentration in TE buffer. The results were correlated against each other and linear regression performed to determine the gradient.

STREAM	GRADIENT	% OFFSET	CORRELATION
PRE-$CACL_2$	0.546	-45.4	0.924
POST-$CACL_2$/ PERMEATE	0.263	-73.7	0.877
DIAFILTRATE 1	0.948	-5.2	0.989
DIAFILTRATE 2/ RECOVERY STREAMS	0.976	-2.4	0.982

Knowing that the Pre-$CaCl_2$ and Post-$CaCl_2$ streams contained species which would corrupt the results, further correlation experiments were performed by preparing fresh standards of known RNA concentration prepared in the buffers, which had been diluted by several degrees. Figure 4-36 plots the results of these investigations. From the figures it can be seen that sample material from the Pre-$CaCl_2$ stream required dilution by 100-fold to remove the corrupting effects of the buffer. However, the same results for the Post-$CaCl_2$ stream suggested that even dilutions of sample material by 200-fold were insufficient to remove the salt effects. The high-salt environment of the Post-$CaCl_2$ solution meant that removing the inhibitory effects would be impossible by dilution alone. Further dilutions could not be attempted as they would take the concentration of the RNA

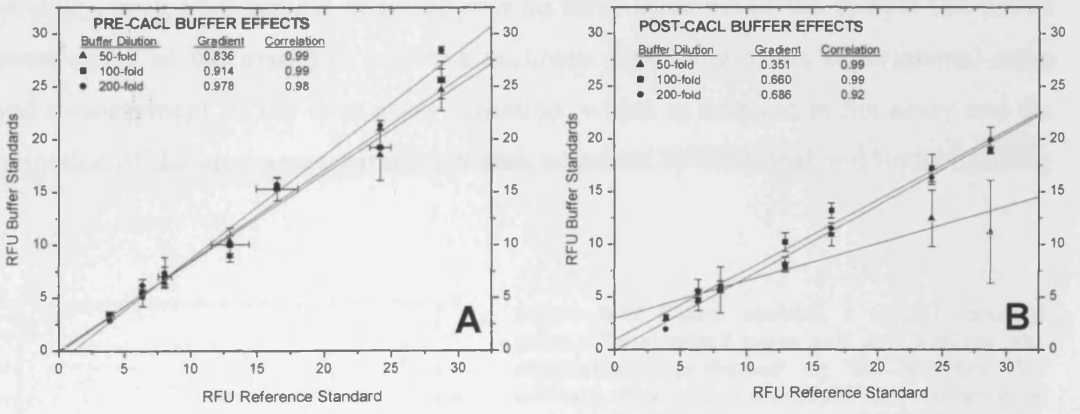

Figure 4-36 Figure A plots the correlation experiments of the RNA standards prepared using Pre-$CaCl_2$ solution of three dilutions against the reference standard. It can be seen that above 100-fold dilution of the solution the corrupting influence of the contaminants is sufficient to reduce the effect to within the 10% acceptable limit. Figure B plots the same results using various dilutions of the Post-$CaCl_2$ buffer to form the standards. The results suggest that even dilutions of 200-fold is insufficient to remove the corrupting effects of the contaminants

in the sample stream out of the linear range of the assay.

For this reason the high-salt streams (Post-$CaCl_2$/ Permeate) would have to be de-salted, prior to analysis, through the use of PD-10 columns. Although this would represent a further processing step, the recoveries of macromolecules from these columns is claimed by the manufacturer to be >95%, meaning that de-salting should not be detrimental to the accuracy (GE Healthcare, 2005). The final dilutions employed for each process stream can be seen in Table 2-13. These experiments gave the confidence that the dilutions were sufficient to remove the effect of any contaminating species in the buffers and that the assay accuracy lay within 10%.

The final consideration concerning the accuracy of this assay lay with the standard curve. The manufacturer's claim that the fluorescence signal from RNA was linearly related to the RNA concentration. However, it was found more accurate to fit a polynomial curve to the data, as shown by Figure 4-37.

4.8.3 Determining the assay precision

As with the other assays, of which the development has been described in this chapter, determining the precision of the Quant-IT RNA assay is central to having confidence in the results it returned. The determination of the assay precision follows the same procedure as outlined for qPCR, with a small difference. The manufacturer's guidelines specify the need to repeat each measurement in triplicate, advice which was followed. Additionally, each DSP sample analysed was on three dilutions of the sample (all within the linear range of the assay) to improve accuracy. Once again this experimental setup allowed measurement of the intra-assay variation, which is inherent in the assay and the determination of the inter-assay variation which is caused by dilutional and liquid handling

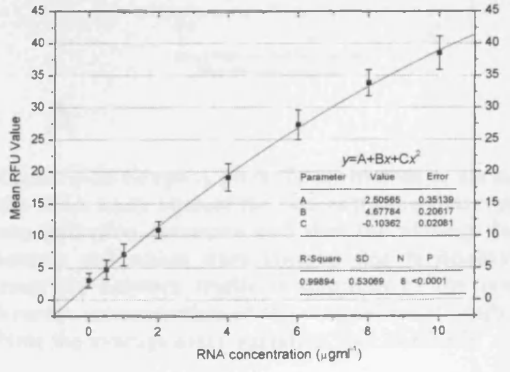

Figure 4-37 Figure showing a typical standard curve. The standard curve and data analysis was automatically performed by the SoftMax Pro software. However, it was found more accurate to employ polynomial regression rather than linear on the standard curve

differences. It was a definite possibility that the inclusion of three dilutions would increase assay variation, which is why it was important to quantify, however doing so would benefit the assay accuracy.

The results of the assay variation are displayed in Figure 4-38. Graph A shows the intra-assay variation encountered between triplicate wells of the same sample, plotted against the concentration of RNA in the well. It can be appreciated that the assay precision decreases as the sample becomes more dilute. For this reason it was decided to ignore the results of triplicate wells where the %CV exceeded 50%.From Figure 4-38A it can be seen that the average %CV of the triplicate samples was 18.6%. This is a high value for intra-assay variation, when compared to the same value for the HPLC, gDNA and BCA assays.

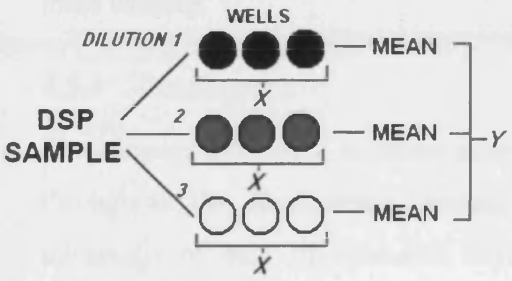

Figure 4-39 Schematic describing the measurement of variation in the Quant-IT assay. Three dilutions of the DSP sample were created, each of which was measured three times on a 96-well plate. The intra-assay variation (X) records the variation inherent in the assay technique, whilst inter-assay variation records the variation between replicate dilutions (Y).

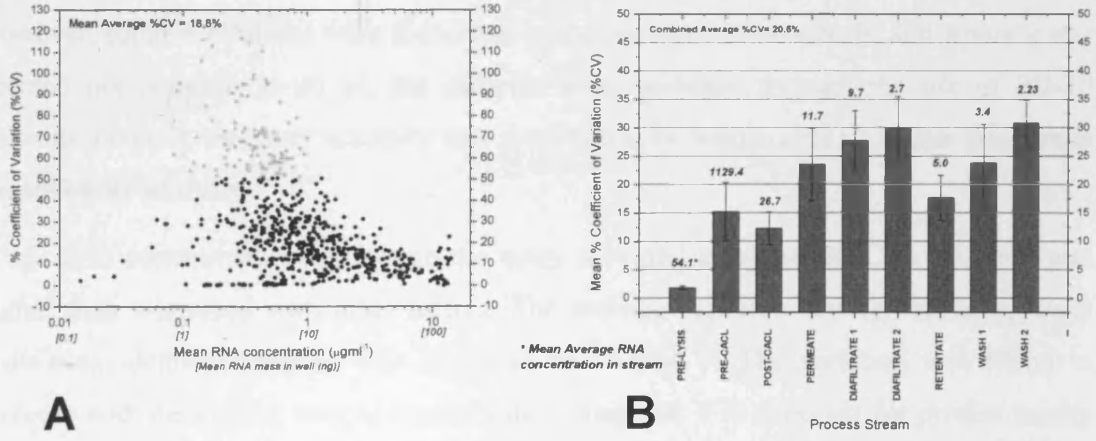

Figure 4-38 Graph A plots the coefficient of variation recorded for every triplicate set of wells recorded in the RNA assay against the concentration determined for the wells. Note that %CV increases as the RNA concentration decreases and that the average %CV for the assay is 18.6%. The grey points represent sample sets which were ignored due to displaying a %CV >50%. Graph B plots the total variation recorded between triplicate dilutions of the same samples as a function of the stream analysed. The average concentration of the sample under study is recorded and is thought to effect the %CV achieved. Note the average assay variation was 20.6%CV

However, little can be done to improve upon this value as it represents the inherent variation within the assay. Figure 4-38B plots the total variation witnessed between the triplicate dilutions. The average value stands at 20.6%, meaning that the vast majority of the variation is a direct result of the assay rather than any liquid handling or dilution effects. It can also be appreciated from that plot that the variation is not fixed but varies between the samples under analysis of the assay variation are displayed in Figure 4-38. Figure 4-38A shows the intra-assay variation encountered between triplicate wells of the same sample plotted against As a general rule, the streams containing the least RNA possessed the greater %CV, something which is a direct result of the assay. It seems that although the assay can quantify RNA solutions less than $1\mu gmL^{-1}$ the precision of the assay becomes less at those concentrations. Although it has been demonstrated that the assay variation increases with sample concentration, the maximum overall variation (~30% for dilute samples) was not deemed high enough not to include the results in the mass balance.

4.8.4 Conclusions

The development of a suitable assay for monitoring the progression of RNA removal throughout the downstream process has been reported. The assay employed had the advantage of ease of operation and the potential to allow the screening of multiple replicates with ease, something not available with alternative methods. It was expected and determined that contaminating species could cause corruption of the results returned. However, suitable dilutions were found that could eliminate these effects, and where it was deemed not possible to do so, the samples were de-salted through the use of PD-10 columns. Overall, the assay accuracy was predicted to be within 10% no matter the sample stream under analysis.

It was also determined that although the assay provided many benefits, its variation was higher than witnessed with other assays. The average variation between replicate wells containing identical samples was found to be 18.9%CV. The variation was found to increase with decreasing sample concentration such that it is expected for precise results the concentration of RNA in the sample wells should not be below $0.1\mu gmL^{-1}$ and ideally $1\mu gmL^{-1}$. Despite this drawback the assay promised to be very suitable for the creation of an RNA balance for the downstream process.

4.9 Protein quantification by BCA assay

4.9.1 Background of BCA assay

Despite the large removal of protein that is achieved over the precipitation step, sufficient mass remains for dissolved protein to form the most abundant contaminant in the downstream process stages. For that reason it is critical that the removal of this contaminant be described by a mass balance. Despite its prevalence, protein represents the least troublesome contaminant to remove during the downstream stages, mainly due to the large physico-chemical differences which exist between proteinaceous molecules and polynucleotides. The same cannot be said for RNA and gDNA, since they share a great deal of similarity to the target plasmid molecule. In order to construct a protein mass balance a suitable assay, capable of monitoring protein concentration through the process was required.

The BCA (Bicinchoninic acid) assay was chosen over competing total protein assays (Modified Lowry and Biuret) namely for ease and accuracy, since the BCA assays was available in 96-well format and the other two were not. The advantage of analysing samples in the plate-based format is that far more samples and sample replicates can be screened more quickly and through the use of less material. The BCA assay was chosen over the Bradford assay, which is available in a 96-well format, because the BCA has a higher sensitivity (~0.5μgmL^{-1}), shows less protein-protein variation and, unlike the Bradford assay, is not strongly affected by trace amounts of SDS (Smith *et al.*, 1985; Brown *et al.*, 1989).

The operation of the BCA assay surrounds the reduction of copper(II) ions by proteins in an alkali environment (Biuret assay). The concentration of copper(I) ions is then determined colourimetrically using the BCA reagent. The reaction produces a purple colour which exhibits strong absorbance at 562nm. More detail concerning the operation of the BCA assay can be found in (2.5.13). In this project the assay was used to determine the protein concentration of all streams of the downstream process enabling the construction of a full mass balance. However, prior to its use, the accuracy of the BCA assay needed to be validated and following the assay's deployment the precision of the assay could be found, so as to give confidence in the results produced.

4.9.2 Determining the accuracy of the BCA assay

As with the RNA assay, the BCA assay required no prior purification of the samples used for analysis. Once again the potential for contaminants in the process samples to effect the BCA reaction and cause misleading results was a distinct possibility, such effects had been reported by (Brown *et al.*, 1989). To determine whether this was the case similar experiments were performed as were described in the RNA assay section. Standard curve material (BSA) of known concentration was prepared using neat solutions of the various solutions encountered during the DSP operations. These samples were run in triplicate against reference standard, consisting of identical concentrations of BSA prepared in PBS buffer. The absorbance results of the buffer standards were then correlated against the same for the reference standards, as shown in Figure 4-40.

From the results of these preliminary experiments it can be seen that the Diafiltrate 1 (DF1) and DF2 buffers did have a small increasing effect (8-10%) on the absorbencies, however, they lay within the 10% acceptable margin, meaning that no dilutions of these solutions would be required. The Pre-$CaCl_2$ and Post-$CaCl_2$ solutions were found to have

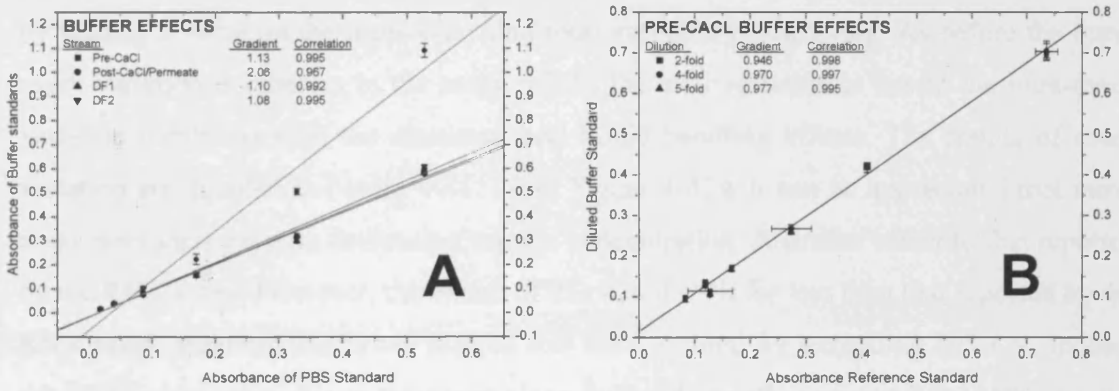

Figure 4-40 Figure A plots the results of correlation experiments performed to determine whether the contents of the solutions of the process stream affected the result obtained by the BCA assay. Known concentration of standard BSA protein were prepared in Pre-CaCl/ Post-CaCl/ DF1 and DF2 buffers. Triplicate volumes of these were loaded onto a plate and read against a reference standard of the same protein solutions made in PBS buffer. The absorbances produced by the buffer standards were then correlated against the reference standard. Note that the gradient produced for the DF1 and DF2 buffers were within the accepted range of accuracy (i.e.10%) but that the same was not true for the solutions made with the Pre-CaCl and Post-CaCl buffers. Figure B shows repeat experiments, using known concentrations of protein made up in Pre-CaCl solution of varying degrees of dilution. Correlating the results against the reference standards demonstrates that dilutions of 2-fold is sufficient to remove the corrupting effects of the contaminants in the Pre-CaCl buffer

more of an impact on the results. The gradient of the Pre-$CaCl_2$ standards suggested that the buffer caused a ~13% increase in the absorbance signal. Further experiments were carried out using various dilutions of this buffer and it was deemed that this effect could be reduced to lie within the acceptable margin (±10%) by a 2-fold dilution of the sample material. The buffer effects demonstrated by the Post-$CaCl_2$ solution (known to be at least a 1M salt-solution) were more dramatic, suggesting that assaying samples in this buffer would cause a >100% deviation from the actual value. It was attempted to remove the effect of this contaminant by dilution, but it was found that even dilutions as 1:100 still produced an effect. Any higher dilutions would take the protein concentration beyond the linear range of the assay. Consequently, for the same reason as described in the RNA assay, high-salt containing streams (Post-$CaCl_2$ and Permeate) would require de-salting prior to assaying. Again, PD-10 columns would be used, which claim to recover >95% of the macromolecules and retain <4% of the salt (GE Healthcare, 2005).

4.9.3 Determining the precision of the BCA assay

The operation of the BCA assay was the same as described for the RNA assay, in that triplicate measurements of three different dilutions of the DSP sample were performed. For that reason determination of the assay precision was carried out in the same fashion, by placing a value on the intra-assay and total variation of the assay. As before the intra-assay variation is inherent in the assay, whilst the total variation is due to the intra-assay variation combined with the dilutional and liquid handling effects. The results of assay variation are detailed in Figure 4-41. From Figure 4-41A it can be appreciated that intra-assay does increase with decreasing sample concentration. A similar effect to that reported by the RNA assay. However, the extent of this variation is far less than that reported by the RNA assay, meaning that fewer sample sets were ignored for exceeding 50%CV. Indeed, the average variation due to the assay alone is less than 10% compared for ~18% for the RNA assay, meaning that the BCA assay is by its nature a more precise assay. Unfortunately, the advantages of this improved assay precision are lost due to dilutional and liquid handling differences as the total variation of the assay was deemed to be 17.8% (Figure 4 41B). As with the gDNA and RNA assays the streams demonstrating the greatest variability are those containing the least amount of protein

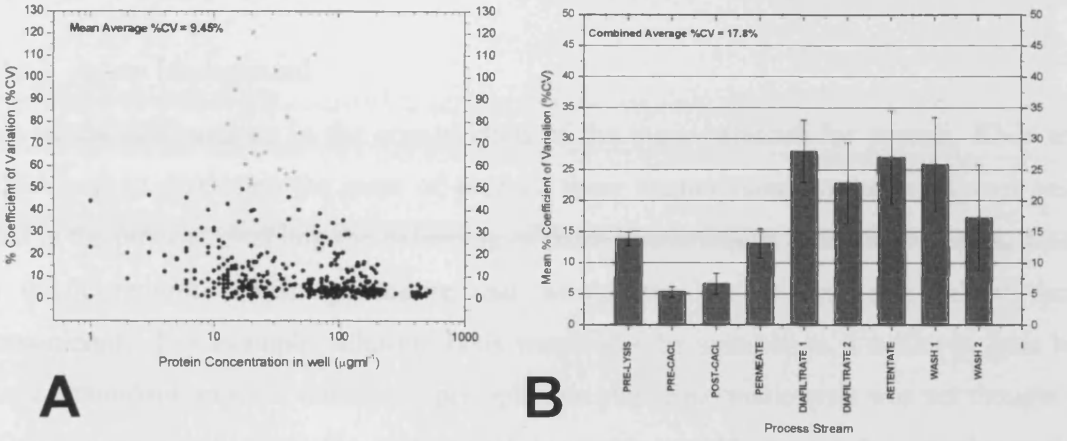

Figure 4-41 Figure A plots the coefficient of variation recorded for every triplicate set of wells run in the BCA assay, against the concentration of protein in the well. Note that %CV does show an increase as protein concentration decreases, but to a lesser extent than for the RNA assay and that the average %CV is 9.45%. The grey points were sample sets that exceeded 50%CV and so where ignored to improve precision. Graph B plots the total variation recorded between triplicate dilutions of the same sample as a function of the stream analysed. Note that the average %CV id 17.8%

The results of the precision analysis suggest that the BCA assay is more precise than the RNA assay. However, it seems to be affected more by dilutional effects between samples, possibly suggesting that the chosen dilutions were not ideal. However, the overall assay precision of 17.8% made it more precise than the RNA assay and was deemed acceptable.

4.9.4 Conclusions

An accurate and precise method of determining protein concentration in all streams of the downstream process has been described. No dilution was required for UF recovered fractions, but a 2-fold dilution of the clarified lysate was deemed required to ensure accuracy. Furthermore, the Post-$CaCl_2$ required de-salting prior to measurement. The intra-assay precision was found to be much improved compared to the RNA assay at 9.45%CV, but that the overall assay variation determined at 17.8%.

4.10 Sonication procedure

4.10.1 Assay Background

One of the final actions in the construction of the mass balances for protein, RNA and gDNA was to determine the mass of each of these contaminants in the initial cell paste used in the process, enabling the balancing of these contaminants over the lysis step. To do so would require a lysis procedure that would not lead to any removal of these contaminants. For example, alkaline lysis would not be suitable as it achieves lysis but also contaminant removal during the precipitation step. Enzymatic lysis was not thought to be an improvement, since the addition of lysozyme would corrupt the protein results. Consequently, it was decided to achieve lysis by a physical mechanism; through the use of ultrasonication.

Ultrasonication of microbial cells in suspension with inaudible ultrasound, results in their physical disruption. The technique utilises the rapid sinusoidal movement of a probe within the suspension. The high frequency (>18 kHz), small displacements (<50 μm) of the probe generate moderate fluid velocities (~1-2ms^{-1}) but cause high shear rates (~4,000s^{-1}) and high acceleration rates (~80,000g). These effects induce cavitation, such that acoustic power is sufficiently high to produce micro-bubbles at nucleation sites in the fluid. The bubbles grow during the rarefying phase of the sound wave but are collapsed during the compression phase. Overall, the collapse of the bubbles converts sonic energy into mechanical energy, in the form of shock waves equivalent to several thousand atmospheres pressure (~300MPa). This energy imparts motion onto cells, which disintegrate when the kinetic energy content exceeds the wall strength. Also, the shear rates produced are enough alone to cause significant damage to the cells (Bailey and Ollis, 1986; Fykse *et al.*, 2003)

This technique would be employed to lyse the cell suspension and the various assays (gDNA/ BCA and Quant-IT RNA) could then be performed on the lysate to determine the concentrations and masses of the contaminants at the beginning of the process. However, to have confidence in the results conditions needed to be isolated that guaranteed that full lysis was being achieved, otherwise not all of the contaminant mass would be accounted for.

4.10.2 Determination of suitable sonication conditions to ensure full cell lysis.

The determination of suitable conditions for the sonication procedure was essential to give confidence that all the intra-cellular contents were released into solution where they could be assayed. Since the achievement of full lysis is dependant on so many factors, varying from the cell strain employed to the shape of the vessel in which the cell suspension is contained, no definitive conditions could be obtained from the literature which would guarantee full lysis. Consequently, studies were required to decide upon the best conditions. It was decided that the lysis would be conducted on 10mL of cell suspension in a 50mL Falcon tube. The ultrasonicator (Braun Labsonic), equipped with a needle-titanium probe of 4-mm diameter and 127-mm length, was kept immersed about 5 mm into the fluid. Sonication experiments were done at 20 kHz meaning that the acoustic power ranged from 35-95W. At all times the cell suspension was kept at ~4°C by incubation in an ice-bath. Determining the extent of cell lysis would employ the BCA assay to record the concentration of dissolved protein in the sonicated lysate.

The two conditions which were thought most likely to impact upon lysis efficiency were the cell concentration of the suspension and the period of time that the cells were sonicated.

4.10.2.1 Determining the optimum cell concentration

From the manufacturer's guidelines a sonication regime was obtained which involved a 10s sonication event followed by a 30s break (the break period prevented sample over heating). This 40s cycle was repeated 10-times for each sample. Cell material extracted from *E.coli* DH1 fermentations was used in the optimisation studies. A series of cell suspensions of varying concentrations ($190gL^{-1}$-$0.39gL^{-1}$) were prepared by dissolving 10g of frozen parental cell paste in 50mL of TE buffer. The WCW of the solution was determined to be $190gL^{-1}$. The remaining cell suspensions were prepared by log_2 dilutions of this starting material in TE buffer. The cell suspensions were then subject to the sonication regime in Falcon tubes. Following sonication, the cell lysate was recovered by centrifugation and the dissolved protein concentration of the supernatant found using the BCA assay. A negative control was also assayed, which involved spinning down an identical cell suspension which had not been subject to sonication. This would account for the protein present due to background cell lysis.

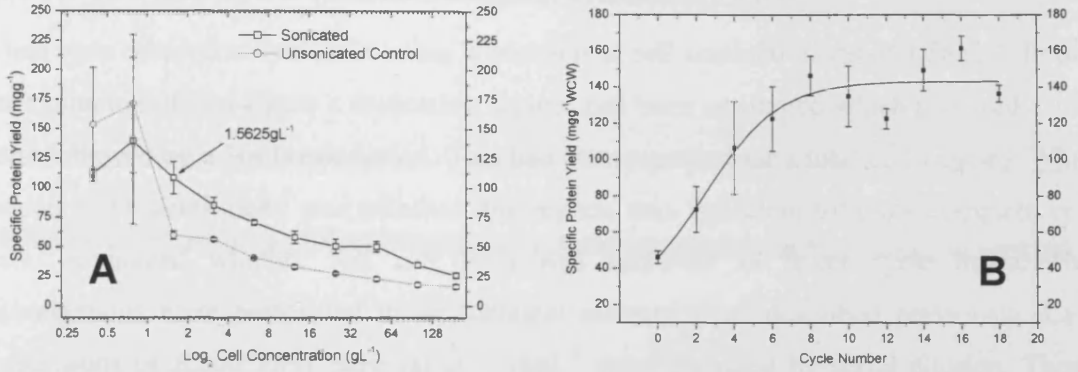

Figure 4-42 Figure A plots the results of investigations to find the optimum cell concentration at which lysis, by sonication, is the most efficient. 10mL solutions of different cell concentration of *E.coli* in TE buffer were subject to a 40s sonication cycle, repeated 10-times. The lysate was centrifuged down and the supernatant assayed to determine total protein concentration. The specific protein yield could then be determined. It was found that lysis at 1.56gL^{-1} gave the highest and most reproducible degree of lysis. Figure B plots the results of investigations to determine the optimum number of sonication cycles required to achieve full lysis of a 1.56gL^{-1} cell solution. It was determined that beyond 8-cycles the increase in lysis achieved was minimal. Additionally, extending lysis longer than this could cause damage to the molecules which were to be assayed, not by shear but by exposure to elevated temperatures.

Figure 4-42A plots the results of these investigations to determine optimum cell concentration. The semi-log plot details the small extent at which lysis occurs at the higher cell concentrations. The efficiency of lysis shows an almost linear increase as the cell concentration is reduced. However, past 1.56gL^{-1} the precision of the assay becomes problematic and as the unlysed control records higher specific protein yield than the lysed value, also the error at that level is high. Consequently, it is decided that a cell concentration of 1.56gL^{-1} (prepared by serial dilution) offers the optimum cell concentration. Visual observations of sonication also recorded the efficiency of lysis, because at the lower cell concentrations the opaque, cloudy suspension became clear following sonication. This was taken as visual evidence of effective lysis. Additionally, the value recorded for specific protein yield at this concentration was ~112mgg^{-1}WCW, representing ~11% WCW. The value for total protein in an *E.coli* cell is ~15% (Bailey and Ollis, 1986) indicating that the lysis was effective. The slightly strange effect noted, was that merely preparing the cell suspension, which does involve pipetting, centrifugation etc. seemed to account for ~50% of the reported lysis. Whether the cells at the end of the fermentation were weakened or that the cells were exposed to osmotic lysis is unsure, but the figure seems high.

4.10.2.2 Determining the optimum number of sonication cycles

It had been decided to lyse cells using sonication at cell concentrations of $1.56gL^{-1}$. In the determination of that figure a sonication regime had been employed which involved a 10s burst followed by a 30s break period. This had been repeated for a total of 10 cycles. What needed to be determined was whether this regime was sufficient to allow complete cell lysis, or indeed whether full cell lysis was achieved in fewer cycle times. The investigations were performed in an identical manner to as described previously. Cell suspensions of *E.coli* DH1 parental at $1.56gL^{-1}$ were prepared by serial dilution. These were then subject to sonication regime of 40s, but the number of cycles was varied from 2-18. Following sonication the lysate was centrifuged and the protein content of the supernatant recorded using the BCA assay.

Figure 4-42B plots the results of the investigations. From the plot it can be appreciated that lysis efficiency rises with the number of sonication cycles, but that a maximum efficiency is recorded at about 8 cycles. Continuing with the sonication past this cycle number did not appear to achieve any higher degree of lysis. Furthermore, it was felt that although the lysis was performed on ice, continuation of sonication for longer than the maximum needed could only lead to damage/denaturation of the contaminants to be assayed.

4.10.3 Conclusions

It had been decided to employ ultrasonication to induce lysis in cells so that the starting amounts of the contaminants could be found. It was believed that this technique was better than alternatives (detergent/ enzymatic lysis) as it efficiently achieved its objective, but with the minimal impact on the concentrations of the contaminants to be assayed. Optimisation studies were performed and it was decided that efficient cell lysis could be achieved at cell concentrations of $1.56gL^{-1}$ using a sonication regime involving 8-cycles. Now that these conditions were known, the cell material used for the downstream processing studies could be subject to the same regime and the lysate assayed for the concentration of gDNA, RNA and protein. This would allow the specific yield of each of these contaminants to be determined for every cell mass processed. Ultimately, this would enable the starting masses of each of the contaminants at the process start to be calculated.

4.11 Conclusions

The importance of accurate analytical techniques was crucial in the development of this project. However, it was understood at the outset that techniques commonly used for plasmid quantification, when recording the concentration of solutions containing small, high-copy number plasmids may not be applicable for quantification of large, low-copy number plasmids. Studies confirmed this. Problems were encountered with the use of PicoGreen, due to the presence of contaminating gDNA. Although this contaminant existed at identical levels whether assaying a high or low copy number plasmid, the ratio of the level of contaminant to plasmid was found to be of key importance. For high-copy number plasmids the small, corrupting influence of background gDNA did not influence results significantly. However, at the low plasmid concentrations encountered with the low-copy plasmids this background signal was found to equal that due to the plasmid, meaning the actual yield results were far more corrupted.

Issues were also identified with processing of these plasmids using Qiagen spin-preps and attempting to quantify the pDNA in the eluents. Due to the low plasmid yields, the presence of protein in the eluent stream had an impact on the accuracy of using A_{260} to quantify large plasmid eluents. Again, this problem was not be encountered when processing small, high-copy plasmids due to that fact that the higher pDNA yields in the eluent were less affected by these trace contaminants. Furthermore, attempting to use PicoGreen to quantify the plasmid in the spin-prep eluents also posed more questions. It was found that to obtain an accurate result the standard curve employed has to mimic closely the topology of the plasmid in the eluent. It was soon realised that the large plasmids in the eluent displayed very little supercoiling and as such assaying against a standard curve composed of native plasmid produced erroneous results. Again, this effect was not witnessed with the smaller plasmids, since the action of spin-prepping did not have the same effect on their level of supercoiling. A method was determined which provides a reasonably accurate method of quantifying large, low-copy number plasmids.

Alternative methods of plasmid quantification were investigated. Development of a HPLC technique led to a very effective assay for the analysis of plasmid (of all sizes) in all elements of the plasmid production process.

Development of an assay for visualising plasmid topology was difficult. The use of Field Inversion Gel electrophoresis (FIGE) was found to reliably separate the isoforms of large plasmids.

Further details are given into the development of the other assays required to construct a mass balance for the key contaminants in the plasmid production process. These included assays for protein, RNA and genomic DNA. Suitable investigation was required to determine the limits of the individual assays, their accuracy and their precision.

Assay development formed a key part of this project and ran concurrently with the progress of the project. All of the assays employed were suitably tested and verified so that confidence can be had in the results these techniques returned.

5 CLONING AND CELL-LINE DEVELOPMENT: RESULTS AND DISCUSSION

5.1 Chapter Aims

From the initial studies it had been determined that the large plasmids of the Oxford series were not particularly useful for investigating the plasmid process. Since the constructs were Bacterial Artificial Chromosomes, their copy number was found to be very low, at about 1-2 copies per cell. The resultant low yields created a multitude of problems, including difficulties in analytical procedures, but also in the investigations performed to study their behaviour when processed. Essentially, it became impossible to differentiate effects recorded when these molecules were processed as being due to the large construct size or the low yields at which they existed. This realisation resulted in a difficult decision as to the direction of the project. The project could continue to investigate the production of the large series of BACs or attempts could be made to construct a series of large plasmids employing origins of replication found in plasmids used for production. As a result, this chapter attempts to cover the following areas;

1. Logical and intuitive reasons why the decision was made to construct large plasmids using conventional plasmid backbones.
2. The chapter will describe the broad methods which were attempted but which failed to produce large constructs.
3. The chapter will describe in more detail the shotgun-cloning method which was successful in producing a series of large constructs.
4. How techniques of statistical design of experiments were adopted to determine optimum conditions at which to produce the large constructs by batch fermentation.
5. Investigations into the stability of the newly constructed plasmids to determine the extent to which losses were accrued by plasmid instability.

5.2 Decision to construct a new series of large plasmids

The Oxford series of plasmids used in the initial investigations were Bacterial Artificial Chromosomes (BACs). As such the constructs' replication was controlled by the F-factor, which stringently maintains plasmid copy number at 1-2 copies per cell, depending on the stage of growth of the culture. This value of 1-2 copies was reported by (Frame and Bishop, 1971) but was also determined by studies into plasmid yield found in Chapter 3. At the outset of this project it was hoped that the large plasmid size would go someway to alleviate the low-copy number by ensuring that there still existed a high amount of pDNA for purification. However, it was soon determined that the yields produced from fermentations of these constructs were very low (~50μgg^{-1}WCW) approximating to about 10-fold less material that un-optimised production systems using high-copy plasmids, and up to 100-fold less than that of optimised production systems. The low yields made it hard to draw any concrete conclusions from investigations into the processing of these macromolecules. The situation was made increasingly difficult by inaccuracies in the analytical procedures, mis-representing plasmid yields because of the relatively high impact of other contaminants on the signal used for quantification. Additionally, it was found that operation of the plasmid production protocol being studied was not feasible using lysate streams containing these plasmids. The reason for this was that the current process employed a UF step which required a certain quantity of plasmid to be present so as to generate an effective gel layer. Attempts to increase the loaded plasmid mass, by either reducing membrane area or increasing the volume of lysate loaded, were tried but found not to be applicable as it led to the rapid and complete blockage of the membrane.

As a result of these issues it was believed that in order to generate meaningful data the specific yield of plasmid to be purified would need to be increased, at least to within comparable yields generated by small, high-copy number constructs. It is important to remember that the cells were not close to the estimated maximum limit of extrachromosomal DNA when they were propagating the BAC series of plasmids (Figure 3-14), meaning there existed a large scope to improve on the pDNA specific yield. With most commercial processes increasing plasmids can be achieved by one of two methods; genetic and process strategies.

These are outlined in 3.3 and either involve increasing the plasmid copy number (and hence specific yield) by employing replicons which ensure high copy numbers or by

adjusting fermentation conditions (media recipe, fermentation strategy, growth rate) to amplify plasmid copy number.

Table 5-1 Decision matrix used in an attempt to objectify the decision making process. The pros and cons of the two courses of action s were summarised. Each pro and con was then rated numerically, a pro given a positive score and a con a negative. The magnitude of the score varied from -5-+5 with each judged on the criteria of relevancy and likelihood. The net score is the sum of the values for pros and cons.

ACTION	PROS	CONS
Continue with the use of the Oxford Series **Net result (-10)**	- Could continue without taking time out to construct new plasmids (+5)	- Unable to differentiate the effect of low yields or large size (-3) - Unsure if meaningful results could be obtained (-2) - Would not be possible to study the whole process, only unit operations (-3) - A commercial process would never make use of these constructs (-1) - Had obtained data relating the difficulty of purifying these constructs using the conventional process (-4) - Constructs' copy number stringently controlled, and as such no methods available to increase copy number. (-2)
Alter replicon of large plasmids **Net result (0)**	- If created high-copy number large plasmids the resultant information would be more relevant to existing processes. (+2) - Creation of a series of plasmids with more realistic sizes. (+4) - Could allow the studying of the whole process- enabling construction of a mass balance. (+3) - Would make use of plasmid backbones used in current production processes. (+3) - Make use of relaxed plasmid backbones which would allow a degree of control over plasmid yields during fermentation (+2)	- Time required to construct/alter the plasmids (-5) - Unsure whether the constructs could be produced. (-5) - New constructs may not improve situation (-4)

Unfortunately, it has been shown in Chapter 1 that none of the process strategies described in the literature can be used with stringently controlled plasmids. In short the only viable

option of increasing plasmid specific yield was to employ a genetic strategy. This would involve replacement of the F-replicon with a relaxed origin of replication which would increase the plasmid copy number. Table 5-2 details the origins of replication and copy number of various plasmids.

Table 5-2 Table describing the replication and copy number of various plasmids. The origin of replication determines whether the plasmid is under relaxed or stringent control. Plasmids such as pUC/pTZ have mutations which allow them to reach very high copy numbers. The copy number of relaxed plasmids is not fixed and can vary depending on the nature and size of the insert. Table adapted from (Sambrook *et al.*, 1989) and (Qiagen, 2005).

PLASMID CONSTRUCT	ORIGIN OF REPLICATION (*ORI*)	COPY NUMBER	CLASSIFICATION
pTZ vectors	pMB1	>1000	High copy
pUC vectors	pMB1	500-700	High copy
pBluescript vectors	ColE1	300-500	High copy
pGEM vectors	pMB1	300-400	High copy
pBR322 and derivatives	pMB1	15-20	Low copy
pSC101	p15A	~5	Low copy
pML31	F-factor	1-2	Very Low copy
pBAC108L (Oxford series)	F-factor	1-2	Very Low copy

However, it was realised that this strategy would be technically difficult and there would be no guarantee of a successful outcome. On the other hand, the alternative of continuing to use the Oxford series was not attractive either. In order to choose the best strategic course of action a decision matrix was drawn as shown in Table 5-1. The decision matrix was used in an attempt to objectify the decision process by rating the reasons for pursuing the two different strategies.

The main pro towards continuing use of the Oxford series was that no time would be required to develop more suitable constructs. However, a number of disadvantages were identified with continuing with this course of action. From the initial studies it had been shown impossible to determine whether the low mass recoveries produced at the end of the process were a result of the low starting yields or the large size of the constructs.

Additionally, with such low starting yields it was unsure whether meaningful results, in the form of a plasmid mass balance, could be obtained using these constructs. The low initial

yields would make detection and mass balancing difficult, and as such it would be hard to determine which steps in the process were the most problematic, since only trace amounts of plasmid were present to begin with.

Furthermore, from the initial studies it had been found that insufficient plasmid mass was present in the lysate to build up an effective gel-layer on the membrane surface. As a result, it probably would not be possible to study the downstream process in its entirety. This would require the application of scale-down studies to mimic each process step, using pre-concentrated plasmid stock as the feedstream. However, investigation of the plasmid process, by studying each unit operation using scaled-down mimics and concentrated feedstock, would not represent the process as accurately and holistically as actually performing pilot-scale downstream runs. Also, generating sufficient material to perform these studies promised to be problematic.

Further reasoning led to the belief that a sea-change in the operation of the plasmid production process would be required to produce such low-copy vectors. Traditional plasmid processes operate by removing the contaminants away from the plasmid product. This strategy works by ensuring that each unit operation delivers a large clearance of the major contaminants, which as a side-effect also leads to the loss of a small proportion of the plasmid product. The losses accrued are generally accepted since the initial plasmid mass would be sufficiently high. With BACs, the mass of plasmid is so small to begin with that it is believed that conventional methods of processing would not be applicable. Instead, the purification strategy would need to focus around selectively purifying the BAC away from the other contaminants. Investigating the potential to do so would be well beyond the scope and capability of this project. Evidence for this opinion is provided by the contaminant ratios shown in Table 5-3, which detail that the low plasmid yields found with BACs are very detrimental to ratios achieved.

Table 5-3 Table detailing the ratio plasmid mass to the contaminant masses in typical clarified lysates of a 50g prep prior to any RNA removal step. The masses of the contaminants are the average of the values determined from later sections for each as they exist in the clarified lysates. The plasmid masses are calculated from specific yield data taken by experiment (50μgg^{-1}WCW for BAC and 1400μgg^{-1}WCW for a high-copy plasmid typically encountered commercially).

Plasmid construct / Contaminant	Bacterial Artificial Chromosome (2.5mg)	High-copy optimised plasmid system (70mg)
Protein [~865mg]	1:346	1:12
Genomic DNA [~32mg]	1:13	1:0.5
RNA [~1100mg]	1:440	1:15

It was also supposed that the practical application of BAC constructs in a commercial process was highly unlikely. It was reasoned that a commercial process, no matter the plasmid size, would at the outset optimise the copy number to be as high as possible, together with making use of relaxed plasmid replicons which allow for a degree of control over copy number during the fermentation.

In contrast to the strategy of continuing with the Oxford series, several advantages were identified with altering the plasmid replicon to increase plasmid specific yield. It was reasoned that the use of large plasmids constructed using a high-copy replicon would be more representative of the course of action which would be taken should large plasmids needed to be produced commercially. It was hoped that the high-copy number replicon would increase the plasmid specific yield to levels that would enable accurate and precise detection and as such allow for the construction of a more representative plasmid mass balance. The reasoning behind this being that if more plasmid is present in the initial streams used for processing, the effect on yield by processing can be more confidently described.

An added advantage of pursuing this strategy, was that constructs could be generated which had more realistic sizes. Historically, the plasmid process being investigated, and indeed the overwhelming majority of alternative processes reported, had been used for the production of plasmid molecules less than 10kb in size. To immediately attempt to process plasmid constructs with size ranges in the order of 116kb – 242kb seemed too large an increment to increase the plasmid size by, without first having described the effects of processing on plasmids ranging from 10-100kb.

The advantages of probing the production process with plasmids constructed using relaxed replicons would not only be beneficial to the downstream stages but also to the upstream steps, since they provide scope for further increases in plasmid specific yield through alteration of process conditions.

The disadvantages of this strategy centred on the time required to create the new constructs and whether it was technically achievable. However, several reports have been published citing the creation of large plasmids under the control of relaxed replicons. Most notable and certainly influential in the decision to clone were (Wild *et al.*, 2002; Wild *et al.*, 1998) and (Tao and Zhang, 1998). Wild *et al.*, (1998/2002) reported a strategy solely based around correcting the problem of low yields produced from cultures bearing BACs. The principle involves retrofitting BAC plasmids with an inducible origin of replication (*oriV*). When the culture is induced using L-arabinose the BAC copy number is reported to increase from 1-2copies/cell to ~10-20copies/cell. Tao *et al.*, (1998) report the creation and stable maintenance of constructs over 300kb using conventional, relaxed plasmid vectors. Thus, it seemed that the strategy was indeed achievable.

To conclude this section involves summarising why the decision was taken to improve the specific yield of large plasmids using genetic based strategies. Although the decision matrix retains a degree of subjectivity, it was the most objective method which could be used to help in making the decision. It clarified the situation by highlighting the intuitive belief that continuing to use the Oxford series of plasmids was not a strategy which would capable of generating useful data. The problems surrounding the processing of these vectors had been demonstrated and it was judged that the issues remain pretty insurmountable. The fact that techniques as described by Wild *et al.*, (1998/2002) had been developed specifically to increase the yield of BACs when they were being used for small-scale, lab-based studies crystallised the notion that the troubles of making BACs on the lab-scale would be magnified if attempts were made to produced these constructs on a pilot-scale.

Consequently, although the cloning strategy was risky and unknown in its outcome, it was favoured as at least it promised to go to someway to alleviate the issues. Additionally, it was felt that it would be the strategy employed if this project were to be attempted commercially.

5.3 Attempts to create large constructs with a relaxed origin of replication

The methods attempted to create large plasmid constructs with relaxed replication control can be divided into three broad techniques.

1. Retrofitting of BACs with relaxed origin of replications
2. Sub-cloning of BAC inserts into relaxed plasmid backbones.
3. Shotgun cloning of large DNA fragments into relaxed plasmid backbones.

Of these three broad strategies only the last two were practically attempted but the first strategy was considered and as a result it is important to describe why it was not attempted. In the following sections details about the three strategies will be outlined.

5.3.1 Retrofitting BAC constructs with relaxed origin of replication

BAC vectors were developed by (Shizuya *et al.*, 1992) for use in genome research mainly for genome mapping and DNA sequencing. The main advantage of these constructs were that they enabled the stable propagation of large DNA fragments, but the main disadvantage was the low-yields at which they were propagated. It should be noted that this drawback was reported even on the laboratory scale where more intensive methods of preparation (not applicable to larger scale processes), such as caesium gradient centrifugation, could be pursued. In an attempt to alleviate this disadvantage Wild *et al.*, (1998, 2002) developed a method to retrofit the control elements of BACs such that copy number could be increased through an inducible origin of replication. (Wild *et al.*, 2002; Wild *et al.*, 1998).

The method involves an in vitro transposition reaction based on bacteriophage *Mu,* to insert a transposon sequence into the target BAC (Figure 5-1). The transposon, derived from bacteriophage *Mu*, is a linear, non-replicating dsDNA sequence containing *MuA* Transposase binding sites (R1 and R2) which flank an inducible origin of replication (*oriV*). It also contains a marker (Kan^R) for selection of recombinants in *E. coli*. In the method, *MuA* Transposase brings the ends of the transposon into close proximity to an homologous sequence in the BAC, forming a loop structure. The enzyme then cleaves the target BAC and covalently joins it to the transposon ends.

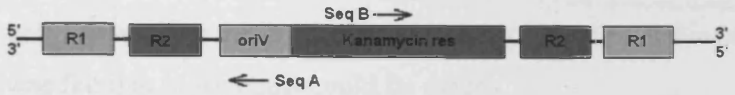

Figure 5-1 Schematic detailing the transposon used to increase the BAC copy number. The 690bp sequence contains the inducible origin (*oriV*) which initiates BAC replication upon binding to the TrfA protein. The sequence codes for Kan resistance allowing selection of recombinants. The flanking R1/R2 sequences are recognised by the *MuA* Transposase protein and used to insert the sequence into the BAC.

The recombinant BAC is then inserted into an engineered cell line and the transformants selected by kanamycin resistance. The cell line is engineered to express the replication initiation protein, TrfA under the control of an L-arabinose regulated promoter. When induced, by the addition of L-arabinose to the culture medium, the genome-based *trfA* gene is expressed and the resultant protein initiates the replication of the BAC through its action on the inserted *oriV* sequence. The inducible replication step is reported to raise the copy number of the BAC from 1-2 copies per cell to ~10-20copies per cell. The method was developed by Wild *et al.,* (1998) but the technology and materials sold under licence by Invitrogen (Invitrogen, 2006). An addition to this system was made in 2004 by the marketing of a BAC vector which already possessed the F-factor and *oriV* combination into which sequences could be cloned, thus removing the need to retrofit.

This method offered several advantages over competing methods. The product information (Invitrogen, 2006) states that the *in vitro* retrofitting reaction is relatively simple and short. Additionally, the technique effects no change upon the actual BAC molecule, except the transposon insertion, which would allow for the comparison of the original BAC vectors to the improved constructs. However, the method was accompanied by several disadvantages which resulted in this method not being attempted. The primary reason was that the system was designed for lab-scale systems, essentially the technique was developed to overcome the problem of low-yields faced by researchers attempting to purify sufficient BAC to sequence or to conduct gene-function studies. There existed, at the time of writing, no reports of the use of this technology at any scale larger than shake-flask. Furthermore, the materials are all supplied by the manufacturers, including the L-arabinose solution used to induce the culture, and sufficient provided to accommodate only small-scale reactions. Since no information was accessible as to the make-up of the L-arabinose solution used for inducement, it would be difficult to produce sufficient quantities to enable induction of pilot-scale fermentations.

An added problem was that the technology only promised to increase copy number up to 10-20 copies per cell. Comparing this to the 500-1000 copy number achievable with high-copy replicons it was felt that more gains could be made.

Furthermore it was felt that there remained several unknowns as to the feasibility of adopting this technique to the larger scale. A major consideration was the requirement to culture the plasmids in an engineered cell line of which little was known and which would be unlikely to be as adapted to the culture media as the in-house *E.coli* strain. Additionally, this protocol involved the expression of further sequences (kanamycin resistance and TrfA) which most likely would have a detrimental effect on the growth rates and productivity of the fermentation step.

As a result of the unknowns it was decided not to pursue this strategy. However, the technology should not be dismissed and it is suggested that this strategy could be investigated should serious attempts be made to manufacture Bacterial Artificial Chromosomes on the large scale. The strategy shares many of the advantages to those of inducible expression systems developed for recombinant protein production in that during the growth and exponential phase the copy number, and thus metabolic burden, can be minimised and that inducement towards the end of the fermentation leads to large increases in yield (Grabherr and Bayer, 2002).

5.3.2 Sub-cloning of BAC inserts into relaxed plasmid vectors

The first strategy attempted to create large plasmids under the control of a relaxed plasmid replicon, was to sub-clone the DNA inserts of the BAC Oxford series into a vector with a high-copy replicon. It was hoped by following this strategy that high copy number constructs could be generated which possessed the same insert as the original plasmids. In this way the direct effect of the replicon could be compared, by investigating the difference in yields between the original BACs and the high-copy derivatives. Figure 5-2 displays the principle behind the sub-cloning strategy.

Multiple rounds of cloning were attempted using this strategy. Three cloning vectors were employed; pBluescript, pUC4K and p7313-mi (a GSK DNA vaccine cloning vector). The methodology attempted was that commonly encountered during cloning regimes.

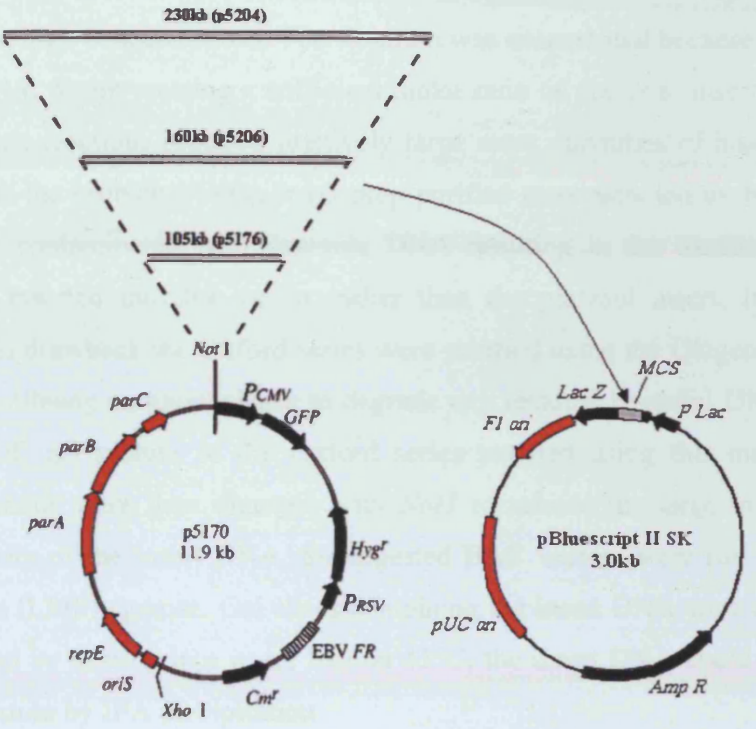

Figure 5-2 Schematic displaying the principle of the sub-cloning strategy. The large DNA inserts from the BAC vectors were excised by digestion with *Not1*. The fragments were then purified by gel electrophoresis and cloned into a *Not1* linearised high-copy vector. In the figure pBluescript is shown but other vectors were employed, including p7313-mi and pUC4K.

5.3.2.1 Preparing linear vector

Sufficient vector DNA was produced from a 5mL overnight culture of the *E.coli* strain bearing the relevant vector and purified using a Qiagen spin-prep. The vector was linearised at the multiple cloning site (MCS) using *Not1* and dephosphorylated to prevent vector religation using Shrimp Alkaline Phosphatase (SAP). The linear plasmid was then purified away from any remaining intact plasmid and restriction enzyme by gel electrophoresis. After staining, the linear vector was excised from the gel and purified using Qiagen gel extraction kit (Promega, 2004; Sambrook *et al.*, 1989)

5.3.2.2 Preparing insert DNA

The insert DNA was prepared from the BAC vectors of the Oxford series; p5176 (105kb), p5206 (160kb) and p5204 (230kb). Purified constructs were digested with *Not1* which released the insert DNA and left the insert fragments with complementary 'sticky ends' to those of the linearised cloning vector.

A major problem encountered with this cloning regime was obtaining sufficiently pure insert DNA at high concentrations. The situation was exacerbated because the large size of the insert DNA, meant creating a sufficient molar ratio of vector to insert DNA (e.g. 1:1) for the ligation reactions required relatively large mass quantities of insert DNA. Figure 5-3 highlights the problem. Using maxi-prep purified constructs led to the insert mixture being highly contaminated with genomic DNA resulting in the likelihood of genomic DNA being inserted into the vector rather than the plasmid insert. In an attempt to overcome this drawback the Oxford series were purified using the Qiagen Large construct kit (2.5.8.3) utilising an exonuclease to degrade any residual bacterial DNA. Figure 5-3B shows a FIGE gel picture of the Oxford series purified using this methodology. The purified plasmids were then digested with *Not1* to release the large inserts. To ensure complete purity of the insert DNA, the digested BAC vectors were run by FIGE in low melting point (LMP) agarose. Gel slices containing the insert DNA were then excised and the gel melted by heating in a water bath at 45°C, the insert DNA could then be purified from this mixture by IPA precipitation.

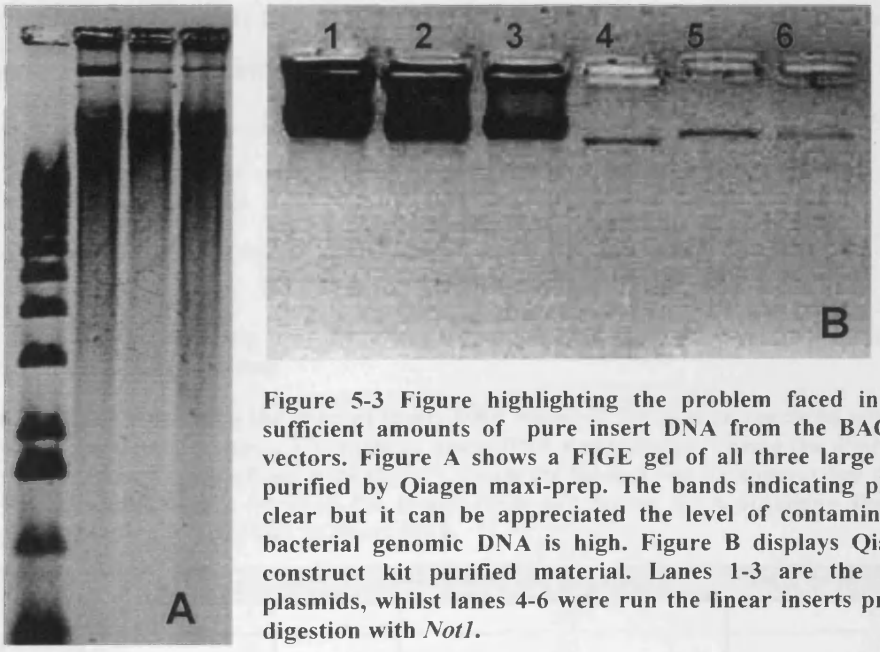

Figure 5-3 Figure highlighting the problem faced in obtaining sufficient amounts of pure insert DNA from the BAC series of vectors. Figure A shows a FIGE gel of all three large constructs purified by Qiagen maxi-prep. The bands indicating plasmid are clear but it can be appreciated the level of contamination with bacterial genomic DNA is high. Figure B displays Qiagen large construct kit purified material. Lanes 1-3 are the undigested plasmids, whilst lanes 4-6 were run the linear inserts prepared by digestion with *Not1*.

5.3.2.3 Ligations

During the ligation reactions the linearised cloning vector was mixed with the insert DNA. Because the vector had been dephosphorylated, it was prevented from religating spontaneously and since the insert DNA has complementary cohesive termini to the linear vector, there was a high probability of the insert and vector annealing. To maximise the chance of this occurrence the molar ratio of vector DNA to insert DNA was paramount. Included in the ligation mixture was *T4 DNA Ligase* (and ATP), added to promote the formation of phosphodiester bonds between the annealed insert and vector DNA, so as to create a stable recombinant DNA molecule (Sambrook *et al.*, 1989). Although the optimum activation temperature of this enzyme is 25°C, the ligation reactions were carried out, as is the norm, at 4°C. The lowered temperature would facilitate the formation of hydrogen bonds between the cohesive termini, which would be less likely to form at higher temperatures due to the greater molecular motion. In order to compensate for the low temperature causing low activity of the ligase enzyme, the reactions were allowed to proceed for ~24hrs.

Theoretically, the higher the ratio of insert DNA to vector DNA, the greater the probability of generating a recombinant molecule, however, this is not always the case so several ratios were attempted. The mass of insert DNA required for the individual ligation reactions was calculated using the relationship detailed in Equation 5-1

$$\text{Mass of insert DNA (ng)} = \left(\frac{\text{Mass of Vector DNA (ng)} \, x \, \text{Size of Insert DNA (kb)}}{\text{Size of Vector DNA (kb)}} \right) x \left(\frac{\text{Insert Ratio}}{\text{Vector Ratio}} \right)$$

Equation 5-1 Relationship used to determine the mass amount of insert DNA required when preparing a ligation reaction.

Table 5-4 Table detailing the mass of insert DNA required for ligation reactions when using three different insert:vector ratios. The mass of insert DNA was calculated using the above equation for ligation reactions using pBluescript (3.0kb). From the table it can be appreciated that due to the large differences in size between the insert DNA and vector DNA obtaining the molar ratios requires large mass quantities of insert DNA.

Insert DNA	Vector: Insert Ratio	Mass of vector DNA(ng)	Mass of Insert DNA (ng)
p5176 insert	1:1	20	693
(104kb)	1:3	20	2080
	3:1	20	231
p5206 insert	1:1	20	1067
(160kb)	1:3	20	3200
	3:1	20	355
p5204 insert	1:1	20	1533
(230kb)	1:3	20	4600
	3:1	20	511

Table 5-4 highlights the main problem encountered with this sub-cloning strategy, which was obtaining sufficient amounts of insert DNA to prepare the ligation reactions. The simple reason for this was that the large size of the DNA inserts required a far greater DNA mass to obtain the desired molar ratios. It should be noted that in traditional ligation reactions the mass of vector DNA typically used is 100-200ng (Promega, 2004). Using such a mass of vector DNA is achievable, for example, when cloning an insert fragment of 0.5kb (typical gene size) into pBluescript (3kb), as this would require only ~17ng of insert DNA to achieve a 1:1 ratio. However, using 100ng of vector was not applicable in this scenario, as to do so, each ligation reaction would require 10-20μg of pure insert DNA. Since restriction enzyme reactions are typically conducted on 1μg of plasmid, trying to generate such large quantities of insert DNA for a single ligation reaction would have been impractical, especially when considering the fact that multiple ligation reactions are commonly prepared in a single protocol. As a result, the starting mass of vector DNA had to be reduced to 20ng per reaction, such that the masses of insert DNA required were not as great. Although necessary, lowering the mass of vector DNA in a ligation reaction by $4/5^{ths}$ would have reduced the probability of a successful annealing event by the same proportion.

A second consideration concerns the concentration of the DNA segments used in the ligation mixture. As outlined before, the annealing of vector to insert DNA is a diffusion driven process. The low temperature incubation would have reduced the molecular motion of the ligation components, in order to allow formation of hydrogen bonds between cohesive termini when they come into contact. However, the reduced molecular motion would also reduce the occurrence of successful 'collisions', as predicted by the Arrhenius equation. Therefore, it is important that the insert and vector DNA are in high concentrations to improve the probability of successful 'collisions'. The problem in this protocol was that despite the insert DNA required being as concentrated as possible, the large masses required resulted in greater reaction volumes. For example, in a typical ligation reaction the total reaction volume is 10μL. In this protocol the lowest volume employed was 20μL, with the highest being 40μL. The larger volumes meant that the probability of successful collisions was further reduced. It was for this reason that in every ligation protocol carried out, a 3:1 ratio of vector to insert was prepared as this preparation requires less insert DNA and so the total ligation volume is reduced.

5.3.2.4 Transformation

The ligation mixtures were left for 24 hours in a 4°C water-bath, after which it was hoped that recombinant DNA molecules would have formed from the large insert DNA annealing with a linear, vector molecule. In order to clone this recombinant molecule it would need to be propagated in cells. In this project, in all but a few instances, it was decided to introduce DNA into cells using electroporation rather than chemical transformation. There are several reasons for this. The main one being that the electroporation has been demonstrated to be up to 10-fold more efficient than chemical transformation, with one study reporting 80% of cells receiving the foreign DNA (Miller and Nickoloff, 1995). It was hoped that this would go some way to alleviate the expected reduced efficiency of the ligation reactions by ensuring that any large recombinant molecules created would be transformed. Also, it had been demonstrated that this method is more applicable to the transformation of large DNA molecules (Sheng *et al.*, 1995; Siguret *et al.*, 1994).

Electroporation involves subjecting bacterial cells to high-voltage pulses, which are thought to lead to the transient formation of pores in the cell wall, through which DNA is driven by the electric field. The electric field is produced by the exponential discharge of a capacitor. Two parameters are key in determining the efficiency of electroporation; the field strength and the duration of the pulse. The field strength is determined by the potential applied as well as the width of separation of the plates found in the electroporation cuvette. In this project, the conditions employed were taken directly from Sheng *et al.*, (1995) using a voltage of 1.3kV across a plate separation of 0.1cm, meaning a field strength of $13kVcm^{-1}$. The second factor concerns the rate at which the potential is discharged. Again, using the parameters from Sheng *et al.*, (1995) the 10μF capacitor was set to discharge with an exponential waveform constant lasting 5ms.

Triplicate rounds of electroporation were conducted using 1μL samples from the same ligation mixture to maximise the chance of capturing any large recombinant plasmids. The electro-competent *E.coli* DH1 cells were prepared as outlined in (2.6.6) being careful to always maintain them at ~0°C. 24μL of electro-competent cells ($\sim10^9$ $cellsmL^{-1}$) were gently pipetted with the 1μL ligation mixture and placed between the conducting plates of a chilled 0.1cm width electroporation cuvette. Following pulsing, the cells were respuspended in pre-warmed SOC media and revived for two hours. The extended recovery period was used to increase the concentration of transformed cells prior to selective plating.

5.3.2.5 Selection

Selection of transformants was straight-forward since the revived cells could be plated out on LB agar plates containing ampicillin. Any cells capable of growing on the substrate must posses the vector-encoded Amp^r gene. Additional to this form of selection, in most cases blue-white screening could be employed (where the vector permitted it) to differentiate which of the transformants contained constructs where the insert had successfully ligated into the vector. Specifically, when attempting to clone into pUC4K and pBluescript vectors, the surface of the ampicillin selective plate could be spread with the chromogenic substrate (X-gal) and the *lacZ* inducer (IPTG) since these vectors carried the *lacZ* gene enabling blue-white selection. This technique exploited the fact that the MCS site, where the vector was linearised, falls in the open-reading frame (ORF) of the *lacZ* gene. If the vector was linearised and then re-ligated to itself, the ORF would have remained intact allowing full expression of the *lacZ* protein product; β-galactosidase. However, should the insert DNA have ligated into the vector, the ORF would be displaced meaning that no β-galactosidase would be produced. No expression of the β-galactosidase means that the chromogenic X-gal remains unhydrolysed and colourless. Hence, whilst the blue colonies could be ignored the white colonies contained possible constructs of interest (Ullmann *et al.*, 1967). It should be mentioned that in every cloning protocol controls were employed. The control ligations consisted of vector DNA ligation mixtures containing no insert DNA. From the colonies produced it was possible to record the efficiency of the ligation reaction.

5.3.2.6 Recombinant Screening

Colonies growing on the selective plates were sure to have contained vector DNA, and where blue-white screening had been employed, white colonies suggested the propagation of plasmids containing large, insert DNA. However, this was not a certainty since the vector could have re-ligated improperly causing incorrect expression of β-galactosidase, or the inserted fragment could be small, contaminating DNA. To identify large recombinant plasmids, sufficient material was purified and sized by gel electrophoresis. To do so involved picking off multiple colonies and inoculating 5mL of sterile, selective media in Universal bottles. Incubating these overnight generated sufficient cell material from which plasmid could be isolated by IPA precipitation of the clarified lysate. These were then be analysed by gel electrophoresis.

The colonies which were picked off were marked and the plates returned to the incubator to allow them to regenerate.

It was decided to attempt to identify colonies bearing large constructs by conventional gel electrophoresis. The simple reason for this being the large number of colonies which needed to be screened. To do this using FIGE would have been impractical since the system can run only 12 samples at a time with a run-time of ~20hrs. Using conventional gel electrophoresis the number of samples which could be processed concurrently was ~25, but also there was more than one gel tank enabling up to 70 colonies to be screened at the same time. Additionally, the run-time was ~2-3hrs. Although conventional gel electrophoresis could not determine the size of any large constructs, as it is only capable of resolving plasmids <20kb, it could be used to determine which clones were large, since they would run far behind the vector standards. Those that did so could be further characterised by FIGE.

Unfortunately, there were no instances where a large construct was identified using this sub-cloning protocol. Despite multiple rounds of cloning using different vectors and all three insert DNA fragments (104kb, 160kb and 230kb). In all cases, although white colonies were generated on the selective plates, when the constructs propagated by these colonies were screened they invariably consisted of re-ligated vector molecules which had incorrectly re-ligated causing improper expression of the β-galactosidase.

In a few cases, plasmids were seen which were larger than the original vector (e.g. Figure 5-4 Lane 8) but by only a small amount indicating the insertion of rogue DNA fragments.

5.3.2.7 Conclusions

The repeated failures of this sub-cloning protocol led to its abandonment after many

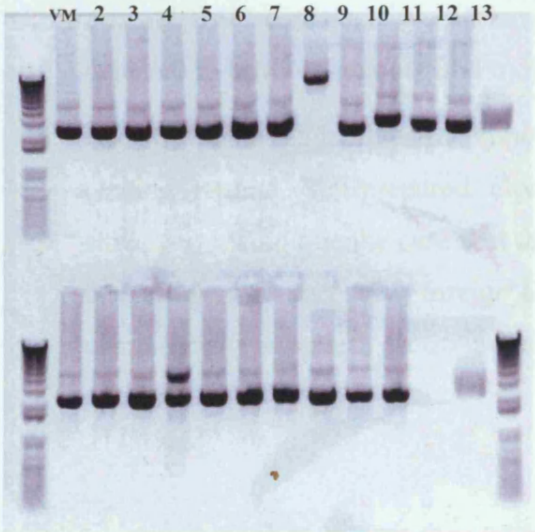

Figure 5-4 Example of a conventional gel run to identify whether any of the colonies transformed and selected contained large constructs. It was hoped that running conventional gels, any large constructs could be identified by moving far behind the vector marker (VM). However, apart from a few cases where small DNA fragments had ligated into the vector (e.g lane 8), no large constructs were identified. The colonies were found to be propagating re-ligated vector constructs since their size matched that of the vector standard on the gels.

attempts. It was reasoned that the failures could be due to a number of possibilities. Much was learnt from the failed attempts which led to alterations of later protocols used to generate large, high-copy plasmids. The reasons for failure could have included many of the following;

1. Difficulty of obtaining sufficient insert material. As with many issues faced so far with the Oxford series plasmids, obtaining sufficient amounts to prepare insert DNA was troublesome. Additionally, measures were needed to reduce the presence of contaminating gDNA in the preparations. All these factors led to great difficulty in preparing sufficient insert DNA. On top of this was the fact that to prepare ligation reactions using suitable vector:insert molar ratios required far more insert DNA, due to the large size of the insert DNA.
2. Reduction in the amount of vector material used to clone. To create the correct ratios of vector to insert DNA, the amount of vector DNA used in each ligation reaction was reduced so that the masses of insert DNA required were realistically obtainable. Doing so also reduced the chance of creating recombinant molecules.
3. Large ligation reaction volumes. The molar ratios employed dictated the use of set masses of insert DNA. Although the insert solutions were made as concentrated as possible (~100ngμL^{-1}), the large masses required led to larger ligation volumes. The final ligation mixture would be more dilute and so would have reduced the possibility of successful annealing.
4. Reduced probability of such large fragments ligating into the vector. The ligation reaction is essentially a stochastic process. The probability of fragments, over 30-fold larger than the vector, successfully ligating would be much lower than a conventional sub-cloning regime. However, it certainly must be possible since the original BAC constructs would have been created by the same techniques, but is believed to be more random and tricky procedure.
5. Use of 'home-made' electrocompetent cells. When attempting a standard sub-cloning regime, self-prepared electro-competent cells are normally adequate. However, it could be the case that for such large constructs the cells used were not that efficient at accepting foreign DNA. For this reason it may be useful to use commercially supplied electro-competent cells.

6. Use of *E.coli* DH1 cells. The electrocompetent cells were prepared from cultures of *E.coli* DH1 cells, since this was the host cell line most commonly used in this project and the one for which the media had been adapted. However, it may not be the most suitable cell line for accepting large, foreign DNA. Evidence from manufacturers suggests that DH10β is a better host-cell line for propagating large plasmids. Indeed, this was the cell line originally used for the propagation of the Oxford series.

5.3.3 Shotgun cloning

Having tried and failed several times to clone the inserts from the Oxford series into high-copy number vectors, a new strategy was attempted. The protocol for this was taken directly from (Tao and Zhang, 1998) who describe the 'cloning and stable maintenance of DNA fragments over 300kb in *Escherichia coli* with conventional plasmid based vectors'. In the report the authors cloned large fragments of eukaryotic DNA into several conventional plasmid vectors, notably the conventional plasmid vector (pGEM11), the binary plasmid vector (pSLJ1711) and the binary cosmid vector (pCLD04541). Contact was initiated with the group, but unfortunately they were unable to provide the clones created in the work. Consequently, it was decided to replicate their work using the pGEM11 vector from Promega, in which they managed to generate constructs ranging

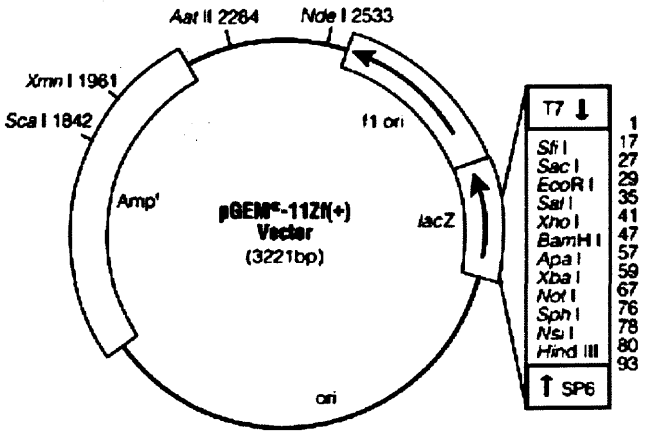

Figure 5-5 Map of the pGEM11 vector employed by (Tao and Zhang, 1998) to clone large segments of eukaryotic DNA. The vector is reported to have a copy number of 300-400 copies per cell, with the replication under control of the pMB1 replicon. Resistance is conferred by the beta-lactamase gene and it contains the *lacZ* gene allowing for blue-white screening.

from 40-100kb (Tao and Zhang, 1998). This vector is a high-copy number reported to have a copy number of 300-400 (Qiagen, 2005) under the control of the pMB1 replicon.

The precise cloning method used by (Tao and Zhang, 1998) was taken from (Hong-Bin Zhang *et al.*, 1995) who describe the technique of shotgun cloning. The technique is traditionally employed for the sequencing of entire genomes. The principle is simple and involves digesting genomic DNA using a restriction enzyme, followed by random ligation of the fragments into vectors. In this project that would be the main aim, whereas when sequencing the recombinant vectors would be sequenced and the sequence data patched together, from the linkage of overlapping sequences, to generate the sequence of the entire genome. The crucial end-point in this project was the generation of large, high-copy number vectors and as a result the actual content and make-up of the insert DNA was rather immaterial.

5.3.3.1 Vector Preparation

Vector DNA was prepared in an identical fashion to before. Sufficient pGEM11 was purified from an overnight culture. 1μg of plasmid was linearised by either *Not1* or *HindIII,* before being dephosphorylated by the addition of Shrimp Alkaline Phosphatase. The linear DNA species was purified away from the other contaminants in the mixture by gel electrophoresis. Following electrophoresis the marker lanes were cut away and stained in SYBR-Gold and the distances travelled used to identify the region on the gel where the linear plasmid would be. These regions were excised from the gel and the linear vector purified from the gel slices by Qiagen gel extraction kit.

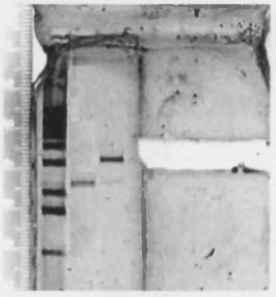

Figure 5-6 Figure displaying the preparation of linear vector DNA for cloning. The vector was linearised with either *Not1* or *HindIII* and dephosphorylated with SAP. The linear vector was purified away from the reaction components and other plasmid forms by electrophoresis. The marker lanes were cut-out and stained and used to mark the position of the desired fragments.

5.3.3.2 Insert Preparation

Insert DNA was prepared by the digestion of *Saccharomyces cerevisiae* gDNA with a single restriction enzyme. The main advantages of this method over the sub-cloning strategy were;

(i) The DNA used to generate the insert fragments could be obtained and digested in large amounts and was of high purity, since it was manufacturer supplied.

(ii) The large masses of DNA which could be used to create the insert DNA meant that the concentration of the insert DNA, following its purification from the gel, was far higher than could be obtained using the sub-cloning strategy.

(iii) The DNA could be digested into a range of fragments sizes, which meant that a series of plasmids could be produced and also allowed multiple ligations to be prepared for each cloning round, increasing the chances of success.

Two restriction enzymes were employed, in separate digestions, to create fragments of suitable length. These fragments were separated on a size basis by electrophoresis and then ligated into the linear pGEM11 vector.

The sizes of the fragments generated by digesting genomic DNA are dependent on the restriction enzyme employed and the extent to which digestion is allowed to run to completion. Figure 5-7 shows the extent of this variation, as it displays a gel on which samples of genomic *S.cerevisiae* DNA have been digested using three different restrictions enzymes. The three restriction enzymes recognise different sequences of DNA at which they cut the DNA. Naturally, the fewer bases the enzyme recognises, the more frequently it will cut the DNA molecule.

For example, *HindIII* recognises a 6bp sequence, so should cut the DNA every 4^6

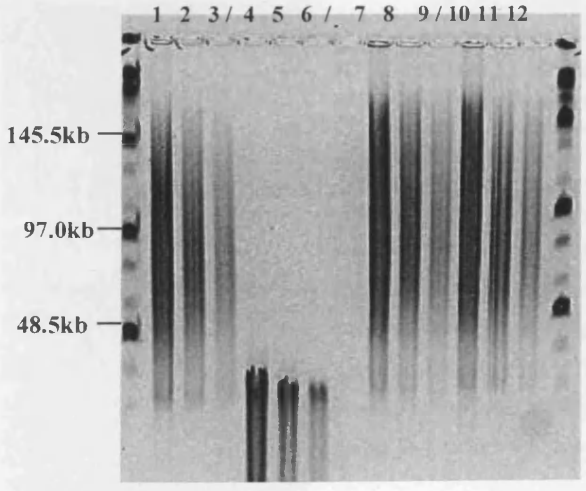

Figure 5-7 Figure displaying the effect of the restriction enzyme and the extent of digestion has on the size of the DNA fragments produced when digesting genomic DNA.

Lane 1-3: *Not1* (8bp cutter) [full digest]

Lane 4-6: *HindIII* (6bp cutter) [full digest]

Lane 7-9: *Not1* (8bp cutter) [partial digest]

Lane 10-12: *HindIII* (6bp cutter) [partial digest]

The three lanes for each are for digests on 2µg, 1µg and 0.5µg

(~4,000bp), whereas *NotI* is an 8bp cutter so should the cut the DNA only every 4^8 (~65,000bp). This frequency driven process dictates that the range of fragment sizes produced will be spread over a large range, but that that most occurrent would be fragments of the predicted size order. From Figure 5-7 it can be seen that the sizes of the fragments are smaller when exposed to *HindIII* than when using *Not1*.

The effect of incomplete digestion is also shown by the gel. Three different masses of DNA (2µg, 1µg, 0.5µg) were exposed to the same quantity of restriction enzyme and the effect of the extra substrate can be seen by the fact that the fragment sizes extend over a larger range. Control over the level of digestion can also be achieved by alteration of the temperature of the digestions. Shown in Figure 5-7 (Lanes 10-12) are partial digestions of DNA using *HindIII,* where the samples were kept on ice. The overall effect of this was to reduce the activity of the enzyme and so reduce the efficiency of the digestion step and hence increase the sizes of the DNA fragments produced.

During this cloning protocol two digestions were prepared; complete digestion of the gDNA using *Not1* and partial digestion of the gDNA using *HindIII.* The digests were prepared as outlined in Table 5-5, using the exact method of (Hong-Bin Zhang *et al.*, 1995).

A large amount of DNA (10µg) was prepared for Digestion 2, since *HindIII* is such a frequent cutter that providing excess substrate increased the size range of the fragments. Furthermore, the digests were incubated on ice for 2 hours and then at 37°C for 30 minutes to promote incomplete digestion.

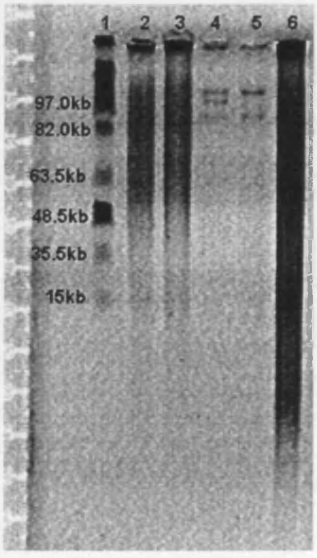

Figure 5-8 FIGE gel marker lanes. The digested *Saccharomyces* DNA was run by FIGE in 0.8% LMP agarose. The marker lanes were cut from the gel, stained and used to determine the position of the DNA fragments in the unstained section of the gel. Digestions of p5176 (116kb) are also shown to demonstrate the difficulty of obtaining sufficient DNA by the sub-cloning method compared to the shotgun cloning method.

Lane 1: Mid-range marker

Lane 2: *HindIII* digested gDNA (10µg)

Lane 3: *NotI* digested gDNA (10µg)

Lane 4: Undigested p5176 (3µg)

Lane 5: *NotI* digested p5176 (3µg)

Lane 6: Undigested *S.cerevisiae* gDNA

Table 5-5 Table displaying the digestions prepared to generate large fragment insert DNA. Two digestions were prepared one using *Not1* which was carried out to completion and once using *HindIII* which was only setup to partially digest the genomic DNA.

	DIGEST REACTION	gDNA VOLUME [MASS]	BSA VOLUME	BUFFER VOLUME	*NOT1* VOLUME [UNITS]
Digestion 1	Complete gDNA digestion (*Not1*)	11.8µL [2µg]	0.2µL	1.4µL	2µL [2U]
Digestion 2	Partial gDNA digestion (*HindIII*)	60µL [10µg]	1µL	6.3µL	1µL [10U]

Five sets of Digestion 1 were prepared separately, and the digests pooled afterwards, in order to prevent excessive substrate causing partial digestion. The reason being that *Not1* is an infrequent cutter, so as the preliminary gel shows, is capable of generating fragments in the right size order without enforcing partial digestion. These digestions were incubated at 37°C for 3 hours to promote complete digestion. All digestions were terminated by incubating at 65°C for 20 minutes.

The digested samples were run on a 0.8% Low Melting Point Agarose gel using the FIGE system, as shown by Figure 5-8. The digestions were run in duplicate, 10µg in each well, such that one half of the finished gel could be cut away, stained and used for determining the position of the fragments. The sections of gel lanes containing large fragments of interest were excised using a scalpel, placed in individual eppendorf tubes and dialysed in 1xTE+30mM NaCl overnight at 4°C. The gel slices excised contained fragments ranging from 30-85kb, in approximately 5kb increments.

Following dialysis, the TE buffer was replaced with twice the gel-slice volume (~100µL) of β-agarase buffer and left on ice for 30 minutes. This step was repeated twice. The gel slices were than melted by heating to 65°C for 10 minutes before being transferred to a 42°C waterbath to equilibrate. To each tube was added 3 units of β-agarase, an enzyme which facilitates the digestion of the carbohydrate in the agarose, which after 2 hours was almost fully digested. The tubes were then placed on ice for 30 minutes to coagulate any remaining agarose moieties, before they were sedimented away by centrifugation at 13,000rpm for 5 minutes. The DNA fragments in the liquour were then purified by IPA precipitation before being resuspended in 100µL of TE buffer. These solutions were then quantified by absorbance.

5.3.4 Ligations

Ligations were prepared as described by (Hong-Bin Zhang *et al.*, 1995) by using a 5:1 ratio of vector DNA to genomic insert DNA. In contrast to the sub-cloning strategy, the ligations were prepared using a constant mass (50ng) of insert. The ligations were prepared as detailed in (2.6.3). The mass of vector required was calculated using the relationship shown in Equation 5-2.

Equation 5-2 Relationship employed to calculate the mass of linearised vector required to form a 5:1 molar ratio of vector to insert DNA in the ligation mixtures.

$$\text{Mass of pGEM11 vector required (ng)} = \text{size of vector (kb)} \times \left(\frac{\text{mass of insert (ng)}}{\text{molar ratio} \times \text{insert size (kb)}} \right)$$

The size of the insert was an estimation based upon the region of the gel from which the slice was extracted. Ligation controls were also prepared to determine the efficiency of the ligation and transformation steps. The negative control consisted of linearised pGEM11 vector, which had not been dephosphorylated, whilst the positive control consisted of linearised vector which had been dephosphorylated. Once the insert and vector DNA solutions had been mixed together, but prior to the addition of the T4 ligase and ligase

Table 5-6 Table outlining the makeup of the ligations. Ligation reactions were prepared using a constant mass of purified insert DNA (50ng). The mass and volume of the vector required was then calculated on the basis of a 5:1 vector to insert molar ratio. The sizes of the insert DNA was estimated from the region of the gel the slice was extracted as measured against the linear DNA marker. T4 DNA ligase was added at volume rate of 0.02U/µL together with the ligase buffer in 0.1vol proportion.

		Insert Size (kb)	Insert Conc. (ng/µl)	Insert Volume (µl)	Mass of Vector (ng)	Vector Volume (µl)	Units of Ligase (U)	Ligase Volume (µl)	Ligase 10x Buffer Vol (µl)	Total Volume (µl)
Not I Digested	A	30	1.38	36.2	27	2.7	0.8	0.3	3.9	43
	B	50	1.45	34.5	16	1.6	0.7	0.2	3.6	40
	C	55	1.54	32.5	15	1.5	0.7	0.2	3.4	38
	D	60	1.99	25.1	13	1.3	0.5	0.2	2.7	29
	E	65	2.09	23.9	12	1.2	0.5	0.2	2.5	28
	F	70	2.5	20.0	11	1.1	0.4	0.1	2.1	23
	G	75	2.89	17.3	11	1.1	0.4	0.1	1.8	20
	H	80	2.44	20.5	10	1.0	0.4	0.1	2.2	24
	I	85	1.57	31.8	9	0.9	0.7	0.2	3.3	36
Hind III Digested	A	20	0.48	104.2	40	4.0	2.2	0.7	10.9	120
	B	25	0.73	68.5	32	3.2	1.4	0.5	7.2	79
	C	30	0.82	61.0	27	2.7	1.3	0.4	6.4	70
	D	35	0.27	185.2	23	2.3	3.7	1.2	18.9	208
	E	40	0.38	131.6	20	2.0	2.7	0.9	13.4	148
	F	45	0.62	80.6	18	1.8	1.6	0.5	8.3	91
	G	50	0.58	86.2	16	1.6	1.8	0.6	8.8	97
	H	55	0.31	161.3	15	1.5	3.3	1.1	16.4	180
	I	60	0.42	119.0	13	1.3	2.4	0.8	12.1	133
	J	65	0.37	135.1	12	1.2	2.7	0.9	13.7	151

buffer, the solution was incubated at 56°C for 10 minutes to promote molecular motion and annealing. The solutions were left to cool to room temperature before addition of the T4 ligase. Ligase was added at a volume of 0.02 units per μL ligation volume. All the ligation reactions were then incubated overnight (~16hrs) at 4°C as described by (Promega, 2005). The setup of the ligation reactions is detailed in Table 5-6.

5.3.4.1 Transformation

Following overnight incubation, 1μL of each ligation reaction was transformed into *E.coli* by electroporation using the same methodology and parameters as detailed before in 5.3.2.4. One adaptation was made to the protocol in order to improve the success rate, which was to use commercially supplied electrocompetent cells. It was reasoned, after the failures of the sub-cloning strategy, that one possible cause of no large constructs being isolated was that there could have been problems in the electroporation step. The sub-cloning strategy employed self-prepared electrocompetent cells which had been washed several times with a 10%(v/v) glycerol solution to remove any media components, namely salts and other electrolytes. The presence of these lead to conductance when electroporation is attempted and so reduce the step's efficiency. However, it was felt that self-prepared cells would still contain some of these contaminants. Secondly, the sub-cloning strategy used *E.coli* strain DH1, which is believed to be not the most suitable strain for accommodating large constructs. There is data to suggest that DH10β is a more suitable strain for cloning and transforming of large constructs (Hanahan *et al.*, 1991; Donahue, 1998; Eastman and Durland, 1998) due to mutation in the *deoR* gene. In response to these issues it was decided to use the ligation mixtures to transform commercially obtained ElectroMAX DH10β cells (Invitrogen).

5.3.4.2 Selection

Following electroporation the transformed cells were revived and selected as outlined before in 5.3.2.5. Blue-white screening was used since the vector did contain the *lacZ* gene. The results of the screening were mixed. Cells transformed using DNA inserts prepared using *Not1* digestion of genomic DNA were few and not really above the background level of ligation, as determined by comparison to the negative control plates. As a result no colonies were picked from these plates as it was reasoned that there would not be a great possibility that they contained large constructs.

The results from the ligations using *HindIII* digestion of genomic DNA were more successful. Many more white colonies were present than on the control plates, suggesting that ligations had been successful. Consequently, ten colonies from every insert size ligation plate (Table 5-6 *HindIII* A-J) were picked off and transferred to fresh, selective plates (25μgmL^{-1} ampicillin) which were incubated at 30°C overnight. This was done to prevent the selection of satellite colonies. All of the selected colonies grew on the plates indicating that they were not satellite colonies and did posses the β-lactamase gene encoded on the pGEM11 plasmid. These strains were then used to inoculate 5mL of sterile, selective media in Universal bottles and incubated overnight to generate sufficient cell mass from which to extract plasmid for screening.

5.3.4.3 Screening

Since 10 colonies were selected from each of the ten plates, 100 colonies were passed to the screening stage. As described before this involved culturing sufficient cell mass from which to purify plasmid, which could then be analysed by electrophoresis to identify colonies bearing large constructs. Several rounds of electrophoresis were required to

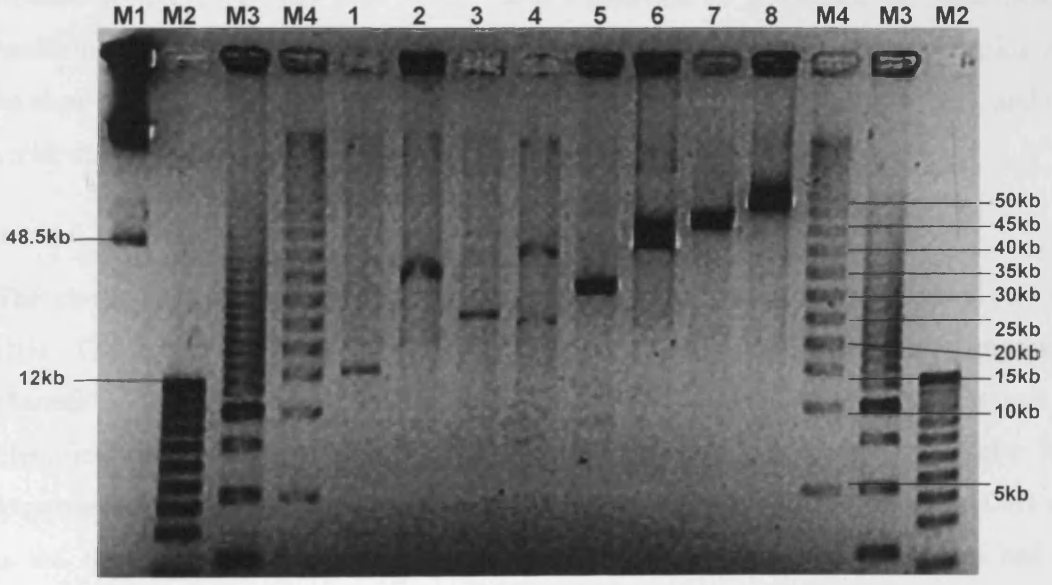

Figure 5-9 FIGE gel image of four large constructs isolated from the screening stage. Several rounds of screening were required to identify large constructs from the 100 colonies selected for scrutiny. The plasmids were run in their native state and also linearised using *Not1*.

M1: λ DNA	**Lane 1: Clone 3 (linearised)**	**Lane 5: Clone 52(linearised)**
M2: 1kb ladder	**Lane 2: Clone 3 (native)**	**Lane 6: Clone 52 (native)**
M3: 2.5kb ladder	**Lane 3: Clone 31 (linearised)**	**Lane 7:Clone 74 (linearised)**
M4: 5kb ladder	**Lane 4: Clone 31 (native)**	**Lane 8: Clone 74 (native)**

Gel was run for 20hrs/ 0.8% PFGE agarose/ Fwrd 180V/ Reverse 120V/ 0.1s-1s/ 0.5xTBE

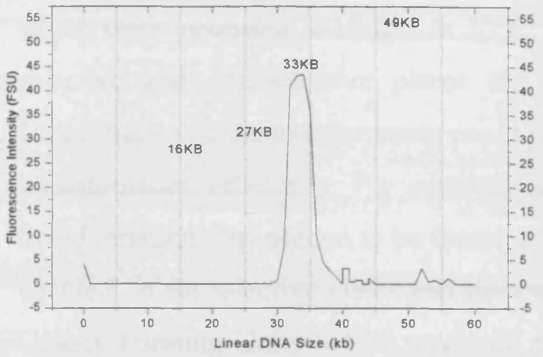

Figure 5-10 Results of a gel scan on the lanes carrying the linearised forms of the newly created plasmids (Lanes 1, 3, 5, 8). After staining the gel was visualised under a UV transilluminator. The image was analysed using UVP software and the positions of the marker bands marked and the software plotted the fluorescence levels recorded down the lanes and subtracted the background noise. The results of this indicates the size of the constructs.

identify large constructs using FIGE system. Fortunately, the presence of large constructs was confirmed, meaning that this method of cloning had been successful. However, it had been hoped to obtain a range of plasmids ranging between 10-100kb. Unfortunately, the approximate size of the largest construct isolated was ~50kb. The final four constructs were identified in the gel shown in Figure 5-9 and the results of the gel scan shown in Figure 5-10.

From the FIGE gel and the associated scan it can be appreciated that this shotgun cloning strategy had been more successful than the sub-cloning attempts. Four constructs had been isolated with sizes greater than 10kb. These constructs all possessed the same pGEM11 backbone, the replication of which is high-copy. It was hoped that these plasmids would be more conducive to investigation as they should exist at higher copy numbers, and hence yield, than the BACs.

5.3.4.4 Cell Banking

The clones selected by the initial screening procedure were transferred to *E.coli* strain DH1. The ligation mixtures were initially transformed into DH10β cells to improve the chances of isolating large constructs. Since colonies bearing large constructs had been identified, these could be transformed into prepared electrocompetent DH1 cells. It was important for reasons of consistency to use the same cell line and also since the DH1 strain is the strain to which the media, fermentations and downstream operations had been optimised for.

This step allowed the investigation into the efficiency by which large plasmids are transformed. Both (Siguret *et al.*, 1994; Sheng *et al.*, 1995) report the decreasing efficiency by which cells are transformed as plasmid size increases. The electroporation was carried out, as detailed earlier, using 200ng of each purified construct, and after revival, dilutions of the broth were plated out on to both selective and non-selective plates,

which were incubated overnight at 30°C. By counting the colonies produced on both the selective and non-selective plates the concentration of cells in the broth and the concentration of the transformants could be found. The ratio between these is a measure of transformation efficiency. For comparison to published data the molar efficiency of the transformation step needed to be found. This requires the number of transformant colonies counted on the selective plates and the measures efficiency on the basis of the number of Colony Forming Units (CFU) produced per unit mass of DNA used. The details of how these measures of efficiency were calculated are detailed in Equation 5-3.

$$\text{(A) Transformant Ratio} = \frac{\text{Concentration of transformed cells}}{\text{Concentration of cells}}$$

$$\text{(B) Molar Transformation Efficiency (CFU/}\mu\text{g)} = \left(\frac{\text{CFU on selective plate}}{\text{Mass of DNA used (ng)}}\right) x\,1x10^{3}\, x \left(\frac{\text{Volume of Transformants}}{\text{Volume plated}}\right) x\,\text{Dilution Factor}$$

Equation 5-3 Equations used to calculate the efficiency of the electroporation event. Published data has described how increasing plasmid size reduces the efficiency of the electroporation. These relationships were used to determine whether a drop in transformation efficiency could be seen when electroporating the large constructs generated into *E.coli* DH1. The transformation efficiency measure shown in A records the proportion of cells transformed by the electroporation step, whilst equation B was used calculate the efficiency of the transformation in terms of the number of transformants generated per unit mass of DNA used.

The results of this investigation into plasmid transformation can be seen in Table 5-7. As a control, the investigation employed a commercially supplied pUC plasmid (2.8kb). The table lists the colony number from which the construct was isolated which are listed in the order of increasing size. The figures in the ratio column displays the ratio of transformed cells to cell non-transformed cells. A slight decrease in transformation efficiency with increasing plasmid size was witnessed, but not in any large amount.

For instance, (Sheng *et al.*, 1995) described a 20-fold drop in transformation efficiency when the plasmid size increased from 150kb to 240kb. In this study the level of transformation stood at one cell in every 2,000-3,000.

Table 5-7 Table describing the two measures used to record transformation efficiency (emboldened) . The first method calculates the proportion of cells transformed, whilst the second method records the efficiency of transformation on the basis of the number of cells transformed per unit mass of DNA.

Colony No.	CFU(Non Selective Plate)	Cell Conc. (Cells/Ml)	Cfu (Selective Plate)	Transformed Cell Conc. (Cells/Ml	Transform Ratio	Mass Of DNA Used (ng)	Transform Efficiency (CFU/mg DNA)
pUC (2.8kb)	130	$1.30x10^9$	26	$5.20x10^3$	250,000	0.2	$2.6x10^8$
3 (16kb)	115	$1.15x10^9$	509	$5.09x10^5$	2,260	200	$2.55x10^6$
31 (27kb)	120	$1.20x10^9$	108	$1.08x10^5$	11,100	200	$5.40x10^3$
52 (33kb)	81	$8.10x10^8$	244	$2.44x10^5$	3,319	200	$1.22x10^6$
74 (49kb)	77	$7.70x10^8$	197	$1.97x10^5$	3,908	200	$9.85x10^5$

This ignores the result obtained for the construct obtained from colony 31, which has the poorest level of transformation at one cell in every 11,000. This result is reasoned to be anomalous and thought to be due to poor electroporation conditions rather than the actual construct. The apparent poor transformation efficiency of the pUC plasmid is explainable due to the reduced amount of DNA which was used in the electroporation. The reason for the difference was that the instructions supplied by the vendor were being followed, which outlined the use of 200pg of vector per transformation. Since the control reaction used a 1000-fold less DNA, the corrected transformation ratio would stand at 1 cell transformed in every 250 cells, roughly a 10-fold improvement on the other constructs.

This requirement for correction is removed when the compared efficiencies are those determined on a unit mass of DNA transformed, as shown in the last column of Table 5-7. From these figures it can be appreciated that the average transformation efficiency for the pGEM series is ~$1.5x10^6$ CFUs/μgDNA. These values are far below comparable figures reported by (Sheng *et al.*, 1995) where efficiencies in the order of $4.4x10^8$CFUs/μgDNA were reported for electroporation of 80kb BAC using identical conditions as used in this study. The value for the efficiency of the pUC transformation is very comparable to those reported in the cited report. It is believed that poor preparation of the DNA used for transformation must be the reason for the reduced efficiency. Overall, there is a ~60% reduction in transformation efficiency between the transformation of the construct isolated from colony 3 (16kb) to the construct isolated from colony 74 (49kb).

However, as evidence by the pUC control and the poor result of the transformation for colony 31, it is thought that the overriding factor influencing transformation efficiency is the quality of the DNA used for the electroporation and not the size of the constructs per se.

One colony from each of the construct transformations was picked from the selective plates and transferred to 5mL of sterile media in Universal bottles. These were incubated overnight and used to seed 50mL of selective media in shake-flasks. These were incubated in a shaking incubator until the optical density reached 2-3OD, when they were aliquoted into cryovials as 20%(v/v) solutions of glycerol and stored at -80°C. These represented the master cell bank.

5.3.5 Conclusions

After numerous cloning attempts large constructs had been isolated by employing a shotgun cloning strategy. The main aim of the cloning effort had been to create a series of large plasmids under the control of a high-copy number replicon. In that sense the operation had been a success. It had also been hoped that the series of plasmids produced would be in the size order of 10-100kb. It was felt that since the vast majority of published data, and current production systems, were concerned with the manufacture of plasmids in the 3-10kb size range a jump to plasmids of 116-242kb in size was too large an increment. Consequently, by obtaining plasmid constructs in this size order should allow a more reasoned approach to determining potential problems with large-plasmid manufacture.

It was decided to drop the 27kb pGEM construct from further investigation. It was felt that the size increment between 27kb and 33kb was not great enough to justify the additional investigation of this construct. As a control, the pGEM11 (3.2kb) would be studied, as would the smallest of the Oxford series used so far; p5176 (116kb). Although this BAC was under the control of a completely different replicon, its inclusion was warranted since it represented the alternative strategy of producing large plasmids i.e. through the use of large, low copy constructs. Figure 5-11 displays a FIGE gel of the five constructs taken on to further study.

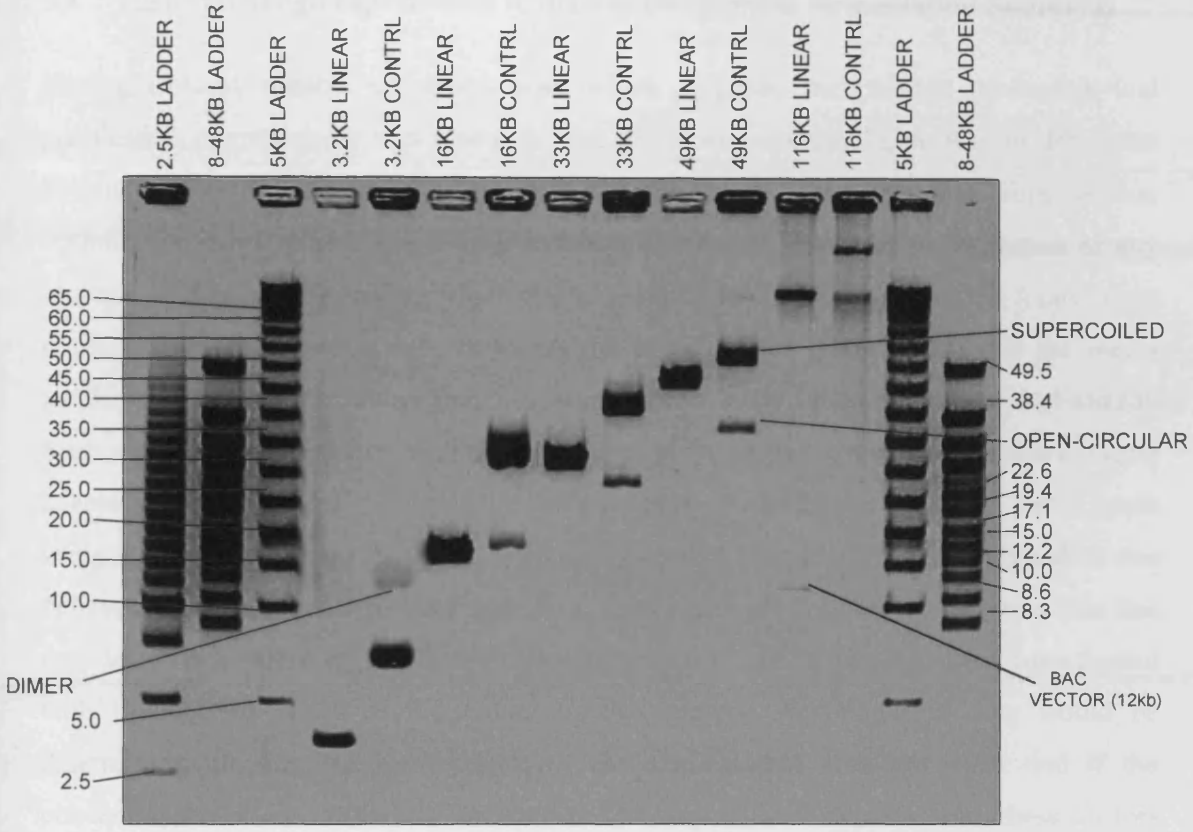

Figure 5-11 FIGE gel of the plasmid constructs which were taken on to further study. The constructs were analysed in both their native and linearised form. Five constructs were taken on to further study; pGEM11 (3.2kb), pGEM16 (16kb), pGEM33 (33kb), pGEM49 (49kb) and p5176 (116kb).

5.4 Factorial design experiments to determine optimum fermentation conditions

Having isolated suitable constructs with which to probe the plasmid production and purification operations, it was reasoned that the most important issue was to determine optimum conditions by which to produce the constructs by fermentation. Fermentation optimisation is of critical importance to the efficient and economical production of any biologic, and is key in deciding whether a process is permissible. Much of the focus, when optimising a fermentation step, concerns the mode of the fermentation and the media employed. However, for the production system under study, these parameters had already been optimised. The process would utilise a glycerol supplemented, complex media adapted to the DH1 cell line, and the fermentation would be conducted in batch mode using enriched air toward the finish to improve harvest biomass (volumetric) yield. It was believed that the more important aspects to ascertain were whether the plasmid size had any deleterious effect on the fermentation progression; much like had been investigated with the Oxford series at the outset of this project. Additional to this, would be determining whether the temperature of the fermentation was important and if the concentration of the antibiotic employed had any effect. Reports into these factors suggested that they were important when propagating large plasmids (Promega, 2005).

Due to the number of continuous variables which were to be investigated it was felt that the most efficient method of achieving the aims was to conduct the optimisation studies in shake-flasks, where more replicates could be analysed. Furthermore, as is common when optimising media for fermentations, the investigations would employ techniques of experimental design to improve the results obtained, as well as reducing the number of runs required.

5.4.1 Design of Experiments (DOE)

Conventional experimental methods are based upon the "one factor at a time" (OFaT) methodology, involving the manipulation of one variable, while keeping the remaining factors constant. The drawback with this methodology is that it is very inefficient, a fact that becomes apparent when the studies require the investigation into the effects of multiple continuous variables. In addition, traditional OFaT methods of experimentation provide an estimate of the effect of a single variable at a selected, fixed set of conditions of all other variables.

For such an estimate to have a general relevance, it is necessary to assume that the effect would be the same at other settings of the other variables, that is, over the ranges of current interest the variables are said to act on the response additively (Box *et al.*, 1978). Because of this, OFaT experiments can only provide information on the main effect that is being varied and give no indication of any interactions which may exist between the factors.

The application of statistical design techniques, such as factorial design and response surface methodology (RSM), to process optimisation offers numerous advantages when compared to traditional experimental techniques including;

(i) Greater efficiency and less time consuming than OFaT techniques, allowing the determination of optimum conditions through a relatively smaller number of systematic experiments (Box *et al.*, 1978; Ficarra *et al.*, 2002).

(ii) Generation of equivalent data to traditional techniques but with additional precision.

(iii) If the variables do not act additively, statistical design techniques, unlike the OFaT design, can also detect and estimate interactions that measure the non-additive effects and gives an accurate description of an experimental region around a centre of interest with validity of interpolation (Box *et al.*, 1978).

(iv) Experimental measurements are performed by varying all the factors simultaneously, providing the ability to estimate the effect of a factor at several levels of other factors and thereby allowing the conclusions made to be valid over a much wider range of experimental conditions (Ficarra *et al.*, 2002).

(v) Compared to empirical methods, statistical design can greatly simplify optimisation. When the concern is which combination of two independent variables will produce a maximum or minimum response the factorial will give a combination near the maximum, whereas OFaT would not (Hicks and Turner, 1999).

(vi) In cases where maximum or minimum has not been reached, factorial techniques will indicate the direction to be followed in the next experiment to get closer to such a maximum (Hicks and Turner, 1999).

With these advantages, statistical design techniques, coupled with an appropriate knowledge of the subject matter, can provide the most effective means of analysing a process. Techniques such as response surface methodology have been successfully used since the 1950s on a wide range of investigations in numerous disciplines. (Chakravarti, 2002; Arroyo *et al.*, 2005; Garcia-Arrazola *et al.*, 2005; He *et al.*, 2004) applied the methodology to establish the optimum operational conditions, including pH, temperature, aeration rate, feed rate and media composition to maximise the performance of a fermentation operation in terms of product yield. The motivation for the use of these techniques in this project was to identify optimum conditions for the fermentations of large plasmids. A full description of factorial design and RSM techniques may be found elsewhere (Montgomery, 2001).

5.4.2 Experimental setup

Response surface methodology (RSM) can be used to map the effect on a measured (response) parameter made by manipulation of a set of defined variables (factors). The methodology which is described in greater detail in (Montgomery, 2001) consists of a number of steps including;

1) *Recognition of the problem and development of all the ideas about the objective of the experiment that is to be designed.*
2) *Establish the factors and the levels and range at which they are to be varied.*
3) *Selection of response variable(s).*
4) *The choice of experimental design involves the consideration of the sample size (i.e. the number of replicates), selection of a suitable run order for the experimental trials and establishment of any blocking, other randomisation restrictions or identification of any additional design features to be applied.*
5) *Set up of a mathematical model to describe the experiment (Use of Stat-Ease)*
6) *Experimental data collection can begin with the investigations performed in run and block order.*

The identification of each factor and the range over which it will be allowed to change in the investigations requires prior knowledge of the process under study. The factors believed to be the most influential are used in the response surface design.

In all statistical designs, presented in this investigation, three levels were assigned to each variable and represent the allowable limit, which are the maximum and minimum and an intermediate value. The final relationship determined would hold within these limits. Additionally, in all the designs the centre repetitions were carried out in order, as this allowed the derivation of the experimental error variance and to test the predictive validity of the model (Ficarra *et al.*, 2002). In this case, three response parameters were to be mapped by experimental design investigations, using a mathematical model which was created using Design-Expert 5® Software and which analysed the results.

As described earlier the chosen factors were temperature, ampicillin concentration and plasmid size. The chosen responses which would be recorded were those felt to be the most important to optimise and were; culture growth rate, final plasmid specific yield and final volumetric yield (a response dependent on the final biomass and specific yield). The required factors and responses were inputted into Design Expert and a D-optimal design was chosen. It was decided to conduct all the runs in parallel, as this would require only one experimental block, and so reduce the possibility of intra-block experimental variation.

Table 5-8 Table outlining the creation of the D-optimal model used to monitor the effect that manipulating the three factors (Temperature, Ampicillin concentration and Plasmid size) had on three recorded responses (Growth rate, Final specific yield and Final volumetric yield) in 50mL cultures in shake-flasks. The model predicted that 18 shake-flask runs would be required to gather the information and gave the model a very acceptable G-efficiency of 74.3%

Design Summary							
Study Type	Response Surface		Experiments	18			
Initial Design	D-optimal		Blocks	No Blocks			
Design Model	Quadratic						
Response	Name	Units	Obs	Minimum	Maximum	Trans	Model
Y1	Growth rate	hrs-1	18	0.3698	0.8798	None	RQuadratic
Y2	Final specific yield	mg/L	18	6.63317	290.594	None	RQuadratic
Y3	Final Volumetic Yield	g/L	18	27.15	51.55	None	Linear
Factor	Name	Units	Type	Low Actual	High Actual	Low Coded	High Coded
A	Temperature	C	Numeric	25	37	-1	1
B	Ampiciliin conc	ug/mL	Numeric	0	200	-1	1
C	Plasmid size	kb	Numeric	16	49	-1	1

Maximum Prediction Variance = 0.748
Average Prediction Variance = 0.556
Condition Number of Coefficient Matrix = 4.07325
G Efficiency = 74.3%
Scaled D-optimality Criterion = 2.247

Table 5-9 Table describing the experimental setup of the D-optimal design. The model predicted that 18 shake-flask runs would be sufficient to gather the required information. The experiments allow the detailed prediction of the effect of manipulating each of the factors together with recording effects produced by interaction which may occur between the manipulated variables. The table also shows the measured responses produced after the experimentation, which were inputted into the model and used to create the response curves.

	FACTORS			RESPONSES		
RUN	Temperature (°C)	Ampicillin (μgmL^{-1})	Plasmid size (kb)	Growth Rate (hrs^{-1})	Final Specific Yield (μgg^{-1})	Final Vol. Yield (mgL^{-1})
1	25	0	49	0.404	7.25	0.339
2	25	200	49	0.445	8.62	0.399
3	37	200	49	0.774	12.69	0.464
4	31	100	16	0.709	177.8	8.274
5	25	0	16	0.374	106.8	4.0
6	31	0	33	0.788	8.76	0.337
7	37	0	16	0.723	246.5	6.97
8	31	100	16	0.725	219.5	11.32
9	37	0	49	0.815	6.63	0.194
10	37	200	16	0.723	235.3	9.022
11	25	0	33	0.417	11.63	0.456
12	37	0	49	0.880	6.75	0.227
13	37	100	33	0.860	8.91	0.308
14	25	200	33	0.424	10.17	0.401
15	31	200	49	0.698	10.10	0.389
16	37	0	16	0.810	290.59	8.718
17	25	200	16	0.370	107.9	4.851
18	37	200	16	0.705	279.7	7.594

As a result, the chosen model possessed a G-efficiency (a measure of accuracy) of 74.3%. Model efficiency between 70-80% is highly desirable when designing the experimental setup. The software determined that a series of 18 shake-flask runs were required to be run in parallel.

The 1L Shake-flasks were prepared as outlined in Table 5-9 using 50mL of sterile media, and the desired volume of selective agent to produce the required concentration. One vial of working cell bank, of the appropriate construct, was used to inoculate the media to a starting optical density of 0.2. The shake-flasks were then placed one of the corresponding shaking incubators, which had been temperature mapped to ensure each was at the desired temperature of either 25°C, 31°C or 37°C.

Growth of the cultures was monitored on an hourly basis by recording optical density progression. These points were used to calculate the growth rate. When the cultures were deemed to have reached stationary growth phase their incubation was stopped. Samples were extracted and used to determine the final biomass yield.

Additionally, triplicate 5OD volumes of broth were taken from each shake-flask, spun-down and the plasmid extracted by Qiagen spin-prep and used to calculate the plasmid specific yield at harvest. Once the data had been collated, as demonstrated in Table 5-9, it was inputted into the Stat-Ease model which generated the response curves.

5.4.3 Data Analysis

The results from the factorial design experiments were inputted into the D-optimal model and used to create response curves. It was found that altering the ampicillin concentration had minimal effect on any of the responses measured. The response curve where changing the ampicillin concentration had the greatest demonstrable effect is shown in Figure 5-12. The profile shows a slight downwards skew, but less than a 5% decrease in growth rate, as the ampicillin concentration was increased from 0 to 200μgmL^{-1}. For that reason, the response curves shown in Figure 5-13 are normalised with respect to ampicillin concentration, which is fixed at 100μgmL^{-1}. What is important to note from the response curve, shown in Figure 5-12, is the effect that plasmid size has on growth rate. The response is not linear, rather the fastest growth rates are witnessed for the intermediate sized construct, with the maximum and minimum sized plasmids causing a reduction from this maximum rate.

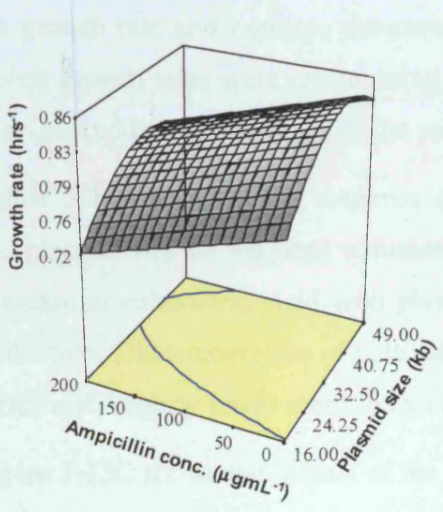

Figure 5-12 Response curve generated for the combined effect of ampicillin concentration and plasmid size on culture growth rate, normalised at 37°C. The small contributory effect of altering the antibiotic concentrations is evidenced by the downward skew in growth rate produced by increasing the antibiotic concentration from 0-200μgmL^{-1}. The graph also shows the effect of the construct size on the growth rate, which was found to be the greatest for the intermediate sized construct, with propagation of the 16kb and 49kb constructs reducing growth rate.

The curves generated for the effect of the other two factors (temperature/ plasmid size) on the three responses are shown overleaf in Figure 5-13. Figure A plots how the temperature and size of the plasmid combine to affect the growth rate of the cultures.

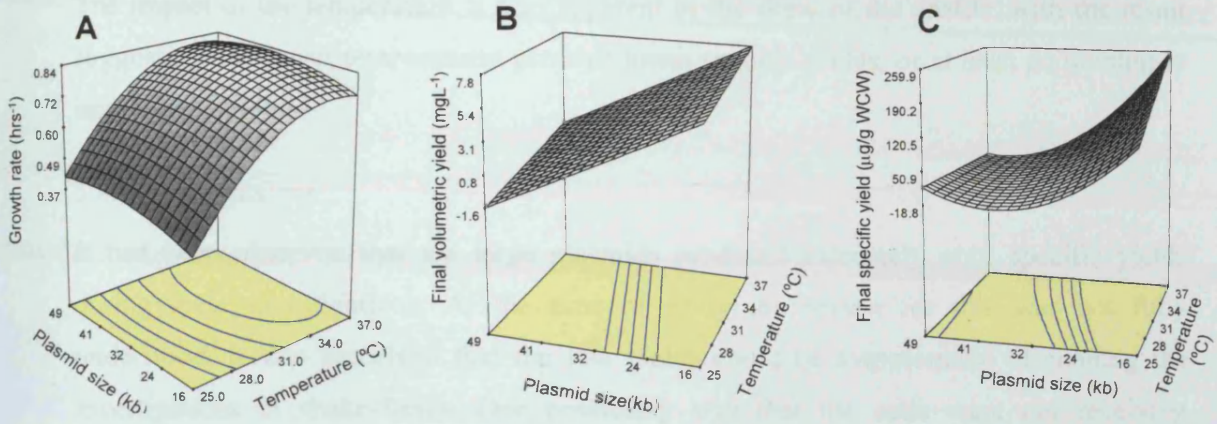

Figure 5-13 Response curves showing the combined effects of manipulating the temperature of incubation and plasmid size on the three measured responses; growth rate (A), volumetric yield at harvest (B) and specific yield at harvest (C).

From the plot it can be seen the temperature is the overriding variable of the two in its effect on culture growth rate. The profile plots a predictable curved increase with temperature. This is the expected case, since growth can be assumed to a collection of enzyme catalysed reactions, and the profile mimics well what occurs with increasing temperature on the rate of enzyme catalysis. It can be seen that the peak rate is reached at 37°C, the optimum temperature for enzymic reactions, with a maximum recorded growth rate of $0.88hrs^{-1}$. Closer inspection reveals the contributory effect of the plasmid size on the growth rate and explains the curves contour lines. As highlighted in Figure 5-12 the fastest growth rates were encountered with the intermediate sized construct and this effect is evidenced by the curvature of the profile in Figure 5-13A.

Figure 5-13B displays the response curve which characterises the effect of temperature and plasmid size on the final volumetric plasmid yield. The graph shows an almost linear decrease in volumetric yield with plasmid size, the variable which has the strongest effect of the two. The temperature of cultivation does appear to have a slight effect on volumetric yield, with slightly lower recorded yields at the reduced temperatures.

Figure 5-13C shows the impact of the two factors on specific plasmid yield at harvest. The reported responses show a higher degree of interaction between the two variables as the response curve is heavily skewed. It is very apparent that the plasmid specific yield decreases with increasing plasmid size to disappointingly low levels. The decrease is not linear as the smallest plasmid size (16kb) reports reasonably high specific yields ($\sim 220\mu gmL^{-1}$), unlike the two larger constructs.

The impact of the temperature is also apparent in the skew of the profile, with the result suggesting that lower temperatures produce lower specific yields, or at least do nothing to improve the yields.

5.4.4 Conclusions

It had been observed that the large plasmids produced extremely poor specific yields during these investigations. At the time of study the reason for this was not fully understood. It was perceived that the low yields could be symptomatic of running the investigations in shake-flasks. One possibility was that the cells were not receiving sufficient oxygen and that running the fermentations in the stirred tanks would alleviate the issue. For that reason it was decided to press ahead with the pilot-scale fermentations. Consequently, to conclude this section involves deciding upon the optimum conditions at which to run the fermentations. The factorial design of experiments had provided good data by which to judge the best conditions at which to operate.

Firstly, the concentration of ampicillin was found to have a minimal effect on any of the responses, so it was decided to maintain its concentration at $100\mu gmL^{-1}$ during the pilot-scale fermentations. The effect of temperature on growth rate was predictable and as expected. Higher temperatures resulted in faster growth, with growth rates at 37°C being up to 100% greater than at 25°C (Figure 5-13A). So in terms of fermentation productivity (yield per unit time), the best option would be to culture at 37°C, providing that this did not impact negatively on the yield responses considered. In both the case of volumetric and specific yields, cultivation temperature was found to have a distinguishable impact, but in both cases the higher yields were generated at the elevated temperature of 37°C (Refer to Figure 5-13B and C). This is also displayed by the response curves shown in Figure 5-14, which plot the effect of temperature and ampicillin concentration on the harvest specific yields, standardised for each of the three constructs under investigation. Again, the effect of the ampicillin concentration is shown to be minimal. In the cases of the 16kb and 33kb constructs, there is an interpolated, linear increase of specific yield with temperature. In the case of the 49kb construct, increasing temperature seems to decrease harvest specific yield but by negligible amounts

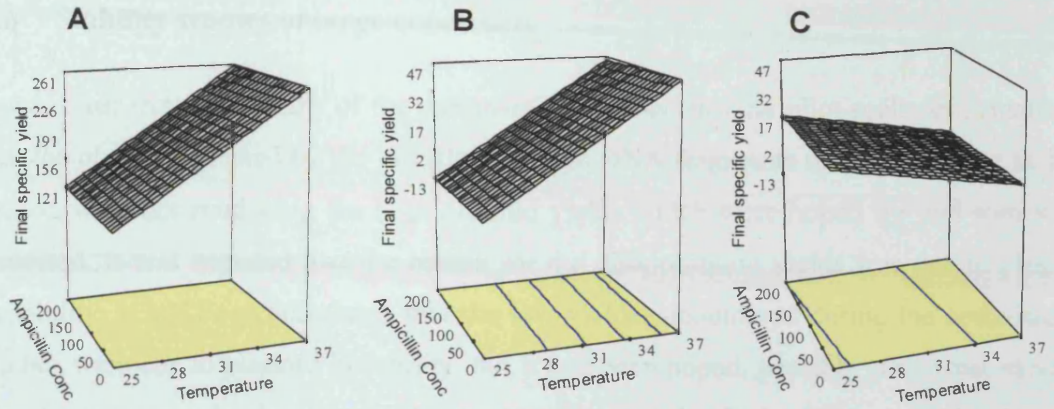

Figure 5-14 Response curves modelling the effect of temperature and ampicillin concentration on plasmid specific yield at harvest. The graphs are normalised with respect to plasmid size, such that figure A plots the response for the 16kb plasmid, figure B for the 33kb construct and figure C for the 49kb. From the plots it can be seen that temperature is the most influential of the two factors with ampicillin concentration barely registering any impact on the response. For the 16kb and 33kb plasmids temperature clearly effects harvest specific yield with an interpolated relationship between temperature and specific yield which is linear.

As a result of these conclusions duplicate 4L fermentations of each of the large pGEM plasmid series (3kb, 16kb, 33kb and 49kb) were conducted at 37°C in media supplemented with 100μgmL^{-1} ampicillin. As described previously, the mode and media of the fermentation had already been optimised to the DH1 strain, and consisted of a glycerol supplemented complex media with the fermentations conducted in batch mode with enriched air aeration toward the end of cultivation.

5.5 Pilot-scale Fermentations of the large plasmid series

Having pursued optimisation studies it was decided to complete duplicate 4L fermentations of the large constructs. Details of these investigations are outlined in the Upstream processing chapter of this report (6.3). Unfortunately, the problem, as flagged by the optimisation studies, was that the plasmid yields from the fermentations of the large constructs were extremely poor. The low yields warranted further studies to identify the nature of the problem as it was believed to be related to the stability of the large plasmid series.

5.6 Stability studies of large constructs

It was clear from the results of the optimisation studies, and the pilot-scale fermentations, that the plasmids created by the insertion of large DNA fragments of DNA into the pGEM vector, were not producing the high plasmid yields which were hoped for and somewhat expected. It was deduced that the reason for the disappointing yields was due to plasmid instability. It had been postulated that the low yields encountered during the optimisation studies were due to plasmid instability, but it had been hoped, possibly somewhat naively, that the cause may be due to poor oxygen transfer in shake-flasks. However, with the poor yield results from the fermentation, this notion had to be abandoned. The reason for the misplaced optimism was due to the stability studies conducted by (Tao and Zhang, 1998) who concluded that the large pGEM constructs created in their own study were stably maintained, a claim even summarised in the publication title. However, it is this author's belief that their investigation into the stability of the large pGEM plasmid was flawed and as such the claim of stable maintenance was misleading. In their report, the stability of the constructs was assessed by passaging a culture, bearing the large constructs, into fresh medium for a total of five days. Because the cells continued to grow on the selective media it was deduced that the cells must be plasmid bearing, however, no details were given into the proportions of cells bearing plasmids and therein lies the flaw in the claim of stable maintenance.

5.6.1 Segregational Plasmid Instability

The type of instability reasoned to be the cause of the poor plasmid yields was segregational stability. The successful partitioning of plasmids to the daughter cells is a central problem in any system utilising plasmids as vectors. Plasmids are always a metabolic burden on the cells, which leads to preference of plasmid–free cells during cultivation, since they are able to replicate at faster rates and so come to dominate the cell population. The probability of plasmid loss during cell division becomes more problematic as plasmid size increases, for the simple reason that the copy number decreases and as a result the likelihood of a daughter cell not receiving a copy of a plasmid increases (Warnes and Stephenson, 1986; Wojcik *et al.*, 1993; Smith and Bidochka, 1998). Bacterial Artificial Chromosomes (BACs), of which the Oxford series are a variety, are very large plasmids but avoid segregational instability by employing active partitioning mechanisms.

Modelling segregational plasmid stability is complex since the phenomenon is influenced by a variety of different factors, including plasmid type and biological properties, culture conditions and host-strain. Non-segregated models only distinguish between cells bearing plasmids and those without, whilst segregated models take more differences into account, namely the difference in plasmid copy numbers in cells. (Imanaka and Aiba, 1981) developed a simple, non-segregated model to describe plasmid loss in batch culture taking into account the probability of plasmid loss per generation of cells and the difference between the growth rates of the plasmid-bearing and plasmid-free cells, assuming exponential growth. This is shown in Equation 5-4. The model itself makes many assumptions and is of limited practical application, as placing a value of the probability of plasmid loss could be somewhat qualitative.

More complicated segregated models attempt to take into account the metabolic burden of plasmids, their copy number, the presence of multimers and the timing of their replication. These models are beyond the scope of this report but examples can be found in (Summers,

$$\text{Growth Rate (Plasmid - bearing)} \quad r_X{}^{+} = (1-p)\mu^{+}x^{+} \qquad (i)$$

$$\text{Growth Rate (Plasmid - free)} \quad r_X{}^{-} = (p\mu^{+}x^{+}) + (\mu^{-}x^{-}) \qquad (ii)$$

$$\text{Proportion of Plasmid - bearing cells} \quad F = \left(\frac{x^{+}}{x^{+} + x^{-}}\right) \qquad (iii)$$

$$\frac{\int_{X0}^{X+} r_X{}^{+}}{\int_{X0}^{X-} r_X{}^{-}}$$

$$F = \left(\frac{1-\alpha-p}{1-\alpha-2^{n(\alpha+p-1)}p}\right) \quad \text{Where}: \alpha = \left(\frac{\mu^{-}}{\mu^{+}}\right) \quad n = \left(\frac{\mu^{+}t}{\ln 2}\right) \qquad (iv)$$

Equation 5-4 A brief description of the non-segregated model developed by (Imanaka and Aiba, 1981) to describe the kinetics of plasmid loss during batch cultivation. The important parameters considered in the model are the probability of plasmid loss per generation (p) and the difference between the growth-rate of the plasmid bearing cells (μ^{+}) and the plasmid-free cells (μ^{-}). The non-segregated nature of the model means that it assumes exponential growth, that all plasmid containing cells have an identical growth rate and that the copy number is the same. Although not particularly helpful in predicting the actual proportions of cells bearing plasmid at any point is does serve to highlight the important issues affecting plasmid stability.

1991; Chatwin and Summers, 2001; Paulsson and Ehrenberg, 1998; O'Kennedy *et al.*, 1995; Summers *et al.*, 1993; Ataai and Shuler, 1986; Leipold *et al.*, 1994; Ganusov *et al.*, 2000; Ridha Mosrati, 1993).

The sheer number of publications in this field goes someway to highlight the industrial implications of plasmid instability and its effect on heterologous protein production and indeed, but to a lesser extent, plasmids themselves. As a direct result of the importance of

this issue to the application of recombinant DNA technology, numerous strategies have been devised, many utilising stabilisation systems employed naturally, to reduce plasmid segregational instability. Some of the strategies developed are detailed in Table 5-10. One of the simplest methods for enhancing segregational plasmid stability, widely used in laboratories and up to pilot-scale, is to add an antibiotic to the medium against which plasmid-bearing cells are resistant. This strategy can be effective in reducing instability, as evidence by Figure 5-15A, and is employed with the pGEM series of large constructs which carry the *bla* gene encoding β-lactamase, an enzyme capable of degrading ampicillin. For historical reasons, this resistance gene has been included on cloning vectors in an almost *de facto* fashion. However, the strategy is not entirely effective due to the nature of the encoded resistance. Once synthesised, β-lactamase is transported into the periplasm and over-expression leads to secretion of the enzyme into the culture medium (Georgiou, 1988). As a result, ampicillin may have a stabilising effect during the lag phase of growth, but is completely degraded by the exponential phase (Korpimaki *et al.*, 2003). Furthermore, the inoculum used in the seeding of the fermentation may have such a high-level of β-lactamase already present that the ampicillin is degraded so rapidly that no overall stabilising effect is witnessed.

An example of the rapidity of ampicillin degradation is shown in Figure 5-15B. This graph is extracted from (Kim *et al.*, 1998) and demonstrates the dramatic rise in the activity of β-lactamse during a fermentation of *E.coli* carrying pAA182.

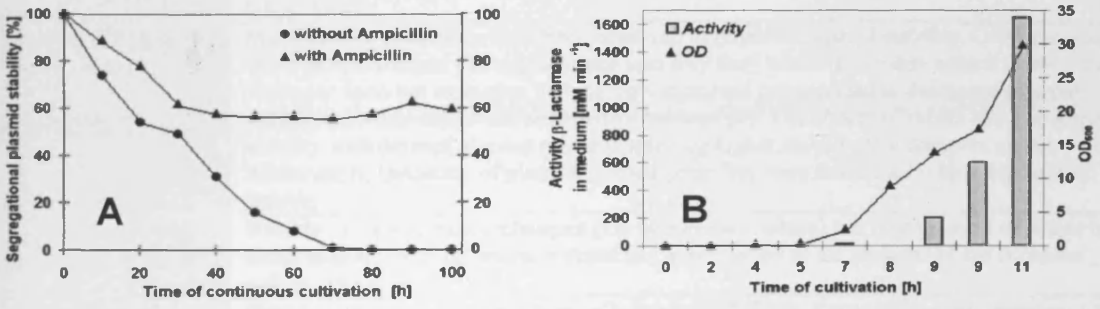

Figure 5-15 Figures highlighting the use of ampicillin as a selective agent to reduce segregational instability. Figure A highlights how the use of ampicillin in continuous cultures does improve plasmid retention compared to a negative control. However, figure B shows how the use of ampicillin in batch culture can be ineffective due to the accumulation of β-lactamase in the culture medium and the associated rapid degradation of the selective agent. Adapted from (Friehs, 2004)

Table 5-10 Table detailing a selection of the numerous mechanisms employed to enhance the stability of plasmids. Many utilise techniques encountered naturally. The vast number of techniques relate the importance of this issue to the application of rDNA technology.

TECHNIQUE	OUTLINE OF MECHANISM
Resistance against toxic substances	Simplest method involves adding a selective antibiotic to the media, against which cells develop resistance due to plasmid encoded genes. Impractical on the large-scale.
Repressor Titration	Again, utilises antibiotic but the resistance gene is encoded in the bacterial genome under the regulation of the *lac* operon. Expression of this resistance gene requires the presence of the *lac* promoter encoded on the plasmid. (Williams *et al.*, 1998a)
Complementation of chromosomal mutations	Propagation of the plasmid in a host-cell line incapable of synthesising an essential metabolite/protein. The required gene is expressed on the plasmid, ensuring only plasmid bearing cells could survive.(Skogman and Nilsson, 1984; Curtiss, III *et al.*, 1989)
Post-segregational killing of plasmid-free cells	Found on natural plasmids. Based upon intracellular mechanisms which kill plasmid-free cells. Mechanism consists of a genome based gene for a toxic substance and a plasmid located antidote which neutralises the lethal toxin i.e. CcdB/ CcdA from F-factor and *hok/sok*.(Jensen *et al.*, 1995; Jensen and Gerdes, 1995)
Stabilisation of plasmid forms	The size of plasmids leads to increased probability of segregational instability. Multimerisation can be a cause of segregational instability. Inclusion of genes leading to the monomerisation of multimers can lead to enhanced plasmid stability. Gene for resolvase in the *parCBA* system is an example. (Gerlitz *et al.*, 1990)
Active plasmid partitioning	*Par* genes can be used to ensure correct segregation of plasmids to daughter cells. Employed by BACs. The mechanism of action of these genes can be either attachment of the plasmid to specific places on the cell membrane or active movement of plasmid to younger zones(Bignell *et al.*, 1999; Lemonnier *et al.*, 2000)
High-copy number probability	Simple, non-segregated models predict that plasmid copy numbers >20 per cell lead to 100% segregational stability (Bentley *et al.*). High plasmid copy numbers increase the probability of successful partitioning. Also important is the variance of copy number, such that the distribution of plasmid copy number is narrow so that the population does not display high and low copy numbers. Inclusion of the Rom protein can reduce copy number variance.
Lowering the difference in specific growth rates	The major disadvantage once plasmid-free cells appear is that they are able to replicate at faster rates that plasmid-bearing cells. Decreasing the difference between the growth rates can increase segregational stability. Industrially inducement of cultures at high biomass reduces the occurrence of plasmid loss during the growth phase. Alternative strategies utilise lowering the temperature of cultivation or by ensuring that plasmid-free cells a forced to express a certain proteinto increase the burden placed upon the cells (Corchero and Villaverde, 1998; Glick, 1995)
Modifying culture conditions	Many culture conditions have been observed to improve plasmid stability. Often these are just observations without full explanations into why they occur. Too many effects observed to comment upon but examples include; low dissolved oxygen lead to decreased plasmid stability a similar effect was seen with a lowered pH. The choice of media can also impact stability with defined glucose media displaying higher stability that complex media. Additionally, induction of plasmid –based genes has been associated with a decrease in stability.
Clone selection	Suitable clone selection techniques (i.e. continuous culture) can be employed to isolate highly stable plasmid-bearing strains without full appreciation of the reasons for the enhanced stability (Vyas *et al.*, 1994).
Separation of plasmid-free and bearing cells	Plasmid bearing and plasmid-free cells can have different flocculation characteristics. Could be employed as part of a purification regime but not ideal when considering fermentation economics (Henry *et al.*, 1990)
Integration into chromosome	Impractical if the aim is to produce plasmid DNA. Can be used if only low gene dosage is required. Integration can lad to negative changes on the host-cell.

From the graph, the harvest point activity of β-lactamase in the broth is ~23mmols/s (1400mmols/min). Considering that the 4L fermentations conducted with the pGEM series were supplemented with 100mgL^{-1} ampicillin, it can be estimated that the total 400mg of ampicillin used (~1.1mmols) could be degraded in within 1s of the addition of the inoculum to the fermenter. This realisation is important as it demonstrates the flaw in the claim made by (Tao and Zhang, 1998) when they specificied that large (up to 100kb) pGEM constructs created in their study were stably maintained. By simply passaging a sample of culture into fresh selective media, a great deal of β-lactamase activity would also have been transferred, most probably sufficient to degrade all of the ampicillin present very quicky. Providing a small proportion of the cells retained the plasmid, sufficient β-lactamase could be generated to do the same when passaged again. Consequently, only a minute proportion of cells need be plasmid bearing for the assumption to be made that the plasmid is maintained, but by not detailing the proportion of cells actually bearing the plasmid, then the claim of stable maintenance is unsubtantiated.

With these considerations in mind it was decided that the stability of the large constructs needed to be investigated by describing the actual proportion of plasmid bearing cells.

5.6.2 Assessing the stability of the pGEM series of large plasmids

Assessment of the stability of the series of large pGEM plasmids was conducted in shake-flasks. The selective media in the first shake-flask was inoculated from an appropriate cell-bank vial and incubated. The growth was monitored by following OD progression and samples taken hourly for the analysis of plasmid stability. At the end of the growth period, sufficient culture broth was passaged and used to inoculate a shake-flask containing fresh selective media to 0.1OD. The whole trial was conducted over a sixty hour period involving four passages of the culture broth into fresh media. Designing the stability trials in this fashion mimicked a fermentation train which would take the culture from the initial master cell vial through to the end of a large-scale fermentation.

The method chosen for monitoring plasmid segregational stability was replica plating. More detail into the assay is provided in (2.6.8). The method involved the appropriately diluted samples of broth being plated out on to non-selective agar plates, which were incubated to allow colony formation. These represented the master plates. The colonies from the master plates were then imprinted on to separate, sterile velveteen cloths and used to inoculate fresh non-selective plates as well as selective plates, in that order.

The plates were then incubated to allow colony formation. The broth was diluted to ensure ~100-200 colonies would form on the master plate; the dilution factor required being determined from the OD at the time of sampling. The ratio of the colonies on the selective plate to the non-selective plate is the ratio of plasmid bearing cells. Each time point for each stability trial was assessed using triplicate plates. To improve accuracy the number of colonies on both the selective and non-selective plates were totalled, and the proportion of plasmid bearing cells calculated using a binomial distribution equation show in (Equation 2-1).

The results of the first stability trials can be seen in Figure 5-16. This stability trial was designed to monitor the likely changes which would have occurred to the proportion of plasmid bearing cells during the pilot-scale 4L fermentations (including the inoculum development period) of the pGEM series of large constructs. To ensure comparability to the fermentations the same media formulation, including an identical concentration of ampicillin ($100\mu gmL^{-1}$) was used for the stability trials. Additionally, all the shake-flasks were incubated at 37°C.

As can be appreciated from the figure, the loss of plasmid was a likely occurrence during the pilot-scale fermentations of the larger constructs. The figures demonstrate that ampicillin selection is not as effective as hoped. Only the pGEM11 culture displayed 100% stability at these conditions and as a direct result of this also recorded the slowest growth rates of all the constructs, at $0.7hrs^{-1}$ on the first day, rising to $0.74hrs^{-1}$ on the final day. It could be postulated that the increase in growth rate witnessed demonstrated some form of adaptation of the culture. The results for the pGEM16 were less successful as even this sized plasmid displayed instability. On the first day of the trial, stability was around 100%, but instability became apparent during the end of the first day and during the overnight passage. By the second day, the 16kb demonstrated a large drop-off in the proportion of plasmid-bearing cells. The drop off in stability followed the roughly sigmoidal curve reported by others investigating segregational plasmid instability and likely caused by the growth-rate differential between plasmid-bearing and plasmid-free cells (Smith and Bidochka, 1998; Warnes and Stephenson, 1986).

It is believed that the loss of plasmid from the cells also accounts for the increase in specific growth rate, which was found to rise from $\sim 0.71hrs^{-1}$, when stability was at is highest, to $\sim 0.80hrs^{-1}$ when the proportion of plasmid bearing cells was at its lowest.

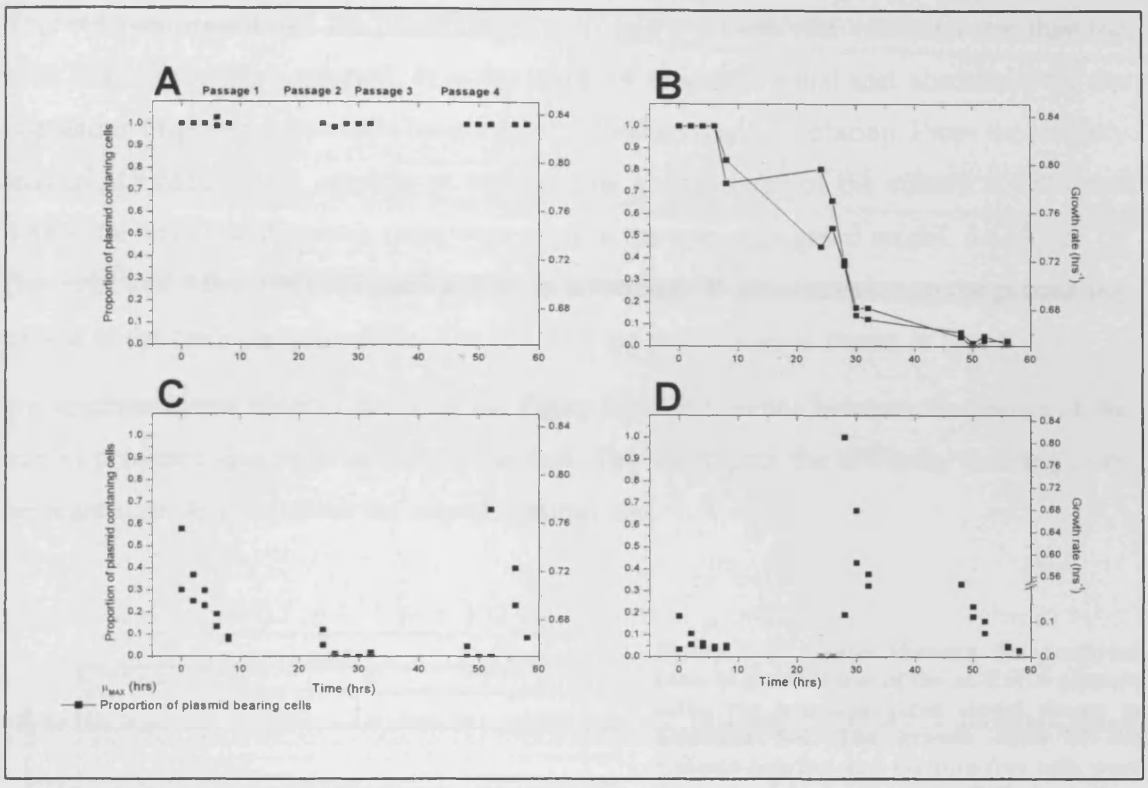

Figure 5-16 Stability studies of the pGEM series of plasmids propagated in DH1, displaying the change in the proportion of plasmid bearing cells through the course of a 60-hour passaging run. In each case, 50mL of sterile media (in 1L baffled shake-flasks) supplemented with 100μgmL^{-1} ampicillin was inoculated from a banked vial of cells to a starting OD of 0.1. For each construct duplicate shake-flasks were incubated at 37°C/ 230rpm in a shaking incubator. In a hood, samples of broth from each flask were removed at regular intervals over an eight-hour period. Optical density measurements were recorded to measure growth rate and samples of the broth were diluted appropriately in sterile PBS. 100μl of the diluted broth was plated on to non-selective TSA plates which were incubated for 20hrs at 37 ° C in a benchtop incubator. At the end of the eight-hour time-point sufficient inoculum was drawn from each shake-flask to inoculate a corresponding flask containing fresh sterile, selective media to 0.1OD. The passaged flasks were incubated in an identical fashion overnight, after which the process was repeated for a total of four passages.

The proportion of plasmid bearing cells was determined for each time point from each flask in duplicate by replica plating. The colonies on each of the master plates were transferred on to a sterile velveteen cloth which was then used to inoculate another non-selective TSA plate followed by a selective plate (TSA+100μg,l^{-1} Amp). The replica plates were then incubated for ~20hrs at 37°C. The proportion of plasmid bearing cells was determined by counting the number of colonies present on the selective plate in comparison to the non-selective control plate.

[A: pGEM11 (3.2kb) B: pGEM16 (16kb) C: pGEM33 (33kb) D: pGEM49 (49kb)]

This outcome meant that the plasmid-free cells had a growth rate ~15% greater than the cells bearing the 16kb plasmid. It is the result of this differential that accounted for the population of plasmid-free cells becoming the dominant cell population. From the stability trial of pGEM16 it was possible to estimate the growth rates of the culture at ~0% and 100% stability. These growth rates were used in the non-segregated model, developed by (Imanaka and Aiba, 1981) (Equation 5-4) in an attempt to place a value on the probability of loss of the 16kb per generation. The result of the predictions is shown in Figure 5-17.

An unsubstantiated observation from the figure is the difference between the shapes of the curves predicted and those actually observed. This highlights the difficulty in using non-segregated models to predict the rate of plasmid loss.

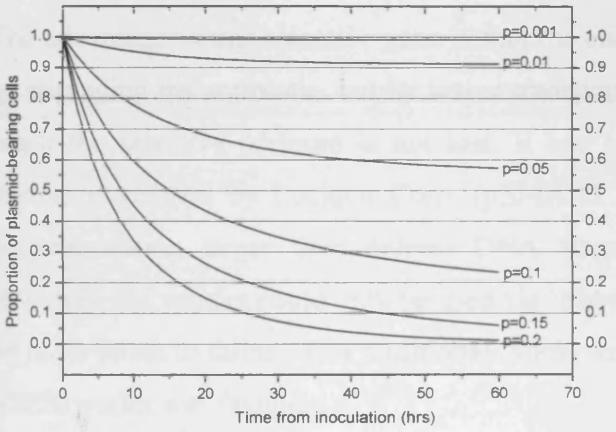

Figure 5-17 Graph showing the predicted rates of plasmid loss of the pGEM16 plasmid using the non-segregated model shown in Equation 5-4. The growth rates of the plasmid-bearing and plasmid-free cells were determined by experiment. Differing values were placed upon the probability of plasmid loss per generation ranging from 0.1% (1:1000) probability to 20% probability (1:5). The predicted rates could be compared to those derived from observation.

Segregational instability is a complex process, dependent on the magnitude of numerous variables, so simple non-segregated models cannot be relied on to accurately predict the event. However, from the predictions it could be estimated that the generational probability of a daughter cell being created which was plasmid-free was ~15%. This probability was estimated as by the end of the 60 hour period it leads to a predicted population of plasmid-bearing cells to be ~5%, in-line with the observed proportion. It can only be assumed that the probability of loss for the 33kb and 49kb constructs would be greater.

The stability profiles of the 33kb and 49kb constructs demonstrate that at no point during the trial did they display 100% stability, suggesting that even the master cell bank used to inoculate was prepared from a culture of cells with reduced stability. In both cases the proportion was reduced, rising only temporarily when the culture was passaged into fresh, selective media, but soon dropping. As a result the growth rates of the cultures were found

to be higher than those reported for the stably maintained 3kb construct ~ 0.75-0.8 hrs^{-1}. One interesting occurrence was seen during the second day of the pGEM49 stability trial, where elevated stability caused a dramatic drop-off in growth rate, or indeed, vice-versa.

To summarise the results of the first stability trial involves confirming that the large pGEM constructs do display reduced segregational stability. More than likely this reduced stability was the reason for the poor plasmid yields obtained during the pilot-scale fermentations. It had been hoped that because stable maintenance was reported by Tao *et al.* (1998), when they created large plasmids using the same vector backbone, that this would be achievable with these constructs. However, in hindsight more care should have been taken over the selection of a suitable cloning vector. Ideally, the vector would not have utilised ampicillin resistance as the selective agent but kanamycin resistance instead. The advantage of this selective gene is that the encoded protein does not confer resistance by degrading the antibiotic, but by active transport of the kanamycin out of the cells. As a result the selective pressure is not lost. It had been thought to use a range of cloning vectors developed by Lucigen Corp. (pSMART vectors) which claim to be capable of accommodating larger than normal DNA fragments and which use Kan resistance. However, the vectors could only be used via 'blunt-end' cloning strategy which was felt to be more prone to failure than traditional 'sticky-end' cloning protocols. Consequently, the pGEM vector was favoured.

The main focus of the stability studies now became trying to improve the stability characteristics of the pGEM large constructs, as in doing so would improve plasmid yield.

5.6.3 Attempts to improve segregational stability of pGEM series

The first attempts to improve the stability profile of the pGEM series of plasmids involved determining whether propagation of the plasmids in an alternative host-cell line or selection with an improved antibiotic, increased plasmid stability. The stability trial was conducted in an identical fashion to before, using shake-flasks and replica plating. The changes included propagation of the plasmids in *E.coli* DH10β and the use of carbenicillin as the selective agent. It was felt that propagation of large plasmids in the DH10β cell line, as reported previously, may aid large plasmid propagation and stability (Hanahan *et al.*, 1991; Donahue, 1998; Eastman and Durland, 1998). Carbenicillin is an analogue of ampicillin, as shown by Figure 5-18.

Its use is recommended over ampicillin since the modifications to the groups surrounding the β-lactam ring mean that it is hydrolysed at a far slower rate by β-lactamase than ampicillin (Sambrook *et al.*, 1989). As such, the selective pressure should be maintained for longer periods.

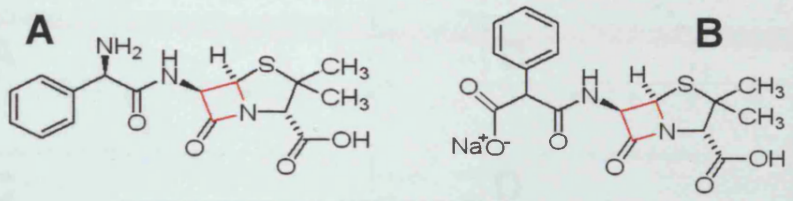

Figure 5-18 Figure showing the structural similarities between ampicillin (A) and carbenicillin (B). Both possess the β-lactam ring (highlighted in red). This is the target for β-lactamase which hydrolyses the ring to break up the molecule. Due to slight differences in the R-groups this process of hydrolysis is slower with carbenicillin than with ampicillin.

The combined results of the use of DH10β host-cell and carbenicillin are shown in Figure 5-19. Once again, the smallest plasmid; pGEM11 (3.2kb) is the only construct which displays 100% stability. pGEM16 (16kb) shows a very similar pattern in stability to as before when using carbenicillin. However, overall the results do not show any real improvement in the stability profile of the large constructs.

Simple cost-benefit analysis suggested that pursuing the use of either carbenicillin or DH10β as the host is not particularly useful. The benefit of either strategy on the stability characteristics of the large constructs was found to be minimal. Furthermore, the use of DH10β would involve the use of an unoptimised strain which has been found before to demonstrate slower growth rates and biomass yields on the DH1 optimised media (3.5.2). As for carbenicillin, the cost multiple is a big disadvantage. It may be found advantageous to increase the concentration of selective agent in the media or even to add it in fed-batch mode. Doing so would require more quantities of antibiotic, however, carbenicillin is ~20-fold more expensive per gram than ampicillin, which reduces the feasibility of using more selective agent. (Ampicillin; £4.20/g Carbenicillin; £76.40/g) (Sigma-Aldrich). As a result of these findings it was decided not to employ either of these techniques.

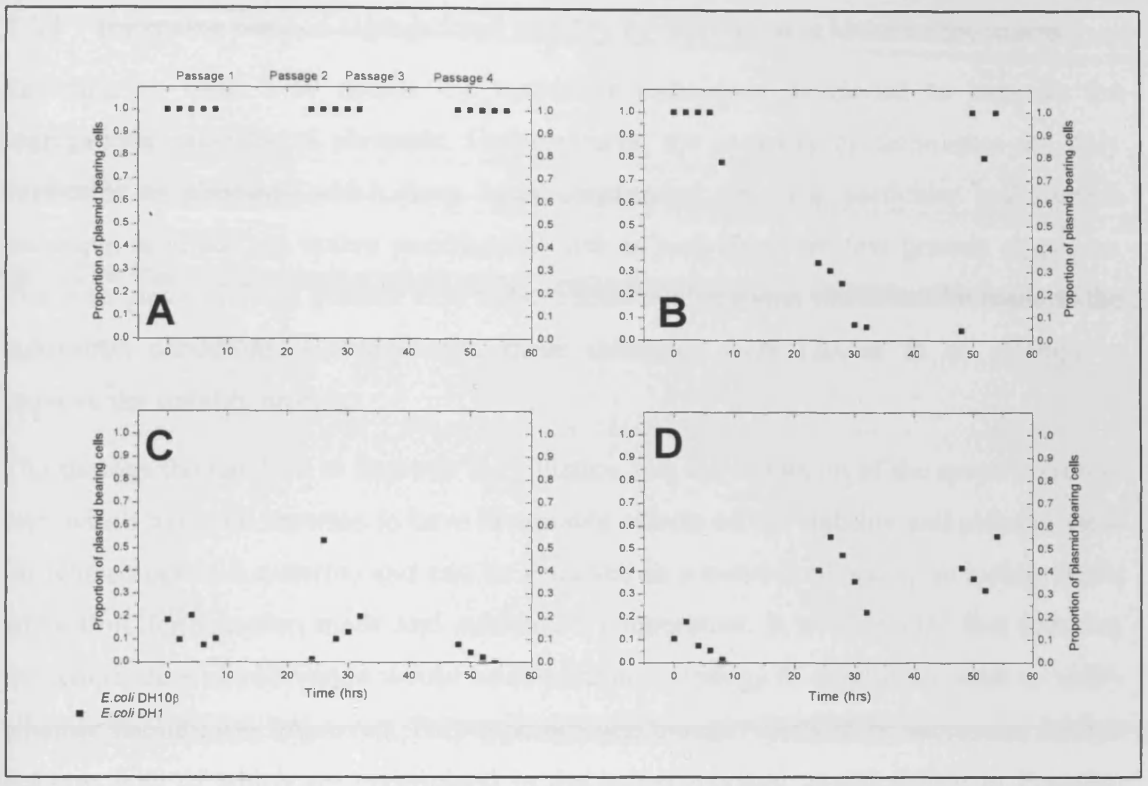

Figure 5-19 Stability studies of the pGEM series of plasmids propagated in DH1 and DH10β, displaying the change in the proportion of plasmid bearing cells through the course of a 60-hour passaging run. In each case, 50mL of sterile media (in 1L baffled shake-flasks) supplemented with 100μgmL^{-1} Carbenicillin was inoculated from a banked vial of cells to a starting OD of 0.1. For each construct duplicate shake-flasks were incubated at 37°C/ 230rpm in a shaking incubator. In a hood, samples of broth from each flask were removed at regular intervals over an eight-hour period. Optical density measurements were recorded and samples of the broth were diluted appropriately in sterile PBS. 100μl of the diluted broth was plated on to non-selective TSA plates which were incubated for 20hrs at 37 ° C in a benchtop incubator. At the end of the eight-hour time-point sufficient inoculum was drawn from each shake-flask to inoculate a corresponding flask containing fresh sterile, selective media to 0.1OD. The passaged flasks were incubated in an identical fashion overnight, after which the process was repeated for a total of four passages.

The proportion of plasmid bearing cells was determined for each time point from each flask in duplicate by replica plating. The colonies on each of the master plates were transferred on to a sterile velveteen cloth which was then used to inoculate another non-selective TSA plate followed by a selective plate (TSA+100μg,l^{-1} Carbenicillin). The replica plates were then incubated for ~20hrs at 37°C. The proportion of plasmid bearing cells was determined by counting the number of colonies present on the selective plate in comparison to the non-selective control plate.

[A: pGEM11 (3.2kb) B: pGEM16 (16kb) C: pGEM33 (33kb) D: pGEM49 (49kb)]

5.6.4 Improving plasmid segregational stability by cultivation at lower temperatures

Referring to Table 5-10 details the numerous techniques developed to improve the segregational stability of plasmids. Unfortunately, the majority of techniques are only applicable to plasmids which have been constructed with the particular stabilisation technique in mind (e.g. active partitioning) and as such there are few generic strategies. The strategies which are generic tend to be related to alterations which can be made to the cultivation conditions. Consequently, these strategies were chosen in an attempt to improve the stability profile.

The strategy thought best to improve the situation was the reduction of the specific growth rate, which has been reported to have favourable effects on the stability and plasmid yield (in relaxed plasmid systems) and can be achieved in a number of ways; including media adaptation, fermentation mode and cultivation temperature. It was decided that reducing the temperature of cultivation would be the simplest strategy to employ in order to verify whether stability was improved. This approach was thought likely to be successful for two reasons, both of which are highlighted in the non-segregated model shown in Equation 5-4. It was reasoned that reducing growth rate would reduce the growth rate differential (α) and the probability of plasmid-free cell generation (p), both should have a positive impact on stability.

The first mechanism exploits the fact that reducing the cultivation temperature would reduce the growth rate differential between the plasmid-free and plasmid-bearing cells. The result is that when/if plasmid-free cells appear their rate of replication should be not much faster than the plasmid-bearing cells. As such, the plasmid-free cells would require far longer periods to become the dominant cell population. Secondly, it is postulated that decreasing the incubation temperature should reduce the probability of plasmid-free cells appearing. The reason behind this is that slower growth rates have been shown to have a positive effect on plasmid copy numbers (Seo, 1986; Bailey and Seo, 1985; Kim *et al.*, 1998; Reinikainen and Virkajaervi, 1989; Reinikainen *et al.*, 1989). Therefore, it was envisioned that incubation at a lower temperature would decrease growth-rate, which would up-regulate the plasmid copy number, which in turn would decrease the probability of plasmid loss (Bentley, 1989). The stability trials were conducted in an identical fashion to before, using shake-flasks and replica plating, the only difference being the temperature at which the shake-flasks were incubated at which were both 30°C and 25°C.

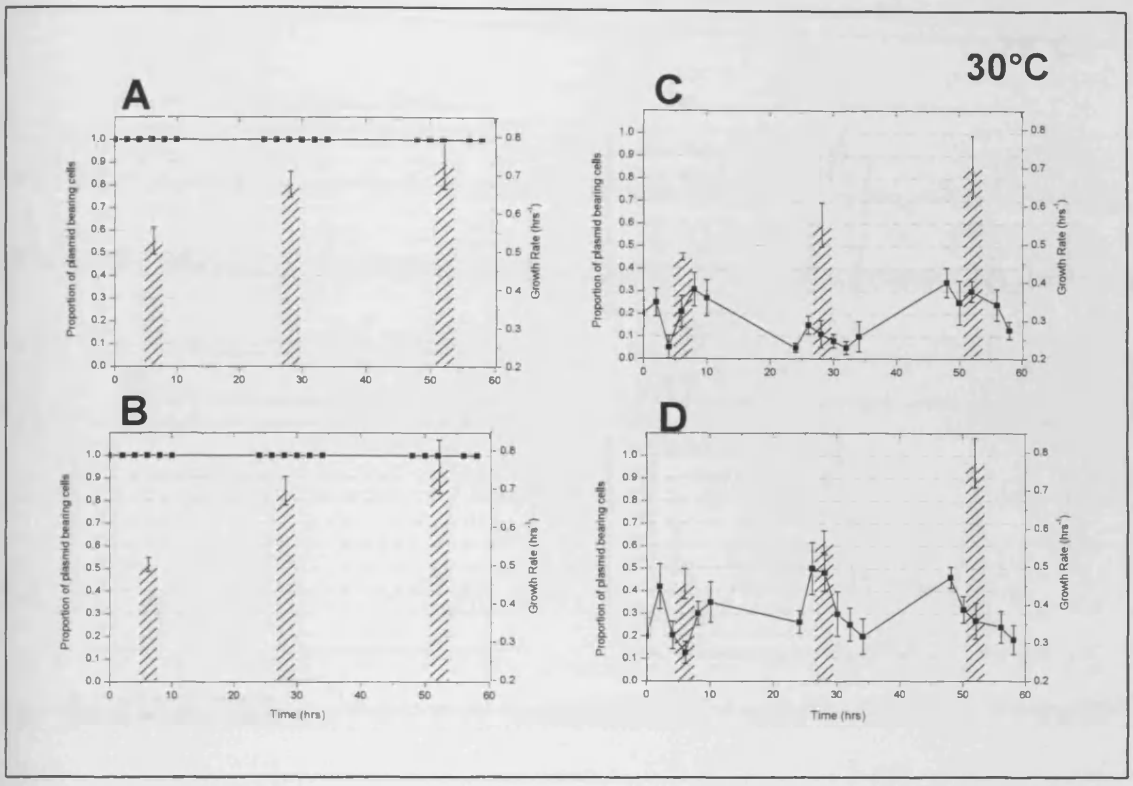

Figure 5-20 Stability studies of the pGEM series of plasmids propagated in DH1, displaying the change in the proportion of plasmid bearing cells through the course of a 60-hour passaging run. In each case, 50mL of sterile media (in 1L baffled shake-flasks) supplemented with 100µgmL^{-1} ampicillin was inoculated from a banked vial of cells to a starting OD of 0.1. For each construct duplicate shake-flasks were incubated at 30°C/ 230rpm in a shaking incubator. In a hood, samples of broth from each flask were removed at regular intervals over an eight-hour period. Optical density measurements were recorded to measure growth rate and samples of the broth were diluted appropriately in sterile PBS. 100µl of the diluted broth was plated on to non-selective TSA plates which were incubated for 20hrs at 30 ° C in a benchtop incubator. At the end of the eight-hour time-point sufficient inoculum was drawn from each shake-flask to inoculate a corresponding flask containing fresh sterile, selective media to 0.1OD. The passaged flasks were incubated in an identical fashion overnight, after which the process was repeated for a total of four passages.

The proportion of plasmid bearing cells was determined for each time point from each flask in duplicate by replica plating. The colonies on each of the master plates were transferred on to a sterile velveteen cloth which was then used to inoculate another non-selective TSA plate followed by a selective plate (TSA+100µg,l^{-1} Amp). The replica plates were then incubated for ~20hrs at 30°C. The proportion of plasmid bearing cells was determined by counting the number of colonies present on the selective plate in comparison to the non-selective control plate.

[A: pGEM11 (3.2kb) B: pGEM16 (16kb) C: pGEM33 (33kb) D: pGEM49 (49kb)]

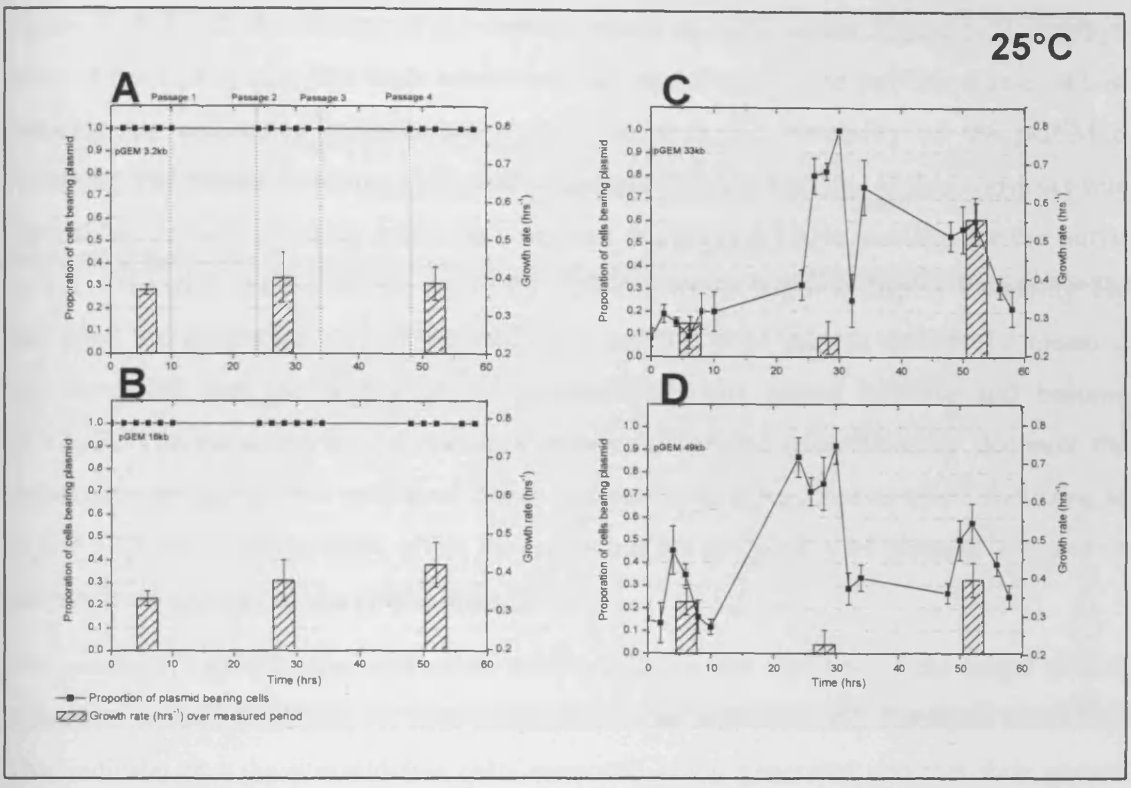

Figure 5-21 Stability studies of the pGEM series of plasmids propagated in DH1, displaying the change in the proportion of plasmid bearing cells through the course of a 60-hour passaging run. In each case, 50mL of sterile media (in 1L baffled shake-flasks) supplemented with 100μgmL^{-1} ampicillin was inoculated from a banked vial of cells to a starting OD of 0.1. For each construct duplicate shake-flasks were incubated at 25°C/ 230rpm in a shaking incubator. In a hood, samples of broth from each flask were removed at regular intervals over an eight-hour period. Optical density measurements were recorded to measure growth rate and samples of the broth were diluted appropriately in sterile PBS. 100μl of the diluted broth was plated on to non-selective TSA plates which were incubated for 20hrs at 25 ° C in a benchtop incubator. At the end of the eight-hour time-point sufficient inoculum was drawn from each shake-flask to inoculate a corresponding flask containing fresh sterile, selective media to 0.1OD. The passaged flasks were incubated in an identical fashion overnight, after which the process was repeated for a total of four passages.

The proportion of plasmid bearing cells was determined for each time point from each flask in duplicate by replica plating. The colonies on each of the master plates were transferred on to a sterile velveteen cloth which was then used to inoculate another non-selective TSA plate followed by a selective plate (TSA+100μg,l-1 Amp). The replica plates were then incubated for ~20hrs at 25°C. The proportion of plasmid bearing cells was determined by counting the number of colonies present on the selective plate in comparison to the non-selective control plate.

[A: pGEM11 (3.2kb) B: pGEM16 (16kb) C: pGEM33 (33kb) D: pGEM49 (49kb)]

Figure 5-20 details the results of the stability study at 30°C whilst Figure 5-21 displays those of the 25°C study. The most interesting fact about both of the stability studies is that reducing the cultivation temperature entirely corrects the instability of the pGEM16 construct. The results from the 37°C trial suggested that the stability of this construct was correctable. In both previous trials the construct maintained 100% stability for the initial period of the trial, but toward the end of the first day would begin to display instability. By that point the generation of plasmid-free cells and the large growth differential meant it was inevitable that the proportion of plasmid-free cells would increase and become dominant. The reduction in cultivation temperature seemed to sufficiently decrease the probability of plasmid-loss such that it does not occur, or at least not as often. Referring to Figure 5-17 shows the positive effect that reducing the probability of plasmid loss had on the predicted stability of the 16kb construct.

The results of reducing the cultivation temperature on the stability of the larger pGEM constructs were more mixed. At both temperatures the constructs still displayed instability. This indicates that the plasmid-free cells were still being generated and that their growth persisted in being faster than the plasmid-bearing cells. On the positive side, the equilibrium proportion of plasmid-bearing cells was higher. This is directly attributable to the lowered temperature, as although plasmid-loss is still occurring, it must have been reduced by some degree. Similarly, the growth-rate differential between the plasmid-free and plasmid-bearing cells must have been reduced since the proportion of plasmid-free cells does not come to dominate the cell population as quickly. However, it establishes the fact that, unlike the pGEM16 construct, the instability of these constructs cannot be entirely rectified by simply reducing the temperature.

The stability profile of the 30°C trials of the pGEM33 and 49 constructs displays predictable sawtooth kinetics, as the proportion of plasmid-bearing cells is highest just following passaging. This is to be expected since the presence of ampicillin would neutralise the plasmid-free cells, but due to the rapid action of β-lactamase the selection pressure is soon lost and the proportion of plasmid-bearing cells begins to fall as growth-rate differential becomes noticeable. Although it is difficult to exactly quantify, it was felt that the stabilising effect was greatest at the lower temperature of 25°C. Theoretically, this would be expected as the growth rate and plasmid copy number would be lower and as such the growth-rate differential and probability of plasmid loss would be reduced.

Observations from the stability profiles back up this belief with the proportion of plasmid bearing cells being higher during the 25°C stability trials than in any previous trial. In the hope that this cultivation temperature did promise the best conditions for improving stability it was chosen.

5.6.5 Clone Selection

Results from the stability trials suggested that cultivation at 25°C would improve the stability profile of the large plasmids. Therefore, pilot-scale fermentations would be carried out using the lower temperature conditions. Before doing so it was felt applicable to attempt a further level of optimisation. Table 5-10 details a generic strategy of improving stability by the selection of more stable clones. Traditionally this would be achieved through the use of continuous culture. For example, (Vyas *et al.*, 1994) employed 72hr continuous culture to select clones which displayed more favourable stability (+60%) profiles during batch culture. The exact mechanism of why the stability improved is unknown, and is likely due to a combination of factors. However, the fact remains that the forced evolution environment of continuous culture enables the generation and selection of clones with improved stability phenotypes.

Unfortunately, it was reasoned that the design and setup of continuous culture systems for clone selection was out of the capability of this investigation. However, it is maintained that the use of this technique as a means of generating and selecting favourable clones, capable of bearing large, high-copy plasmids, could be a successful strategy and would be recommended should further attempts be made at producing these constructs.

Although continuous culture would have been the optimal method of clone selection a less sophisticated method was attempted to identify and select suitable clones. Streaks of the master cell bank of each large construct were made on to selective plates and incubated at 25°C to allow colony formation. Five colonies from each construct plate were inoculated into sterile, selective media and incubated overnight at 25°C. These cultures were then used to inoculate five shake-flasks. In an identical fashion to the stability studies, the cultures were grown in shake-flasks and passaged at 12 hour periods into fresh, selective media. This selection regime was continued for a 60 hour period. At the end of the 60 hour period, samples of the culture broth were streaked on to selective plates and 5OD volume samples of culture broth taken and spun down.

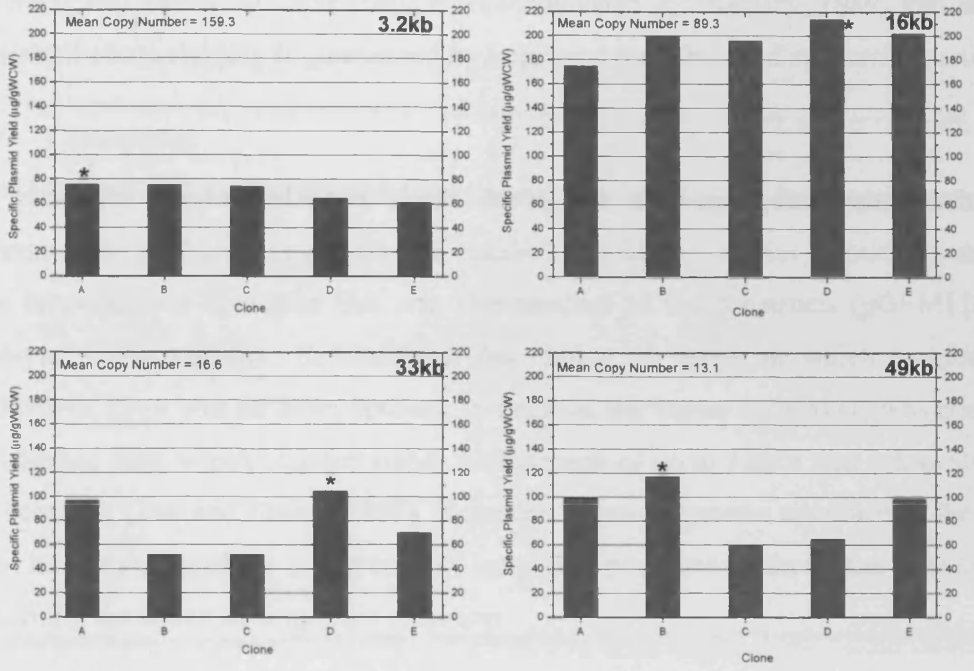

Figure 5-22 Figure displaying the specific yields of each of the five clones, bearing each of the pGEM series of plasmids, at the end of the 60 hour selection period. The asterisk marks the clone which was selected and banked.

The plasmid specific yield of each of the clones was then determined by HPLC on IPA precipitated samples. The results are detailed in Figure 5-22.

The results show that there was a level of variation in the yields of each clone. The clones which produced the highest yield at the end of the selection procedure were selected. The results also gave the first indications of expected yields from this series of large plasmids and their associated copy number. The most noticeable are the poor yields of the pGEM11 construct, which were below 100µg/gWCW. This was surprising since in the product literature it is claimed that this construct has a copy number of 300-400, but the estimates from this study placed the value at ~150 (Qiagen, 2005). The yields for the pGEM16 were far greater due to the greater quantity of cloned DNA, but as the estimates show, the value for copy number is reduced by ~50% due to the increased plasmid size. The yields of the two larger constructs would be expected to be even greater than the 16kb construct, due to the increased cloned DNA mass, but the instability issue brought the overall yields down. However, the clones selected both returned yields above 100µg/gWCW.

It may be coincidental, but the estimates placed on the copy number of both the larger constructs was below 20 copies/cell. It was calculated by (Bentley, 1989) that above 20 copies/cell 100% stability is guaranteed by improved probability of successful partitioning.

5.6.6 Conclusions

The cause for the low plasmid yields during the pilot-scale fermentations has been determined to be due to segregational instability. Stability studies mimicking the pilot-scale fermentations identified that only the smallest of the constructs (pGEM11[3.2kb]) displayed 100% stability. In hindsight, the choice of vector in which to clone large segments of DNA was far from optimal. In defence, the vector (pGEM11) was chosen due to published data, which claimed stable maintenance of up to 100kb was achievable using this construct (Tao and Zhang, 1998). However, a more reasoned approach to the cloning could have anticipated the occurrence of instability problems as there was published data concerning the action of ampicillin selection.

Attempts at further cloning using a more optimal vector were ruled out due to time constraints and the potential for the same problem occurring. As a result attempts were made to improve the stability of the plasmid using generic techniques. Initially, these attempts included changing the host cell line and the use of a more degradation resistant antibiotic. Unfortunately, these efforts did not yield significant improvements in stability and it was deduced that the cons from utilising these approaches outweighed their minimal benefits. As a result, the final strategy employed was to reduce the temperature of cultivation from 37°C to 25°C. Shake-flask evidence suggested that this had the action of reducing the probability of plasmid loss as well as reducing the growth-rate differential between the plasmid-free and plasmid-bearing cells. Clone selection was also conducted to try and select more stable clones.

Although a major disappointment, the stability issues serve as a reminder of a technical hurdle which must be overcome in the production of large constructs. However, it is believed it is a hurdle which could be overcome. In contrast, the low-yields presented by the stringently controlled Oxford series have no margin for improvement. Described in this chapter (Table 5-10) are mechanisms which could be employed to optimise the stability of the large plasmids. It is believed that rational design of large constructs with plasmid stabilisation in mind could generate suitable candidates for large-scale production.

Unfortunately, due to the highly technical nature of many of these approaches it was not possible to attempt them in this project. As a result only the simplest strategies were attempted, but some improvement in stabilisation can be reported. Consequently, pilot-scale fermentations using these improved conditions could now be conducted to determine the plasmid yields resulting from growth in a more controlled environment.

5.7 Conclusions

Attempts to produce the Oxford series of Bacterial Artificial Chromosomes were described in Chapter 3. From these studies it was reasoned that the low yields produced from the fermentations of these constructs did not allow effective study of their processing. Problems with analytical procedures and the setup of the downstream processing steps, highlighted that these constructs were not really applicable to large-scale manufacture. With little that could be done to improve the yields of these constructs, the decision was taken to produce large plasmids under the control of a high-copy number replicon, with the intention that they would improve the yields achievable and so allow further study into their processing.

Initial attempts at sub-cloning the insert DNA from the Oxford series constructs into high-copy number vectors were not successful. As a result, a new strategy was attempted that involved the cloning of large fragments of *S.cerevisiae* genomic DNA into pGEM vectors, as first reported by (Tao and Zhang, 1998). These efforts were more successful in generating large constructs. However, optimisation studies, designed to identify suitable conditions at which to produce these constructs, reported low yields of these constructs, as did further pilot-scale fermentations. Investigations into the cause of the low-yields determined that the problem lay with the unstable nature at which these construct were propagated. In response to this, attempts were made at trying to identify suitable conditions which would increase the stability of the plasmids. Following these investigations, higher-producing clones were isolated and it was decided that reducing the temperature of cultivation to 25°C improved the stability by a significant degree. Consequently, attempts could now be made to produce these constructs on the pilot-scale using these conditions. The results of these efforts will be outlined in the next section of this report which deals with the upstream processing of these constructs.

6 UPSTREAM PROCESSING: RESULTS AND DISCUSSION

6.1 Chapter Aims

The aims of this chapter are to outline the results of pilot-scale fermentations conducted on strains bearing the large plasmid series created in the previous chapter. The fermentations were studied as a separate unit operation since their importance to any process cannot be easily estimated. Too often upstream and downstream processes are considered as completely separate, unconnected unit operations; when in reality fermentations have a huge impact on the proceeding steps. Attempts have been made to avoid such an approach since previous studies have demonstrated the impact that fermentation-driven factors, namely specific yield, can have on the performance of downstream operations. Despite this, the fact remains that the main aim of the fermentations was to produce sufficient cell material with which to attempt purification of the large plasmids. It was fully understood that far longer could have been spent investigating and optimising this section of the overall process so as to further increase productivity, but due to time pressures, many of the more elegant strategies which could have been applied were not attempted. More detail into the background of fermentations for plasmid production is described in Chapter 3.

The main issues which will be investigated by this chapter include the following;

1. At the outset of this project fermentation calibration was identified to be of critical importance. Many calculations required the understanding of how factors such as cell concentration and optical density relate to one another. Detailed in this section will be the results of runs performed to prepare calibration curves for such purposes.
2. Prior to the realisation of the stability issues plaguing the propagation of these large plasmids, 'conventional' 37°C fermentations were carried out in an attempt to produce the constructs. The results from these fermentations will be outlined.

3. Following poor yields from the 37°C fermentations, the stability studies detailed in 5.6 were carried out. From these investigations it was decided to proceed with fermentations at 25°C. The results of these fermentations will be outlined.

4. Together with assessment of the fermentation characteristics such as growth and final biomass levels, perhaps the most important measurable are the actual plasmid yields. As such details will be given in to the plasmid yields of the fermentations.

5. Finally, high plasmid yields are only desirable if the plasmid is produced in supercoiled form. Since supercoiling is a driven by an energy requiring process the level of supercoiling can vary throughout the course of a fermentation. The results from gel analysis will be outlined to describe the observed flux in plasmid supercoiling during the fermentations.

6.2 Fermentation Calibration

In many instances throughout this project it has been necessary to perform calculations which required the conversion of values such as optical density into figures such as cell concentration, so enabling the determination, of amongst other things, plasmid copy number. In order to have confidence in the values returned by these calculations, an accurate and precise description of how these factors relate to one another was required. To this end quadruplicate fermentations of *E.coli* DH1 [parental] were carried out in which all possible measurements were recorded allowing the construction of calibration curves♦.

♦ It should be emphasised that the creation of these calibration curves did not replace direct measurement where possible and the curves were never created with this aim in mind. In every fermentation conducted WCW and optical density were measured as standard.

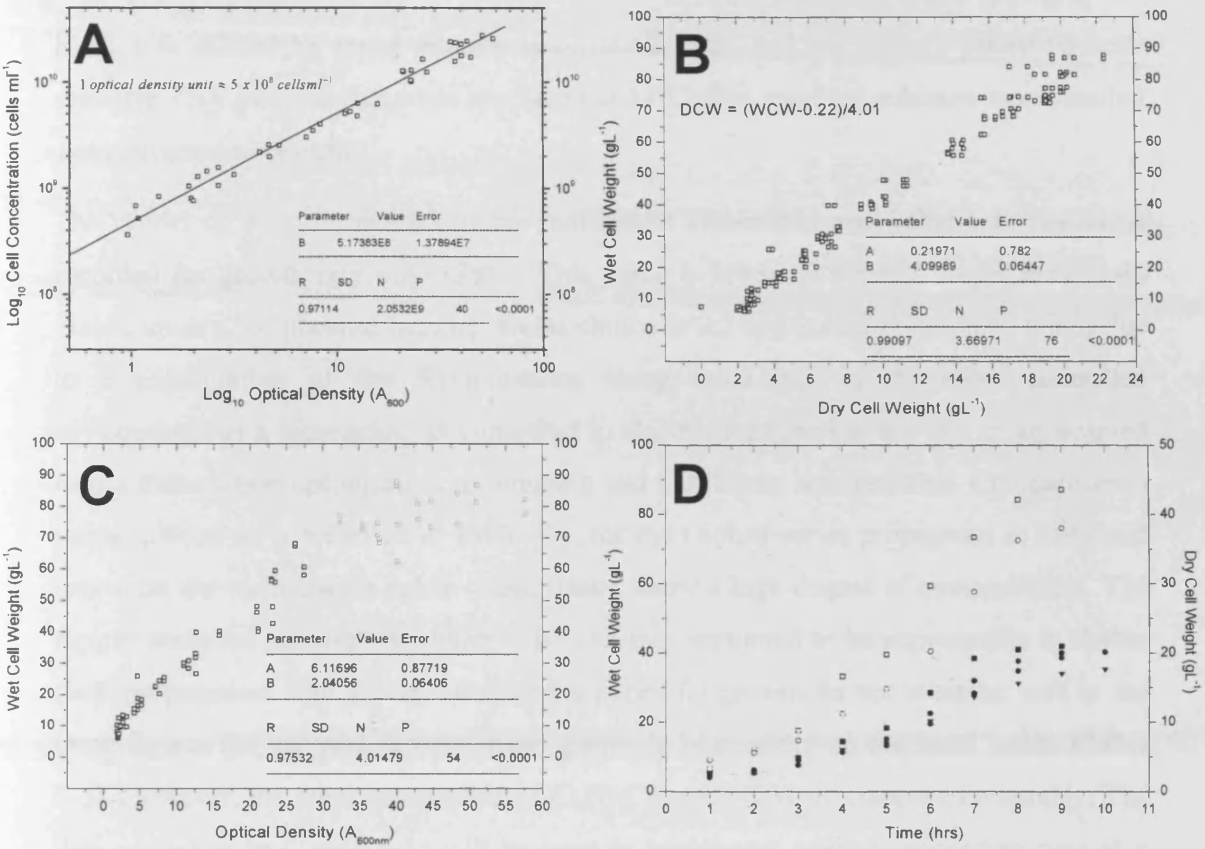

Figure 6-1 Results from quadruplicate fermentations of DH1 parental were used to prepare the calibration curves shown. During the runs wet cell weight (WCW), dry cell weight (DCW), optical density and cell concentration measurements were taken. Figure A correlates cell concentration against optical density and establishes that 1OD unit ~$5x10^8$cellmL^{-1}. Figure B correlates dry cell weight against wet cell weight and shows that DCW is roughly ¼ of WCW. Figure C attempts to correlate optical density against wet cell weight. Figure D plots the WCW and DCW progression of the parental fermentations

Table 6-1 Table summarising the key growth data extracted from quadruplicate 4L pilot-scale fermentations of DH1 Parental at 37°C.

	Vessel 1	Vessel 2	Vessel 3	Vessel 4	Average
Specific Growth Rate	0.359	0.408	0.410	0.399	0.394
Final WCW (gL^{-1})	87.2	76.1	79.9	79.2	80.6
Final DCW (gL^{-1})	17.6	20.9	19.3	20.0	19.5
Final optical density	40.1	32.4	57.7	48.4	44.7

The results of the fermentations also provide a useful benckmark, representing a negative control against which to compare the other fermentations. Four-litre working volume fermentations were conducted as outlined in 2.7.3. Optical density, wet-cell weight (WCW), dry cell weight were calculated as described in 2.5.1, 2.5.2, 2.5.3. Cell concentration was determined using a method similar to that used for replica plating (2.5.4).

Broth was diluted by serial dilution using sterile PBS and the dilutant plated on non-selective TSA plates which were incubated at 37°C. The resultant colonies were counted and converted to cellsmL^{-1}

The results of these fermentations are outlined in Figure 6-1 and Table 6-1. The value recorded for growth rate was 0.39h^{-1}. This value is lower than many values previously placed upon μ for plasmid bearing strains shown in 3.2 and 3.4. It is reasoned this is due to a combination of the fermentations being conducted in the more controlled environment of a bioreactor, as compared to shake-flasks, and to the use of an adapted media formulation optimised to minimise μ and a different host cell-line. Comparison to values placed on μ recorded in Table 3-4, for the Oxford series propagated in DH1 and grown on the same media but in shake-flasks, show a high degree of comparability. The figures recorded are slightly higher (~10%) a fact presumed to be accountable to shake-flask propagation. The values calculated for specific growth do not compare well to the same figures for parental fermentations grown in bioreactors on the same media (Table 3-5). However, the other measurables; OD, WCW and DCW do compare favourably. The data portrayed in (Table 6-1) will be used to benchmark against proceeding runs as a negative control.

The main point to this exercise was to use the data produced by these fermentations to construct calibration curves. From Figure 6-1A it can be appreciated that 1OD unit was found to be equivalent to a cell concentration of 5x10^{8} cellsmL^{-1}.

The second calibration curve Figure 6-1B correlates wet cell weight (WCW) against dry cell weight (DCW). This curve was used since recording DCW progression for each fermentation would have been laborious and quite variable. However, on many occasions in the literature plasmid yields are recorded as a proportion of DCW. In order to allow direct comparison of the figures determined for yield in these studies to those reported in the literature, this calibration curve allowed conversion.

The final calibration curve confirms the accuracy of the optical density assay. Good linearity exists between OD and WCW until high optical densities are reached. As reported in 2.5.1 the linear range of the OD assay is 0.1-0.6OD. Consequently, the higher the broth OD e.g. >45 the more extreme the dilution required (i.e.90-100-fold), the larger the dilution the greater the likelihood of dilutional errors and liquid handling differences. However, in the batch fermentations described here the OD did not often exceed 45 so the accuracy of the measurements was never in doubt, however, this limitation should be acknowledged if utilising more intensive modes of operation i.e. fed-batch.

6.3 Duplicate 4L fermentations at 37°C

6.3.1 Introduction

Following the successful creation of large constructs using the pGEM11 vector and their successful transformation into *E.coli* DH1, statistical design studies were performed to identify optimum cultivation conditions (5.4) with which to produce the large constructs. The results of those investigations were ambiguous because poor yields were returned. However, without knowledge of the stability problems it was decided to progress to pilot-scale (4L) fermentations using the conditions chosen as being the most optimal; 37°C, 100μgmL^{-1} Ampicillin. This section details the results of these duplicate fermentations and how it came to be realised that the plasmids were being plagued by instability issues.

6.3.2 Results and discussion

The results of the fermentations are detailed in Figure 6-2 and the results summarised in (Table 6-2). The first noticeable fact are the differences in the growth profiles between the smaller constructs (pGEM11 [3.2kb]/ pGEM16) and the larger pGEM33 and pGEM49. The two larger constructs displayed much longer lag-phase periods of about 4.5 hours compared to 3 hours for the smaller constructs. The explanation for this was only realised after appreciation of the stability issues with the larger series. According to the stability profiles of these larger constructs at 37°C (Figure 5-19) at this stage of the fermentation train it is predicted that only a small proportion of the cells used to inoculate the fermenters

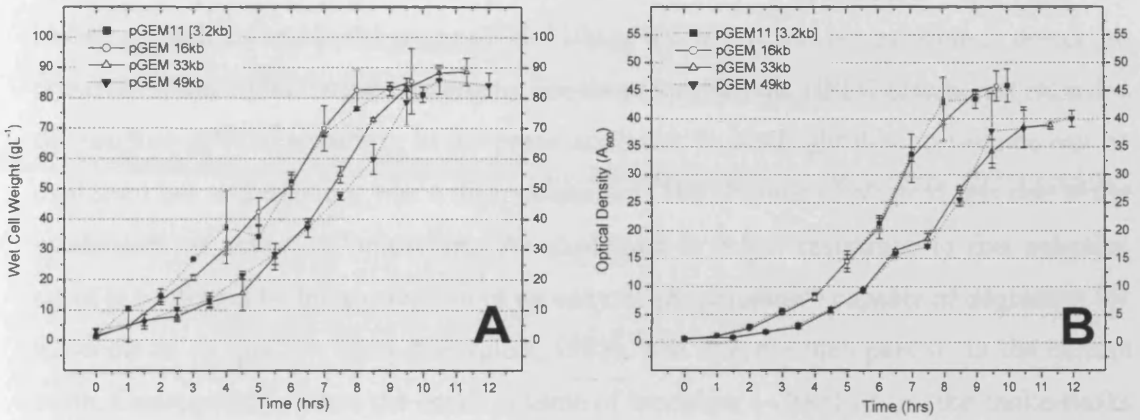

Figure 6-2 Results from duplicate 4L pilot-scale batch fermentations of the large pGEM series of plasmids created by shotgun cloning. Fermentations were conducted at 37°C on complex media supplemented with 100μgmL^{-1} Ampicillin. Figure A plots the progression of wet cell weight and B plots OD progression.

Table 6-2 Table summarising the key growth measurables obtained from 4L pilot-scale fermentations of the pGEM series of plasmids at 37°C.

	Final WCW (gL^{-1})	Final OD (A_{600})	Growth Rate (h^{-1})	Growth Rate % of parental rate
pGEM11 (3.2kb)	81.4	45.9	0.367	93.1%
pGEM16 (16kb)	85.6	45.9	0.372	94.3%
pGEM33 (33kb)	88.7	38.9	0.35	88.8%
pGEM 49 (49kb)	84.3	40.1	0.351	89.0%
Average	85	42.7	0.36	91.3%

would have been plasmid-bearing. Throughout inoculum preparation the plasmids would have been lost and with them the resistance to ampicillin. Consequently, when the cells were passaged into the fermenter containing fresh selective agent the growth of the vast majority of cells would have been inhibited. As such when it was thought the fermenters were being inoculated to a starting OD of 0.1, in reality the figure would have been lower. The lower value would have represented the small portion of plasmid bearing cells capable of resisting the ampicillin and any cells remaining which were not destroyed by the ampicillin before it was degraded. The lower starting optical density explains the extended lag-phase demonstrated by the most unstable plasmids.

Samples extracted from the fermentations were analysed for the presence of plasmid using HPLC (2.5.5 and 2.5.11). Presence of pGEM11 (3.2kb) plasmid was confirmed as having a specific yield in the range of 90-110μggWCW^{-1}. It was not possible to detect the presence of any of the larger constructs. For these samples the HPLC results just recorded the residual gDNA remaining in the preps analysed. In hindsight this occurrence can be explained but at the time it was a disappointment. The absence of plasmid was due to the mechanism of action of ampicillin. As explained in 5.6.1, resistance to this selective agent is conferred by the expression of an enzyme *(β-lactamase)* capable of degrading the molecule to an inactive form (Georgiou, 1988). The enzyme then persists in the culture broth. Consequently, when the small volume of inoculum (~30mL) from the shake-flasks was added to the fresh media in the bioreactor there already existed a significant level of *β-lactamase* activity. Estimates place the activity of the enzyme at such a magnitude that all the selective agent in the bioreactors could have been degraded in less than 10s (5.6.1). With such rapid degradation of the selective agent the pressure for the bacterial cell to maintain and propagate these plasmids was lost. Due to the large size the metabolic burden meant propagation of these constructs was unfavourable and as such the plasmid-bearing population was soon outgrown by the plasmid-free population. This did not occur with the smaller pGEM11 construct since its propagation was perhaps not as disadvantageous but certainly the probability of loss was much less. More information concerning the stability issues faced by these plasmids is outlined in 5.6.

6.3.3 Conclusions

The results of these fermentations were disappointing. The likelihood of instability issues was thought likely after the results from the optimisation experiments failed to demonstrate significant plasmid yields. It was hoped that the situation may improve in the more controlled environment of the bioreactors. This was not found to be the case.

In light of these results, investigations were performed to confirm that plasmid instability was the cause of the absence of plasmid DNA. The results of these runs were outlined in 5.6 confirming the hypothesis. With limited options available the few methods which could be employed to discourage the loss of plasmids were attempted. These included the use of the more degradation resistant antibiotic (carbenicillin), a different host-strain (DH10β) and reduced temperature of incubation (25°C). It was decided that the most applicable method was to reduce the temperature of cultivation in order to reduce the growth differential between plasmid-free and plasmid bearing cells. Additionally, more

stable clones were selected. After conducting these optimisation studies, repeat pilot-scale 25°C fermentations were conducted as described in the next section.

6.4 Fermentations at 25°C

6.4.1 Introduction

Duplicate pilot-scale 4L working volume fermentations of each of the constructs were conducted in an identical fashion to as outlined in 2.7.3, except that the cultivation temperature was adjusted to 25°C, including for the inoculum development steps prior to the fermentations. As described in the stability studies the aim was to reduce the specific growth rate of the culture with the hope that plasmid copy number would be up-regulated and that the growth rate differential between the plasmid-free and plasmid-bearing cells would be minimised. It was outlined in 3.3 how judicious control of the culture growth rate can have a positive impact on plasmid specific yield and this was demonstrated for fermentations of relaxed plasmids as shown in Figure 3-10 (Vasuki, 1989). In addition, there are reports that reducing growth rate increases plasmid stability by reducing the differential between plasmid-free and plasmid-bearing cells (O'Kennedy *et al.*, 1995).

It was appreciated that reducing the incubation temperature by such a degree would massively extend the periods required for growth. To assess the extent of this change preliminary fermentations were conducted and it was discovered that fermentations at this temperature required ~20-24 hours from inoculation to harvest[♦] (with the additional 24 hours required to prepare sufficient inoculum by shake-flask fermentation). At 37°C batch fermentations using the conditions outlined in 2.7.3 could be completed within 12 hours. Due to the extended operation monitoring the entire fermentation in terms of recording WCW and OD would not be possible. To overcome this the reactors were inoculated in the evening and the initial lag-phase period of growth (0.1→~6OD) was left to proceed unmonitored. As a result no growth or yield data was obtained for the first 8-9hrs of growth. However, it was felt that this was not a major limitation since not much could be gleaned from this initial period.

[♦] Fermentations were harvested, as before, following the spike in DOT indicative of the culture being O_2 limited and repiring anaerobically. Often accompanied by a decrease in pH as the catabolites of anaerobic respiration are released into the media. (Figure 9-14 to Figure 9-25)

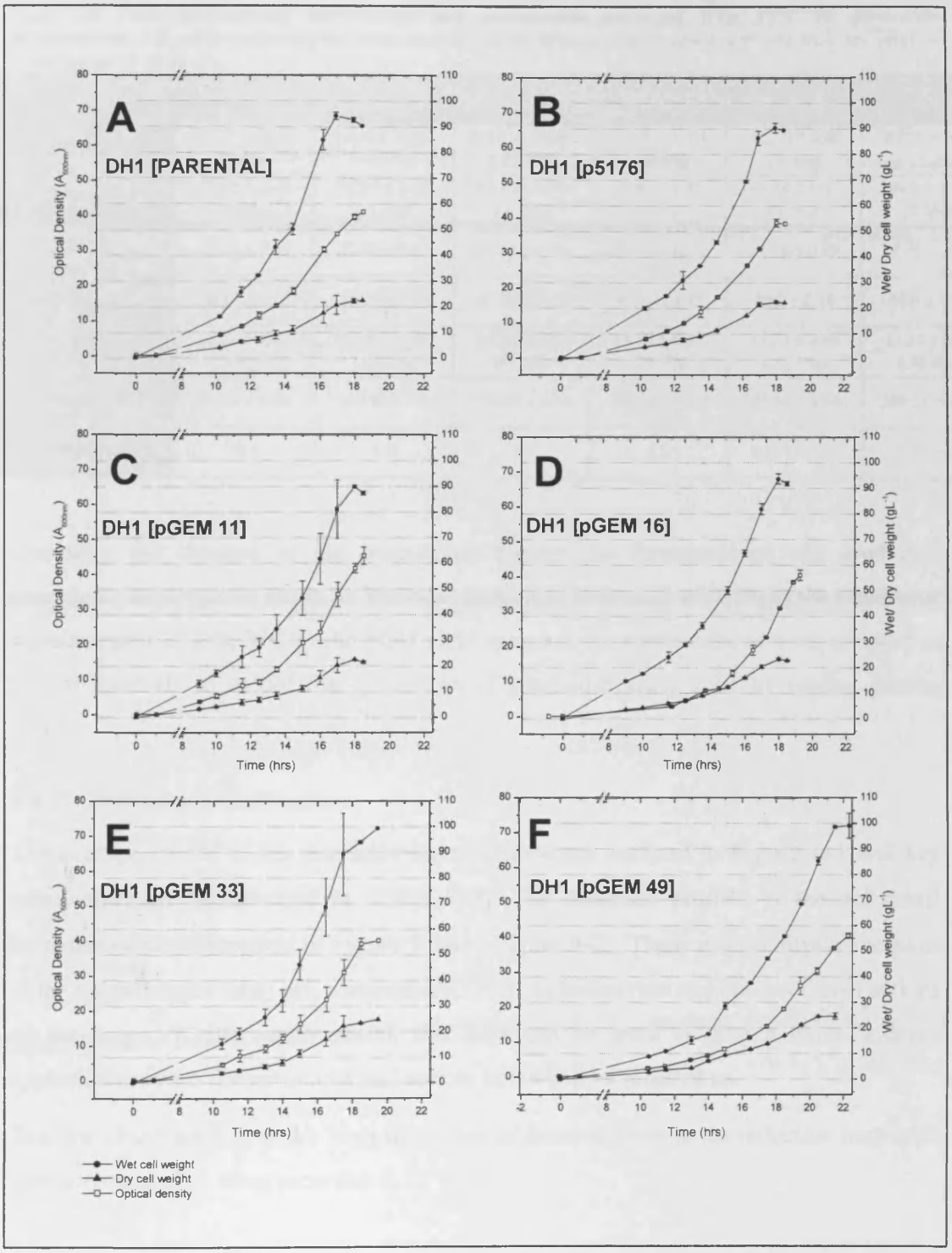

Figure 6-3 Chart displaying the mean progression of optical density, wet and dry cell weight through the course of 4L duplicate fermentations on GSK proprietary media at 25°C [100μgmL^{-1} ampicillin]. [A; DH1 parental / B; DH1 p5176 / C; pGEM 3.2kb / D; DH1 pGEM 16kb / E; pGEM 33kb / F; pGEM 49kb]

Table 6-3 Table summarising the average key measurables extracted from 25°C 4L pilot-scale fermentations of *E.coli* propagating the large plasmid series. Where percentages are shown they are relative to the parental value

Strain / Parameter	DH1 parental	P5176 (116kb)	pGEM11 (3.2k)b	pGEM16 (16kb)	pGEM33 (33kb)	pGEM49 (49kb)
Final Growth Rate (h^{-1})	0.266 ± 0.019 (100%)	0.215 ± 0.002 (-18.8%)	0.220 ± 0.006 (-17.3%)	0.215 ± 0.004 (-19.0%)	0.25 ±0.008 (-5.8%)	0.225 ± 0.03 (-15.3%)
Final WCW (gL^{-1})	91.88 ± 2.16 (100%)	90.55 ± 1.48 (-1.5%)	87.33 ± 0.74 (-5.0%)	91.85 ± 0.85 (0.0%)	96.78 ± 3.57 (5.3%)	99.1 ± 4.88 (7.9%)
Final DCW (gL^{-1})	22.10 ± 0.54	22.56 ± 0.41	21.55 ± 0.43	22.85 ± 0.212	24.08 ± 0.89	24.65 ± 1.22
Final OD	38.15 ± 4.17	38.25 ± 0.35	45.45 ± 2.47	40.55 ± 1.48	40.2 ± 0.14	40.5 ± 0.71
Max OUR ($mmolsL^{-1}h^{-1}$)	17.89 ± 0.19 (100%)	14.98 ± 0.088 (-16.3%)	16.94 ± 0.29 (-5.3%)	14.46 ± 0.97 (-19.2%)	15.51 ± 0.88 (-13.3%)	11.37 ± 0.61 (-36.4%)
Total O_2 Demand (mmols)	219.3 ± 8.84	187.85 ± 2.6	194.34 ± 6.14	146.98 ± 0.14	205.54 ± 0.544	169.74 ± 12.6
Final Plasmid Stability	N/A	1.0	1.0	1.0	0.22 ± 0.042	0.12 ± 0.017

Excepting the changes in the inoculation regime the fermentations and analytical procedures were carried out in an identical fashion to before. In addition to the traditional measurements of OD, WCW and 5OD yield samples, the fermentations were sampled at regular intervals to record the proportion of plasmid-bearing cells by replica plating (2.6.8).

6.4.2 Results and Discussion

The average results of the duplicate fermentations are outlined in Figure 6-3 and key measurables are summarised in (Table 6-3). The complete profiles of the individual fermentations are displayed in Figure 9-14 to Figure 9-25. These graphs display the plots of the online logged data; pH, temperature, DOT, agitation rate and the associated actions on the loops. Whilst supplemental, this data can be used to give a more in-depth appreciation of the fermentations and certain items will be referred to.

The first observation to make from this series of fermentations is the reduction in growth rate as compared to those recorded at 37°C.

For example, the parental negative control fermentations recorded an average of growth rate of $0.394h^{-1}$ at 37°C (Table 6-1) whilst at 25°C the same figure had dropped to $0.266h^{-1}$ representing a 33% decrease. Similar decreases were recorded for the other fermentations. The aim of cultivation at 25°C was to reduce the growth rate, so in that sense the fermentations had been successful.

More information about the growth rates is provided by the relative performance of the plasmid bearing strains to the parental negative control. From Table 6-3 it can appreciated that culture growth rate did decrease for strains bearing plasmids. However, there did not appear to be any logical trend in the reported growth reductions, with all (except pGEM 33) recording ~15-20% relative reductions. It is postulated that a more linear decrease would have been witnessed had each of the constructs been propagated at the same copy number, since as plasmid size increased the amount of extrachromosomal DNA propagated by the strains would have increased proportionately and so placed more pressure on the host cell replication. As it was, stability issues meant that direct comparison on this front was not possible.

The table also details the mean maximum oxygen uptake rates and the total oxygen demand required over the course of the fermentations. Maximum oxygen uptake rates (OUR) were obtained from mass spectroscopy of the fermentation exit gas plotted in Figure 9-14 to Figure 9-25 and calculated using the method described in (2.7.6). Values for total oxygen demand were obtained by integration of the curves describing oxygen uptake rate. The figures for plasmid-bearing strains all describe a similar relative decrease in the relative oxygen uptake rates and total oxygen demands. This suggests that there is no significant relationship between increasing construct size and increased oxygen requirement. This is in agreement with other authors who described no significant impact on OUR by increasing plasmid size (Kay *et al.*, 2003). The fact that all the constructs reported a decrease in relative oxygen uptake rate/demand may also be significant. It suggests that the demand for oxygen is more related to the culture growth rate than the actual plasmid size, consequently, the parental strain records the highest value.

The fermentations all recorded similar biomass yields in the order of 40-45OD and WCW in the order of $85\text{-}90gL^{-1}$.

More information on the fermentations is provided by the graphs plotting the online data which was continually logged (Figure 9-14 to Figure 9-25). Of interest are the plots of pH and temperature. Although these variables were maintained constant by the action of the control, the % action plots are interesting. The % action on the heating loop demonstrated a smooth decrease with time displaying the decreased action (heating) required on the temperature loop with time. It is believed that this mirrors very precisely the growth of the cultures for as the cell density increased the heat produced by the culture increases proportionately and the control moves from needing gentle heating to an increasing level of cooling. Similarly for pH, as the fermentation progressed the action on the pH loop increased with more base required to neutralise the acidic metabolites created by respiration.

6.4.3 Stability profiles

Having identified plasmid instability as the cause of the absence of plasmid when fermentations were conducted at 37°C, it was felt essential to monitor plasmid stability during this series of fermentations. The results are detailed in Figure 6-4. Figure B details the proportion of plasmid-bearing cells during the fermentations. From the profiles it can be appreciated that pGEM11, as has always been the case, was maintained at 100% stability. The reduction in cultivation temperature also corrected the instability demonstrated by the 16kb plasmid at 37°C. Unfortunately, the temperature reduction was not sufficient to eliminate the problems with instability found in the larger two constructs of 33kb and 49kb.

Considering pGEM 33kb first. The profile demonstrates the increase in plasmid–bearing cells following inoculation. This has been seen before (Figure 5-21) and is due to most plasmid-free cells being destroyed upon passage of the inoculum to broth containing fresh selective agent and so increasing the relative proportion of plasmid-bearing cells. However, after this initial peak the stability decreased over the course of the fermentation, but an equilibrium was reached toward the end of the fermentation. It is also proposed that there was an increase (at least a stabilisation) of plasmid stability in the last couple of hours of the fermentation.

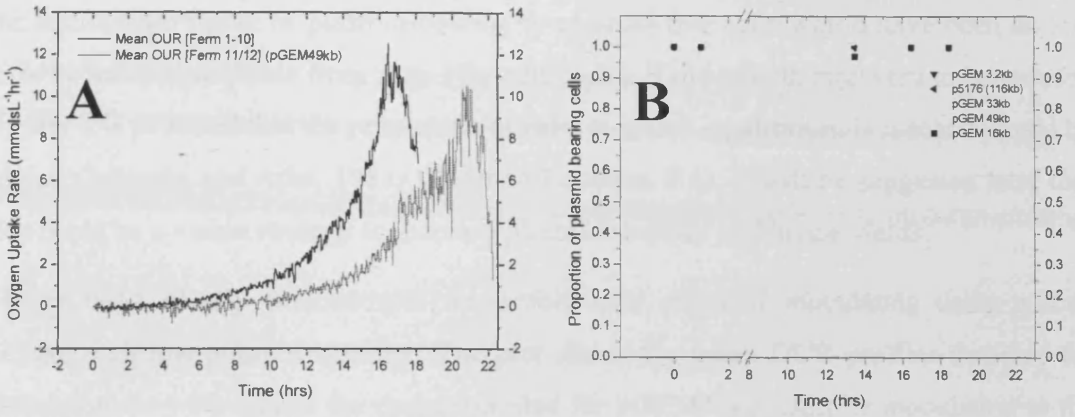

Figure 6-4 Figures profiling the plasmid stability during the course of the 25°C fermentations. Figure B plots the mean proportion of plasmid bearing cells recorded during the duplicate fermentations for each of the plasmid bearing strains. pGEM 11 (3.2kb) recorded 100% stability throughout the fermentation. The graph also shows that the reduced temperature did lead to stabilisation of the pGEM16 construct as predicted by stability studies. Unfortunately, the reduced temperature was not sufficient to correct the stability profiles of the larger constructs. It can be seen that pGEM 33 showed a dramatic increase in the proportion of plasmid bearing cells shortly following inoculation. This is simply due to the ampicillin causing a reduction in the number of plasmid-free cells. The stability does decrease following this event. For the pGEM49 constructs no dramatic rise was witnessed possibly suggesting even more rapid loss of plasmid in that the majority of plasmid-free cells were inhibited following inoculation but that the loss of plasmid was so rapid that this was not recorded. It is expected that at the point of the first sample (T+1) the ampicillin had largely been degraded. However, both strains did record presence of plasmid-bearing cells through the course of the fermentation albeit ~10-20% but that suggests an equilibrium was reached.
Figure A plots the mean OUR profiles of fermentations 1-10 compared against the same for the pGEM 49kb plasmids. The delay hints at a phenomenon previously witnessed in that the poor stability profile lead to an extension of the lag-phase and hence an extension of the fermentation.

This would be expected as toward the end of the fermentation a combination of the competition for nutrients and the increasing presence of toxins leads to the wholly expected drop-off in culture growth rate. Again, any reduction in growth rate is advantageous as it leads to a reduction in the relative growth rates between plasmid-free and plasmid-bearing cells. Additionally, as is outlined in the next section this decrease in growth also leads to an up-regulation of plasmid copy number. By harvest, the proportion of cells bearing the 33kb plasmid was found to be ~22%.

The profile of the 49kb plasmid differs to that of the 33kb construct. It did not demonstrate the same increase one hour following inoculation. This could be due to the increased instability shown by this construct. However, the culture did seem to reach equilibrium again as the fermentation progressed and again showed an increase/ stabilisation toward the end of its growth. At harvest the proportion of cells bearing the 49kb was determined to be ~12%. The fact that both cultures reached a detectable equilibrium, demonstrates the effectiveness of reducing the growth rate and hence the

growth differential that persists between plasmid-free and plasmid-bearing cells. At 37°C the equilibrium figure of plasmid-bearing to plasmid-free cells would have been so low as to be indistinguishable from zero. Hypothetically, if the growth rate were to be reduced further it is expected that the proportion of cells at which equilibrium is reached would be higher (Imanaka and Aiba, 1981) (Refer to Equation 5-4). It will be suggested later that this could be a viable strategy to increase plasmid stability and hence yields.

Figure 6-4A clearly demonstrates the problematic effect of inoculating using a seed culture with low plasmid stability. The plot shows the mean OUR profiles detected for fermentations 1-10 against the mean recorded for pGEM49kb. Despite inoculation to the same final OD of 0.1 it is clear that the lag-phase of the 49kb is extended by the inhibitory effect of the selective agent on the plasmid-free cells.

6.4.4 Conclusions

This series of fermentations has demonstrated that cultivation of strains bearing large constructs at the reduced temperature of 25°C is feasible. The results suggested that growth rate was reduced by ~30% relative to 37°C incubation. Also, it was suggested that increasing construct size did reduce growth rate but not in any linear fashion. It was also shown that oxygen uptake rate was not related to the size of the construct. The conclusions being drawn cannot be relied upon to be definitive since despite the reduced temperature, the stability of the larger 33kb and 49kb plasmids remained troublesome. Despite this, significant improvements were made in improving the overall stability of the plasmids in that at least plasmid-bearing cells could be detected at the harvest of the fermentation. A slight increase in plasmid stability was recorded toward the end of the fermentations, which provides further evidence of the advantages offered by operating at a reduced growth rate.

6.5 Analysis into the plasmid yields of the duplicate 25°C fermentations

6.5.1 Introduction

Results from the fermentation growth analysis suggested that the reduced temperature fermentations had been a success in that the aim of lowering specific growth rate had been achieved. Additionally, the stability profiles suggested that a proportion of cells propagating the larger 33kb and 49kb constructs were plasmid-bearing at harvest. Therefore, unlike the 37°C runs, plasmid was expected from these fermentations. As with all other fermentations, multiple 5OD volume-equivalent samples were taken throughout the duplicate fermentations and prepared as described in 2.7.5. To record specific yield progression the 5OD cell pellets were lysed in a typical fashion and the clarified lysate concentrated by precipitation using 0.7 volumes of IPA (2.5.5). The plasmid pellet was then resuspended in 100µL of TE buffer and the concentration of the solution quantified by HPLC (2.5.11).

Knowing the concentration of the plasmid solution allowed simple calculation of the plasmid mass. Since both the volume of broth processed to obtain a 5OD sample and the wet cell weight at the time of sampling were known, calculation of the mass of the cell pellet was a simple manipulation. From both the mass of plasmid and cell pellet it was extracted from, the plasmid specific yield could be found simply by division of one by the other. Duplicate 5OD samples were processed for each time point of each fermentation. (For more information concerning the calculation of specific yield refer to Figure 9-29). From plasmid specific yields simple manipulations could be used to calculate plasmid volumetric yield and plasmid copy number (Equation 2-2 and Equation 2-3). For each fermentation a sample of the inoculum was processed as described above to calculate the specific yield of the culture from time 0. This value was the same for both duplicates as both vessels were seeded from the same inoculum. At the end of the fermentation the cell paste was recovered by batch centrifugation and frozen at -80°C for later use in DSP studies.

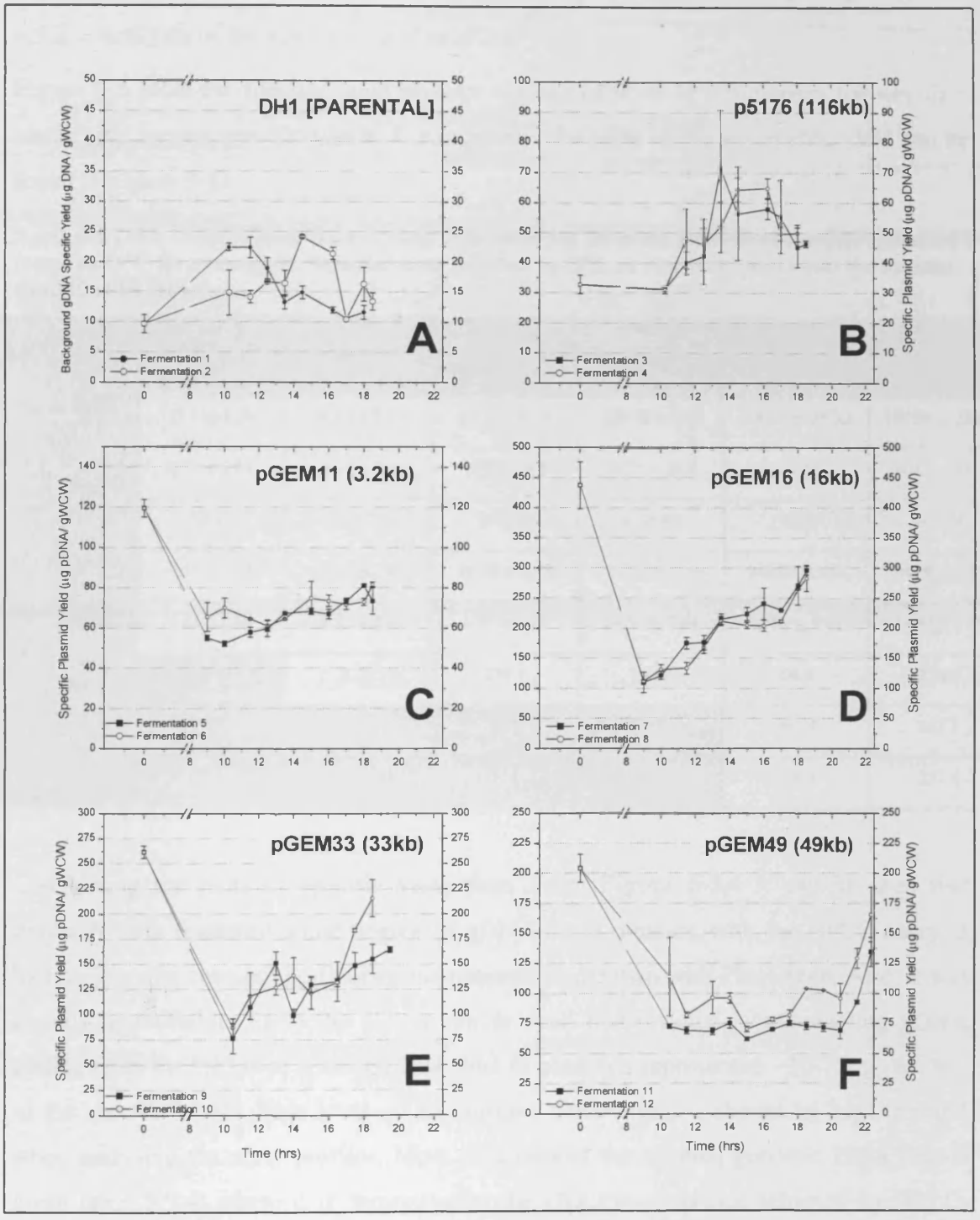

Figure 6-5 Plots displaying the specific yield progression of the fermentations carried out at 25°C. It should be appreciated that whilst the majority of the gDNA contamination was removed when the 5OD sample pellets were lysed and purified by IPA some remained in the samples for analysis by HPLC. The overwhelming majority of gDNA remaining was sufficiently small to avoid co-elution with the plasmid DNA, however some large fragments did persist. The full background into the HPLC assay is outlined in (REF). When analysing the plasmid specific yield curves it must understood that the small amount of contamination shown in Figure A will contribute to the above profiles. In the majority of cases this is not that important but it is for lower copy constructs i.e. (p5176).

6.5.2 Analysis of the specific yield profiles

Figure 6-5 plots the specific yield profiles whilst (Table 6-4) summarises the key data concerning harvest specific yields. For reference, the plots of the volumetric yield can be found in Figure 9-13.

Table 6-4 Table summarising the key yield data recorded from the analysis of samples extracted from the 25°C fermentations. Samples were purified by IPA on clarified lysates and the streams quantified by HPLC.

Strain / Parameter	DH1 parental	P5176 (116kb)	pGEM11 (3.2k)b	pGEM16 (16kb)	pGEM33 (33kb)	pGEM49 (49kb)
Final Specific Yield (µgpDNA/ gWCW)	12.51± 1.29	48.13 ± 2.53	77.53 ±5.79	289.48 ± 9.33	190.07 ± 36.19	150.06 ± 22.01
Inoculum Spec. Yield (µgpDNA/ gWCW)	9.65 ± 1.51	32.8 ± 3.1	119.4 ± 4.4	437.5 ± 38.8	261.4 ± 6.2	204.1 ± 11.7
Final Spec. Yield (µg pDNA/ gDCW)	50.19	193.01	310.89	1160.83	762.2	601.74
Final Spec. Yield from Maxi-preps(µg/gWCW)	7.11 ± 2.06	5.77 ±0.08	86.58 ± 8.78	272.02 ± 13.94	144.88 ± 1.06	64.08 ± 7.35
Final Volumetric Yield (mg pDNA L^{-1})	1.15 ± 0.09	4.36 ± 0.3	6.77 ± 0.45	26.59 ± 0.61	18.33 ± 2.82	14.82 ± 1.45
Final Copy Number (copies/cell)	N/A	3.59	270.1	149.6	50.4	27.29
Specific Yield assuming 100% stability (WCW)	N/A	N/A	N/A	N/A	863.9	682.1
Copy Number assuming 100% stability	N/A	N/A	N/A	N/A	229.4	227.4

Considering the plots of specific yield first. From Figure 6-5A it can be seen that although there remained some degree of gDNA contamination with the HPLC assay, it had far less of a corrupting effect on the plasmid signal than with PicoGreen. Also, it was directly quantifiable. From the plot it can be seen that residual, contaminating gDNA eluting from the HPLC at a comparable time to plasmids represented ~10-15µggWCW^{-1} of the specific yields. This level of background contamination should be kept in mind when analysing the other profiles. More detail about the residual genomic DNA data is given later (6.5.4) where it is demonstrated the effective clearance achieved by HPLC. (Also refer to Figure 4-22).

Turning attention to the specific yield plot of the BAC p5176 (116kb). From the graph the increase in specific yield can be seen to coincide with the period of maximum growth. This has been reported previously (Figure 3-5) and is because the replication of this BAC is maintained in-line with host genome replication. As such, it is a growth-linked product, such that during periods of high growth there are more copies in existence. When

analysing Figure 6-5B it should be appreciated that its high-point, in mid-point of the exponential phase, is also when the genomic DNA contamination will be at the greatest (Figure 6-7). A point worth noting concerns the inoculum specific yield. In contrast to the other strains it can be seen that the specific yield of the inoculum is not significantly higher than the specific yields reported throughout the course of the fermentations. Again this is because this plasmid is growth-linked, which is in direct contrast to the other constructs where higher yields are associated with periods of slower growth. From Figure 6-5 the final specific yield of this construct was placed at ~50μggWCW^{-1}, a value consistently reported throughout this project due to the very controlled nature of its replication. However, a fraction of the specific yield can be attributed to gDNA contamination (~25%) which would bring the actual figure down. This would also mean that the specific yield reported in the table would be more like 2.5 copies per cell, more in line with predicted values (Frame and Bishop, 1971). As outlined several times previously, improvement on this yield is impossible by manipulation of environmental parameters due to the nature of the plasmid's replication.

Considering the 3.2kb plasmid (Figure C), the yield profile shows a gradual increase in specific yield over the course of the fermentation from ~60 to 80μggWCW^{-1}. However, overall the yields of this construct were disappointing. In the product information the copy number of this plasmid was reported to be between 400-600 copies per cell. Such a copy number would only be recorded if the specific yield was double those reported at harvest in these fermentations (Promega, 2004). It is assumed that the figure for 400-600 may have been reported following a period of slow growth. For example, consider the value for the specific yield for the inoculum (~120μggWCW^{-1}). The increased yield is a result of period of sustained low-growth, since the culture used for inoculation had been in the stationary phase of growth for some time. As outlined before slow growth is very beneficial to plasmid copy number. It will be discussed later whether the fermentations were harvested too early when on fact the cultures should have been cultured past the DOT spike.

The pGEM16kb showed a similar increase in specific yield over the course of the fermentation to as witnessed before with another relaxed plasmid model; pSVβ (Figure 4-12). Once again the cultures did demonstrate a steep increase in the yield toward the end of the fermentations. This increase, toward the end of the fermentation is well documented and the reason is as discussed earlier (Prather *et al.*, 2003; Reinikainen *et al.*,

1989). Once more it must be suggested that the fermentation was harvested too early, as judging from the inoculum results it could be predicted that the increase in plasmid specific yield could have continued and taken the specific yield to ~450μggWCW^{-1}. The harvest specific yield was found to average ~300μggWCW^{-1} meaning an extra 50% increase in yield could have been attained. The increase in harvest yield relative to pGEM11 is wholly attributable to the extra 13kb of DNA being propagated per plasmid. However, as can be seen from the table, the predicted copy number actually fell from 270 to 150 upon the insertion of the 13kb DNA fragment into pGEM11 to create pGEM16. This is to be expected and is reported that copy number is related to plasmid size (Sambrook *et al.*, 1989; Qiagen, 2005). Overall the yields of this plasmid are poor being at a similar level to that of pSVβ (6.9kb) a plasmid ½ its size (Figure 4-12). The reason for the low yields are due to the lower copy number. It had been expected that copy number may have decreased upon insertion of large fragments but that it was hoped since the copy number of the original vector was 400-600 meant that high copy numbers would still be obtained. However, it has to be stated that compared to the 50μggWCW^{-1} harvest yield of p5176, yields of 300μggWCW^{-1} (with the potential for 450μggWCW^{-1}) is an improvement.

The specific yield profiles of the two larger pGEM constructs (33kb and 49kb) do show a higher degree of variation between vessels. A rise of specific yield was recorded over the course of the fermentations with yield increasing from ~75 to 200μggWCW^{-1}. Again, the increase toward the end of the fermentation was more pronounced. It is suggested that the increase in specific yields toward the end of the fermentations for both 33kb and 49kb is more dramatic than for the other pGEM models. This is believed to be due to the slow down on growth recorded during these periods as impacting positively on both plasmid copy number (copy number is inversely related to specific growth (Vasuki, 1989)) and plasmid stability (stability is inversely related to specific growth (Imanaka and Aiba, 1981)). As a result for one vessel culturing pGEM33 the specific yield recorded an increase from 125μggWCW^{-1} to 225μggWCW^{-1} over the last two hours of cultivation. From Table 6-4 it can be seen that the average harvest value for this construct was a specific yield of 190μggWCW^{-1} and so a copy number of ~50 per cell. This yield is recorded with only ~20% of the cells bearing plasmid (Table 6-3). If the diluting effect of the non-plasmid bearing cells is ignored the copy number of the plasmid-bearing cells in the vessel is closer ~230 copies per cell. This can only be an estimate since it relies on

the value placed on the culture stability being accurate. However, it means that the cells actually bearing plasmid are propagating a massive ~7,500kb of extrachromosomal DNA (~1.7 genome equivalents). This analysis is essential to the conclusions of this project for it means that if the problems with stability were overcome, then large yields from fermentations of large plasmids could be expected.

Finally considering the largest pGEM construct pGEM 49kb. Once more the extreme increase in yield toward the end of the fementation can be seen. The harvest specific yields were placed at ~150μggWCW^{-1}, meaning the potential existed for a maximum specific yield of ~700μggWCW^{-1} should 100% stability be attained. The result is that each cell would be propagating 11,000kb of plasmid DNA

6.5.3 Specific Yields determined by HPLC on Qiagen maxi-prepped harvest paste

Following the 25°C fermentations the samples taken during the fementation were analysed for the presence of plasmid and the specific yields reported as detailed in the preceeding section. To allow comparision it was decided to determine the specific yield of the constructs by Qiagen max-prep studies. As such, duplicate 2.0g masses of frozen cell paste were processed by this technique♦ (2.5.8.1) and the eluents quantified by HPLC. The results are detailed in Figure 6-6.

When the calculated specific yields from the Qiagen studies were compared to those recorded by HPLC on harvest IPA samples, the results were mixed. From Figure 6-6A it can be seen that the values for specific yield align vey well when comparing the smaller pGEM 3kb and 16kb constructs but that the yields reported for the larger 33kb, 49kb and 116kb were increasingly reduced as compared to harvest IPA values.

♦ It was decided to perform the extractions using standard Qiagen maxi-preps. It was felt that the additional time and variation involved in pursuing Qiagen Large construct kit purification was not justified. In the technique an exonuclease is employed to degrade any gDNA. It was the technique used to generate the material used for HPLC calibration.

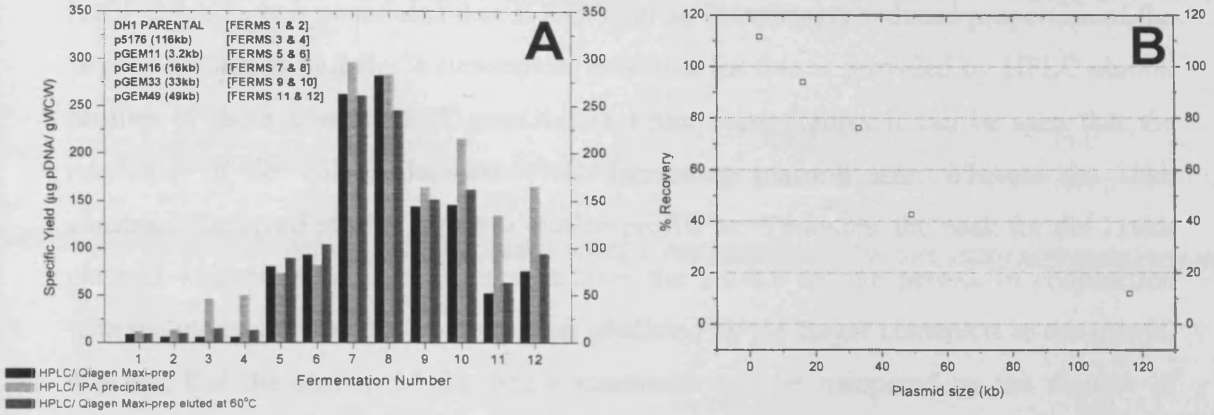

Figure 6-6 Figures plotting the results of investigations into the specific yields of the plasmid as determined by HPLC on harvest material purified using Qiagen Maxi-prep columns. Figure A compares the values for specific yields obtained from the harvest samples taken at the end of the fermentations and determined by HPLC on IPA precipitated clarified lysates to those produced by Qiagen maxi-prep. Two different protocols were employed for the maxi-prep with duplicates run for both. In one the plasmid was eluted using room-temperature buffer and for the other the plasmid was eluted from the columns using buffer at 60°C. Figure B plots the specific yield recorded for Qiagen maxi-prep (60°C elution) as a percentage of that recorded for the harvest specific yields determined by HPLC on IPA precipitated lysates.

A similar issue was encountered in the early stages of this project (3.4.3) when investigating the yields of p5176 from fermentation cell paste. It was suspected that the larger constructs were not eluting effectively from the anion-exchange resin of the Qiagen Tip-500 columns. To investigate this further, repeat Qiagen maxi-preps were conducted on the same batches of cell paste but the elution buffer temperature was heated to 60°C prior to use. This technique is suggested by the manufacturers when dealing with larger constructs (Qiagen, 2005). Referring back to Figure 6-6A it can be appreciated that increasing the elution buffer temperature did have a positive effect on the resultant specific yields. However, as demonstrated by Figure 6-6B the yields produced by increased temperature elution were still below those identified by HPLC, directly on IPA precipitated harvest samples, for the larger constructs. The plot of the recovered yields as a percentage of IPA harvest yields clearly shows a decrease in recovery with increasing plasmid size.

There could be several reasons for this. Due to the increasing sizes of the plasmids each plasmid molecule would bind the matrix at more points and so increase the strength of the overall interaction. Due to the operation of the Qiagen protocol there is no increase in salt gradient, rather the level of salt in the the buffer is fixed at 1.25M

NaCl (2.4.1.3). It is postulated that at this level an increasingly reduced proportion of the larger plasmids is eluted. Circumstantial evidence for this is provided by HPLC elution profiles of these constructs (Figure 4-19). From these figures it can be seen that the resolution of the curves decreases with increasing plasmid size. Whereas the 16kb construct displayed at very uniform elution profile at ~7minutes, the peak for the 116kb plasmid was much broader and spread over the 6.0-8.0 minute period. In conjunction with the increased strength of interaction predicted by the larger constructs to the matrix, it is felt that the elution of the larger constructs will be hampered by the number of conformations larger molecules can exist in, and as such the broader range of charge densities displayed by a population of larger plasmids.

Despite the high temperature elution not all of the specific yield was accounted for, suggesting that this was not sufficient to achieve total elution of the larger molecules. Although it is incorrect to state defintively (since no experiements were conducted employing increasing salt gradients), this fact leads to the conclusion that maybe other factors, other than the strength of the interaction, may be responsible. Increasing the size of the plasmid molecules may mean that they are incapable of penetrating the column effectively. Such an issue was at the heart of a problem with another analytical coumn step employed in this project. As will be outlined later in section 7.4 it was not possible to balance plasmid over the $CaCl_2$ step of the downstream process, because attempts to desalt larger plasmid samples for analysis using gel-base (SEC) PD-10 coulumns resulted in limited plasmid being eluted. It is believed that the larger plasmids were incapable of penetrating the gel matrix. Whilst no direct comparison can be made between the AEX resin and the gel-based columns it remains a possibility.

If studies confirm that larger plasmids are incapable of effective prentration in to Qiagen AEX resins then it does not bode well for AEX column stages in this process, where resins of comparable dimensions are employed. It was found that the plasmids did penetrate the HPLC columns effectively but that could be by virtue of the large pressures employed.

6.5.4 Investigations into the levels of contaminating gDNA

The main flaw determined in the PicoGreen assay, as applied to plasmid samples of low concentration, was the large contributory effect that contaminating gDNA had on the signals used for plasmid DNA quantification. From this realisation every effort has been made to confirm that the signals used for plasmid quantification were produced from the plasmid and not gDNA. For this reason HPLC was employed as studies confirmed that the signal it produced was not affected strongly by residual gDNA contamination (4.5.2.1). However, the studies did demonstrate some carryover of residual gDNA, assumed to be large fragments. In this section the contamination will be investigated further.

Figure 6-7 plots the results of gDNA quantification of samples taken from the DH1 Parental fermentations. In the yield profiles shown in Figure 6-5 the figures for gDNA contamination are those derived from HPLC analysis of IPA precipitated clarified lysates, since this was the method used to quantify the plasmid-containing samples. The intent of these studies was to compare the values of gDNA contamination produced by this measure against other methods. It was realised that during DSP studies plasmid was to be balanced by HPLC and the hope was to do so directly on samples.

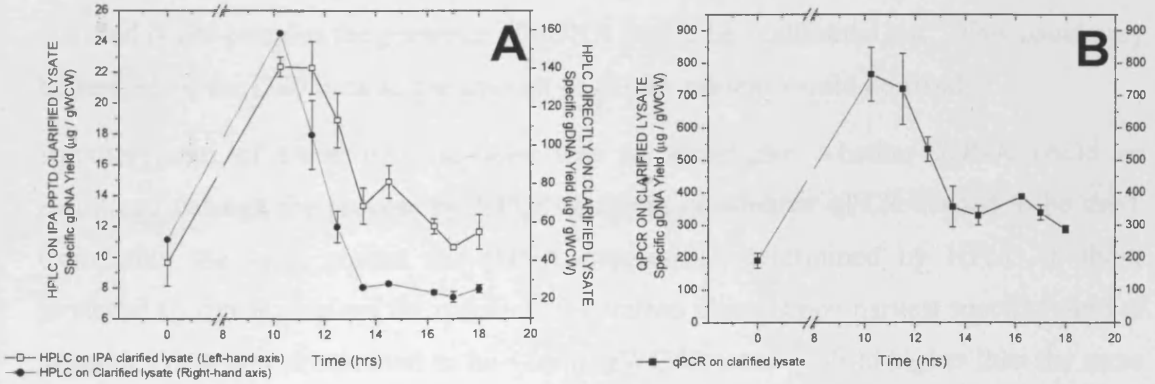

Figure 6-7 Studies conducted to assess the progression of gDNA contamination in fermentation samples used for analysis. The studies were performed to place a definitive value on the level of background detectable gDNA in the samples used for plasmid analysis during the fermentations. Secondly it was decided to perform preliminary runs to assess whether gDNA in process streams could be reliably monitored using HPLC or whether qPCR was needed to track the progression of this contaminant in downstream studies. Both figures plt the specific yield of gDNA from samples taken during a DH1 Parental fermentation but quantified by three different methods. HPLC on IPA clarified lysates (as was used for the plasmid samples), HPLC directly on clarified lysate samples and qPCR directly on clarified lysate

From Figure 6-7A it can be seen that gDNA quantification on IPA precipitated samples produced the lowest values for contamination at harvest, ~8μggWCW^{-1}, in-line with the values reported alongside the plasmid yield curves. This value is much lower than for the direct clarified lysate where values placed upon gDNA contamination at harvest were 60μggWCW^{-1} and demonstrates the removal of gDNA achieved by IPA precipitation. It is belived that the technique is capable of removing much of the small molecular weigtht gDNA contamination since it does not precipitate with the larger (plasmid) species.

The gDNA value of 60μggWCW^{-1}when analysing clarified lysate samples directly meant that a great deal of gDNA contamination would be present if clarified lysate samples taken during the DSP runs were run directly. As such it would be hard to trust HPLC results conducted in clarified lysate without some accommodation being made for this contamination. Again this is due to the relative plasmid concentrations. For high-copy (therefore high-concentration) plasmids, gDNA contamination of ~60μggWCW^{-1} could be ignored if the plasmid existed at ~500μggWCW^{-1}, however, with lower-copy plasmids doing so would be inaccurate. Therefore, the HPLC assay for the plasmid quantification from DSP clarified lysate had to be adjusted. As described in 4.5.2.2 for the analysis of plasmid quantification during clarified lysate a separate HPLC standard curve was developed. The standard curve was prepared by spiking blank, parental clarified lysate with known masses of plasmid. As such, when using the curve to quantify plasmid in clarified lysate samples the presence of gDNA would be "calibrated out". This could only be performed for DSP runs as the amount of gDNA present would be fixed.

Another point of these investigations was to investigate whether gDNA could be monitored through the process by HPLC analysis, or whether qPCR needed to be used. Comparing the yield curves for gDNA progression determined by HPLC to those produced by qPCR answers the question.The values placed upon harvest specific yield of genomic DNA was determined to be ~280μggWCW^{-1}some ~5-fold higher than the same value placed upon the figure by HPLC of clarified lysate. Ultimately, it is believed that HPLC is unable to resolve the small genomic fragments which form the bulk of the gDNA contamination, only the larger species are retained detected by the column. This means that HPLC could not effectively be used to monitor gDNA progression through the DSP process and that qPCR should be used.

A final point to be taken from all of the curves shown in Figure 6-7 concerns their profile. An interesting insight can be gleaned into the progression of genomic DNA

throughout the course of a bacterial fermentation. As described before the p5176 was found to be growth linked since its replication was coupled to that of the bacterial genome. From the curves it can be seen that during the exponential phase cells are propagating double the amount of DNA as to when the cells are in the quiescent stages of growth, indicative of the additional genome copies.

6.5.5 Conclusions

It has been demonstrated that the problems with the instability of the larger pGEM series were alleviated slightly by cultivation at reduced temperatures. Plasmid DNA arising from the propagation of large plasmids under the control of relaxed replicons could be detected. However, the yields were not spectacular even for the strains demonstrating 100% stability. The reported copy numbers of the pGEM11 vector were not achieved. For the larger constructs correcting for the instability, revealed that large yields of plasmid DNA could be expected by virtue of the increased DNA propagated by the plasmids. Analysis of the yield profiles indicated the substantial impact of stabilisation and up-regulation of copy number toward the end of the fermentations. Knowledge of this could allow for improved design of the fermentation process, such that with improved construct design and optimised fermentations 100% stability could be possible.

Also outlined were the problems faced with purification of these large constructs using Qiagen packed bed columns. The poor yields warrant futher investigation since it could suggest potential problems with larger constructs penetrating chromatographic matrices commonly used for plasmid purification.

Further work was conducted concerning the contamination of plasmid samples by residual gDNA. The likely contamination from the HPLC analysis was reported alongside the plasmid yield curves. It was determined that HPLC was not a viable technique for gDNA quantification and that a qPCR assay should be developed.

6.6 Plasmid Topology through the fermentations

6.6.1 DNA Supercoiling

With an average molecular weight of 660Da per base pair, even small pDNA constructs can be considered large, heavy molecules. Thus, in order to fit into the bacterial cell (or ultimately a eukaryotic nucleus) DNA molecules must be condensed. This is achieved by plasmid supercoiling. Supercoilinng in plasmids is achieved by the over/under winding of the plasmid molecule. In addition to reducing the molecule's size, supercoiled plasmids contain a large amount of free energy (ΔG) that can be used to drive biological reactions such as replication and transcription. More details in to the thermodynamics of supercoiling can be found in (Bonilla et al., 1991; Pavlicek et al., 2004). Supercoiling is characterised by the linking number (Lk) which is the number of times the two DNA strands interwind when the molecule is laid on a flat plane. A molecule with no supercoiling has a linking number of (Lk_0) equal to the number of base pairs divided by the helical repeat. Most plasmid molecules display negative supercoiling such that Lk $<Lk_0$ and the supercoiling is in the opposition rotation to the right-handed DNA helix.

DNA topoisomerases catalyse the supercoiling and relaxation of plasmid DNA. These nuclease-active enzymes are divided into two groups. Type I topoisomerases introduce temporary single-strand breaks in DNA. This relaxes the supercoiled molecule into open-circular (OC) form allowing transcription and replication. DNA gyrases introduce supercoiling into plasmid molecules by an ATP-driven process. The degree of supercoiling is regulated by the opposing activities of both types of enzyme, such that the balance of these activities keeps the plasmid DNA at a precisely tuned level of supercoiling. It also suggests that achieving 100% supercoiling during fermentation is an impossibility.

6.6.2 Introduction

Having established that large plasmids had been produced by the reduced temperature fermentations it remained to be confirmed that the plasmids existed in an acceptable form. In an industrial setting, tests for structural homogeneity are required to be performed to characterise plasmid DNA prior to its release. In addition to the strict requirements on the levels of the contaminants it is specified that the plasmid DNA must exhibit >95% supercoiling (Zoon, 1996). There is no accepted reason why supercoiling is

desired. It is commonly argued that eukaryotic cells are more likely to accept SCC pDNA upon administration of a plasmid as a therapeutic agent, however, studies have not confirmed this (Bergan *et al.*, 2000). More likely is that the attainment of 95% SCC is indicative of an acceptable and reproducible process.

Despite the dubious reasoning, it is important to track the supercoiling of the plasmid molecules for other reasons. As is shown in the Chapter 7, a clear understanding of the topology changes which occur during processing can reveal a great deal about the process. Admittedly tracking the changes of topology during downstream processing is probably more critical since the plasmid molecules are free of the protective environment of the cell wall and as such subject to the full impact of physical forces. However, since supercoiling is a biologically driven process, dependent on the relative activities of gyrases and topoisomerases, fluctuations can occur during fermentation which must be understood. Several authors have reported changes in plasmid topology with the progression of fermentation. (O'Kennedy *et al.*, 2003) reported that % supercoiling decreased with progression of batch fermentation but that the same effect was not demonstrated during fed-bacth operation. However, (Schleef, 2001) maintains that fed-batch processing does have a detrimental effect on plasmid quality.

Topology changes were recorded by performing field inversion gel electrophoresis (2.5.19) on IPA precipitated lysates obtained from samples taken during the fermentations. The gels are shown in Figure 9-1 to Figure 9-5. The gels were run for a period of 40 hours at 4°C in attempt to improve resolution. After which time the gels were stained with SYBR-Gold for 24 hours and destained followed by gel densitometry using UVP software (2.5.20 and 2.5.21). Due to the long period require for separation, only single sample sets could be analysed.

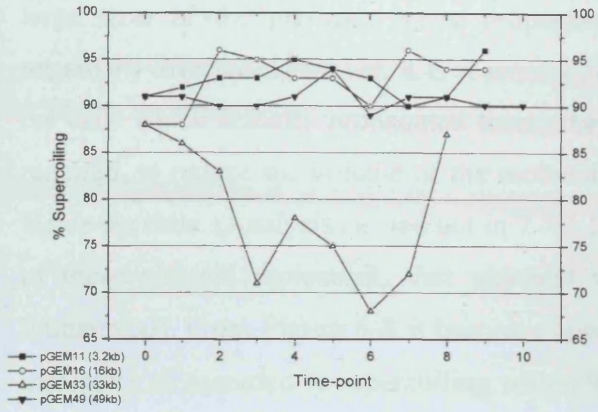

Figure 6-8 Plot displaying the changes in % supercoiling observed during the 25°C temperature fermentations of the large pGEM series of plasmids. It is clear that despite the more pronounced fluctutations displayed by the pGEM33 construct the results for the other plasmids show no major changes in %SCC with the values consistently being between 90-100%. Despite this the smaller two plasmids (3kb and 16kb) did record slightly higher %SCC at harvest.

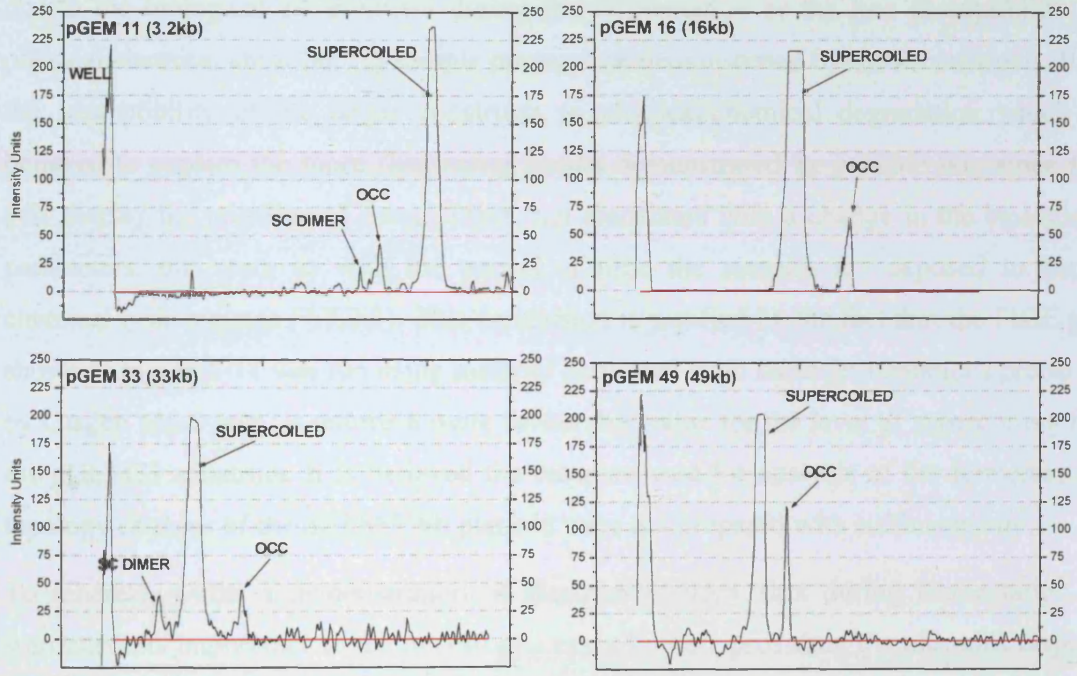

Figure 6-9 Figure displaying the gel scan profiles of the four pGEM constructs normalised against the baseline determined for the lanes. The profiles are those taken from the harvest point of each fermentation and show the relative proportions of the different isomeric plasmid forms.

6.6.3 Results of the Topology Analysis

The changes observed in plasmid supercoiling during fermentation are tracked in Figure 6-8, whilst examples of the gel scan produced by which the relative proportions are shown in Figure 6-9. From the first graph it can be seen that, with the exception of pGEM33, no large variations in plasmid supercoiling were witnessed

during the fermentations. This is encouraging since it was a possibility that due to the large sizes of the plasmids being propagated the resultant toplogy may have been negatively affected. However, it is reasoned that in order to propagate these plasmids (in the cells which actually propagated them) then a high degree of supercoiling would be required, to reduce the volume of the molecules such they would be capable of packing inside the cells. (Analysis carried out in 7.7.3.1 suggests that due to the large size of some of these plasmid molecules, that physical volume of a bacterial cell may become limitational). From Figure 6-8 it becomes apparent that the 3kb, 16kb and 49kb plasmid molecules all recorded % supercoiling within 90-100%. The smaller constructs did record higher degrees of supercoiling upon harvest but it remains debatable whether that was due to the biological environment during the fermentation or the less susceptibility to physical/chemical shear during sample preparation demonstrated by these constructs. It is the susceptibility of the larger constructs to physical/chemical degradation which is believed to explain the more fluctuating results demonstrated by pGEM33kb, since the gels display the presence of linear forms, not associated with a change in the biological parameters, but more so with the period of time the samples are exposed to harsh chemical lysis regimes (7.7.2.3). This conclusion is justified by the fact that the FIGE gel shown in Figure 5-11 was run using material harvested from these fermentations prepared by Qiagen Maxi-prep. It returns a more favourable value for the level of supercoiling for the pGEM33 construct. It is believed the samples used for analysis of the fermentation topology changes of the pGEM33kb plasmid were not prepared with sufficient care.

To reiterate, whilst a demonstration of plasmid topology flux during fermentation is warranted, its importance to the overall process is limited, providing the plasmids display a significantly high level of supercoiling at harvest. This is because supercoiling cannot be improved upon downstream and as such the proportion of SCC plasmid at harvest represents the total product available for purification. However, as will be demonstrated in the proceeding chapter, topology fluctuations are much more likely when the plasmid is free of the protection provided by the bacterial cell wall.

6.7 Upstream Processing Conclusions

Work in this chapter has described how large plasmids, created by cloning fragments of DNA into pGEM series of vectors, are hampered by instability issues. This was unexpected since others describe stable maintenance of such constructs as an attribute (Tao and Zhang, 1998). Had it been realised that instability would have been an issue, vectors employing a more optimal form of selection (i.e.kanamycin) would have been used.

Despite the disappointment it was found that reducing the growth rate of cultivation had a positive impact on both plasmid stability and yield. The importance of this technique was made clear in these studies. It is concluded that if attempts were made to produce large plasmids, employing a reduced growth rate would be a good strategy to follow because of the positive effect it has on both copy number and stability. However, it is envisioned that a more elegant and reproducible strategy could be tried than simple temperature reduction, namely exponential fed-batch fermentation. This method of cultivation allows direct control over the culture growth rate meaning that stability and copy number could be positively influenced. Additionally, higher biomass yields could be attained. It would mean an extension in the period required for fermentation but this is not too harmful a drawback. It is plausible to entertain the notion that if this fementation regime was used in conjunction with a more judicious method of selection (kanamycin or repressor titration) then stabilities of 100% could be attained.

Although the yields of the large plasmids were not in the ranges hoped for, an insight into the possible yields was provided by adjustment of the final yields accounting for the levels of stability. The values achieved are due entirely to the increased DNA being propagated per plasmid, since a reduction in the copy number with increasing plasmid size was seen. However, if the stability were improved, the main problem faced this far in the processing of large plasmids; low yields, could be alleviated. As such, although the decision to clone large constructs under the control of high-copy number replicons represented a fundamental change of direction for this project, the strategy has been partially validated.

Evidence was also provided that the propogation of these large constructs was not accompanied by any significant decrease in plasmid topology. This was important to

ascertain since there would be little to be gained from designing processes to accomodate the production of large plasmids if the resultant plasmid quality was poor.

A rather unfortunate aspect of large plasmid purification was identified in that recoveries of the large plasmids from packed-bed chromatographic matrices were poor. It was not possible to state whether this was due to unoptimised elution conditions or the more troublesome possibility that the larger sizes means that the plasmids were incapable of penetrating the resin.

Overall through the use of an understanding of the potential that manipulation of environmental conditions can have on relaxed plasmid yields it was possible to obtain cell material containing large plasmids. It was realised that the yield increases were not by the large increment desired but it was hoped that sufficient plasmid mass existed to perform meaningful analyses into the purification of such constructs. With this aim the purification of these molecules forms the subject of the next chapter.

7 DOWNSTREAM PROCESSING: RESULTS AND DISCUSSION

7.1 Chapter Aims

The aims of this chapter are to describe the attempts made at purifying the large constructs produced from the pilot-scale fermentations. The process for the purification of the plasmid DNA was already in place and had previously been demonstrated to be effective for the purification of small plasmid DNA (Eon-Duval and Burke, 2004; Eon-Duval *et al.*, 2003b). The investigations described in this section would help to decide the feasibility of applying the process to the purification of larger plasmid DNA molecules and to determine any potential problems which could be encountered, should further attempts be made to manufacture larger plasmid constructs.

As such the main questions which hope to be answered in this section are;

1. Whether the process was capable of purifying larger constructs with the same degree of efficiency as attained with smaller constructs. This would be determined from a plasmid mass balance enabling the calculation of percentage recovery levels of larger constructs over the process. However, an additional consideration with any plasmid process are any changes to the form of the plasmid during its processing, an issue of increasing importance when processing larger, and therefore, more shear sensitive plasmids. As such, a further question to be answered was whether the act of processing had a more detrimental effect on the topology of the larger constructs.
2. The mixing conditions employed during these investigations will be subject to scrutiny in order to decide whether improvements could be made.
3. Of key importance in any plasmid process is the removal of contaminants. Of the contaminants, the most critical is reasoned to be the bacterial genomic DNA, with the regulators requiring increasingly strict levels of clearance (Zoon, 1996). Consequently, this section will describe the clearance levels achieved of genomic DNA.

4 Together with genomic DNA, any plasmid production process must demonstrate effective clearance of other contaminants. Consequently, this chapter will outline the mass balances constructed of the two other contaminants; protein and RNA.

4. Finally, this section will consider the impact of the plasmid size on any chromatographic procedures which would need to conducted in a plasmid process. This would be achieved by investigating the binding kinetics and maximum binding capacities of the large constructs to two commercially supplied anion-exchange resins.

7.2 Introduction

There are several strategies which can be employed to improve the "manufacture" of plasmid DNA by fermentation. As explained in 3.3.1, the methods centre on genetic strategies and process strategies (medium and mode of operation). Consequently, when optimising the fermentation step the choice of strategy is somewhat constrained. The same cannot be said for the design of processes for the purification of the plasmid DNA once synthesised. There are innumerable publications which describe the different strategies, techniques and technologies which have been investigated for plasmid DNA purification (Table 7-1). The aim of this introduction is not to attempt to cover them all but to get an overview of some of main processes employed in this area.

Downstream processing consists of a sequence of unit operations designed to release the plasmid DNA molecules from the host cells and to remove impurities and contaminants until the desired level of purity and other specifications are reached. The major components of the starting mass of cell paste are detailed in Table 7-2 and the specifications for release shown in Table 7-10. The plasmid will, even when considering a high-copy plasmid, account for less than 1%(w/w) and as reiterated through out this project, many of the contaminants have very similar physico-chemical profile to that of the plasmid product (Ciccolini *et al.*, 2002; Shamlou, 2003).

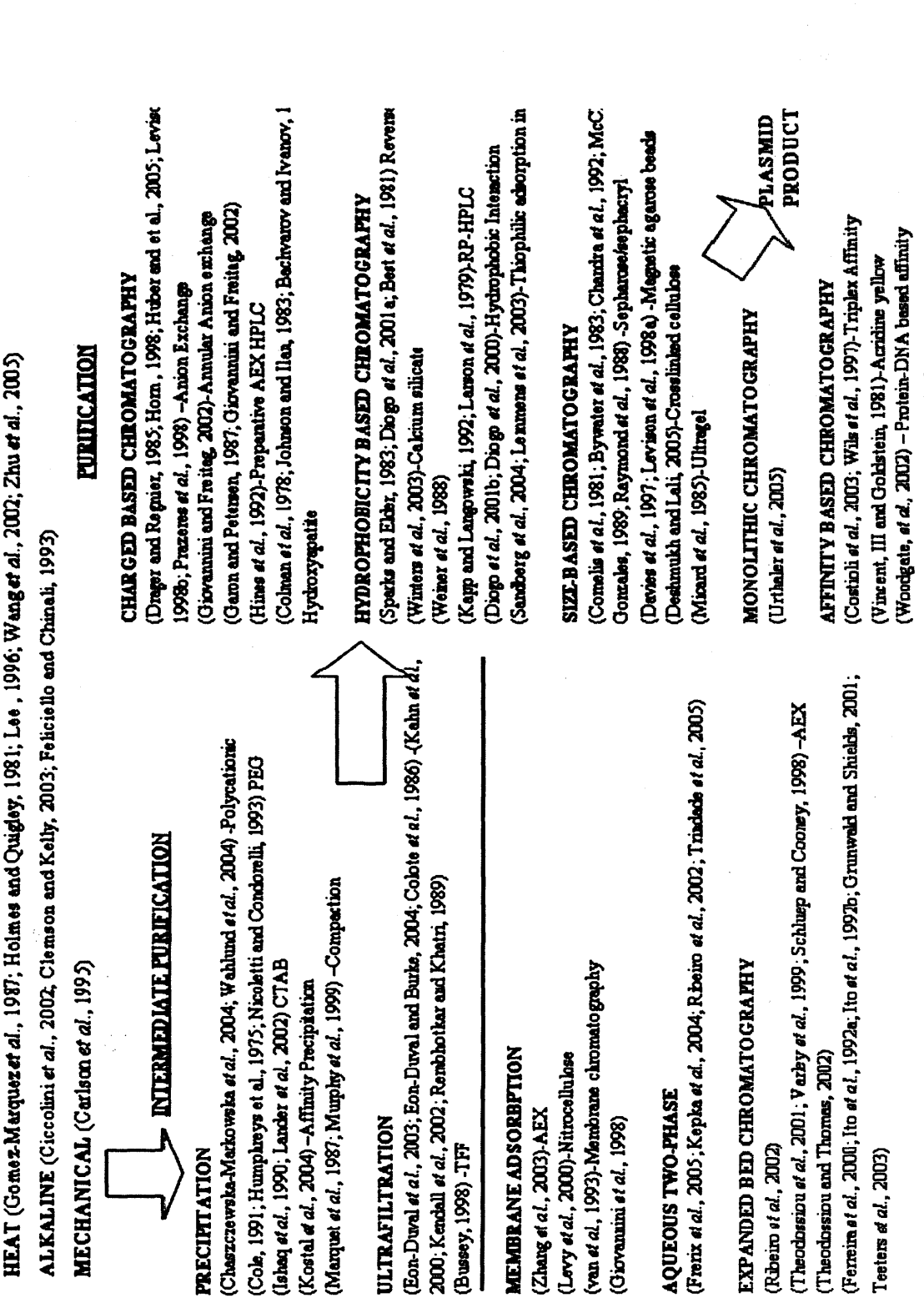

Table 7-1 Table detailing the possible methods which could be used for the manufacture of plasmid DNA. From the table it can be seen that alkaline lysis is the most obvious choice for the initial step, due the capacity of the step to release the plasmid together with achieving a large degree of purification. Following lysis the number of process options are increased. More traditional approaches would employ a form of intermediate purification such as precipitation / ultrafiltration to concentrate the plasmid solution prior to a chromatographic step. However, more recently process options are appearing which like intermediate steps accept clarified lysate but achieve more concentration and purification in a single step. These process options include membrane chromatography, ATPS and expanded bed adsorption.

7.2.1 Primary isolation

Table 7-2 Composition of a rapidly growing *E.coli* cell. [A] Assumes the total nucleic acid complement excluding plasmid DNA. [B] Assumes that a rapidly growing cell can have more than 1 genome copy. [C] Assumes a plasmid molecule of 5kb in size.

Species	Amount (% w/w)	No of different kinds	Average MW (kDa)
Water	70	1	18
Nucleic Acids	6.5 [a]		
gDNA	0.5	1 [b]	2.8×10^6
Transfer RNA	4.8	40	28
Ribosomal RNA	0.9	3	500-1,000
Messenger RNA	0.3	400-800	660-990
Plasmid DNA			
pGEM 3.2kb		1	2,100
pGEM 16kb		1	10,500
pGEM 33kb		1	21,800
P5176 116kb		1	76,600
Proteins	15	1,100	8-200
Endotoxins	5		10
Small molecules/ ions[d]	3	800-2,000	<1

Downstream processing begins with the recovery of cells from the fermentation broth. In this project this was achieved by batch centrifugation but on the larger scale microfiltration or continuous centrifugation are employed (Stanbury and Whitaker, 1984). The cell paste is then resuspended in a buffer which contains agents capable of disrupting the ionic and hydrogen bonds which lend strength to the outer wall of the bacterial cell. Commonly the chelating agent EDTA is used which binds divalent cations from the cell wall destabilising the overall structure and so facilitating lysis (Feliciello and Chinali, 1993). The chelation of Mg^{2+} ions has the added advantage of inhibiting endonucleases which can degrade the released plasmid. In these investigations the resuspension buffer also contained dextrose in order to increase the solution viscosity in an attempt to minimise any shear damage to the plasmid.

Cell disruption can be achieved by mechanical methods such as sonication or homogenisation but they are not commonly employed as the shear damage to the plasmid is too great (Carlson *et al.*, 1995). Heat based techniques have also been studied as a potential ways of lysing bacterial cells (Zhu *et al.*, 2005) however for this method to be effective requires pre-treatment of the cells with agents such as lysozyme.

Variations on the alkaline lysis procedure described by Birnboim and Doly remain the method of choice (Birnboim and Doly, 1979). This operation disrupts the cells to release

plasmid and at the same time removes a large amount of the genomic DNA and protein, which are precipitated together with the cell debris and other impurities. More information on the lysis step is provided in 2.8.2 and 3.8.3. The lysis step is the most crucial step in the downstream process and the one where most problems arise (Ciccolini *et al.*, 1999). Lysis is initiated by the addition of the lysis reagent to the *E.coli* cell suspension. The reagent contains the alkali solution (~0.2M NaOH) and a detergent (~1% SDS). The detergent solubilises cell membranes by eliminating interfacial *van der Waals* interactions between proteins and phospholipids. The actual lysis reaction is rapid and only 30-40s are required to reach completion (Ciccolini *et al.*, 1999).

The alkali in the solution raises the pH and so promotes the irreversible denaturation of the gDNA, whilst keeping plasmid denaturation reversible. The complementary strands of gDNA are completely separated and the hydrophobic bases exposed. This denaturation of the genomic DNA leads to an associated increase in fluid viscosity peaking at 35-160mPas (shear rate dependent) 120-140s after the addition of the lysis reagent (Ciccolini *et al.*, 1999). Although plasmid is denatured during this operation the circular conformation of the molecule mean sufficient bases remain in register to act as nuclei for the renaturation of the molecule, provided that the solution pH does not exceed 12.5.

Mixing during lysis is extremely important. The lysis must be added and mixed rapidly so as to avoid localised regions of high pH which could lead to irreversible plasmid denaturation (Prazeres *et al.*, 1998). This is made more difficult by the increase in viscosity of the lysate which makes the flow and handling of the material very difficult (Stephenson *et al.*, 1992). In addition, following the release of plasmid the agitation intensity should not be too great as to cause the shearing of plasmid DNA or genomic DNA into small fragments which do not precipitate out and so remain as contamination. However, gentle mixing leads to shear thickening of the lysate and so the deterioration of mixing conditions. Refer to Table 3-6.

The following step in the lysis procedure is the addition of a chilled high salt neutralisation buffer (3M Potassium acetate pH 5.5) which causes the renaturation of the plasmid molecules and the precipitation of the gDNA and protein. Genomic DNA precipitates whilst the SDS-protein complexes to form a buoyant, shear sensitive matrix which entraps the cell debris, RNA and gDNA (Theodossiou *et al.*, 1999).

Alkaline lysis and neutralisation are typically carried out sequentially in the same tank with each operation taking 5-10 minutes. In these investigations the lysis and neutralisation operations were conducted for 30 minutes each.

This fact will prove controversial but was found to be required due to the gentler agitation conditions employed in this protocol. Following neutralisation a solid-liquid separation step is used to remove the contaminant floc. This is either centrifugation or filtration with the latter becoming more common due to improved performance. Flotation can be employed to remove the bulk of the floc material prior to loading on to filter.

Often overlooked, but of equal importance to the shear sensitivity of the plasmid molecules, is their chemical stability during the lysis/ neutralisation stage (Monteiro *et al.*, 1999). In spite of the harsh alkali treatment endogenous nucleases (DNases/RNases) may persist in the process streams. If adequate measures are not taken, such as not extending lysis or by failing to lower the temperature of the solutions, damage to the supercoiled molecules can result (Monteiro *et al.*, 1999). Attempts have been made to exploit the persistence of the RNases to degrade the RNA remaining, by incubating the lysate. However, on the larger scale the technique has been plagued by damage to the plasmid caused by exposure to endogenous DNases.

7.2.2 Intermediate purification

The main aim of intermediate processing steps is to decrease the volume of the plasmid containing stream prior to chromatography. However, increases in purity can be obtained in parallel. As shown by Table 7-1, traditional intermediate purification steps such as ultrafiltration and precipitation produce a cleaner and smaller process streams. However, there is evidence that they can be by-passed all together by the use of expanded-bed chromatography, membrane chromatography or aqueous-two phase systems (ATPS). These techniques are grouped with the other intermediate techniques by virtue of the fact that all can accept clarified lysate directly; generally traditional packed-bed chromatography is unable to do so. In contrast to the UF/precipitation these techniques are capable of achieving remarkable levels of purification in one step. It is these impressive clearances combined with ease of use which are driving the uptake of these technologies.

7.2.2.1 Precipitation

Precipitation can be used to either precipitate the plasmid or contaminants. Precipitation of plasmid from clarified lysate with ethanol/isopropanol can recover >95% of plasmid

(Diogo *et al.*, 2000). This technique is common on the laboratory scale and indeed was utilised in this project in analytical studies 2.5.6 but the technique is not feasible to the larger scale.

Another method of precipitation of plasmid utilises polyethylene glycol (PEG). In this technique the size of the DNA molecules precipitated depends on the concentration and molecular weight of the PEG. As such the technique can be used to fractionate DNA according to its MWt or to precipitate the total DNA content (Horn *et al.*, 1995; Marquet , 1996). Whilst the technique is applicable to lager scale operation there remain inconsistencies and a degree of empiricism in its application.

Small cationic molecules, known as compaction agents have also been used to selectively precipitate plasmid DNA. These molecules (spermidine/spermine) bind into the grooves of the DNA neutralising the charge and compacting the molecule's size (Plum *et al.*, 1990).

When considering the use of precipitation it has to understood that the operation entails a solid-liquid step which may be deleterious to the resultant plasmid quality. Precipitation can be used to remove contaminants including proteins, gDNA, LPS and RNA. In these studies Calcium chloride is used to precipitate out the RNA.

7.2.2.2 Ultrafiltration

UF can achieve good levels of concentration and purification in one unit operation as well as buffer exchange. The use of tangential flow filtration with UF polyethersulfone membranes (MWCO 500-1,000kDa) has been claimed to remove 99% of RNA and 95% of protein from clarified lysates, with the plasmid being retained on the membrane side and the protein/RNA passing through (Butler *et al.*, 2000; Kahn *et al.*, 2000). It is this technique which forms the basis of these investigations and with which similar levels of clearance are achieved as described by (Eon-Duval and Burke, 2004).

7.2.2.3 Aqueous two-phase systems (ATPS)

Clarified lysates can be concentrated and purified by liquid-liquid extraction using aqueous two-phase systems. ATPS consist of a PEG enriched top-phase and a salt enriched bottom phase. Partition of nucleic acids depends on many factors such as the size/chemistry of the macromolecule and the ionic composition of the buffer which can be manipulated to achieve the desired partitioning (Cole, 1991; Frerix *et al.*, 2005; Kepka *et al.*, 2004a; Trindade *et al.*, 2005). Promising results have been reported and the technology

is becoming a more fashionable area of development for plasmid manufacture. Plasmid recoveries of 100% were reported using a PEG1,000/ K_2HPO_4 [15%/13% (w/w)] with no protein detected in the purified stream and the gDNA content reduced 60-fold (Ribeiro *et al.*, 2002). There are several advantages to ATPS. It can achieve impressive concentrations and purifications in one low-shear, low-cost unit operation using non-hazardous reagents.

7.2.2.4 Expanded Bed Chromatography

Expanded bed chromatography is being finally being accepted on an industrial scale in a variety of processes due to its significant advantages over standard packed bed-chromatography. Indeed, it can even supersede unit operation upstream of chromatographic steps. The technology exploits the fluidisation of adsorbent particles by up-pumping flow. This increases the voidage between particles, something not achievable by standard packed-bed techniques. This increased voidage enables the passage of unclarified feedstocks which would block traditional packed-bed columns in a matter of seconds. This capacity to handle unclarified feed stocks minimises the number of unit operations (solid-liquid separation/ UF/Precipitation) which in turn results in higher yields, lower processing times and running costs. Overall significant improvements in process economic can be achieved. The investigation of the technology to plasmid purification is described by (Ferreira *et al.*, 2000b; Theodossiou *et al.*, 2001; Theodossiou and Thomas, 2002; Theodossiou *et al.*, 2002; Varley *et al.*, 1999).

7.2.2.5 Membrane Adsorption/Chromatography

As will be outlined in the following section the major limitation of porous particles for chromatographic separations of plasmid DNA is the low binding capacity of the resins due to inability of plasmid to diffuse into the pores of the matrix particles. Developments in this field are led by the aim to reduce the limitations posed by intra-particle binding. One approach is to use a continuous stationary phase, where the internal surface area is completely accessible by convective flow and thus reducing the need for diffusive intra-particle transport. This strategy forms the basis for membrane chromatography. Membrane chromatography systems consist of multiple microporous membranes in series onto which adsorptive ligands have been attached. The technology is receiving increased attention due to several advantages. Convective binding means shorter residence times, diffusional limitations are overcome by having mainly through pores and thus higher binding capacities can be attained. Additionally, any problems with column packing and uneven

flow are eliminated. The strategy has also has the capacity to accept quite impure feedstocks (Giovannini *et al.*, 1998; Grunwald and Shields, 2001; Teeters *et al.*, 2003; van *et al.*, 1993; Zhang *et al.*, 2003).

7.2.3 Purification

Chromatography is typically the last step in the downstream processing of plasmid DNA. The role of chromatography is to remove impurities such as RNA, gDNA, endotoxins and plasmid variants. To achieve these wide-ranging aims several varieties of chromatography are available. In this section the different types of chromatography will be outlined. However, it should be understood that the achievement of process objectives is dependent on both the adsorbent phase used and how they are deployed i.e. the nature of the support material/ chromatography system used. For instance, anion-exchange resins have been utilised for expanded-bed chromatography but have achieved different process objectives due to the different setup♦.

This section assumes that the chromatography being employed is standard packed-bed mode. This is important because historically the majority of chromatographic matrices have been designed for the purification of proteins and due to their massive size plasmids cannot penetrate the pores of the majority of commercial chromatographic matrices. This means that only the outer surface of the matrix is available for binding, a fact that constitutes an important capacity limitation (Ljunglof *et al.*, 1999);(Ferreira *et al.*, 2000a). For example, 2.5mg plasmid are obtained as opposed to 110mg of protein per mL of the anion-exchanger Streamline QXL (Ferreira *et al.*, 2000a).

7.2.3.1 Anion-exchange chromatography (AEX)

Purification of plasmid DNA by anion exchange chromatography utilises the interaction between negatively charged phosphate groups on the DNA backbone and positively charged ligands on the stationary phase. Suitable ligands include the weak exchangers such as DEAE and DMA coupled to silica, polymeric or composite matrices or strong exchangers such as quaternary amines coupled to polymeric matrices (Diogo *et al.*, 2005). A salt gradient is used to displace the different nucleic acid species.

The order in which the species elute should be in order of charge density, a factor governed by the DNA molecule's chain length and conformation. However, variations in

♦ For example elution profiles of the different chromatographic techniques refer to Figure 4-16. Although they are HPLC traces the principle mechanism of the chromatography remains the same.

the base sequence, size and conformation impact to affect the elution order. However, anion exchangers can and have been employed to remove OC plasmid from SCC plasmid (Prazeres *et al.*, 1998).

Anion exchange is also useful for ensuring the removal of RNA, oligoribonucleotides and some proteins. However, the technique should not be relied upon to clear other polyanionic molecules such as short gDNA fragments and endotoxins due to their similar binding affinities (Wicks *et al.*, 1995).

7.2.3.2 Size-exclusion chromatography (SEC)

Size exclusion chromatography (SEC) or gel filtration chromatography has been used to fractionate and purify plasmid molecules on the basis of their relative size. SEC can be used alone but more often is used sequentially to other chromatographic steps such as anion exchange (as is the case in the process under study)(Ferreira *et al.*, 1999; Varley *et al.*, 1999). It constitutes an ideal polishing step enabling the removal of trace gDNA and RNA, partial separation of OC from SCC forms, reduction of endotoxin loads and the transferral of the plasmid product into a suitable storage buffer. DNA exits the column as a broad non-Gaussian peaks (Figure 4-16), gDNA elutes first as the leading edge followed by the open-circular and then supercoiled forms. Smaller solutes such as salts and RNA are eluted behind the larger DNA species and can easily be separated. A judicious choice of the fractions collected enables recovery of almost pure SCC pDNA. The disadvantages with this technology are associated with its limited capacity and the fact that there are few gels which have the adequate selectivity to be used for plasmid purification.

7.2.3.3 Hydrophobic Interaction chromatography (HIC)

Hydrophobic interaction chromatography has been described for the purification of plasmid DNA (Diogo *et al.*, 2003; Diogo *et al.*, 2001a; Diogo *et al.*, 2000; Yuan Li, 2005). The technology uses matrices derivatised with mildly, hydrophobic ligands (e.g.PEG) to separate relaxed and supercoiled plasmids from RNA, gDNA, endotoxins and denatured pDNA on the basis of differences in surface hydrophobicity. HIC takes advantage of the higher hydrophobicity of single-stranded nucleic acids, a characteristic resulting from the exposure of the organic bases. With dsDNA molecules the bases are shielded inside the helical structure by the phosphate background and so there is little scope for interaction with the hydrophobic stationary phase. However, the high quantity of single-stranded nucleic acid forms which compose the gDNA/RNA contamination bind strongly as do

endotoxins by virtue of the lipdic moiety. It has been reported that HIC is straight-forward to scale-up with no losses in purity and only marginal losses in yield, additionally, run-to-run consistency is high even after sanitation and cleaning cycles of caustic washing (Diogo *et al.*, 2005).

7.2.3.4 Affinity chromatography

Affinity chromatography is based upon the recognition of a very precise structure in the target plasmid molecule by the immobilised ligand. Triplex-affinity chromatography utilises the formation of triple helices between plasmid molecules and sequence-specific immobilised oligonucleotides. Proponents claim that the technique can purify pDNA in one-step whilst significantly reducing the levels of impurities. This specificity makes it an attractive option but the same sequence specificity could potentially limit its adoption since the ligand is base specific. Similar to the deployment of this technique for the purification of proteins the associated costs are high (Ito *et al.*, 1992a; Schluep and Cooney, 1998). Other forms of affinity chromatography for the purification of plasmids have been investigated (Table 7-1) but overall the use of this technology for pDNA purification remains lab-based at present.

7.2.4 Process schematic

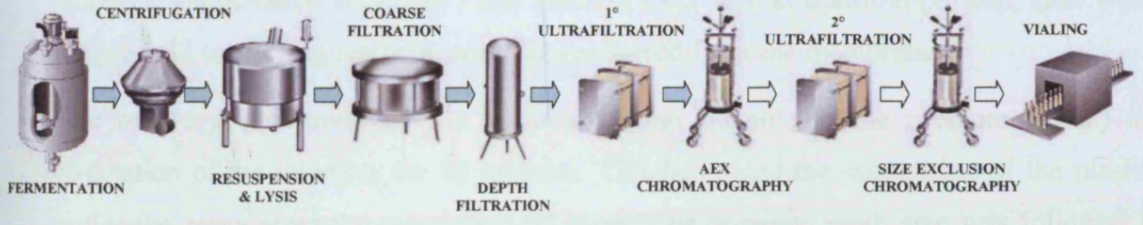

Figure 7-1 Schematic of the process studied in this project in its entirety. The steps which were studied in detail are highlighted by the blue arrows. The fermentation broth is centrifuged and the cell paste resuspended in the lysis vessel. Following lysis, neutralisation and RNA removal by $CaCl_2$ addition the lysate is clarified by a series of filtration steps. The first filtration step is a coarse, mesh filter which removes the majority of the large floc material. To achieve clearance of remaining micron/sub-micron particulates, which could block the UF membrane, the lysate is further clarified by two depth filtration steps in series. The clarified lysate is then subject to ultrafiltration. During the 1°UF step the clarified lysate is first concentrated by 10-fold. This removes the majority of protein and RNA. The concentrated solution is then purified further by a diafiltration step which removes small MWt RNA. A second diafiltration step is then used for buffer exchange to transfer the plasmid into a buffer suitable for loading on to an anion exchange column. The AEX column facilitates the removal any traces RNA but can also be used to purify SCC topology and achieve some removal of gDNA. The remaining steps are designed to ensure clearance of any trace endotoxin/ gDNA material and so use size-based approaches.

7.3 Process Outline

A process developed for pilot-scale purification of plasmid DNA was utilised for these studies. The procedure was conducted on 50g of frozen cell paste from the fermentations.

It involved the resuspension of the cell paste in a Tris-based resuspension buffer. Concurrently, the lysis buffer was prepared in a 1.5L round-bottomed vessel fitted with a 45° pitched-blade impeller and surrounded by ice. Lysis was achieved by addition of the cell suspension to the alkaline lysis buffer, a method similar to that described by (Birnboim and Doly, 1979). The removal of RNA from the lysate was achieved through the addition of the divalent salt calcium chloride, first demonstrated by (Mukhopadhyay and Mandal, 1983) and further improved by (Eon-Duval *et al.*, 2003a; Eon-Duval *et al.*, 2003b). Clarification was performed by batch ultracentrifugation. This step replaced a course filter train typically employed on the larger scale for ease and simplicity and due to the fact that the course clarification has little, if any, effect on final plasmid recoveries. Small particulates were removed from the liquor, to prevent any blockage of the UF membrane, by depth microfiltration.

The central concentration and purification step of this downstream process utilised ultrafiltration. Primary concentration of the clarified lysate involved reducing its volume from 1205mL to 100mL and was achieved by permeation. The plasmid remained on the Retentate side of the membrane. Removal of protein and remaining small molecular weight RNA was achieved by diafiltration using 30 volumes of a Tris-based buffer. Further purification and buffer exchange (placing the plasmid in a suitable buffer for anion-exchange chromatography) was enabled by a second diafiltration step, after which the plasmid containing retentate could be recovered from the membrane.

The recovery step involved the removal of the transmembrane pressure (TMP) and circulation of the retentate for 20 minutes. This facilitated the suspension of the plasmid molecules away from the membrane gel layer. The retentate wash step was followed by two further wash steps, involving the addition of 80mL of the second diafiltration buffer to the membrane and the subsequent recirculation and collection.

Table 7-3 Table outlining the sequential steps of the downstream processing steps. Brief details are given into the actions performed in each step as well as the samples taken and the name assigned to the samples stage.

STEP	ACTION	SAMPLING
Cell Resuspension	50g of frozen cell paste resuspended to homogeneity in 250mL of Tris based buffer.	Samples taken to determine WCW of suspension. Sonication to reveal starting amounts of RNA, Protein and gDNA. **[Pre-Lysis samples]**
Cell Lysis	Lysis achieved by addition of cell suspension to 395mL ice-cold 0.96 %(w/v) NaOH and 78mL 6%(w/v) SDS in lysis vessel. Mixed at 100rpm for 30 minutes.	No samples taken
Neutralisation	Lysis mixture neutralised by addition of 246mL ice-cold Potassium acetate. Mixing continued for 30 minutes	1mL samples taken, centrifuged and frozen for retrospective analysis of pDNA, RNA, gDNA and Protein. **[Pre-$CaCl_2$ samples]**
RNA Removal	RNA removal achieved by addition of 246mL of r.tp 5M $CaCl_2$. Mixing continued for 10 minutes	No samples taken.
Clarification	Lysate aliquoted into centrifuge pots and centrifuged for 30 mins at 20,000g. Small particulates removed from liquor by depth microfiltration.	1mL samples taken, centrifuged and frozen for retrospective analysis of RNA and Protein. **[Post-$CaCl_2$ samples]**
UF Concentration	Clarified lysate concentrated from 1205mL to 100mL by permeation. Cross-flow at either 250 or 500mLmin^{-1}. Permeate collected. Flux rate recorded.	1mL samples of permeate taken and frozen for retrospective analysis of pDNA, RNA and Protein. **[Permeate samples]**
UF Diafiltration 1	Protein and small mol.wt. RNA removed from retentate by diafiltration with 20 volumes (2L) of a Tris-based buffer. Flux rate recorded.	Diafiltrate collected and samples taken and frozen for retrospective analysis of pDNA, RNA and Protein. **[Diafiltrate 1 samples]**
UF Diafiltration 2	Further purification and buffer exchange achieved by diafiltration with 30 volumes (3L) of DF2 buffer. Flux rate recorded.	Diafiltrate collected and samples taken and frozen for retrospective analysis of pDNA, RNA and Protein. **Diafiltrate 2 samples]**
Retentate Recovery	TMP removed and Retentate allowed to circulate for 20 mins prior to collection in a pre-weighed Nalgene bottle.	Retentate collected and samples taken and frozen for retrospective analysis of pDNA, gDNA, RNA and Protein. Volume determined by weight. **[Retentate samples]**
Wash 1 Recovery	80mL of DF2 buffer added to the membrane and allowed to circulate for 20 minutes prior to collection in a pre-weighed Nalgene bottle.	Retentate collected and samples taken and frozen for retrospective analysis of pDNA, gDNA, RNA and Protein. Volume determined by weight **[Wash 1 samples]**
Wash 2 Recovery	80mL of DF2 buffer added to the membrane and allowed to circulate for 20 minutes prior to collection in a pre-weighed Nalgene bottle.	Retentate collected and samples taken and frozen for retrospective analysis of pDNA, gDNA, RNA and Protein. **[Wash 2 samples]**

7.4 Process Analytics

One of the main objectives of these investigations was the construction of mass balances for the plasmid and the key contaminants. To do so required accurate determination of the concentration of each at various stages of the process. Once the concentration was determined the masses could easily be calculated from knowing the volume of the different streams. The development of the assays employed is outlined in the analytical development chapter. There remain a few points to explain here though.

Table 7-4 outlines the assays employed to determine the concentration of the various constituents and where sampling was recorded. Of note was the fact that measurements could not be made of plasmid mass before the lysis stage. Essentially, alkaline lysis is a lysis procedure that also enables removal of a majority of protein and genomic DNA. Feasibly it could also lead to losses of plasmid. Determination of the plasmid mass in the cells before lysis would have enabled a more complete plasmid balance. However, sonication could not be employed, as was used for the other contaminants, because the act of sonication shears the plasmid to the extent that it could not be recorded. Alternative methods of determining the plasmid mass at outset, through the use of different lysis regimes (e.g. enzymatic and detergent based lysis) were attempted but no sensible results, from the analysis of the samples by HPLC, were forthcoming.

Furthermore, it was not found possible to record the plasmid concentration of streams containing high-levels of the calcium chloride salt. The high-salt content of the streams meant that the samples did not run well on HPLC. Estimates could be placed upon the concentration by applying samples diluted 10-fold with TE buffer. This was done for permeate samples to check that the permeate did not contain high-levels of plasmid. However, the results returned, when using this method for the Post-CaCl2 samples, were too variable to be included and so were discarded. As with the other constituents, it was hoped that desalting the Post-CaCl2 samples would alleviate the issue. However, when the desalted samples were analysed by HPLC no plasmid could be detected. It is believed that the plasmid did not run well through the gel matrix of PD-10 columns.

Table 7-4 Table outlining the assays used to determine the concentrations of the various constituents. The table also shows the streams on which these assays were used on.

CONSTITUENT	ASSAY	DETAILS	SAMPLING STAGES
Plasmid Quantification	HPLC	Directly on samples	Pre-$CaCl_2$/ Permeate / DF1 / DF2 / Retentate / Wash 1 / Wash 2.
Plasmid Quantification	A_{260}	On UF recovered material	Retentate / Wash 1 / Wash 2
Plasmid Topology	FIGE	On IPA purified samples	Pre-$CaCl_2$ / Post-$CaCl_2$ / Retentate / Wash 1 / Wash 2
Protein	BCA	In triplicate on 3 appropriate dilutions	Pre-Lysis / Pre-$CaCl_2$/ Post-$CaCl_2$ / Permeate / DF1 / DF2 / Retentate / Wash 1 / Wash 2.
RNA	Quant-IT	In triplicate on 3 appropriate dilutions	Pre-Lysis / Pre-$CaCl_2$/ Post-$CaCl_2$ / Permeate / DF1 / DF2 / Retentate / Wash 1 / Wash 2.
Genomic DNA	qPCR	Purified robotically by MagNA-Pure.	Pre-Lysis / Pre-$CaCl_2$ / Retentate / Wash 1 / Wash 2
Flux Rate	Manually	Measuring cylinder and stopwatch	Permeation / Diafiltration 1 & 2

The plasmid topology assay could only be performed on streams containing sufficient plasmid material to enable concentration. As a result, only the streams shown in the table were analysed by FIGE. However, this was not a major problem since the streams with low plasmid masses were the exit streams which were less critical.

The concentration of plasmid solutions recovered from the UF step were concentrated by both HPLC and checked against those returned by A_{260}. This could be done since the plasmids were sufficiently pure by the end of the UF step to allow for A_{260} quantification. However, in all the balances the HPLC results were used for reasons of consistency. It was this double-check that highlighted the issue found with the HPLC concerning the detection of sheared plasmid DNA, when the results from A_{260} did not match those from the HPLC.

7.5 Experimental order

Having outlined the way in which the DSP operations were conducted and the various analytical techniques employed to determine the concentration of the different constituents, the run order in which these investigations were performed can now be outlined.

Twenty-four individual DSP runs were completed, the details of which are outlined in Table 7-5. From the table it can be seen that each of the five plasmid constructs was processed in duplicate runs. Also the investigations were designed to determine whether the cross-flow velocity had any impact on the recovery and topology of the plasmid product. This was done as it was reasoned that the high shear environment of the UF rig may lead to severe damage to the larger constructs. Normally the UF process is operated at a cross-flow velocity of $500mLmin^{-1}$, so performing investigations at $250mLmin^{-1}$ should provide data to make useful comparisons.

Furthermore, HPLC determination of the pDNA concentration in the samples taken from the Post-$CaCl_2$ stream of the process was found to be unachievable. As a result it was not possible to balance pDNA mass across this step. In order to determine whether the addition of $CaCl_2$ resulted in any plasmid loss control runs were performed. In these control runs RNA removal was achieved through the action of RNase by replacing the

	Construct size (kb)	Crossflow velocity (ml/min)	RNA removal
RUN 1	3.2	500	CACL
RUN 2	3.2	500	CACL
RUN 3	16	500	CACL
RUN 4	16	500	CACL
RUN 5	33	500	CACL
RUN 6	33	500	CACL
RUN 7	49	500	CACL
RUN 8	49	500	CACL
RUN 9	116	500	CACL
RUN 10	116	500	CACL
RUN 11	3.2	250	CACL
RUN 12	3.2	250	CACL
RUN 13	16	250	CACL
RUN 14	16	250	CACL
RUN 15	33	250	CACL
RUN 16	33	250	CACL
RUN 17	49	250	CACL
RUN 18	49	250	CACL
RUN 19	116	250	CACL
RUN 20	116	250	CACL
RUN 21	33	500	RNASE
RUN 22	49	500	RNASE
RUN 23	33	250	RNASE
RUN 24	49	250	RNASE

Table 7-5 Table describing the twenty-four separate DSP operations conducted on 50g of cell paste obtained from the fermentations. All five constructs were analysed in duplicate. Two cross-flow velocities were also used; $250mLmin^{-1}$ and $500mLmin^{-1}$. Determination of the plasmid concentration in the streams immediately following the addition of calcium chloride was found unachievable. Consequently control runs were performed to determine whether the addition of this salt had any impact on the plasmid yields. In these controls the addition of 246mL of 5M $CaCl_2$ was replaced by the addition of the same volume of 1xTE buffer containing $500\mu gmL^{-1}$ RNase. This produced a solution of RNase of $100\mu gmL^{-1}$ in the lysate. The remainder of the procedure was conducted in the same fashion as the other runs.

addition of 246mL of 5M $CaCl_2$ with the same volume of 1xTE buffer supplemented with 500μgmL^{-1} RNase. This solution formed an RNase concentration of 100μgmL^{-1} in the lysate. The remainder of the process was performed in an identical fashion to the other runs.

7.6 Plasmid recovery and topology

7.6.1 Plasmid Yields following alkaline lysis

The plasmid balances of the different runs are show in the individual mass balance breakdowns shown in (Figure 9-31 to Figure 9-49). The figures used in this analysis are the averages of the quadruplicate runs performed.

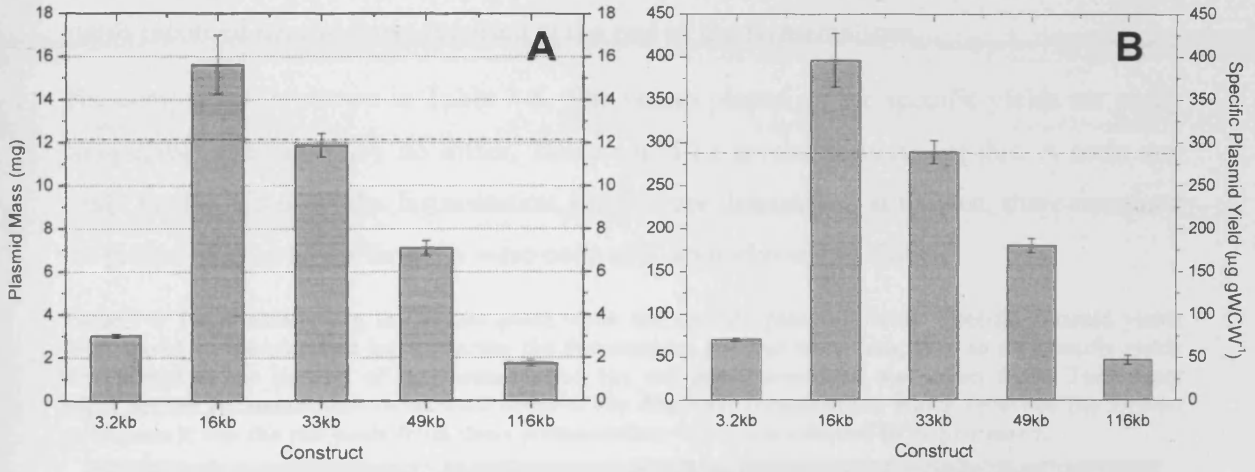

Figure 7-2 Figures detailing the masses of the different constructs at the Pre-$CaCl_2$ stage of the process. This step is directly after the completion of neutralisation and before the addition of the Calcium chloride. The figures record the average of four runs for each construct. This was allowable, since there was no difference between the different runs at this stage, the different processing technique (crossflow velocity) appear later in the UF step. Figure A shows the total plasmid masses determined by HPLC directly on clarified lysate. These mass values represent the starting masses of plasmid DNA. Figure B shows the plasmid specific yields determined from the mass quantities and the WCW of the individual cell suspensions. It was not possible to plot the graphs on the same graph because although they appear equivalent small differences in the WCW between runs mean they are not quite equivalent. The dashed line represents the lower limit of starting yields determined to be acceptable by this process.

Figure 7-2 details the initial starting masses of plasmid DNA for each construct. These were determined following the neutralisation stage of the process by HPLC on the clarified lysate. The average of the four runs is displayed in the graph.

This could be done since up until the UF stage the operation of all the processes was equivalent. The WCW of each suspension was determined prior to lysis. This value could be used to determine the specific yields of the constructs and see how close they compared to the values reported at the end of the fermentations since they should be equivalent. It was noted that although 50g of frozen cell paste was lysed in these reactions the actual WCW of the solutions deemed that there was only on average ~42g of cell mass present. The reason for this disparity was reasoned to be due to the relative dewatering capabilities of the centrifuge used to recover the cell paste from the fermentations. It seems from the results that it was only capable of achieving 80-90% dewatering. This meant assuming that the 50g used was all cell paste would have been wrong and as such would have under-represented the specific plasmid yields at this point. Determination of the WCW of the cell suspension highlighted the issue and as such allowed for direct comparison of the specific yields recorded here to those reported at the end of the fermentations.

The comparison is shown in Table 7-6. The values placed on the specific yields are pretty comparable although they do differ. There could be several reasons for this. A main one could be that although the fermentation yields were determined at harvest, there remained the period of time when the cells were collected, spun-down and frozen.

Table 7-6 Table comparing the values place upon the specific plasmid yields. Specific plasmid yields determined on the clarified lysate during the downstream process were compared to the specific yields determined at the harvest of the fermentation the cell paste processed was taken from. The values taken for the fermentations yields were those of the duplicate fermentation which recorded the highest yield since it was the cell paste from these fermentation which was selected to be processed.

	Fermentation Specific Plasmid Yield (µg pDNA/ gWCW)	DSP Specific Plasmid Yield (µg pDNA/ gWCW)	% Difference
pGEM 11 [3.2kb]	81.6	70.4	-16.0
pGEM 16 [16kb]	296.1	396.2	+ 25.3
pGEM 33 [33kb]	215.7	289.0	+ 25.4
pGEM 49 [49kb]	165.6	180.0	+ 7.97
P5176 [116kb]	49.9	47.2	- 6.2

Before the cells were frozen there remains the distinct possibility that specific yield could have increased, especially considering how rapidly the specific yields were increasing toward the end of the fermentations. Additionally, there would have been variations in the assay. Although in both scenarios the yield values were determined by HPLC, the sample for the fermentations was performed on IPA precipitated clarified lysate, whilst the DSP samples were run directly (Refer to 4.5.2.2 for the reason). However, it was felt that the values aligned sufficiently to give confidence.

7.6.2 Plasmid Recoveries from the UF rig

The plasmid recoveries of the individual runs were calculated from the total masses recovered from the Retentate and wash fractions of the UF stage, and the starting masses determined by HPLC on the clarified lysate prior to $CaCl_2$ addition. The full breakdown of the individual runs can be seen in the mass balances (Figure 9-31-Figure 9-49).

Figure 7-3A plots the calculated % recoveries of every run against the size of the plasmids processed. From the graph it can be appreciated that there is a roughly linear drop-off in the percentage of plasmid recovered with increasing plasmid size.

The poor results for the smallest construct (pGEM11) seem to break the trend, but are explainable. Details from the mass balances show that the low recoveries of this construct are due to its appearance in the permeate streams, and as a result, the vast majority of this plasmid can be accounted for. Unfortunately, it seems that by virtue of the small size of this construct, it was capable of penetrating the membrane. From the full plasmid balances shown in (Figure 9-31to 9-49) it seems that a great deal of this plasmid appears specifically in the Diafiltrate 2 stream, exiting the membrane. The most likely cause of this is that since the DF2 buffer is relatively high-salt (0.54M NaCl), the high ionic

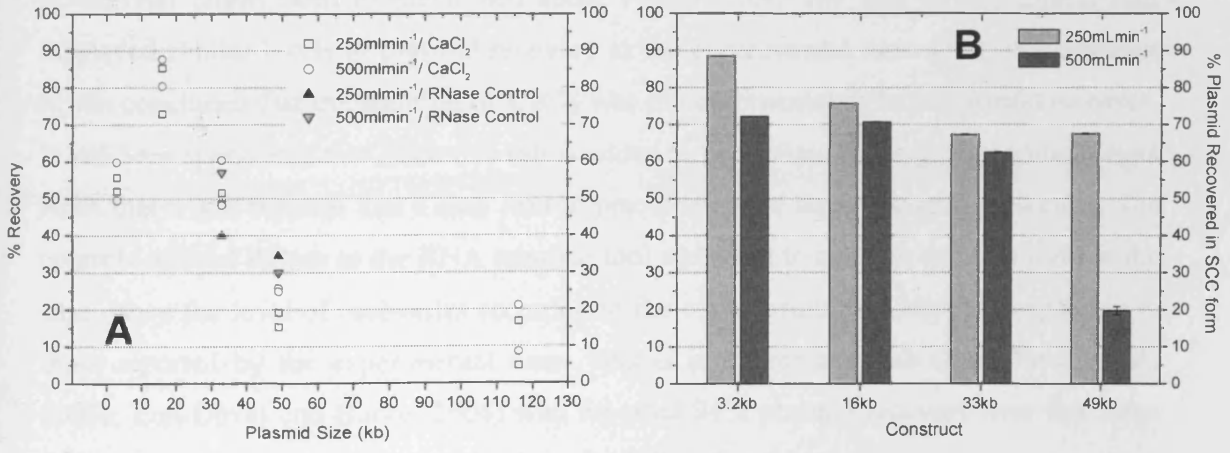

Figure 7-3 Figures detailing the recovery of plasmid DNA from the process and the proportion of supercoiling displayed. Figure A records the % plasmid recovery as a function of plasmid size at the different cross-flow rates. This was calculated from the amount of plasmid mass determined to be present in the clarified lysate at the Pre-Lysis stage (Figure 7-2) and the total mass of pDNA recovered from the process in the Retentate and wash fractions. Figure B shows the % supercoiling displayed by the different constructs at the end of the process in the recovered stream. This was calculated on a mass basis from determination of the plasmid topology by densitometric scanning the process gels.

environment would have caused greater compaction of the plasmid molecule, reducing its size sufficiently to allow it to permeate the membrane. It is well documented how high-ionic environments induce better packing in supercoiled plasmid molecules as cations reduce electrostatic repulsion between phosphate groups in the DNA backbone (Schlick, 1994). Unfortunately, this meant that only small amounts of this plasmid could be recovered from the UF rig at the end of the operation. In some ways it highlights the importance of pursuing pilot-scale process runs.

Turning attention to the other constructs, the recoveries of the different sized plasmids did demonstrate intra-run variation, which would be expected due to the multi-step nature of the downstream process. Despite the variation it is clear that decreasing levels of recovery were evident with increasing plasmid size. The question which was asked was where was the plasmid mass disappearing to? Evidence from the plasmid balances suggested that, unlike the smaller construct, the larger plasmids were not penetrating the membrane an outcome that would not be expected anyhow, due to the increased size. Additionally, the poor recoveries were only seen with the larger constructs and not with the 16kb plasmid which displayed highly acceptable ~80% recoveries. The determination of where the plasmid mass was escaping to requires the analysis of plasmid topology and will be discussed in the next section.

Some final points need to mentioned about Figure 7-3A. The first is that control runs displayed similar levels of plasmid recovery to the experimental runs. From this evidence it was concluded that the addition of $CaCl_2$ was not detrimental to large plasmid recovery. It had been speculated that since this salt is added to precipitate the large molecular weight RNA that it was feasible that it may lead to precipitation of larger plasmid molecules. The controls utilised RNase as the RNA removal tool and seem to confirm that this was not the case, since the level of recoveries recorded in the control runs was highly comparable to those reported by the experimental runs. This is in agreement with (Eon-Duval *et al.*, 2003a; Eon-Duval and Burke, 2004) who reported 94% plasmid recovery over this same $CaCl_2$ step when investigating production of a 5.5kb plasmid.

They concluded that the less hydrophobic nature of SCC pDNA meant that it was less likely to precipitate than ssRNA molecules, which are more hydrophobic by virtue of their exposed base sequences.

The second point about Figure 7-3A is that the different cross-flow velocities had no discernable effect on the % recoveries. Accepting that reasonable levels of variation would be encountered due to the complex, multi-step nature of the procedure there appears no real evidence that the cross-flow velocity had a large impact on recovery levels.

7.6.3 Plasmid Topology changes witnessed during processing

Explanation of the poor recoveries of the larger plasmids only came following analysis of the topology changes of the constructs during their processing. IPA precipitated samples from five points during the process for each plasmid run were analysed by gel electrophoresis. The gel images are shown in (Figure 9-6-Figure 9-11). The gels were scanned as described in (2.5.21). The data describing the proportional breakdown of the isomeric forms is described in graphical form in this section. The five sampling points were; Pre-$CaCl_2$ (following neutralisation), Post-$CaCl_2$ addition, Retentate, Wash 1 and Wash 2 fractions. Also described are the proportions of isomer forms taken as being the case at the Pre-Lysis stage. These values were obtained from the gel shown in (Figure 5-11). These were taken as the Pre-Lysis form of the plasmids because the samples analysed were prepared by maxi-prep (large construct kit) on cell paste recovered from the fermentations. It was assumed that the gentle processing regime of these preparations meant that the plasmid forms would have remained unchanged to as they were at the end of the fermentations.

Figure 7-4 plots the topology proportions of the constructs pGEM11, pGEM16, pGEM33 and pGEM49 at the different stages. As shown by Figure 9-9 it was not possible to extract sufficient information from the gel of the p5176 (116kb) plasmid to be of use. Numerous attempts were made at trying to prepare sufficient p5176 material, from the different streams, with which to prepare a useful gel. However, on each occasion visualisation of the actual plasmid, not to mention the different topologies, remained elusive.

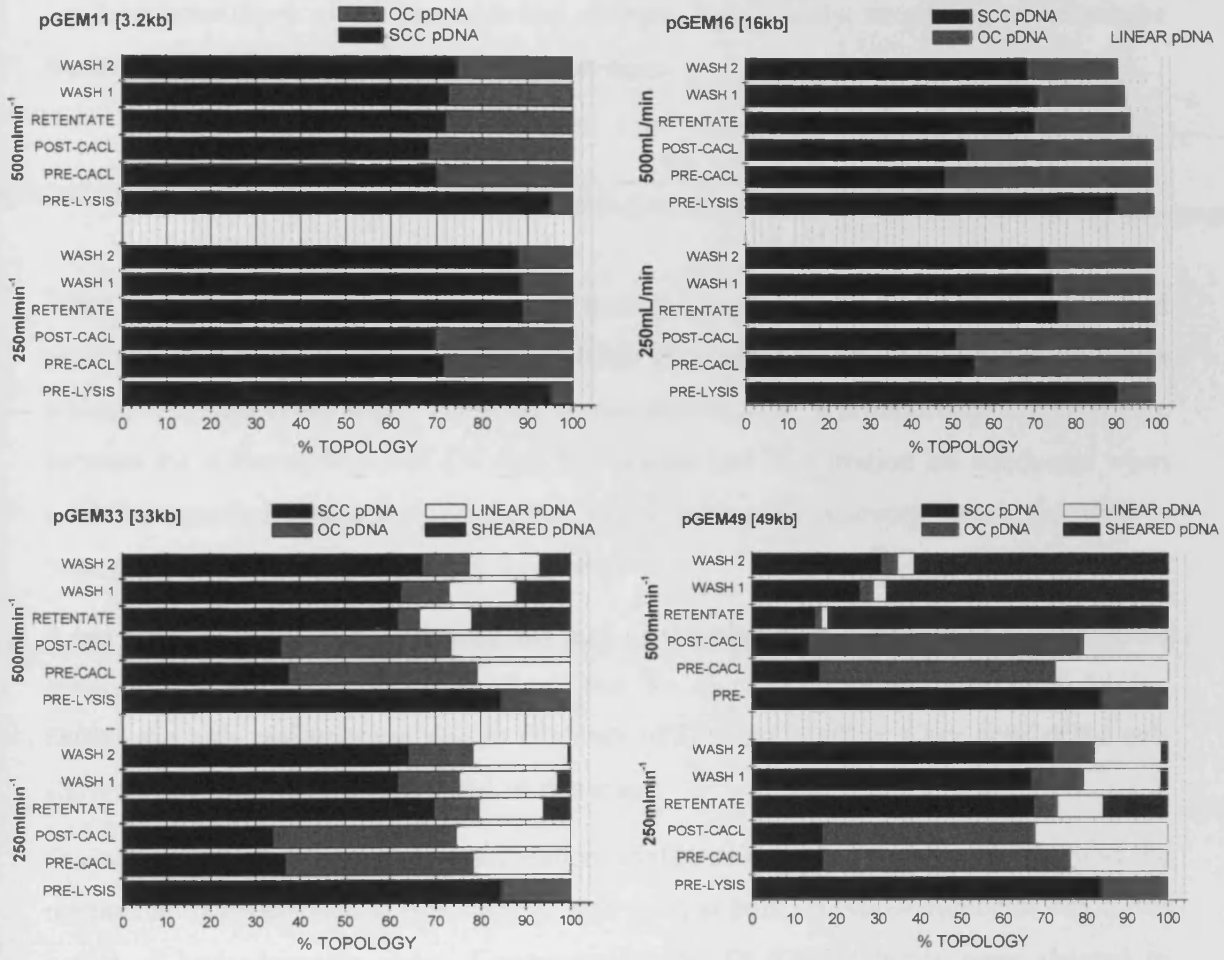

Figure 7-4 Bar charts describing the proportions of the different plasmid forms at various stages during the downstream process. The data was obtained from densitometric scanning of the gel images shown in Figure 9-6 to Figure 9-11.

Close inspection of the topology graphs, and indeed the gels themselves, clarifies the issue surrounding the poor plasmid recoveries. On a general level it can be seen that before lysis all the plasmid display a high level of supercoiling. The actual levels vary slightly between constructs but it can be said that they all display between 85-95% supercoiling. What becomes apparent with every construct is that this level of supercoiling drops over the lysis step. The level of the reduction of the supercoiling is very much related to the plasmid size and is discussed separately in the following section. What also should be noted is how linear plasmid form is generated over the lysis stage for the two largest constructs; pGEM33 and pGEM49.

So, at the end of the lysis stage a large amount of both linear and open-circular forms of plasmid had been generated. For the larger constructs the levels of these isomeric forms were greater than the level of supercoiling. However, after the ultrafiltration steps the

topology breakdown of the plasmids had changed significantly, something which can be appreciated by visual inspection of the gel images.

$$\text{SCC} \xrightarrow{k_1} \text{OC/LIN} \xrightarrow{k_2} \text{Sheared pDNA}$$

When describing the events, which it is believed explain both the changes in plasmid topology and decreases in % recoveries, it helps to consider the kinetics of the mechanisms which are central to the issue. These are shown above. Also, it is important to differentiate between the different stages of UF step. Permeation and Diafiltration are conducted when a TMP is applied across the membrane, whilst during the recovery stages the TMP is removed. At all times a crossflow is in operation.

It has been outlined how increasing the size of the plasmid causes more OC form to be generated during the lysis regime, such that for increasing plasmid size k_1 is greater. During the lysis regime there was no evidence of k_2 being in effect, since none of the gels show the presence of sheared pDNA at this stage.

During the UF operation stage (permeation/ diafiltration) a TMP was applied across the membrane. It is reasoned at this stage k_2 was rapid at both crossflow velocities due to the action of hydrodynamic shear. Consequently, the OC/Linear forms were sheared to fragments ~15kb in size (Figure 9-10 and Figure 9-11). Due to the TMP these fragments were able to penetrate the membrane and escape the process. However, it is also believed that during this stage k_1 was low, due to the smaller hydrodynamic diameter of the SCC form and the relative protective environment of the gel layer. The high rate of k_2 and low rate of k_1 would explain why %SCC would increase. This also means that the recovery of plasmid from the membrane becomes a function of the proportion of the plasmid loaded on in OC form. Since a higher proportion of the larger constructs were converted from SCC to OC form during the lysis step meant that the yields of these constructs would be correspondingly lower, a fact reported in Figure 7-3A. The OC form having been sheared would have passed through the membrane as short dsDNA fragments and so would not be accounted.

Similarly, it is reasoned that the rate of k_2 was high enough at both crossflow velocities to shear OC plasmid forms, explaining why at both velocities the % plasmid recoveries were similar.

It is believed that this rate differential explains the similar recoveries reported for the different crossflow velocities and why % recovery decreased with plasmid size, but this is not a complete explanation. As can be seen from Figure 7-3A and Figure 7-4, although the % recoveries were similar at both crossflow rates, the resultant topology breakdowns differ, with the slower crossflow rate reporting higher %SCC form and less sheared plasmid. This again can be logically explained.

At the end of the UF operation stage (by DF2) it is deduced that selective degradation of the OC/Lin form had occurred at both crossflow velocities. This was sufficient to account for the similar recovery levels and it is reasoned that the majority of plasmid form in the plasmid gel-layer, at this stage, for both scenarios would have been SCC. However, the UF operation stages (Permeation and Diafiltration) were followed by the UF recovery stages (Retentate, Washes 1 and 2). During these periods the TMP was removed from the membrane, such that no flow occurred across the membrane, but the same crossflow rates were in effect. The objective of these steps is to scour the membrane to recover the plasmid from the gel layer. It is believed that these steps account for the difference in plasmid topologies witnessed between the two crossflows for every construct. It is reasoned that during these recovery phases both k_1 and k_2 are in action. K_1 would have been higher because the protective environment of the gel-layer, a result of the applied TMP, would have been absent. Additionally, it is believed that the magnitude of k_1 would have been greater at the faster crossflow velocity of $500mLmin^{-1}$ than $250mLmin^{-1}$. Consequently, more SCC plasmid would have been converted into OC/Lin form during the investigations employing higher crossflow rates. For the larger constructs, this form would have been rapidly converted to sheared plasmid form (k_2), but because no flow existed across the membrane these fragments were unable to escape and so were detected.

It is believed that the sequence of events just described occurred with all the plasmids investigated from the smallest to the largest, the only difference being the rates of the two processes described. It is therefore maintained that to improve the recovery of plasmid from a UF membrane, whatever its size, it is important that little plasmid is converted to OC form during the lysis step. Had this been the case for the larger plasmids it is believed

that their recoveries would have been greater. Additionally, it was found that recovery at slower cross-flow rates would be advantageous to plasmid topology.

7.6.4 Plasmid topology changes over the lysis step

The recovery and topology results from the DSP investigations suggested that the action of ultrafiltration on OC/Linear plasmid form was particularly damaging. From those results it was postulated that the majority of plasmid loaded on to the membrane in OC/Linear form was degraded to small DNA fragments capable of penetrating the membrane. This meant that the recovery levels from the UF step were heavily influenced by the amount of OC form generated during the lysis stage of the process. Information from the gels suggested that as plasmid size increased the amount of plasmid degraded to OC/Linear form increased. (Figure 9-6 to Figure 9-11)

In this section this degradation of plasmid form from SCC to OC/Linear during the lysis step will be investigated.

Figure 7-5A displays the supercoiled proportion of the four plasmids, capable of being analysed by FIGE, at the end of the lysis stage of the investigations. The samples scanned were those at the Pre-$CaCl_2$ stage but identical levels of supercoiling were apparent at the Post-$CaCl_2$ stage of the process (Refer to gels Figure 9-6 to Figure 9-11). The plot shows a very linear decrease in supercoiling with increasing plasmid size. For the smaller construct, roughly 70% supercoiling was witnessed by the end of the lysis step, compared

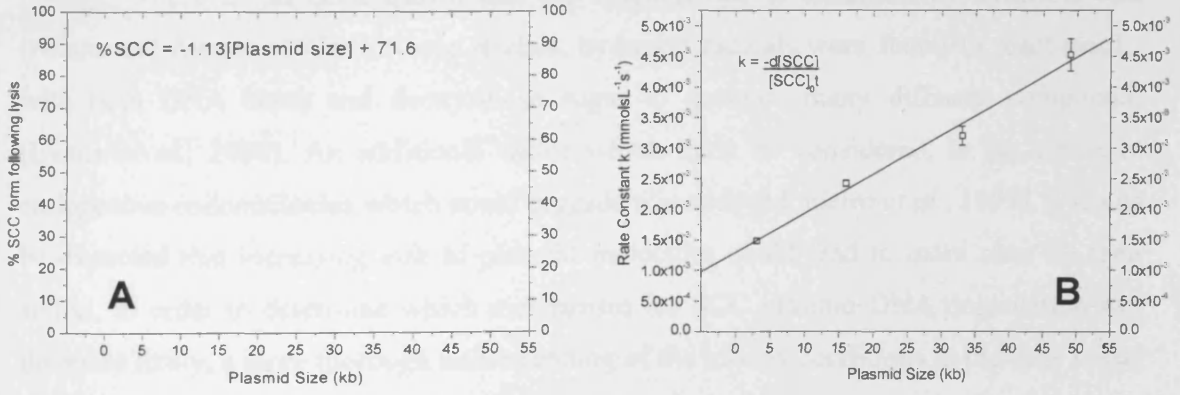

Figure 7-5 Figures describing the degradation of SCC plasmid form during the lysis stages of the DSP operations. Figure A shows the proportion of the different sized plasmids determined to be in supercoiled form at the end of neutralisation reaction (Pre-$CaCl_2$ stage) as determined by densitometric scanning of the gels shown in Figure 9-6 to Figure 9-11. Figure B plots the estimated rate constants for the degradation of SCC topology over the lysis steps for the different sized constructs.

to only 15% with the larger 49kb construct. The linearity suggested the action of a first-order reaction rate with respect to plasmid size. Using the values for plasmid concentration and the pre-lysis levels of supercoiling, the rate constants could be determined. Figure 7-5B plots the calculated reaction rate constants for the degradation of supercoiling over the entire lysis procedure. From the plot it can be seen how the rate constant of degradation increased from ~$1.5x10^{-3}$mmolsL^{-1}s^{-1} for the smallest construct to ~$4.5x10^{-3}$mmolsL^{-1}s^{-1} for the largest construct. This threefold increase in reaction rate explains the prevalence of OC form for the larger constructs at the end of the process and the subsequent effect on the recovered plasmid yields.

It was known that the increased presence of OC form post-lysis was directly related to the increased plasmid size. The unknown remained of what caused the increased degradation of SCC form during the lysis period. It was reasoned that the degradation of supercoiled form could be caused by two mechanisms; physical shear or chemical degradation since, both of these could be increasingly likely with increased plasmid size.

Physical shear could be expected to increase with plasmid size since the plasmid molecule would be larger and hence more susceptible to hydrodynamic shear forces. The causes of fluid stresses sufficient to degrade plasmid molecules could be found to be due to either the action of turbulent eddies on the surface of the particle or the deforming effects of elongational flows. Similarly, chemical degradation could be expected to increase with plasmid size due to the increased sites for action. One mechanism of DNA chain breakage in fluid flows has been shown to be a base-catalysed hydrolysis of the phosphate-ester linkage, where it has been shown that the reaction rate is enhanced by hydroxyl ions (Adam and Zimm, 1977). In these studies, hydroxyl radicals were found to react readily with both DNA bases and deoxyribose sugar to generate many different compounds (Evans *et al.*, 2000). An additional factor which must be considered, is the action of endogenous endonucleases which could degrade plasmids (Monteiro *et al.*, 1999). It would be expected that increasing size of plasmid molecules could lead to more sites for their action. In order to determine which mechanism for SCC plasmid DNA degradation was the more likely, a more thorough understanding of the mixing conditions in the lysis vessel was required. This will be the subject of the next section.

7.7 Characterising the mixing in the lysis vessel

During the DSP investigations the lysis procedure was carried out in an agitated vessel, a schematic of which is shown in Figure 7-6. In this section attempts will be made at describing the mixing conditions encountered during the scaled-down process and what effects would be predicted to plasmid form. As described in (3.8.3) efficient mixing is a key parameter in successful lysis. Shear rates must be large enough to promote good macro and micromixing patterns to ensure rapid blending and dissolution of the NaOH solution. However, high shear forces may impact negatively on the plasmid structure but also lead to fragmentation of genomic DNA creating hard-to-remove gDNA fragments.

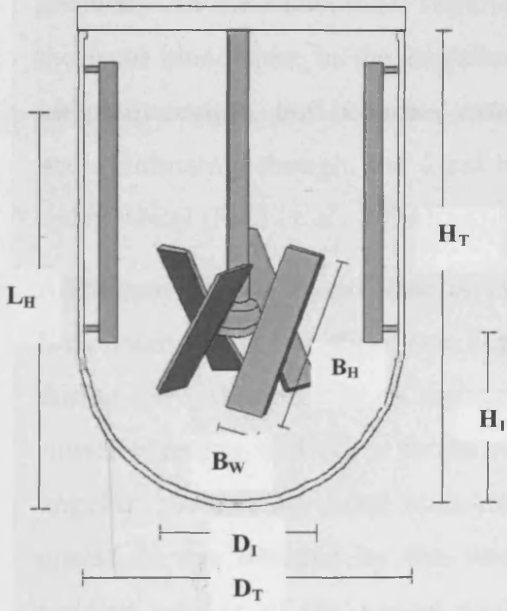

Figure 7-6 Schematic of the lysis vessel in which the lysis, neutralisation and $CaCl_2$ operations were conducted.

H_T = Vessel height = 0.19m

D_T = Vessel width = 0.12m

D_I = Impeller width = 0.065m

H_I = Height from base = 0.04m

B_H = Blade height = 0.045m

B_W = Blade width = 0.014m

L_H = Neutralisation liquid height = 0.128m

7.7.1 Analysis of the Macromixing conditions in the lysis vessel

The lysis operation can be divided into two distinct phases; lysis and neutralisation. During the first phase the cell membranes are solubilised by the SDS, and the DNA and protein denatured by the sodium hydroxide. The release of the intracellular contents causes a dramatic increase in the fluid viscosity and the fluid assumes non-Newtonian, pseudoplastic behaviour, which makes describing the mixing conditions complicated. The addition of the potassium acetate neutralises the solution and causes the precipitation of the majority of the intracellular contaminants. This precipitation leads to a dramatic decrease in the fluid viscosity as it returns to a value close to that of water and displays highly Newtonian behaviour.

When characterising mixing in stirred tanks it is common to describe the efficacy of the operation by calculating the mixing time. Mixing time is defined as the time required to achieve a prescribed degree of homogeneity of the vessel contents, and is dependent on the level of macromixing or distribution of fluid in the vessel. However, the objective of this lysis operation was the blending of two miscible fluids (*cell suspension* + *lysis buffer* and *cell lysate* + *neutralisation buffer*) and as such the measure of mixing time is less useful in describing the operation. More useful is the blend time or macroscale mixing time, which is a measure of the time taken to blend two fluids to a predetermined degree of homogeneity, in this case set to 95%. Blend time (θ) in turbulent regimes is a constant, independent of Reynolds and Froude numbers, and dependent only on vessel and impeller geometry. In the transitional regime, where Reynolds value lies between 10 and 20,000, the local blend time in the impeller region is the same as the vessel blend time for the turbulent regime, but becomes extended when recording local blend time at the vessel wall. Ultimately though, the local blend time at the wall controls the blend time for the entire vessel (Paul *et al.*, 2004).

Additional to this, blend time is viscosity (μ) dependent, a factor which is constant in Newtonian fluids but shear rate dependent in viscoelastic fluids of the type encountered during the lysis operation. Consequently, since viscosity is a function of the shear rate, slower blending will occur in the regions of low shear typically found furthest from the impeller, such as the vessel wall. Ultimately, this means that the overall blend time of this operation was dictated by the viscosity and macromixing conditions at the less well agitated regions of the vessel wall. Therefore, to estimate the blend time for a non-Newtonian fluid, the appropriate shear rate at the vessel wall must be identified and the blend time can then be estimated using Newtonian correlations.

In order to estimate the blend time, the rheological properties of the lysate needed to be understood. This was achieved using data from (Ciccolini *et al.*, 1999) where they listed the steady-state viscosity of lysate fluid, prepared from *E.coli* C600/pR26 suspension, at various shear rates. A plot of these results (Figure 9-12) suggests a power law relationship between the viscosity and shear rate. From the curve, the values for K (consistency index) and n (flow-behaviour index) could be extracted. (Metzner A.B and Otto R.E., 1957) described how shear rate is directly proportional to agitator speed using an impeller dependent constant k.

Using the obtained values and relationships it was possible to estimate the blend time in the vessel used for lysis in both the lysis period of operation (*cell suspension + lysis buffer*) and the neutralisation period of operation (*cell lysate + potassium acetate*). The calculations performed are detailed in Table 1-5. The calculation for the blend time in these stages used derivations described by (Grenville, 1992; Paul *et al.*, 2004). Estimating the blend time taken to reach 95% homogeneity during the lysis step was based upon the premise that the blend time for viscoelastic fluid mixing is governed by the rate limiting point furthest from the impeller region, where mixing and so shear rates are at the lowest. The calculation makes use of a correlation for estimating shear rate at the vessel wall derived for the agitation of shear-thinning fluids in torispherical bottomed, baffled vessels as described by (Grenville, 1992). The blend time was then calculated using equations derived for Newtonian fluids in transitional regimes (Paul *et al.*, 2004). The calculation for blend time for the neutralisation step was more straight-forward, since Newtonian behaviour was assumed and hence constant viscosity. A value was placed upon the viscosity of the neutralised lysate at 10-fold greater than water, in order to place an upper value on blend time.

Considering the lysis stage first, it can be seen that the time estimated to blend the two fluids to 95% homogeneity is 24.5 minutes. This value is close to the 30 minutes actually employed for the mixing during the experimental protocol. However, the estimation placed upon blend time is probably an underestimate since it uses historical data from (Ciccolini *et al.*, 1999) for the rheological properties of cell lysate. In that study the cells were resuspended to $125gL^{-1}WCW$, whereas in these studies the value was $162gL^{-1}WCW$. The higher cell concentration would tend to increase the overall blend time. Certainly, the blend time was observationally verified, as even late into the lysis operation (~20mins) distinct 'sections' of the bulk fluid could be seen to be poorly mixed. Similar blend time analysis during the neutralisation stage estimated the required period to reach 95% homogeneity to be just 1.3 minutes. The difference at this stage of the process was that the viscosity of the fluid was assumed to drop to 0.01mPas, since the majority of the macromolecular species responsible for the viscoelastic behaviour during the lysis stage were precipitated out. Additionally, the fluid was assumed to be Newtonian in behaviour. However, the predicted rate of operation is much quicker than measured experimentally and may be due to the fact that the calculation assumes the viscosity of the

Table 7-7 Table outlining the calculation of the blend time of the two steps of the lysis procedure. For the lysis stage the calculation involved determination of the shear rate at the vessel wall and so the apparent viscosity. From this value the blend time could be calculated using traditional Newtonian correlations. Because during the neutralisation procedure the fluid was assumed to display Newtonian behaviour and constant value for viscosity could be used. This constant value was assumed to be 10-fold greater than water to place an upper value on the blend-time for the neutralisation operation. Furthermore, the value for density of the lysate solution was taken as being 1100kgm^{-3}. All equations used are described in (Paul *et al.*, 2004; Grenville, 1992).

TERM	EQUATION	LYSIS	NEUTRALISATION
Reynolds (pseudoplastic fluid) at impeller	$\mathrm{Re}_I = \left(\frac{\rho N_I^{(2-n)} D_I^2}{k^{(n-1)} K} \right)$	124.1	N/a
Reynolds (Newtonian)	$\mathrm{Re} = \left(\frac{\rho N_I D_I^2}{\mu} \right)$	N/a	774.6
Torque on shaft (Λ)	$\Lambda = \left(\frac{P_0 \rho N_I^2 D_I^5}{2\pi} \right)$	1.13x10^{-3} Nm	0.72x10^{-3} Nm
Shear stress at vessel wall (τ_W)	$\tau_W = \frac{1}{1.622} \left(\frac{\Lambda}{D_T^3} \right)$	0.403 Pa	N/a
Shear rate at vessel wall (γ_W)	$\gamma_W = \left(\frac{\tau_W}{K} \right)^{(1/n)}$	1.54 s^{-1}	N/a
Apparent viscosity at wall (μ_W)	$\mu_W = \left(K \gamma_W^{(n-1)} \right)$	262 mPas	N/a
$P_0^{1/3}$ x Reynolds number at vessel wall	$P_0^{1/3} \mathrm{Re}_W = P_0^{1/3} \left(\frac{\rho N_I D_I^2}{\mu_W} \right)$	37.1 (transition)	838.8 (transition)
Fourier number at wall (Fo_W)	$\frac{1}{\sqrt{Fo_W}} = \left(\frac{P_0^{1/3} \mathrm{Re}_W}{183} \right)$	0.203	4.58
Fourier number at wall (F_oW)	$\frac{1}{Fo_W} = \left(\frac{\rho D_T^2}{\mu_W \theta} \right)$	0.0411	21.0
Blend-time (θ)	$\theta = \left(\frac{\rho D_T^2}{\mu_W (1/Fo_W)} \right)$	**24.5 mins**	**1.3 mins**

solution dropped immediately upon addition of the neutralising agent. In practice this was not the case since the final viscosity of the solution would only be reached upon homogeneity. It was also noted that once the potassium acetate solution was added a distinct, clear layer at the base of the vessel, with the lysate solution above, was formed by virtue of the higher density of the neutralisation buffer (1143kgm^{-3} at 25°C). The compartmentalisation of the lysate and neutralisation buffer meant blending took much longer, despite the use of an up-pumping, mixed-flow impeller which transported material across the interface.

7.7.1.1 Conclusions

To conclude the macromixing analysis requires assessment of the efficacy of each of the steps. The long blend time for the lysis was verified observationally and the blend-time for the neutralisation reaction was found to be far longer than predicted. Predicting bulk mixing during cell lysis and neutralisation is known to be difficult because of the large viscosity changes and density differentials causing compartmentalisation during the neutralisation reaction. By way of a comparison, the calculated blend-time for two solutions with similar μ and ρ to water, in the same vessel, was determined to be 8.5s. This value was found to be comparable to the experimental result using coloured, aqueous solutions.

In all, the long periods required for bulk mixing can only be assumed to be detrimental to plasmid quality. Several reports link extended lysis periods to decreases in plasmid supercoiling (Clemson and Kelly, 2003; Meacle *et al.*, 2004; Sayers *et al.*, 1996). However, analysis of the bulk mixing conditions does not help in determining whether the decrease in supercoiling witnessed is a result of a physical or chemical mechanism, just that the extended periods of operation required make more likely the effect of either to occur and to increase their impact. Further analysis of the micromixing conditions and shear forces in the vessel are required and are the subject of the next sections. In all it has to be reasoned that if this lysis vessel were to be scaled-up, on a constant power to unit volume ratio, the blend time estimations suggest that the mixing regime and parameters employed would be far from optimal.

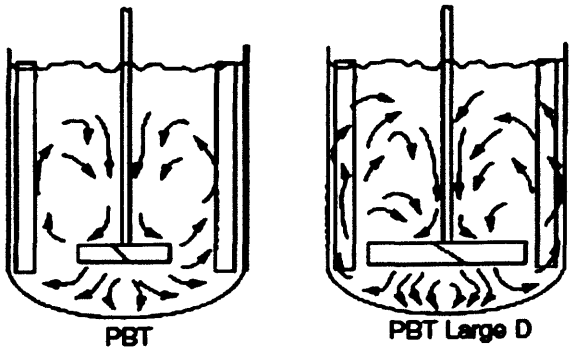

Figure 7-7 Schematic demonstrating the improved flow characteristics of a larger diameter pitched blade turbine (PBT) impeller. Better flow and higher shear rates at the vessel wall would improve the overall blend time (Paul *et al.*, 2004).

However, it is envisioned that two approaches could be employed to reduce the blend times in the vessel. Increasing the swept diameter of the impeller would improve mixing by increasing the bulk flow and thus raise the shear rates around the vessel wall.

Figure 7-7 sketches out improved flow characteristics expected from the use of a larger pitched-blade turbine (PBT). A second approach would increase the agitation rate of the impeller

7.7.2 Analysis of the Micromixing conditions in the lysis vessel

Both the lysis and neutralisation stages involve chemical reactions between two fluids, which means that it is important to consider the level of micromixing occurring in the vessel. Micromixing is the mixing encountered on the smallest scales of motion (Kolmogorov scale, η_K) and at the final scales of molecular diffusivity (Batchelor scale, λ_B). Micromixing can be the limiting step in the progress of reactions because effective micromixing dramatically accelerates the rate of production of interfacial area available for diffusion. Additionally, analysing the micromixing environment provides information on the hydrodynamic forces likely to be impacting on particles (i.e. plasmid DNA) at this scale. This is important since during the lysis and neutralisation operations, the plasmid product is in the bulk solution and no longer protected from hydrodynamic forces by the bacterial cell wall.

Table 7-8 details some of the key parameters which impact upon the vessel micromixing during the lysis and neutralisation reactions. All the values listed describe the situation in the impeller region, where the shear and energy dissipation rates are at their highest, and as such represent the most efficacious micromixing conditions likely to be encountered in the vessel. At the less well agitated areas of the vessel, lower shear rates would mean higher viscosities, lower energy dissipation rates and so poorer micromixing conditions.

Table 7-8 Table describing the key parameters which influence mixing and reaction on the microscale. The values were all determined for the impeller region of the vessel where the energy dissipation and shear rates are at their greatest. The smaller the turbulent length scales, the finer the scale of micromixing, and the faster the rate of mixing at the smallest scales of motion.

NOTATION	MEANING	LYSIS STAGE (100RPM)	NEUTRALISATION STAGE (100RPM)
$\eta_K = \left(\frac{\nu^3}{\varepsilon_T}\right)^{1/4}$	*Kolmogorov's length scale* Eddy size at which viscous forces equal inertial forces	288μm	38μm
$t_K = \left(\frac{\eta_K^2}{\varepsilon_T}\right)^{1/3}$	*Kolmogorov's time scale* Time taken to dissipate the energy contained in the smallest eddies	4.8ms	1.6ms

$\lambda_B = \left(\frac{\nu D^2}{\varepsilon_T}\right)^{1/4}$	*Batchelor's length scale* Size of a pure 'drop' that will diffuse into bulk fluid in time t_B	2.7μm	1.2μm
$t_B = \left(\frac{0.5\eta_K^2}{4D}\right)$	*Batchelor's time scale* Time required for pure 'drop' of size λ_B to diffuse into the bulk fluid. (Micromixing Time τ_{mm})	6.9s	0.21s
Reaction rate (k_r) (mols $L^{-1}s^{-1}$)	(a) HCl + NaOH (b) CH_3COOH + NaOH	(a) $1.4x10^{11}$	(b) $4.7x10^{1}$
$Da = k_r C_0 t_K$	*Damkoehler number (Da)* Ratio of mixing rate to reaction rate. Values <0.02 imply reaction is limiting.	$1.6x10^{8}$	0.0144

7.7.2.1 Micromixing environment during lysis

During the lysis step the maximum shear rate at the impeller was calculated using an empirical correlation (Paul *et al.*, 2004) that suggests the maximum shear experienced at the impeller is roughly equal to 150N, giving a value of $2.5x10^2 s^{-1}$. This rate is ~1000-fold lower than the shear rates at which plasmid supercoiling is damaged (Levy *et al.*, 1999b). Indeed others report that shear rates of this magnitude have no adverse effects on plasmid supercoiling and do not cause further fragmentation of the genomic DNA (Meacle *et al.*, 2004; Chamsart *et al.*, 2001).

Using the maximum shear rate the apparent viscosity of the lysate fluid at the impeller region was estimated at 19mPas. Ultimately, this meant that the Kolmogorov microscale of turbulence, and therefore the size of the smallest eddies, was ~300μm. Such relatively large sizes are a direct result of the high viscosity of the system causing viscous damping, such that the inertial forces of the fluid in motion would have been quickly dissipated in the fluid.

During the lysis procedure the cell suspension was mixed with the sodium hydroxide/ SDS solution with the aim of solubilising the cell membranes and raising the pH of the solution, in order to denature macromolecules. The pH and molarity of the neutralisation solution was 14 and 0.24M respectively, decreasing to ~12 and 0.13M upon reaching full homogeneity with the cell suspension. It has been demonstrated that during lysis,

irreversible denaturation of plasmid molecules occurs if they are exposed to pH's >12.5 and molarities >0.15M (Meacle *et al.*, 2004; Thatcher , 1997).

This means that a key process objective is the rate at which the sodium hydroxide enters the bulk solution; a faster rate being desired to avoid creating localised regions of high pH in the vessel, where plasmid molecules could be denatured.

Using the value for the diffusion coefficient of sodium hydroxide in water at room temperature of $1.51x10^{-9}m^2s^{-1}$ (Coulson *et al.*, 1996), the size of the Batchelor length scale could be estimated. Below this size 'drops' of sodium hydroxide are small enough such that diffusion becomes the driving force for mass transfer. Because of the relatively high diffusivity of sodium hydroxide in water, the Batchelor length scale is larger than the same value for acetic acid in water (Coulson *et al.*, 1996). However, the time taken for a 'drop' of this size to diffuse into the bulk fluid, the Batchelor time-scale (t_B) (or micromixing time) is much longer than for the neutralisation reaction. The reason for this being that the Batchelor length scale is proportional to the square of the size of the smallest eddy, so as η_K increases the time taken for the NaOH to diffuse into the bulk solution increases rapidly. Ultimately, the viscous damping occurring during lysis results in rapid dissipation of the fluid energy, increasing the size of η_K and so extending the diffusion time for NaOH. The resulting micromixing time scale is reliably assumed to be longer than the reaction rate, so as the Damkoehler number suggests, micromixing is the limiting factor in the lysis reaction. The estimation of the Damkoehler number assumed that the lysis reaction is rapid once the NaOH is in the solution, the figure of $1.4x10^{11}molsL^{-1}s^{-1}$ being typical value for a neutralisation reaction (Paul *et al.*, 2004). With such a fast reaction rate, micromixing will always be limiting irrelevant of the mixing conditions as for the reaction rate to become limiting η_K would need to be $\sim10^{-19}m$, which would be impossible.

Even though the micromixing would always be the limiting factor in the lysis reaction, reduction of the Batchelor time scale would be an effective way of lessening the heterogeneity of the NaOH and so reduce the exposure time of plasmid molecules to high NaOH molarities and pH's. Because of the square relationship between the η_K and the time taken for a drop of size λ_B to diffuse into the bulk fluid, reducing the size of η_K would have a large impact on the diffusion rates. Figure 7-8 describes the estimated impact of increasing the agitation (shear) rate on some of the key parameters influencing macro and micromixing during lysis. The graph shows the dramatic improvements expected in blend

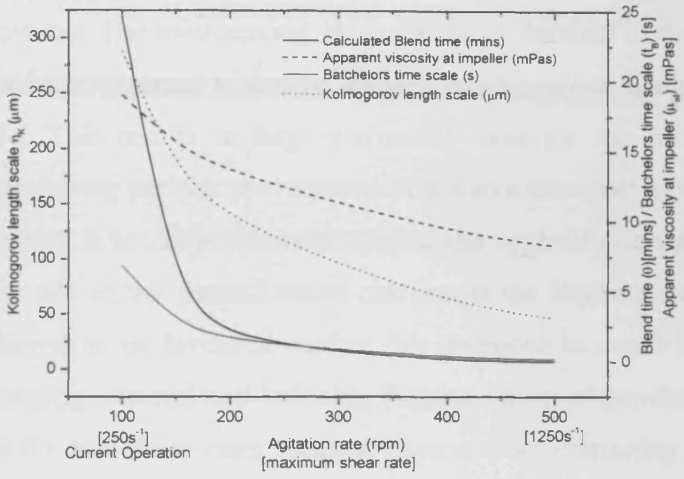

Figure 7-8 Schematic displaying the calculated impact that increasing the agitation rate would have on some of the key parameters affecting macro- and micromixing during the lysis operation. A constant power number was assumed during the regime since the Reynolds number at impeller did not exceed 10^3.

time, Kolmogorov's length and micromixing time scale, which can be attributed to the simultaneous increase in ε_T and decrease in apparent viscosity of the lysate.

7.7.2.2 Micromixing environment during neutralisation

Referring to Table 7-8 shows that by virtue of the viscosity drop (assumed to be $1x10^{-2}$Pas) the size of the Kolmogorov length and time scales are much reduced than those estimated for the lysis stage. However, because of the slower rate of diffusivity of acetic acid in water ($0.88x10^{-9}m^2s^{-1}$ (Coulson *et al.*, 1996)) the size of the 'drop' at which diffusion becomes the driving force for mass transfer (Batchelor length scale) is smaller than for NaOH. But, due to the smaller values for η_K the time taken for mass transfer is much reduced. Similar to the situation for the lysis procedure, rapid micromixing is desired in the neutralisation stage as the longer the plasmid molecules are exposed to high pH's the more chance of irreversible plasmid denaturation. The production of OC pDNA under strongly alkaline conditions due to the alkaline-scission of the phosphodiester bonds in DNA has been reported (Uhlenhopp *et al.*, 1974; Sayers *et al.*, 1996). However, the reported reaction rate of the NaOH-CH_3COOH neutralisation reaction at $4.7x10^1molsL^{-1}s^{-1}$ (Paul *et al.*, 2004) is far slower than those seen for strong acid-strong base neutralisation. Because of this, the calculated Damkoehler number for the neutralisation step suggests that the reaction rate and not the level of the micromixing represents the limiting step in the reaction. Because of this increasing the level of micromixing would not improve the efficacy of the neutralisation step.

7.7.2.3 Conclusions

To conclude requires judging the efficacy of the micromixing encountered during the lysis operation. The micromxing environment is deemed to be poor. The low shear rate results in a high apparent viscosity leading rapid viscous damping of the inertial forces of the fluid. This results in large estimated sizes for the microscale of turbulence which in ensures long periods are required to achieve transport of the NaOH into bulk solution. The situation is not as problematic during the neutralisation stage since it is suspected that the slow rate of the neutralisation reaction is the limiting step. The use of low shear rates is believed to be favoured during this protocol in order to reduce the possibility of both damaging plasmid and inducing fragmentation of genomic DNA. However, it is believed that the low shear rates adopted have a more damaging effect by virtue of creating poor conditions for mass transfer.

7.7.3 Characterising the possibility for shear induced plasmid damage during lysis

When considering shear damage to biological particles it is commonly accepted that if the particle is smaller than the Kolmogorov length scale then shear damage is unlikely, since under these conditions eddies will be larger than the particles and so would be entrained within the eddy. If the eddies are smaller than the particle then they would act on the particle surface and induce relative motion, possibly resulting in damage. This reasoning does not include the possibility of elongational flows, present in all fluid in motion, causing shear damage, but these are rarely studied.

To understand whether the size of the smallest eddies induced by mixing in the impeller region were small enough to inflict damage on the plasmid DNA, the hydrodynamic diameter of the supercoiled plasmid molecules needs to be known. It is quite hard to place an exact figure on this value.

7.7.3.1 Estimating the size of the plasmid molecules

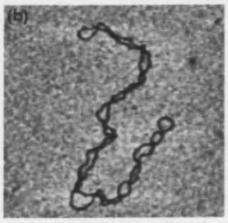

Figure 7-9 Electronmicrograph of a supercoiled 6kb plasmid molecule represented on a 2D surface from (Levy *et al.*, 2000b) with a measured hydrodynamic diameter ~500nm. Length of plasmid DNA is (6000x 3.4A) is 2µm, meaning the hydrodynamic diameter is roughly 3/4 plasmid diameter.

Figure 7-9 shows an electronmicrograph of a 6kb plasmid with a measured hydrodynamic diameter of 500nm. It is known that B-DNA rises 3.4Å with each base pair (Voet and

Voet, 1995), giving this plasmid a total linear length of 2μm. If this represents the plasmid circumference then the outstretched diameter would be 636nm, and as such means the hydrodynamic diameter is ~3/4 the total plasmid diameter. However, this assumes a maximum value, since the plasmid molecule is splayed out on a 2D surface. In solution, it could be expected to be a more tightly coiled three dimensional structure.

To estimate the approximate dimensions of the plasmid when in solution, it could be assumed it behaves like a globular protein and adopts a spherical morphology. By such logic and knowing the density of supercoiled DNA to be 1.709gcm^{-3} (Davidson, 1972) and the molecular weight of the plasmid, the particle diameter can be calculated. The calculated diameter for the 6kb plasmid becomes 19.4nm. Obviously, the difference between the calculated value and the value obtained from the electronmicrograph is very large.

The problem with both measures is that each makes assumptions about the state of the plasmid in solution. The maximum measure assumes that the diameter is that of the plasmid molecule when splayed out on a 2D surface, whilst the calculation method assumes that the topology of the plasmid molecule is such that it forms a tightly coiled ball. However, the chemical composition of DNA makes the thermodynamics of this assumption unlikely. The phosphate groups forming the backbone of the DNA are charged molecules and as such will be hydrophilic.

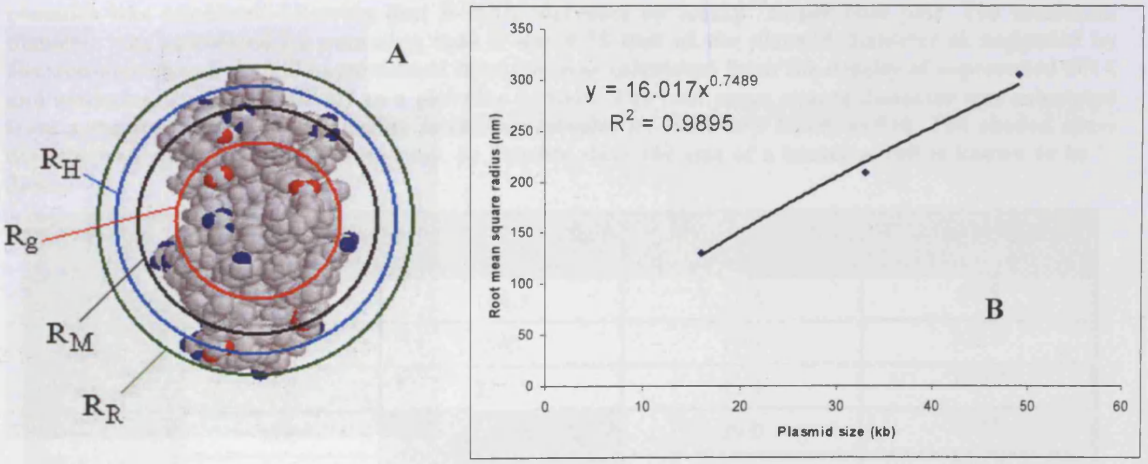

Figure 7-10 Schematic of the different radii used to describe the size of a globular protein; lysozyme. R_G is the radius of gyration (root mean square radius) and is a measure of the mass distribution of a molecule around its centre of mass. R_M is the particle radius calculated from knowing the density of the molecule. R_H is the hydrodynamic radius and represents the full radius of the particle including the solvation shell. R_R is the radius of rotation and describes the maximum radius of the particle when rotated. Figure B shows the linear fit of the three data points produced for the R_G of three plasmids of different sizes from FFF.

For the molecule to assume its lowest energy state these groups would need to be solvated and as such be exposed to the bulk solution. This situation differs from globular proteins, which contain hydrophobic amino acids, and so the thermodynamics of the system force the protein molecule to assume a tightly coiled configuration. Structural analysis of plasmids is complicated by the conceptual belief that the plasmid molecule would assume a more tightly coiled formation with associated water molecules trapped within the supercoiled structure.

An estimate can be placed on plasmid size using information gained from field-flow fractionation (FFF). Three large plasmids of size 16kb, 33kb and 49kb were run once on such a system. It should be mentioned that the data is very limited.

Field-flow fractionation outputs the root-mean square radius of the particles under study. This is a size value weighted by the mass distribution about the centre of mass of the molecule, also known as the radius of gyration. The root mean square radius is not necessarily representative of globular protein size, though for a plasmid since its tertiary structure will not be as compact as a globular protein, it may provide a more useful measure. Ultimately, what has to be considered when estimating the size of plasmids using the various methods is that it cannot exceed the size of the bacterial cell it as synthesised in i.e 1-2μm.

Table 7-9 Predicted plasmid diameters calculated by three different means. The linear length of the plasmids was calculated knowing that B-DNA increases by $3.4x10^{-10}$m per base pair. The maximum diameter was calculated by assuming that it was 0.75 that of the plasmid diameter as suggested by electronmicrograph data. The minimum diameter was calculated from the density of supercoiled DNA and assuming it coiled similarly to a globular protein. The root mean square diameter was calculated from a standard curve generated by analysing samples by field-flow fractionation. The shaded areas display predicted sizes which would not be feasible since the size of a bacterial cell is known to be 1-2μm.

Plasmid length (kb)	Linear length (μm)	Max. supercoiled diameter (nm)	Min. supercoiled diameter (nm)	Root mean square diameter (nm)
2	0.68	166.5	13.5	53.8
6	2.0	500	19.4	122.6
10	3.4	832.5	23.1	179.7
20	6.8	1,665.0	29.0	302.0
40	13.6	3,330.0	36.6	507.5
80	27.2	6,660.0	46.0	852.8
100	34	8,325.0	49.7	1,007.9
116	39.4	9,657.0	52.2	1,126.4

Table 7-9 details the diameters of various sized plasmids estimated by the three methods. The maximum measure assumes that the plasmid diameter is 0.75 its outstretched diameter but the values estimated soon reach levels unsustainable by the bacterial cell. The minimum values predicted for plasmid size, by calculating the particle radius from supercoiled DNA density, are deemed to be too small as the method overestimates supercoiling by assuming the same level of coiling seen in globular proteins.

The most plausible estimates of plasmid diameter are those provided by FFF. From these estimates the predicted plasmid diameters reach a level of just over 1μm for the largest constructs. These values will be taken as the closest estimates but are themselves subject to large variations depending on the system in which the plasmids are in, for instance changes in the ionic strength of the buffers are known to have large effects on the plasmid diameters (Schlick, 1994). An interesting analysis produced from these size assumptions is that for a 116kb plasmid (i.e. p5176) there exists only enough physical volume in a 1μm radius bacterial cell to accommodate 6 constructs, which could give an indication of the maximum level of copy number.

Having estimated the plasmid sizes being investigated to be ~1μm, it can be stated that they are smaller than the Kolmogorov length scales witnessed in the impeller region during the lysis and neutralisation stages (Table 7-8) and as such would be unlikely to be sheared by these forces. However, it must be expected that if the plasmid molecules were to lose a degree of supercoiling when released into solution, a possibility due to changes in the ionic/biological environment, then it does not take much to extend the diameters of these molecules to very large sizes, in the order of 10μm, such that shear forces would be effective. This acknowledgment has ramifications for the UF step where selective degradation of the OC plasmids form was witnessed. It is hypothesised from these size estimations that the size difference between the SCC and OC plasmid forms becomes greater with the increased linear length of the pDNA molecule. As such in the higher shear environment of the UF membrane the outstretched OC plasmid forms were within the size ranges of hydrodynamic shear but that the compacted nature of the SCC forms meant that these particles were below the size range of hydrodynamic shear and thus were relatively unscathed.

7.7.4 Conclusions

To conclude this section requires assessment of the mixing conditions created in the vessel and deciding on whether the degradation of SCC→OC plasmid form, witnessed during the lysis procedure, was the result of a physical or chemical action. It has to be reiterated at this point that whilst a decrease in SCC plasmid topology was witnessed for the smaller plasmid (3.2kb) the issue only became more apparent for the larger constructs. As such, it must be appreciated when assessing the conditions used for this lysis procedure, that they were deemed to be sufficient for plasmids in that size order (3-10kb). It is only during these recent investigations, utilising larger plasmids that the efficacy of this lysis procedure needed to be questioned. Analysis of the macromixing found blend time to be extensively long in both the lysis and neutralisation steps. The long periods estimated to achieve 95% homogeneity, at the conditions employed, were found to be required in practice. The blending of viscoelastic fluids will continue to be a difficult problem due to the large increases in fluid viscosity. Again, despite evidence showing that extended exposure to alkaline environments can lead to OC generation, the magnitude of the problem may not have been apparent with smaller plasmids. However, it is believed that the extended periods required to reach homogeneity have a more detrimental effect when processing larger constructs.

Similarly, the micromixing conditions were found to be far from ideal during the lysis period of the process. It was estimated that due to viscous damping, sizes of the smallest eddies were ~300μm. Due to the square relationship which exists between the sizes of these eddies and the resultant micromixing time, the time required for the NaOH to diffuse into the bulk solution was extended. The only result of this is that at the microscale, plasmid molecules would have been exposed to regions of high pH and NaOH for longer periods, a detrimental occurrence. During the neutralisation reaction the situation with the micromixing environment was deemed to be less of a problem as it was suggested that the actual reaction rate rather than the micromixing was the limiting step.

Overall it is felt that the mixing conditions employed during the lysis procedure are sub-optimal. The low shear rate is at the heart of the poor macro and micromixing. It is suspected that the protocol is too cautious in the belief that the lower the shear-rate, the less likelihood of fragmentation of gDNA and plasmid shearing. However, it is believed that the shear rates required to cause those problems are far above those employed in this protocol (Chamsart *et al.*, 2001; Meacle *et al.*, 2004).

Characterising the potential for physical damage to the plasmid molecules by hydrodynamic shear, required estimation of the plasmid diameter of the constructs under investigation. The values thought best to represent the sizes were determined by FFF and suggested that the supercoiled plasmid form of all the constructs were $\leq$ 1μm. At such sizes the plasmids were deemed to be out of the size range of the smallest eddies (~40μm) calculated to be generated during the neutralisation. It was also established by these analyses that as linear plasmid DNA length increased the estimated sizes for OC plasmid form could be expected to become very large indeed ~10μm. It is reasoned that these large size increases lie at the heart of the issue surrounding selective OC degradation during UF.

In all, it is believed that the SCC to OC degradation witnessed during lysis was largely the result of chemical action rather than a physical mechanism. Both the macro and micromixing analysis suggested poor mixing conditions were generated, meaning that the plasmid molecules would have been exposed to high molarities and pHs for the long periods required to blend. This would not necessarily been apparent when processing smaller plasmids but certainly became more so with the larger constructs. Secondly, the impact of hydrodynamic shear was estimated not to be in the region to cause damage to the plasmid molecules. These suspicions are backed up by visual inspection of the gels of the lysate samples. The gels describe an accumulation of OC and in the cases of the larger plasmids linear plasmid form during lysis. Conceptually had this been caused by physical shear then it is reasoned that the process would not stop there, but the OC/ Linear forms to would have been further sheared to fragments, as occurred during the UF step. This would be expected since the hydrodynamic diameters of the OC/Lin forms would be larger than the same plasmid in SCC form and so more prone to shear degradation. The fact that this degree of shearing was not witnessed suggests the action of more precise degradation of the type expected from chemical degradation. The reason that the extent of degradation would increase with plasmid size, is thought to be unrelated to the actual physical size of the plasmids and more to do with the increased linear length of DNA providing an proportional increase in the number of sites for degradative action.

So in short, poor mixing conditions leading to extended mixing operations and poor mass transfer led to the plasmid damage by a chemical mechanism. The exact mechanism is unknown but likely to be due to the combination of alkaline-scission of phosphodiester bonds (Adam and Zimm, 1977) and the endonucleases actions of endogeneous DNases (Monteiro *et al.*, 1999).

7.8 Balances of the major contaminants

The main aim of this downstream process is the recovery and concentration of the desired plasmid product, but of equal importance is the purification of the product away from any contaminants. One of the main aims of conducting these downstream investigations was to monitor the clearance levels of the major contaminants encountered when processing plasmids. As such samples taken during each of the 24 runs were analysed by BCA, Quant-IT and qPCR in order to quantify the levels of dissolved protein, RNA and genomic DNA. In this section the levels of removal exacted by the process will be presented and judged. Judgement will be made against the criteria required for plasmid release as shown in Table 7-10.

Table 7-10Specifications required for release of plasmid DNA (Ferreira *et al.*, 2000c; Zoon, 1996)

Specification	Acceptance criteria	Analytical method
Plasmid		
Appearance	Clear, colourless solution	Visual inspection
Identity of plasmid	Restriction map, sequence homology	Restriction mapping, PCR
Plasmid homogeneity	>90% supercoiled (SCC) form	Agarose gel + densitometry
Plasmid concentration	According to application	A_{260}, HPLC, Fluorescence
Potency	According to application	Cell transfection studies
Impurities		
Protein	Not detectable, <0.01µg/ dose	BCA assay, SDS-PAGE
RNA	Not detectable	0.8% Agarose gel
gDNA	<0.05µg/ µg plasmid, <0.01µg/dose	Southern blot, qPCR,
Endotoxins	0.1EU/ µg plasmid, <5EU/kg body weight	*Limus* ameobocyte lysate (LAL)

It should be noted that the results displayed in this section are the averages of the runs conducted, the full breakdowns for each run can be seen in the respective mass balance (Figure 9-31 to Figure 9-49). Averages were taken for the masses of the contaminants at the respective points of the process for all runs excluding the controls. The controls were excluded since they utilised a different mechanism of RNA removal, involving the addition of RNase (a protein), and as such were thought to be unequivalent. It was deemed that the other runs were equivalent since they made use of identical batches of cell paste. Taking averages in this way allowed for comparison between the different crossflow rates

on contaminant clearance. As such, each point recorded is the average of 10 individual runs, and the value for each of those points is the average of multiple assay results.

7.8.1 Genomic DNA

It has been reiterated several times in this report about the importance of demonstrating clearance of genomic DNA during plasmid production, as well as highlighting the unique difficulties presented by this contaminant (Ferreira *et al.*, 1999). The philosophy of any downstream process is to employ appropriate techniques which enable separation by exploiting any differences either physical (e.g. size, charge) or chemical (e.g. solubility, binding) between the desired product and the contaminants (Bailey and Ollis, 1986). As was demonstrated in the analytical section of the report, in this project recording the relative amounts of plasmid DNA and genomic DNA was troublesome. With high-copy number plasmids the importance of this was reduced, since the plasmid DNA was commonly far in abundance of gDNA in the samples used for analysis, and so the presence of gDNA could be ignored. However, with low-copy plasmids this was not the case. Fluorescence and absorbance techniques were found not capable of distinguishing between pDNA and gDNA. Similarly, with HPLC, although the impact of gDNA was reduced, small amounts were still found to co-purify with the plasmid DNA. In all, this anecdotal evidence displays the problems faced in removing this contaminant, in that for most criteria, gDNA and pDNA are essentially identical molecules, making separation troublesome.

The greatest selective removal of gDNA is achieved across the alkaline lysis step, which exploits a differences connected to the relative size and form of pDNA and gDNA. Due to the larger size of gDNA, when denatured during the lysis step, it is unable to re-anneal properly when the solution is neutralised. However, due to the smaller size of pDNA and its circular conformation, it is capable of re-annealing properly. Due to this behaviour pDNA returns to soluble form upon neutralisation, whilst the amorphous mass of mismatched gDNA does not and so is precipitated out (Birnboim and Doly, 1979; Ferreira *et al.*, 2000c). However, this removal is not complete as small fragments of gDNA can be found dissolved in the neutralised solution. It is these fragments that present the problem to the steps downstream of lysis. The creation of these fragments is an inherent drawback with the alkaline lysis procedure, however, there are no alternative methods which have been shown to outperform this step, which is why it is the industry standard..

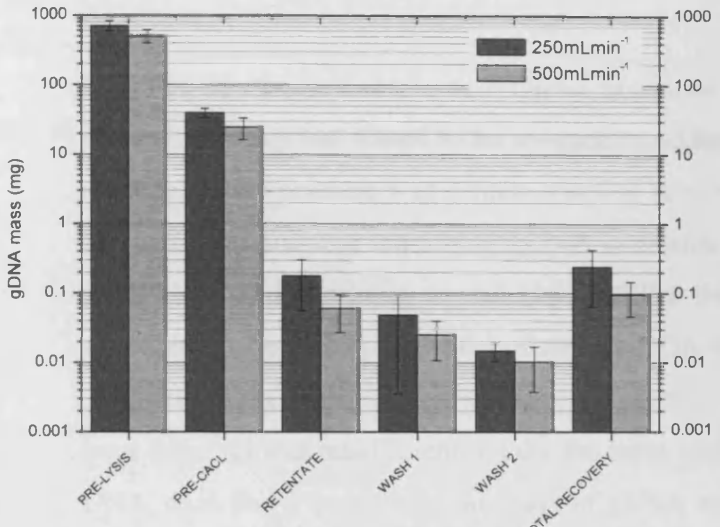

250ml/min	MASS(MG)	%
PRE-LYSIS	709.06	100.00
PRE-CACL	39.64	5.59
RETENTATE	0.1797	0.0253
WASH 1	0.0484	0.0068
WASH 2	0.0149	0.0021
TOTAL RECOVERY	0.2431	0.0343
CLEARANCE	708.82	99.966

500ml/min	MASS(MG)	%
PRE-LYSIS	504.93	100.00
PRE-CACL	24.86	4.92
RETENTATE	0.0608	0.0120
WASH 1	0.0252	0.0050
WASH 2	0.0103	0.0020
TOTAL RECOVERY	0.0964	0.0191
CLEARANCE	504.83	99.981

Figure 7-11 Figures outlining the step removal of gDNA during these investigations. The results represent the averages of the 10 individual runs for each crossflow rate (Table 7-5). The results for the individual runs are shown in the mass balances and each point in those was determined by quadruplicate analysis of samples by qPCR. The pre-lysis values were obtained by sonication of a 1.56gL^{-1} sonication of the relevant cell paste and subsequent qPCR of the lysate. The starting masses were then calculated by knowing the WCW of each of the individual DSP runs.

However, one of the most important considerations when optimising the alkaline lysis step is that the shear rates employed do not lead to fragmentation of the precipitated floc and the associated increase in gDNA fragments such an event would cause.

Figure 7-11 details the results of the investigations into the removal of gDNA through the downstream process. Whilst not a full mass balance, the data is useful in describing the clearances produced by the process. At the outset, the total mass of genomic DNA was determined to range between 500-700mg. The large difference between the two starting masses for the different investigations is reasoned to be due to variations produced by the analytical procedures, since the cell paste in which the investigations were conducted upon were deemed equivalent. The difference is not too problematic since the different investigations are also compared on a proportionate basis taking the initial value as 100%. Taking the average value of 607mg and knowing that the average mass of cells lysed was 42g♦ produces a value of 1.44% (w/w). This is larger than the value listed in Figure 7-2, taken from (Ferreira *et al.*, 2000c), but values do vary. (Bailey and Ollis, 1986) place the value at 1% (w/w). In all, the figure was deemed acceptable since variation in cell line,

♦ As outlined earlier, even though the procedure was conducted on 50g of frozen cell paste, determination of the WCW of the cell suspension recorded the average cell concentration of 168gL^{-1} equating to 42g of cells lysed. The difference was reasoned to be due to differences in the dewatering capabilities of the batch centrifuges used for fermentation harvest.

extraction methodology and analytical technique could all combine to account for the difference.

It can be appreciated the large removal produced by the alkaline lysis procedure, as the starting ~607mg was found to be reduced to ~32mg in the neutralised lysate. Overall, the alkaline lysis procedure was demonstrated to remove 94.5-95% of the total genomic DNA. It is reasoned that the remaining gDNA consisted of small dsDNA fragments capable of re-anealing and returning to solution. Whilst this level of removal is impressive the situation is effected by the ratio of genomic DNA to plasmid DNA. As shown by Table 7-11, for all the plasmids under investigation the final specific yields meant that even the large removal was insufficient to take the mass of the genomic DNA below that of plasmid DNA, such that it every case the mass of gDNA exceeded that of pDNA in the neutralised lysate. The factor by which this occurred being dependent on the mass of pDNA in the lysate and so the final specific yield of the fermentations.

Table 7-11 Table showing the mass levels of each of the plasmids at the pre-$CaCl_2$ stage of the process, as described in Figure 7-2. The table also shows the ratio of genomic DNA to plasmid DNA at this stage. Also, detailed is the expected mass of a hypothetical high-copy number construct of 5kb with a copy number of 1000 per cell. The mass value was calculated by determining the mass of plasmid DNA produced from each cell (5.48×10^{-15} g pDNA/cell) and using the calibration curves shown in the fermentation chapter to determine the level of mass expected from a cell suspension containing 42g of cells (2.5×10^{9} cellsmL^{-1} ~ 16.32gL^{-1}WCW).

Construct	Mass of pDNA (mg) in clarified lysate	Ratio of gDNA to pDNA at lysate stage
Genomic DNA	32.25	1
pGEM 11 [3.2kb]	3.04	10.6
pGEM 16 [16kb]	15.62	2.06
pGEM 33 [33kb]	11.87	2.72
pGEM 49 [49kb]	7.10	4.54
P5176 [116kb]	1.73	18.6
pUC [5kb]	35	0.92

By way of analysis the table describes the hypothetical situation for a high-copy number 5kb plasmid existing at a copy number of 1000 at the end of the fermentation. Calculations estimate that the mass of pDNA present in the lysate at the pre-$CaCl_2$ stage for this construct would be ~35mg. As a result of these higher masses it could be expected that for such a plasmid it would exist in excess of the genomic DNA. Obviously, this would be a more favourable position to be in. This analysis goes someway to highlighting the importance of specific plasmid yields to the downstream process. Had the large plasmids demonstrated 100% stability the situation would have been much improved.

Indeed higher masses, in the order of 100-200mg of plasmid in the lysate at this stage could be obtainable, depending on the construct and the fermentation strategy employed (Chen *et al.*, 1997). The result of obtaining these higher masses would mean that plasmid DNA was far more in excess of gDNA than the situation encountered with these constructs.

Further processing led to reductions in genomic DNA. It has been reported that some gDNA removal (especially denatured gDNA) would be likely over $CaCl_2$ addition step, but no data is available to state this definitively for these investigations (Eon-Duval *et al.*, 2003a). Certainly, the UF step removes a large proportion of the remaining gDNA fragments. The logic behind this step being that the smaller, linear form of the gDNA fragments allows them to pass through the membrane and so exit the process. The DNA would have been cleared either during the permeation or diafiltration procedures and as can be seen by the clearance data the removal is almost total. The permeation of these fragments is perceived to be comparable to what occurred to the sheared plasmid fragments during the same operation. The losses described in the plasmid section were reasoned to be due to the small, sheared pDNA fragments being small enough to pass through the membrane when a TMP was applied.

The clearance of gDNA by this process is deemed to be good, in that both situations >99.9% of the gDNA is removed. As can be seen from the gDNA clearance data and as will be described with the other contaminants, higher proportionate clearances were achieved during using the higher crossflow velocity of $500mLmin^{-1}$. It is reasoned that due to the greater scouring effect of the faster crossflow rate, the resultant equilibrium thickness of the gel layer would have been smaller (Darnon *et al.*, 2003; Butler *et al.*, 2000). A direct result of a thinner boundary layer would be improved transport of material across it. Since at the boundary layer mass transfer becomes a diffusion driven process, the narrower layer produced during faster crossflow operation, would allow more material to cross and be cleared from the process.

A final level of information to be extracted from the clearance data is the final co-recovery levels of gDNA. Although both procedures resulted in >99.9% clearance, the amount of gDNA co-recovered from the UF step with the plasmid product has very important implications. It is important that the UF stages of this process remove the majority of gDNA, since following the UF step the plasmid recovery fractions are subjected to anion-exchange chromatographic purification. Although there are more sophisticated

chromatography systems being developed for plasmid purification (Diogo *et al.*, 2005), the one utilised in this process is a packed bed TMAE resin. It is accepted, that due to the relatively unsophisticated nature of anion-exchange chromatography and the physicochemical similarities of gDNA and pDNA, that no great clearances of gDNA can be expected from this step. By personal communication (Cora Henwood, GSK) it has been determined that 0.5log clearances are the best that can be achieved.

For argument's sake it will be assumed that the levels of gDNA recorded to be co-purified along with the plasmid at the end of the UF step, represent the final situation. Regarding Table 7-10 shows that the specifications for plasmid release require the gDNA contamination to be below 0.05μg gDNA/ μg pDNA. However, industry pressure is leading to further stringency, such that processes should be able to demonstrate clearances down to 0.01μg gDNA/ μg pDNA (personal communication). These clearances have implications to this process as the data suggests that the average co-recovery of gDNA was 96.4μg gDNA for the 500mLmin^{-1} operation but 243.1μg gDNA for the 250mLmin^{-1} procedure. These results can be used to estimate the limits of this process. Using the lower value (96.4μg) means that to be acceptable the total plasmid recovered must be 9.6mg. If 80%[♦] recovery of plasmid is assumed across the process then this requires a starting mass of pDNA in the lysate to be 12.05mg, which assuming 42g of cells are lysed, equates to a specific yield of 287μg pDNA / gWCW. From the calibration curves outlined in the fermentation chapter, it was found that 1g WCW ~ 1.5x10^{11} cells. As such, the specific yield equates to 1.91x10^{-15} g pDNA/ cell, a mass equivalent to 1.15x10^{9}Da of extrachromosomal DNA. Since 1bp ~ 660Da, the total amount of extrachromosomal DNA required, per cell, is 1.75x10^{6}bp. This value represents the lower acceptable limit of this process, if each of the cells produces pDNA at values below this level, then the clearance of gDNA exacted by this process will be insufficient for the plasmid to pass the acceptance criteria.

The value of 1.75x10^{6}bp has important implications in judging whether this process can be employed to process large constructs. The results from previous sections have highlighted problems faced with plasmid recoveries and topology changes encountered during operation of this process for the purification of large plasmids. This result demonstrates a

[♦] 80% recovery was found to be achievable with the 16kb construct and would be expected for constructs smaller than this, as shown by Figure 7-3. However, the recoveries of the larger constructs was found to fall below this level due to the greater abundance of OC plasmid form being created during lysis and subsequently sheared during UF operation. As such, when assuming 80% recovery this should be appreciated and that poorer recoveries would lead to the levels of gDNA clearances being unacceptable

physical cut-off point, dictated by the clearance of gDNA, below which the process cannot be operated since the contamination remaining at the end would be too high to pass the acceptance criterion of 0.01μg gDNA/ μg pDNA.

Figure 7-12 shows the minimum copy number required by plasmids of different sizes such that sufficient pDNA is present at the end of the process such that ratio of plasmid DNA to genomic DNA is above the acceptance criterion for this contaminant. From the graph it can be appreciated that under no circumstances could this process be used to effectively purify the Oxford series of BAC plasmids. Considering the construct p5176 (116kb), for sufficient plasmid material to be present to meet the acceptance criteria (even assuming 80% recovery, which as the process stands is unlikely) the copy number of this construct would have to be ~ 15 per cell. At present the copy number of this construct is deemed to be 1-2 copies per cell and as such way below the minimum acceptable limit. Indeed the situation is not much improved for the other constructs. Referring back to Figure 7-2, the point at which the lower limit of acceptability is demarcated by dashed lines on the graphs plotting plasmid mass and specific yields of the constructs employed in these investigations. It can be seen that only pGEM16 and pGEM33 have specific yields high enough to expect that this process would be capable of their purification. The other constructs fall too low. However, even though the two constructs have specific yields within the acceptable range they are too close to the cut-off point to be likely to be trusted in practice. Consequently, for such a process, specific yields double the limit would probably be required for the process to be deemed operational i.e. ~600μg pDNA/ gWCW.

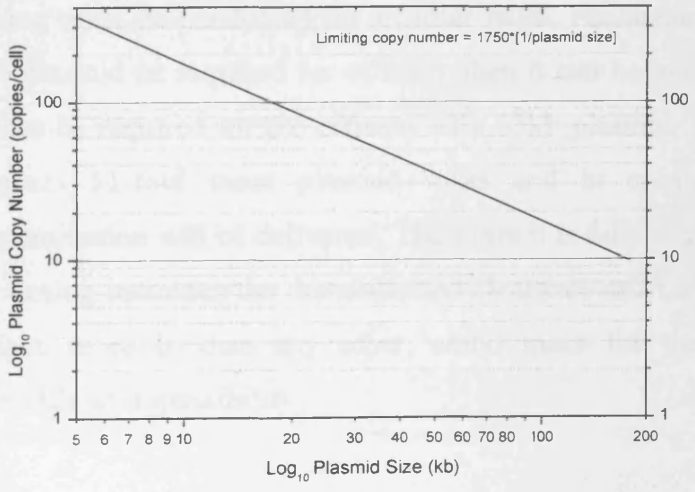

Figure 7-12 Plot showing the lower level at which this process is capable of operating. The graph plots plasmid size against the required copy number which must be ensured such that the total mass of extrachromosomal pDNA available for purification exceeds $1.75x10^6$bp per cell. This amount of pDNA is estimated to be required such that the ratio of plasmid DNA to genomic DNA at the end of the process is high enough to pass the acceptance criterion of 0.01μg gDNA/ μg pDNA.

The importance of acknowledging this process constraint cannot be understated for the production of large plasmids using this or similar processes. The process can only be relied upon to clear a certain majority of the gDNA present, which is reasonably fixed by the process design. Whether the process is acceptable is reliant on the mass of plasmid purified from it and as such the mass of plasmid present initially i.e. the harvest specific yield. If that yield is not high enough, the process, as it stands, would not be capable of producing a sufficiently pure plasmid fraction. With small plasmids this has been reasonably unproblematic since the constructs and production strategies have been designed and optimised to ensure plasmid DNA is maintained at high enough levels, such that the mass of extrachromosomal DNA exceeds the minimum level. With larger constructs, such as BACs, the unoptimised nature of their replication elements and their stringent control means that the levels of pDNA remain below the level acceptable by this process.

Similarly, had the cloned large constructs been maintained at 100% stability, sufficient pDNA would have been present to reach the minimum requirements. Extrapolation of the yield and stability data of the larger pGEM33kb and 49kb in Table 6-4 demonstrated that the specific yields of these constructs if stability were 100% specific would have been in the range of 700-800μggWCW^{-1}, and as such above the 600μggWCW^{-1} limit. However, with the poor stability profile the plasmids it was found that sufficient pDNA was not being produced per unit mass of cells.

A final caveat must also be outlined. The specifications for use of plasmid DNA in therapeutic applications has been assumed to be 0.01μg gDNA/μg pDNA. However, when dosing plasmid DNA it is assumed that for the protocol to be effective the gene dosing must be conducted on a molar basis. For instance, should 10,000 copies of a 3kb plasmid be required for efficacy then it can be assumed that the same number of copies be required for the efficacy of a 33kb plasmid. However, to achieve that level requires 11-fold more plasmid mass and in conjunction 11-fold more gDNA contamination will be delivered. Therefore it is fully expected that as the mass required for dosing increases the demonstrated clearance must also be shown to increase. Such a fact, more so than any other, could make the therapeutic application of large plasmids an impossibility.

7.8.2 Ribonucleic acid (RNA)

An additional nucleic acid which any plasmid process needs to demonstrate clearance of is RNA, for exactly the same reasons as gDNA, the fear being that these fragments may contain oncogenes or cause activation of oncogenes once delivered (Schleef, 2001). Again, RNA is physically and chemically similar to the plasmid DNA being produced. Historically, this contaminant was removed using RNase and indeed this approach is still commonly employed on the analytical scale. However, there are concerns regarding RNase because it is purified from bovine pancreas and regulatory authorities recommend that bovine-derived material should be avoided in the production of biopharmaceuticals, following the outbreak of new-variant CJD.

Precipitation techniques are a convenient way of separating pDNA from RNA and can be divided into two categories. First, plasmid precipitation can be employed, using either isopropanol (IPA) (Chakrabarti *et al.*, 1992), spermine (Murphy *et al.*, 1999), polyethylene glycol (PEG) (Lis and Schleif, 1975) or cetyltrimethylammonium bromide (CTAB) (Ishaq *et al.*, 1990). However, the scaling up of plasmid precipitation is troublesome since the delicate plasmid needs to be centrifuged out and resuspended for further processing. Consequently, selective precipitation of the RNA impurity with the plasmid remaining in solution is deemed preferable. High-salt is the main RNA precipitant. Lithium chloride is most commonly used on the analytical scale (Chakrabarti *et al.*, 1992) but its adverse toxicological effects prevent its use on a commercial scale, as such sodium acetate, ammonium acetate, ammonium sulphate, magnesium chloride and calcium chloride have all been studied.

In these investigations RNA precipitation was achieved through the addition of Calcium chloride (Eon-Duval *et al.*, 2003a; Eon-Duval and Burke, 2004). The high modal surface tension of this salt means it is anti-chaotropic and so reduces the solubility of molecules. Its mechanism of action has been linked to the presence of divalent cation binding sites within RNA structures (Bukhman and Draper, 1997). However, (Semancik and Szychowski, 1983) found RNA precipitation by divalent salts to be reversible and as such more likely to be caused by the 'salting-out' effect described by (Wu and Karger, 1996), an occurrence commonly seen with proteins, rather than metal-ion mediated cleavage. The selective nature of the nucleic acid precipitation may be explained by the flexible single-stranded structure of the RNA molecule. This form results in more hydrophobic bases being exposed, which leads to increased aggregation and precipitation. By contrast, SCC

plasmid DNA is less hydrophobic since the bases are sheltered within the compact double helix structure. This may also explain why denatured gDNA has been found to co-precipitate with RNA (Eon-Duval *et al.*, 2003a). In all these studies the concentration of RNA at the various sample points was determined using the Quant-IT RNA assay, the background of which is explained in (2.5.16 and 4.8)

Figure 7-13 details the results of the investigations into the clearance of RNA from the process. From the figures the starting RNA mass was deemed to be ~1384mg, which equates to ~3.3% (w/w). Both (Bailey and Ollis, 1986) and Table 7-2 estimate the actual figure to be 6%(w/w). The difference is perceived to be down to preparatory and analytical differences centred on the action of endogenous RNases. If the action of these is not blocked then they can quickly degrade the RNA present. A blocking agent was employed when the samples were sonicated, but how effective it was remains questionable, since the result produced is ~50% that reported in the literature.

As a result of the difference between the published value for RNA mass and the figure reported in these studies, background RNA removal over the lysis and neutralisation step differs. If the value of 6%(w/w) is assumed then RNA removal over lysis is ~55%,

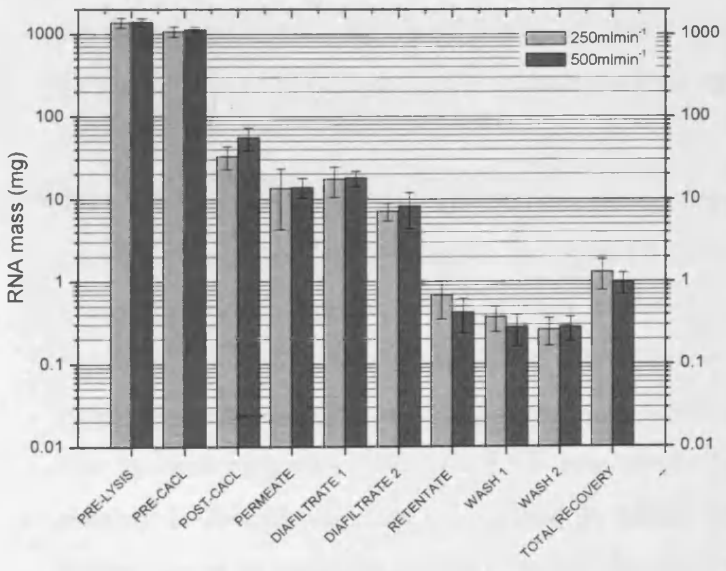

250ml/min	MASS (MG)	%
PRE-LYSIS	1373.983	100.000
PRE-CACL	1071.026	77.950
POST-CACL	32.887	2.394
PERMEATE	13.640	0.993
DIAFILTRATE 1	17.464	1.271
DIAFILTRATE 2	7.136	0.519
RETENTATE	0.683	0.050
WASH 1	0.371	0.027
WASH 2	0.263	0.019
TOTAL RECOVERY	1.315	0.096
CLEARANCE	1372.668	99.904

500ml/min	MASS (MG)	%
PRE-LYSIS	1395.661	100.000
PRE-CACL	1129.634	80.939
POST-CACL	55.635	3.986
PERMEATE	14.056	1.007
DIAFILTRATE 1	17.918	1.284
DIAFILTRATE 2	8.203	0.588
RETENTATE	0.426	0.031
WASH 1	0.280	0.020
WASH 2	0.282	0.020
TOTAL RECOVERY	0.988	0.071
CLEARANCE	1394.673	99.929

Figure 7-13 Figures outlining the removal of RNA during these investigations. The results represent the averages of the 10 individual runs for each crossflow rate (Table 7-5). The results for the individual runs are shown in the mass balances and each point in those was determined by quadruplicate analysis of samples by Quant-IT RNA. The pre-lysis values were obtained by sonication of a 1.56gL^{-1} sonication of the relevant cell paste and subsequent analysis of the lysate. The starting masses were then calculated by knowing the WCW of each of the individual DSP runs.

whereas if the reported figure of 3.3%(w/w) is taken then removal is ~23%. Background RNA removal over this step would be expected through both the precipitation of larger RNA species combined with the action of endogenous RNases, however, it is felt that the level of removal would fall in between the range of 23%-55%.

The mass value of the RNA following the lysis stage is not in doubt and at 1.0-1.1g still represents a large mass of contaminant. Compared to the level of gDNA, which was determined to be in excess of pDNA at this stage, the mass of RNA is ~34-fold higher, making it by far the most abundant nucleic acid. The large step removal produced by the addition of $CaCl_2$ can be seen in that the mass of RNA falls from an average of 1100mg to 44.2mg representing a 96% step clearance. This figure is very much in line with those reported by (Eon-Duval *et al.*, 2003a) using the same reaction conditions. It is accepted that RNA precipitation cannot lead to 100% clearance and that the action of $CaCl_2$ is more effective at precipitating larger MWt RNA molecules than the smaller species (Semancik and Szychowski, 1983). As such, a further step is required to ensure full removal of RNA. In this process that step is ultrafiltration.

With the high MWt RNA molecules removed by precipitation the UF step removes the smaller Mwt RNA molecules in the same fashion as small gDNA fragments. Their smaller size allows them to penetrate the UF membrane and be cleared from the process. From the clearance breakdown shown in Figure 7-13 the vast majority of the remaining RNA is cleared in the permeate and DF1 streams, with a smaller proportion cleared by the DF2 buffer.

The final recoveries of the RNA contaminant from the system estimate that for both crossflow velocities >99.9% RNA is removed from the process, most of which can be accounted for. As reported with gDNA, recoveries of RNA were found to be slightly reduced at the higher crossflow rate, an effect reasoned to be due to the same reason of the narrower boundary layer resulting from the higher fluid velocity. What is also noticeable is that in both instances ~1mg of RNA was co-purified along with the plasmid product, roughly 10-fold the amount co-purified as gDNA (Figure 7-11). This high figure is not deemed to be as problematic as for the gDNA since there exists sufficient size and charge differences between RNA and the plasmid product that more effective clearance of this contaminant can be expected over the chromatographic steps.

7.8.3 Protein

The final contaminant important to demonstrate clearance of was dissolved protein. On a mass basis this species represents the most abundant contaminant, but it is fair to say it is the least problematic one to reduce. The reason for this being that there exists many more differences between proteins and nucleic acids, than between different types of nucleic acids, which a purification strategy can exploit for the removal of this contaminant.

Figure 7-14 describes the average clearances of protein at the two crossflow velocities employed. The data suggests that the starting mass of dissolved protein to be ~3000mg representing 7.2% (w/w). Again this figure represents 50% of the value described by (Bailey and Ollis, 1986) and Table 7-2 which both place the starting mass of protein at 15%(w/w). The reason again for this anomaly is deduced to be due to preparatory and analytical differences. It is believed that the figure in this report accurately represents the total soluble protein but it is believed that the other 50% of the protein may have been membrane-bound protein. It is believed that these were not recorded by the sonication

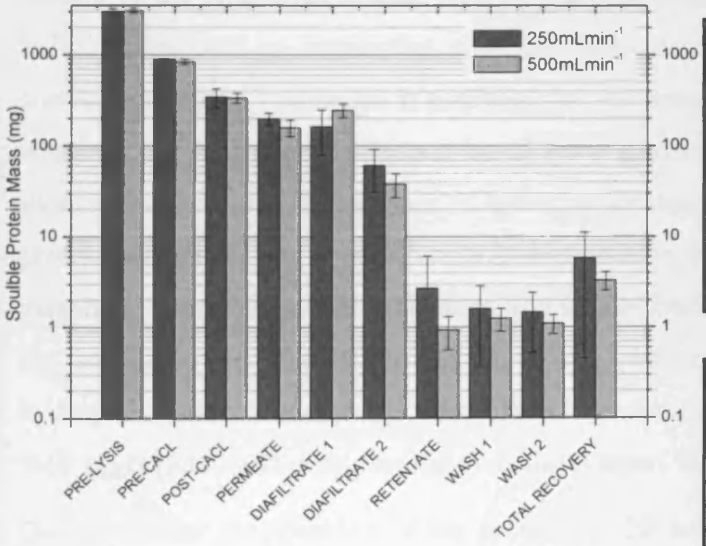

250mlmin	MASS (MG)	%
PRE-LYSIS	3015.687	100.000
PRE-CACL	894.716	29.669
POST-CACL	343.325	11.385
PERMEATE	198.658	6.587
DIAFILTRATE 1	163.237	5.413
DIAFILTRATE 2	60.932	2.021
RETENTATE	2.708	0.090
WASH 1	1.609	0.053
WASH 2	1.475	0.049
TOTAL RECOVERY	5.792	0.192
CLEARANCE	3009.895	99.808

500mlmin	MASS (MG)	%
PRE-LYSIS	3058.983	100.000
PRE-CACL	837.047	27.364
POST-CACL	336.557	11.002
PERMEATE	158.573	5.184
DIAFILTRATE 1	246.267	8.051
DIAFILTRATE 2	38.100	1.246
RETENTATE	0.931	0.030
WASH 1	1.252	0.041
WASH 2	1.105	0.036
TOTAL RECOVERY	3.288	0.107
CLEARANCE	3055.695	99.893

Figure 7-14 Figures outlining the removal of dissolved protein during these DSP investigations. The results represent the averages of the 10 individual runs for each crossflow rate (Table 7-5). The results for the individual runs are shown in the mass balances and each point in those was determined by multiple analysis of samples using the BCA assay. The pre-lysis values were obtained by sonication of a 1.56gL^{-1} sonication of the relevant cell paste and subsequent analysis of the lysate. The starting masses were then calculated by knowing the WCW of each of the individual DSP runs. Post-$CaCl_2$ samples were desalted prior to analysis.

method employed in these investigations, since after sonication and prior to analysis, the lysate was clarified by centrifugation to remove cellular debris. The cellular debris must have contained the other 50% of the total protein mass.

Due to the differences in the starting mass of protein, the value placed upon protein removal over the lysis step can be taken as either of two values. If total protein is recorded then the lysis and neutralisation step removed ~86% of the total protein. If the soluble protein is recorded then the value is ~72% removal. Despite the differences it can be appreciated that the lysis step is effective at bulk removal of this contaminant.

Total dissolved protein at the pre-$CaCl_2$ stage was determined to be ~865mg and the data suggests that a considerable amount of protein removal occurs over the $CaCl_2$ precipitation step, for which the step was not strictly designed. Approximately 60% of the protein remaining in the neutralised lysate is precipitated by the addition of $CaCl_2$. The mechanism behind this is believed to be identical to that employed by ammonium sulphate precipitation of proteins. In brief, protein folding is a thermodynamic driven process which results in the hydrophobic amino acids regions of proteins being contained within the interior of the protein molecule, with the charged, hydrophilic amino acids exposed to the bulk solution and so interacting with the molecules of solvation. This interaction with surrounding water molecules is essential for the protein molecule to be stable. However, when the $CaCl_2$ is added, a proportion of water molecules are attracted by the Ca^{2+} and Cl^- ions, which decrease the number of water molecules interacting with the charged part of protein molecules. As a result of this competition between the salt ions and the other dissolved solutes for water molecules, the solute-solute interactions become stronger than the solvent-solute interaction. As such, the protein molecules coagulate by forming hydrophobic interactions with each other in order to stabilise themselves. This leads to their aggregation and precipitation (Wu and Karger, 1996; Doran, 1995)

Despite further precipitation of the protein by the addition of $CaCl_2$, ~340mg of protein was found remaining in the clarified lysate prior to the ultrafiltration step. The very small size of proteins means that they were able to pass through the membrane quite easily. The breakdown shows that the majority of protein was removed during the permeation and diafiltration stages.

Despite quite effective clearances, on a mass basis, protein represents the most abundant contaminant co-recovered along with the plasmid product. At the faster crossflow ~3.3mg

was remaining compared to ~5.8mg for the slower crossflow velocity♦. Again, on average, higher co-recovery was reported with the slower crossflow velocity rates. Also, despite the higher mass recoveries of this contaminant the clearance levels of >99.8% were deemed acceptable in the knowledge that further clearances of this contaminant would be achieved by following chromatographic procedures.

7.8.4 Conclusions

To conclude this section requires summarising the clearances of the major contaminants achieved by this process. This is shown in Table 7-12. From the table it can be appreciated that the process is effective at clearing the three contaminants. If the starting masses of each contaminant are assumed to be those listed in (Bailey and Ollis, 1986) then the process achieves >99.9% clearance of every contaminant at both crossflow rates.

It has been noted from these studies that % clearances were found to be higher for the faster crossflow velocity. This may be an important factor to bear in mind when adapting such a process for the manufacture of large plasmids. This is because lower crossflow rates were found to be beneficial to plasmid form recovered from the membrane, with higher %SCC recovered at the slower crossflow rates.

If the decision was made to operate at a slower velocity for the sake of improved topology then the increased contamination may become an issue. It could be possible to conduct the UF operation stages (permeation/ diafiltration) at the faster crossflow velocity and the recovery phases at the lower speed. This would mean that higher contaminant clearances would be achieved with no negative outcomes on plasmid topology, since it is believed that SCC pDNA is protected when TMP is applied by the plasmid gel-layer.

♦ It should be mentioned that detection of both RNA and protein in the Retentate and wash fractions was almost out of the linear range of both assays, since the concentrations were so low. However, as mentioned in the analytical section it was found more accurate to fit a polynomial curve to the standard curves, doing so also extended the range of the assays to these lower levels. Calibration on a standard linear fit resulted in negative values. In a way this validates the process for the clearance of these contaminants in that they were at such low concentrations that the assays employed were at their very limit of detection.

Table 7-12 Table detailing the average co-recovered masses of the major contaminants for the two different crossflow rates. The table also describes the % clearances of these contaminants over the process. The non-italicised values represent the % clearances calculated using the starting masses of the different species determined by assays performed on sonicated cell samples. The italicised % clearances are calculated using the %(w/w) starting masses described by (Bailey and Ollis, 1986) on 42g of cells.

	Mass co-recovered (mg) 500mLmin^{-1}	% Clearance	Mass co-recovered (mg) 250mLmin^{-1}	% Clearance
Genomic DNA [1% (w/w)]	0.0964	99.981 *[99.977]*	0.243	99.966 *[99.942]*
RNA [6% (w/w)]	0.988	99.929 *[99.961]*	1.315	99.904 *[99.948]*
Protein [15% (w/w)]	3.288	99.893 *[99.948]*	5.792	99.808 *[99.908]*

It was determined that severe damage to the SCC plasmid form was found to occur during the recovery operations especially at the higher crossflow rate. If the crossflow rate was reduced for the recovery stage the result would combine the better clearances with improved plasmid topology. However, the logistics of such an operation remains unknown since a variable speed pump would be required.

Clearance of protein and RNA by this process was deemed acceptable. The concentration of these contaminants in the membrane recovery fractions was lower enough such that they were at the very limit of assay detection. Additionally, it was reasoned that further clearance of these species would be achieved over the chromatographic steps which follow the membrane. The most important issue determined by these investigations into contaminant clearance was the impact of residual gDNA contamination.

The mass of 0.0964mg gDNA co-recovered from the membrane was used to set the limit of operation of this process. It was reasoned that unlike protein and RNA, assuming further clearance of this molecule over the chromatography steps could not be guaranteed. Using the acceptance criteria of 0.01μg gDNA/ μg pDNA it was determined that for the process to be effective an initial starting mass of pDNA of 12.05mg was required. Back-calculation set the required mass of extrachromosomal DNA per cell to be 1.75×10^6bp. If the total amount of pDNA per cell falls shy of this limit then the process will not be capable of producing an acceptably pure product.

7.9 Binding studies

7.9.1 Introduction

During regular operation of this pilot-scale process the retentate and wash fractions, collected from the UF membrane, are pooled and further purified by an anion-exchange chromatography step (Figure 7-1). However, due to the low mass yields (and hence low concentrations) of plasmid recovered from the membrane using these large constructs, it was deemed that there was insufficient material to load on to the column and as such little could be determined by carrying out investigations with this aim in mind. Additionally, much of the larger plasmid mass recovered from the membrane existed in sheared form, meaning limited data could be extracted about the binding behaviour of intact large plasmid molecules. It was reasoned that more useful information would be provided by the determination of whether the large size of these plasmids would pose any problems to the actual level of binding and associated kinetics when using the anion-exchange resins employed in the process. As such, it was decided to investigate the binding behaviour of these large constructs through batch adsorption studies.

7.9.2 Chromatographic matrices for plasmid purification

The separation and purification of pDNA by chromatography is associated with two significant limitations (Diogo *et al.*, 2005)

1. Physical and chemical similarities between impurities and pDNA. The most problematic contaminant being gDNA but RNA and protein can also be troublesome. The result of the contamination can be poor selectivity due to competition and the co-elution of impurities. Reduction of the impurities prior to chromatography is one strategy to overcome this limitation and has already been covered in the earlier sections of this chapter.
2. The large size of pDNA molecules combined with the small pore sizes of chromatographic matrices. This limitation causes a number of problems when separating plasmids by chromatography;
    i. Low diffusion coefficients and poor internal mass transfer
    ii. Broad peaks and low recovery
    iii. Small flow-rates and long separation times

iv. Poor capacity for pDNA due to lack of accessibility.

Importantly, the diffusion coefficients of pDNA in solution are significantly lower than those of proteins. This is a result of the greater mass of plasmids and also their size and structure. Most proteins are small (2-10nm) and globular whilst plasmids are micron size (0.2-1μm) with a structure intermediate between a flexible coil and a rigid interwound superhelix. A typical diffusion coefficient for a plasmid is $10^{-8}cm^2s^{-1}$, whilst proteins can be expected to display a coefficient over 10-fold greater.

The larger size and reduced diffusion coefficients are associated with poor internal mass transfer leading to long binding times and therefore long-separation times, poor flow rates and low binding capacities. These drawbacks are reported for plasmids of the size range 3kb-10kb. The point of these investigations was to determine whether these issues worsen when the plasmids being purified are larger still.

7.9.3 Experimental setup

Much of the design and setup of these experiments was a direct repeat of published studies, which investigated the batch binding behaviour of smaller plasmids on to anion exchange resins (Ferreira *et al.*, 2000a). The main difference exploited the advantages offered by the NanoDrop spectrophotometer. As outlined in (2.5.9.2) this device enables direct absorbance measurement on plasmid solutions using only 2μL of solution. More detail into the methodology of the studies can be found in (2.8.7).

Briefly, the studies employed the matrix from 20μL volumes of two common anion-exchange resins; DEAE-Fractogel and TMAE-Fractogel to which were added 1mL volumes of $50\mu gmL^{-1}$ solutions of the different constructs (Qiagen Large Construct kit purified 2.5.8.3). These were combined in sterilised eppendorf tubes and agitated on an inversion mixer. At periodic intervals, 2μL samples of the solution were extracted and the level of unbound plasmid measured by direct A_{260} absorbance using the NanoDrop spectrophotometer. Each binding study for each plasmid on each resin was performed in triplicate. The concentration of the free, unbound plasmid was recorded over a 90 minute period. For examples of the NanoDrop recordings refer to Figure 9-49 and Figure 9-50. At the end of this period the tubes were left to agitate at room temperature

for a total of 24 hours, after which a final absorbance measurement was taken. It is reported that the level of binding would have reached equilibrium by this point, such that the value represents the maximum-binding capacity of the resin (Ferreira *et al.*, 2000a).

In order to perform studies into the binding behaviour of the large plasmids on to anion-exchange resins certain information was required about the resins themselves. Specifically, when reporting the binding capacity of the resins it is standard to report the level on a specific, mass-basis so as to eliminate differences in the relative density differences between different resins. To do so required determination of the mass-volume coefficients of the resins being studied. This was achieved by evaporation of the suspending fluid as described in 2.8.6. The values from this analysis are recorded in Table 7-13.

7.9.4 Binding kinetics of plasmids on to two commercially available AEX resins

Figure 7-15 plots the adsorption isotherms from the studies into the binding kinetics of the different constructs on to TMAE Fractogel and DEAE Fractogel. There are several points to be extracted from these two figures. Primarily, it can be appreciated that plasmid binding rates are very much dependent on plasmid size. This is to be expected since binding is a diffusion driven process requiring the transport of plasmid molecules from the bulk-solution to binding sites on the matrix particles[♦]. Rates of diffusion can be described by Fick's Law which uses a value for diffusivity coefficient to determine diffusion rates. As shown by Equation 7-1 a particle's diffusivity coefficient is directly related to its size.

$$D = \frac{kT}{f} \quad \because f = 6\pi\eta r \qquad D = \frac{kT}{6\pi\eta r}$$

Equation 7-1 Relationship describing the link between a particle's diffusivity and its size. Einstein proposed that diffusivity (D) is governed by a particle's kinetic energy (k-Boltzman constant and T-temperature) and the frictional coefficient of the solute molecule (f). The frictional coefficient is a direct result of the solution viscosity (η) and particle radius (r).

♦ Plasmids are known only to bind to shallow depths within the chromatographic matrices. Intra-particle binding is severely reduced because the plasmid molecules are too large to penetrate deeply in to the pores in the Fractogel matrix particles (Ljunglof *et al.*, 1999).

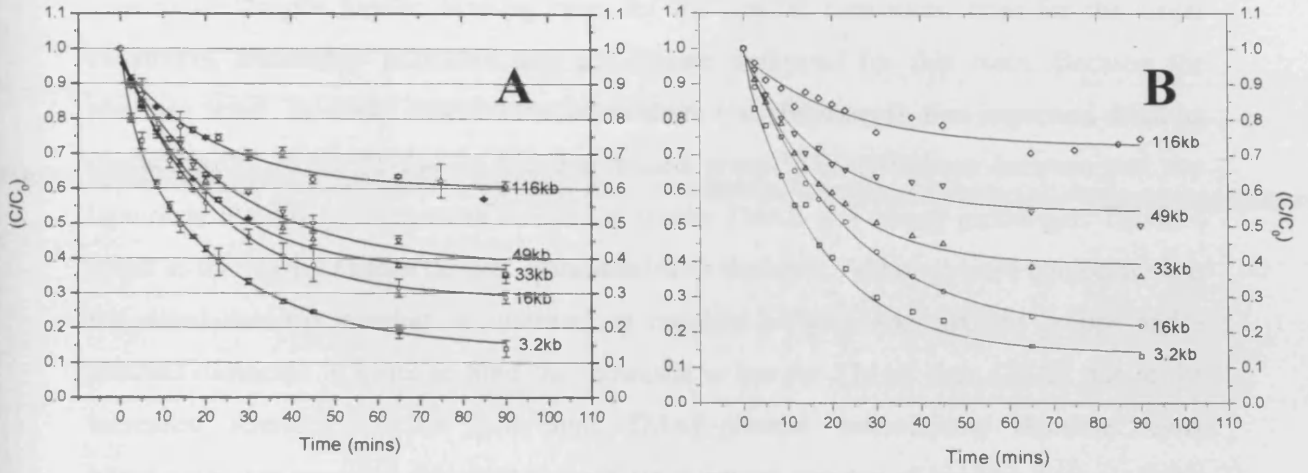

Figure 7-15 The results of the NanoDrop binding studies were converted into mass values describing the levels of plasmid remaining unbound in solution. These values were then described as a proportion of the amount of mass (50μg) originally present in the solution under study. Plotted in A are the results for TMAE Fractogel and in B are the results for DEAE Fractogel. Each of the points represent the average of triplicate runs.

Additional to the lower rates of diffusion it is postulated that steric hindrances between larger plasmid molecules may extend the time required for binding. From the figures it can be seen that by the end of the recorded period an in both examples ~85% of the small plasmid pGEM11 had been removed from bulk solution by binding to the matrix particles. In contrast binding levels of the larger pGEM49kb and p5175 <50% of the free plasmid had bound by the end of the same period.

The pattern of the isotherms are also interesting since they suggest that plasmid adsorption on to these anion-exchangers can be modelled by Langmuir-type isotherms (Ferreira *et al.*, 2000a).

$$\theta = \frac{\alpha C^*}{1+(\alpha C^*)} \qquad K = \frac{\theta}{(1-\theta)C^*}$$

Equation 7-2 Expressions used to describe the Langmuir isotherm. Θ is the equilibrium concentration or coverage of the adsorbent by the adsorbed particle. C* is the equilibrium concentration of the solute in the fluid phase and α is a constant. K describes the equilibrium constant determined by ratio of bound to unbound substrate.

It is appreciated that assuming a Langmuir adsorption makes several assumptions about the system including that there are no interactions between bound molecules and that each site for adsorption is equivalent.

A final point concerns the relative performance of the two different resins. The data suggests that TMAE Fractogel produced superior binding rates especially for larger

constructs. Despite similar binding rates for the smaller constructs, rates for the larger constructs, noticeably pGEM49 and p5176, are improved for this resin. Because the particles used in both cases were equivalent (i.e. Fractogel) the improved binding characteristics must be due to the derivatized group. The difference between the two ligands is that DEAE is a weak exchanger whilst TMAE is a strong exchanger. This is a result of the higher charge density associated with the latter. Although pure conjecture it is suggested that the number of interactions required between the charged groups and a plasmid molecule in order to bind the molecule is less for TMAE than DEAE due to the increased strength of the individual TMAE-plasmid interactions. Because fewer interactions are required means that there are a greater number of binding sites available per unit mass of TMAE resin. For smaller constructs this lower number of binding sites is not immediately noticeable since fewer interactions are required. However, for the larger molecules more interactions will be required and as such the rate of binding will be effected by the number of sites available. More binding sites are required for larger molecules by virtue of their larger size and the fact that steric hindrances may appear between competing plasmid molecules.

7.9.5 Specific Binding Capacities

The results of the binding capacities highlight other potential issues with the attachment of these plasmids to the available resins. The results are reported in Table 7-13 and Figure 7-16. As outlined before these resins are not specifically designed for plasmids and this fact is reflected in the binding capacities of the plasmids compared to proteins. Even for the smallest construct; [pGEM11] the maximum binding capacity is ~2.3mgmL^{-1}. This capacity is 40-fold lower than that reported for proteins. This effect has been described by several authors and the reason determined to be due to plasmids only binding to the outer surface of the matrix particles (Ljunglof *et al.*, 1999; Lyddiatt and O'Sullivan, 1998). The large size of plasmids prevents them from accessing the full complement of potential binding sites which lie inside the pores of the particles.

Table 7-9 displays the results of attempts to place figures on plasmid diameters of the constructs under study. The most reliable estimate was determined to be provided by field-flow fractionation which sized the diameter of

Table 7-13 Table highlighting the differences between the two anion exchange resins studied in these investigations. Shown are the mass-volume coefficients determined by evaporation of the suspending fluid. The maximum specific binding capacities were obtained by calculating the level of plasmid bound to the matrix following 24 hours of incubation. They are reported on both a volumetric and specific basis. The % difference described the relative improvement offered by TMAE Fractogel.

	DEAE-Fractogel	TMAE-Fractogel	% Difference
Particle diameter (µm)	40-90	40-90	0
Average pore Ø (nm)	800	800	
Mass-Volume coefficient (g dry matrix/ mL)	0.133 ± 0.0036	0.125 ± 0.0053	- 6%
Max. Binding capacity (mg protein/ mL resin)	100		
	Maximum. Binding capacity (mg pDNA mL^{-1}resin)		
3.2kb	2.27 ± 0.028 *(100%)*	2.34 ± 0.007 *(100%)*	+ 3.1
16kb	2.35 ± 0.011 *(104%)*	2.24 ± 0.007 *(96%)*	- 4.7
33kb	2.05 ± 0.014 *(90%)*	2.23 ± 0.035 *(95%)*	+ 8.8
49kb	1.74 ± 0.074 *(77%)*	2.07 ± 0.028 *(88%)*	+ 19.0
116kb	1.56 ± 0.046 *(69%)*	1.96 ± 0.039 *(84%)*	+ 25.6
	Specific Maximum. Binding (mg pDNA/ g dry matrix)		
3.2kb	17.03 ± 0.21	18.72 ± 0.056	+ 9.9
16kb	17.69 ± 0.08	17.88 ± 0.042	+ 1.1
33kb	15.38 ± 0.106	17.84 ± 0.28	+ 16.0
49kb	13.10 ± 0.56	16.52 ± 0.23	+ 26.1
116kb	11.75 ± 0.35	15.70 ± 0.31	+ 33.6

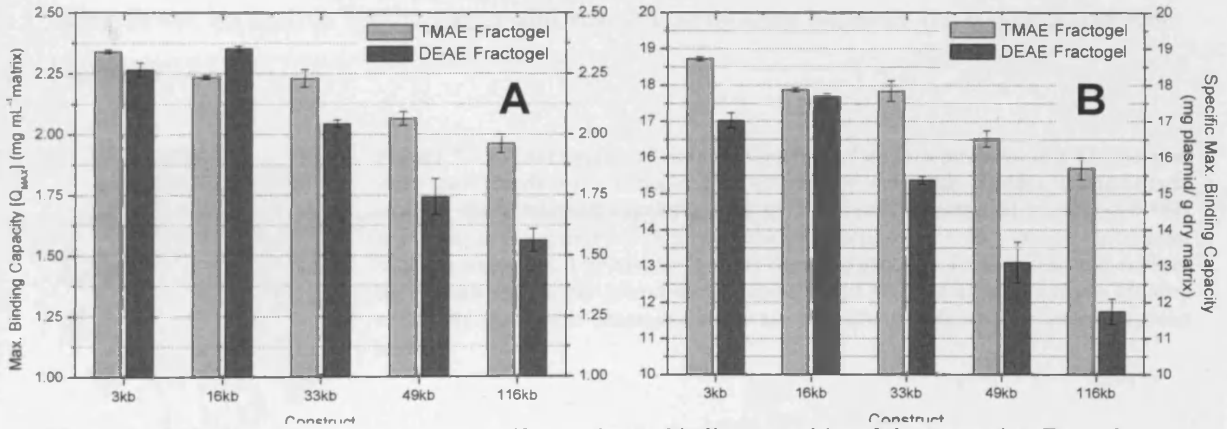

Figure 7-16 Plots of the maximum and specific maximum binding capacities of the two resins. From the graphs it can be seen that for both measures the binding capacity decreases with plasmid size an interesting occurrence was that the maximum specific binding capacities for the 3kb and 16kb plasmids were quite equivalent and that the decrease in capacity only became apparent for the larger constructs. This suggests that with plasmid sizes over 16kb the drop in binding capacities is due to steric hindrance. Again TMAE displayed superior binding performance

a 3.2kb plasmid at ~77nm.and the largest plasmid (116kb) at ~1100nm. The figure of 77nm is much larger than the average protein size of 2-10nm but is still smaller than the 800nm pore size of the matrix particles of the resins under study. The results of this analysis suggests that a plasmid of 3.2kb would be capable of penetrating the 800nm pores on the Fractogel particle. It is believed that some intra-particle penetration does occur and that the limited intra-particle diffusion accounts for the decrease in the specific maximum binding capacity with increasing plasmid size.

Referring to Figure 7-16 and Table 7-13 there are two main observations to explain. Firstly that maximum binding capacity does decrease with plasmid size, for example in the case of DEAE a 30% decrease is witnessed between 3.2kb and 116kb binding capacities. The decrease is not linear with plasmid size. Secondly the binding capacities of TMAE resin is greater than that for DEAE for all plasmid sizes.

In order to explain these results requires consideration of what is occurring on the micron-scale. Again this is pure conjecture, but it is reasoned that a 3kb plasmid molecule is capable of penetrating the pores on the particle surface but that the intra-particle diffusion is limited to a very shallow penetration due to the plasmid size. This limitation increases with plasmid size such that less and less penetration is possible with the result in their being fewer accessible binding sites and hence less binding capacity for larger constructs. Figure 7-17

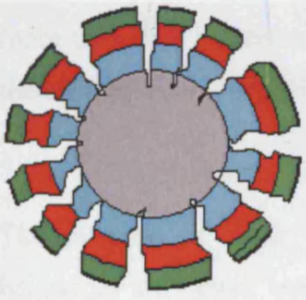

Figure 7-17 A schematic of the cross-section of a resin particle. It is known that intra-particle delivery is dependent on particle size. This schematic attempts to explain the witnessed results and is by no means to scale. It is reasoned that proteins are capable of full penetration (blue-layer) and hence maximum binding capacity. The smaller plasmids can penetrate further into the surface layer than the larger plasmids (red-layer) and so have access to more binding sites than the larger plasmids which are capable of only surface binding (green layer).

The explanation for the improved binding capacity demonstrated by TMAE resin has quite a simple explanation. TMAE, by virtue of its higher charge density, is considered a strong exchanger. Since the results for maximum binding capacity were obtained after 24 hrs incubation it is safe to assume that equilibrium had been reached.

$$k = \frac{[B-P]}{[B][P]} \qquad [B] = Binding\ sites \quad [P] = Plasmid$$

Due to the stronger interaction between plasmid and binding site which would occur in TMAE resins the rate of dissociation would be lower and so the equilibrium concentration of bound [B-P] plasmid would be greater than for DEAE. Additionally, as described previously the stronger interactions provided by TMAE groups mean that more sites are available since fewer sites will be required per plasmid. An interesting point is raised by Table 7-13 which demonstrates that the percentage improvement offered by TMAE increases with plasmid size. The reason for this is a more rapid decrease in binding capacity with plasmid size offered by DEAE resin. Overall this suggests that the rate of dissociation found in DEAE resins increases more rapidly with increasing plasmid size. Therefore as plasmid size increases it becomes more likely for a plasmid to dissociate from DEAE resins. Perhaps the weaker exchange characteristics limit the ability of this resin to bind increasingly large plasmids as strongly such that they are more likely to dissociate.

It is appreciated that the extent of the analysis into the results of the maximum binding capacities is likely to be an over-simplification of what is occurring. No explanation can be offered for why the results suggest the binding capacities for the 16kb and 3kb should be equivalent. It could be anomalous but the studies were conducted in triplicate and the effect is witnessed for both resins. It is likely that the binding capacities are dictated by more than size limitations. Possibly steric hindrances could be playing a part in reducing the binding capacities witnessed for larger constructs.

7.9.6 Conclusions

The purpose of these investigations was to identify any limitations in the binding behaviour of larger constructs on anion-exchange resins commonly used for plasmid purification. The data can now be used to predict any problems which could be expected should plasmids of this size order be subject to anion-exchange chromatography on a larger scale. Overall, the results have suggested that limitations currently witnessed with chromatographic separation of plasmids are exacerbated by the increased size of the constructs. The adsorption isotherms suggest that binding rates decrease with increasing plasmid size due in part to the reduced diffusivity of the plasmid molecules and the associated reduction in the number of accessible binding sites. The reduction in the

number of available binding sites also reduces the maximum binding capacities. Although TMAE Fractogel offered an improvement, the difference was not great. The results of these limitations will be as described earlier in that broad peaks and low recoveries could be expected. Additionally, the chromatography step would require slower flowrates resulting in longer separation times.

The limitations posed by the increasing size may never be completely eliminated but improvements could be achieved. The sizes of the plasmid DNA could be reduced prior to loading with compaction agents (e.g.spermine) but that may be unfavourable since it represents an addition of an added impurity. The bead size of the matrix particles could be reduced to improve mass transfer, but this strategy would introduce new challenges caused by the expected increased pressure drops over the column. Certainly worth investigating would be "superporous" stationary phases designed with plasmid purification in mind. These are reported to improve intra-particle mass transfer with the introduction of much more rapid convective pore flow to take place. Reports suggest these matrices allow the attainment of binding capacities in the range of $10 mgmL^{-1}$ (Diogo *et al.*, 2005).

One strategy thought very worthy of investigating for such large constructs would be the use of membrane chromatography (7.2.2.5). In these systems (e.g.Pall Mustang Q columns) diffusional limitations are overcome by having through-pores rather than dead-end pores associated with particle based stationary phases. The pores could be engineered to accommodate larger constructs and the more rapid adsorption would allow for faster mobile phase flow rates.

7.10 Conclusions

The conclusion to this section requires summarising the key observations and whether the questions posed at the section beginning have been satisfactorily answered.

7.10.1 Plasmid Purification

The key point from the analysis of large plasmid purification by this process was that % recoveries of plasmid (% of plasmid in clarified lysate recovered from the UF membrane) decreased with increasing plasmid size (Figure 7-3A). The smaller 3.2kb plasmid was found to be capable of penetrating the membrane but the 16kb plasmid recorded ~80% recovery levels. The loss of the other plasmids was determined by careful analysis of the gels tracking the change in plasmid topology levels (Figure 9-6 to Figure 9-11). It was

noted that the level of supercoiling increased for all the plasmids, including the 3.2kb (Figure 9-6), over the course of the ultrafiltration step. Such an unlikely occurrence was not envisioned since supercoiling is an energy intensive process. The only explanation which could be offered was that the % supercoiling increased due to selective reduction in the proportion of the open-circular and linear fractions. The gels suggested that increased degradation of supercoiling occurred with increasing plasmid size over the course of the lysis operation (Figure 7-4). As such plasmid recovery became a function of the amount of plasmid loaded on to the membrane in supercoiled form. The more plasmid loaded in SCC form, the higher the recovery. Since the %SCC at the end of the lysis period was found to be directly related to the size of the plasmid there was a comparable decrease in plasmid recoveries from the membrane.

Experiments were conducted which compared the effect of the cross-flow rates on recovery levels. It was found that the crossflow rate had no real effect on recovery levels (Figure 7-3A). Essentially at both rates the shear forces were of sufficient magnitude to exact the degradation of OC/Linear form to sheared fragments, which when a TMP was applied, were capable of penetrating the membrane. The effect of the cross flow rate only manifested itself during the recovery steps of the operation. At the outset of this stage it was envisioned that the overriding plasmid form was SCC, due to the selective degradation of OC/ linear forms. However, with the removal of the TMP and the purposeful disruption of the plasmid gel layer, the SCC form was damaged by the shear forces. It was found that the plasmid degradation was not specific and that the plasmid was sheared randomly into fragments ~15kb in size. Had a TMP in place these fragments would have penetrated the membrane but due to the system being closed they were recovered. It is believed that this sequence of events accurately explains the recovery levels.

Overall, the results of this section suggests that ultrafiltration of plasmid containing lysates remains a reasonably viable technique for the purification of constructs up to 50kb and plausibly larger. However, two caveats must be acknowledged. Firstly, that the recovery levels are directly effected by the form of the plasmid loaded on to the membrane. Secondly, the recovery of the plasmid from the membrane following processing promises to be difficult since this step was found to cause shear damage. Evidence was provided that shearing was reduced by operating the recovery steps at a low cross-flow but that a degree of shearing was still in effect.

7.10.2 Analysis of the Lysis step

Having demonstrated that the % recovery of plasmid from the UF membrane was a function of its supercoiling it was decided to investigate the lysis step utilised in this protocol. It had been shown that the rate of loss of supercoiling during this step was linearly relate to the plasmid's size (Figure 7-5). What remained to be determined was whether this was the result of the action of a physical or chemical process.

Reasonable estimates were placed upon the size of the plasmid molecules from the results of field-flow fractionation (Table 7-9). Analysis of the macromixing conditions in the vessel suggested that the loss of supercoiling was not due to physical shear, since the size of the eddies produced were determined to be too large to impact upon a particle of the size of the plasmids being studied. Additionally evidence from the gels suggested that the conversion of SCC form to OC/Linear form was unlikely to be the result of random physical shear. Further analysis of the mixing conditions produced in the lysis vessel, suggested that both the macro and micromixing conditions were poor. This was a direct result of the low shear rate utilised. In the belief that the low shear environment would minimise damage to the plasmid and precipitated gDNA, the low shear rates actually led to an extension of the period required for both bulk mixing and mass transfer. It was suggested that the effect of the extended lysis period may have escaped notice when processing plasmids of the size order 3-10kb. However, with increasing plasmid size there is a linear increase in the number of sites for action and as such a linear decrease in plasmid supercoiling displayed by the end of the lysis period.

In effect this lysis procedure requires optimisation. Even when considering smaller plasmids where 70-80% SCC is displayed following lysis, it is believed that judicious optimisation could lead to increase in %SCC displayed by the end of the lysis period, and hence better recoveries from the UF rig. It is suggested that the agitation rate be increased to improve both bulk mixing and mass transfer. This will decrease the amount of time required for lysis, improve mass transfer and so reduce the occurrence of regions of heterogeneity in the vessel. For the processing of these larger constructs it may not be enough to increase agitation rate. As such, it is felt that the adoption of a continuous lysis protocol could be highly beneficial to recoveries and topologies.

7.10.3 Contaminant Profiles

Mainly performed to complement the results for the plasmid recoveries, it was possible to describe in some detail the removal of key contaminants exacted by this process. Of key importance were the results describing the removal of genomic DNA from the process. Effective clearance was demonstrated (Figure 7-11) but the remaining trace amounts served as a reminder of optimising the specific yields of large plasmids from the fermentation. It was found that the process could remove >99.9% of the starting mass. Using the best case scenario it was found that ~100μg of gDNA could be expected to be co-purified by this process. Using the latest purity requirements this co-purification means that for the process to be validated (assuming an optimistic 80% recovery of plasmid from the system) the minimum specific yield that is capable of being handled by this process is ~280μg pDNA $gWCW^{-1}$. For plasmid specific yields lower than this the ratio of contaminating gDNA to pDNA at the end of the process will be too high as to be approvable. Such a figure for specific yield equates to $1.75x10^{6}$bp of extrachromosomal pDNA per cell. This means that a plasmid of size 116kb must be present at 15 copies per cell to be even close to being acceptable.

This analysis also suggests that the 33kb and 49kb series of plasmids created by cloning were present at too low a yield to process effectively. However, for these constructs the problems of instability led to reduced yields. As predicted by (Table 6-4) the predicted yields of these constructs (assuming 100%) are 600-800μg$gWCW^{-1}$ and should be able to be purified effectively. However, again this assumes 80% recovery which as was seen with larger constructs was not achieved due to extensive damage in the lysis step.

Further contaminant profiles were generate for RNA and protein. The description of the RNA removal was achieved through the use of a novel assay, which although not applicable for QA/QC purposes would be suggested for process optimisation studies. A final point was found concerning the relative clearances achieved at the different cross-flow velocities. It was found that more co-purification of all the contaminants occurred at the slower crossflow rate.

7.10.4 Chromatographic studies

Batch binding studies in to the adsorption of these larger constructs on to commercially available resins suggests that problems could be expected to arise during the chromatographic separation of these macromolecules. Binding rates and binding capacities

were found to be reduced with increasing plasmid size. It is suggested that should attempts be made to produce constructs of this size order on a commercial scale that investigations should be made in to the application of membrane chromatography systems or at least "superporous" stationary phases. The necessity for such studies is even more justified when the results from the poor binding are considered in light of the possibility that large plasmids may face problems in penetrating packed-bed columns of such resins (6.5.3).

8 CONCLUSIONS AND FUTURE WORK

8.1 Introduction

To conclude this thesis first involves reiteration of the objective of the investigations which was; to identify any problems which may be encountered should attempts be made to produce large plasmids using currently adopted techniques. As such, the project had quite a broad remit since the current processes for the manufacture of these macromolecules involves numerous steps. Rather than concentrate on specific operations the aim was to observe, through experimentation, where the potential bottlenecks were likely to be encountered. This required taking a holistic view of the process, since each section of the process impacts on the next. However, in concluding it is felt more digestible to divide the process up into sections and describe the main observations.

8.1.1 Construct design

The start of any plasmid production process begins with the design of the construct to be produced. In a commercial setting the design of the construct will be mainly dictated by the condition to which the therapeutic plasmid is being targeted. However, since within the plasmid sequence are contained the instructions for its propagation and replication, its design becomes of fundamental importance to the parties involved in its manufacture. This fact cannot be overstated.

At the outset of this project, the constructs with which investigations were begun had not been designed with any form of manufacture in mind. The Oxford series of plasmids were Bacterial Artificial Chromosomes, designed for shuttling DNA between eukaryotic and prokaryotic cells, so as to investigate the functionality of proteins encoded on the huge sections of DNA it was capable of propagating. The desire for high plasmid yields was not a key driver in the design of these plasmids, since only small masses were required with which to perform such studies. Sufficient mass with which to conduct such functional studies could be obtained by lab-based procedures. What was deemed important when these constructs were being designed, was stable propagation of the plasmid, such that strains could be maintained and banked. Consequently, the plasmids were built around F-factor replicons. This naturally occurring plasmid replicon maintains a very low plasmid copy number by coupling the replication of the plasmid to the replication of the host

genome, as such only 1-2 copies persist within any given cell. Consequently, when initial yield investigations into fermentations of strains bearing this plasmid were performed it was found that little pDNA could be recovered (3.3). Also, downstream purification investigations were conducted but little useful information could gathered concerning issues faced with the purification of large plasmid, since the initial plasmid masses were too low (3.8).

This forms the first conclusion. If large plasmids are to be manufactured the use of low-copy number replicons should be avoided simply because insufficient plasmid mass is produced with which to enable purification. It was detailed in the downstream processing chapter that even had 100% of the large construct p5176 been purified the initial starting mass still would not be sufficient to produce a validatable contaminant profile (7.8.1). It is speculated that to produce such plasmids would require a fundamental overhaul in the currently adopted techniques for plasmid purification. Rather than the aim of the purification train being the bulk removal of contaminants from the plasmid, as is the current philosophy, the selective removal of the plasmid from the contaminants would need to be attempted. The feasibility of such a course of action remains debatable. Should there be a strong desire to make BACs (>100kb) then there is a potential strategy which may be worth investigating, which involves the propagation of inducible BACs. However, these only promise to increase the copy number to the 10-20 copies per cell level. Estimates show that even this may be insufficient. (5.3.1).

A final note on BACs must include the correction to a belief that due to the massive size of the average BAC (>100kb) compared to a regular plasmid (3-10kb) is that it needs to be maintained at 1-2 copies per cell in order to avoid over-burdening the host-cell machinery. With commercially designed vectors of 3-10kb being reliably propagated at 1000 copies per cell, the notion that 2 copies of a plasmid 100kb in size would cause an excessive burden is a misnomer (Figure 3-14).

In a change of course of this project, it was decided to attempt the creation of large plasmids under the control of relaxed, high-copy number replicons. It is concluded that this strategy is the only reasonable course of action were attempts be made at large plasmid manufacture. It was demonstrated (from extrapolation (Table 6-4)) that the yields which could be expected from the fermentations of such constructs could allow purification. However, a few considerations need to be taken in the choice of vector. It is recommended that the vector employed should use an alternative selection method than

that of ampicillin. It is reasoned that kanamycin may be a more judicious choice due to the mode of action of this agent. However, in a more commercial setting, where the use of antibiotics is discouraged, then design of the construct should employ a system such as repressor titration. What has to be concluded from the investigations conducted in the course of this project is that a form of selective pressure is definitely required since the probability of loss of larger constructs is increased (Table 5-10).

8.1.2 Upstream Processing

Following construct design the next step of a plasmid production process involves optimisation and characterisation of the fermentation step. Initial studies concluded that the propagation of the large BACs did not pose a significant burden to the growing cells (3.2). Indeed the results confirmed previous reports suggesting that any metabolic burden suffered by cells, and manifested by reduced growth rates and biomass yields, were more likely to be the result of proteins expressed by the construct rather than the construct itself. Furthermore, it is concluded that the small amount of extrachrmomosomal DNA being propagated by cells bearing BACs is unlikely to present a significant burden to any growing cell.

Another unfortunate consequence of the design of the Oxford series concerned the limitation that the stringent nature of their replication eliminated any prospect of increasing plasmid yields by manipulation of the environmental parameters influencing culture growth rate. Had this been a possibility then the feat of cloning large constructs could have been avoided by employing sophisticated cultivation techniques to amplify the BAC copy number.

Upstream investigations revealed the true extent by which manipulation of the fermentation growth conditions could positively influence specific yields. Having determined that the series of pGEM plasmid were plagued by instability issues, after 37°C pilot-scale fermentations failed to generate plasmids (6.3), it was decided to culture the plasmids at reduced temperatures (6.4). The more optimal control mechanism of the pGEM plasmids meant that their replication was relaxed. As such the copy number was not linked to host-genome replication but more connected to the growth rate of the cells bearing the constructs. Had it been realised, prior to conducting the pilot-scale fermentations, the extent to which the plasmid specific yield would increase toward the end of the fermentations (Figure 6-5), then fermentation time would have been extended

to exploit the full magnitude of this effect. As it were, it was only realised following the completion of the fermentations. It is concluded that the large increases seen in plasmid specific yields toward the end of the fermentation were feasibly larger than those described by other researchers. The reason being that the increase was being fuelled by not only the up-regulation of plasmid replication, but also by the increase in the relative proportions of plasmid-bearing cells, caused as a result of the reduction in the growth differential existing between plasmid-free and plasmid bearing cells. It was this observation that leads to the conclusion that should fermentations of high-copy number, large plasmids, be conducted that problems of instability should be expected, which will push down plasmid yields. However, unlike stringent plasmids, there are strategies which could be employed to counteract this issue so as to correct the problem and restore high yields. One has already been mentioned; the judicious choice of the selection system. However, the second concerns the choice of the mode of operation of the fermentation. It is suggested that exponential fed-batch control of culture growth at a levels $<0.2h^{-1}$ would be very effective in increasing the yields of large plasmids by exploiting the two outcomes previously mentioned.

Overall the extrachromosomal DNA yields which could be expected from a fermentation of a large, high-copy plasmid in which stability was maintained at 100%, are predicted to reach levels several multiples that of the genome of the host cell (Table 6-4). However, it must be concluded that this increase is in the large part driven by the proportionate increase in plasmid size, as a decrease in plasmid copy number with increasing plasmid size was recorded. Whilst not a critical issue, if the plasmid product is considered on a molar basis, as must be considered when dosing, then the fermentations do become less efficient with increasing plasmid size, since fewer copies are being propagated.

Finally it can be concluded that propagation of larger constructs was not hampered by any reduction in supercoiling. Indeed it has been shown that the larger plasmids recovered from the fermentations did show a favourable level of supercoiling (Figure 6-8/Figure 5-11).

8.1.3 Intermediate purification

The conclusions to be drawn from the studies in to the downstream purification steps are considered quite profound. It is concluded that the potential exists for constructs up to

50kb to be purified by the currently adopted process. However, it must be stated that for the manufacture of large plasmids, the current process is far from optimal.

It was demonstrated that recovery levels of increasingly sized plasmids from the UF demonstrated a reasonably linear decrease (Figure 7-3). It was only from detailed investigations into the topology changes (Figure 7-4) occurring to the plasmid molecules that a mechanism for the losses was elucidated. It is believed that the lysis operation is the real culprit in reducing plasmid yields. It was found that increasingly severe damage to plasmid topology was enacted upon plasmids as the size of the constructs increased, such that by the end of the lysis period an increasing proportion of the larger plasmid molecules existed in open-circular form (Figure 9-10). Analysis into the macro and micromixing environments achieved in the vessel suggested that the damage was not inflicted by a physical process but rather a chemical one (7.7). It can only be concluded that the precise nature of the chemical process responsible was either base-catalysed hydrolysis of the phosphodiester bonds in the pDNA backbone or the action of endogenous nucleases, or a combination of the two. It can be quite reliably concluded that the effect was not produced by physical forces, since the loss of topology was a clean one, involving the uniform conversion of SCC form to OC form, this would not be typically expected by a random physical process (Figure 9-10).

It is concluded that the mixing condition employed in the lysis vessel are far from ideal. In the mistaken belief that a low-agitation/shear environment would be beneficial to both plasmid and contaminating gDNA form, the result is in reality the creation of poor mixing conditions. The poor mixing conditions in turn lead to an extension of the time required for the lysis and neutralisation steps to be completed (Table 7-7). It is the extended periods required for these unit operations which are responsible for the damage to the plasmids, since they prolong the period for the action of either of the two chemical mechanisms outlined. It is concluded that the chemical damage is in action for plasmids of all sizes, but that with increasing plasmid size the effect became more noticeable since more sites were available for action.

Whilst it is concluded that the lysis operation lies at the root of the losses of plasmid from the system, it is not the direct cause of the plasmid losses. From the plasmid balances (Figure 9-31), all the plasmid expected from harvest sample comparison was still detectable following lysis, it is just that the gels recorded that the larger plasmid were

increasingly detected in OC form. The actual loss of plasmid mass was believed to occur during the ultrafiltration operation.

During the operation stages of the UF step a crossflow was in action and a transmembrane pressure applied. It is concluded that during this period the crossflow quickly degraded the open-circular pDNA leading to a relative increase in the proportion of supercoiled plasmid, an occurrence which can be appreciated by direct visualisation of the gels (Figure 9-10). It is maintained that the supercoiled form was relatively unaffected during this period of operation being quite protected from the physical forces by the action of the plasmid-gel layer. The losses of the plasmid were accrued since the shearing of the OC plasmid forms was believed to create small linear fragments capable of penetrating the membrane. It is believed that the shearing of the OC plasmid form with the effect of increasing % supercoiling to be an occurrence which is independent of plasmid size. This can be concluded since the effect was witnessed even with the smallest construct (Figure 9-6). As a result of the selective degradation of the OC form, the recovery levels of plasmid from the UF membrane became a function of the proportion of plasmid loaded in OC form. Since the proportion of OC form generated by the lysis step was found to be linearly related to plasmid size (Figure 7-5), by virtue of an increased likelihood of chemical degradation, the larger plasmids recorded the most severe losses.

Following the period of UF operation follows the recovery of the plasmid from the UF membrane. During this operation the TMP is removed from the membrane and the crossflow allowed to scour the membrane so as to recover the plasmid on the surface. It is this scouring of the membrane which is thought to explain the difference in the final topologies between runs performed on the same plasmids at crossflows 250mLmin^{-1} and 500mLmin^{-1} (Figure 7-3). It is also this period of operation which creates the sheared pDNA which can be observed on the gel scans of many of the larger constructs (Figure 9-10). From the results it is concluded, as would be expected, that operation of the membrane at 250mLmin^{-1} rather than 500mLmin^{-1} is more beneficial to final plasmid quality. However, it must also be concluded that the final form of the larger plasmid recovered from the membrane would not pass the >95% supercoiling criterion (Figure 7-3).

From these conclusions it was speculated that the operation of this process could be applied to the purification of larger constructs since it was found that the reported losses were due to the high proportions of OC pDNA in the clarified lysate at the time of

ultrafiltration. It will be suggested that should a process for the manufacture of larger plasmid DNA be attempted, intermediate purification by UF could work as a viable strategy, providing attempts were made to ensure that the plasmid loaded on to the membrane was primarily supercoiled. As such, when commenting on this process it is recommended that the lysis step be optimised since, even for smaller constructs, its operation is concluded to be far from optimal. It is suggested that lysis needs to be achieved more rapidly and increasingly so for larger constructs. The employment of a continuous lysis and neutralisation procedure should be considered. The fact also remains that recovery of plasmid from the membrane promises to be problematic in terms of the quality of the pDNA recovered as plasmid size increases.

8.1.4 Contaminant profiles

The level of clearance achieved of the major contaminants achieved by the process was detailed and deemed to be very effective (7.8). A large swathe of contaminants was found to be removed by precipitation during the lysis regime and another large majority removed by the proceeding diafiltration steps. Incidentally, it was determined that a slightly more effective clearance of all the contaminants was realised using the faster ($500mLmin^{-1}$) crossflow rate. This is believed to be due to the greater scouring action, resulting from the faster velocity, reducing the thickness of the gel-layer which inhibits the transit of the contaminant moieties across the membrane. A drawback with this is that were large plasmids to be produced a trade-off would need to be established between the faster crossflow velocity, at which greater contaminant clearances are demonstrated, and the slower velocities at which damage to plasmid topology is less pronounced. It was suggested that the use of a faster crossflow could be employed during the membrane operation stages, with a slower velocity used for the recovery stages. However, the demands for a variable speed pump might prevent the application of such a proposal.

The level of gDNA was deemed the most critical contaminant to track (7.8.1). The resultant profiles produced by monitoring the clearance of this contaminant are concluded to have important implication to the manufacture of large plasmids. It was found that this process is capable of achieving a set level of clearance of this contaminant. Although the process was only studied up to the anion-exchange column stage, due to the similar physico-chemical properties of pDNA and gDNA it was deemed that the ratio between the two at the end of the UF step could be used to assess the likelihood of the process being accepted. Strict requirements surrounding the ratio of gDNA to pDNA demanded by the

regulators, combined with the fixed level of clearance achieved by the plasmid process means that the final plasmid mass obtained comes to influence whether a process would be acceptable or not.

Employing such as process as the one outlined here, with a plasmid maintained at high-copy numbers will almost always ensure that there is sufficient plasmid mass at the end of the process such that the small amount of gDNA co-purified is massively exceeded by the mass of plasmid purified. However, the situation for large plasmids may not be as simple. If the specific yields of large plasmids from the fermentations are low then the poor yield of pDNA purified by the end means that the ratio of gDNA to pDNA may be too high as to be acceptable. This was found to be the case in these investigations. This provides a definitive reason why high plasmid yields from the fermentation are a necessity and not just a matter of process efficiency. It can be concluded that for this process to be accepted, in that the ratio of pDNA to gDNA by the process end meets the acceptance criteria, then a minimum specific yield of ~290μgpDNA $gWCW^{-1}$must be obtained. If not then the level of clearance of gDNA will be insufficient. This specific yield figure was obtained assuming an 80% recovery of plasmid across the UF steps. As has been demonstrated, as the process stands this level of recovery remains unachievable for larger constructs.

8.1.5 Chromatographic Separations

The use of chromatography in processes for the manufacture of plasmid DNA is essential, despite the matrices not being particularly well adapted for the purpose. From these investigations it can be concluded that the purification of larger plasmids can be expected to be increasingly troublesome (7.9). It was demonstrated that the binding kinetics of larger constructs were reduced as compared to the smaller plasmid controls (Figure 7-15) . This would mean that slower flow rates would be required and less well defined elution peaks could be expected. Additional studies demonstrated the decreasing maximum binding capacities displayed by the resins under study with increasing plasmid size (Figure 7-16), the result of which could be poorer recoveries from column steps.

Another observation made through the course of the project were the poor recoveries produced from Qiagen resins when purifying larger constructs. Investigations concluded that whilst heating the elution buffer alleviated the problem it was not completely resolved (6.5.3). As such it was proposed that the plasmids may have had difficulty entering the resins and as such poor recoveries were recorded. It is recommended that further studies be

conducted to confirm whether this is the case. It was certainly established that the larger plasmids were not capable of effectively penetrating PD-10 gel columns used for de-salting. The results from the chromatographic investigations suggest that should attempts be made to produce large plasmids alternative chromatographic strategies are worth pursuing, namely membrane chromatography.

8.1.6 Analytical

Effective analytical techniques are essential if confidence is to be had in the results returned since it from these that conclusions will be drawn. In these investigations the two assays for which a great deal of development was required were the plasmid quantification assay and the plasmid topology assay.

Studies found that the accurate quantification of large plasmids was hampered by their size and their yield. Low yields often meant that contributory signals produced as a result of the relatively high levels of contaminants lead to misleading results regarding plasmid yield (4.3). For instance, the presence of contaminating gDNA was found to completely distort the reading produced by PicoGreen. In the end a suitable HPLC assay was developed. It has to be concluded that HPLC remains a valid technique for large plasmid quantification but the caveat must be applied that plasmid resolution decreases with plasmid size. However, it must be outlined that if this project were to be repeated then time spent developing a qPCR based assay for plasmid quantification would be well spent. Results from qPCR for gDNA contamination were impressive in the level of sensitivity and specificity displayed. It can only be expected that the same could be said of a qPCR assay for plasmid quantification.

The second assay regards the plasmid topology. Due to the larger size of these constructs the use of conventional gel electrophoresis was prevented since DNA molecules >20kb are not effectively resolved (4.6.1). As such a great deal of trial and error was spent developing a FIGE based assay. Although useful results were eventually forthcoming the turn around of the assay was incredibly slow. It was found that 40 hours was required for the running of the gel followed by another 24 hours for effective staining to be achieved. Therefore it was far from being a user-friendly assay. As with a plasmid qPCR assay, if this project were to be started from the outset then it would be considered a good move to investigate the use of capillary electrophoresis for the analysis of plasmid topology. The

turnaround time for this assay is a matter of minutes, meaning that many more replicates could be processed.

8.1.7 Future Work

(i) There is a pressing need to further investigate the lysis step of the current process. It was postulated that the lysis step was the real cause of plasmid topology damage, and as such the root cause of plasmid loss. Investigations are required to further quantify the damage to plasmid molecules by this lysis regime. If the plasmid topology changes are reduced, through the use of more suitable conditions, it may be found that the remainder of the current process could be applicable to the manufacture of larger constructs.

(ii) Further work needs to be conducted into optimising large plasmid's replication machinery in order to improve plasmid yield and stability. Whilst it was found favourable to use a high-copy number replicon to improve plasmid copy-number, the consequences this had on the plasmid stability were disappointing. As such it is thought that large yield gains could be found by optimising the plasmid's machinery such that high-copy numbers were obtained in conjunction with high stability. Several approaches would be required including the choice of a more effective selection mechanism which could be as simple as kanamycin or more complicated such as post-segregational killing.

(iii) It would be worth investigating the use of inducible BACs. Whilst it is maintained that standard vectors e.g. pGEM11 are capable of maintaining up to 100kb of DNA, for larger amounts BACs remain the only option. However, as described in Chapter 3, it is believed that at copy numbers of 1-2 per cell, they would never represent a feasible strategy. The arrival of inducible BACs, whose copy number can be amplified upon the addition of IPTG may promise to rectify the issue of low copy number.

(iv) Further investigations need to focus on the chromatographic steps to be used in any process for the manufacture of large plasmids. It was highlighted during these studies how the specific binding capacity decreased with increasing plasmid size.

Such a phenomenon would reduce the overall efficiency of any chromatography step. More explanation is needed into why this is the case. It was hypothesised to be due to the lack of binding sites created by hindrances resulting from the molecules' size. It would be useful investigating the use of more porous supports. Furthermore, no studies were conducted into the use of expanded bed strategies. The low shear environment of this option may be found to be favourable.

(v) One recurring problem throughout this project was the corruption of plasmid quantification by changes in plasmid topology. Whilst minimal effect is noticeable when assaying smaller plasmids, with larger constructs the distorting effect became increasingly apparent when using many of the analytical procedures. It is believed that for large plasmid studies it would be worth investing time in creating a qPCR based assay for the highly accurate quantification of plasmid in all process streams.

9. APPENDICES

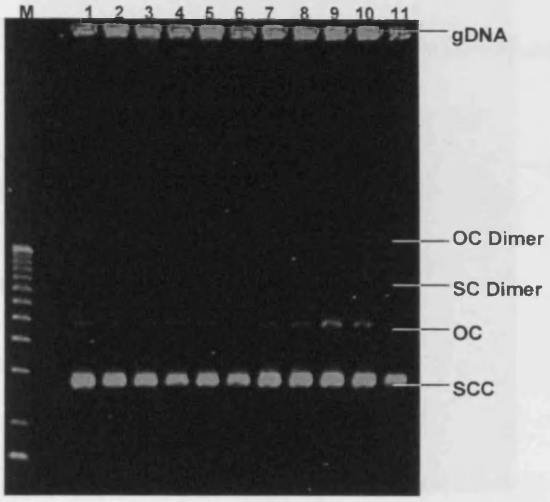

Figure 9-1 Conventional AGE of the smallest construct (pGEM11 [3.2kb]) used to determine the topology changes of the construct through the fermentation. The gel was scanned and the proportions used to plot the change in supercoiling with time.

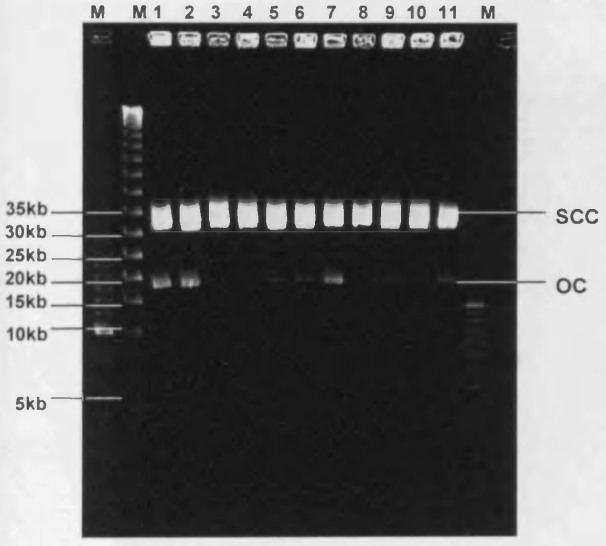

Figure 9-3 FIGE of the construct (pGEM16 [16kb]) used to determine the topology changes of the construct through the fermentation. The gel was scanned and the proportions used to plot the change in supercoiling with time.

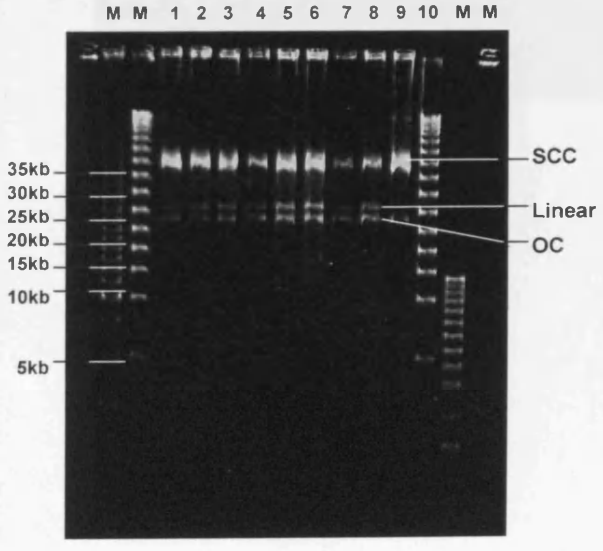

Figure 9-2 FIGE of the construct (pGEM33 [33kb]) used to determine the topology changes of the construct through the fermentation. The gel was scanned and the proportions used to plot the change in supercoiling with time.

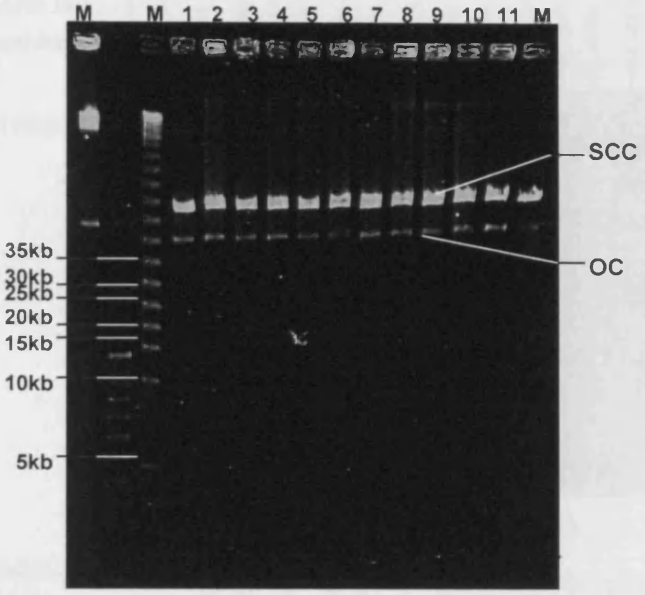

Figure 9-5 FIGE of the construct (pGEM49 [49kb]) used to determine the topology changes of the construct through the fermentation. The gel was scanned and the proportions used to plot the change in supercoiling with time. The right-hand marker consisted of the 49kb which had been subjected to vigourous pipetting to attempt to damage the plasmid. Some shearing is evident.

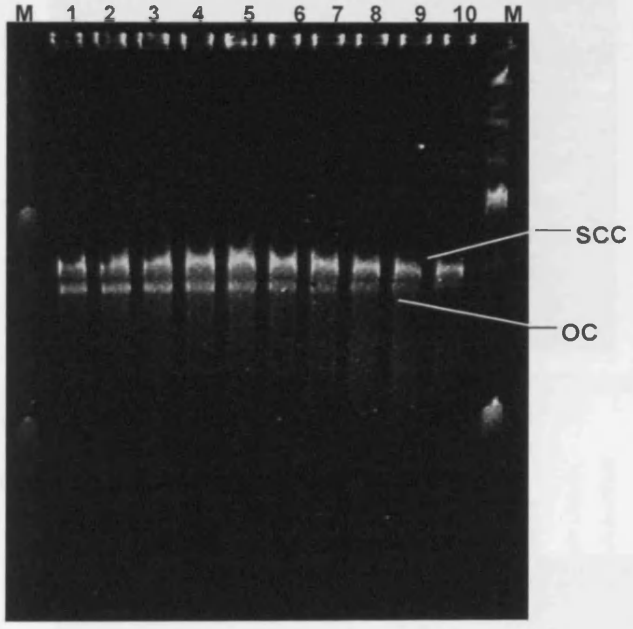

Figure 9-4 FIGE of the construct (p5176 [116kb]) used to determine the topology changes of the construct through the fermentation. The gel was scanned and the proportions used to plot the change in supercoiling with time.

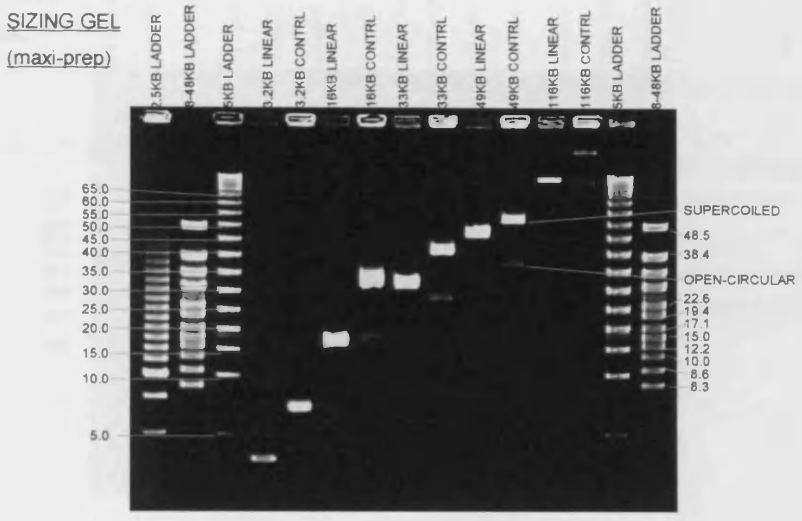

Figure 9-7 FIGE gel of maxi-prep (large construct kit) purified constructs. This gel was scanned and the topology information taken to be the proportions at the start of the process (Pre-Lysis), since the gentle processing regime of the maxi-preps should not have caused significant changes to the topology.

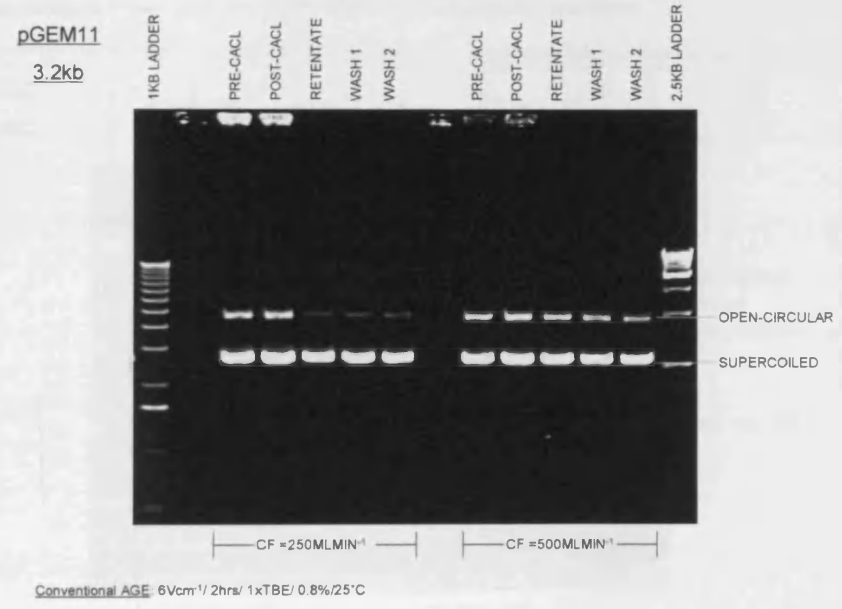

Figure 9-6 Conventional AGE of the smallest construct (pGEM11 [3.2kb]) used to determine the topology changes of the construct through the production process. Samples were taken from five points during the process and from runs at both crossflow velocities; 250 and 500mLmin^{-1}.

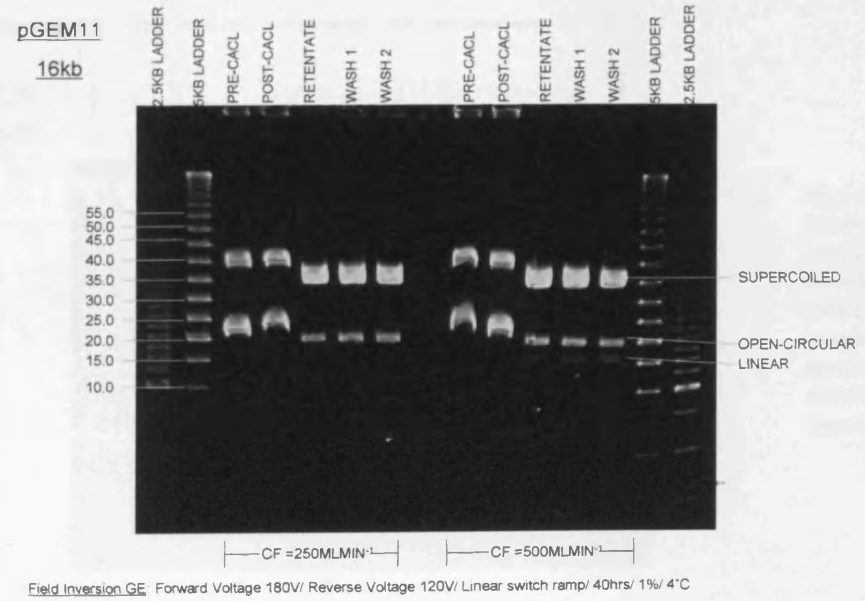

Figure 9-8 FIGE of the pGEM 16kb construct used to determine the topology changes of the construct through the production process. Samples were taken at five points during the process and from runs at both crossflow velocities; 250 and 500mLmin^{-1}.

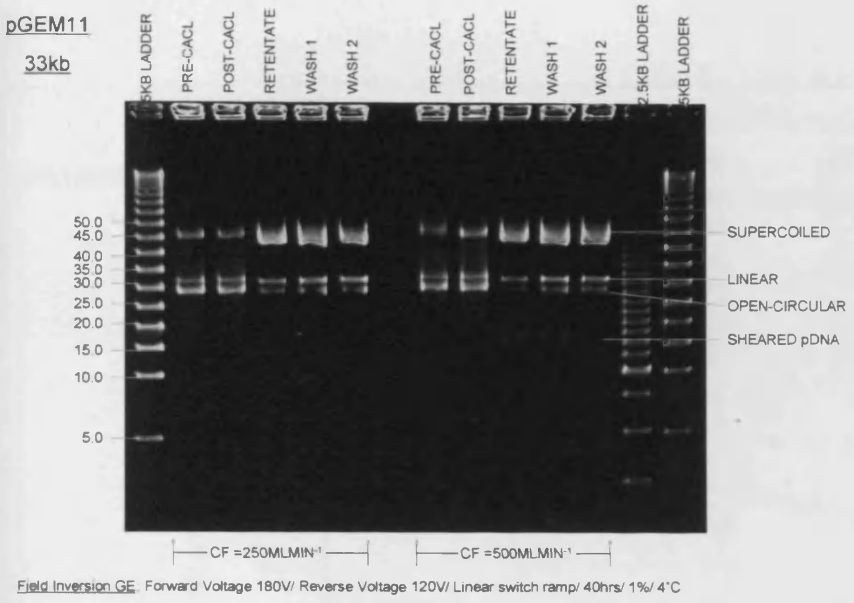

Field Inversion GE: Forward Voltage 180V/ Reverse Voltage 120V/ Linear switch ramp/ 40hrs/ 1%/ 4°C

Figure 9-11 FIGE of the pGEM 33kb construct used to determine the topology changes of the construct through the production process. Samples were taken at five points during the process and from runs at both crossflow velocities; 250 and 500mLmin^{-1}

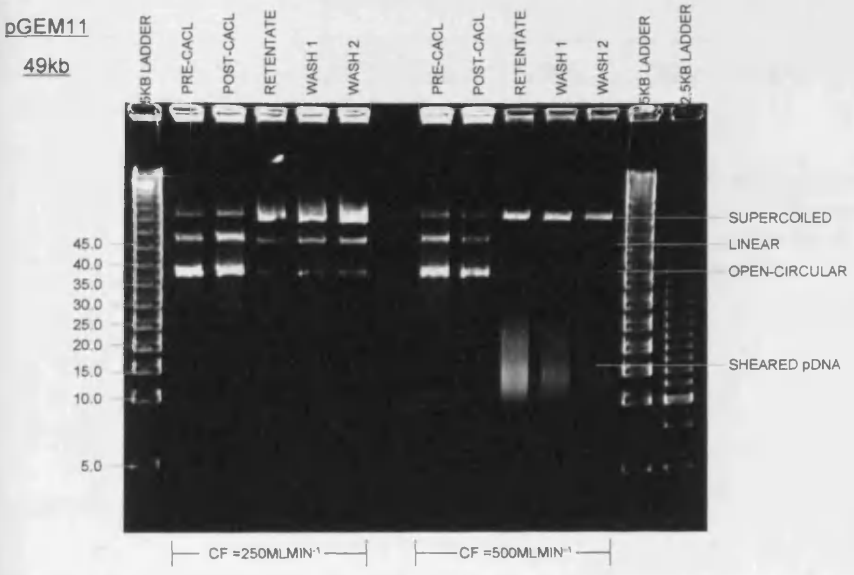

Field Inversion GE: Forward Voltage 180V/ Reverse Voltage 120V/ Linear switch ramp/ 40hrs/ 1%/ 4°C

Figure 9-10 FIGE of the pGEM 49kb construct used to determine the topology changes of the construct through the production process. Samples were taken at five points during the process and from runs at both crossflow velocities; 250 and 500mLmin^{-1}

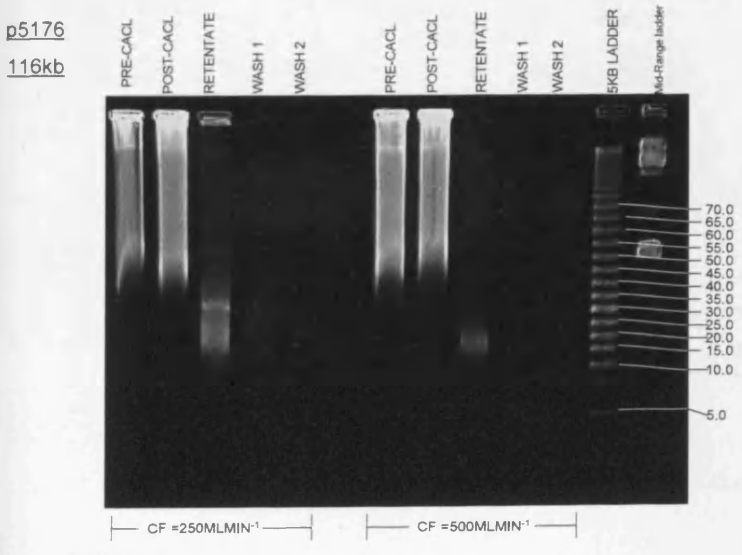

Field Inversion GE: Forward Voltage 180V/ Reverse Voltage 120V/ Linear switch ramp/ 40hrs/ 1%/ 4°C

Figure 9-9 FIGE of BAC p5176. Numerous attempts were made to extract sufficient plasmid material with which to run a reliable gel but to no avail. The plasmid existed in such small amounts that insufficient could be concentrated and purified without the masking effect of the genomic DNA smear appearing

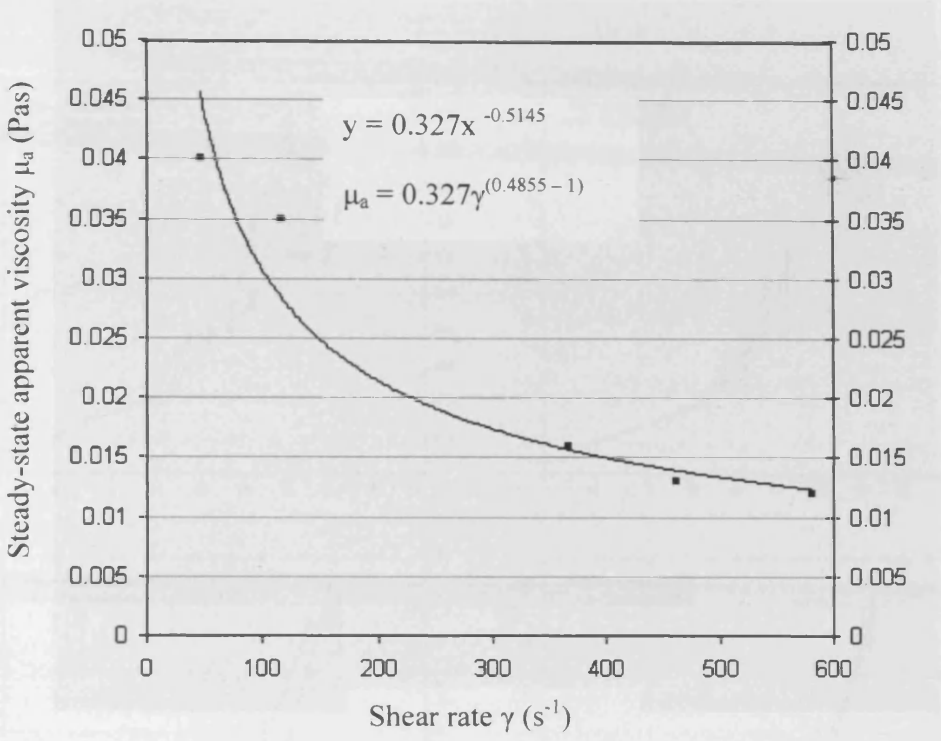

Figure 9-12 Graph plotting a line of best fit through the data for apparent viscosity of lysate fluid at various shear rates as determined from (Ciccolini *et al.*, 1999) Table 7-7. From the data the values for *K* (consistency index) and *n* (flow-behaviour index) have been extracted.

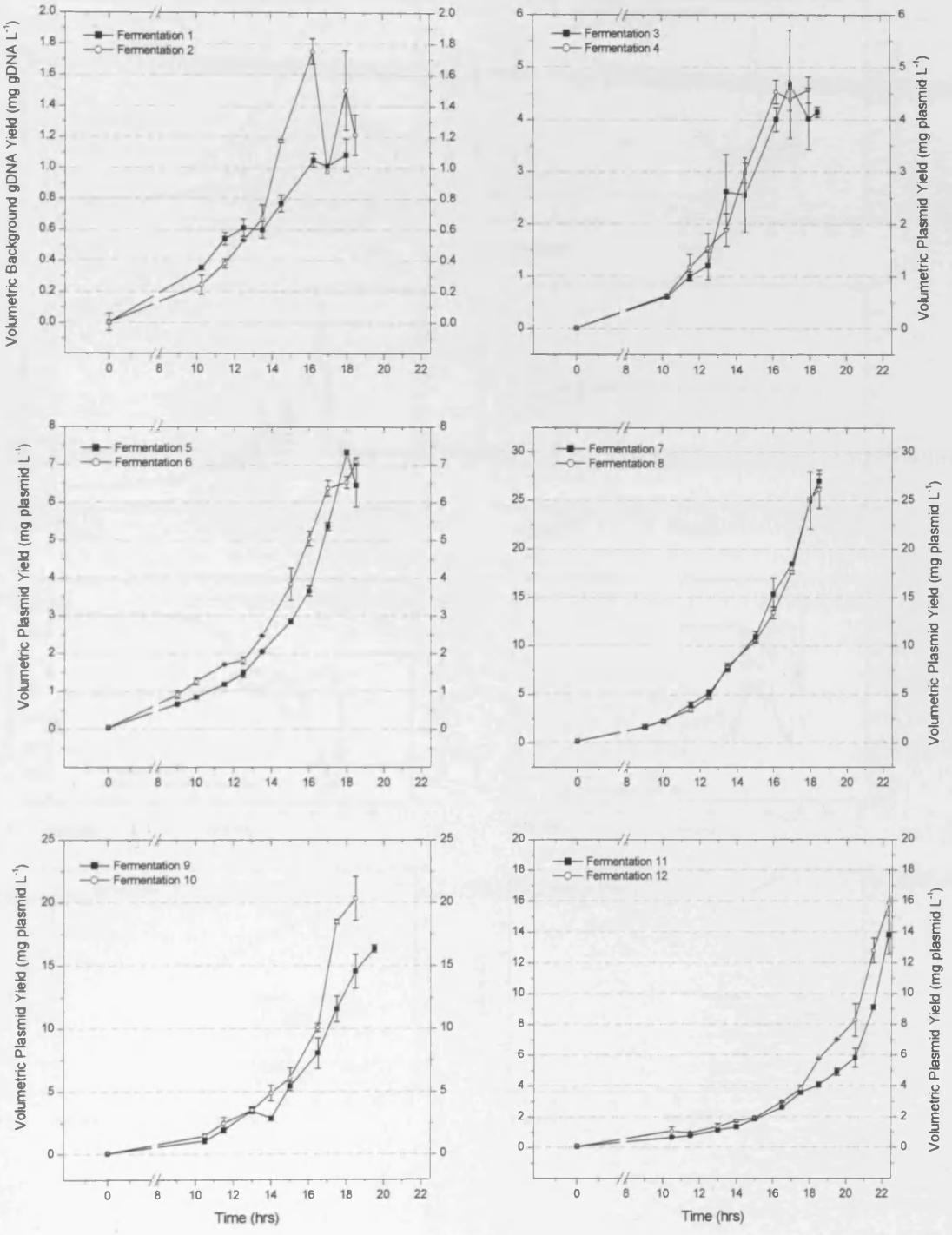

Figure 9-13 Volumetric Yield profiles from the 25°C 4L fermentations

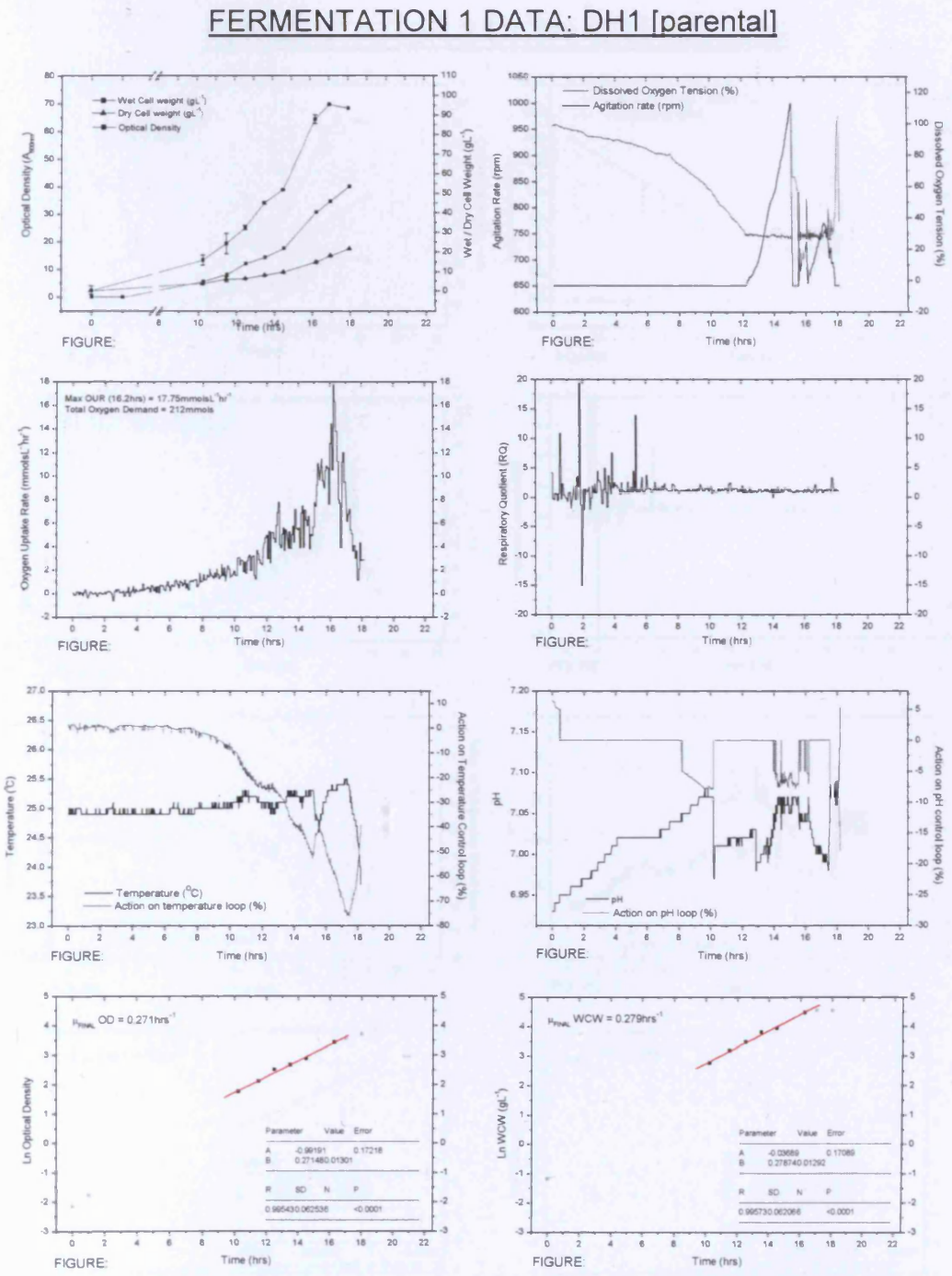

Figure 9-14 Online data for 4L working volume 25°C fermentation of DH1 parental. 4L of sterile media (GSK proprietary media) was inoculated to a starting OD of 0.1 using a starter culture grown at 25°C. Oxygen saturation was maintained at 30% by cascade control of impeller speed and maintained through the sparging of enriched air. Online data was logged using BioXpert

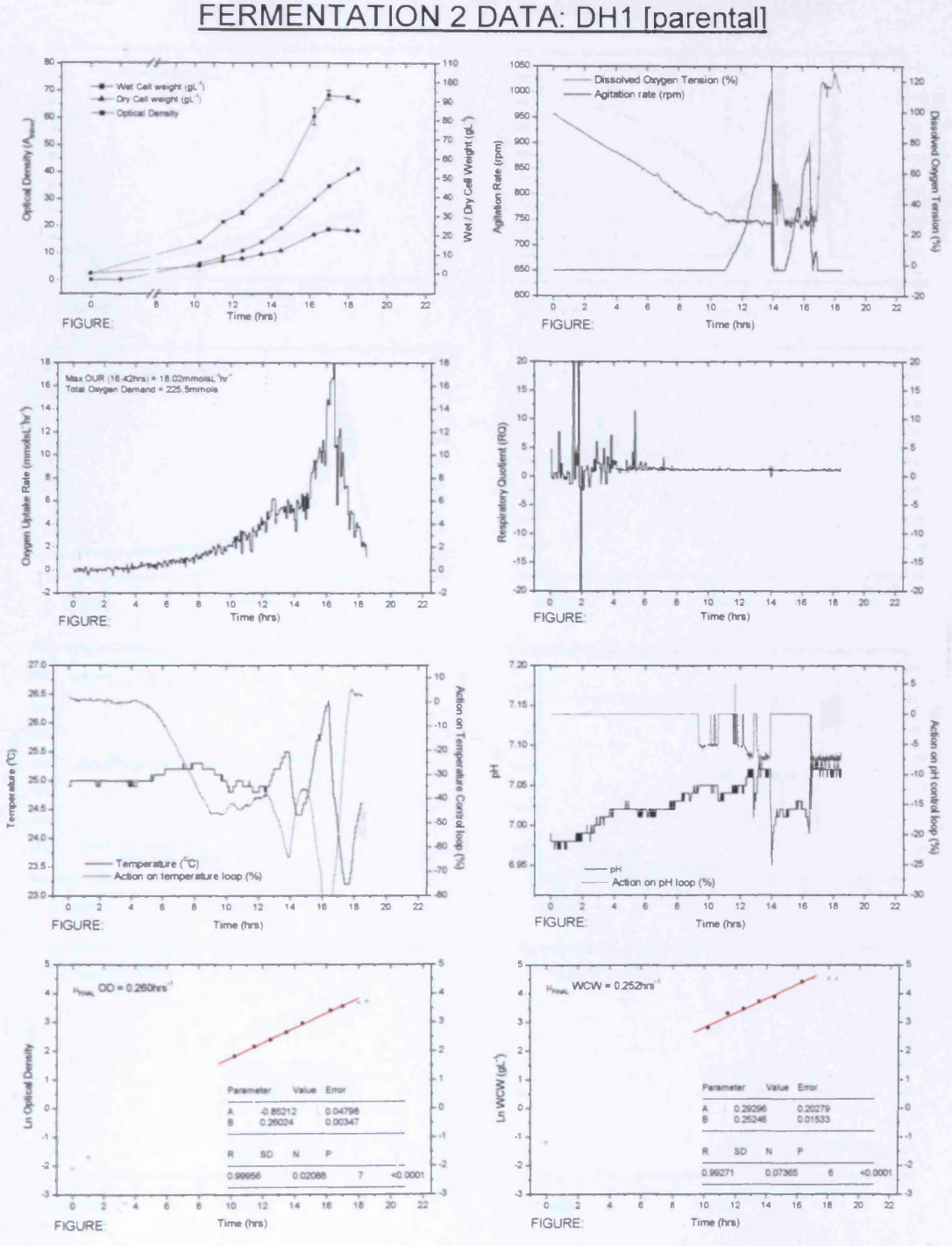

Figure 9-15 Online data for 4L working volume 25°C fermentation of DH1 parental. 4L of sterile media (GSK proprietary media) was inoculated to a starting OD of 0.1 using a starter culture grown at 25°C. Oxygen saturation was maintained at 30% by cascade control of impeller speed and maintained through the sparging of enriched air. Online data was logged using BioXpert

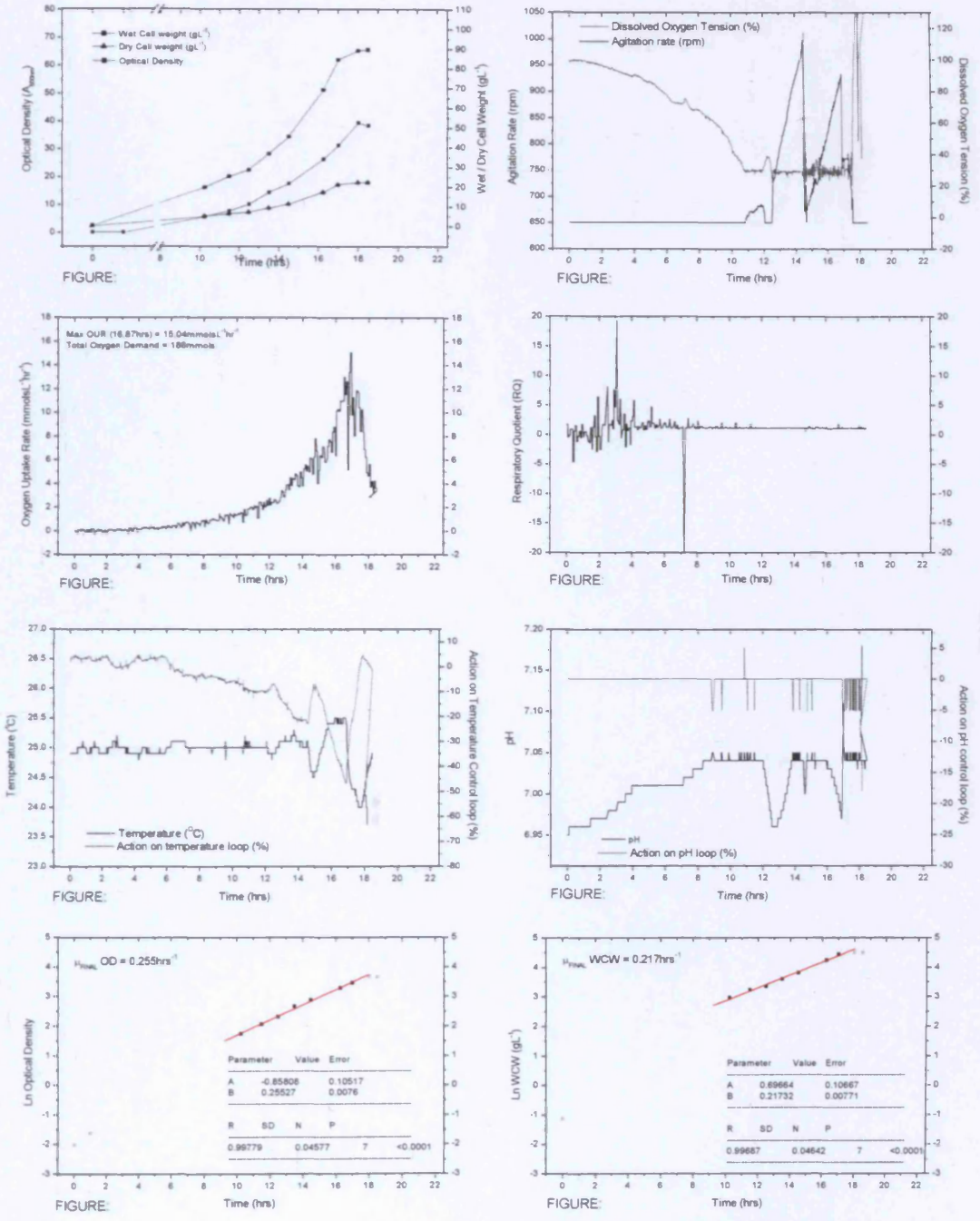

Figure 9-16 Online data for 4L working volume 25°C fermentation of DH1 p5176. 4L of sterile media (GSK proprietary media) was inoculated to a starting OD of 0.1 using a starter culture grown at 25°C. Oxygen saturation was maintained at 30% by cascade control of impeller speed and maintained through the sparging of enriched air. Online data was logged using BioXpert

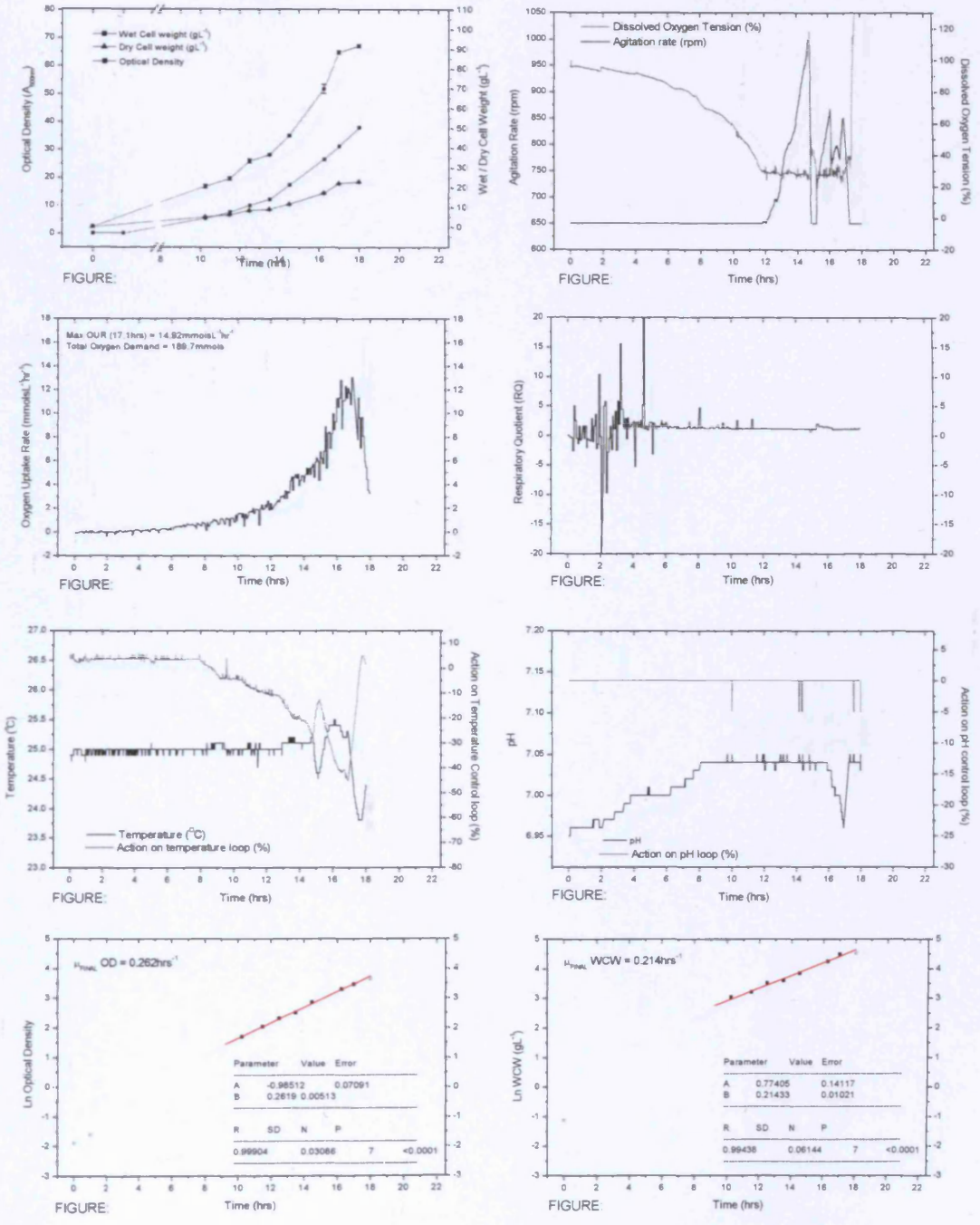
FERMENTATION 4 DATA: DH1 [p5176] (116kb)
Wet Cell weight (gL-1)
Dry Cell weight (gL-1)
Optical Density
Optical Density (A600nm)
Wet / Dry Cell Weight (gL-1)
Time (hrs)
FIGURE:
Dissolved Oxygen Tension (%)
Agitation rate (rpm)
Agitation Rate (rpm)
Dissolved Oxygen Tension (%)
Time (hrs)
FIGURE:
Max OUR (17.1hrs) = 14.82mmolsL-1hr-1
Total Oxygen Demand = 189.7mmols
Oxygen Uptake Rate (mmolsL-1hr-1)
Time (hrs)
FIGURE:
Respiratory Quotient (RQ)
Time (hrs)
FIGURE:
Temperature (°C)
Action on temperature loop (%)
Action on Temperature Control loop (%)
Time (hrs)
FIGURE:
pH
Action on pH loop (%)
Action on pH control loop (%)
Time (hrs)
FIGURE:
μmax OD = 0.262hrs-1
Ln Optical Density
Parameter Value Error
A -0.98512 0.07091
B 0.2619 0.00513
R SD N P
0.99904 0.03086 7 <0.0001
Time (hrs)
FIGURE:
μmax WCW = 0.214hrs-1
Ln WCW (gL-1)
Parameter Value Error
A 0.77405 0.14117
B 0.21433 0.01021
R SD N P
0.99438 0.06144 7 <0.0001
Time (hrs)
FIGURE:

Figure 9-17

FERMENTATION 5 DATA: DH1 pGEM11 (3.2kb)

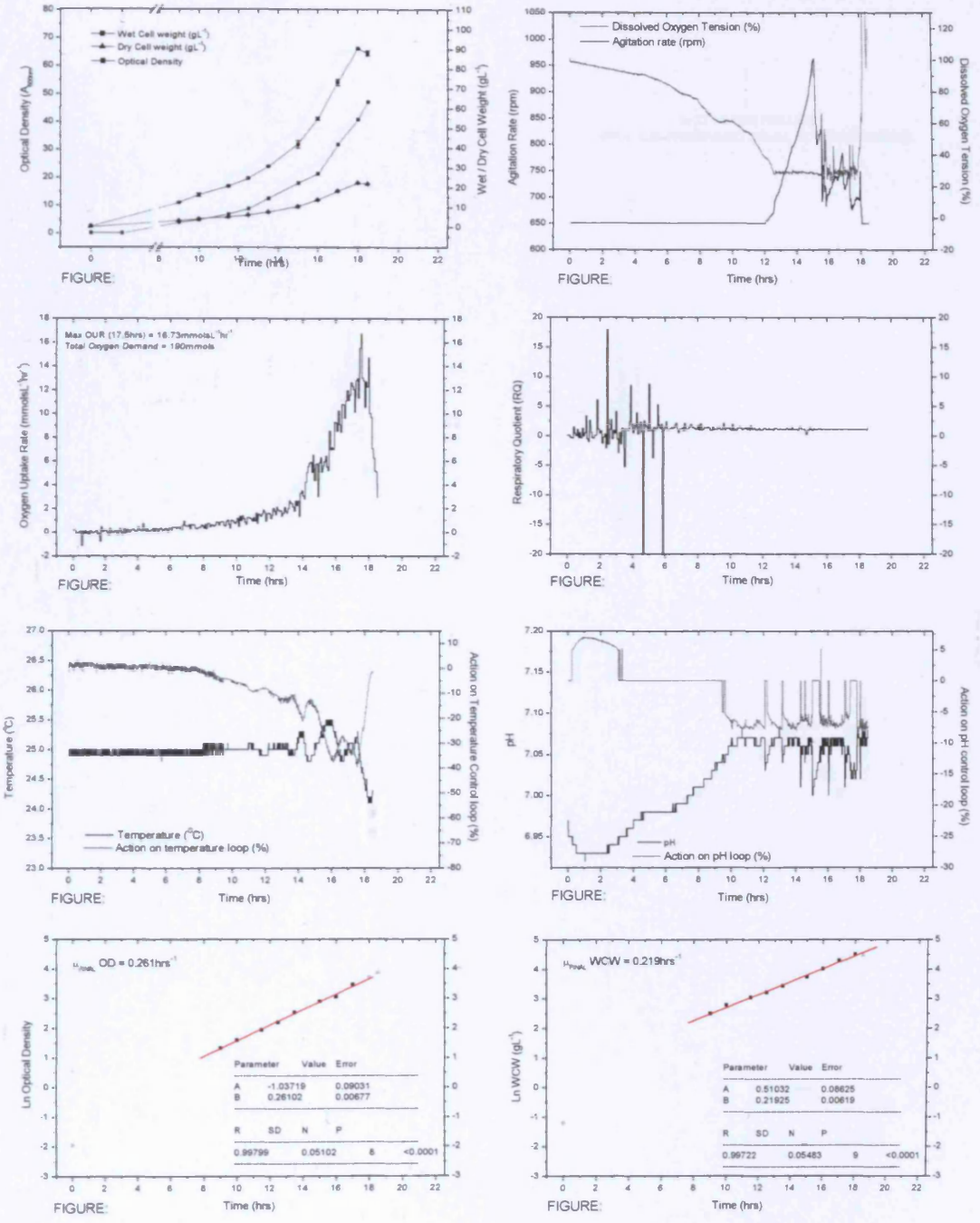

Figure 9-18

FERMENTATION 6 DATA: DH1 pGEM11 (3.2kb)

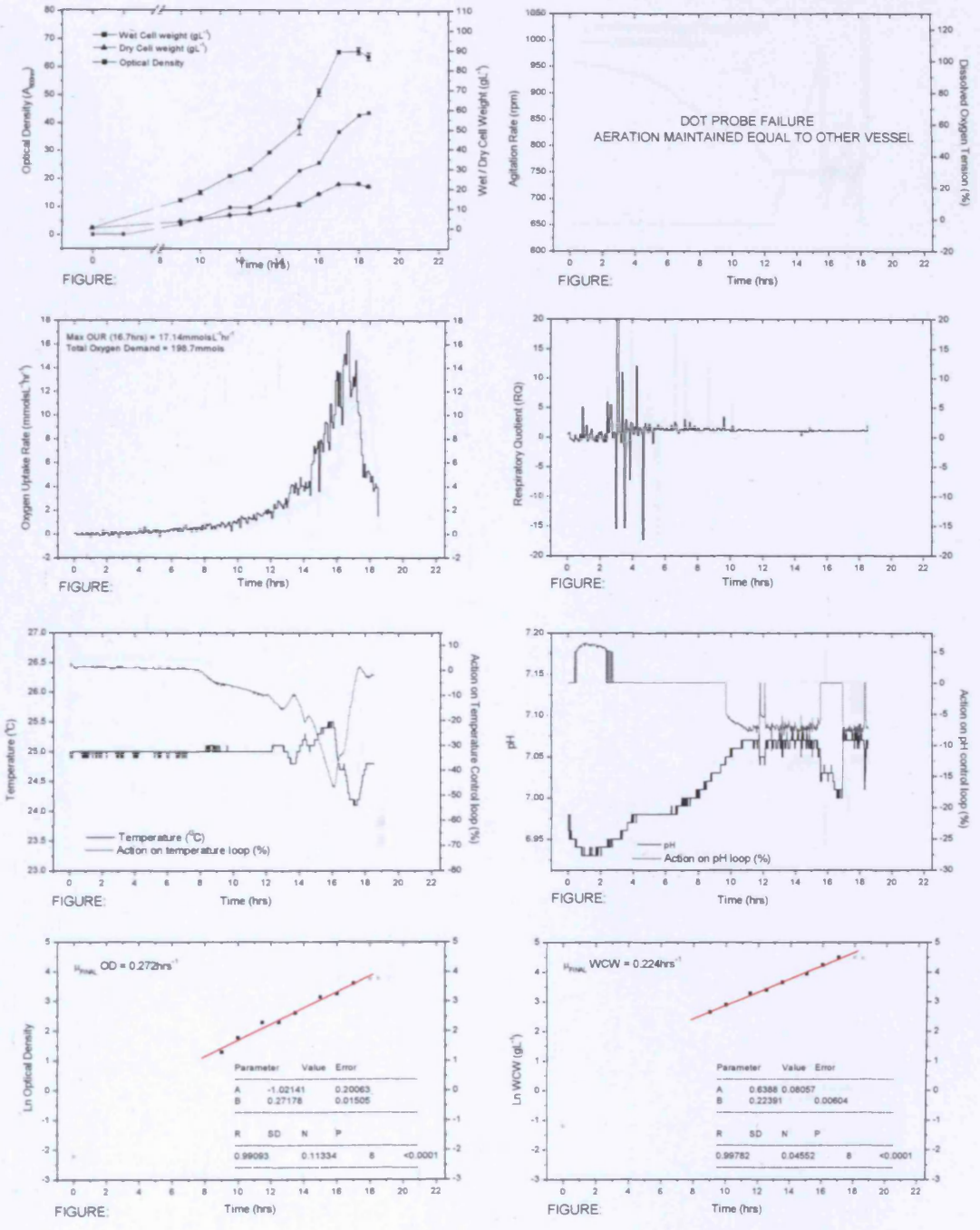

Figure 9-19

FERMENTATION 7 DATA: DH1 pGEM 16kb

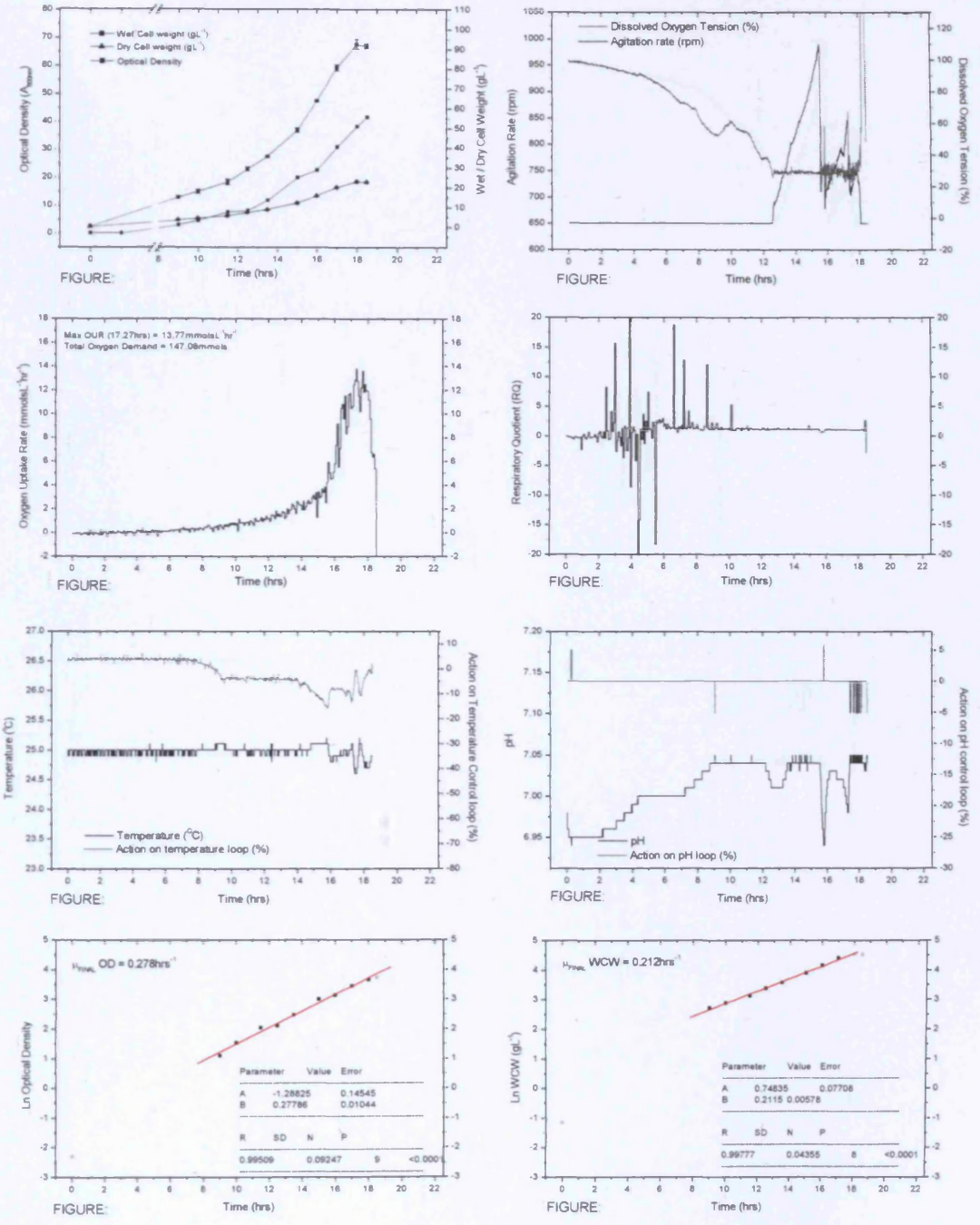

Figure 9-20

FERMENTATION 8 DATA: DH1 pGEM 16kb

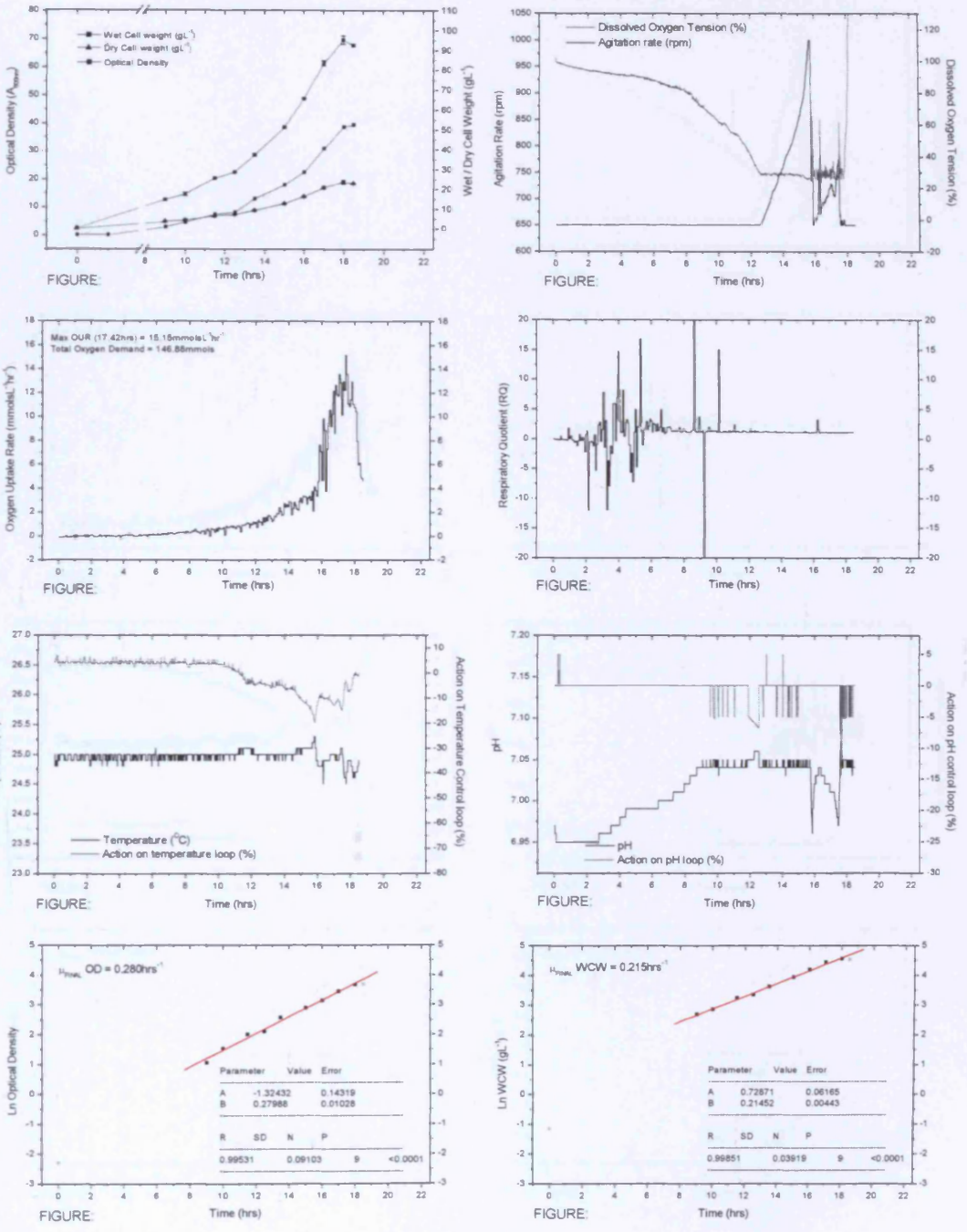

Figure 9-21

FERMENTATION 9 DATA: DH1 pGEM 33kb

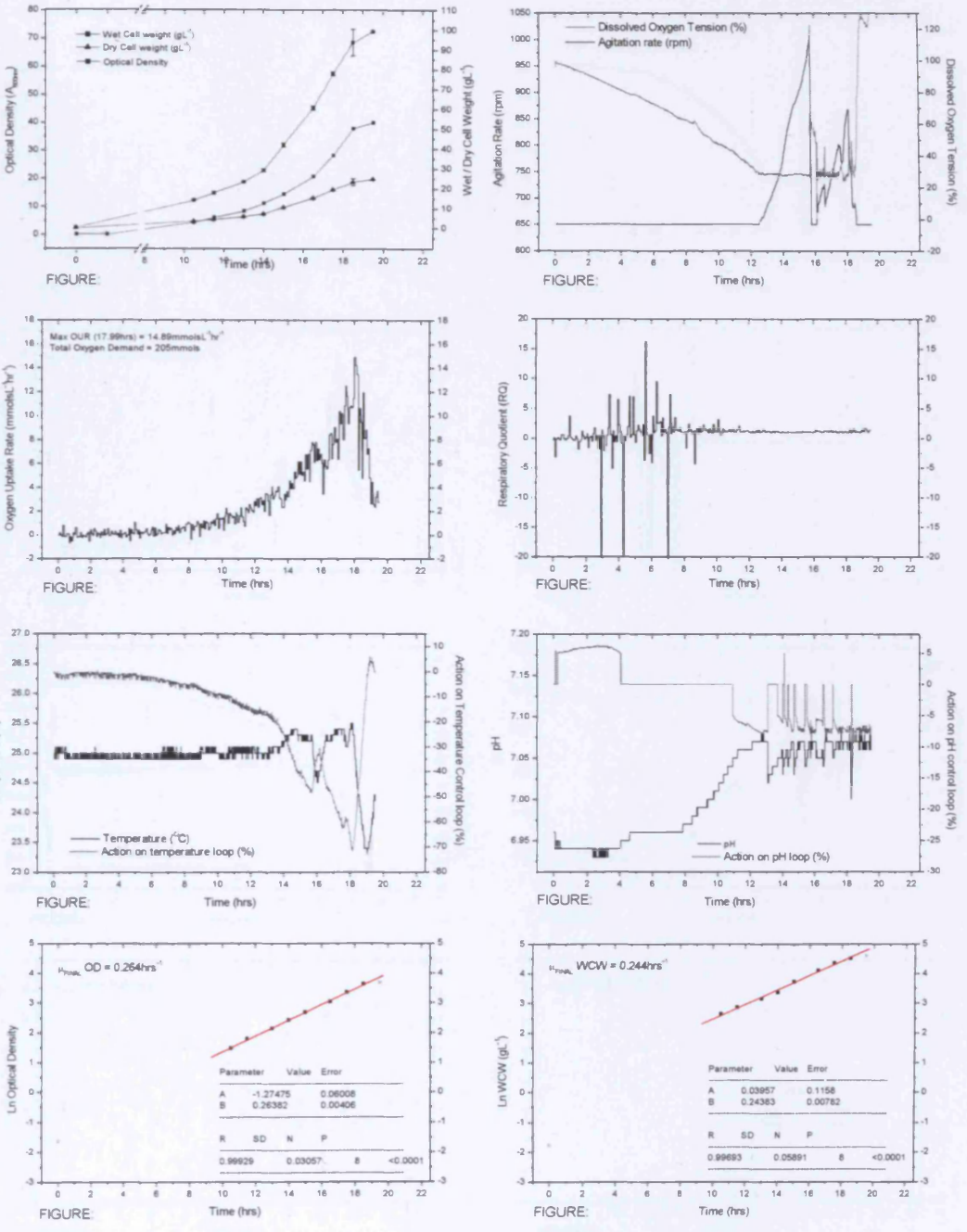

Figure 9-22

FERMENTATION 10 DATA: DH1 pGEM 33kb

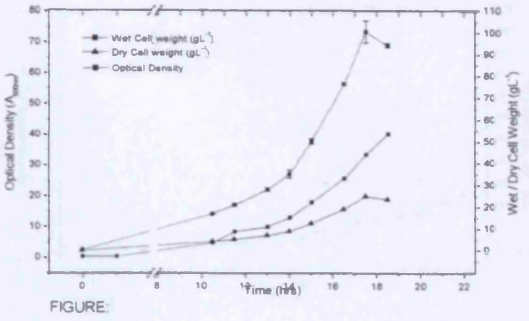

FIGURE:

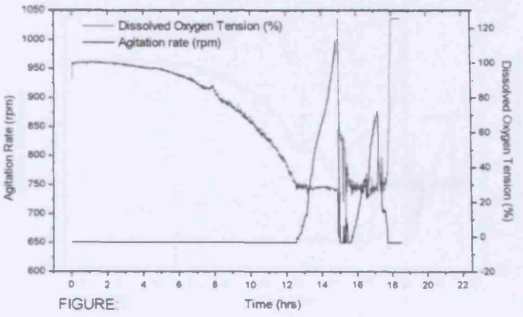

FIGURE:

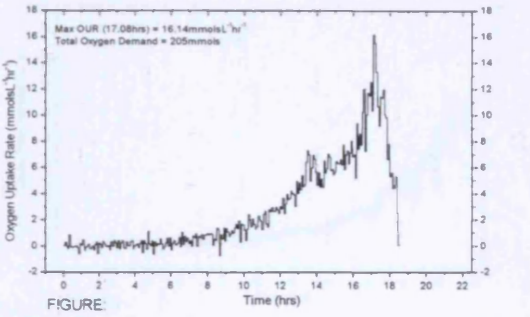

FIGURE:

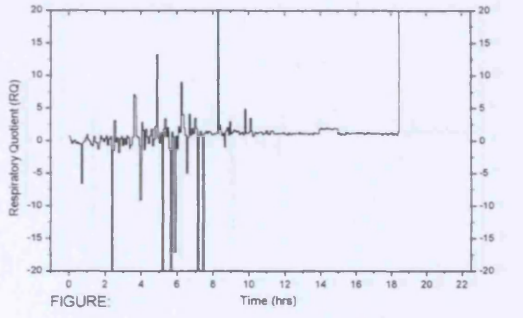

FIGURE:

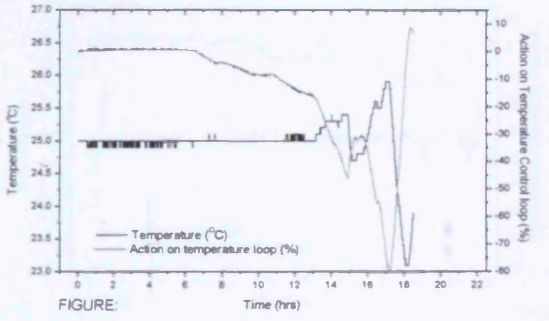

FIGURE:

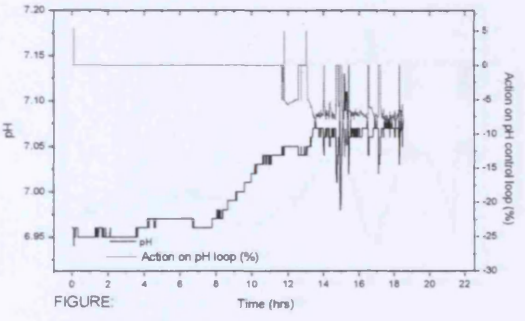

FIGURE:

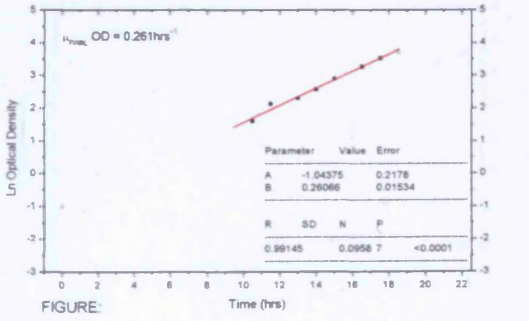

FIGURE:

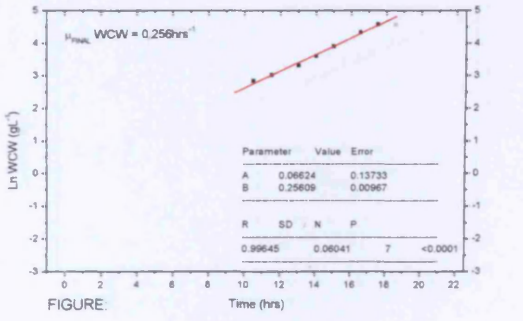

FIGURE:

Figure 9-23

FERMENTATION 11 DATA: DH1 pGEM 49kb

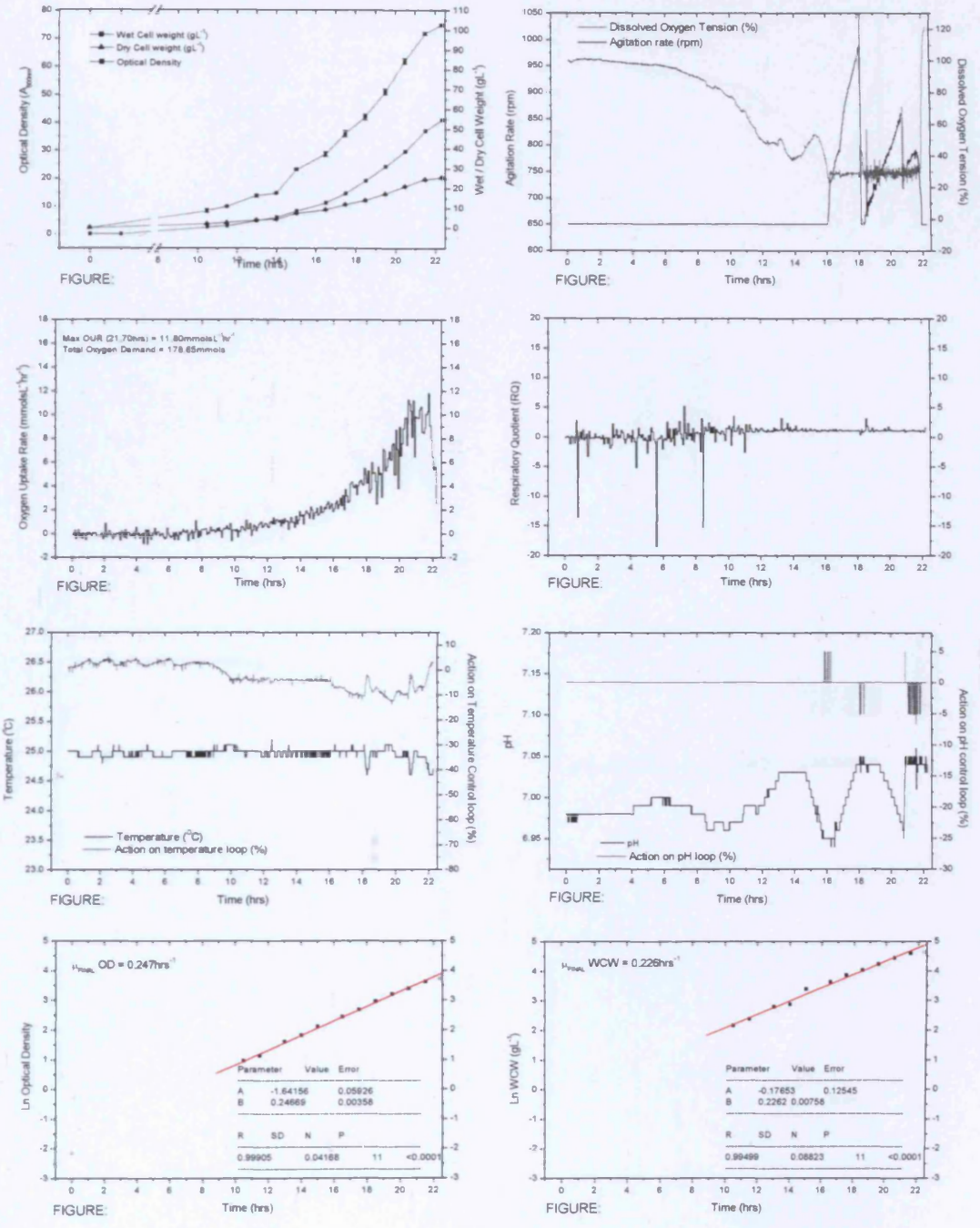

Figure 9-24

FERMENTATION 12 DATA: DH1 pGEM 49kb

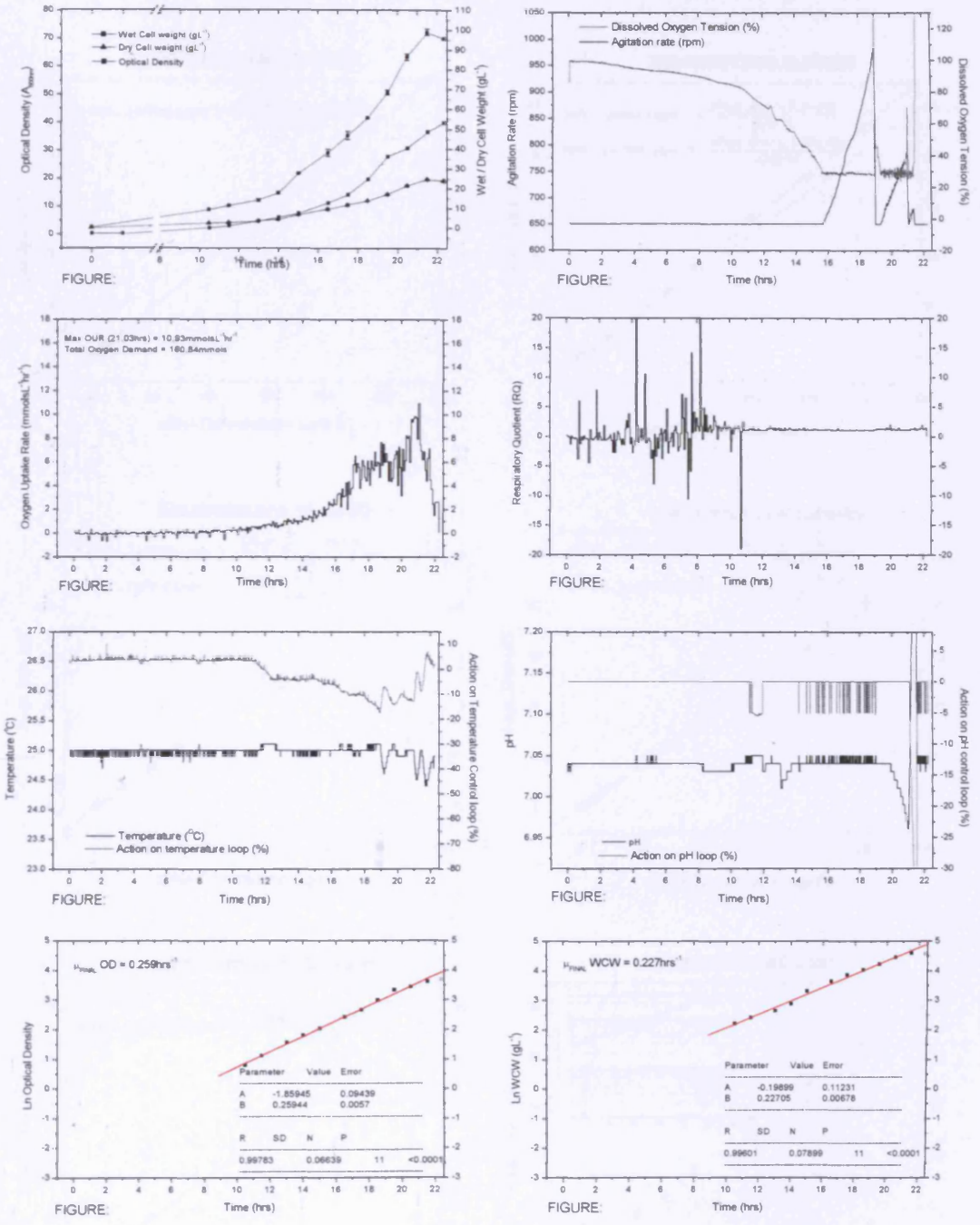

Figure 9-25

(vi) Upstream HPLC curves

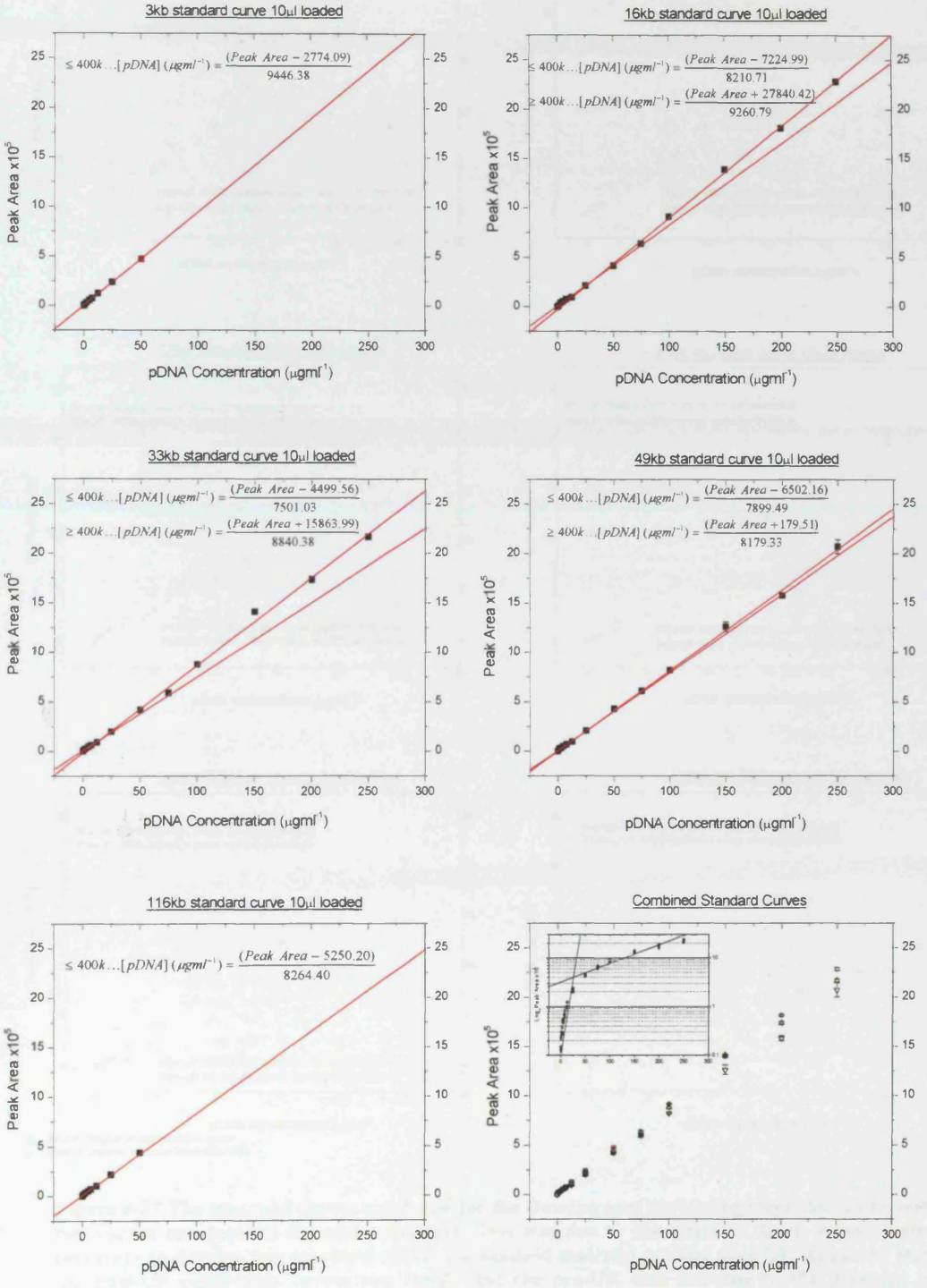

Figure 9-26 HPLC calibration curves used determination of plasmid concentration in samples taken during the fermentations. A standard curve was prepared for each construct under investigation ranging between 0-250µgmL^{-1} in concentration. As can be seen from the figures it was not always possible to purify some of the constructs to the high concentrations so only the more dilute points were used in the standard curves.

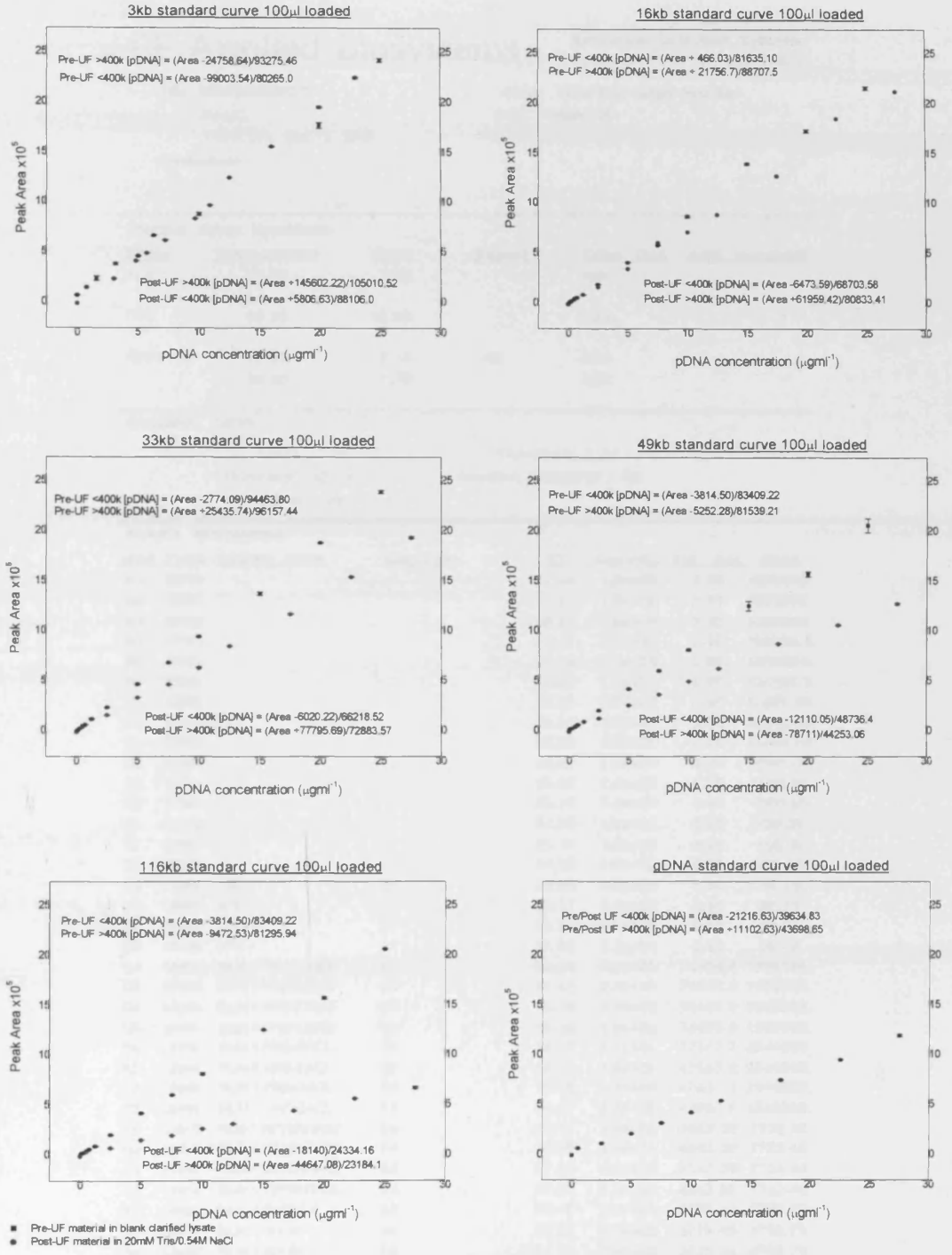

Figure 9-27 The standard curves employed for the Downstream processing steps. As can be seen two curves are detailed for each construct. This was due to the effect of shear. It was found necessary to develop two standard curves for plasmid material pre and post-UF. As can be seen the Post-UF calibration curves run lower that the pre-UF, this was due to the presence of sheared pDNA being unaccounted for during peak integration

PE Applied Biosystems

Sequence Detection Systems 1.6.3

File Name: untitled 2
User:
Date: Thu, Sep 15, 2005
Comments:

Plate Type: 7700 Single Reporter
PCR Volume: 30

Thermal Cycle Conditions

Cycle	Temperature	Time	Repeat	Ramp Time	Auto Increment
Hold	50.00	2:00		Auto	
Hold	95.00	10:00		Auto	
Cycle	95.00	0:15	40	Auto	
	60.00	1:00		Auto	

Standard Curve

Slope: -4.05
Intercept: 42.18
Fit R: 0.99
Threshold: 0.04
Baseline Range: (3 , 13)

Sample Information

Well	Type	Sample Name	Replicate	Ct	Quantity	Std. Dev.	Mean
A1	STND			17.89	1.0e+06	0.00	1000000.
A2	STND			17.81	1.0e+06	0.00	1000000.
A3	STND			18.34	1.0e+06	0.00	1000000.
B1	STND			21.57	1.0e+05	0.00	100000.0
B2	STND			21.49	1.0e+05	0.00	100000.0
B3	STND			21.47	1.0e+05	0.00	100000.0
C1	STND			26.31	1.0e+04	0.00	10000.00
C2	STND			26.41	1.0e+04	0.00	10000.00
C3	STND			26.63	1.0e+04	0.00	10000.00
D1	STND			30.04	1.0e+03	0.00	1000.00
D2	STND			29.75	1.0e+03	0.00	1000.00
D3	STND			30.15	1.0e+03	0.00	1000.00
E1	STND			34.03	1.0e+02	0.00	100.00
E2	STND			33.17	1.0e+02	0.00	100.00
E3	STND			34.85	1.0e+02	0.00	100.00
A4	UNKN	NTC	01	35.38	4.8e+01	6.60	50.18
A5	UNKN	NTC	01	35.17	5.4e+01	6.60	50.18
B4	UNKN	NTC	01	35.61	4.2e+01	6.60	50.18
B5	UNKN	NTC	01	35.08	5.7e+01	6.60	50.18
C4	UNKN	RUN 1 PRE-LYSIS	02	16.66	2.0e+06	74605.9	1955786.
C5	UNKN	RUN 1 PRE-LYSIS	02	16.67	2.0e+06	74605.9	1955786.
D4	UNKN	RUN 1 PRE-LYSIS	02	16.75	1.9e+06	74605.9	1955786.
D5	UNKN	RUN 1 PRE-LYSIS	02	16.80	1.9e+06	74605.9	1955786.
E4	UNKN	RUN 1 PRE-CACL	03	16.28	2.5e+06	47657.2	2544000.
E5	UNKN	RUN 1 PRE-CACL	03	16.21	2.6e+06	47657.2	2544000.
F4	UNKN	RUN 1 PRE-CACL	03	16.28	2.5e+06	47657.2	2544000.
F5	UNKN	RUN 1 PRE-CACL	03	16.27	2.5e+06	47657.2	2544000.
G4	UNKN	RUN 1 RETENTATE	04	25.77	1.1e+04	4942.09	7732.48
G5	UNKN	RUN 1 RETENTATE	04	25.59	1.3e+04	4942.09	7732.48
H4	UNKN	RUN 1 RETENTATE	04	27.78	3.6e+03	4942.09	7732.48
H5	UNKN	RUN 1 RETENTATE	04	27.92	3.3e+03	4942.09	7732.48
A6	UNKN	RUN 1 WASH 1	05	26.40	7.9e+03	3725.44	4793.79
A7	UNKN	RUN 1 WASH 1	05	26.37	8.1e+03	3725.44	4793.79
B6	UNKN	RUN 1 WASH 1	05	29.21	1.6e+03	3725.44	4793.79
B7	UNKN	RUN 1 WASH 1	05	29.29	1.5e+03	3725.44	4793.79

Figure 9-28 An example of the PDF report generated by the MagNA Pure machine as part of the gDNA assay. Note that four independent samples are combined into 1 result. The results were reported in copies per well, figures which were then converted into mass based units.

Calculation of specific yields

Yield calculations for Fermentation 1: DH1 Parental A

Par V1 Time point	Elapsed Time (hrs)	HPLC Area A	HPLC Area B	Mean Area	Plasmid Conc. (µg/ml)	Plasmid Mass (µg)	Pld Mass [St Dev]	WCW (g/L)	WCW [St Dev]	Optical Density (A600)	WCW Pellet Mass (g)	Plasmid Specific Yield (µg/gWCW)	Spec Yld [St Dev]	Volumetric Yield (mg/L)	Vol Yield [St dev]
0	0	16103	18806	17454.5	1.48	0.15	0.0231	36.8	2.121	12.02	0.0153078	9.65	1.511	0.0030	0.056
2	10.25	30000	31000	30500	3.06	0.31	0.0086	15.85	2.616	5.8	0.0136638	22.36	0.626	0.35	0.010
3	11.5	33663	30751	32207	3.26	0.33	0.0249	24.3	5.233	8.3	0.0146386	22.28	1.702	0.54	0.041
4	12.5	27341	24598	25969.5	2.51	0.25	0.0235	32.4	1.131	12.2	0.0132787	18.88	1.767	0.61	0.057
5	13.5	21285	23426	22355.5	2.07	0.21	0.0183	45.1	0.636	14.5	0.0155517	13.31	1.178	0.60	0.053
6	14.5	22210	24013	23111.5	2.16	0.22	0.0154	51.7	0.212	17.8	0.0145225	14.88	1.062	0.77	0.055
7	16.25	18894	19711	19302.5	1.70	0.17	0.0070	87.7	2.192	30.9	0.0141909	11.98	0.493	1.05	0.043
8	17	17260		17260	1.45	0.15	0.0000	95.3	0.071	34.8	0.0136925	10.61	0.000	1.01	0.000
9	18	15633	17151	16392	1.35	0.13	0.0130	93.4	0.000	40.2	0.0116169	11.61	1.118	1.08	0.104

Yield calculations for Fermentation 2: DH1 Parental B

PAR V2 Time point	Elapsed Time (hrs)	HPLC Area A	HPLC Area B	Mean Area	Plasmid Conc. (µg/ml)	Plasmid Mass (µg)	Pld Mass [St Dev]	WCW (g/L)	WCW [St Dev]	Optical Density (A600)	WCW Pellet Mass (g)	Plasmid Specific Yield (µg/gWCW)	Spec Yld [St Dev]	Volumetric Yield (mg/L)	Vol Yield [St dev]
0	0	16103	18806	17454.5	1.48	0.15	0.0231	36.8	2.121	12.02	0.0153078	9.65	1.511	0.0030	0.056
2	10.25	18806	24701	21753.5	2.00	0.20	0.0504	16.5	0.283	6.13	0.0134584	14.84	3.748	0.24	0.062
3	11.5	22688	24593	23640.5	2.23	0.22	0.0163	27.05	0.495	8.6	0.0157267	14.15	1.036	0.38	0.028
4	12.5	25585	25480	25532.5	2.45	0.25	0.0009	31.95	1.061	10.84	0.0147371	16.65	0.061	0.53	0.002
5	13.5	26812	23187	24999.5	2.39	0.24	0.0310	41.15	0.354	14.12	0.0145715	16.40	2.129	0.67	0.088
6	14.5	30824	30519	30671.5	3.08	0.31	0.0026	48.65	0.212	19.08	0.0127490	24.13	0.205	1.17	0.010
7	16.25	28744	30358	29551	2.94	0.29	0.0138	82.15	4.344	29.8	0.0137836	21.33	1.002	1.75	0.082
8	17	16850		16850	1.40	0.14	0.0000	93.3	2.404	34.8	0.0134052	10.47	0.000	0.98	0.000
9	18	23026	19193	21109.5	1.92	0.19	0.0328	92.1	0.849	39.1	0.0117775	16.29	2.785	1.50	0.256
10	18.5	16514	18376	17445	1.48	0.15	0.0159	90.35	0.354	41.1	0.0109915	13.42	1.449	1.21	0.131

Yield calculations for Fermentation 3: DH1 p5176 (116kb) A

p5176 116kb V1 Time point	Elapsed Time (hrs)	HPLC Area A	HPLC Area B	Mean Area	Plasmid Conc. (µg/ml)	Plasmid Mass (µg)	Pld Mass [St Dev]	WCW (g/L)	WCW [St Dev]	Optical Density (A600)	WCW Pellet Mass (g)	Plasmid Specific Yield (µg/gWCW)	Spec Yld [St Dev]	Volumetric Yield (mg/L)	Vol Yield [St dev]	Moles of Plasmid	Plasmid Copy No. (copies/cell)	Copy No [St Dev]
0	0	46328	52232	49280	5.33	0.53	0.0505	36.55	1.344	11.24	0.0162589	32.77	3.107	0.011	0.001	4192039545	3.35	0.32
2	10.25	49088	50600	49844	5.40	0.54	0.0129	19.5	0.354	5.66	0.0172261	31.32	0.751	0.61	0.015	4245737502	3.40	0.08
3	11.5	61496	54598	58047	6.39	0.64	0.0590	25.1	0.354	7.84	0.0160077	39.91	3.687	1.00	0.093	5026738106	4.02	0.37
4	12.5	46773	62022	54397.5	5.95	0.59	0.1305	28.5	0.071	10.12	0.0140810	42.23	9.266	1.20	0.264	4679272337	3.74	0.82
5	13.5	65945	94679	80312	9.08	0.91	0.2458	36.7	0.212	14.44	0.0127078	71.47	19.346	2.62	0.710	7146569686	5.72	1.55
6	14.5	76638	53328	64983	7.23	0.72	0.1994	45.35	0.318	17.72	0.0127963	56.48	15.586	2.56	0.707	5687108725	4.55	1.26
7	16.25	65387	70468	67927.5	7.58	0.76	0.0435	69.06	0.369	26.4	0.0130795	57.98	3.324	4.00	0.230	5967452048	4.77	0.27
8	17	57265	76373	66819	7.45	0.74	0.1635	84.4	0.424	31.4	0.0134395	55.43	12.165	4.68	1.027	5861912713	4.69	1.03
9	18	42973	51644	47308.5	5.09	0.51	0.0742	89	0.141	39.5	0.0112658	45.17	6.585	4.02	0.586	4004334719	3.20	0.47
10	18.5	49036	50503	49769.5	5.39	0.54	0.0126	89.5	0.636	38.5	0.0116234	46.35	1.080	4.15	0.097	4238644421	3.39	0.08

Figure 9-29 Tables showing examples of the tables used to calculate specific plasmid yield of of the ferntations aswell as volumetric yield and plasmid copy number.

(vii) Topology Balance

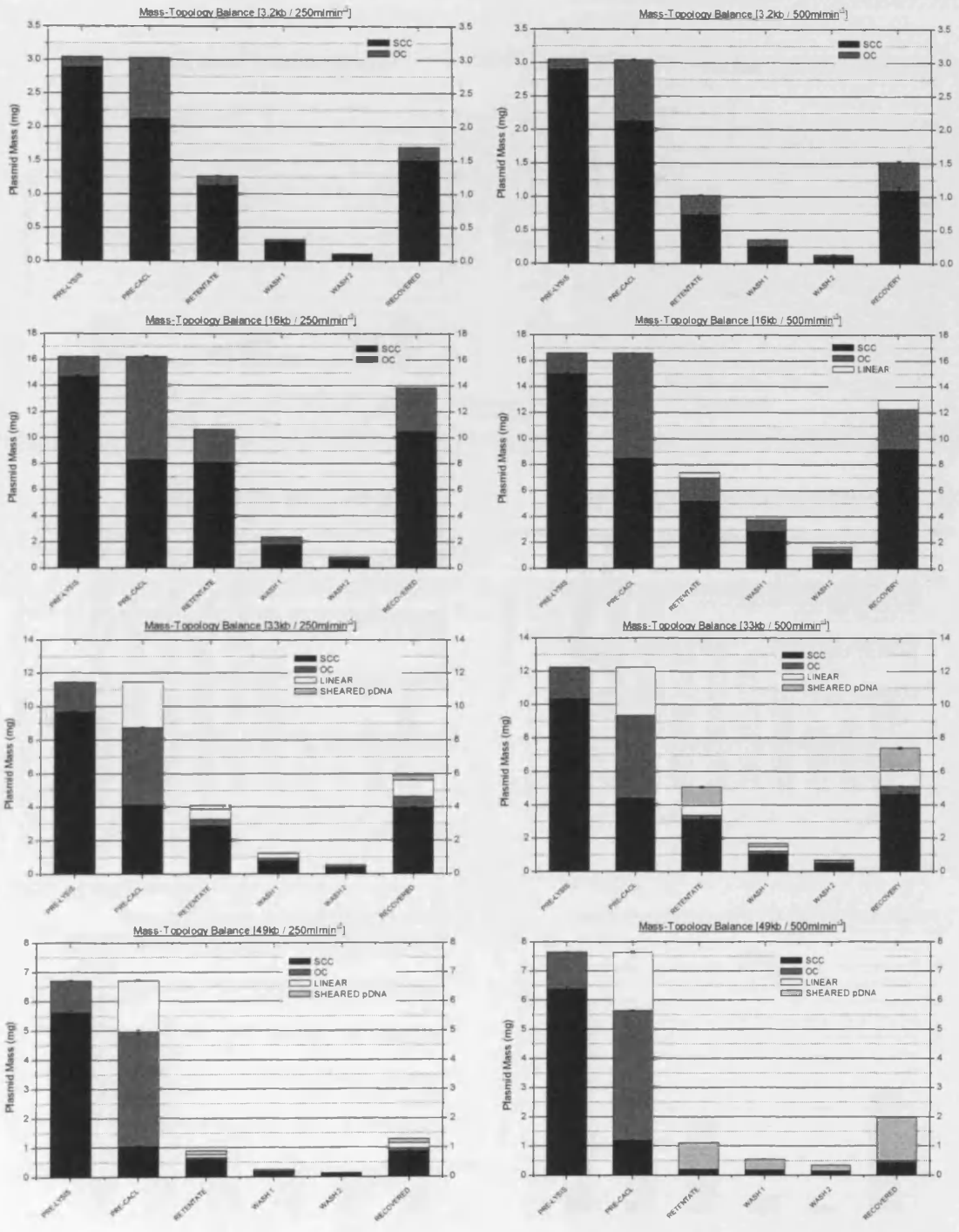

Figure 9-30 Figures applying the percentage toplogy results produced by gel analysis of the different streams to the plasmid mass balance data so as to indicate the proportion of plasmid mass in each form. Avergaes from each of the two runs were taken.

RUN 1 [pGEM11]

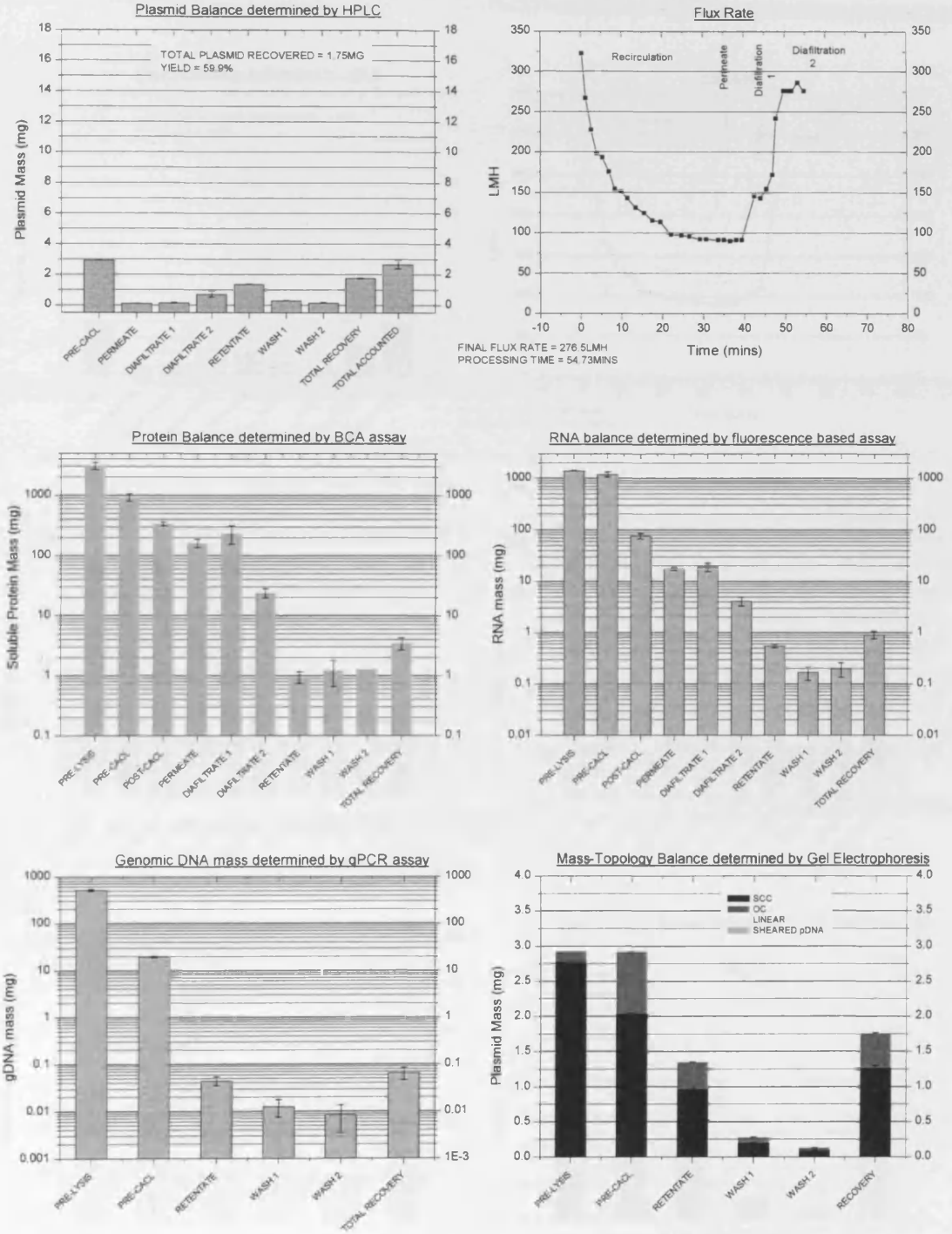

Figure 9-31 Run 1 Data from a single DSP operation. Shown is the plasmid mass balance, the flux recorded during the UF operation, the soluble protein, RNA and gDNA masses recorded at each stage and the plasmid toplogy balance.

RUN 2 [pGEM11]

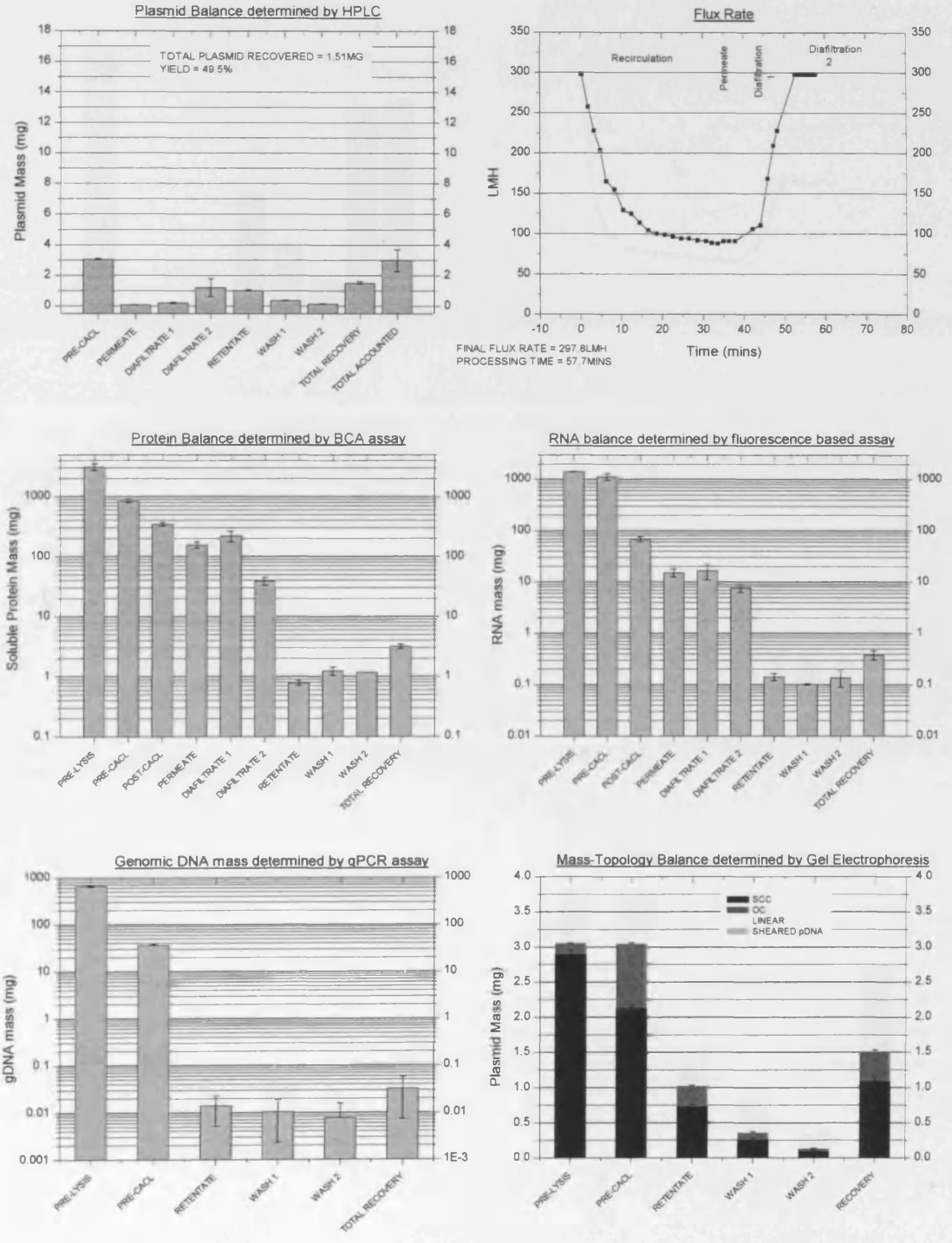

Figure 9-32 Data from a single DSP operation. Shown is the plasmid mass balance, the flux recorded during the UF operation, the soluble protein, RNA and gDNA masses recorded at each stage and the plasmid toplogy balance.

RUN 3 [pGEM16]

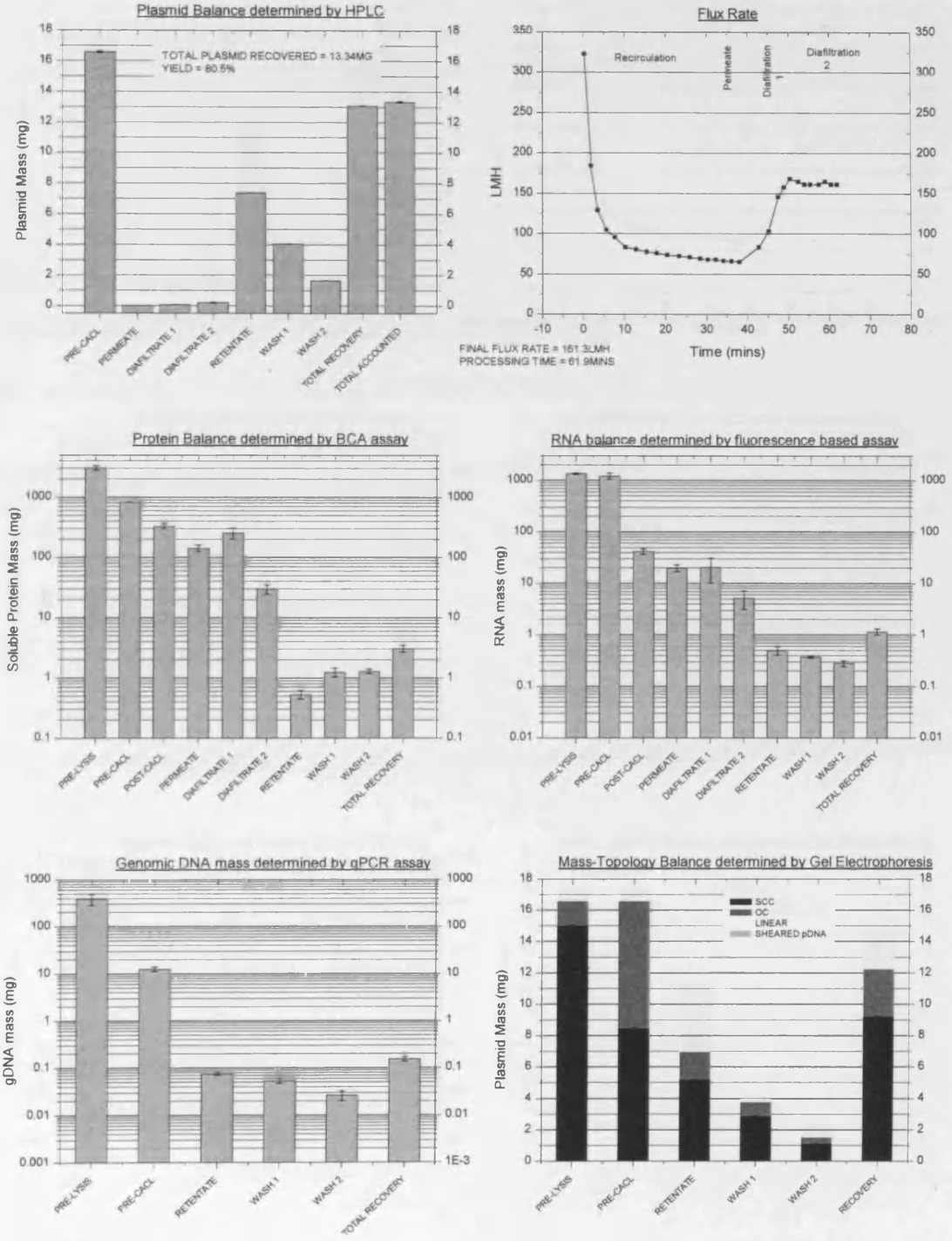

Figure 9-33

RUN 4 [pGEM16]

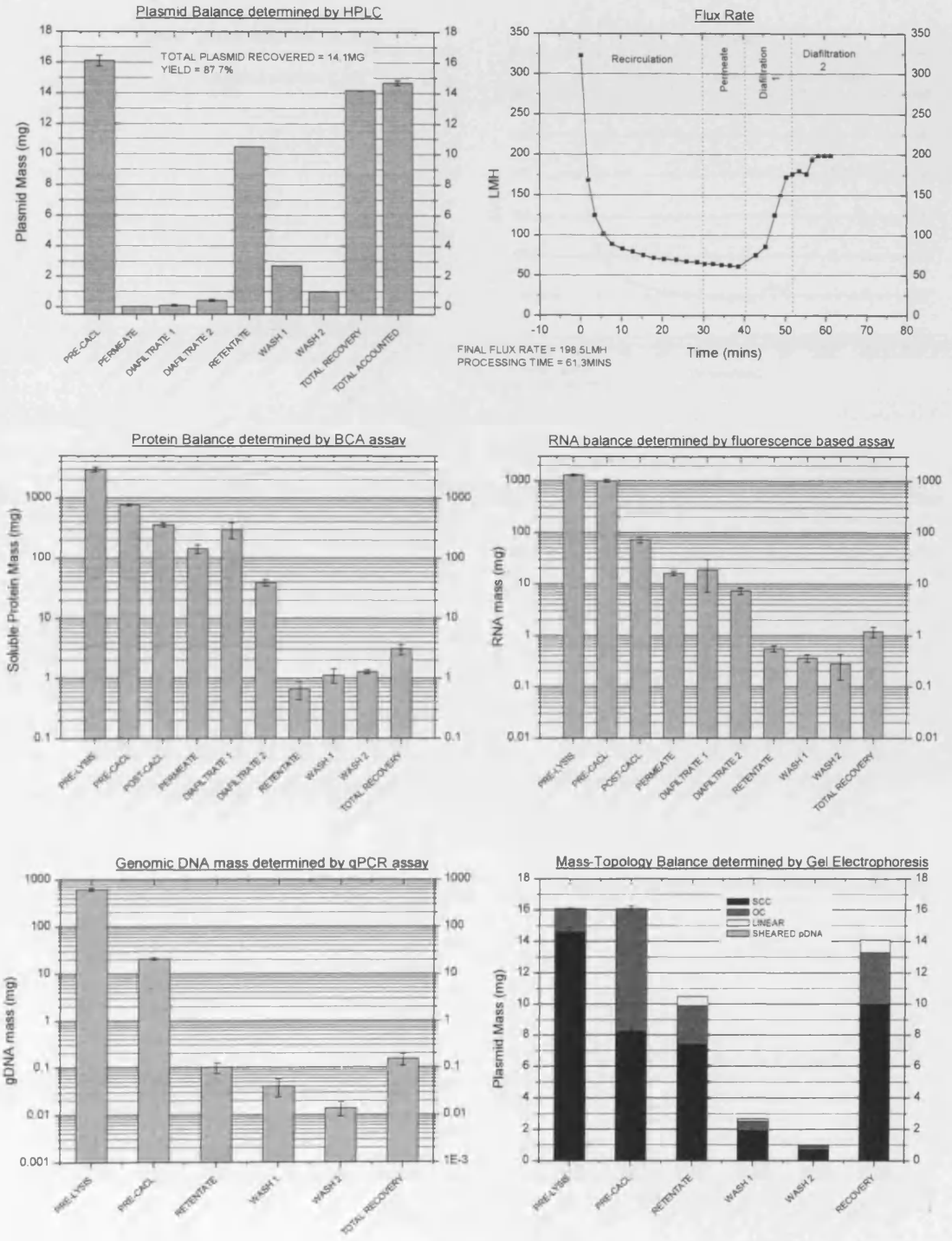

Figure 9-34

RUN 5 [pGEM33]

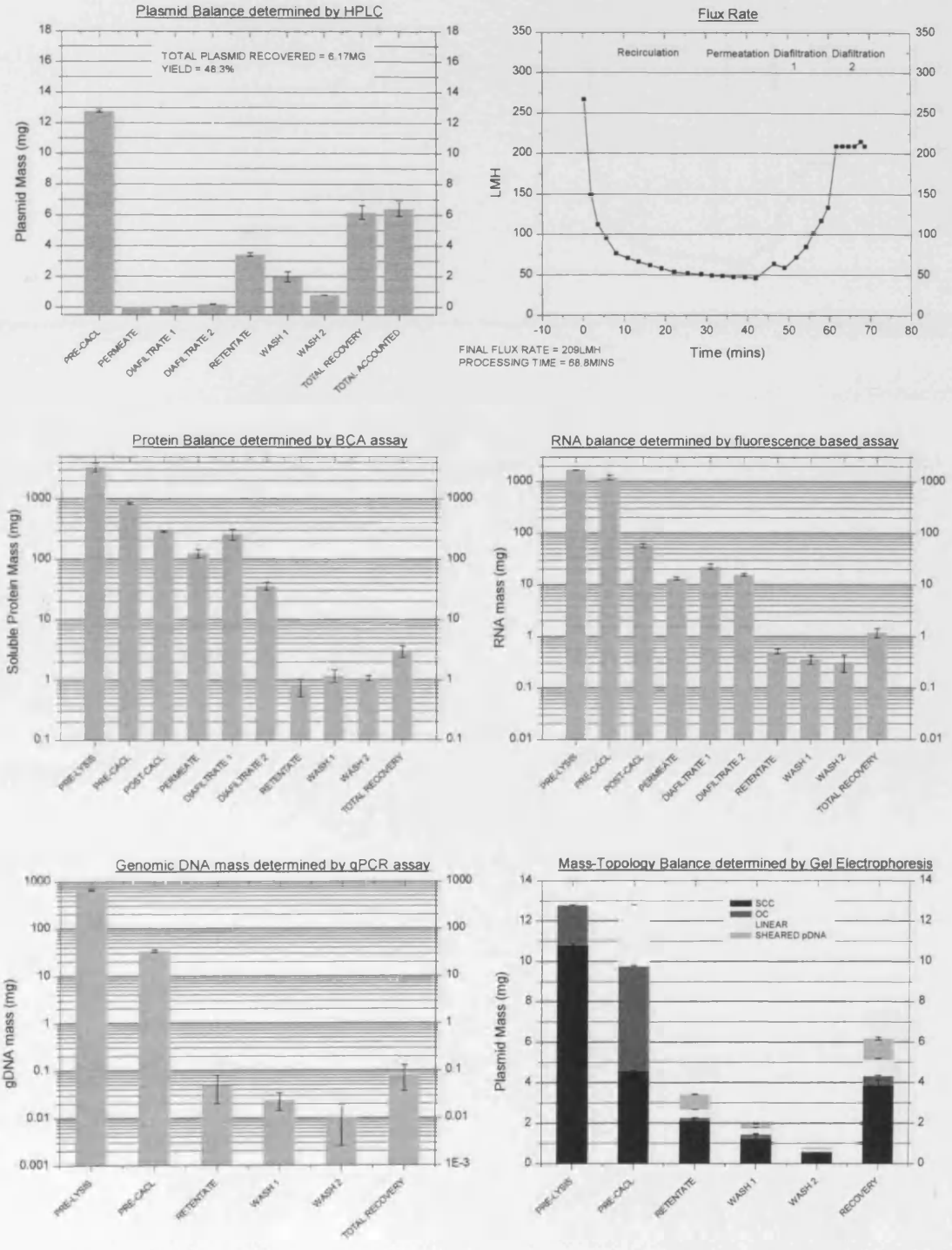

Figure 9-35

RUN 6 [pGEM33]

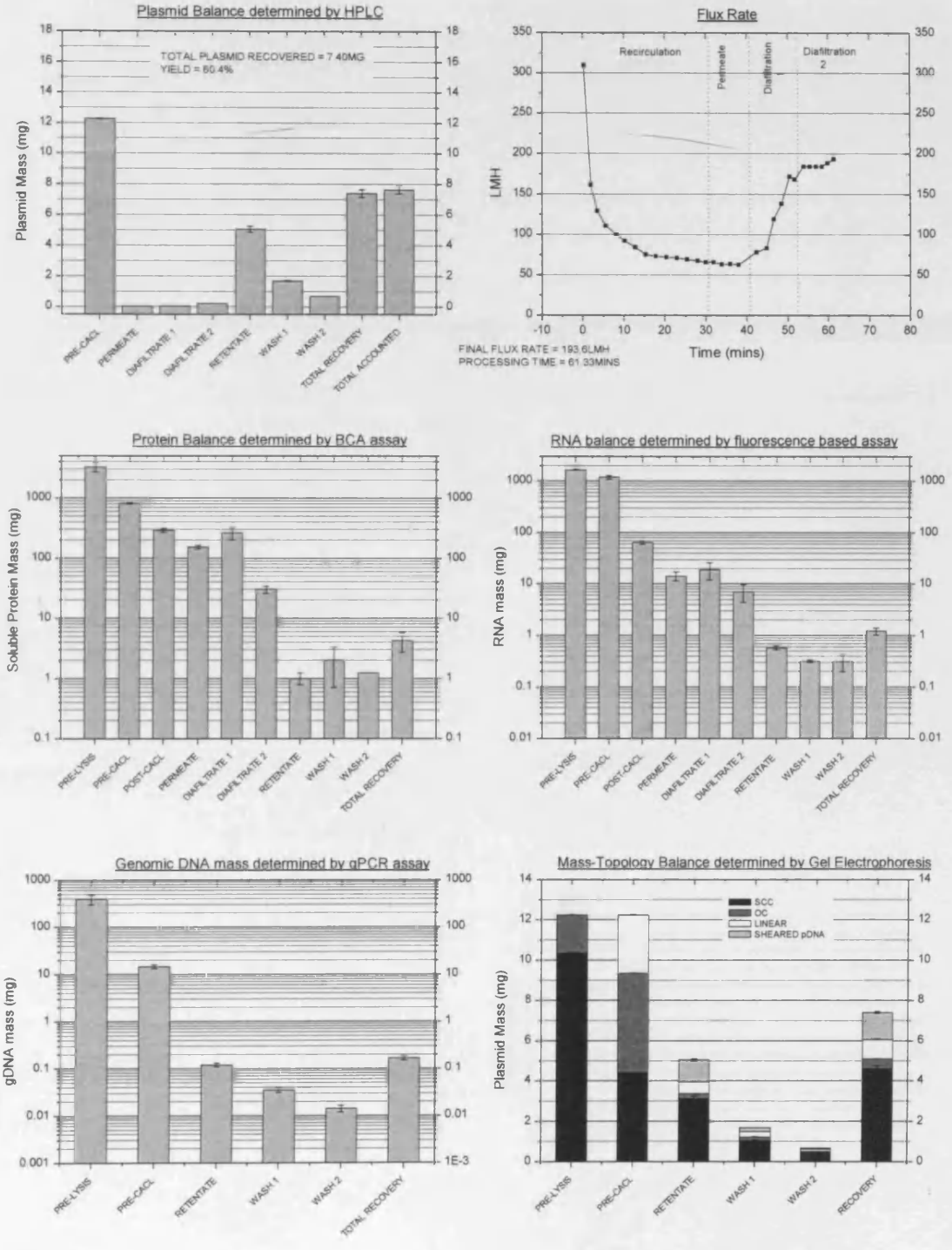

Figure 9-36

RUN 7 [pGEM49]

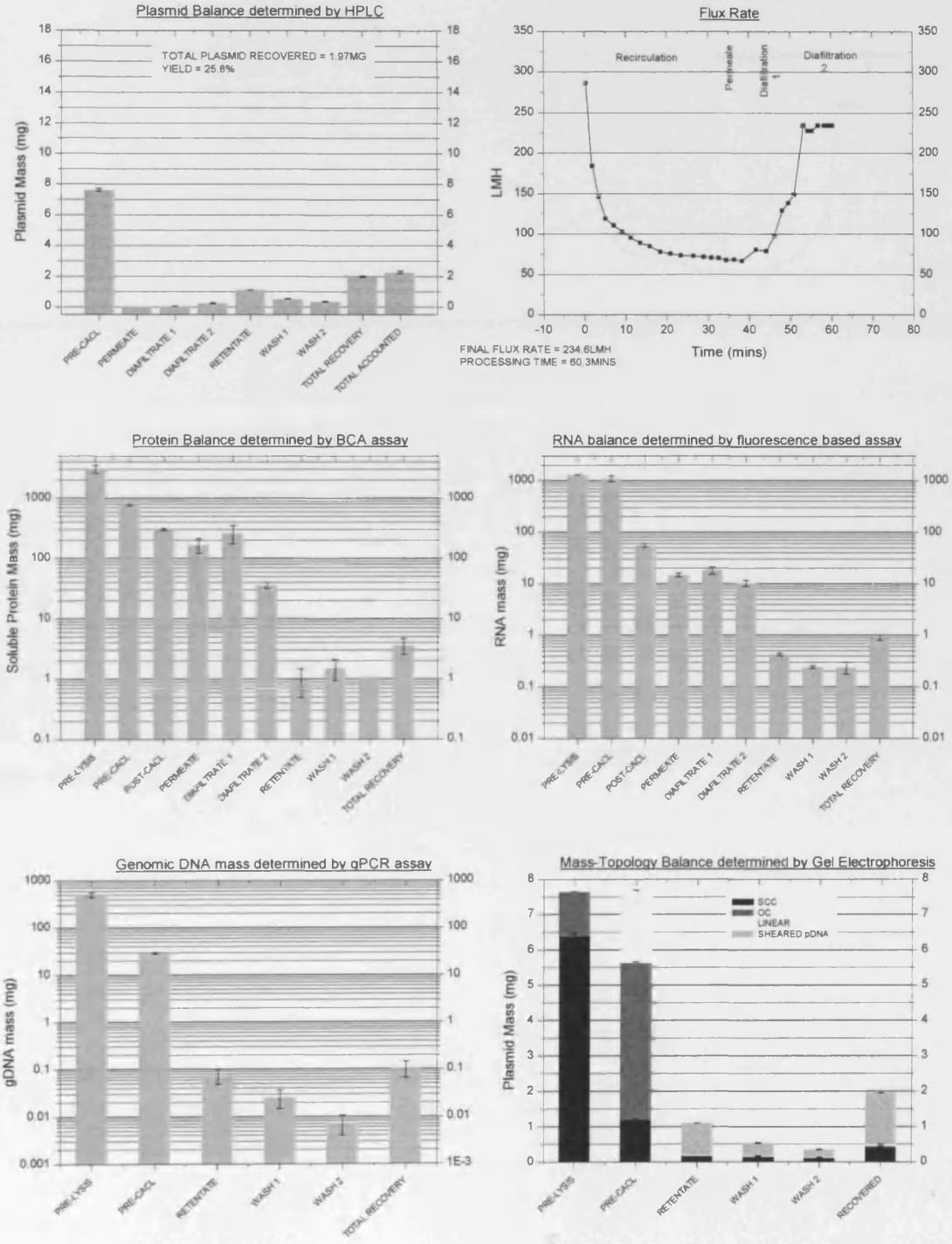

Figure 9-37

RUN 8 [pGEM49]

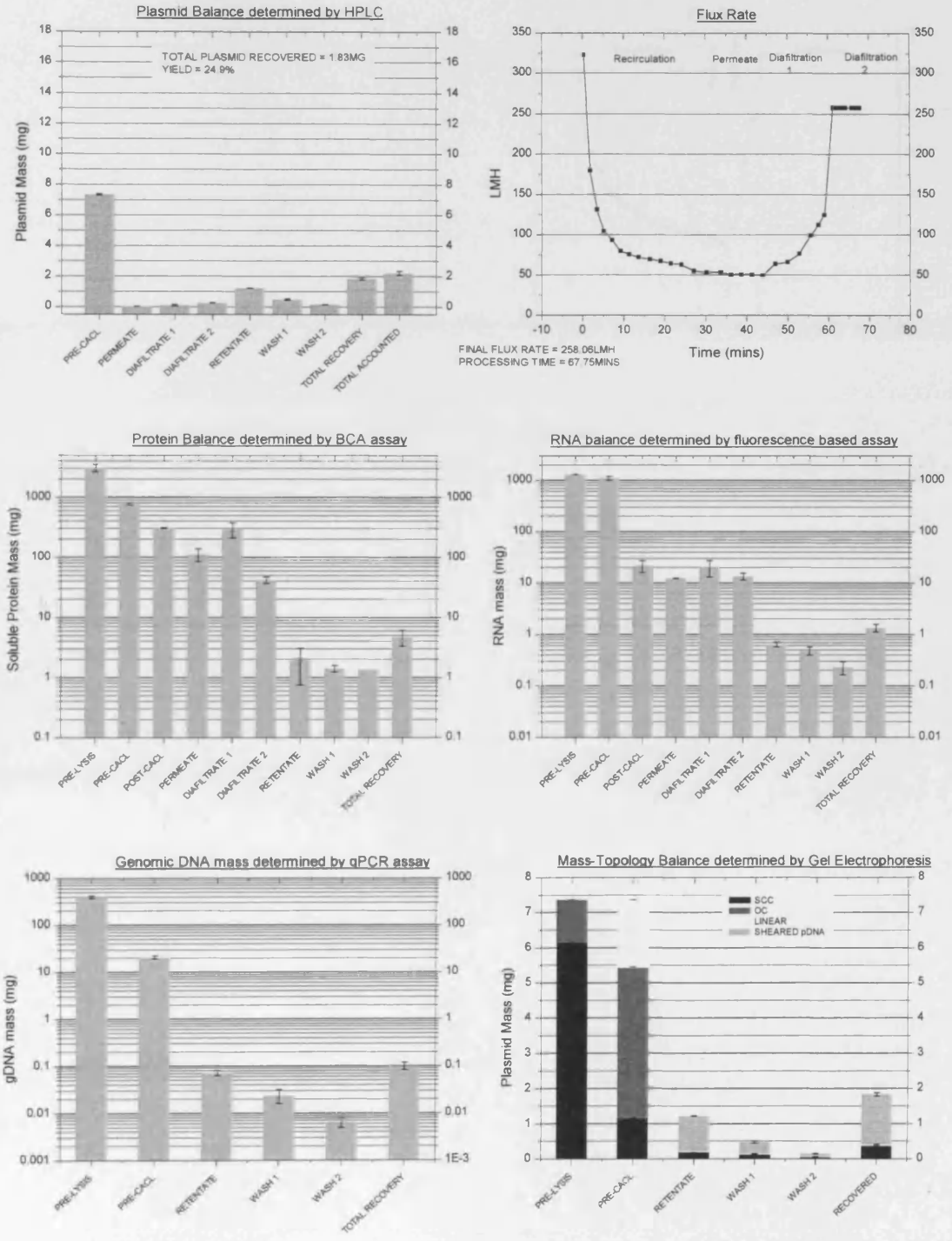

Figure 9-38

RUN 9 [P5176]

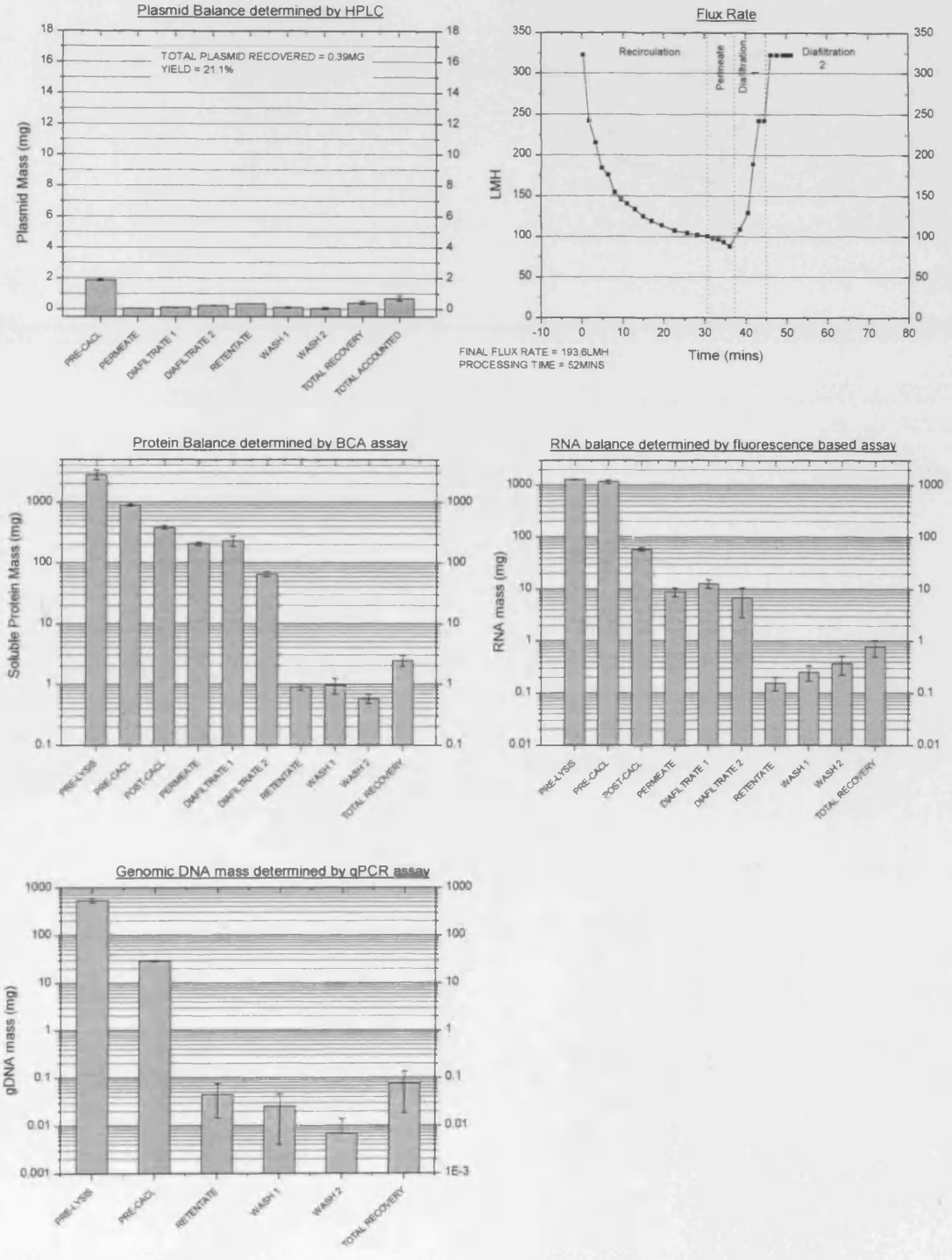

Figure 9-39

RUN 10 [p5176]

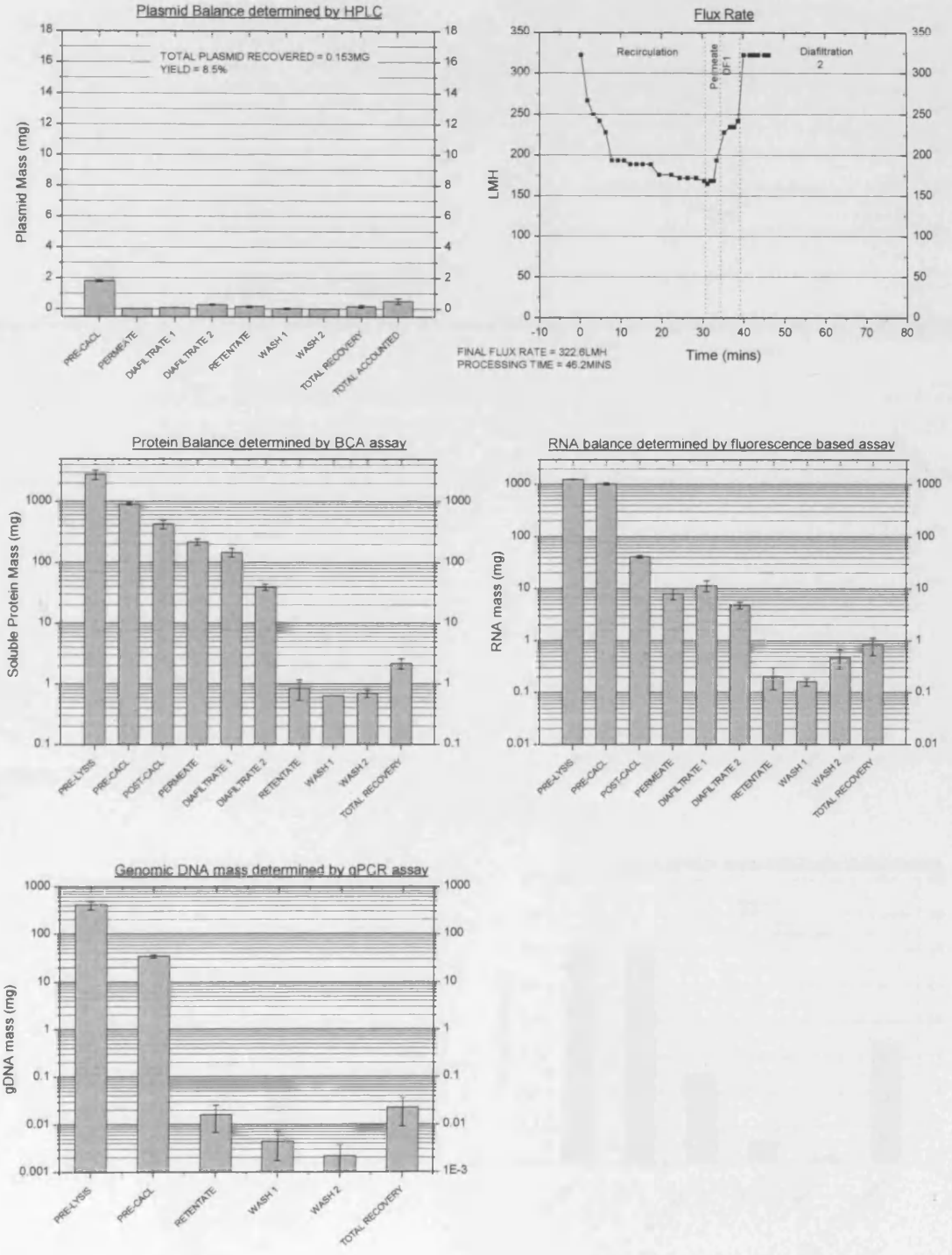

Figure 9-40

RUN 11 [pGEM11] 250mLmin^{-1}

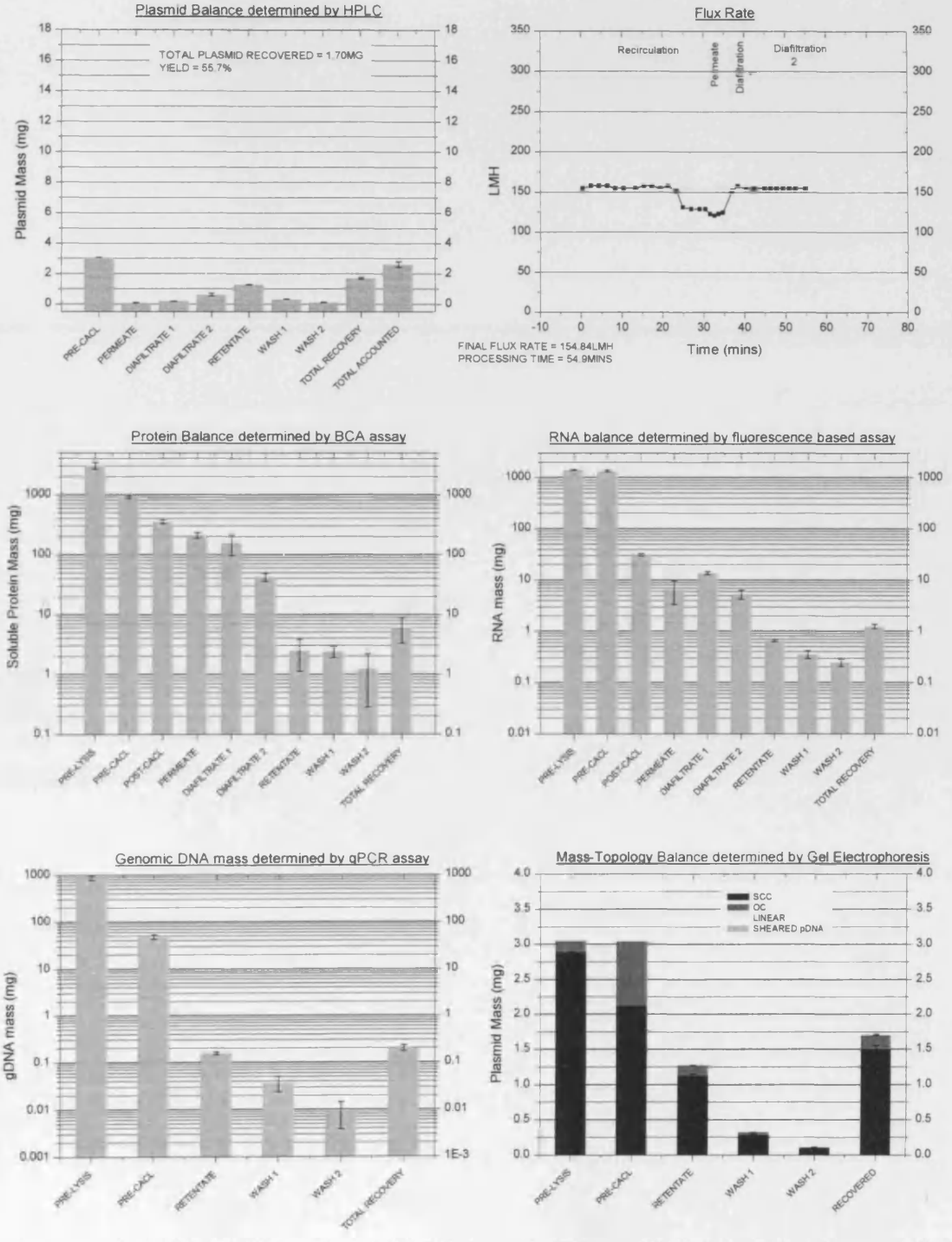

Figure 9-41

RUN 12 [pGEM11] 250mLmin^{-1}

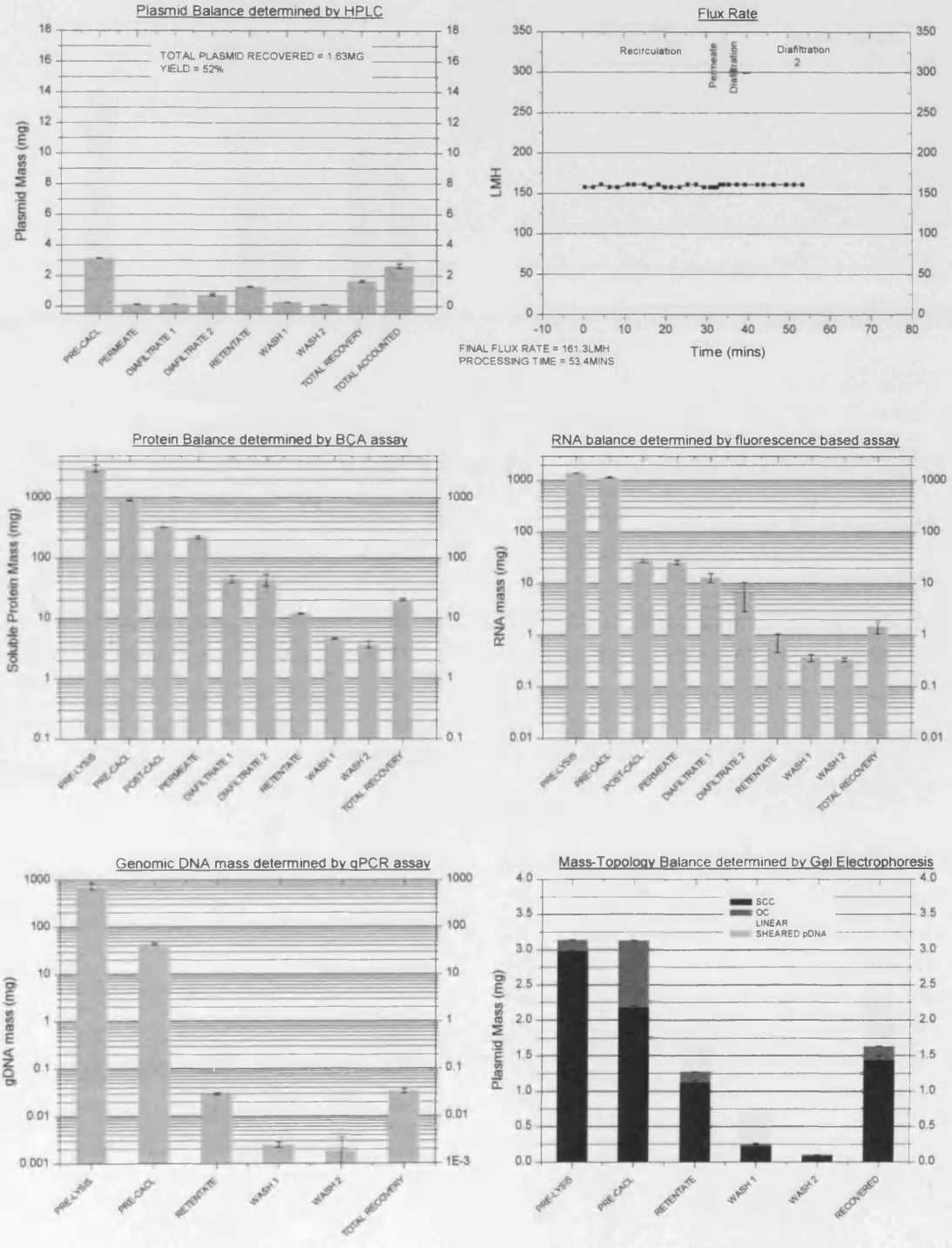

Figure 9-42

RUN 13 [pGEM16] 250mLmin^{-1}

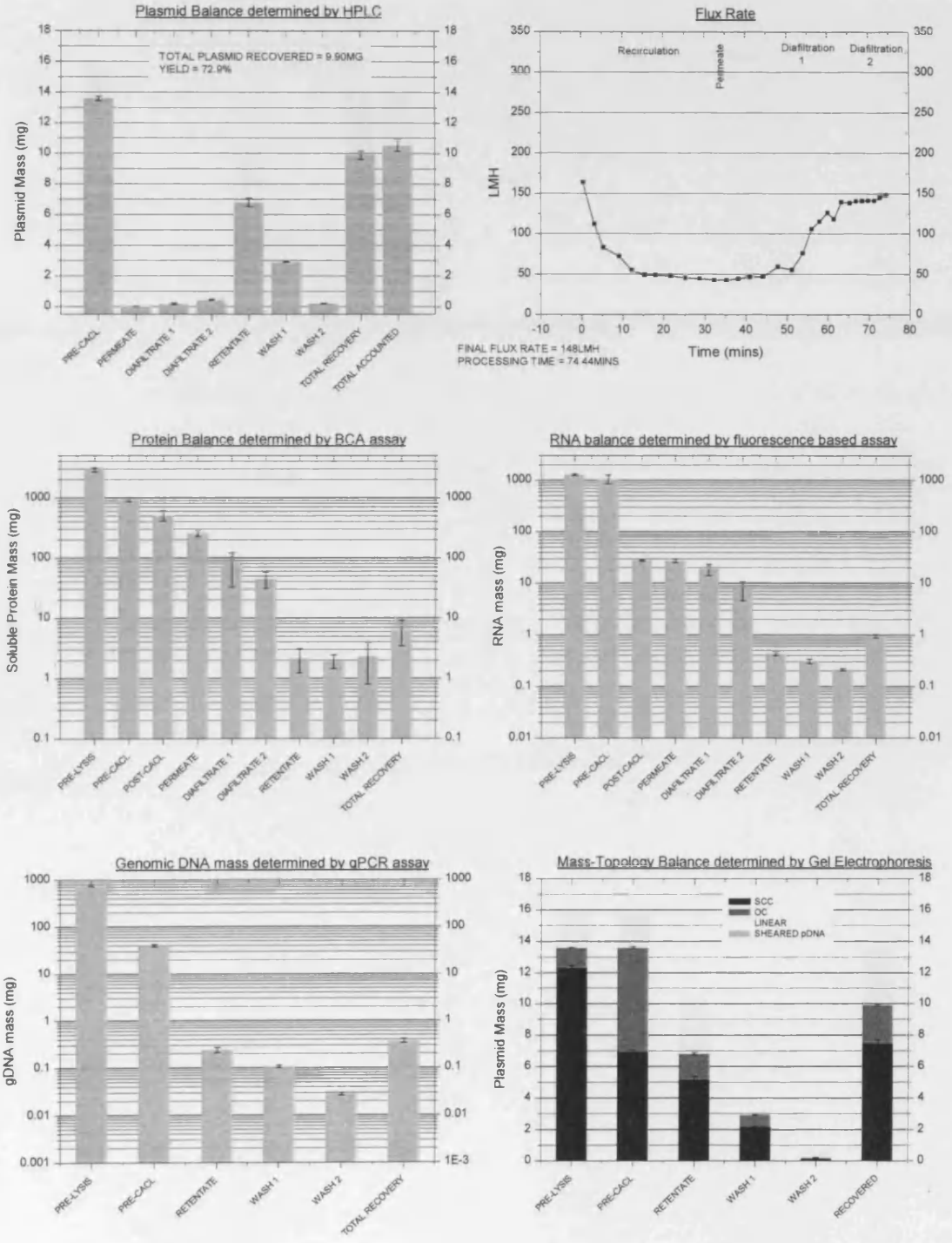

Figure 9-43

RUN 14 [pGEM16] 250mLmin^{-1}

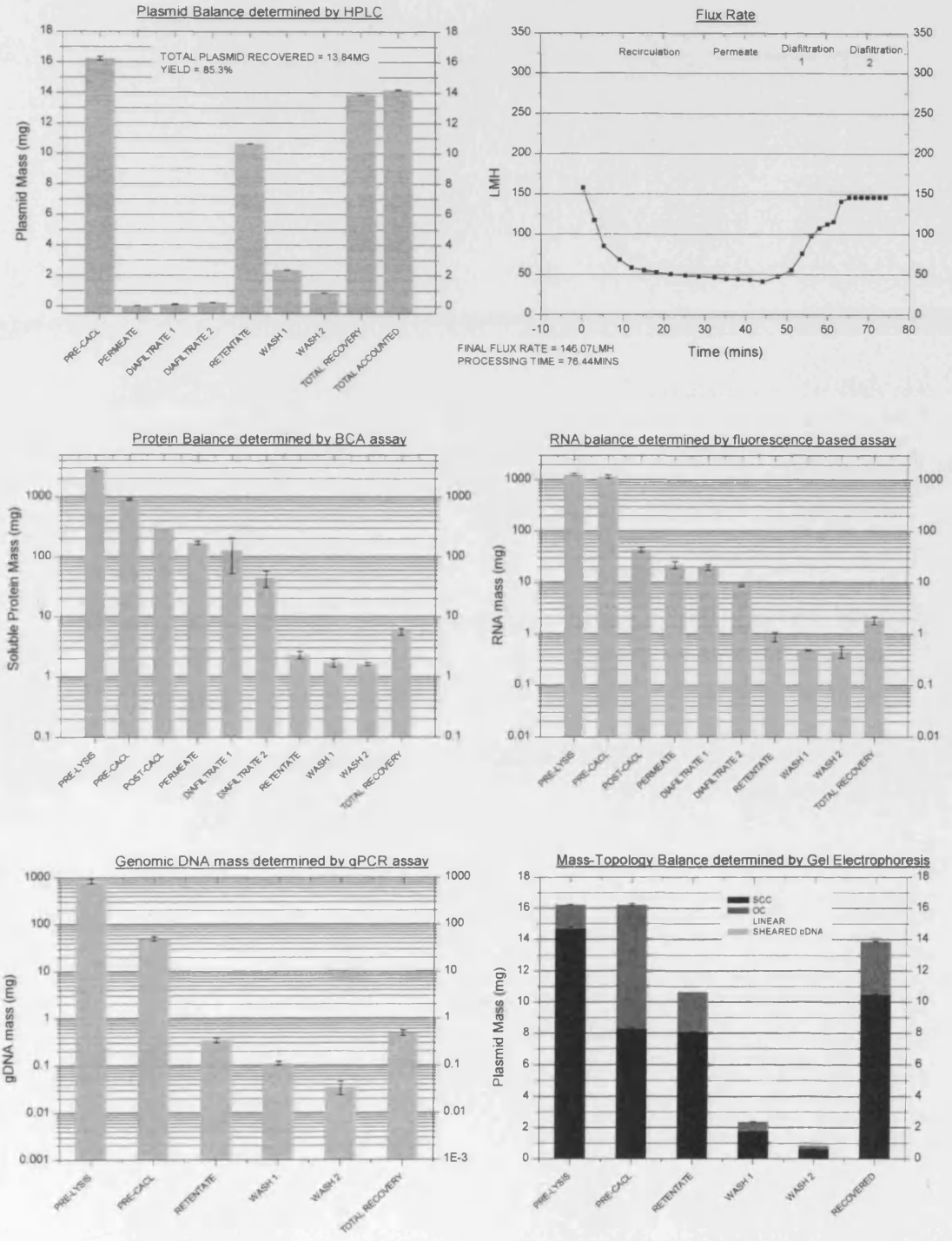

Figure 9-44

RUN 15 [pGEM 33] 250mLmin^{-1}

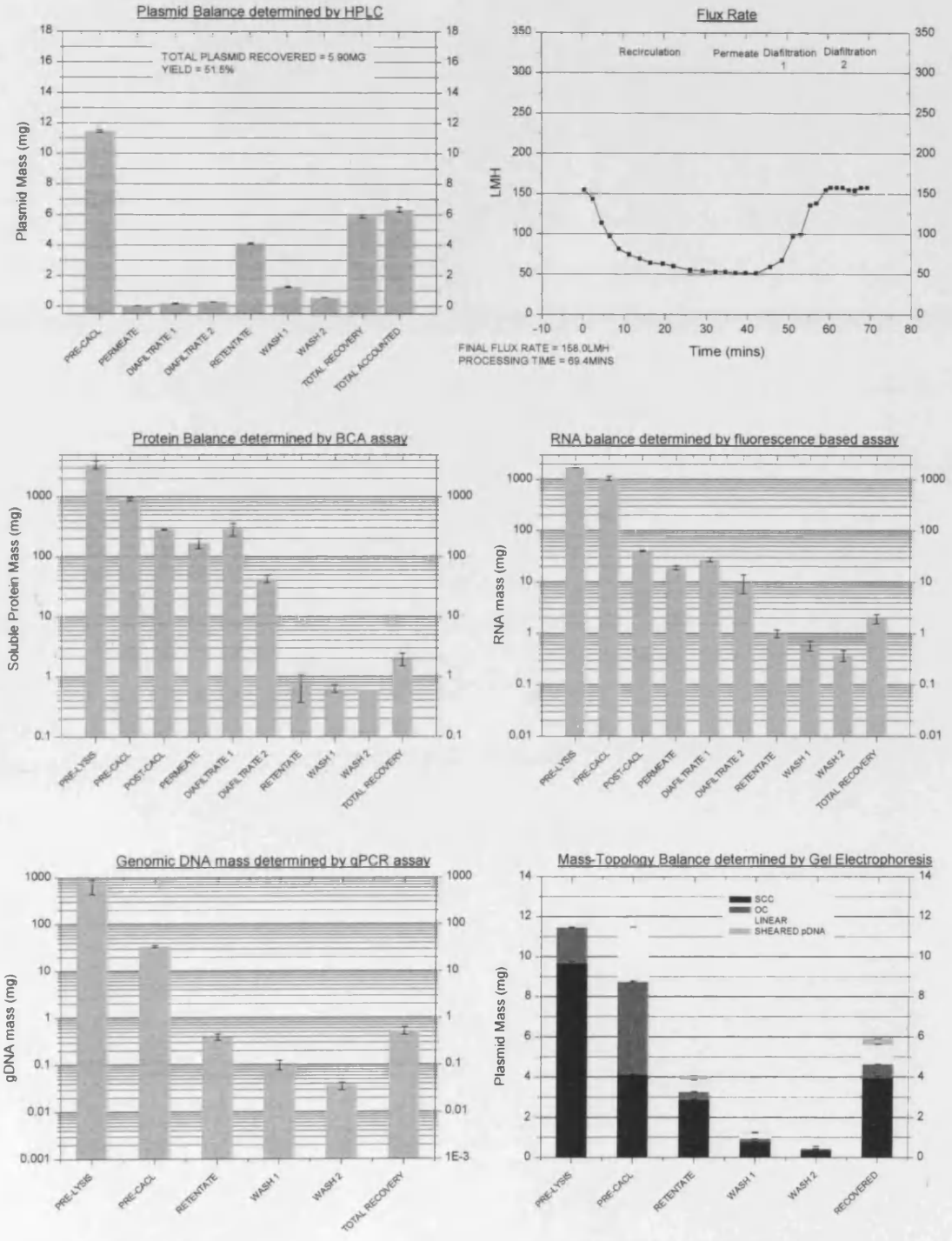

Figure 9-45

RUN 16 [pGEM 33] 250mLmin^{-1}

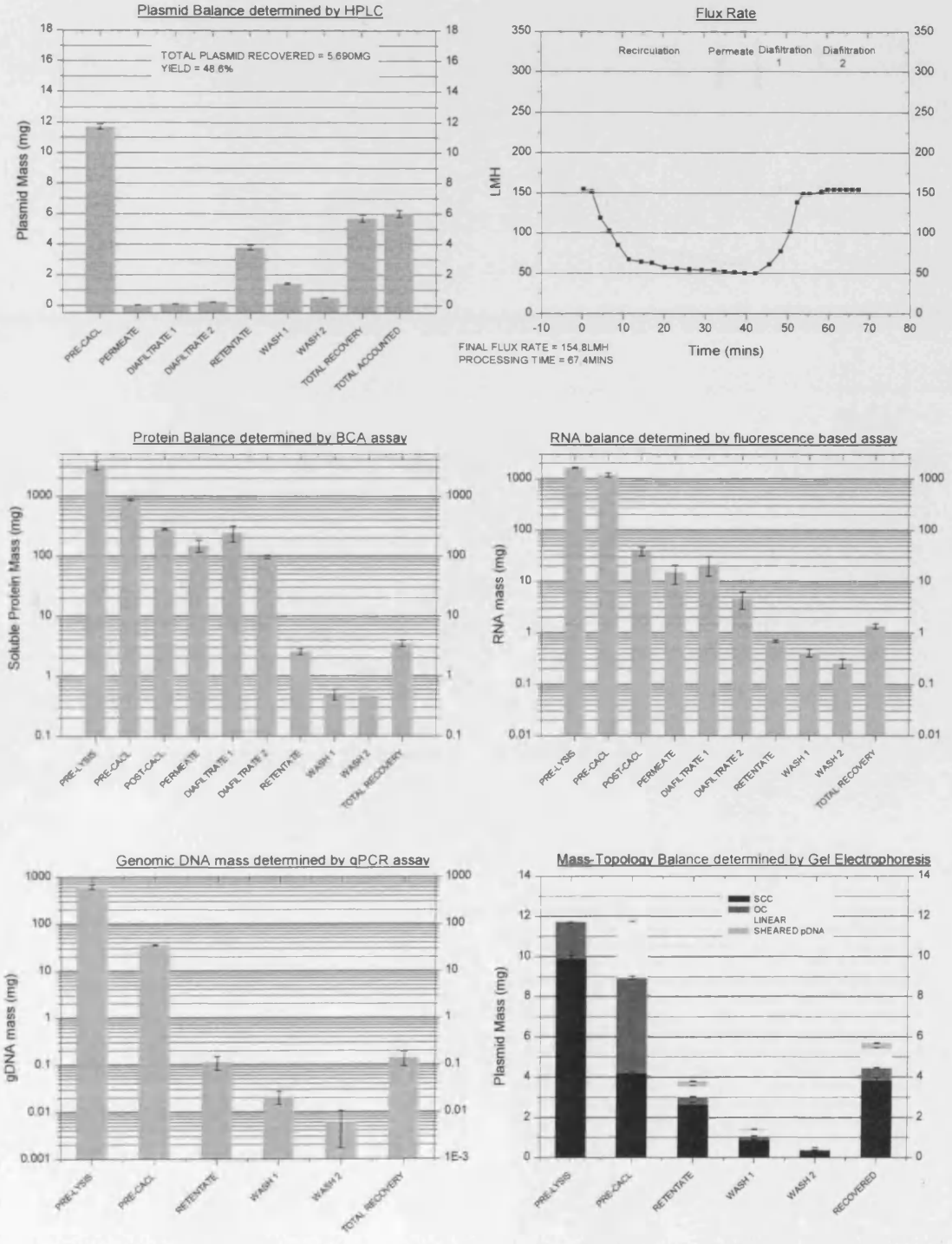

Figure 9-46

RUN 17 [pGEM 49] 250mLmin^{-1}

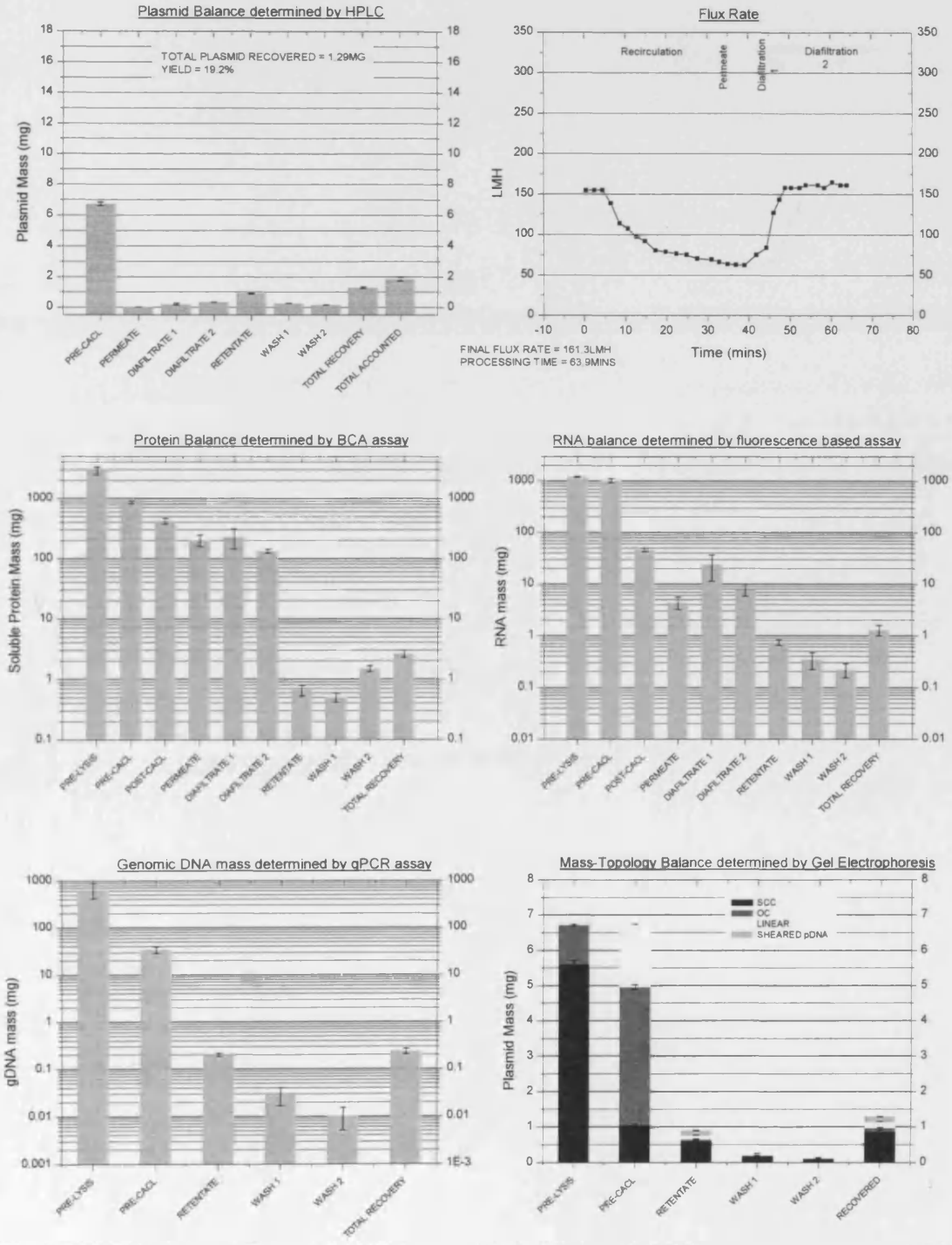

Figure 9-47

RUN 18 [pGEM 49] 250mLmin^{-1}

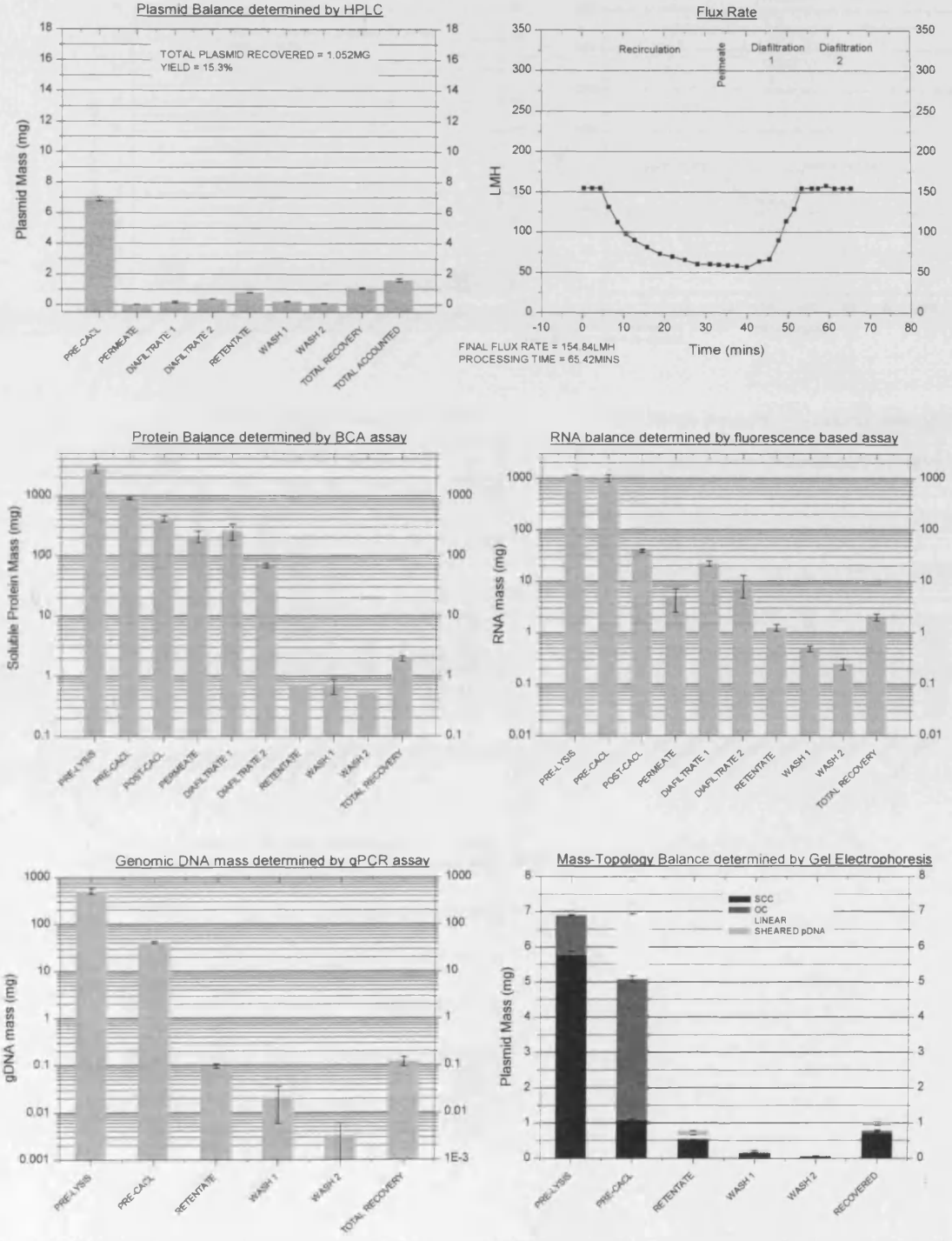

Figure 9-48

RUN 19 [p5176] 500mLmin^{-1}

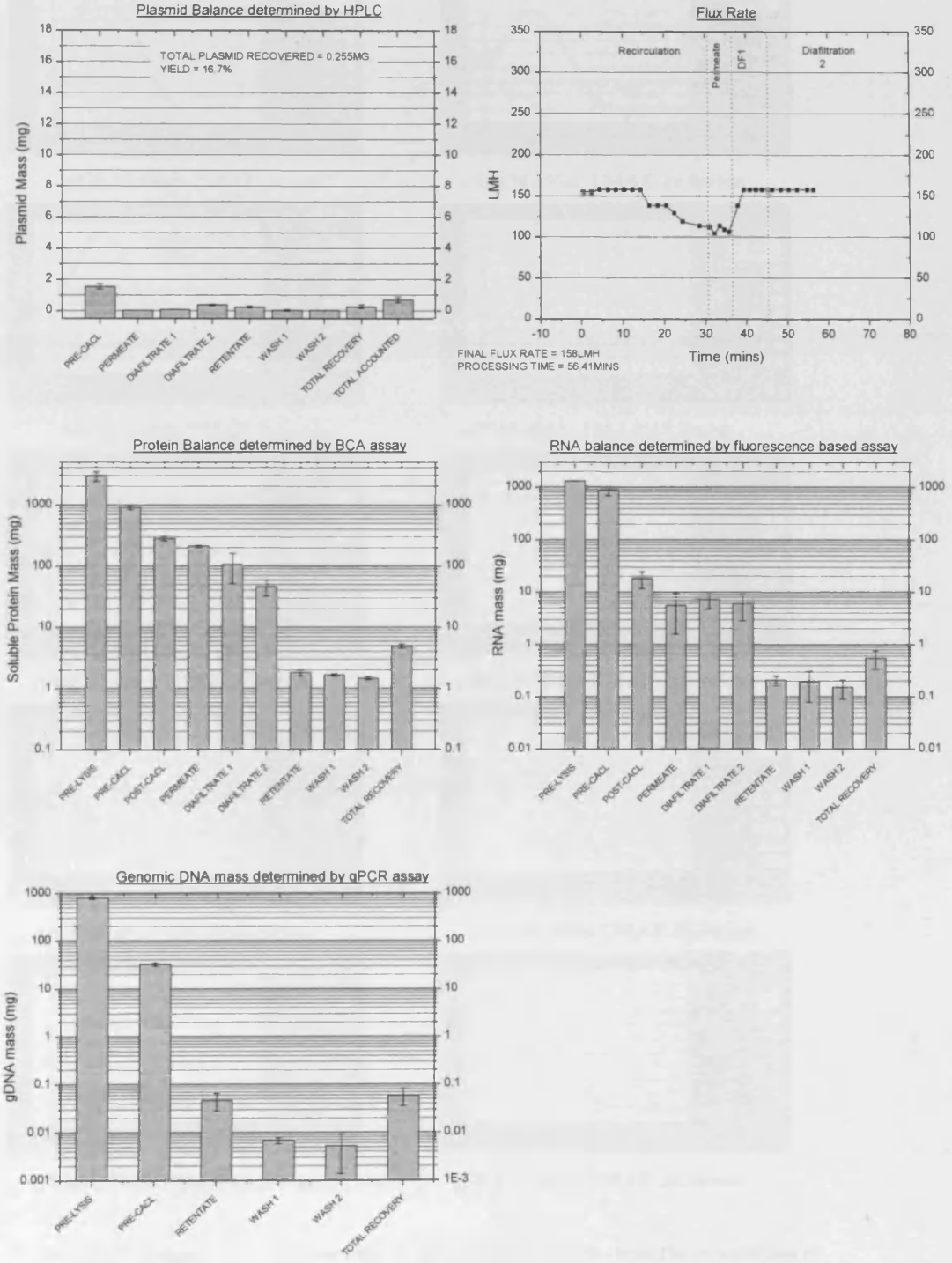

Figure 9-49 Run 19

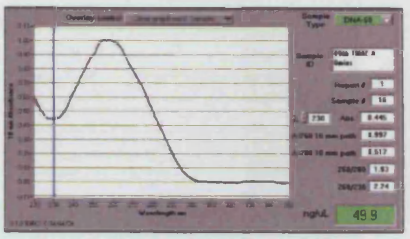

pGEM 49kb TMAE 0mins

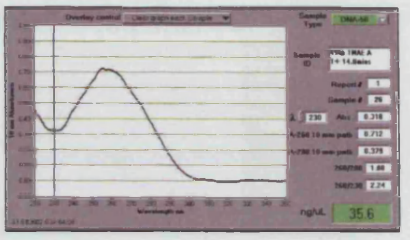

pGEM 49kb TMAE 14.0mins

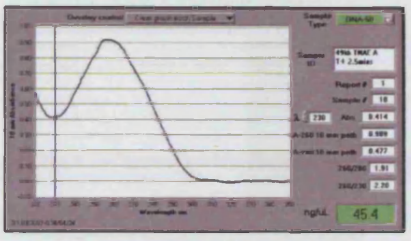

pGEM 49kb TMAE 2.5mins

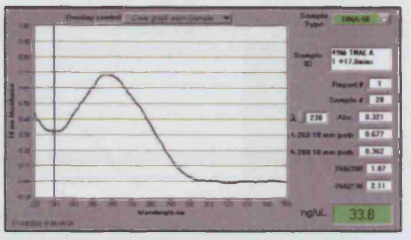

pGEM 49kb TMAE 17.0mins

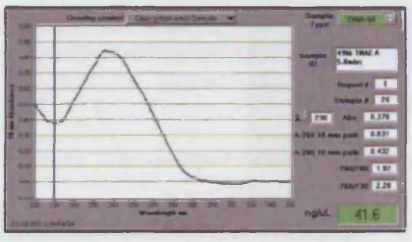

pGEM 49kb TMAE 5.0mins

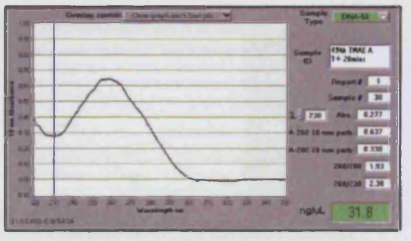

pGEM 49kb TMAE 20.0mins

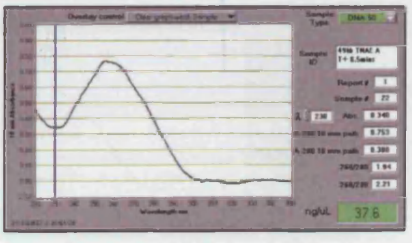

pGEM 49kb TMAE 8.5mins

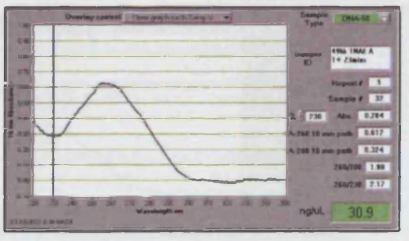

pGEM 49kb TMAE 23.0mins

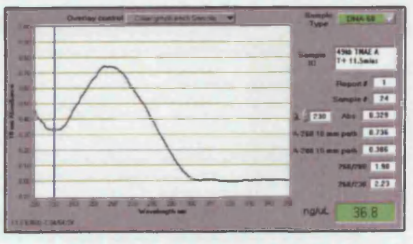

pGEM 49kb TMAE 11.5mins

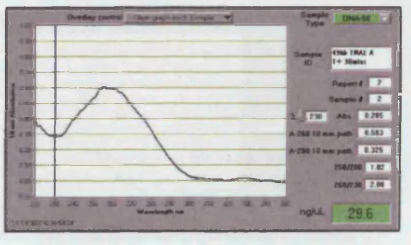

pGEM 49kb TMAE 30.0mins

Figure 9-50 Images recorded from the binding studies which show the proportion of plasmid remaining in solution at various points from the addition of the plasmid solution to the chromatographic matrix – pGEM49kb

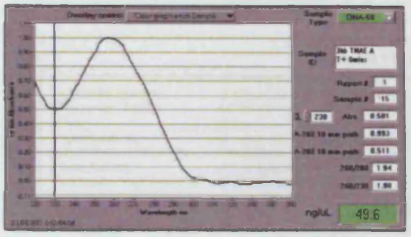

pGEM 3.2kb TMAE 0mins

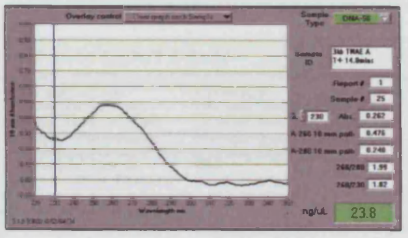

pGEM 3.2kb TMAE 14.0mins

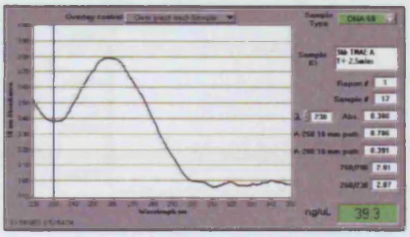

pGEM 3.2kb TMAE 2.5mins

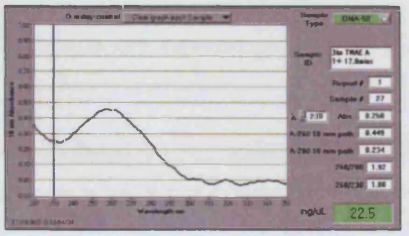

pGEM 3.2kb TMAE 17.0mins

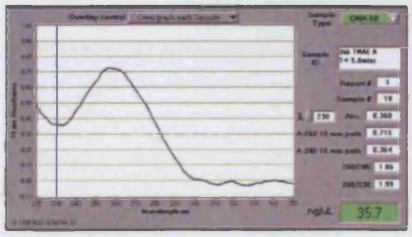

pGEM 3.2kb TMAE 5.0mins

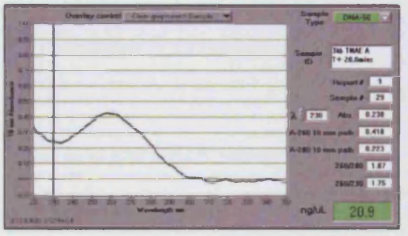

pGEM 3.2kb TMAE 20.0mins

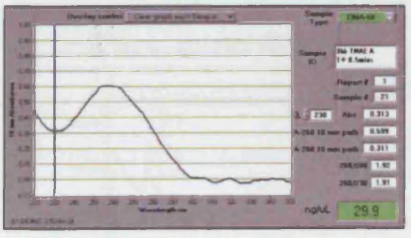

pGEM 3.2kb TMAE 8.5mins

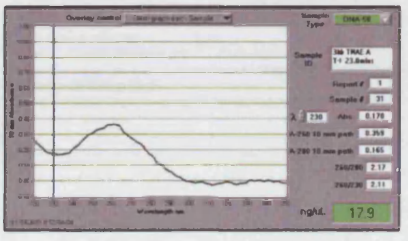

pGEM 3.2kb TMAE 23.0mins

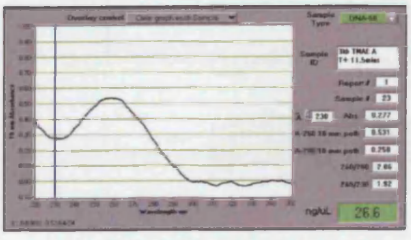

pGEM 3.2kb TMAE 11.5mins

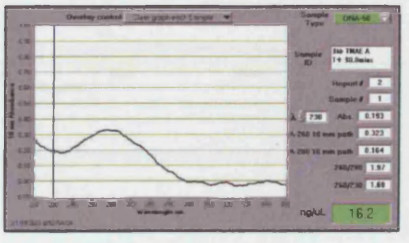

pGEM 3.2kb TMAE 30.0mins

Figure 9-51 Images recorded from the binding studies which show the proportion of plasmid remaining in solution at various points from the addition of the plasmid solution to the chromatographic matrix – pGEM 11 3.2kb

SAMPLE INFORMATION

Sample Name:	V1T11A	Acquired By:	thb30228
Sample Type:	Unknown	Date Acquired:	08-Apr-2005 04:25:23
Vial:	41	Acq. Method Set:	Dionex BAD 2 Meth
Injection #:	1	Date Processed:	09-Apr-2005 11:04:51
Injection Volume:	10.00 ul	Processing Method	Dionex BAD P
Run Time:	14.0 Minutes	Channel Name:	486
Sample Set Name:	DIO TB 07APR05	Proc. Chnl. Descr.:	

Auto-Scaled Chromatogram

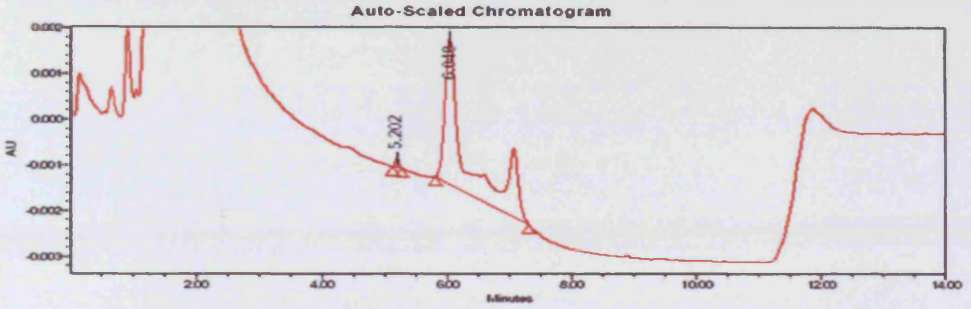

Peak Results

	Name	RT	Area	% Area
1		5.202	767	1.09
2		6.049	71327	98.94

SAMPLE INFORMATION

Sample Name:	V2T11A	Acquired By:	thb30228
Sample Type:	Unknown	Date Acquired:	07-Apr-2005 22:52:10
Vial:	19	Acq. Method Set:	Dionex BAD 2 Meth
Injection #:	1	Date Processed:	08-Apr-2005 10:59:53
Injection Volume:	10.00 ul	Processing Method	Dionex BAD P
Run Time:	14.0 Minutes	Channel Name:	486
Sample Set Name:	DIO TB 07APR05	Proc. Chnl. Descr.:	

Auto-Scaled Chromatogram

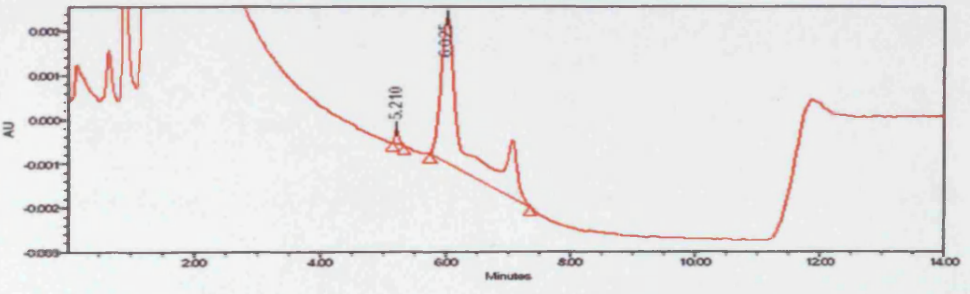

Peak Results

	Name	RT	Area	% Area
1		5.210	1481	1.82
2		6.025	79870	98.18

REFERENCES

1. **Adam,R.E. and Zimm,B.H.** (1977) *Shear degradation of DNA 1.* Nucleic Acids Res., 4, 1513-1537.

2. **Anderson,W.F.** (1998) *Human gene therapy 1.* Nature, 392, 25-30.

3. **Anderson,W.F.** (1984) *Prospects for human gene therapy 1.* Science, 226, 401-409.

4. **Andersson,L., Yang,S., Neubauer,P. and Enfors,S.O.** (1996) *Impact of plasmid presence and induction on cellular responses in fed batch cultures of Escherichia coli 2.* J. Biotechnol., 46, 255-263.

5. **Arroyo,F.N., Duran Quintana,M.C. and Garrido,F.A.** (2005) *Evaluation of primary models to describe the growth of Pichia anomala and study of temperature, NaCl, and pH effects on its biological parameters by response surface methodology.* J. Food Prot., 68, 562-570.

6. **Ataai,M.M. and Shuler,M.L.** (1986) *Mathematical model for the control of ColE1 type plasmid replication.* Plasmid, 16, 204-212.

7. **Ausubel,F.M.** (1987) *Current protocols in molecular biology.*

8. **Bachvarov,D.R. and Ivanov,I.G.** (1983) *Large scale purification of plasmid DNA 1.* Prep. Biochem., 13, 161-166.

9. **Bailey,J.E. and Seo,J.H.** (1985) *Effects of recombinant plasmid content on growth properties and cloned gene product formation in Escherichia coli* . Biotechnol. Bioeng., 27, 1668-1674.

10. **Bailey,J.E. and Ollis,D.F.** (1986) Biochemical engineering fundamentals. McGraw-Hill, New York.

11. **Balbas,P., Soberon,X., Merino,E., Zurita,M., Lomeli,H., Valle,F., Flores,N. and Bolivar,F.** (1986) *Plasmid vector pBR322 and its special-purpose derivatives--a review 1.* Gene, 50, 3-40.

12. **Baracchini,E. and Bremer,H.** (1988) *Stringent and growth control of rRNA synthesis in Escherichia coli are both mediated by ppGpp.* J. Biol. Chem., 263, 2597-2602.

13. **Barton,B.M., Harding,G.P. and Zuccarelli,A.J.** (1995) *A general method for detecting and sizing large plasmids 1.* Anal. Biochem., 226, 235-240.

14. **Bentley W.E.,M.N.A.D.C.D.R.H.K.D.S.** (1990) *Plasmid-encoded protein: The principal factor in the ?metabolic burden? associated with recombinant bacteria.* BIOTECHNOLOGY AND BIOENGINEERING, 35, 668-681.

15. **Bentley,W.E.K.D.S.** (1989) *A novel structured kinetic modeling approach for the analysis of plasmid instability in recombinant bacterial cultures.* Biotechnol. Bioeng., 33, 49-61.

16. **Bergan,D., Galbraith,T. and Sloane,D.L.** (2000) *Gene transfer in vitro and in vivo by cationic lipids is not significantly affected by levels of supercoiling of a reporter plasmid.* Pharm. Res., 17, 967-973.

17. **Best,A.N., Allison,D.P. and Novelli,G.D.** (1981) *Purification of supercoiled DNA of plasmid col E1 by RPC-5 chromatography 2.* Anal. Biochem., 114, 235-243.

18. **Bignell,C.R., Haines,A.S., Khare,D. and Thomas,C.M.** (1999) *Effect of growth rate and incC mutation on symmetric plasmid distribution by the IncP-1 partitioning apparatus.* Mol. Microbiol., 34, 205-216.

19. **Bio-Rad Labs.** (2000) *CHEF-DR® III Pulsed Field Electrophoresis Systems Instruction Manual and Applications Guide.*

20. **Bio-Rad Labs.** (2003) *MicroPulser Electroporation Apparatus; Operating Instructions and Applications guide 165-2100.*

21. **Birnboim,H.C. and Doly,J.** (1979) *A rapid alkaline extraction procedure for screening recombinant plasmid DNA.* Nucleic Acids Res., 7, 1513-1523.

22. **Blattner,F.R., Plunkett,G., III, Bloch,C.A., Perna,N.T., Burland,V., Riley,M., Collado-Vides,J., Glasner,J.D., Rode,C.K., Mayhew,G.F., Gregor,J., Davis,N.W., Kirkpatrick,H.A., Goeden,M.A., Rose,D.J., Mau,B. and Shao,Y.** (1997) *The complete genome sequence of Escherichia coli K-12 1.* Science, 277, 1453-1474.

23. **Bolivar,F., Rodriguez,R.L., Greene,P.J., Betlach,M.C., Heyneker,H.L. and Boyer,H.W.** (1977) *Construction and characterization of new cloning vehicles. II. A multipurpose cloning system 1.* Gene, 2, 95-113.

24. **Bonilla,P.J., Freytag,S.O. and Lutter,L.C.** (1991) *Enhancer-activated plasmid transcription complexes contain constrained supercoiling.* Nucleic Acids Res., 19, 3965-3971.

25. **Box,G.E.P., Hunter,J.S. and Hunter,W.G.** (1978) Statistics for experimenters an introduction to design, data analysis, and model building. Wiley, New York.

26. **Brown,R.E., Jarvis,K.L. and Hyland,K.J.** (1989) *Protein measurement using bicinchoninic acid: elimination of interfering substances 3.* Anal. Biochem., 180, 136-139.

27. **Buhler,H. and Ingold,W.** (1976) *Measuring pH and oxygen in fermenters.* Proc. Biochem, 11, 19-22.

28. **Bukhman,Y.V. and Draper,D.E.** (1997) *Affinities and selectivities of divalent cation binding sites within an RNA tertiary structure.* J. Mol. Biol., 273, 1020-1031.

29. **Burke,D.T., Carle,G.F. and Olson,M.V.** (1987) *Cloning of large segments of exogenous DNA into yeast by means of artificial chromosome vectors 2.* Science, 236, 806-812.

30. **Bussey,L.B.** (1998) *Methods for purifying nucleic acids.*

31. **Butler ,e.al., Kahn, Cohen and Winkler** (2000) *Purification of plasmid DNA.*

32. **Byung Gee Kim,M.L.S.** (2006) *Analysis of pBR322 replication kinetics and its dependency on growth rate.* BIOTECHNOLOGY AND BIOENGINEERING, 36, 233-242.

33. **Bywater,M., Bywater,R. and Hellman,L.** (1983) *A novel chromatographic procedure for purification of bacterial plasmids 1.* Anal. Biochem., 132, 219-224.

34. **Carle,G.F., Frank,M. and Olson,M.V.** (1986) *Electrophoretic separations of large DNA molecules by periodic inversion of the electric field 1.* Science, 232, 65-68.

35. **Carlson,A., Signs,M., Liermann,L. and Boor,R.** (1995) *Mechanical Disruption of Escherichia coli for Plasmid Recovery.* BIOTECHNOLOGY AND BIOENGINEERING, VOL 48; NUMBER 4, -303.

36. **Chakrabarti,A., Sitaric,S. and Ohi,S.** (1992) *A procedure for large-scale plasmid isolation without using ultracentrifugation 1.* Biotechnol. Appl. Biochem., 16, 211-215.

37. **Chakravarti,R.a.S.V.** (2002) *Optimisation of compactin production in chemically defined production medium by Penicillin citrinum using statistical methods.* Proc. Biochem.

38. **Chamsart,S., Patel,H., Hanak,J.A., Hitchcock,A.G. and Nienow,A.W.** (2001) *The impact of fluid-dynamic-generated stresses on chDNA and pDNA stability during alkaline cell lysis for gene therapy products 1.* Biotechnol. Bioeng., 75, 387-392.

39. **Chandra,G., Patel,P., Kost,T.A. and Gray,J.G.** (1992) *Large-scale purification of plasmid DNA by fast protein liquid chromatography using a Hi-Load Q Sepharose column 1.* Anal. Biochem., 203, 169-172.

40. **Chaszczewska-Markowska,M., Ugorski,M. and Langner,M.** (2004) *Plasmid condensation induced by cationic compounds: hydrophilic polylysine and amphiphilic cationic lipid.* Cell Mol. Biol. Lett., 9, 3-13.

41. **Chatwin,H.M. and Summers,D.K.** (2001) *Monomer-dimer control of the ColE1 P(cer) promoter 1.* Microbiology, 147, 3071-3081.

42. **Cheah,U.E., Weigand,W.A. and Stark,B.C.** (1987) *Effects of recombinant plasmid size on cellular processes in Escherichia coli.* Plasmid, 18, 127-134.

43. **Chen,W., Graham,C. and Ciccarelli,R.B.** (1997) *Automated fed-batch fermentation with feed-back controls based on dissolved oxygen (DO) and pH for production of DNA vaccines.* J. Ind. Microbiol. Biotechnol., 18, 43-48.

44. **Chu,G.** (1990) *Pulsed-field electrophoresis: theory and practice.* In Birren,B. and Lai,E. (eds.), *Methods: A Companion to Methods of Enzymology. Pulsed-Field Electrophoresis.* Academic Press, San Diego.

45. **Ciccolini,L.A., Shamlou,P.A. and Titchener-Hooker,N.** (2002) *A mass balance study to assess the extent of contaminant removal achieved in the operations for the primary recovery of plasmid DNA from Escherichia coli cells.* Biotechnol. Bioeng., 77, 796-805.

46. **Ciccolini,L.A.S., yazi Shamlou,P., Titchener-Hooker,N.J., Ward,J.M. and Dunnill,P.** (1999) *Rheological properties of chromosomal and plasmid DNA during alkaline lysis reaction.* Bioprocess and Biosystems Engineering, 21, 231-237.

47. **Clark,S.M., Lai,E., Birren,B.W. and Hood,L.** (1988) *A novel instrument for separating large DNA molecules with pulsed homogeneous electric fields*
3. Science, 241, 1203-1205.

48. **Clemson,M. and Kelly,W.J.** (2003) *Optimizing alkaline lysis for DNA plasmid recovery*
1. Biotechnol. Appl. Biochem., 37, 235-244.

49. **Cole,K.D.** (1991) *Purification of plasmid and high molecular mass DNA using PEG-salt two-phase extraction.* Biotechniques, 11, 18, 20, 22-18, 20, 24.

50. **Colman,A., Byers,M.J., Primrose,S.B. and Lyons,A.** (1978) *Rapid purification of plasmid DNAs by hydroxyapatite chromatography*
1. Eur. J. Biochem., 91, 303-310.

51. **Colote,S., Ferraz,C. and Liautard,J.P.** (1986) *Analysis and purification of plasmid DNA by reversed-phase high-performance liquid chromatography*
1. Anal. Biochem., 154, 15-20.

52. **Colpan ,e.al.** (1999) *Process for the separation and purification of nucleic acids from biological sources.*

53. **Coppella,S.J., Acheson,C.M. and Dhurjati,P.** (1987) *Isolation of high-molecular-weight nucleic acids for copy number analysis using high-performance liquid chromatography*
1. J. Chromatogr., 402, 189-199.

54. **Corchero,J.L. and Villaverde,A.** (1998) *Plasmid maintenance in Escherichia coli recombinant cultures is dramatically, steadily, and specifically influenced by features of the encoded proteins.* Biotechnol. Bioeng., 58, 625-632.

55. **Cornelis,P., Digneffe,C., Willemot,K. and Colson,C.** (1981) *Purification of Escherichia coli amplifiable plasmids by high-salt sepharose chromatography*
1. Plasmid, 5, 221-223.

56. **Costioli,M.D., Fisch,I., Garret-Flaudy,F., Hilbrig,F. and Freitag,R.** (2003) *DNA purification by triple-helix affinity precipitation.* Biotechnol. Bioeng., 81, 535-545.

57. **Coulson,J.M., Richardson,J.F., Backhurst,J.R. and Harker,J.H.** (1996) Chemical engineering. Butterworth-Heinemann, Oxford, U.K.

58. **Cranenburgh,R.M., Hanak,J.A., Williams,S.G. and Sherratt,D.J.** (2001) *Escherichia coli strains that allow antibiotic-free plasmid selection and maintenance by repressor titration 24.* Nucleic Acids Res., 29, E26.

59. **Crystal,R.G.** (1995) *The gene as the drug.* Nat. Med., 1, 15-17.

60. **Cserjan-Puschmann,M., Kramer,W., Duerrschmid,E., Striedner,G. and Bayer,K.** (1999) *Metabolic approaches for the optimisation of recombinant fermentation processes.* Appl. Microbiol. Biotechnol., 53, 43-50.

61. **Curtiss,R., III, Nakayama,K. and Kelly,S.M.** (1989) *Recombinant avirulent Salmonella vaccine strains with stable maintenance and high level expression of cloned genes in vivo.* Immunol. Invest, 18, 583-596.

62. **Darnon,E., Morin,E., Belleville,M.P. and Rios,G.M.** (2003) *Ultrafiltration within downstream processing: some process design considerations.* Chemical Engineering and Processing, 42, 299-309.

63. **Davidson,J.N.** (1972) The biochemistry of the nucleic acids. Chapman and Hall, London.

64. **Davies,M.J., Smethurst,D.E., Howard,K.M., Todd,M., Higgins,L.M. and Bruce,I.J.** (1997) *Improved manufacture and application of an agarose magnetizable solid-phase support 11.* Appl. Biochem. Biotechnol., 68, 95-112.

65. **Davis,M.E.** (2002) *Non-viral gene delivery systems 1.* Curr. Opin. Biotechnol., 13, 128-131.

66. **Deshmukh,N.R. and Lali,A.M.** (2005) *Adsorptive purification of pDNA on superporous rigid cross-linked cellulose matrix.* J. Chromatogr. B Analyt. Technol. Biomed. Life Sci., 818, 5-10.

67. **Dieffenbach C W, Lowe TMK and Dveksler** (1995) General concepts for primer design. Cold Spring Harbour Laboratory Press, New York.

68. **Diogo,M.M., Queiroz,J.A., Monteiro,G.A., Martins,S.A., Ferreira,G.N. and Prazeres,D.M.** (2000) *Purification of a cystic fibrosis plasmid vector for gene therapy using hydrophobic interaction chromatography.* Biotechnol. Bioeng., 68, 576-583.

69. **Diogo,M.M., Queiroz,J.A., Monteiro,G.A. and Prazeres,D.M.** (1999) *Separation and analysis of plasmid denatured forms using hydrophobic interaction chromatography.* Anal. Biochem., 275, 122-124.

70. **Diogo,M.M., Queiroz,J.A. and Prazeres,D.M.** (2005) *Chromatography of plasmid DNA.* J. Chromatogr. A, 1069, 3-22.

71. **Diogo,M.M., Queiroz,J.A. and Prazeres,D.M.** (2001a) *Studies on the retention of plasmid DNA and Escherichia coli nucleic acids by hydrophobic interaction chromatography.* Bioseparation., 10, 211-220.

72. **Diogo,M.M., Queiroz,J.A. and Prazeres,D.M.** (2003) *Assessment of purity and quantification of plasmid DNA in process solutions using high-performance hydrophobic interaction chromatography.* J. Chromatogr. A, 998, 109-117.

73. **Diogo,M.M., Ribeiro,S.C., Queiroz,J.A., Monteiro,G.A., Tordo,N., Perrin,P. and Prazeres,D.M.** (2001b) *Production, purification and analysis of an experimental DNA vaccine against rabies.* J. Gene Med., 3, 577-584.

74. **Donahue,R.B.F.R.** (1998) *Transformation Efficiency of E.coli Electroporated with Large Plasmid DNA.*

75. **Dong,H., Nilsson,L. and Kurland,C.G.** (1995) *Gratuitous overexpression of genes in Escherichia coli leads to growth inhibition and ribosome destruction*
1. J. Bacteriol., 177, 1497-1504.

76. **Doran,P.M.** (1995) Bioprocess engineering principles. Academic Press, London.

77. **Drager,R.R. and Regnier,F.E.** (1985) *High-performance anion-exchange chromatography of oligonucleotides*
1. Anal. Biochem., 145, 47-56.

78. **Eastman,E.M. and Durland,R.H.** (1998) *Manufacturing and quality control of plasmid-based gene expression systems*
1. Adv. Drug Deliv. Rev., 30, 33-48.

79. **Edelstein,M.L., Abedi,M.R., Wixon,J. and Edelstein,R.M.** (2004) *Gene therapy clinical trials worldwide 1989-2004-an overview*
130. J. Gene Med., 6, 597-602.

80. **Eon-Duval,A. and Burke,G.** (2004) *Purification of pharmaceutical-grade plasmid DNA by anion-exchange chromatography in an RNase-free process.* J. Chromatogr. B Analyt. Technol. Biomed. Life Sci., 804, 327-335.

81. **Eon-Duval,A., Gumbs,K. and Ellett,C.** (2003a) *Precipitation of RNA impurities with high salt in a plasmid DNA purification process: use of experimental design to determine reaction conditions*
2. Biotechnol. Bioeng., 83, 544-553.

82. **Eon-Duval,A., MacDuff,R.H., Fisher,C.A., Harris,M.J. and Brook,C.** (2003b) *Removal of RNA impurities by tangential flow filtration in an RNase-free plasmid DNA purification process*
3. Anal. Biochem., 316, 66-73.

83. **Evans,R.K., Xu,Z., Bohannon,K.E., Wang,B., Bruner,M.W. and Volkin,D.B.** (2000) *Evaluation of degradation pathways for plasmid DNA in pharmaceutical formulations via accelerated stability studies*
1. J. Pharm. Sci., 89, 76-87.

84. **Even-Chen,S. and Barenholz,Y.** (2000) *DOTAP cationic liposomes prefer relaxed over supercoiled plasmids*
1. Biochim. Biophys. Acta, 1509, 176-188.

85. **Fangman,W.L.** (1978) *Separation of very large DNA molecules by gel electrophoresis*
1. Nucleic Acids Res., 5, 653-665.

86. **Feliciello,I. and Chinali,G.** (1993) *A modified alkaline lysis method for the preparation of highly purified plasmid DNA from Escherichia coli*
1. Anal. Biochem., 212, 394-401.

87. **Ferreira,G.N., Cabral,J.M. and Prazeres,D.M.** (2000a) *Studies on the batch adsorption of plasmid DNA onto anion-exchange chromatographic supports.* Biotechnol. Prog., 16, 416-424.

88. **Ferreira,G.N., Cabral,J.M. and Prazeres,D.M.** (1999) *Development of process flow sheets for the purification of supercoiled plasmids for gene therapy applications.* Biotechnol. Prog., 15, 725-731.

89. **Ferreira,G.N., Cabral,J.M. and Prazeres,D.M.** (2000b) *Anion exchange purification of plasmid DNA using expanded bed adsorption.* Bioseparation., 9, 1-6.

90. **Ferreira,G.N., Monteiro,G.A., Prazeres,D.M. and Cabral,J.M.** (2000c) *Downstream processing of plasmid DNA for gene therapy and DNA vaccine applications.* Trends Biotechnol., 18, 380-388.

91. **Ficarra,R., Calabro,M.L., Cutroneo,P., Tommasini,S., Melardi,S., Semreen,M., Furlanetto,S., Ficarra,P. and Altavilla,G.** (2002) *Validation of a LC method for the analysis of oxaliplatin in a pharmaceutical formulation using an experimental design.* J. Pharm. Biomed. Anal., 29, 1097-1103.

92. **Fox,J.L.** (1999) *Gene therapy safety issues come to fore.* Nat. Biotechnol., 17, 1153.

93. **Frame,R. and Bishop,J.O.** (1971) *The number of sex-factors per chromosome in Escherichia coli*
1. Biochem. J., 121, 93-103.

94. **Frerix,A., Muller,M., Kula,M.R. and Hubbuch,J.** (2005) *Scalable recovery of plasmid DNA based on aqueous two-phase separation.* Biotechnol. Appl. Biochem., 42, 57-66.

95. **Friehs,K.** (2004) *Plasmid copy number and plasmid stability*
1. Adv. Biochem Eng Biotechnol., 86, 47-82.

96. **Fykse,E.M., Olsen,J.S. and Skogan,G.** (2003) *Application of sonication to release DNA from Bacillus cereus for quantitative detection by real-time PCR*
32. J. Microbiol. Methods, 55, 1-10.

97. **Ganusov,V.V., Bril'kov,A.V. and Pechurkin,N.S.** (2000) *[Mathematical modeling of population dynamics of unstable plasmid-containing bacteria during continuous cultivation in a chemostat].* Biofizika, 45, 908-914.

98. **Garcia-Arrazola,R., Dawson,P., Buchanan,I., Doyle,B., Fearn,T., Titchener-Hooker,N. and Baganz,F.** (2005) *Evaluation of the effects and interactions of mixing and oxygen transfer on the production of Fab' antibody fragments in Escherichia coli fermentation with gas blending.* Bioprocess. Biosyst. Eng, 27, 365-374.

99. **Garon,C.F. and Petersen,L.L.** (1987) *An improved method for the isolation of supercoiled DNA molecules using ion-exchange column chromatography*
1. Gene Anal. Tech., 4, 5-8.

100. **GE Healthcare** (2005) *PD-10 Desalting Columns [Instructions 52-1308-00 AP].*

101. **Gehrke,C.W. and Kuo,K.C.** (1989) *Ribonucleoside analysis by reversed-phase high-performance liquid chromatography.* J. Chromatogr., 471, 3-36.

102. **Gelfand, David H., Holland, Pamela M., Saiki, Randall K., Watson and Robert M.** (1993) *Homogeneous assay system using the nuclease activity of a nucleic* ***5,210,015*** .

103. **Georgiou,G.S.M.L.W.D.B.** (1988) *Release of periplasmic enzymes and other physiological effects of B-lactamase overproduction in Escherichia coli.* BIOTECHNOLOGY AND BIOENGINEERING, 32, 741-748.

104. **Gerlitz,M., Hrabak,O. and Schwab,H.** (1990) *Partitioning of broad-host-range plasmid RP4 is a complex system involving site-specific recombination.* J. Bacteriol., 172, 6194-6203.

105. **Gibson,U.E., Heid,C.A. and Williams,P.M.** (1996) *A novel method for real time quantitative RT-PCR.* Genome Res., 6, 995-1001.

106. **Giovannini,R. and Freitag,R.** (2002) *Continuous isolation of plasmid DNA by annular chromatography.* Biotechnol. Bioeng., 77, 445-454.

107. **Giovannini,R., Freitag,R. and Tennikova,T.B.** (1998) *High-performance membrane chromatography of supercoiled plasmid DNA.* Anal. Chem., 70, 3348-3354.

108. **Glick,B.R.** (1995) *Metabolic load and heterologous gene expression.* Biotechnology Advances, 13, 247-261.

109. **Gomez-Marquez,J., Freire,M. and Segade,F.** (1987) *A simple procedure for large-scale purification of plasmid DNA*
1. Gene, 54, 255-259.

110. **Grabherr,R. and Bayer,K.** (2002) *Impact of targeted vector design on ColE1 plasmid replication.* Trends in Biotechnology, 20, 257-260.

111. **Grenville,R.K.** (1992) *Blending of viscous and pseudo-plastic fluids.* Cranfield Institute of Technology, Bedfordshire, UK.

112. **Grunwald,A.G. and Shields,M.S.** (2001) *Plasmid purification using membrane-based anion-exchange chromatography*
1. Anal. Biochem., 296, 138-141.

113. **Hanahan,D., Jessee,J. and Bloom,F.R.** (1991) *Plasmid transformation of Escherichia coli and other bacteria.* Methods Enzymol., 204, 63-113.

114. **Haque,K.A., Pfeiffer,R.M., Beerman,M.B., Struewing,J.P., Chanock,S.J. and Bergen,A.W.** (2003) *Performance of high-throughput DNA quantification methods.* BMC. Biotechnol., 3, 20.

115. **He,G.Q., Kong,Q. and Ding,L.X.** (2004) *Response surface methodology for optimizing the fermentation medium of Clostridium butyricum.* Lett. Appl. Microbiol., 39, 363-368.

116. **Hecker,M., Schroeter,A. and Mach,F.** (1983) *Replication of pBR322 DNA in stringent and relaxed strains of Escherichia coli.* Mol. Gen. Genet., 190, 355-357.

117. **Heid,C.A., Stevens,J., Livak,K.J. and Williams,P.M.** (1996) *Real time quantitative PCR 6.* Genome Res., 6, 986-994.

118. **Henry,K.L., Davis,R.H. and Taylor,A.L.** (1990) *Continuous recombinant bacterial fermentations utilizing selective flocculation and recycle.* Biotechnol. Prog., 6, 7-12.

119. **Hicks,C.R. and Turner,K.V.** (1999) Fundamental concepts in the design of experiments. Oxford University Press, New York.

120. **Hightower,R.C., Metge,D.W. and Santi,D.V.** (1987) *Plasmid migration using orthogonal-field-alternation gel electrophoresis.* Nucleic Acids Res., 15, 8387-8398.

121. **Hines,R.N., O'Connor,K.C., Vella,G. and Warren,W.** (1992) *Large-scale purification of plasmid DNA by anion-exchange high-performance liquid chromatography 1.* Biotechniques, 12, 430-434.

122. **Holland,P.M., Abramson,R.D., Watson,R. and Gelfand,D.H.** (1991) *Detection of specific polymerase chain reaction product by utilizing the 5'----3' exonuclease activity of Thermus aquaticus DNA polymerase 1.* Proc. Natl. Acad. Sci. U. S. A, 88, 7276-7280.

123. **Holmes,D.S. and Quigley,M.** (1981) *A rapid boiling method for the preparation of bacterial plasmids 3.* Anal. Biochem., 114, 193-197.

124. **Hong-Bin Zhang, Sangdun Choi, Sung-Sick Woo, Zhikang li and Rod A.Wing** (1995) *Construction and characterization of two rice bacterial artificial chromosome libraries from the parents of a permanent recombinant inbred mapping population.* Molecular Breeding, 2, 11-24.

125. **Horn ,e.al.** (1998) *Purification of plasmid DNA during column chromatography.*

126. **Horn,N.A., Meek,J.A., Budahazi,G. and Marquet,M.** (1995) *Cancer gene therapy using plasmid DNA: purification of DNA for human clinical trials.* Hum. Gene Ther., 6, 565-573.

127. **Huber,C.G.** (1998) *Micropellicular stationary phases for high-performance liquid chromatography of double-stranded DNA*
3. J. Chromatogr. A, 806, 3-30.

128. **Huber,H. and et al.** (2005b) *Method for producing plasmid DNA on a manufacturing scale.*

129. **Huber,H. and et al.** (2005a) *Fed-batch fermentation process and culture medium for the production of plasmid DNA in E. coli on a manufacturing scale.*

130. **Humphreys,G.O., Willshaw,G.A. and Anderson,E.S.** (1975) *A simple method for the preparation of large quantities of pure plasmid DNA*
1. Biochim. Biophys. Acta, 383, 457-463.

131. **Imanaka,T. and Aiba,S.** (1981) *A perspective on the application of genetic engineering: stability of recombinant plasmid.* Ann. N. Y. Acad. Sci., 369, 1-14.

132. **Invitrogen** (2006) *The GeneJumper oriV Kit.*

133. **Ishaq,M., Wolf,B. and Ritter,C.** (1990) *Large-scale isolation of plasmid DNA using cetyltrimethylammonium bromide*
1. Biotechniques, 9, 19-20, 22, 24.

134. **Ito,T., Smith,C.L. and Cantor,C.R.** (1992b) *Triplex affinity capture of a single copy clone from a yeast genomic library*
1. Nucleic Acids Res., 20, 3524.

135. **Ito,T., Smith,C.L. and Cantor,C.R.** (1992a) *Sequence-specific DNA purification by triplex affinity capture*
2. Proc. Natl. Acad. Sci. U. S. A, 89, 495-498.

136. **Iuliano,S., Fisher,J.R., Chen,M. and Kelly,W.J.** (2002) *Rapid analysis of a plasmid by hydrophobic-interaction chromatography with a non-porous resin.* J. Chromatogr. A, 972, 77-86.

137. **Jensen,R.B. and Gerdes,K.** (1995) *Programmed cell death in bacteria: proteic plasmid stabilization systems.* Mol. Microbiol., 17, 205-210.

138. **Jensen,R.B., Grohmann,E., Schwab,H., az-Orejas,R. and Gerdes,K.** (1995) *Comparison of ccd of F, parDE of RP4, and parD of R1 using a novel conditional replication control system of plasmid R1.* Mol. Microbiol., 17, 211-220.

139. **Johnson,T.R. and Ilan,J.** (1983) *Large-scale isolation of plasmid DNA and purification of lambda phage DNA using hydroxylapatite chromatography*
3. Anal. Biochem., 132, 20-25.

140. **Jones,K.L. and Keasling,J.D.** (1998) *Construction and characterization of F plasmid-based expression vectors*
4. Biotechnol. Bioeng., 59, 659-665.

141. **Kahn,D.W., Butler,M.D., Cohen,D.L., Gordon,M., Kahn,J.W. and Winkler,M.E.** (2000) *Purification of plasmid DNA by tangential flow filtration.* Biotechnol. Bioeng., 69, 101-106.

142. **Kapp,U. and Langowski,J.** (1992) *Preparation of DNA topoisomers by RP-18 high-performance liquid chromatography*
1. Anal. Biochem., 206, 293-299.

143. **Kay,A., O'Kennedy,R., Ward,J. and Keshavarz-Moore,E.** (2003) *Impact of plasmid size on cellular oxygen demand in Escherichia coli.* Biotechnol. Appl. Biochem., 38, 1-7.

144. **Kendall,D., Lye,G.J. and Levy,M.S.** (2002) *Purification of plasmid DNA by an integrated operation comprising tangential flow filtration and nitrocellulose adsorption.* Biotechnol. Bioeng., 79, 816-822.

145. **Kepka,C., Lemmens,R., Vasi,J., Nyhammar,T. and Gustavsson,P.E.** (2004a) *Integrated process for purification of plasmid DNA using aqueous two-phase systems combined with membrane filtration and lid bead chromatography.* J. Chromatogr. A, 1057, 115-124.

146. **Kepka,C., Rhodin,J., Lemmens,R., Tjerneld,F. and Gustavsson,P.E.** (2004b) *Extraction of plasmid DNA from Escherichia coli cell lysate in a thermoseparating aqueous two-phase system.* J. Chromatogr. A, 1024, 95-104.

147. **Kim,B.G., Good,T.A., Ataai,M.M. and Shuler,M.L.** (1987) *Growth behavior and prediction of copy number and retention of ColE1-type plasmids in E. coli under slow growth conditions.* Ann. N. Y. Acad. Sci., 506, 384-395.

148. **Kim,C.H., Lee,J.Y., Kim,M.G., Song,K.B., Seo,J.W., Chung,B.H., Chang,S.J. and Rhee,S.K.** (1998) *Fermentation strategy to enhance plasmid stability during the cultivation of Escherichia coli for the production of recombinant levansucrase.* Journal of Fermentation and Bioengineering, 86, 391-394.

149. **Knorre,W.A., Deckwer,W.D., Korz,D., Pohl,H.D., Riesenberg,D., Ross,A., Sanders,E. and Schulz,V.** (1991) *High cell density fermentation of recombinant Escherichia coli with computer-controlled optimal growth rate*
1. Ann. N. Y. Acad. Sci., 646, 300-306.

150. **Korpimaki,T., Kurittu,J. and Karp,M.** (2003) *Surprisingly fast disappearance of beta-lactam selection pressure in cultivation as detected with novel biosensing approaches.* J. Microbiol. Methods, 53, 37-42.

151. **Kostal,J., Mulchandani,A. and Chen,W.** (2004) *Affinity purification of plasmid DNA by temperature-triggered precipitation.* Biotechnol. Bioeng., 85, 293-297.

152. **Lahijani,R., Hulley,G., Soriano,G., Horn,N.A. and Marquet,M.** (1996) *High-yield production of pBR322-derived plasmids intended for human gene therapy by employing a temperature-controllable point mutation.* Hum. Gene Ther., 7, 1971-1980.

153. **Lander,R.J., Winters,M.A., Meacle,F.J., Buckland,B.C. and Lee,A.L.** (2002) *Fractional precipitation of plasmid DNA from lysate by CTAB*
1. Biotechnol. Bioeng., 79, 776-784.

154. **Larson,J.E., Hardies,S.C., Patient,R.K. and Wells,R.D.** (1979) *Factors influencing fractionation of DNA restriction fragments by RPC-5 column chromatography 3.* J. Biol. Chem., 254, 5535-5541.

155. **Le Pecq,J.B. and Paoletti,C.** (1966) *A new fluorometric method for RNA and DNA determination 11.* Anal. Biochem., 17, 100-107.

156. **Lee ,e.al.** (1996) *Method for large scale plasmid purification.*

157. **Lee,C., Kim,J., Shin,S.G. and Hwang,S.** *Absolute and relative QPCR quantification of plasmid copy number in Escherichia coli.* Journal of Biotechnology, In Press, Corrected Proof.

158. **Lee,S.W. and Edlin,G.** (1985) *Expression of tetracycline resistance in pBR322 derivatives reduces the reproductive fitness of plasmid-containing Escherichia coli.* Gene, 39, 173-180.

159. **Lee,S.Y.** (1996) *High cell-density culture of Escherichia coli 15.* Trends Biotechnol., 14, 98-105.

160. **Leipold,R.J., Krewson,C.E. and Dhurjati,P.** (1994) *Mathematical model of temperature-sensitive plasmid replication 1.* Plasmid, 32, 131-167.

161. **Lemmens,R., Olsson,U., Nyhammar,T. and Stadler,J.** (2003) *Supercoiled plasmid DNA: selective purification by thiophilic/aromatic adsorption.* J. Chromatogr. B Analyt. Technol. Biomed. Life Sci., 784, 291-300.

162. **Lemonnier,M., Bouet,J.Y., Libante,V. and Lane,D.** (2000) *Disruption of the F plasmid partition complex in vivo by partition protein SopA.* Mol. Microbiol., 38, 493-505.

163. **Levene,S.D. and Zimm,B.H.** (1987) *Separations of open-circular DNA using pulsed-field electrophoresis 1.* Proc. Natl. Acad. Sci. U. S. A, 84, 4054-4057.

164. **Levison,P.R., Badger,S.E., Dennis,J., Hathi,P., Davies,M.J., Bruce,I.J. and Schimkat,D.** (1998a) *Recent developments of magnetic beads for use in nucleic acid purification.* J. Chromatogr. A, 816, 107-111.

165. **Levison,P.R., Badger,S.E., Hathi,P., Davies,M.J., Bruce,I.J. and Grimm,V.** (1998b) *New approaches to the isolation of DNA by ion-exchange chromatography.* J. Chromatogr. A, 827, 337-344.

166. **Levy,M.S., Ciccolini,L.A.S., Yim,S.S.S., Tsai,J.T., Titchener-Hooker,N., yazi Shamlou,P. and Dunnill,P.** (1999a) *The effects of material properties and fluid flow intensity on plasmid DNA recovery during cell lysis.* Chemical Engineering Science, 54, 3171-3178.

167. **Levy,M.S., Collins,I.J., Tsai,J.T., yazi Shamlou,P., Ward,J.M. and Dunnill,P.** (2000a) *Removal of contaminant nucleic acids by nitrocellulose filtration during pharmaceutical-grade plasmid DNA processing.* Journal of Biotechnology, 76, 197-205.

168. **Levy,M.S., Collins,I.J., Yim,S.S., Ward,J.M., Titchener-Hooker,N., yazi Shamlou,P. and Dunnill,P.** (1999b) *Effect of shear on plasmid DNA in solution.* Bioprocess and Biosystems Engineering, 20, 7-13.

169. **Levy,M.S., Kennedy,R.D., yazi-Shamlou,P. and Dunnill,P.** (2000b) *Biochemical engineering approaches to the challenges of producing pure plasmid DNA.* Trends in Biotechnology, 18, 296-305.

170. **Lin-Chao,S. and Bremer,H.** (1986) *Effect of the bacterial growth rate on replication control of plasmid pBR322 in Escherichia coli*
2. Mol. Gen. Genet., 203, 143-149.

171. **Lis,J.T. and Schleif,R.** (1975) *Size fractionation of double-stranded DNA by precipitation with polyethylene glycol*
1. Nucleic Acids Res., 02, 383-389.

172. **Liu,J., Zhang,Q., Bi,J., Wang,X., Gong,P., Ha,X., Wang,Z. and Wu,Z.** (2004) *[Analysis of plasmid pUDKH by anion-exchange high performance liquid chromatogaphy]*
16. Se. Pu., 22, 65-67.

173. **Ljunglof,A., Bergvall,P., Bhikhabhai,R. and Hjorth,R.** (1999) *Direct visualisation of plasmid DNA in individual chromatography adsorbent particles by confocal scanning laser microscopy*
1. J. Chromatogr. A, 844, 129-135.

174. **Lockey,C., Otto,E. and Long,Z.** (1998) *Real-time fluorescence detection of a single DNA molecule.* Biotechniques, 24, 744-746.

175. **Lyddiatt,A. and O'Sullivan,D.A.** (1998) *Biochemical recovery and purification of gene therapy vectors*
1. Curr. Opin. Biotechnol., 9, 177-185.

176. **Mallet,F.** (2000) *Comparison of competitive and positive control-based PCR quantitative procedures coupled with end point detection.* Mol. Biotechnol., 14, 205-214.

177. **Marquet ,e.a.** (1996) *Production of pharmaceutical-grade plasmid DNA.*

178. **Marquet,R., Wyart,A. and Houssier,C.** (1987) *Influence of DNA length on spermine-induced condensation. Importance of the bending and stiffening of DNA*
12. Biochim. Biophys. Acta, 909, 165-172.

179. **McClung,J.K. and Gonzales,R.A.** (1989) *Purification of plasmid DNA by fast protein liquid chromatography on superose 6 preparative grade*
1. Anal. Biochem., 177, 378-382.

180. **Meacle,F.J., Lander,R., Ayazi,S.P. and Titchener-Hooker,N.J.** (2004) *Impact of engineering flow conditions on plasmid DNA yield and purity in chemical cell lysis operations*
1. Biotechnol. Bioeng., 87, 293-302.

181. **Metzner A.B and Otto R.E.** (1957) *Agitation of non-Newtonian fluids.* AIChEJ, 3.

182. **Mhashilkar,A., Chada,S., Roth,J.A. and Ramesh,R.** (2001) *Gene therapy. Therapeutic approaches and implications*
1. Biotechnol. Adv., 19, 279-297.

183. **Micard,D., Sobrier,M.L., Couderc,J.L. and Dastugue,B.** (1985) *Purification of RNA-free plasmid DNA using alkaline extraction followed by Ultrogel A2 column chromatography*
1. Anal. Biochem., 148, 121-126.

184. **Middaugh,C.R., Evans,R.K., Montgomery,D.L. and Casimiro,D.R.** (1998) *Analysis of plasmid DNA from a pharmaceutical perspective*
15. J. Pharm. Sci., 87, 130-146.

185. **Miller,E.M. and Nickoloff,J.A.** (1995) *Escherichia coli electrotransformation.* Methods Mol. Biol., 47, 105-113.

186. **Molecular Probes Inc** (2006) *Quant-iT ™ RNA Assay Kit*
http://probes.invitrogen.com/media/pis/mp33140.pdf.

187. **Molecular Probes Inc** (2003) *SYBR Gold Nucleic Acid Gel Stain*
http://probes.invitrogen.com/media/pis/mp11494.pdf.

188. **Molecular Probes Product Information** (2003) *PicoGreen dsDNA Quantitation Reagent and Kits.*

189. **Monaco,A.P. and Larin,Z.** (1994) *YACs, BACs, PACs and MACs: artificial chromosomes as research tools*
1. Trends Biotechnol., 12, 280-286.

190. **Monteiro,G.A., Ferreira,G.N., Cabral,J.M. and Prazeres,D.M.** (1999) *Analysis and use of endogenous nuclease activities in Escherichia coli lysates during the primary isolation of plasmids for gene therapy.* Biotechnol. Bioeng., 66, 189-194.

191. **Montgomery,D.C.** (2001) Design and analysis of experiments. Wiley, New York.

192. **Mountain,A.** (2000) *Gene therapy: the first decade*
9. Trends Biotechnol., 18, 119-128.

193. **Mukhopadhyay,M. and Mandal,N.C.** (1983) *A simple procedure for large-scale preparation of pure plasmid DNA free from chromosomal DNA from bacteria*
1. Anal. Biochem., 133, 265-270.

194. **Murphy,J.C., Jewell,D.L., White,K.I., Fox,G.E. and Willson,R.C.** (2003) *Nucleic acid separations utilizing immobilized metal affinity chromatography*
11. Biotechnol. Prog., 19, 982-986.

195. **Murphy,J.C., Wibbenmeyer,J.A., Fox,G.E. and Willson,R.C.** (1999) *Purification of plasmid DNA using selective precipitation by compaction agents*
7. Nat. Biotechnol., 17, 822-823.

196. **NanoDrop Tech.Lit** (2005) *NanoDrop Users Manual http://www.nanodrop.com/pdf/nd-1000-users-manual.pdf.*

197. **Nicoletti,V.G. and Condorelli,D.F.** (1993) *Optimized PEG method for rapid plasmid DNA purification: high yield from "midi-prep"*
1. Biotechniques, 14, 532-4, 536.

198. **Noites,I.S., O'Kennedy,R.D., Levy,M.S., Abidi,N. and Keshavarz-Moore,E.** (1999) *Rapid quantitation and monitoring of plasmid DNA using an ultrasensitive DNA-binding dye.* Biotechnol. Bioeng., 66, 195-201.

199. **O'Kennedy,R., Houghton,C.J. and Patching,J.W.** (1995) *Effects of growth environment on recombinant plasmid stability in Saccharomyces cerevisiae grown in continuous culture.* Appl. Microbiol. Biotechnol., 44, 126-132.

200. **O'Kennedy,R.D., Baldwin,C. and Keshavarz-Moore,E.** (2000) *Effects of growth medium selection on plasmid DNA production and initial processing steps.* J. Biotechnol., 76, 175-183.

201. **O'Kennedy,R.D. and Patching,J.W.** (1997) *Effects of medium composition and nutrient limitation on loss of the recombinant plasmid pLG669-z and beta-galactosidase expression by Saccharomyces cerevisiae.* J. Ind. Microbiol. Biotechnol., 18, 319-325.

202. **O'Kennedy,R.D. and Patching,J.W.** (1999) *The isolation of strains of Saccharomyces cerevisiae showing altered plasmid stability characteristics by means of selective continuous culture.* J. Biotechnol., 69, 203-214.

203. **O'Kennedy,R.D., Ward,J.M. and Keshavarz-Moore,E.** (2003) *Effects of fermentation strategy on the characteristics of plasmid DNA production.* Biotechnol. Appl. Biochem., 37, 83-90.

204. **Olson,M.V.** (1989) *Separation of large DNA molecules by pulsed-field gel electrophoresis. A review of the basic phenomenology*
5. J. Chromatogr., 470, 377-383.

205. **Onishi,Y., Azuma,Y. and Kizaki,H.** (1993) *An assay method for DNA topoisomerase activity based on separation of relaxed DNA from supercoiled DNA using high-performance liquid chromatography.* Anal. Biochem., 210, 63-68.

206. **Paul,E.L., Kresta,S.M., tiemo-Obeng,V.A. and North American,M.F.** (2004) Handbook of industrial mixing
science and practice. Wiley-Interscience, Hoboken, N.J.

207. **Paulsson,J. and Ehrenberg,M.** (1998) *Trade-off between segregational stability and metabolic burden: a mathematical model of plasmid ColE1 replication control.* J. Mol. Biol., 279, 73-88.

208. **Pavlicek,J.W., Oussatcheva,E.A., Sinden,R.R., Potaman,V.N., Sankey,O.F. and Lyubchenko,Y.L.** (2004) *Supercoiling-induced DNA bending*
6. Biochemistry, 43, 10664-10668.

209. **Pederson,N.E.** (1996) *Spin-column chromatography for DNA purification 1.* Anal. Biochem., 239, 117-118.

210. **Pierce Scientific** (2006) *BCA Protein Assay Kit Technical Literature* http://www.piercenet.com/files/1296dh4.pdf

211. **Plum,G.E., Arscott,P.G. and Bloomfield,V.A.** (1990) *Condensation of DNA by trivalent cations. 2. Effects of cation structure 3.* Biopolymers, 30, 631-643.

212. **Popper,K.R.** (1975) Objective knowledge: an evolutionary approach 19. Oxford University Press, Oxford.

213. **Prather,K.J., Sagar,S., Murphy,J. and Chartrain,M.** (2003) *Industrial scale production of plasmid DNA for vaccine and gene therapy: plasmid design, production, and purification.* Enzyme and Microbial Technology, 33, 865-883.

214. **Prazeres,D.M., Schluep,T. and Cooney,C.** (1998) *Preparative purification of supercoiled plasmid DNA using anion-exchange chromatography.* J. Chromatogr. A, 806, 31-45.

215. **Promega** (2004) *Promega Subcloning Notebook.*

216. **Promega** (2005) *FAQ: What is the largest insert a Promega plasmid vector will accept?*

217. **Providenti,M.A., O'Brien,J.M., Ewing,R.J., Paterson,E.S. and Smith,M.L.** *The copy-number of plasmids and other genetic elements can be determined by SYBR-Green-based quantitative real-time PCR.* Journal of Microbiological Methods, In Press, Corrected Proof.

218. **Qiagen** (2005) *QIAGEN Plasmid Purification Handbook.*

219. **Raymond,G.J., Bryant,P.K., III, Nelson,A. and Johnson,J.D.** (1988) *Large-scale isolation of covalently closed circular DNA using gel filtration chromatography.* Anal. Biochem., 173, 125-133.

220. **rector-Myska,A.E., Pogozelski,W.K., Lofts,R.S., Prasanna,P.G., Hamel,C.J. and Blakely,W.F.** (2001) *Quantitative plasmid mixture analysis using the fluorogenic 5'-nuclease polymerase chain reaction assay.* Environ. Mol. Mutagen., 37, 147-154.

221. **Reinikainen,P., Korpela,K., Nissinen,V., Olkku,J., Soederlund,H. and Markkanen,P.** (1989) *Escherichia coli plasmid production in fermenter.* Biotechnol. Bioeng., 33, 386-393.

222. **Reinikainen,P. and Virkajaervi,I.** (1989) *Escherichia coli growth and plasmid copy numbers in continuous cultivations.* Biotechnol. Lett., 11, 225-230.

223. **Rembhotkar,G.W. and Khatri,G.S.** (1989) *Large scale preparation of bacteriophage lambda by tangential flow ultrafiltration for isolation of lambda DNA 1.* Anal. Biochem., 176, 373-374.

224. **Rengarajan,K., Cristol,S.M., Mehta,M. and Nickerson,J.M.** (2002) *Quantifying DNA concentrations using fluorometry: a comparison of fluorophores.* Mol. Vis., 8, 416-421.

225. **Ribeiro,S.C., Monteiro,G.A., Cabral,J.M. and Prazeres,D.M.** (2002) *Isolation of plasmid DNA from cell lysates by aqueous two-phase systems 4.* Biotechnol. Bioeng., 78, 376-384.

226. **Ridha Mosrati,N.N.J.B.** (1993) *Variation and modeling of the probability of plasmid loss as a function of growth rate of plasmid-bearing cells of <I>Escherichia coli</I> during continuous cultures.* BIOTECHNOLOGY AND BIOENGINEERING, 41, 395-404.

227. **Riesenberg,D., Schulz,V., Knorre,W.A., Pohl,H.D., Korz,D., Sanders,E.A., Ross,A. and Deckwer,W.D.** (1991) *High cell density cultivation of Escherichia coli at controlled specific growth rate 2.* J. Biotechnol., 20, 17-27.

228. **Roche Diagnostics** (2004) *MagNA Pure LC DNA Isolation Kit 1* http://www.roche-applied-science.com/pack-insert/3003990a.pdf.

229. **Roche Diagnostics** (2006) *MagNA Pure LC Tech. Lit* http://www.roche-applied-science.com/sis/automated/magna_lc/.

230. **Rozkov,A., vignone-Rossa,C.A., Ertl,P.F., Jones,P., O'Kennedy,R.D., Smith,J.J., Dale,J.W. and Bushell,M.E.** (2004) *Characterization of the metabolic burden on Escherichia coli DH1 cells imposed by the presence of a plasmid containing a gene therapy sequence.* Biotechnol. Bioeng., 88, 909-915.

231. **Saiki,R.K., Scharf,S., Faloona,F., Mullis,K.B., Horn,G.T., Erlich,H.A. and Arnheim,N.** (1985b) *Enzymatic amplification of beta-globin genomic sequences and restriction site analysis for diagnosis of sickle cell anemia.* Science, 230, 1350-1354.

232. **Saiki,R.K., Scharf,S., Faloona,F., Mullis,K.B., Horn,G.T., Erlich,H.A. and Arnheim,N.** (1985a) *Enzymatic amplification of beta-globin genomic sequences and restriction site analysis for diagnosis of sickle cell anemia.* Science, 230, 1350-1354.

233. **Sambrook,J., Russell,D.W. and Cold Spring,H.L.** (1989) Molecular cloning: a laboratory manual. Cold Spring Harbor Laboratory, Cold Spring Harbor, N.Y.

234. **Sandberg,L.M., Bjurling,A., Busson,P., Vasi,J. and Lemmens,R.** (2004) *Thiophilic interaction chromatography for supercoiled plasmid DNA purification.* J. Biotechnol., 109, 193-199.

235. **Sayers,J.R., Evans,D. and Thomson,J.B.** (1996) *Identification and eradication of a denatured DNA isolated during alkaline lysis-based plasmid purification procedures 2.* Anal. Biochem., 241, 186-189.

236. **Schleef,M.** (2001) Plasmids for therapy and vaccination 1. Weinheim ; Chichester : Wiley-VCH.

237. **Schlick,T.L.B.O.W.K.** (1994) *The influence of salt on the structure and energetics of supercoiled DNA.* Biophys. J., 67, 2146-2166.

238. **Schluep,T. and Cooney,C.L.** (1998) *Purification of plasmids by triplex affinity interaction.* Nucleic Acids Res., 26, 4524-4528.

239. **Schwartz,D.C. and Cantor,C.R.** (1984) *Separation of yeast chromosome-sized DNAs by pulsed field gradient gel electrophoresis.* Cell, 37, 67-75.

240. **Semancik,J.S. and Szychowski,J.** (1983) *Enhanced detection of viroid-RNA after selective divalent cation fractionation.* Anal. Biochem, 135, 275-279.

241. **Seo,J.H.B.J.E.** (1986) *Continuous cultivation of recombinant Escherichia coli: Existence of an optimum dilution rate for maximum plasmid and gene product concentration.* Biotechnol. Bioeng., 28, 1590-1594.

242. **Shamlou,P.A.** (2003) *Scaleable processes for the manufacture of therapeutic quantities of plasmid DNA*
3. Biotechnol. Appl. Biochem., 37, 207-218.

243. **Sheng,Y., Mancino,V. and Birren,B.** (1995) *Transformation of Escherichia coli with large DNA molecules by electroporation*
1. Nucleic Acids Res., 23, 1990-1996.

244. **Shizuya,H., Birren,B., Kim,U.J., Mancino,V., Slepak,T., Tachiiri,Y. and Simon,M.** (1992) *Cloning and stable maintenance of 300-kilobase-pair fragments of human DNA in Escherichia coli using an F-factor-based vector*
1. Proc. Natl. Acad. Sci. U. S. A, 89, 8794-8797.

245. **Shoham,Y. and Demain,A.L.** (1990) *Effect of medium composition on the maintenance of a recombinant plasmid in Bacillus subtilis*
1. Enzyme Microb. Technol., 12, 330-336.

246. **Siguret,V., Ribba,A.S., Cherel,G., Meyer,D. and Pietu,G.** (1994) *Effect of plasmid size on transformation efficiency by electroporation of Escherichia coli DH5 alpha*
1. Biotechniques, 16, 422-426.

247. **Singer,V.L., Jones,L.J., Yue,S.T. and Haugland,R.P.** (1997) *Characterization of PicoGreen reagent and development of a fluorescence-based solution assay for double-stranded DNA quantitation*
6. Anal. Biochem., 249, 228-238.

248. **Singh,R., Pantarotto,D., McCarthy,D., Chaloin,O., Hoebeke,J., Partidos,C.D., Briand,J.P., Prato,M., Bianco,A. and Kostarelos,K.** (2005) *Binding and condensation of plasmid DNA onto functionalized carbon nanotubes: toward the construction of nanotube-based gene delivery vectors*
14. J. Am. Chem. Soc., 127, 4388-4396.

249. **Sinnett,D., Richer,C. and Baccichet,A.** (1998) *Isolation of stable bacterial artificial chromosome DNA using a modified alkaline lysis method*
1. Biotechniques, 24, 752-754.

250. **Skogman,S.G. and Nilsson,J.** (1984) *Temperature-dependent retention of a tryptophan-operon-bearing plasmid in Escherichia coli.* Gene, 31, 117-122.

251. **Smith,G.J., III, Helf,M., Nesbet,C., Betita,H.A., Meek,J. and Ferre,F.** (1999) *Fast and accurate method for quantitating E. coli host-cell DNA contamination in plasmid DNA preparations*
3. Biotechniques, 26, 518-22, 524, 526.

252. **Smith,M.A. and Bidochka,M.J.** (1998) *Bacterial fitness and plasmid loss: the importance of culture conditions and plasmid size.* Can. J. Microbiol., 44, 351-355.

253. **Smith,P.K., Krohn,R.I., Hermanson,G.T., Mallia,A.K., Gartner,F.H., Provenzano,M.D., Fujimoto,E.K., Goeke,N.M., Olson,B.J. and Klenk,D.C.** (1985) *Measurement of protein using bicinchoninic acid*
1. Anal. Biochem., 150, 76-85.

254. **Sparks,R.B. and Elder,J.H.** (1983) *A simple and rapid procedure for the purification of plasmid DNA using reverse-phase C18 silica beads*
1. Anal. Biochem., 135, 345-348.

255. **Stanbury,P.F. and Whitaker,A.** (1984) Principles of fermentation technology. Pergamon Press, Oxford.

256. **Stephenson,D., Norman,F. and Cumming,R.H.** (1992) *Shear thickening of DNA in SDS lysates*
1. Bioseparation., 3, 285-289.

257. **Stouthamer A.H.** (1973) *A theoretical study on the amount of ATP required for synthesis of microbial cell material.* Antonie Van Leeuwenhoek, 39, 545-565.

258. **Stowers,D.J., Keim,J.M., Paul,P.S., Lyoo,Y.S., Merion,M. and Benbow,R.M.** (1988) *High-resolution chromatography of nucleic acids on the Gen-Pak FAX column*
1. J. Chromatogr., 444, 47-65.

259. **Strege,M.A. and Lagu,A.L.** (1991) *Anion-exchange chromatography of DNA restriction fragments.* J. Chromatogr., 555, 109-124.

260. **Summers,D.K.** (1991) *The kinetics of plasmid loss*
1. Trends Biotechnol., 9, 273-278.

261. **Summers,D.K., Beton,C.W. and Withers,H.L.** (1993) *Multicopy plasmid instability: the dimer catastrophe hypothesis.* Mol. Microbiol., 8, 1031-1038.

262. **Tao,Q. and Zhang,H.B.** (1998) *Cloning and stable maintenance of DNA fragments over 300 kb in Escherichia coli with conventional plasmid-based vectors*
1. Nucleic Acids Res., 26, 4901-4909.

263. **Teeters,M.A., Conrardy,S.E., Thomas,B.L., Root,T.W. and Lightfoot,E.N.** (2003) *Adsorptive membrane chromatography for purification of plasmid DNA.* J. Chromatogr. A, 989, 165-173.

264. **Thatcher ,e.al.** (1997) *Method of plasmid DNA production and purification.*

265. **Theodossiou,I., Elsner,H.D., Thomas,O.R. and Hobley,T.J.** (2002) *Fluidisation and dispersion behaviour of small high density pellicular expanded bed adsorbents 10.* J. Chromatogr. A, 964, 77-89.

266. **Theodossiou,I., Sondergaard,M. and Thomas,O.R.** (2001) *Design of expanded bed supports for the recovery of plasmid DNA by anion exchange adsorption 1.* Bioseparation., 10, 31-44.

267. **Theodossiou,I. and Thomas,O.R.** (2002) *DNA-induced inter-particle cross-linking during expanded bed adsorption chromatography. Impact on future support design 9.* J. Chromatogr. A, 971, 73-86.

268. **Theodossiou,I., Thomas,O.R.T. and Dunnill,P.** (1999) *Methods of enhancing the recovery of plasmid genes from neutralised cell lysate.* Bioprocess and Biosystems Engineering, 20, 147-156.

269. **Thwaites,E., Burton,S.C. and Lyddiatt,A.** (2002) *Impact of the physical and topographical characteristics of adsorbent solid-phases upon the fluidised bed recovery of plasmid DNA from Escherichia coli lysates 1.* J. Chromatogr. A, 943, 77-90.

270. **Trindade,I.P., Diogo,M.M., Prazeres,D.M. and Marcos,J.C.** (2005) *Purification of plasmid DNA vectors by aqueous two-phase extraction and hydrophobic interaction chromatography.* J. Chromatogr. A, 1082, 176-184.

271. **Tuma,R.S., Beaudet,M.P., Jin,X., Jones,L.J., Cheung,C.Y., Yue,S. and Singer,V.L.** (1999) *Characterization of SYBR Gold nucleic acid gel stain: a dye optimized for use with 300-nm ultraviolet transilluminators 3.* Anal. Biochem., 268, 278-288.

272. **Uhlenhopp,E.L., Zimm,B.H. and Cummings,D.J.** (1974) *Structural aberrations in T-even bacteriophage : VI. Molecular weight of DNA from giant heads.* Journal of Molecular Biology, 89, 689-690.

273. **Ullmann,A., Jacob,F. and Monod,J.** (1967) *Characterization by in vitro complementation of a peptide corresponding to an operator-proximal segment of the beta-galactosidase structural gene of Escherichia coli.* J. Mol. Biol., 24, 339-343.

274. **Urthaler,J., Schlegl,R., Podgornik,A., Strancar,A., Jungbauer,A. and Necina,R.** (2005) *Application of monoliths for plasmid DNA purification development and transfer to production.* J. Chromatogr. A, 1065, 93-106.

275. **van,H.N., Motte,J.C., Pilette,J.F., Decleire,M. and Colson,C.** (1993) *Sequential elution of denatured proteins, hydrolyzed RNA, and plasmid DNA of bacterial lysates adsorbed onto stacked DEAE-cellulose membranes 1.* Anal. Biochem., 211, 61-65.

276. **Varley,D.L., Hitchcock,A.G., Weiss,A.M., Horler,W.A., Cowell,R., Peddie,L., Sharpe,G.S., Thatcher,D.R. and Hanak,J.A.** (1999) *Production of plasmid DNA for human gene therapy using modified alkaline cell lysis and expanded bed anion exchange chromatography.* Bioseparation., 8, 209-217.

277. **Vasuki,N.S.** (1989) *A generalized model of plasmid replication.* BIOTECHNOLOGY AND BIOENGINEERING, 33, 1135-1144.

278. **Vilalta,A., Whitlow,V. and Martin,T.** (2002) *Real-time PCR determination of Escherichia coli genomic DNA contamination in plasmid preparations.* Anal. Biochem., 301, 151-153.

279. **Vincent,W.S., III and Goldstein,E.S.** (1981) *Rapid preparation of covalently closed circular DNA by acridine yellow affinity chromatography*
1. Anal. Biochem., 110, 123-127.

280. **Voet,D. and Voet,J.G.** (1995) Biochemistry. J. Wiley & Sons, New York.

281. **Voß,C., Schmidt,T., Schleef,M., Friehs,K. and Flaschel,E.** (2003) *Production of supercoiled multimeric plasmid DNA for biopharmaceutical application*
46. J. Biotechnol., 105, 205-213.

282. **Vyas,V.V., Gupta,S. and Sharma,P.** (1994) *Stability of a recombinant shuttle plasmid in Bacillus subtilis and Escherichia coli.* Enzyme Microb. Technol., 16, 240-246.

283. **Wade-Martins,R., Frampton,J. and James,M.R.** (1999) *Long-term stability of large insert genomic DNA episomal shuttle vectors in human cells*
1. Nucleic Acids Res., 27, 1674-1682.

284. **Wahlund,P.O., Gustavsson,P.E., Izumrudov,V.A., Larsson,P.O. and Galaev,I.Y.** (2004) *Precipitation by polycation as capture step in purification of plasmid DNA from a clarified lysate*
69. Biotechnol. Bioeng., 87, 675-684.

285. **Wang,L., Blasic,J.R., Jr., Holden,M.J. and Pires,R.** (2005) *Sensitivity comparison of real-time PCR probe designs on a model DNA plasmid.* Anal. Biochem., 344, 257-265.

286. **Wang,M. and Lai,E.** (1995) *Pulsed field separation of large supercoiled and open-circular DNAs and its application to bacterial artificial chromosome cloning*
6. Electrophoresis, 16, 1-7.

287. **Wang,Z., Le,G., Shi,Y. and Wegrzyn,G.** (2001) *Medium design for plasmid DNA production based on stoichiometric model.* Process Biochemistry, 36, 1085-1093.

288. **Wang,Z., Le,G., Shi,Y. and Wegrzyn,G.** (2002) *Studies on recovery plasmid DNA from Echerichia coli by heat treatment.* Process Biochemistry, 38, 199-206.

289. **Warnes,A. and Stephenson,J.R.** (1986) *The insertion of large pieces of foreign genetic material reduces the stability of bacterial plasmids*
1. Plasmid, 16, 116-123.

290. **Weiner,M.P., Thannhauser,J.H., Laity,M.H., Benning,D.P. and Lee,H.A.** (1988) *Plasmid purification using reverse-phase high performance liquid chromatography resin PRP-infinity.* Nucleic Acids Res., 16, 8183.

291. **Weissensteiner,T. and Lanchbury,J.S.** (1996) *Strategy for controlling preferential amplification and avoiding false negatives in PCR typing* *1.* Biotechniques, 21, 1102-1108.

292. **White,R.E., Wade-Martins,R., Hart,S.L., Frampton,J., Huey,B., sai-Mehta,A., Cerosaletti,K.M., Concannon,P. and James,M.R.** (2003) *Functional delivery of large genomic DNA to human cells with a peptide-lipid vector.* J. Gene Med., 5, 883-892.

293. **WHO,G.** (1997) *WHO Expert Committee on Biological Standardisation. WHO Technical Report Series No 878.*

294. **Wicks,I.P., Howell,M.L., Hancock,T., Kohsaka,H., Olee,T. and Carson,D.A.** (1995) *Bacterial lipopolysaccharide copurifies with plasmid DNA: implications for animal models and human gene therapy* *1.* Hum. Gene Ther., 6, 317-323.

295. **Wild,J., Hradecna,Z. and Szybalski,W.** (2002) *Conditionally amplifiable BACs: switching from single-copy to high-copy vectors and genomic clones* *1.* Genome Res., 12, 1434-1444.

296. **Wild,J., Sektas,M., Hradecna,Z. and Szybalski,W.** (1998) *Targeting and retrofitting pre-existing libraries of transposon insertions with FRT and oriV elements for in-vivo generation of large quantities of any genomic fragment.* Gene, 223, 55-66.

297. **Williams,S.G., Cranenburgh,R.M., Weiss,A.M., Wrighton,C.J., Sherratt,D.J. and Hanak,J.A.** (1998a) *Repressor titration: a novel system for selection and stable maintenance of recombinant plasmids.* Nucleic Acids Res., 26, 2120-2124.

298. **Williams,S.G., Cranenburgh,R.M., Weiss,A.M., Wrighton,C.J., Sherratt,D.J. and Hanak,J.A.** (1998b) *Repressor titration: a novel system for selection and stable maintenance of recombinant plasmids* *5.* Nucleic Acids Res., 26, 2120-2124.

299. **Wils,P., Escriou,V., Warnery,A., Lacroix,F., Lagneaux,D., Ollivier,M., Crouzet,J., Mayaux,J.F. and Scherman,D.** (1997) *Efficient purification of plasmid DNA for gene transfer using triple-helix affinity chromatography.* Gene Ther., 4, 323-330.

300. **Winters,M.A., Richter,J.D., Sagar,S.L., Lee,A.L. and Lander,R.J.** (2003) *Plasmid DNA purification by selective calcium silicate adsorption of closely related impurities* *1.* Biotechnol. Prog., 19, 440-447.

301. **Wojcik,K., Wieckiewicz,J., Kuczma,M. and Porwit-Bobr,Z.** (1993) *Instability of hybrid plasmids in Bacillus subtilis.* Acta Microbiol. Pol., 42, 127-136.

302. **Woodcock,D.M., Crowther,P.J., Doherty,J., Jefferson,S., DeCruz,E., Noyer-Weidner,M., Smith,S.S., Michael,M.Z. and Graham,M.W.** (1989) *Quantitative evaluation of Escherichia coli host strains for tolerance to cytosine methylation in plasmid and phage recombinants* *2.* Nucleic Acids Res., 17, 3469-3478.

303. **Wu,S.L. and Karger,B.L.** (1996) *Hydrophobic interaction chromatography of proteins.* Methods Enzymol., 270, 27-47.

304. **Yoshida,A., Nagata,T., Uchijima,M., Higashi,T. and Koide,Y.** (2000) *Advantage of gene gun-mediated over intramuscular inoculation of plasmid DNA vaccine in reproducible induction of specific immune responses.* Vaccine, 18, 1725-1729.

305. **Yuan Li,X.-Y.D.a.Y.S.** (2005) *High-speed chromatographic purification of plasmid DNA with a customized biporous hydrophobic adsorbent.* Biochemical Engineering Journal, 27, 33-39.

306. **Zagon,I.S., Sassani,J.W., Verderame,M.F. and McLaughlin,P.J.** (2005) *Particle-mediated gene transfer of opioid growth factor receptor cDNA regulates cell proliferation of the corneal epithelium.* Cornea, 24, 614-619.

307. **Zhang,S., Krivosheyeva,A. and Nochumson,S.** (2003) *Large-scale capture and partial purification of plasmid DNA using anion-exchange membrane capsules.* Biotechnol. Appl. Biochem., 37, 245-249.

308. **Zhu,K., Jin,H., Ma,Y., Ren,Z., Xiao,C., He,Z., Zhang,F., Zhu,Q. and Wang,B.** (2005) *A continuous thermal lysis procedure for the large-scale preparation of plasmid DNA.* J. Biotechnol., 118, 257-264.

309. **Zipper,H.B.H.B.J.V.F.** (2004) *Investigations on DNA intercalation and surface binding by SYBR Green I, its structure determination and methodological implications.* Nucleic Acids Res., 32.

310. **Zoon,K.C.** (1996) *Points to Consider on Plasmid DNA Vaccines for Preventive Infectious Disease Indications [Food and Drug Administration]*(http://www.fda.gov/cber/gdlns/plasmid.pdf).